Journal of Mathematics

Application of Fractional-order Models in Management and Economic Systems

Lead Guest Editor: Lifeng Wu
Guest Editors: Utkucan Şahin and Shuhua Mao

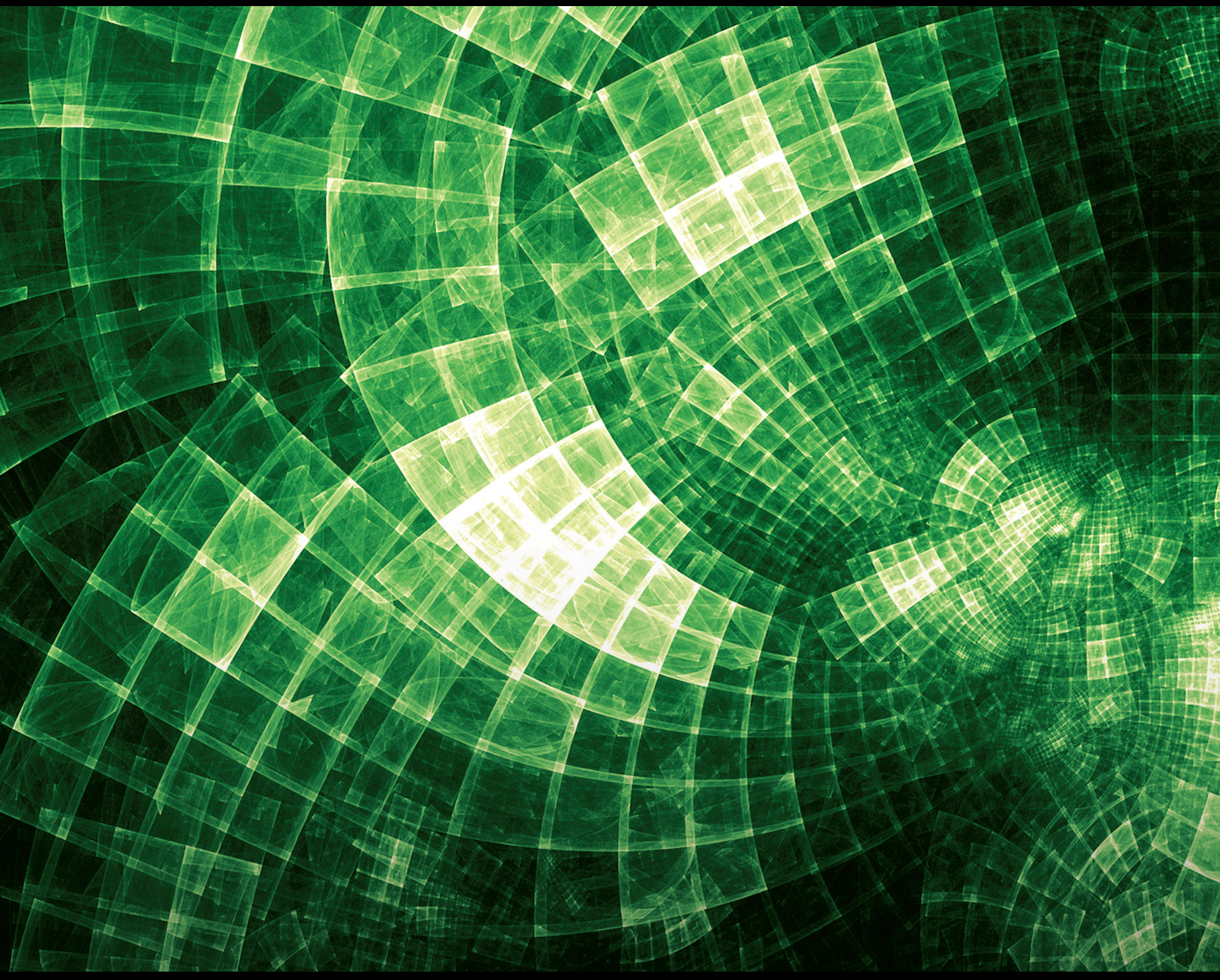

Application of Fractional-order Models in Management and Economic Systems

Journal of Mathematics

Application of Fractional-order Models in Management and Economic Systems

Lead Guest Editor: Lifeng Wu
Guest Editors: Utkucan Şahin and Shuhua Mao

Probability and Statistics

Contents

Contents

Hindawi
Journal of Mathematics
Volume 2021, Article ID 3023385, 7 pages
https://doi.org/10.1155/2021/3023385

Research Article

Prediction of Agricultural Water Consumption in 2 Regions of China Based on Fractional-Order Cumulative Discrete Grey Model

Yunhong Xu,[1] Huadong Wang,[1] and Nga Lay Hui[2]

[1]*School of Management Engineering and Business, Hebei University of Engineering, Hebei, Handan 056038, China*
[2]*Faculty of Business, Economics and Accountancy, Universiti Malaysia Sabah, Kota Kinabalu 11800, Malaysia*

Correspondence should be addressed to Huadong Wang; 16176535@qq.com

Received 10 June 2021; Revised 3 November 2021; Accepted 6 November 2021; Published 6 December 2021

Academic Editor: Efthymios G. Tsionas

In this paper, a new forecasting method of agricultural water demand, fractional-order cumulative discrete grey model, is proposed. Firstly, the best fitting of historical data is used to construct the optimization model. MATLAB programming is applied to solve the optimization model and obtain the optimal order. Secondly, the fractional-order cumulative discrete grey model in this paper is compared with GM (1, 1) model to verify the performance of the model. Finally, Handan region of Hebei Province and Jingzhou region of Hubei Province were selected as the study areas to predict their agricultural water consumptions. The results show that the fractional-order cumulative discrete grey model has better prediction performance than the GM (1, 1) model. It can be used as an effective method for forecasting agricultural water consumption.

1. Introduction

Water is an important basic resource and necessity for agricultural production. Affected by regional and natural environment changes, the contradiction between supply and demand of water resources in various regions in China is prominent, which seriously affects the process of economic development in various regions. The key to solve the contradiction between the supply and demand of water resources lies in the accurate prediction of water demand. There are few historical data of agricultural water consumption, and it is affected by many factors, such as economic development level, agricultural structure adjustment, natural climate conditions, and irrigation management level, which shows great randomness and fluctuation between years.

The prediction of agricultural water consumption is an important part of the optimal allocation of regional water resources, and it is the basic work to realize the optimal scheduling of regional water supply. Accurately predicting of regional water consumption is the key to the optimal allocation of water resources in the region. There are many forecasting methods of agricultural water consumption, including principal component analysis method, index analysis method, regression analysis method, grey prediction method, and artificial neural network method.

There are few historical data of agricultural water consumption in general areas. The purpose of this study is to select one forecasting method reasonably and collect the required data for effective forecasting based on the changing law of water consumption. In this paper, based on the existing literature review results and the research focus of the sustainable development of the water resource-environment-economy-society system, a fractional discrete grey model is proposed to predict the agricultural water demand.

The rest of the paper is organized as follows. Literature review is introduced in Section 2. The proposed method, including DGM (1, 1) model and $\mathrm{DGM}^{p/q}(1,1)$ model, is introduced in Section 3. A numerical example is illustrated in Section 4, and conclusions are discussed in Section 5.

2. Literature Review

2.1. Research on Forecasting Methods of Agricultural Water Consumption. Agricultural water consumption is the focus and hotspot in the field of water resources research, but the influencing factors of water consumption are many, and the research methods are endless.

In the research of agricultural water demand forecasting, more scholars are devoted to integrating forecasting methods into concrete practice. Fu et al. [1] applied the back propagation neural network model to predict regional water demand. The quota quantitative method is used to predict and analyze water demand in Zhengzhou region and Aksu region [2, 3]. Lv et al. [4] used principal component analysis to find out the main influencing factors of domestic water, industrial water, and agricultural water in Sichuan Province; they also use regression analysis to model and predict the three aspects of water consumption. Wen et al. [5] used the trend surface analysis method to predict agricultural water demand.

However, the prediction accuracy of each method above is not ideal. The quota method is mainly based on crop characteristics and current irrigation quota, but the preparation of irrigation quota has certain subjectivity and uncertainty. Therefore, it is difficult to achieve accurate prediction by the quota method. The back propagation neural network method requires a large number of data for model training, and there is also the problem of overfitting. Autoregressive and moving average model have high requirements for data stability. Since the actual water consumption series do not fully conform to the exponential relationship, it also limits the application range of the exponential model method. The trend surface analysis requires that the selected trend surface model is not enough, and the fitting accuracy may not reach sufficient accuracy.

2.2. Grey Model Research. Since Professor Deng [6] proposed grey system theory, the grey prediction model has been widely used in industry, agriculture, water conservancy, geology, science and education, military, and many other fields. The grey model is a method to study the "poor information," "small sample," and uncertainty problems, which requires less data and has simple principle. Among them, the GM (1, 1) model is the most widely used model [7]. It is mainly for single-variable systems. The randomness of the weakening sequence is generated by accumulation to find the change law of the system. Based on this, the prediction model of time is established.

After more than 20 years of development, scholars have studied the grey prediction model from different aspects, and these research results have greatly promoted the development of the grey model.

Shu-Hui et al. [8] forecasted agricultural water consumption based on the GM (1, 1) model. Zhang [9] predicted the agricultural water consumption in Korla region based on the GM (1, 1) model. Xiao et al. [10] studied agricultural water use in Shaanxi based on the uncertainty grey model. Zhao et al. [11] predicted agricultural water consumption in Shiyang River Basin based on a combined model. Jiang et al. [12] based on regression analysis and grey model GM (1, 1) method predicted the water demand of Minqin County. Li et al. [13] predicted agricultural water consumption in Tongliao and Baoji by using the fractional-order reverse accumulation grey model.

However, with the expansion of the application scope of the grey prediction model, various new problems emerge one after another, and it is necessary to do more extensive research on the GM (1, 1) model. Since the fractional-order calculus is proposed by Leibniz in 1965, it has shown strong vitality and superiority in control theory, image processing, and other aspects. It is the extension of the integer-order calculus in the usual sense to the fractional-order calculus. Compared with GM (1, 1), the fractional-order grey model improved the prediction accuracy.

To sum up, scholars have carried out different degrees of research on agricultural water consumption in different regions, but a generally accepted viewpoint has not been formed in the research on forecasting methods of water consumption, and there are still shortcomings as follows:

(1) The forecasting methods of agricultural water consumption all have their defects, especially the qualitative research methods are mixed with a few personal subjective factors, so it is necessary to adopt objective methods to reduce the impact of subjective factors and determine the importance of research methods for forecasting.

(2) There are few historical data of agricultural water consumption in general areas, and it is affected by many factors at the same time which is oscillatory. Therefore, it is applicable to use the grey model to predict agricultural water consumption. However, the prediction results show the approximate exponential growth patterns, which is only suitable for short-term prediction. Although researchers have improved and optimized the GM (1, 1) model in many ways, they cannot overcome the inherent error of the grey model from discrete estimation to continuous prediction.

Therefore, based on the idea of the discrete grey model, this paper constructs a kind of direct discrete grey model—fractional accumulated discrete grey model—to overcome the inherent error from discrete estimation to continuous prediction and studies the accumulated generation method of the discrete grey GM (1, 1) model so as to reduce the disturbance bound of the prediction model and improve the accuracy of GM (1, 1) prediction ability and modeling accuracy of the model and expand the theoretical research and application scope of the grey prediction model.

3. Methods

3.1. The Discrete Grey Model (1, 1). Grey prediction is a method to construct a model based on the known information of the sequence and predict the future data with the past data through the model. The model can reflect the development trend of data and make reasonable prediction and judgment according to the model. In the grey prediction model, the accumulation of original data weakens the volatility and randomness of random sequence and enhances the certainty. However, many defects of the GM (1, 1) model have been unable to meet the theoretical basis for our exploration of complex uncertain systems. The discrete grey prediction model proposed by Liu et al. [14] has made us have a deeper understanding of the grey system theory. The proposed discrete grey prediction model theoretically solves

the error caused by the jump between the discrete parameter estimation equation and the continuous prediction equation of the original GM (1, 1) model, which has the coincidence of the white exponent, and greatly improves the simulation effect and prediction accuracy of the model.

The theoretical framework is as follows.

Assuming that the nonnegative original sequence is $X^{(0)} = (x^0(1), x^0(2), \ldots, x^0(n))$, first-order summation of the original sequence $X^{(0)}$ by $(1-\text{AGO})$, the sequence is produced which is $X^{(1)} = (x^1(1), x^1(2), \ldots, x^1(n))$. In this sequence, $x^1(k) = \sum_{i=1}^{(0)} x^{(0)}(i), \quad k = 1, 2, \ldots, n$.

Definition 1. Assuming $x^{(0)}(k)$ and $x^{(1)}(k)$ as already pointed out, the grey equation

$$x^{(1)}(k+1) = \beta_0 + \beta_1 k^{\gamma} + \beta_2 x^{(1)}(k), \tag{1}$$

is called the discrete grey model, where γ is called a power exponent.

Theorem 1. *It is assumed that $X^{(0)}$ is a nonnegative sequence and that $X^{(0)}$ and $X^{(1)}$ are as described in Definition 1. Assume that the power exponent γ of the discrete grey power model is known, and if $\widehat{\beta} = (\beta_0, \beta_1, \beta_2)^T$ is a parameter column, then*

$$\widehat{\beta} = \left(B^T B\right)^{-1} B^T Y, \tag{2}$$

where

$$B = \begin{bmatrix} 1 & 1^{\gamma} & x^{(1)}(1) \\ 1 & 2^{\gamma} & x^{(1)}(2) \\ \vdots & \vdots & \vdots \\ 1 & (n-1)^{\gamma} & x^{(1)}(n-1) \end{bmatrix}, \; Y = \begin{bmatrix} \mathrm{x}^{(1)}(2) \\ \mathrm{x}^{(1)}(3) \\ \vdots \\ \mathrm{x}^{(1)}(\mathrm{n}) \end{bmatrix}. \tag{3}$$

Two corollaries are drawn.

Corollary 1. *When $\gamma = 0$, the discrete grey power model changes to $x^{(1)}(k+1) = \beta_1' + \beta_2 x^{(1)}(k)$; that is, the discrete grey model degenerates to the discrete grey GM (1, 1) model [14].*

Corollary 2. *When $\gamma = 1$, the discrete grey power model is $x^{(1)}(k+1) = \beta_0 + \beta_1 k + \beta_2 x^{(1)}(k)$; that is, the discrete grey power model degenerates into an approximate nonhomogeneous discrete grey GM (1, 1) model [14].*

(3) If $\widehat{\beta} = (\beta_0, \beta_1, \beta_2)^T$ is as stated in Theorem 1 and the initial value condition is $\widehat{x}^1(1) = x^{(0)}(1)$, then the solution of the discrete grey power model is

$$\widehat{x}^{(1)}(k+1) = \begin{cases} k\beta_0 + \beta_1 \sum_{i=1}^{k} i^{\tau} + x^{(0)}(1), \beta_2 = 1, \\ \beta_0 \dfrac{1-\beta_2^k}{1-\beta_2} + \beta_1 \sum_{i=1}^{k} i^{\tau} \beta_2^{k-i} + x^{(0)}(1)\beta_2^k, \beta \neq 1. \end{cases} \tag{4}$$

According to the time response formula of the discrete grey power model given in (3), the discrete grey power model retains the power exponential diversity of the power model, which makes the discrete grey power model have better adaptability to data prediction. In addition, according to the parameter estimation method of the discrete grey power model and Corollary 1 and Corollary 2, it avoids the inherent defect of the traditional power model from discrete estimation to continuous prediction; that is, it has the advantage of the discrete grey model from discrete estimation to discrete prediction. Therefore, the newly constructed discrete grey power model has the advantages of both the discrete model and the grey power model, which makes the new model constructed more adaptable to the data.

3.2. Fractional-Order Cumulative Discrete Grey Model. The fractional accumulation makes the original data sequence to satisfy the approximate exponential law. The sequence before the accumulation is called the original sequence, and the sequence after the accumulation is called the generated sequence. Accumulation generation is a method to make the grey process from grey to white, which plays an extremely important role in the grey system theory. The development trend of the grey accumulation process can be seen through the accumulation generation, and the integral characteristics or laws contained in the chaotic original data can be manifested. Accumulation generation is a method to generate a new sequence by successively accumulating the data of each moment in the original data column.

The theoretical framework is as follows:

(1) Assume that the nonnegative sequence $X^{(0)} = |x^{(0)}(1), x^{(0)}(2), \ldots, x^{(0)}(n)|$,

$$x^{(r)}(k) = \sum_{i=1}^{k} x^{(r-1)}(i), \tag{5}$$

is an r (r is an integer) order summative operator, denoted as

$$X^{(r)} = \left|x^{(r)}(1), x^{(r)}(2), \ldots, x^{(r)}(n)\right|, \tag{6}$$

Then,

$$x^{(r)}(k) = \sum_{i=1}^{k} C_{k-i+r-1}^{k-i} x^{(0)}(i), \tag{7}$$

where $C_{r-1}^{0} = 1, C_{k-1}^{k} = 0, k = 1, 2, \ldots, n$.

(2) Assume that the nonnegative sequence $X^{(0)} = |x^{(0)}(1), x^{(0)}(2), \ldots, x^{(0)}(n)|$, $x^{(p/q)}(k) = \sum_{i=1}^{k} C_{k-i+(p/q)-1}^{k-i} x^{(0)}(i)$ is an accumulation operator of p/q $(0 < p/q < 1)$ and specify that

$$C_{\frac{p}{q}-1}^{0} = 1, C_{k-1}^{k} = 0, k = 1, 2, \ldots, n \cdot C_{k-i+(p/q)-1}^{k-i} = \frac{(k-i+(p/q)-1)(k-i+(p/q)-2)\cdots(p/q+1)(p/q)}{(k-i)!}, \tag{8}$$

$X^{(p/q)} = |x^{(p/q)}(1), x^{(p/q)}(2), \ldots, x^{(p/q)}(n)|$ is an accumulation sequence of order p/q $(0 < p/q < 1)$.

(3) Assume that the nonnegative sequence $X^{(0)} = |x^{(0)}(1), x^{(0)}(2), \cdots, x^{(0)}(n)|$ and call $\alpha^{(1)}x^{(1-(p/q))}(k) = x^{(1-(p/q))}(k) - x^{(1-(p/q))}(k-1)$ is the $p/q\,(0 < p/q < 1)$ order reduction operator.

$$\alpha^{(p/q)}X^{(0)} = \alpha^{(1)}X^{(1-(p/q))} = \left|\alpha^{(1)}x^{(1-(p/q))}(1), \alpha^{(1)}x^{(1-(p/q))}(2), \ldots, \alpha^{(1)}x^{(1-(p/q))}(n)\right|, \tag{9}$$

is a p/q order descending sequence.

(4) Assume that the nonnegative sequence $X^{(0)} = |x^{(0)}(1), x^{(0)}(2), \ldots, x^{(0)}(n)|$, p/q $(0 < p/q < 1)$ order cumulative sequence is $X^{(p/q)} = |x^{(p/q)}(1), x^{(p/q)}(2), \ldots, x^{(p/q)}(n)|$, and

$$x^{(p/q)}(k+1) = \beta_1 x^{(p/q)}(k) + \beta_2, \quad k = 1, 2, \ldots, n-1, \tag{10}$$

is the order p/q cumulative discrete grey model (it is denoted as $\mathrm{DGM}^{p/q}(1,1)$).

3.3. Modeling Steps of Fractional-Order Cumulative Discrete Grey Model. The modeling steps for $\mathrm{DGM}^{p/q}(1,1)$ are as follows:

Step 1. The cumulative sequence of order p/q is obtained by calculation: $X^{(p/q)} = |x^{(p/q)}(1), x^{(p/q)}(2), \ldots, x^{(p/q)}(n)|$

Step 2. Substitute $x^{(p/q)}(k)\,(k = 1, 2, \ldots, n)$ into step (4) to estimate the parameter $\begin{bmatrix} \widehat{\beta}_2 \\ \widehat{\beta}_1 \end{bmatrix}$ by the least square method

Step 3. We can use $x^{(p/q)}(k) = (x^{(0)}(1) - \widehat{\beta}_2/1 - \widehat{\beta}_1)\,\widehat{\beta}_1^{(k-1)} + \widehat{\beta}_2/1 - \widehat{\beta}_1\,(k = 2, 3, \ldots, n)$ to predict that $\widehat{x}^{(p/q)}(1), \widehat{x}^{p/q}(2), \ldots$

Step 4. So, let us subtract $X^{(p/q)} = |\widehat{x}^{(p/q)}(1), \widehat{x}^{(p/q)}(2), \ldots, \widehat{x}^{(p/q)}(n)|$ by p/q, which is $\alpha^{(p/q)}X^{(0)} = |\alpha^{(1)}\widehat{x}^{(1-(p/q))}(1), \alpha^{(1)}\widehat{x}^{(1-(p/q))}(2), \ldots, \alpha^{(1)}\widehat{x}^{(1-(p/q))}(n), \alpha^{(1)}\widehat{x}^{(1-(p/q))}(n+1), \ldots|$

4. Case Analysis

The above model $\mathrm{DGM}^{p/q}(1,1)$ was applied to the forecasting research of agricultural water consumption. The agricultural water consumption of Handan region in Hebei Province and Jingzhou region in Hubei Province from 2011 to 2020 was used as the basic data to predict the agricultural water consumption of the two regions from 2021 to 2025, and the GM (1, 1) model was used to make a comparison.

4.1. Overview of the Study Area. In this paper, Handan region (36°20′~36°44′N, east longitude 114°03′~114°40′E) and Jingzhou region (29°26′~31°37′N, 111°15′~114°05′E) of Hebei Province are selected as the study areas.

Handan is a large agricultural region with 9.95 million mu of arable land and is plotted in Figure 1. It is an important commodity grain production base and grain production core area in China and a major cotton, egg, and vegetable production base in China. It is one of the five pilot cities (regions) in China to promote high-yield production known as "grain warehouse in the north," "cotton sea in the south of Hebei," and "Beijing Tianjin Vegetable Garden" of reputation.

Jingzhou is a large agricultural region, is the famed based on grain, cotton, oil, fish, meat, eggs production base, and is plotted in Figure 2. The agricultural production of Jingzhou occupies an important position in Hubei Province. The output of main agricultural products ranks the top in the province. Perennially, the output of cotton accounts for 1/3 of the province, the output of aquatic products accounts for 1/4, the output of grain and oil, respectively, accounts for 1/6, the output of pigs accounts for 1/10, and the added value of agriculture, forestry, animal husbandry, and fishery accounts for 1/9 of the province, especially the rapeseed and freshwater products occupy an important position in the country. The area and output of freshwater aquaculture have ranked first in China for 18 consecutive years.

It can be seen that the agricultural planting in both places wins a place in the whole country. Handan region is one of the main bases of corn and wheat in Hebei Province, and Jingzhou region is the main base of rice and cotton production in Hubei Province. Due to the great difference of planting varieties between the two places, the demand for agricultural water consumption is also different. It has the typical representative significance for us to select the two places as the research area.

4.2. Agricultural Water Consumption in the Study Area. According to "Hebei Province water resources communique," "Handan water resources communique," "Hubei Province water resources communique," and "Jingzhou water resources communique" from 2011 to 2020, the agricultural water consumption data of Handan region and Jingzhou region from 2011 to 2020 are collected, as shown in Table 1. It can be seen from Table 1 that agricultural water consumption is the main water users of the two regions, accounting for about 70% of the total water consumption. However, with the development of social economy, other industries are crowding out agricultural water, and water pollution is becoming more and serious. Therefore, it is necessary to predict the agricultural water consumption of the two regions in order to provide the basis for the overall planning of agricultural water supply.

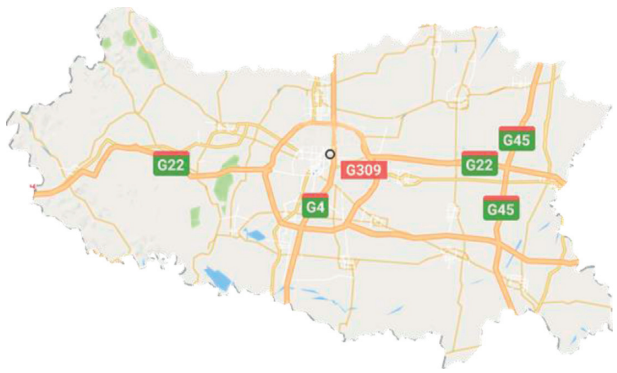

Figure 1: Location map of research area—Handan.

Figure 2: Location map of research area—Jingzhou.

Table 1: Agricultural water consumption in Handan and Jingzhou from 2011 to 2020.

	2011	2012	2013	2014	2015	2016	2017	2018	2019	2020
Agricultural water consumption in Jingzhou region	26.28	24.62	29.55	26.49	25.11	24.01	26.31	26.7	27.68	—
Proportion of water occupied	71%	69%	77%	75%	71%	69%	71%	72%	73%	—
Agricultural water consumption in Handan region	12.86	14.96	14.02	14.62	14.14	12.72	12.98	12.75	12.96	12.61
Proportion of water occupied	69.9%	72.2%	71.2%	72.6%	73.0%	68.9%	69.6%	67.5%	67.5%	67.2%

4.3. Model Comparison and Test. The procedure of data preprocess is illustrated as follows:

Step 1. Normalize the data: Taking the observation data of Handan region from 2011 to 2020 as the modeling sample, the original data sequence was obtained as follows:

$$X_H(0) = \{12.86, 14.96, 14.02, 14.62, 14.14, 12.72, 12.98, 12.75, 12.96, 12.61\}. \tag{11}$$

The observation data of Jingzhou from 2011 to 2019 were taken as modeling samples, and the original data sequence was as follows:

$$X_J(0) = \{26.28, 24.62, 29.55, 26.49, 25.11, 24.01, 26.31, 26.7, 27.68\}. \tag{12}$$

Step 2. Find the optimal order of the model and build a model: In order to illustrate the advantages of the fractional-order cumulative grey model in national economic forecasting, the commonly used order $R = 1/2$ and $R = 1/4$ are selected to compare with GM (1, 1) [15, 16].

However, in order to accurately predict the agricultural water consumption of Handan and Jingzhou in the future, the fractional-order discrete grey optimal model should be constructed, which requires the optimal order number. The optimal order $R = 0.1025$ was obtained by MATLAB software programming. The fractional discrete grey DGM (1, 1) model established according to the observed data is as follows:

$$x^{(0.1025)}(k+1) = 1.2865x^{(0.1025)}(k) + 21.7806, \quad k = 1, 2, \ldots, n-1. \tag{13}$$

Step 3. Solve the model: In order to test the performance of the model proposed in this paper, the prediction effect of the model compared with that of the GM (1, 1) model is shown in Table 2.

Table 2: Comparison of prediction effect of the model.

Study area	Year	Original value	GM (1, 1) model		$DGM^{p/q}(1,1)$ model	
			Predicted value	Relative error	Predicted value	Relative error
Handan region	2011	12.86	12.86	0.00%	12.86	0.00
	2012	14.96	14.73	1.51%	14.49	3.16
	2013	14.02	14.42	2.84%	14.41	2.76
	2014	14.62	14.11	3.51%	14.04	3.98
	2015	14.14	13.80	2.38%	13.68	3.23
	2016	12.72	13.51	6.18%	13.39	5.24
	2017	12.98	13.22	1.82%	13.14	1.25
	2018	12.75	12.93	1.43%	12.94	1.47
	2019	12.96	12.65	2.37%	12.76	1.53
	2020	12.61	12.38	1.81%	12.61	0
	Mean			2.38%		2.26
Jingzhou region	2011	26.28	26.28	0.00%	26.28	0.00
	2012	24.62	26.07	5.91%	25.53	3.70
	2013	29.55	26.147	11.53%	25.50	13.71
	2014	26.49	26.21	1.06%	25.69	3.03
	2015	25.11	26.27	4.64%	26.98	3.48
	2016	24.01	26.34	9.71%	26.34	9.72
	2017	26.31	26.41	0.38%	26.74	1.65
	2018	26.7	26.48	0.84%	27.17	1.78
	2019	27.68	26.54	4.11%	27.63	0.19
	Mean			4.24%		4.14

Table 3: Forecast value of agricultural water consumption in the study area in the next five years.

Region	2020	2021	2022	2023	2024	2025
Handan region	12.61	12.48	12.35	12.25	12.15	12.05
Jingzhou region	28.10	28.58	29.07	29.58	30.09	30.61

Step 4. Contrast and analyze: It can be seen from Table 2 that under the GM (1, 1) model established when the order $r = 1$, the average prediction error of test set water consumption in Handan City and Jingzhou City is 2.38% and 4.24%, respectively. However, the average prediction error of the $DGM^{p/q}(1,1)$ model in Handan region and Jingzhou region is 2.26% and 4.14%, respectively, which is small, indicating that the model in this paper is significantly improved compared with the GM (1, 1) model.

4.4. Forecast of Agricultural Water Consumption in the Study Area in the Next Five Years. The fractional discrete grey GM (1, 1) power model is constructed according to the characteristics of the original data series, which plays an important role in enriching and developing the theory and method of grey prediction. In general, the model in this paper can predict agricultural water consumption well. In order to further test the performance of the model, the model in this paper is used to forecast and analyze agricultural water consumption in Handan region and Jingzhou region in the next five years. The predicted results are shown in Table 3.

5. Conclusion

In this paper, the basic data of agricultural water consumption from 2011–2020 in Hebei Province and Hubei Province were selected to compare the differences between the GM (1, 1) model and the fractional-order discrete grey model, verify the effectiveness of fractional-order discrete grey model, expand the application range of the grey prediction model, and provide a new method for demand prediction of small sample data. It also contributes to the policy formulation and risk control of water resources protection in the two places, so as to ensure the rational use of water resources and provide water resources guarantee for the sustainable development of agriculture in the two places.

(1) In view of the oscillation characteristics and data requirements of agricultural water series, this paper introduces the discrete idea and fractional-order accumulation idea into the grey model and constructs the fractional-order discrete grey model. Compared with the GM (1, 1) model, this model eliminates the error caused by the traditional grey model jumping directly from the differential equation to the difference equation, improves the modeling accuracy of the model, and can be used as an effective method for the prediction of agricultural water consumption.

(2) With the adjustment of agricultural industrial structure, the popularization of water-saving irrigation technology is slow, and the agricultural water consumption will increase year by year. Jingzhou has vigorously developed rice and crayfish industry in

recent years. In 2019, the area of shrimps and rice in Jingzhou is 2.51 million mu, and the output of crayfish is 400,000 tons, which ranks first among cities and states in China. The demand for water is obviously increasing. Handan has made great efforts to carry out high-efficiency water-saving irrigation project and the agricultural project to stabilize the overdrawing of groundwater, and the agricultural water consumption has shown a downward trend. Therefore, the water management department should improve the existing irrigation system and accelerate the promotion of water-saving irrigation to improve the water use efficiency and realize the transformation from traditional agriculture to modern agriculture.

(3) Agricultural water consumption is affected by many factors, especially when the climate conditions change significantly, which will affect the consistency of agricultural water consumption data before and after climate change so that the historical data will show different patterns before and after climate change. To some extent, considering the influence of different meteorological conditions on agricultural water consumption, the prediction of agricultural water consumption is more accurate. Therefore, climate factors should be considered in the future model research to establish a more reasonable prediction model of water consumption.

Data Availability

The relevant data are included within the paper or in Supplementary Information.

Conflicts of Interest

The authors declare that they have no conflicts of interest.

Acknowledgments

The relevant research was supported by Hebei Province Social Science Fund Project (HB19GL062), Handan Science and Technology Bureau Project (19422303008–75), and Research on the Spatio-Temporal Evolution of County Economy in Hebei Province under the background of coordinated development of Beijing-Tianjin-Hebei (SQ182026).

References

[1] D. Fu, C. Wang, Q. Zhang, and Y. Dai guang, "Forecast of area water demand based on BP neural network model," *Urban Roads Bridges & Flood Control*, vol. 4, pp. 93–97, 2011.

[2] L. Yong, L. X. Yun, and J. Wen, "Forecast analysis of Aksu region's Water Demand Based on quantitative quota method," *Journal of Water Resources and Water Engineering*, vol. 23, no. 2, pp. 13–15, 2012.

[3] D. Liu, C.-H. Hu, and Z.-N. Wu, "Predicting method for demand of agriculture water based on quantitative analysis," *Journal of Irrigation and Drainage*, vol. 27, no. 6, pp. 88–91, 2008.

[4] L. Wang-Yong, L. Zhao, and C. Dong, "Prediction of amount of water use in sichuan province based on the principal component analysis," *Journal of Water Resources and Water Engineering*, vol. 20, no. 06, pp. 84–87, 2009.

[5] L. Wen, W. Song, F. Zhang, and D. Liang-fei, "Application of trend surface analysis in prediction of agricultural water demand," *Journal of Anhui Agricultural Sciences*, vol. 40, no. 3, pp. 1624-1625, 2012.

[6] J. Deng, "Properties of grey forecasting models GM (1, 1)," *Journal of Huazhong University of Science and Technology: Natural Science Edition*, vol. 5, pp. 1–6, 1987.

[7] S. Liu and Y. Lin, "Introduction to grey systems theory," *Understanding Complex Systems*, vol. 68, pp. 1–18, 2010.

[8] L. Shu-Hui, C. Wu-Qun, F. Gao, S. Shao-gang, and K. Guo-fang, "Application of GM (1, 1) model in agriculture water demand and water-saving irrigation area forecasting," *Water Saving Irrigation*, vol. 8, pp. 14–16, 2007.

[9] X.-H. Zhang, "Prediction of agricultural water consumption in Korla region based on grey GM (1, 1) model," *Water Saving Irrigation*, vol. 2009, no. 10, pp. 45-46, 2009.

[10] H. Xiao and C. Yin, "Study on agricultural water in shangxi province based on uncertainty grey prediction," *Journal of Anhui Agricultural Sciences*, vol. 39, no. 6, pp. 3161-3162, 2011.

[11] Y.-G. Zhao, C. Hong-Xia, and W. Xing-uang, "Agricultural water consumption forecast in Shiyang River Basin based on combined model," *Yellow River*, vol. 34, no. 1, pp. 99–101, 2012.

[12] T.-L. Jiang, H.-J. Zhang, Y. Shi, and Y. Wang, "Water demand forecast based on regression analysis and grey model GM (1, 1) in Minqin county," *Northwest Hydropower*, vol. 4, pp. 4–9, 2018.

[13] J. Li, S. SONG, T. GUO, and X. WANG, "Prediction of agricultural water consumption based on fractional grey model," *Transactions of the Chinese Society of Agricultural Engineering*, vol. 36, no. 4, pp. 82–89, 2020.

[14] L. Liu, Y. Chen, and L. Wu, "The damping accumulated grey model and its application," *Communications in Nonlinear Science and Numerical Simulation*, vol. 95, p. 105665, 2021.

[15] L. Tu and Y. Chen, "An unequal adjacent grey forecasting air pollution urban model," *Applied Mathematical Modelling*, vol. 99, pp. 260–275, 2021.

[16] Y. Chen, W. Lifeng, L. Lianyi, and Z. Kai, "Fractional Hausdorff grey model and its properties," *Chaos, Solitons & Fractals*, vol. 138, p. 109915, 2020.

Hindawi
Journal of Mathematics
Volume 2021, Article ID 2383473, 9 pages
https://doi.org/10.1155/2021/2383473

Research Article

Performance Prediction of the Ferrous Metal Smelting and Rolling Processing Industry in Supply-Side Structural Reform in China

Kaihe Shi,[1] **Danning Du**,[2] **and Xiaoxuan Zhang**[3]

[1]*School of Management, Tianjin University of Technology, Tianjin 300384, China*
[2]*School of Political Science and Public Administration, Wuhan University, Wuhan 430072, China*
[3]*School of Accounting and Financial Management, University of Waterloo, Waterloo N2L 3G1, Canada*

Correspondence should be addressed to Kaihe Shi; skh1166@163.com

Received 16 June 2021; Accepted 19 November 2021; Published 30 November 2021

Academic Editor: Lifeng Wu

Supply-side structural reforms and environmental protection policies have a great impact on the ferrous metal smelting and rolling processing industry. This paper uses a grey model that introduces a fractional-order cumulative generating operator to study the development of ferrous metal smelting and rolling processing enterprises under the influence of supply-side structural reform in order to derive the future development trend of the industry. The forecast results show that from 2018 to 2022, the number of enterprises and substitute enterprises, inventory, finished products, and assets and liabilities decreases; the scale of income of metal smelting and rolling processing industry increases. The results can serve as a reference for policy makers and industry investors.

1. Introduction

In recent years, the development of China's ferrous metal smelting and rolling processing industry (FRI) has been volatile. Fluctuation in price of ferrous metal has been exerting pressure on ferrous metal smelting and rolling processing companies. The impact of these measures on China's ferrous metal smelting and rolling processing industry continues to increase with the strengthening of supply-side structural reforms and increased environmental protection policies [1]. It is expected that relevant policies will continue to exert pressure on the industry in the future. Currently, China is in the middle to late stage of industrial development [2]. The industry is facing relatively high development pressure [3].

The forecasting of FRI indicators is helpful to provide a reference for the development of FRI. Moreover, it can provide a basis for the government and other departments to formulate relevant policies. At present, the research on the forecast of FRI in China is still limited. There are few studies on FRI development structure, scale, production, and other indicators. In order to discuss the development trend of FRI in China, it is necessary to analyze its indicators. However, there are few data on FRI indicators since the supply-side structural reform only started in 2015. The sample size of the data is small. Statistical methods are not suitable for predicting these indicators. Fortunately, grey system theory is a suitable method for analyzing small sample size data. GM(1, 1) is the core model of the grey system, but it has some drawbacks. For time series with relatively large change rates, its prediction effect is not satisfactory. In response to these defects, many scholars have improved GM(1, 1). Based on the effectiveness characteristics of short-term series forecasting, the fractional cumulative grey model (FGM) has been widely applied in various fields [4], including in the field of economic research and development [5]. Several studies have demonstrated that the accuracy of FGM(1, 1) is higher than that of the traditional GM(1, 1) [6]. FGM(1, 1) not only has higher accuracy but also has better initial validity. In the case of FGM(1, 1) equality perturbation, the sample size of the original series is proportional to the size of the perturbation boundary of the model [7]. This implies that from the perspective of stability, the model is relatively stable when the sample size is small. It not only has high

stability and high fitting accuracy but also can add the weight of new information.

This paper uses FGM(1, 1) to make predictions on corporate data in different FRIs. The forecast targets are the losses, inventory, finished products, assets, and total liabilities of the enterprises, as well as the revenue scale of the FRI. The reason for choosing these variables is that these are the most suitable indicators of industry change. First of all, the number and scale of enterprises comprehensively reflect the industry's market structure and industry development and operating capabilities. The number of enterprises is more convenient for statistics, so it is selected as the forecast target. In order to make the research more rigorous, a forecast of the number of loss-making companies has been added. Second, the output of products and the number of products in stock reflect the company's production capacity as well as the industry's market potential and growth. Sales volume is one of the indicators of enterprise size, and it can also reflect the development capacity of the industry to a certain extent. There are two ways of expressing this indicator, namely, sales volume and sales revenue, which is the sales scale. In addition, the industry's debt ratio indicates how much of the company's assets are debt. It can also be used to provide an indication of a company's long-term repayment ability and the stability of its financial position. The debt ratio is the ratio of total debt to total assets, and it is an important indicator of the debt ratio of the industry under study. The purpose of this paper is to analyze the development prospects of the industry and make recommendations through the observation of FRI development trends. It also provides a reference for investors who want to invest in FRI. The data on the enterprises in the FRI from 2013 to 2018 were obtained from the National Bureau of Statistics of China.

The structure of this paper is as follows. Section 2 is a literature review. Section 3 is the methodology and introduces the construction steps of FGM(1, 1). Section 4 is the prediction and analysis of the data using FGM(1, 1). Conclusions are presented in Section 5.

2. Literature Review

Ferrous metals are iron and its alloys, such as steel, pig iron, and ferroalloys. Ferrous metal smelting generally refers to melting iron ore into pig iron or smelting pig iron into steel billets [8]. FRI is a type of heavy industry and is divided into four industries: iron making, steel making, steel rolling, and ferroalloy smelting [9]. The production of heavy metal industry can have a serious impact on the environment if not well managed [10]. With the deterioration of the environment in recent years, people's awareness of environmental protection has gradually increased. The government has promulgated measures to promote green production in heavy industries. This requires enterprises to save energy, reduce emissions, and adjust the industrial structure. Similarly, in 2015, the supply-side structural reforms proposed by the Party Central Committee and Comrade Xi Jinping also required heavy industry companies to optimize the allocation of factors, with the aim of adjusting the economic structure and improving the quality and quantity of economic growth [11]. Structural reforms on the supply side include demand and supply. The demand-side reform mainly includes investment, consumption, and export, while the supply side has labor, land, capital, institutional creation, and innovation [12]. The supply-side structural reform can improve supply quality and use reforms to promote structural adjustment. It not only corrects the distortion of factor configuration but also expands the effective supply. It also improves the adaptability and flexibility of the supply structure to demand changes and increases total factor productivity [13]. For FRI, the main purpose of supply-side structural reform is to eliminate backward production capacity and improve product quality [14]. The FRI in China is greatly affected by the supply-side structural reform and environmental protection, and its economy loss is relatively high [15]. Some scholars have conducted research on the impact of supply-side structural reforms on the heavy industry. Zhang and Cui [16] analyzed how coal listed companies can assume social responsibilities with regard to supply-side reforms and ecological protection policies and the impact these policies may have on companies. Wang and Quan [17] found through research that supply-side decision-making reforms have a positive impact on enhancing innovation in enterprises. Tang et al. [18] studied the development of state-owned enterprises and heavy industry enterprises in China following the promulgation of supply-side structural reform policies.

Grey system theory can provide accurate predictions using small data sets and limited information [19]. In pursuit of higher prediction accuracy, scholars began to improve the traditional grey model after GM(1, 1) was widely used in many fields. Lei et al. [20] proposed a novel grey prediction model based on GM(1, 1), called neural ordinary differential grey model, with high prediction accuracy. Wang et al. [21] compared the GM(1, 1) and discrete grey model (DGM(1, 1)) in terms of prediction accuracy and found that DGM(1, 1) has better stability. The FGM(1, 1) used in this paper was proposed by Shi and Wu [22]. The introduction of the fractional-order cumulative generating operator makes the grey prediction model have better prediction performance compared with the traditional grey prediction model GM(1, 1). FGM(1, 1) can weaken the randomness of the original data sequence during the operation, and the data fluctuation has less interference with the model prediction results, which can obtain a higher fitting accuracy (the construction principle of FGM(1, 1) is shown in Figure 1). Therefore, this grey forecasting model is also commonly used as a forecasting tool by scholars [23]. Tu and Chen [24] used the unequal fractional-order discrete multivariable grey model to predict the public concern about air pollution in three cities of China. Liu et al. [25] used a fractional-order grey model to analyze the development trend of total retail sales of consumer goods in China and obtained some management insights from numerical examples. Wang and Li [26] analyzed the development trends of the eastern, central, and western regions of China by building a fractional-order multivariate grey model at the level of ecological environment and economic development. The main influencing

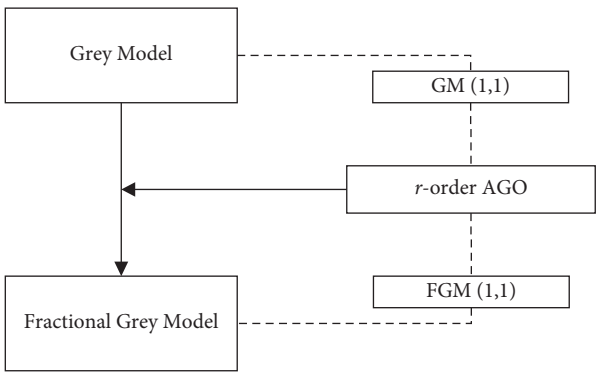

Figure 1: The construction principle of FGM(1, 1).

factors of natural gas consumption in eastern, central, and western regions of China were analyzed by establishing a fractional-order multivariate grey model from the ecological environment and economic development levels.

3. Methodology

The composition of FGM(1, 1) is to introduce the fractional-order cumulant operator into the traditional grey univariate model GM(1, 1). One indicator sequence is $Y^{(0)} = \{y^{(0)}(1), y^{(0)}(2), \ldots, y^{(0)}(n)\}$; the FGM(1, 1) modeling process is as follows. By using

$$Y^{(r)} = \sum_{i=1}^{k} C_{k-i+r-1}^{k-1} y^{(0)}(i), \tag{1}$$

the r-order accumulation sequence is $Y^{(r)} = \{y^{(r)}(1), y^{(r)}(2), \ldots, y^{(r)}(n)\}$.

Here,

$$\begin{aligned} C_{r-1}^{0} &= 1, C_{k}^{k+1} = 0, C_{k-1+r-1}^{k-1} \\ &= \frac{(k-i+r-1)(k-i+r-2)\cdots(r+1)r}{(k-1)!}. \end{aligned} \tag{2}$$

The first-order one-variable differential equation of the r-order cumulative sequence, $Y^{(r)}$, can be expressed as

$$\frac{\mathrm{d}y^{(r)}(t)}{\mathrm{d}t} + ay^{(r)}(t) = b. \tag{3}$$

Among them, a is the development coefficient b is the grey action quantity. The solution is

$$y^{(r)}(t+1) = \left[y^{(0)}(1) - \frac{b}{a}\right]e^{-at} + \frac{b}{a}. \tag{4}$$

The parameters are obtained by using the least squares method. It enables to minimise the square sum of errors. The unknown parameters $\widehat{a}$ and $\widehat{b}$ are obtained by the following calculations:

$$\begin{bmatrix} \widehat{a} \\ \widehat{b} \end{bmatrix} = \left(A^T A\right)^{-1} A^T Z, \tag{5}$$

where

$$\begin{aligned} Z &= \begin{bmatrix} y^{(r)}(2) - y^{(r)}(1) \\ y^{(r)}(2) - y^{(r)}(1) \\ \vdots \\ y^{(r)}(n) - y^{(r)}(n-1) \end{bmatrix}, \\ A &= \begin{bmatrix} -0.5y^{(r)}(1) + y^{(r)}(2) & 1 \\ -0.5y^{(r)}(2) + y^{(r)}(3) & 1 \\ \vdots & \vdots \\ -0.5y^{(r)}(n-1) + y^{(r)}(n) & 1 \end{bmatrix}. \end{aligned} \tag{6}$$

Entering $\widehat{a}$ and $\widehat{b}$ into the time response function $\widehat{y}^{(r)}(k+1) = [y^{(0)}(1) - (\widehat{b}/\widehat{a})]e^{-\widehat{a}k} + (\widehat{b}/\widehat{a})$, $\widehat{y}^{(r)}(k+1)$ is the fitting value at the time $k+1$.

The predictive sequence of $\widehat{Y}^{(r)} = \{\widehat{y}^{(r)}(1), \widehat{y}^{(r)}(2), \ldots, \widehat{y}^{(r)}(n)\}$ is

$$\alpha^r \widehat{Y}^{(r)} = \left\{\alpha^1 \widehat{y}^{(r)(1-r)}(1), \alpha^1 \widehat{y}^{(r)(1-r)}(2), \ldots, \alpha^1 \widehat{y}^{(r)(1-r)}(n)\right\}, \tag{7}$$

where $\alpha^1 \widehat{y}^{(r)(1-r)}(k) = \widehat{y}^{(r)(1-r)}(k) - \widehat{y}^{(r)(1-r)}(k-1)$.

Therefore, the forecasting values are $\widehat{y}^{(0)}(1), \widehat{y}^{(0)}(2), \ldots, \widehat{y}^{(0)}(n)$.

The mean absolute percentage error (MAPE) is used to evaluate the model, and the calculation method is as follows:

$$\mathrm{MAPE} = 100\% \frac{1}{n} \sum_{k=1}^{n} \left| \frac{y^{(0)}(k) - \widehat{y}^{(0)}(k)}{y^{(0)}(k)} \right|. \tag{8}$$

In summary, through the fractional-order accumulation generation process in FGM(1, 1) and the model solving process, the model construction steps are summarized as follows:

Step 1. The original nonnegative sequence $Y^{(0)} = \{y^{(0)}(1), y^{(0)}(2), \ldots, y^{(0)}(n)\}$ is generated by the action of fractional-order accumulation to obtain the sequence $Y^{(r)} = \{y^{(r)}(1), y^{(r)}(2), \ldots, y^{(r)}(n)\}$.

Step 2. The order r in the fractional-order cumulative generation is optimized in the case where the objective function is MAPE minimum. The parameters a and b are obtained according to the above equations.

Step 3. The time response equation of the FGM(1, 1) model can be obtained by substituting the calculated parameters a and b into formula. Subsequently, the fitted and predicted values of the original series can be computed.

4. Forecasting Results and Discussion

4.1. Forecasting the Enterprise's Losses. The sample data are the number of enterprises from 2013 to 2017. The companies' number is taken as the example, and the FGM(1, 1) model is developed to forecast the change in the companies' number in 2018–2022. The modeling process is as follows:

Step 1. The sequence of the enterprise is

$$Y^{(0)} = \{11034, 10564, 10071, 9224, 8545\}. \tag{9}$$

The 0.84-order accumulation sequence is

$$\begin{aligned} Y^{(0.84)} &= \left\{y^{(0.84)}(1), y^{(0.84)}(2), y^{(0.84)}(3), y^{(0.84)}(4), y^{(0.84)}(5)\right\} \\ &= \{11034, 19832.56, 27471.84, 33919.80, 39553.89\}. \end{aligned} \tag{10}$$

Step 2. The unknown parameters $\hat{a}$ and $\hat{b}$ are obtained by the following calculations:

$$\begin{bmatrix} \hat{a} \\ \hat{b} \end{bmatrix} = \left(A^T A\right)^{-1} A^T Z = \begin{bmatrix} 0.1506 \\ 11140.61 \end{bmatrix}, \tag{11}$$

where

$$\begin{aligned} Z &= \begin{bmatrix} 8798.56 \\ 7639.28 \\ 6447.96 \\ 5634.09 \end{bmatrix}, \\ A &= \begin{bmatrix} -15433.28 & 1 \\ -23652.20 & 1 \\ -30695.82 & 1 \\ -36736.84 & 1 \end{bmatrix}. \end{aligned} \tag{12}$$

Step 3. The time response function is

$$\hat{y}^{(0.84)}(k+1) = \left(11034 - \frac{11140.61}{0.1506}\right)e^{-0.1506k} + \frac{11140.61}{0.1506}. \tag{13}$$

Step 4. It can be obtained that

$$\begin{aligned} \hat{Y}^{(0.84)} &= \left\{\hat{y}^{(0.84)}(1), \hat{y}^{(0.84)}(2), \hat{y}^{(0.84)}(3), \hat{y}^{(0.84)}(4), \hat{y}^{(0.84)}(5), \hat{y}^{(0.84)}(6), \hat{y}^{(0.84)}(7), \hat{y}^{(0.84)}(8), \hat{y}^{(0.84)}(9), \hat{y}^{(0.84)}(10)\right\} \\ &= \{11034, 19833.52, 27402.74, 33913.65, 39514.25, 44331.78, 48475.76, 52040.33, 55106.5357744.02\}. \end{aligned} \tag{14}$$

Therefore,

$$\begin{aligned} \hat{Y}^{(0.84)(0.16)} &= \left\{\hat{y}^{(0.84)(0.16)}(1), \hat{y}^{(0.84)(0.16)}(2), \hat{y}^{(0.84)(0.16)}(3), \hat{y}^{(0.84)(0.16)}(4), \hat{y}^{(0.84)(0.16)}(5), \hat{y}^{(0.84)(0.16)}(6),\right. \\ &\quad \left.\cdot\, \hat{y}^{(0.84)(0.16)}(7), \hat{y}^{(0.84)(0.16)}(8), \hat{y}^{(0.84)(0.16)}(9), \hat{y}^{(0.84)(0.16)}(10)\right\} \\ &= \{11304, 21598.96, 31600.06, 40875.89, 49391.03, 57163.68, 64235.94, 70660.00, 76491.10, 81783.94\}. \end{aligned} \tag{15}$$

The predictive sequence is

$$\begin{aligned} \hat{y}^{(0)} &= \left\{\hat{y}^{(0)}(1), \hat{y}^{(0)}(2), \hat{y}^{(0)}(3), \hat{y}^{(0)}(4), \hat{y}^{(0)}(5), \hat{y}^{(0)}(6), \hat{y}^{(0)}(7), \hat{y}^{(0)}(8), \hat{y}^{(0)}(9), \hat{y}^{(0)}(10)\right\} \\ &= \{11034, 10564.96, 10001.09, 9275.84, 8515.13, 7772.65, 7072.27, 6424.06, 5831.10, 5292.83\}. \end{aligned} \tag{16}$$

A comparison of the fitted values with the actual values is shown in Figure 2.

The MAPE calculated by FGM(1, 1) with the number of enterprises as the sample data is 0.4%, which is much less than 10%, indicating that FGM(1, 1) is applicable to the calculation of this data set. The calculation process of other indicators is the same as this process.

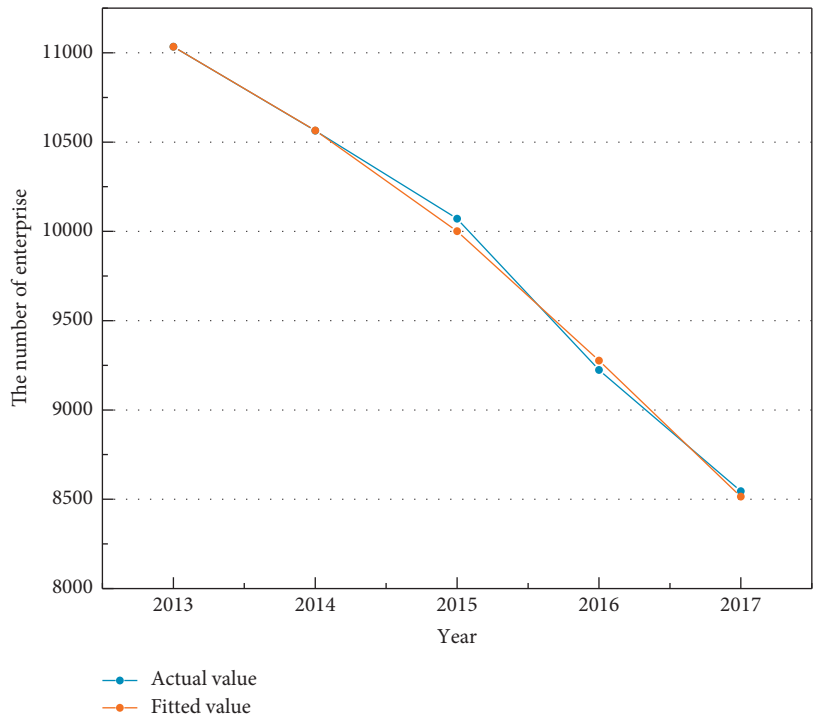

Figure 2: Comparison of actual value and fitting value.

The fitted and predicted values of the number of enterprises are derived based on the above calculation process. The fitted results and MAPE comparisons derived from FGM(1, 1), DGM(1, 1), even GM(1, 1) (EGM(1, 1)), and original difference GM(1, 1) (ODGM(1, 1)) for the same set of data are shown in Table 1. The comparison of each model further illustrates the advanced nature of FGM(1, 1).

The forecasting results of the FGM(1, 1) indicate that the number of enterprises in 2018–2022 is decreasing continuously and will fall to 5293 by 2022, which is half of that in 2013 (Table 2). The number of loss-making enterprises declines at a slow rate and accounts for 13.3% of the total number of enterprises in 2022, which represents a 2% decrease compared with 2017.

The number of smelting and rolling processing enterprises in China was 8545 in 2017. Under the pressure of supply-side structural reform and environmental protection, the number of enterprises decreased by 23% compared with 2013 (11,034). The number of enterprises declaring losses in 2015 was 2,210, accounting for 21.9% of the total number of enterprises. The number of enterprises declaring losses in 2017 dropped to 1,305 (Table 3). Although the number of loss-making enterprises is gradually decreasing, the percentage of the total number of enterprises is still high at 15.3%. This implies that one out of every seven enterprises is declaring a loss.

One of the reasons for the rapid decline in the total number of enterprises is the relatively poor innovation capacity of enterprises. The issue arises in connection with the ability to upgrade the technology of products and the organizational structure of enterprises as well as their management capabilities. It ultimately leads to low market competitiveness. In addition, the market pressure on Chinese FRI is gradually increasing. The enterprises are actively

Table 1: Comparison of fitting values of different models.

Year	FGM(1, 1)	DGM(1, 1)	EGM(1, 1)	ODGM(1, 1)
2013	11034.00	11034.00	11034.00	11034.00
2014	10564.96	10655.98	10651.09	10654.94
2015	10001.09	9919.51	9915.61	9919.27
2016	9275.84	9233.94	9230.92	9234.39
2017	8515.13	8595.75	8593.51	8596.80
MAPE	0.40%	0.77%	0.75%	0.77%

Table 2: The number of enterprise.

Year	Predicted value
2018	7773
2019	7072
2020	6424
2021	5831
2022	5293

Table 3: The number of losing-market enterprise.

Year	Fitted value	Year	Predicted value
2013	1946	2018	1199
2014	2064	2019	1035
2015	1862	2020	901
2016	1620	2021	792
2017	1394	2022	703
MAPE	8.91%		

seeking a way out of restructuring and integration, forced by external pressure. Thus, many companies are being swallowed up and merged. Furthermore, the debt ratio of enterprises is very high. It is possible for many enterprises to collapse due to the breakage of capital chain. It is considered to be the main means for Chinese FRI enterprises to maintain cash flow by borrowing new debts to pay off old ones. However, with the State Council's stricter regulation and control policies on overcapacity industries, the channels for these enterprises to borrow directly from banks are gradually being closed. Under the dual pressure of policies and the market, the number of enterprises has continued to decline; thus, the number of loss-making enterprises has also decreased.

4.2. Forecasting Inventory and Finished Products. From 2013 to 2015, the inventory showed a sharp downward trend and reached 6749.9. After a rebound in 2016, it began to decline again. As of 2017, the inventory of FRI was 7125.9 hundred million Yuan, and the finished product value was 2475.8 hundred million Yuan (Figure 3). It is observed that from 2018 to 2022, changes in inventories and finished products tended to be flat, and development was relatively stable (the modeled MAPEs for the inventory and finished product data sets were 3.20% and 2.43%, respectively).

The marked decline in FRI inventory in 2015 and 2017 was mainly due to the impact of China's national policies. Therefore, China's traditional manufacturing capacity is generally surplus, and there is a problem of oversupply. In 2015, to solve the problem of overcapacity, the "de-capacity" policy based on the supply-side structural reform was proposed by China's President Xi Jinping. In 2017, Premier Li Keqiang of the State Council identified the target for capacity reduction in the government work report. The rationalization of production capacity was accelerated by this policy, and the rationalization level of production capacity has been realized. Therefore, in 2015 and 2017, affected by the relevant policies and regulation, the inventory of the FRI was reduced, especially in 2015 the excess capacity was regulated. The forecasting results show that the development of inventory and finished products is stable. After 2018, it indicates that the implementation of the policy has promoted the steady development of the industry.

4.3. Forecasting Assets and Total Liabilities. In 2016, the assets of the FRI were 64445.1 hundred million Yuan, a decrease of 0.98% compared with the value in 2015. In 2017, the assets and liabilities of the industry were 63818 hundred million Yuan and 40902 hundred million Yuan, respectively, and the asset-liability ratio was 64.09% (Figure 4). The forecasting results indicate that by 2022, the asset-liability ratio will be 51.62%, representing a decrease of 15.83% compared with the value in 2013.

As shown in Figures 4 and 5, FRI's assets, liabilities, and asset-liability ratio have all increased in 2013–2014. Since 2015, they have begun to show a continuous decline. It can be seen from Figure 1 that the debt ratio will drop to 51.62% in 2022, which is 15.83% lower than 2013.

However, it is worth noting that although industrial operations have improved, the current asset-liability ratio is still relatively high. The main reasons for the high asset-liability ratio of the FRI are as follows. On the one hand, the production capacity has expanded rapidly in the early years, which led to the expansion of enterprises (or an increase in the number of new projects). It is difficult to maintain the capital requirements of enterprises by using their own funds. External financing is inevitably necessary. On the other hand, under the market orientation, the ferrous metal industry needs to upgrade its industrial structure. The structural adjustment requires large investment amounts and a long payback period. This depends largely on the financial system, especially bank loans.

In response to these problems, the FRI companies began to improve their profitability by reducing costs. They increased the net assets by increasing income and increasing profits. In addition, some high-debt companies have reached market-based debt-to-equity swap agreements. Debt-to-equity swaps are a direct solution to the high debts of companies. In 2018, the National Development and Reform Commission, the Central Bank, and the Ministry of Finance and other seven ministries and commissions jointly issued the "Notice on Specific Policy Issues in the Implementation of Market-Oriented Banks' Debt-to-Equity Rights." This document loosened the implementation requirements in terms of the combination of stocks and bonds, sources of funds, targets of implementation, types of claims, and financial instruments. This policy has further promoted the implementation of debt-to-equity swaps and had a positive impact on reducing debt ratios. These companies' own adjustments and favorable policies are also the reasons that caused the debt ratio to decrease annually. With the continuous adjustment of the industrial structure, the industry is gradually being standardized, and the operational conditions are expected to improve.

4.4. Forecasting the Revenue Scale. The revenue scale fluctuated considerably, dropping sharply to 64605.70 in 2015. Compared with the amount of 75028.45 hundred million Yuan in 2014, it decreased by 13.89%. Then in 2016, the industry resumed its growth. In 2017, the revenue of the industry was 67429.60 hundred million Yuan, an increase of 22.4% over the same period of the previous year (Table 4).

The prediction results of the FGM(1, 1) show that after a brief decline in 2018, the scale of revenue will rise steadily in 2019–2022 and reach 88082.92 by 2022.

In 2015, the focus of China's macroeconomic policy shifted to supply-side structural reforms and there was a significant withdrawal of capital from the futures market, resulting in price volatility and declines.

The scale of revenues started to increase in 2016, and the overall growth was due to the reasons listed below. To begin with, the implementation of "de-capacity" and the corresponding national policies provided new ideas for the development of FRI. Many backward industries were eliminated. As a result, some resources and capital were

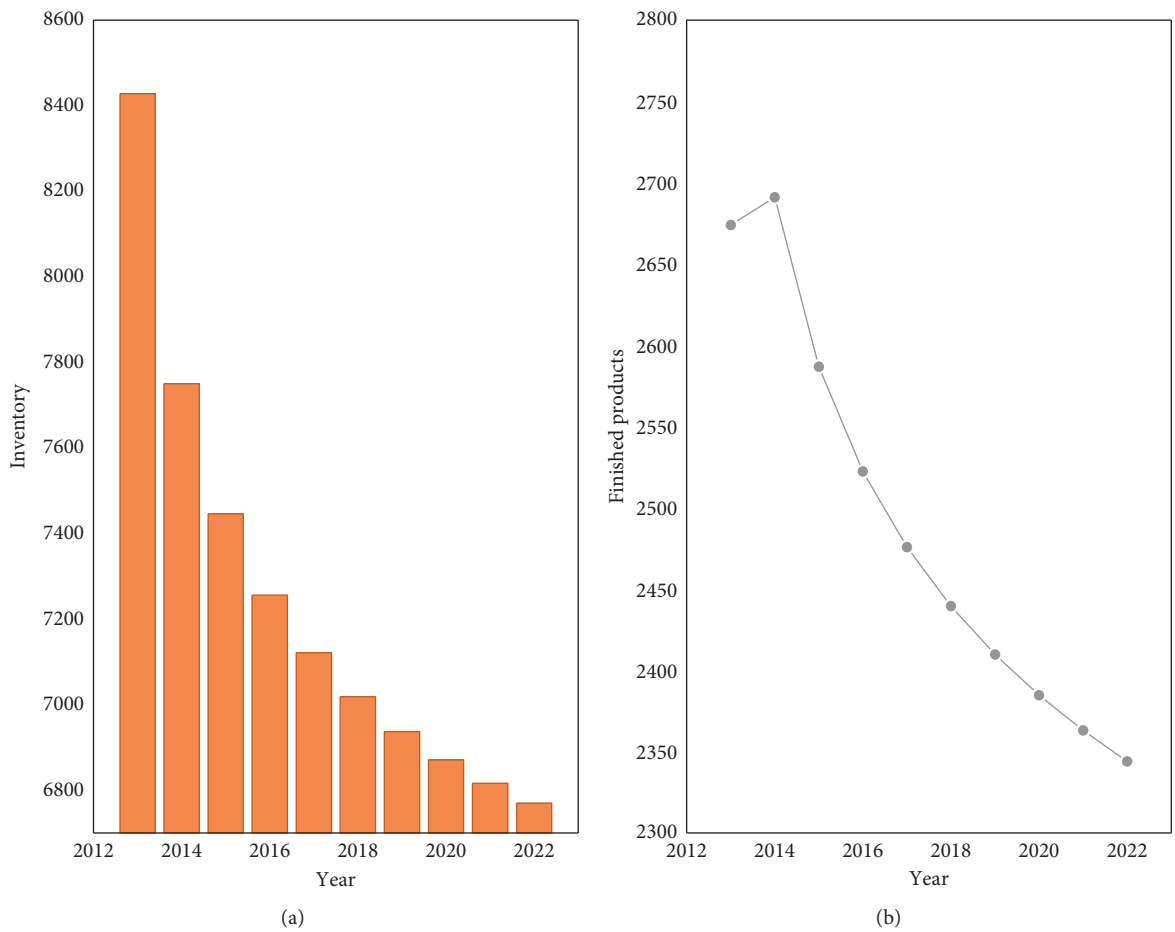

Figure 3: Model calculation results for (a) inventory and (b) finished products.

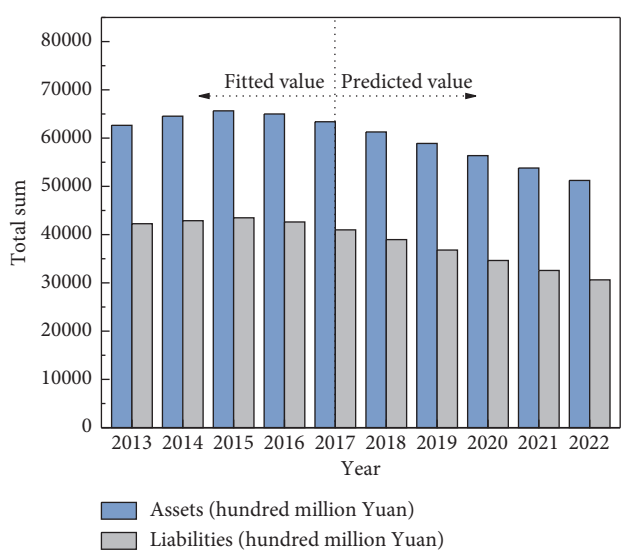

Figure 4: Model calculation results for FRI's assets and liabilities.

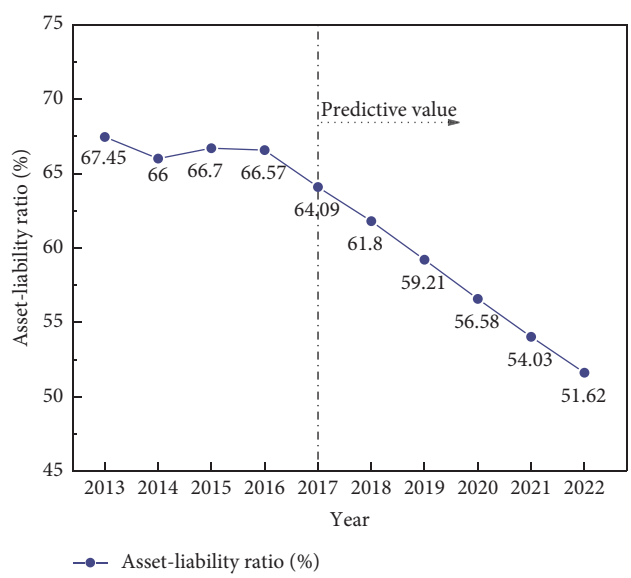

Figure 5: Trend of asset-liability ratio (%).

released and utilized more effectively. Moreover, based on the support of the Belt and Road Initiative and the definition of international division of labor, China's advanced technologies are exported along with other resources. Such development is highly sustainable. Furthermore, the expansion of international FRI is increasing with the economic rise of developing countries and the international demand for ferrous metals. This trend has contributed to the continued increase in market prices for international ferrous

Table 4: Revenue scale (hundred million Yuan).

Year	Fitted value	Year	Predicted value
2013	76316.93	2018	63227.03
2014	68209.31	2019	65172.5
2015	64911.45	2020	69202.97
2016	63259.51	2021	76488.17
2017	62696.86	2022	88983.92
MAPE	4.17%		

metals in 2018. The revenue size of FRI in China is bound to be influenced by the international market.

5. Conclusions

In this paper, FGM(1, 1) was used for the predictive analysis of the FRI data and the MAPEs were less than 10% during the calculation. It indicates that the model is suitable for studying the problem in this field. The prediction results of FGM(1, 1) demonstrate that the number of enterprises, inventories, and finished products in China's ferrous metal smelting and rolling industry will decrease annually due to the structural reform on the supply side and environmental pressure. The number of loss-making enterprises is on a downward trend. The trend of industrial assets, total liabilities, and gearing ratio will also decrease.

The revenue size started to increase after 2017. It shows that the industry is improving. In other words, FRI's decapitalization has achieved milestones. As the decapacity measures continue to strengthen and the industrial structure is adjusted, the profitable development pattern of the FRI in China is likely to maintain the relatively high prices of ferrous metals.

Considering the development status of China's foreign direct investment, the following suggestions are made for China's FRI. First of all, it is necessary to adopt innovative thinking to accelerate the extension of the industrial chain. Extension of the industrial chain helps solve the problem of overcapacity, it also helps seeking new sources of power and improving market competitiveness. This is the most effective way to enhance traditional industries. The second is to promote investor diversification and optimize resource allocation, thereby adjusting the industrial layout to avoid diversified investment and repeated construction. It is also necessary to increase the scale of income by adjusting product structure and reducing production costs.

Data Availability

The data used to support the findings of this study are available from the corresponding author upon request.

Conflicts of Interest

The authors declare that they have no conflicts of interest.

Acknowledgments

The relevant research studies in this paper are supported by the Humanities and Social Sciences Planning Projects of Ministry of Education (20YJAZH141).

References

[1] L. Z. Zhang and X. H. Liu, "Evaluating ecological efficiency of Chinese industrial enterprise," *Renewable Energy*, vol. 178, pp. 679–691, 2021.

[2] Q. H. Huang, "New drivers of China's industrial growth in its late-stage industrialization and new normal," *China Economist*, vol. 3, pp. 4–14, 2016.

[3] W. G. Liu, H. B. Zuo, J. S. Wang, and Q. G. Xue, "The production and application of hydrogen in steel industry," *International Journal of Hydrogen Energy*, vol. 46, no. 17, pp. 10548–10569, 2021.

[4] L. F. Wu, S. F. Liu, Z. G. Fang, and H. Y. Xu, "Properties of the GM(1, 1) with fractional order accumulation," *Applied Mathematics and Computation*, vol. 252, pp. 287–293, 2015.

[5] Q. Xiao, M. Shan, M. Gao, and X. Xiao, "Evaluation of the coordination between China's technology and economy using a grey multivariate coupling model," *Technological and Economic Development of Economy*, vol. 27, no. 1, pp. 24–44, 2021.

[6] W. S. Jiang, Z. Y. Wang, and J. Lv, "A fractional-order accumulative regularization filter for force reconstruction," *Mechanical Systems and Signal Processing*, vol. 101, pp. 405–423, 2018.

[7] M. Gao, H. Yang, Q. Xiao, and M. Goh, "A novel fractional grey Riccati model for carbon emission prediction," *Journal of Cleaner Production*, vol. 282, Article ID 124471, 2021.

[8] G. Cai, M. Ebrahimi, G. Zheng, and A. H. Kaksonen, "Effect of ferrous iron loading on dewaterability, heavy metal removal and bacterial community of digested sludge by Acidithiobacillus ferrooxidans," *Journal of Environmental Management*, vol. 295, Article ID 113114, 2021.

[9] J. B. Huang, Y. M. Luo, and C. Feng, "An overview of carbon dioxide emissions from China's ferrous metal industry: 1991–2030," *Resources Policy*, vol. 62, pp. 541–549, 2019.

[10] S. Z. Salleh, A. H. Yusoff, S. K. Zakaria, and M. A. A. Taib, "Plant extracts as green corrosion inhibitor for ferrous metal alloys: a review," *Journal of Cleaner Production*, vol. 304, Article ID 127030, 2021.

[11] M. Yu, X. T. Zhao, and Y. N. Gao, "Factor decomposition of China's industrial electricity consumption using structural decomposition analysis," *Structural Change and Economic Dynamics*, vol. 51, pp. 67–76, 2019.

[12] D. B. Fang, P. Hao, Q. Yu, and J. C. Wang, "The impacts of electricity consumption in China's key economic regions," *Applied Energy*, vol. 267, Article ID 115078, 2020.

[13] X. N. Guo and S. R. Lu, "Analysis of China's potential economic growth rate under the background of supply-side structural reform," *Economist*, vol. 1, pp. 29–40, 2018.

[14] X. C. Jiang, J. H. N. Shen, C. C. Lee, and C. Chen, "Supply-side structural reform and dynamic capital structure adjustment: evidence from Chinese-listed firms," *Pacific-Basin Finance Journal*, vol. 65, Article ID 101482, 2021.

[15] X. H. Zhu, A. Q. Zeng, M. R. Zhong, J. B. Huang, and H. P. Qu, "Multiple impacts of environmental regulation on the steel industry in China: a recursive dynamic steel industry chain CGE analysis," *Journal of Cleaner Production*, vol. 210, pp. 490–504, 2019.

[16] Y. X. Zhang and M. Z. Cui, "The impact of Corporate Social Responsibility on the enterprise value of China's listed coal enterprises," *The Extractive Industries and Society*, vol. 7, pp. 138–145, 2020.

[17] X. F. Wang and F. G. Quan, "The study of innovation path under the supply-side structural reform," *Shanghai Journal of Economics*, vol. 3, pp. 3–12, 2016.

[18] K. Tang, Y. Qiu, and D. Zhou, "Does command-and-control regulation promote green innovation performance? Evidence from China's industrial enterprises," *The Science of the Total Environment*, vol. 712, Article ID 136362, 2020.

[19] K. H. Shi and L. F. Wu, "Modelling the relationship between population density and air quality using fractional Hausdorff grey multivariate model," *Kybernetes*, vol. 50, no. 11, 2021.

[20] D. J. Lei, K. L. Wu, L. P. Zhang, and W. S. Li, "Neural ordinary differential grey model and its applications," *Expert Systems with Applications*, vol. 177, Article ID 114923, 2021.

[21] Z. X. Wang, D. D. Li, and H. H. Zeng, "Model comparison of GM(1, 1) and DGM(1, 1) based on Monte-Carlo simulation," *Physica A: Statistical Mechanics and Its Applications*, vol. 542, Article ID 123341, 2020.

[22] K. H. Shi and L. F. Wu, "Forecasting air quality considering the socio-economic development in Xingtai," *Sustainable Cities and Society*, vol. 61, Article ID 102337, 2020.

[23] Q. Xiao, M. Shan, M. Gao, and X. Xiao, "Parameter optimization for nonlinear grey Bernoulli model on biomass energy consumption prediction," *Applied Soft Computing*, vol. 95, Article ID 106538, 2020.

[24] L. Tu and Y. Chen, "An unequal adjacent grey forecasting air pollution urban model," *Applied Mathematical Modelling*, vol. 99, pp. 260–275, 2021.

[25] C. Liu, W. L. Xie, W. Z. Wu, and H. G. Zhu, "Predicting Chinese total retail sales of consumer goods by employing an extended discrete grey polynomial model," *Engineering Applications of Artificial Intelligence*, vol. 102, Article ID 104261, 2021.

[26] J. L. Wang and N. Li, "Influencing factors and future trends of natural gas demand in the eastern, central and western areas of China based on the grey model," *Natural Gas Industry B*, vol. 7, no. 5, pp. 473–483, 2020.

Hindawi
Journal of Mathematics
Volume 2021, Article ID 4869135, 10 pages
https://doi.org/10.1155/2021/4869135

Research Article

Prediction of Farmers' Income in Hebei Province Based on the Fractional Grey Model (1,1)

Yongqiang Xu,[1,2] **Lim Thien Sang**,[1] **and Kun Wang**[3]

[1]*Faculty of Business, Economics and Accountancy, University Malaysia Sabah, Kota Kinabalu, Sabah 88400, Malaysia*
[2]*School of Management Engineering and Business, Hebei University of Engineering, Handan 056038, China*
[3]*Department of Management, Handan Polytechnic College, Handan 056000, China*

Correspondence should be addressed to Kun Wang; uthz2013@163.com

Received 17 June 2021; Accepted 6 November 2021; Published 29 November 2021

Academic Editor: Efthymios G. Tsionas

The problem of increasing farmers' income has been a hot issue of social concern. Understanding the farmers' income and the overall development trend is conducive to the rational layout of the social economy and promotes the steady development of a well-off society. Based on this, the paper selects the per capita disposable income (PCDI) of farmers' households from 2012 to 2019 in 11 cities of Hebei Province as the research object and applies the fractional grey model (FGM (1,1)) to predict farmers' income from 2020 to 2024. The results show that the farmers' income will increase in the next five years. However, the growth rate of farmers' income is slow in the areas with a large base of farmers' income and strong in the areas with a small base of farmers' income. The area with the highest trend in the growth rate of farmers' income is Zhangjiakou and the lowest place is Handan. Only Shijiazhuang's income growth rate is on the rise. Finally, suggestions are given to promote farmers' income in Hebei Province.

1. Introduction

In recent years, the government has been focusing on "three rural issues: agriculture, rural areas, and farmers" in rural work and "how to increase farmers' income" has been a long-term work to tread. Only by understanding the development trend of farmers' income can the government better formulate economic plans and achieve a well-off society [1]. Hebei, as a province in China, should also consider the importance of predicting farmers' income to promote the rural economy. As of 2020, the urbanization level of Hebei Province was 45%. It means that the rural population still has an absolute advantage. The precondition for the rapid economic development of Hebei Province is that farmers' income needs to increase substantially. Meanwhile, some studies expressed that increasing farmers' income is also the key step in solving the urbanization and the dual economy between urban and rural areas. In Hebei, farmers' absolute income is increasing, but at a slower rate, wage income is the main income factor. In addition, the PCDI of farmers' households in Hebei Province has no advantage across the country. So, it was necessary to evaluate and predict the future farmers' income, investigate the income channels, and formulate relevant rural policies. The paper takes Hebei farmers' income as the research object, the basic data are obtained from the PCDI of farmers in different cities from 2012 to 2019, and FGM (1,1) is used to predict the farmers' income from 2020 to 2024. Then, the paper analyses the results and gives suggestions of promoting farmers' income in Hebei Province. Meanwhile, the prediction model of farmers' income and the experience of increasing farmers' income also have some guiding significance for other provinces in China.

2. Literature Review

There have been many related studies on farmers' income, which can be divided into the analysis of factors influencing farmers' income and the prediction research of farmers' income. In terms of influencing factors of farmers' income, the agricultural industrial structure had an impact on farmers' income and not all agricultural structures were useful to the growth of farmers' income [2, 3]. In addition, agricultural technology and the degree of agricultural

intensification also affected farmers' income; advanced agricultural technology saved resources and reduced costs, which increased farmers' income [4]. The scale of the agricultural industry and agricultural mechanization would also raise farmers' income [5]. Some researchers introduced the quality of farmers in their studies and found that there was a positive relationship between income and education years, so it was necessary to guide farmers to receive vocational skills training [6]. And, the government support and urbanization development levels had a certain influence on farmers' income [7]. Both national policies and measures to support agriculture could affect farmers' income. The development of industries increased the level of nonagricultural employment and directly promoted the increase of farmers' income [8, 9].

Researchers have also done a lot of work on income prediction. Backpropagation neural network has strong nonlinear mapping ability, and it has high accuracy in farmers' income prediction [10]. The autoregressive integrated moving average model was applied to time-series data, which could accurately reflect the interdependence of dynamic data and provide an effective reference for the prediction of farmers' income in the short term [11]. The "quasi-stepwise regression" method had high accuracy, and the average relative error of farmers' income obtained was around 1%, which had a good validity [12]. Compared with the previous model, the support vector machine model, which had the nonlinear time-series prediction characteristic, greatly improved the prediction accuracy of farmers' income [13]. The advantage of the rough set theory and partial least squares regression method was that both can eliminate the influence of redundant factors on farmers' income and improve the prediction accuracy [14, 15]. To sum up, the above models were able to consider the variables' time variation and structural differentiation and supplied gaps of sectional data or time-series data, which had strong advantages in predicting farmers' income [16].

With the deepening of research, the studies have discovered that many factors affect the farmers' income and it was difficult to screen the main factors. The fuzziness and uncertainty of farmers' income prediction were more consistent with the grey theory [17]. The grey system theory and prediction model originally proposed by Professor Deng can accurately predict the future development trend with "small sample and poor information" data in the real world, which has been widely applied in many fields [18]. The grey model GM (1,1) was a basic predictive model [19, 20]. The advantage of the GM (1,1) model was that it can deal with grey information and poor data, but the model was mainly applicable to the sequence with strong exponential law and could only describe the monotone change process, and it had a big error in some specific fields [21]. In view of the shortcomings of the traditional GM (1,1) model, the fractional grey model (FGM (1,1)) was proposed [22]. In the process of FGM (1,1), the matrix perturbation theory was used to prove that the traditional integer-order cumulative generating operator violated the new information priority principle of grey system theory. Under certain conditions, the FGM (1,1) had a higher accuracy than the GM (1,1) model [23]. The FGM (1,1) was able to effectively reduce the error and obtain a better prediction by choosing the appropriate fractional order. Therefore, in this paper, the PCDI of farmers' households in various cities of Hebei Province from 2012 to 2019 was used as the measurement of farmers' income, the FGM (1,1) model was used to predict farmers' income, and suggestions were put forward to promote farmers' income.

3. Model Introduction of FGM (1,1)

The sequence with the nonnegative samples is $X^{(0)} = \{x^{(0)}(1), x^{(0)}(2), \ldots, x^{(0)}(n)\}$. The FGM (1,1) model is constructed as follows.

Step 1. The R-order accumulation generation sequence is

$$X^{(r)} = \left\{x^{(r)}(1)\ ,\ x^{(r)}(2)\ ,\ \ldots\ ,\ x^{(r)}(n)\right\}. \tag{1}$$

Among them,

$$\begin{aligned} x^{(r)}(k) &= \sum_{i=1}^{k} C_{k-i=r-1}^{k-i} x^{(0)}(i), \quad k = 1, 2, \ldots, n, \\ C_{r-1}^{0} &= 1, C_{k}^{k-1} = 0, \\ C_{k-i+r-1}^{k-i} &= \frac{(k-i+r-1)(k-i+r-2), \ldots, (r+1)r}{(k-i)!}. \end{aligned} \tag{2}$$

We establish the average generation sequence of $X^{(r)}$:

$$Z^{(r)} = \left\{z^{(r)}(2), z^{(r)}(3), \ldots, z^{(r)}(n)\right\}. \tag{3}$$

Among them,

$$z^{(r)}(k) = \frac{1}{2}\left(x^{(r)}(k) + x^{(r)}(k-1)\right), \quad k = 2, 3, \ldots, n. \tag{4}$$

Step 2. We establish the whitening differential equation:

$$\frac{\mathrm{d}x^{(r)}(t)}{\mathrm{d}t} + ax^{(r)}(t) = b, \tag{5}$$

where a is the developmental grey number and b is the grey action.

Since the least squares method can minimize the error of the solution, we use the least squares method to solve $\hat{a}$ and $\hat{b}$:

$$\begin{bmatrix} \hat{a} \\ \hat{b} \end{bmatrix} = \left(B^T B\right)^{-1} B^T Y. \tag{6}$$

Among them,

$$B = \begin{bmatrix} -z^{(r)}(2) & 1 \\ -z^{(r)}(3) & 1 \\ \vdots & \vdots \\ -z^{(r)}(n) & 1 \end{bmatrix}, Y = \begin{bmatrix} x^{(r)}(2) - x^{(r)}(1) \\ x^{(r)}(3) - x^{(r)}(2) \\ \vdots \\ x^{(r)}(n) - x^{(r)}(n-1) \end{bmatrix}. \tag{7}$$

The time response formula is as follows:

$$\hat{x}^{(r)}(t) = \left(x^{(0)}(1) - \frac{\hat{b}}{\hat{a}}\right) \cdot e^{-\hat{a}(t-1)} + \frac{\hat{b}}{\hat{a}}. \quad (8)$$

Using the time response formula, $\hat{X}^{(r)}$ is solved:

$$\hat{X}^{(r)} = \left\{\hat{x}^{(r)}(1), \hat{x}^{(r)}(2), \ldots, \hat{x}^{(r)}(n)\right\}. \quad (9)$$

Step 3. The inverse accumulation generating operator is used to obtain

$$\hat{x}^{(1)} = x^{(r)} x^{(1-r)} = \left\{\hat{x}^{(r)(1-r)}(1), \hat{x}^{(r)(1-r)}(2), \ldots, \hat{x}^{(r)(1-r)}(n)\right\}. \quad (10)$$

Then, the predicted value can be obtained by the following reduction formula:

$$\hat{x}^{(0)}(k) = \hat{x}^{(1)}(k) - \hat{x}^{(1)}(k-1), \quad k = 2, 3, \ldots, n. \quad (11)$$

Step 4. Model Testing. There are many testing methods for grey prediction models. And, the average absolute percentage is a commonly used testing method in grey prediction. The paper uses this method for model testing. Grey systems are often evaluated by using the mean absolute percentage error (MAPE).

$$\text{MAPE} = \frac{1}{n} \sum_{k=1}^{n} \left| \frac{x^{(0)}(k) - \hat{x}^{(0)}(k)}{x^{(0)}(k)} \right| \times 100\%. \quad (12)$$

The evaluation criteria of MAPE are shown in Table 1. When MAPE < 10%, it means that the model fitting effect is better and the prediction result is more reliable. When 10% < MAPE < 20%, the model fit has a certain degree of credibility. When MAPE > 20%, the fitting effect of the model is average and the prediction result has little reference value.

Especially in the FGM (1,1), when $r = 1$, the FGM (1,1) is equivalent to the GM (1,1). The GM (1,1) can be regarded as a special case of the fractional grey model.

Table 1: MAPE evaluation criteria.

MAPE (%)	Predictive performance
<10	Excellent
10~20	Good
20~50	General
>50	Difference

4. Prediction and Result Analysis of Farmers' Income

4.1. Data Sources. The data came from Hebei Statistical Yearbook from 2013 to 2020. From Table 2, the PCDI of farmers in all cities showed an upward trend from 2012 to 2019. In combination with the trend chart of farmers' income in Figure 1 and the average growth rate in Figure 2, it can be concluded that there is a large gap in the income level of farmers in the different areas of Hebei Province. The PCDI of Tangshan farmers is twice that of Chengde farmers. From the average growth rate of farmers' income in different cities, the growth rate of farmers' income in Hebei Province is more than 8%. In addition, income in Zhangjiakou, Hengshui, Chengde, Xingtai, Cangzhou, and Baoding all grew by more than 10% and even income in Zhangjiakou and Hengshui both grew by almost 12%. However, it cannot be ignored that the average growth rate is relatively low in areas with higher farmers' incomes, such as Tangshan and Langfang. This might have a certain relationship with the economic background of the new normal of China's economic growth rate from high-speed growth to medium-high growth [24]. But overall, under the premise of stable development of the economic environment, the slowdown of farmers' income growth in some cities is temporary and it will still keep the rising trend in the future.

4.2. Testing the Validity of FGM (1,1). The FGM (1,1) was established according to the PCDI of farmers' households in different cities of Hebei Province from 2012 to 2019. The FGM (1,1) process was as follows.

Due to the duplication and similarity of calculations, the paper only gives the process of predicting farmers' income in Handan City from 2020 to 2024. The income prediction process of farmers in other cities is omitted.

PCDI of farmers' households in Handan City from 2012 to 2019 as follows:

$$X^{(0)} = (8447, 9307, 10343, 11247, 12153, 13151, 14307, 15695). \quad (13)$$

In MATLAB software, particle swarm optimization was used to calculate the optimal order r of the prediction model, $r = 0.95$, and then the 0.95-order accumulation generation sequence was

$$X^{(0.95)} = (8447.0, 17336.5, 27021.1, 37409.3, 48526.2, 60474.4, 73412.8, 87566.3). \quad (14)$$

We established a first-order one-variable differential equation about t for $X^{(0.95)}$:

$$\frac{\mathrm{d}x^{(0.95)}}{\mathrm{d}t} + ax^{(0.95)} = b. \quad (15)$$

Then, the least squares method was used to solve a and b:

$$\begin{bmatrix} a \\ b \end{bmatrix} = \left(B^T B\right)^{-1} B^T Y_n = \begin{bmatrix} -0.076 \\ 7914.332 \end{bmatrix}, \quad (16)$$

Table 2: PCDI of farmers' households in various cities of Hebei Province from 2012 to 2019 (unit: yuan).

City	Year							
	2012	2013	2014	2015	2016	2017	2018	2019
Shijiazhuang	8993	9682	10691	11442	12345	13345	14518	15853
Tangshan	10698	11674	12867	13935	15023	16229	17656	19316
Handan	8447	9307	10343	11247	12153	13151	14307	15695
Baoding	7696	8649	9704	10558	11612	12779	14108	15618
Cangzhou	7514	8470	9442	10389	11340	12363	13516	14854
Xingtai	6601	7446	8342	9152	10006	10999	12287	13798
Langfang	10447	10985	12115	13159	14286	15487	16865	18467
Chengde	5546	6031	7163	7923	8736	9682	10804	12101
Zhangjiakou	5564	6583	7462	8341	9241	10293	11531	12973
Hengshui	6167	7182	8104	9030	10069	11194	12493	13917
Qinhuangdao	8315	9007	9964	10782	11621	12563	13719	15035

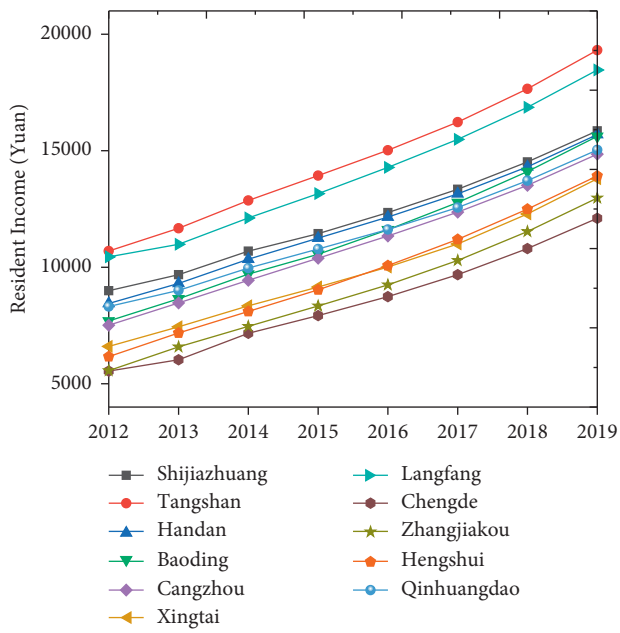

Figure 1: The farmers' income trend of Hebei Province from 2012 to 2019.

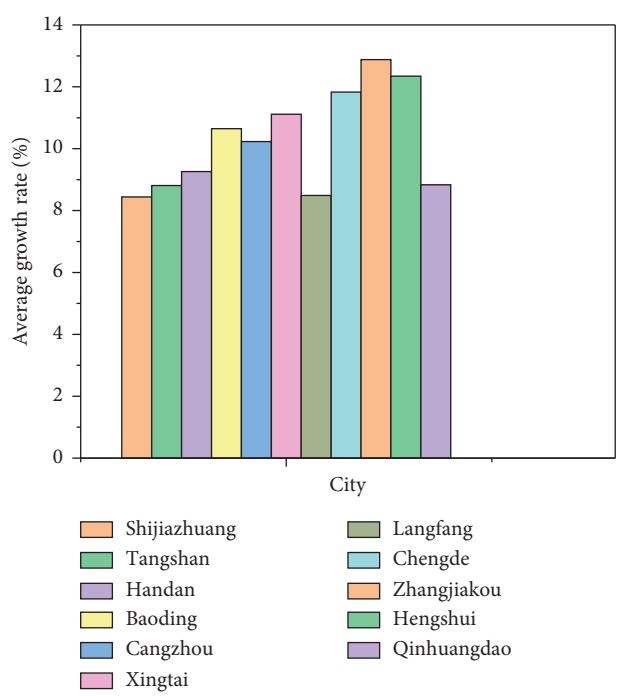

Figure 2: Average growth rate of farmers' income in Hebei Province from 2012 to 2019.

where

$$B = \begin{bmatrix} -12891.8 & 1 \\ -22178.8 & 1 \\ -32215.2 & 1 \\ -42967.8 & 1 \\ -54500.3 & 1 \\ -66943.6 & 1 \\ -80489.6 & 1 \end{bmatrix}, \quad Y_n = \begin{bmatrix} 8889.53 \\ 9684.61 \\ 10388.20 \\ 11116.89 \\ 11948.18 \\ 12938.40 \\ 14153.53 \end{bmatrix}. \tag{17}$$

Table 3: Prediction results of the GM (1,1) model and FGM (1,1) model for Handan data.

Year	PCDI	GM (1,1)	Growth rate	FGM (1,1)	Growth rate
2012	8447	8447		8447	
2013	9307	9417	0.114	9307	0.102
2014	10343	10246	0.088	10250	0.101
2015	11247	11149	0.088	11203	0.093
2016	12153	12132	0.088	12197	0.089
2017	13151	13201	0.088	13249	0.086
2018	14307	14364	0.088	14370	0.085
2019	15695	15630	0.088	15570	0.083
MAPE (%)		0.62		0.52	

We used the corresponding formula of time, and we obtained

$$\widehat{X}^{(0.95)} = \left(\widehat{x}^{(0.95)}(1), \widehat{x}^{(0.95)}(2), \ldots, \widehat{x}^{(0.95)}(13)\right) = \begin{pmatrix} 8447.0, 17336.5, 26927.8, 37326.1, 48441.4, 60488.0, 73485.5, \\ 87509.0, 102639.5, 118964.4, 136577.9, 155581.8, 176085.9 \end{pmatrix}. \tag{18}$$

Then, the 0.95-order reverse accumulation generation operation was performed on $\widehat{X}^{(0.95)}$ to obtain $\widehat{X}^{(1)}$:

$$\widehat{X}^{(1)} = \alpha^{(0.95)} X^{(0)} = \begin{pmatrix} 8447.0, 17754.0, 28003.6, 39206.2, 51403.1, 64652.3, 79022.5, \\ 94952.3, 111448.5, 129686.8, 149411.2, 170735.1, 193781.4 \end{pmatrix}. \tag{19}$$

Finally, the fitting value sequence and the predicted value sequence of $X^{(0)}$ were obtained.

The fitted value sequence of $X^{(0)}$ is

$$\{8447.0, 9307.0, 10249.6, 11202.5, 12197.0, 13249.1, 14370.3, 15569.8\}. \tag{20}$$

The predicted value sequence of $X^{(0)}$ is

$$\{16856.2, 18238.2, 19724.4, 21323.9, 23046.3\}. \tag{21}$$

When $r = 1$, the FGM (1,1) model became the GM (1,1) model. The MAPE of the GM (1,1) model and FGM (1,1) model is shown in Table 3. It can be found that the MAPE of the FGM (1,1) model and GM (1,1) model both meet the requirements, but the MAPE of the FGM (1,1) model was significantly lower than that of the GM (1,1) model. In other words, the FGM (1,1) model had a higher accuracy than the GM (1,1) model. Excluding the second data, the growth rate of GM (1,1) is a constant. But, the growth rate of FGM (1,1) is mutable and data-driven. The growth rate of FGM (1,1) is very consistent with the actual situation. This is an important property. Thus, we used FGM (1,1) to fit the other data. The results are listed in Table 4; the FGM (1,1) model and GM (1,1) model both meet the requirements, but the MAPE of the FGM (1,1) model was significantly lower than or equal to that of the GM (1,1) model. In other words, the FGM (1,1) model had a higher accuracy than the GM (1,1) model.

4.3. Prediction Results of Farmers' Income in Different Cities. Based on the data of farmers' income from 2012 to 2019, the FGM (1,1) model was used to predict farmers' income from 2020 to 2024. The predicted results are shown in Table 5.

Table 4: Prediction results of the GM (1,1) model and FGM (1,1) model.

Year	Shijiazhuang PCDI	Shijiazhuang GM (1,1)	Shijiazhuang FGM (1,1)	Tangshan PCDI	Tangshan GM (1,1)	Tangshan FGM (1,1)	Qinhuangdao PCDI	Qinhuangdao GM (1,1)	Qinhuangdao FGM (1,1)
2012	8993	8993	8993	10698	10698	10698	8315	8315	8315
2013	9682	9730	9701	11674	11752	11674	9007	9068	9007
2014	10691	10544	10498	12867	12756	12759	9964	9855	9857
2015	11442	11427	11377	13935	13846	13884	10782	10711	10741
2016	12345	12383	12343	15023	15029	15075	11621	11641	11677
2017	13345	13420	13402	16229	16313	16346	12563	12652	12679
2018	14518	14543	14563	17656	17706	17710	13719	13751	13755
2019	15853	15761	15835	19316	19219	19176	15035	14945	14912
MAPE (%)		0.52	0.49		0.50	0.47		0.59	0.56
Year	Baoding PCDI	Baoding GM (1,1)	Baoding FGM (1,1)	Cangzhou PCDI	Cangzhou GM (1,1)	Cangzhou FGM (1,1)	Xingtai PCDI	Xingtai GM (1,1)	Xingtai FGM (1,1)
2012	7696	7696	7696	7514	7514	7514	6601	6601	6601
2013	8649	8694	8685	8470	8578	8470	7446	7430	7430
2014	9704	9579	9579	9442	9399	9401	8342	8222	8222
2015	10558	10553	10558	10389	10298	10350	9152	9098	9098
2016	11612	11628	11633	11340	11283	11347	10006	10067	10067
2017	12779	12811	12815	12363	12362	12410	10999	11139	11139
2018	14108	14115	14116	13516	13545	13551	12287	12326	12326
2019	15618	15552	15547	14854	14841	14781	13798	13639	13639
MAPE (%)		0.39	0.38		0.49	0.29		0.80	0.80
Year	Langfang PCDI	Langfang GM (1,1)	Langfang FGM (1,1)	Chengde PCDI	Chengde GM (1,1)	Chengde FGM (1,1)	Zhangjiakou PCDI	Zhangjiakou GM (1,1)	Zhangjiakou FGM (1,1)
2012	10447	10447	10447	5546	5546	5546	5564	5564	5564
2013	10985	11053	10985	6031	6265	6057	6583	6622	6583
2014	12115	12034	12035	7163	6990	6973	7462	7401	7401
2015	13159	13101	13134	7923	7799	7885	8341	8272	8289
2016	14286	14262	14304	8736	8701	8824	9241	9245	9267
2017	15487	15527	15558	9682	9707	9890	10293	10332	10349
2018	16865	16904	16908	10804	10830	10857	11531	11547	11550
2019	18467	18403	18364	12101	12083	11978	12973	12905	12885
MAPE (%)		0.39	0.32		1.28	1.06		0.47	0.44
Year	Hengshui PCDI	Hengshui GM (1,1)	Hengshui FGM (1,1)						
2012	6167	6167	6167						
2013	7182	7235	7182						
2014	8104	8067	8067						
2015	9030	8996	9019						
2016	10069	10031	10061						
2017	11194	11186	11209						
2018	12493	12473	12476						
2019	13917	13908	13880						
MAPE (%)		0.32	0.16						

Table 5: Prediction results of farmers' income from 2020 to 2024.

City	Year 2020	2021	2022	2023	2024
Shijiazhuang	17227	18752	20421	22247	24247
Tangshan	20754	22454	24287	26265	28399
Handan	16856	18238	19724	21324	23046
Baoding	17123	18857	20767	22869	25184
Cangzhou	16108	17545	19100	20785	22611
Xingtai	15092	16699	18478	20446	22624
Langfang	19938	21640	23481	25474	27631
Chengde	13184	14486	15894	17419	19073
Zhangjiakou	14369	16020	17858	19904	22182
Hengshui	15434	17158	19070	21191	23544
Qinhuangdao	16161	17507	18961	20532	22228

4.4. Result Analysis. The farmers' income has been predicted, combining the actual values of farmers' income from 2012 to 2019 and the predicted values from 2020 to 2024 (as shown in Figure 3); obviously, farmers' income in Hebei Province is generally increasing by years and the growth rate of farmers' income in cities with a small income base is higher than that in cities with a large income base (as shown in Figure 4). In particular, 2021 is a turning point for farmers' income. Later, the growth rate tends to stabilize, which is closely related to the economic environment such that the whole country enters a well-off society and the productive forces are fully released. For the convenience of analysis, the farmers' income in 11 cities is divided into three ranges based on the income growth rate. The first growth range: Zhangjiakou and Hengshui (income growth rate > 11%), the second growth range: Baoding, Xingtai and Chengde (10% < income growth rate < 11%), and the third growth range: Shijiazhuang, Tangshan, Handan, Cangzhou, Langfang, and Qinhuangdao (income growth rate < 10%).

In the first range, as shown in Figure 5, the income growth rate of Zhangjiakou and Hengshui is in the leading position in the province. This is inseparable from the local government support and farmers' motivation. In particular, Zhangjiakou's growth rate is the first; it takes the "2022 Winter Olympics" as an opportunity to increase the "ice and snow economy," promoting the development of tertiary industries. Meanwhile, Zhangjiakou actively guides the transfer of rural surplus labor to cities, creates a lot of rural wealth, and increases the farmers' income. Hengshui takes advantage of its proximity to the Xiong'an New District, and it develops characteristic agriculture, such as pears and peaches, uses modern science and technology, optimizes the structure of agricultural industries, and builds modern agricultural parks. At the same time, Hengshui relies on the advantages of the Internet to carry out e-commerce cooperation with large agricultural enterprises. All these have laid a solid foundation for increasing farmers' incomes.

Baoding, Xingtai, and Chengde are in the second range (as shown in Figure 6), where farmers' incomes are growing at a medium speed. Based on the actual situation, Baoding cultivates characteristic and advantageous agricultural products, builds industry-leading enterprises, helps agricultural product clusters, mixes the development of primary, secondary, and tertiary industries in rural areas, and promotes "agriculture and industry," "agriculture and Internet," "agriculture and tourism," and other models to increase farmers' employment and income. While increasing the development of agricultural planting industries in Chengde and Xingtai, two cities take advantage of geographical and labor cost advantages to export rural surplus labor to Beijing and Tianjin, the purpose of which is to increase farmers' income through multiple channels.

The third range is the slower increase in farmers' income, as shown in Figure 7, including Shijiazhuang, Tangshan, Handan, Cangzhou, Langfang, and Qinhuangdao. From the existing statistical yearbook of Hebei Province, it can be found that the farmers' income in the six cities is higher than that in the other five cities, but the growth rate is slow. In particular, Handan and Xingtai have the slowest income growth rates in the province. They are both heavy industrial cities, and their development models are in a transitional period; this influences economic development, but the impact is temporary. Langfang is next to Beijing, and its economic development is inseparable from Beijing. However, the phenomenon of economic and talent "siphoning" is inevitable. Although Qinhuangdao has increased its

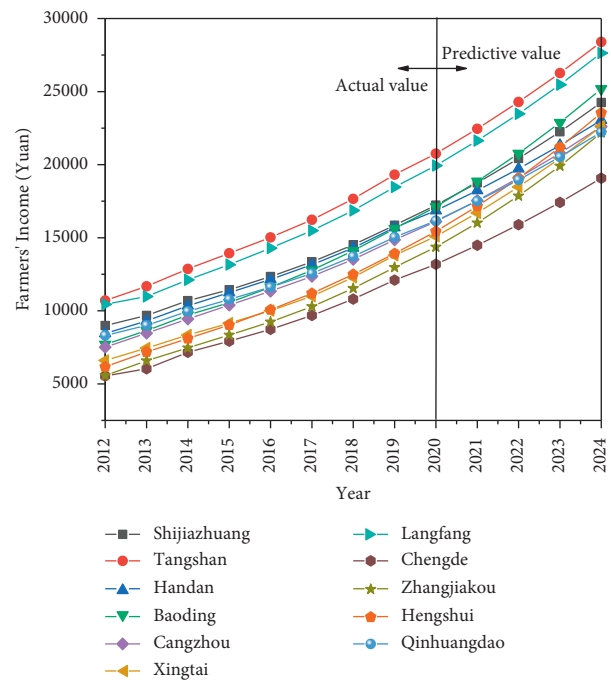

Figure 3: The actual and predicted values of farmers' income in Hebei Province from 2012 to 2024.

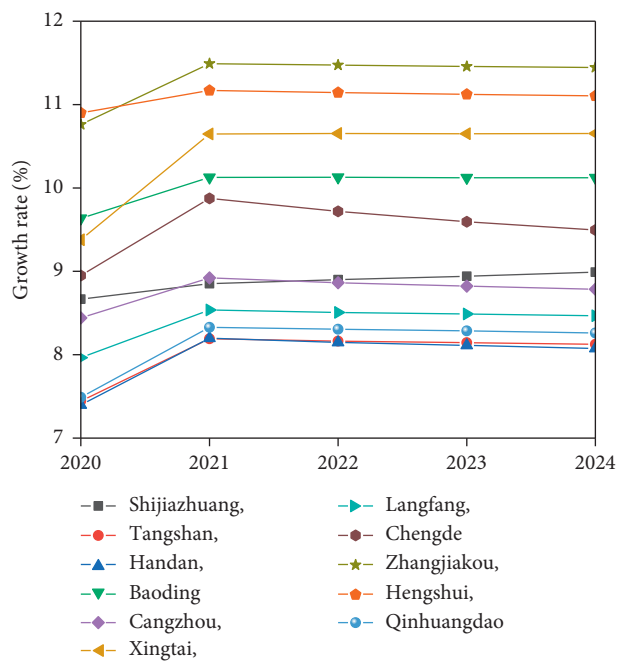

Figure 4: The growth rate of the predicted value of farmers' income from 2020 to 2024.

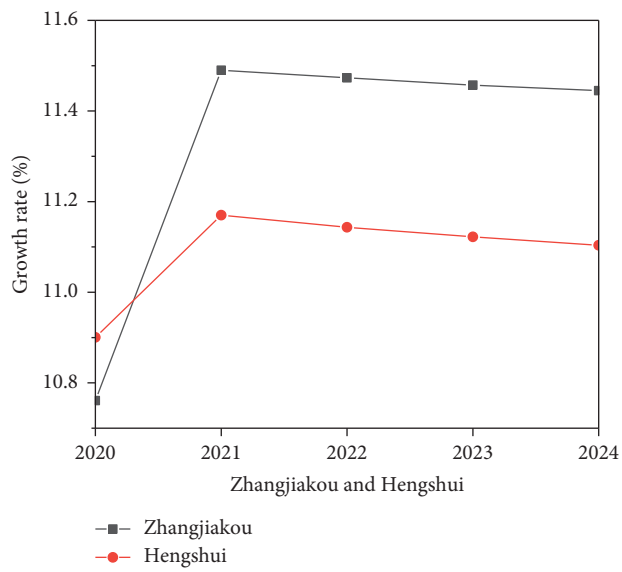

Figure 5: Farmers' predicted income growth rate in the first range.

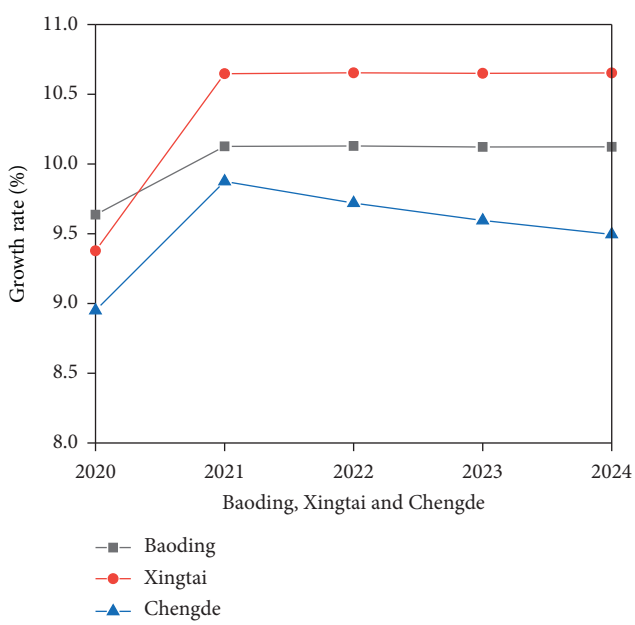

Figure 6: Farmers' predicted income growth rate in the second range.

investment in rural infrastructure construction, the unreasonable structure of agricultural industrialization, backward education, and ecological environmental governance still disturb farmers' income. Cangzhou promotes the cultivation of characteristic agriculture and strengthens the construction of the fruit market such that behaviors have been useful in promoting farmers' income. Shijiazhuang is the capital of Hebei Province, and it is the only city where farmers' income growth rate has been growing steadily. However, it has a slow growth rate, which is completely inconsistent with the characteristics of capital cities. It also proves that the development of urban and rural areas is relatively unbalanced, the economic growth force is still focused on cities, and there is lack of management of rural development.

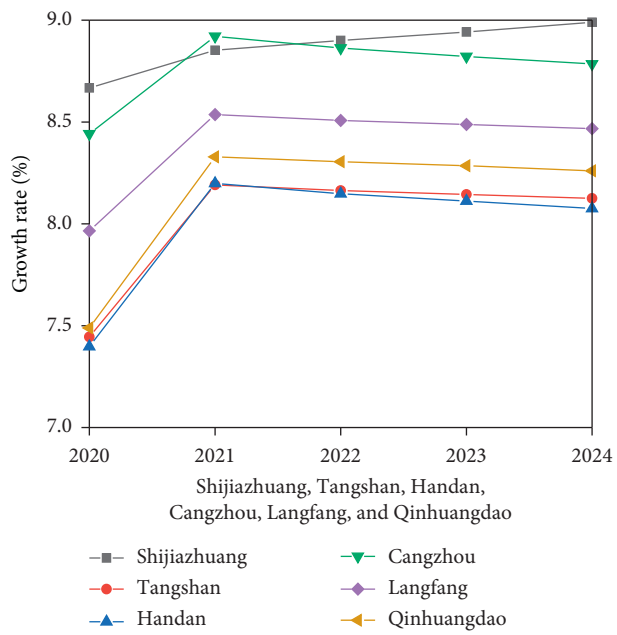

Figure 7: Farmers' predicted income growth rate in the third range.

5. Conclusions and Suggestions

By using the FGM (1,1) model to predict the farmers' income in Hebei province, it can be concluded that the FGM (1,1) model can better predict farmers' income and the FGM (1,1) model has certain advantages over the GM (1,1) model in predicting accuracy. The prediction results show that the farmers' income in Hebei province will continue to increase in the next five years, and from the perspective of the growth rate of farmers' income, the growth rate is slow in the areas with a large base of farmers' income and strong in the areas with a small base of farmers' income. The area with the highest trend growth rate of farmers' income is Zhangjiakou, and the lowest place is Handan. Only Shijiazhuang's income growth rate is on the rise.

According to the prediction results of farmers' income in Hebei Province, combined with national policies, the core of solving the rural issue is to increase farmers' income. Meanwhile, increasing farmers' income is also the basic requirement of a well-off society [25]. Hence, the paper makes the following suggestions for increasing farmers' income:

(1) Strengthen rural infrastructure construction and improve rural production efficiency.

Rural infrastructure is an important material foundation for enhancing rural productivity, developing modern agriculture, increasing farmers' income, and building a new socialist countryside. The government needs to increase capital investment in rural infrastructure. Farmers are the main body of new rural construction, and the government should take various measures to mobilize farmers' enthusiasm, initiative, and creativity so that farmers consciously participate in rural construction.

(2) Improve the quality of farmers and guide the transfer of rural surplus labor.

The low quality and ability of the farmers are the main factors affecting the increase in income. The government has the responsibility to improve the quality of farmers in rural areas. In addition, it is necessary to strengthen rural vocational and technical education based on market demand and promote the transfer of rural labor to cities, to ensure stable employment for farmers and increase income.

(3) Promote the combined development of rural revitalization strategy and new urbanization.

The coupled development of rural revitalization and new urbanization is conducive to promoting the extension of urban public resources and public services to the rural areas, encouraging the flow of urban capital, technology, and talents to the rural areas. Then, the new industrialization, information technology, urbanization, and agricultural modernization are developed simultaneously.

Finally, the prediction of farmers' income is a complex issue. In the next step, the paper will analyze the influencing factors of farmers' income in Hebei Province, establish the GM (1,N) model, and put forward more targeted methods to increase farmers' income.

Data Availability

The research data come from Hebei Statistical Yearbook from 2013 to 2020, available at (http://tjj.hebei.gov.cn/hetj/tjsj/jjnj/).

Conflicts of Interest

The authors declare that there are no conflicts of interest regarding the publication of this paper.

Acknowledgments

This work was supported by the Humanities and Social Science Research Project of Higher Education Institutions in Hebei Province (No. SQ2021127) and Handan City Philosophy and Social Science Planning Project (No. 2020074). Meanwhile, this paper was also partially supported by Dr. Lim and Ms. Wang. Dr. Prof. Li also provided a lot of research suggestions for the paper.

References

[1] D. X. Song, X. Z. Feng, and Y. M. Zhu, "The forecast analysis of rural residents' income in shanxi province based on the GM (1,1) model," *Agriculture and Technology*, vol. 40, no. 009, pp. 142–144, 2020.

[2] Y. H. Gao and S. Zhao, "Study on the influence of county agricultural structure adjustment on farmers' income in gansu province based on fixed effect model," *Journal of Lanzhou University of Finance and Economics*, vol. 36, no. 02, pp. 24–33, 2020.

[3] J. Y. Jing, "Study on adjustment of agricultural industrial structure and farmers' income in changzhou city," *Food Science and Economy*, vol. 44, no. 07, pp. 112–118, 2019.

[4] Z. Zeng and P. M. He, "Study on the influence of food price and agricultural technology progress on farmers' income," *Price Monthly*, vol. 07, pp. 21–26, 2019.

[5] Y. Hu, J. S. Zhang, and M. Miao, "Study on the impact of large-scale land management on urbanization and farmers' income," *World Agriculture*, vol. 08, pp. 47–55, 2018.

[6] S. T. Li and X. Zhou, "Differences in the effect of farmers' education levels on their wage income Based on CH IP2013 Data of Shandong Province," *Journal of Hunan Agricultural University (Social Sciences)*, vol. 19, no. 04, pp. 41–46, 2018.

[7] H. J. Guan, "Characteristics and cause of wage income fluctuation in Chinese farmers," *Journal of Hebei University of Engineering (Social Sciences)*, vol. 31, no. 03, pp. 15–21, 2014.

[8] X. L. Wu and Z. Y. Liu, "Study on impact factors in China based on provincial panel data 2002-2011," *Contemporary Economic Sciences*, vol. 36, no. 01, pp. 46–54, 2014.

[9] X. Y. Mao and T. L. Cheng, "Empirical analysis of the structure of fiscal agriculture consumption and farmers ' income based on 2010 ~ board data of 13 cities in jiangsu province in 2012," *Public Finance Research*, vol. 12, pp. 68–71, 2014.

[10] D. X. Song, X. Z. Feng, and Y. M Zhu, "Prediction analysis of rural residents in shanxi province based on GM (1,1) model," *Agriculture and Technology*, vol. 40, no. 09, pp. 142–144, 2020.

[11] R. Zhou and X. Y. Chen, "Analysis of adjustment factors of engineering price based on grey system theory," *Friends of Accounting*, vol. 01, pp. 61–66, 2021.

[12] Z. H. Han and C. Qi, "Analysis of the impact factors of energy consumption strength based on grey association degree," *Industrial Technical economy*, vol. 35, no. 10, pp. 155–160, 2016.

[13] L. Xu, "Comparative analysis of the main causes of consumption structure of urban and rural residents under grey correlation," *Development Research*, vol. 05, pp. 63–66, 2012.

[14] W. Shan, H. M. Xiao, and X. P. Geng, "Analysis of the impact factors of farmers' income based on the grey correlation model," *Henan Science*, vol. 23, no. 02, pp. 306–309, 2005.

[15] K. L. Lin, Q. L. Chen, and R. Zhao, "Study on classified management of rocky desertification area based on the perspective of farmers' income," *Forestry Economy*, vol. 35, no. 01, pp. 31–37, 2015.

[16] S. F. Liu, Y. J. Yang, and L. F. Wu, *Grey System Theory and its Application*, Science Press, Beijing, China, 2014.

[17] J. J. Li, W. M. Liu, and H. M. Fei, "The forecast of farmers' income in Jilin province based on the grey markov model," *Northeast Agricultural Science*, vol. 45, no. 06, pp. 106–109, 2020.

[18] S. Liu, Y. Yang, N. Xie, and J. Forrest, "New progress of grey system theory in the new millennium," *Grey Systems: Theory and Application*, vol. 6, no. 01, pp. 2–31, 2016.

[19] S. F. Liu, B. Zeng, and J. F. Liu, "Study on the centralized basic form and use scope of the GM (1,1) model," *Systems Engineering and Electronics*, vol. 36, no. 03, pp. 501–508, 2014.

[20] S. F. Liu and J. L. Deng, "Range of GM (1,1) model," *Theory and Practice of Systems Engineering*, vol. 20, no. 05, pp. 121–124, 2000.

[21] L. Pei and J. Liu, "A predictive analysis of the business environment of economies along the belt and road using the fractional-order grey model," *Journal of Mathematics*, vol. 2021, Article ID 3153731, 13 pages, 2021.

[22] L. Wu, S. Liu, L. Yao, S. Yan, and D. Liu, "Grey system model with the fractional order accumulation," *Communications in*

Nonlinear Science and Numerical Simulation, vol. 18, no. 7, pp. 1775–1785, 2013.

[23] H. Chen, Y. Tong, and L. Wu, "Forecast of energy consumption based on FGM (1, 1) model," *Mathematical Problems in Engineering*, vol. 2021, Article ID 6617200, 11 pages, 2021.

[24] D. X. Song, X. Z. Feng, and Y. M. Zhu, "Forecast analysis of the income of rural residents in shaanxi province based on the GM (1,1) model," *Agriculture and Technology*, vol. 04, no. 09, pp. 142–144, 2020.

[25] J. Ding, "Strategic integration and coordinating promotion of rural revitalization and new urbanization in the new era," *Socialism Studies*, vol. 05, pp. 74–81, 2019.

Hindawi
Journal of Mathematics
Volume 2021, Article ID 4318481, 10 pages
https://doi.org/10.1155/2021/4318481

Research Article

Analysis of Rural Talent Scale in Hebei Province Based on Fractional GM (1,1) and the Grey Relational Analysis Model

Yibo Li, Wenbin Bi, Kuo Xiao, Huan Li, Shi Yin, and Chaoyong Tang

College of Economics and Management, Hebei Agricultural University, Baoding 071000, China

Correspondence should be addressed to Yibo Li; lyb_cau@126.com

Received 29 May 2021; Accepted 15 November 2021; Published 26 November 2021

Academic Editor: Lifeng Wu

Talents are the key of rural revitalization. Under the background of Beijing-Tianjin-Hebei Coordinated Development, Hebei Province has always put talent revitalization at the core of rural revitalization. In order to promote the process of rural revitalization in Hebei Province, it is very important to understand the scale of rural talents. Firstly, the GM (1,1) model was used to predict the scale of rural talents in Hebei Province from 2020 to 2025. The prediction results showed that, in the rural development of Hebei Province in the next few years, the scale of production-oriented talents would gradually decline, while the scale of service-oriented, business-oriented, management-oriented, and skilled talents would show varying degrees of growth. Secondly, the grey relational analysis was used to analyze the importance of different factors for rural talents. Through the grey relational analysis, it was found that the infrastructure had the greatest impact on production-oriented talents, the agricultural industrialization operating rate had the strongest impact on service-oriented talents, and the urban-rural income level had the greatest impact on business-oriented talents, management-oriented talents, and skilled talents. Finally, according to the results of the GM (1,1) model and grey relational analysis, aiming at different types of rural talents, this paper puts forward countermeasures and suggestions from the aspects of strengthening rural infrastructure construction, improving rural medical and health conditions and improving income distribution pattern.

1. Introduction

Talent is the first step in rural revitalization. Rural talent revitalization is not only a talent problem in the general sense but also a strategic problem in China's modernization and development. Under the development mode dominated by urbanization and industrialization, the rural development mechanism is weakened, and a large number of rural surplus labor force choose to flow out, which makes the scale of urbanization continue to expand and the rural scale gradually shrink [1]. According to statistics, the proportion of rural population in the total population of Hebei Province decreased from 88.79% in 1978 to 77.14% in 2018. The number of new professional farmers in Hebei Province was 103600 in 2018, accounting for only 0.315% of the total rural population [2].

Hebei Province is a big province of agriculture and human resources. Under the background of the Beijing-Tianjin-Hebei Coordinated Development strategy, it is necessary to study the scale of rural talent development and the influencing factors of talent development in Hebei Province. Talent as a resource of "special assets" is an indispensable and important factor in economic development [3].

Through the research on the scale of rural talents in Hebei Province, we can enrich the theoretical research on rural talents revitalization under the background of rural revitalization, provide theoretical reference for party and government departments at all levels to formulate rural talents training and introduction strategies, and provide theoretical basis for the construction of rural talents in other regions of China.

In previous studies, most of them took rural human resources and rural labor force as the research objects. Under the background of rural revitalization, the research on the scale of rural talents needs to be expanded. This study

classifies rural talents and then studies their scale, which can more comprehensively cover all types of rural talents, and puts forward more targeted countermeasures and suggestions.

2. Journals Reviewed

Talents are the key of rural revitalization, "human" development is the basic problem of rural revitalization [4], and human resource development practice can enhance people's ability, skills, and knowledge [5]. The lag of talent team construction is the key factor restricting rural revitalization [6]. Without talents as the first factor, rural revitalization is impossible. If we cannot attract and retain talents and effectively play the initiative of all kinds of rural talents, rural revitalization will not be realized. Haq believed that human resources played an important role in promoting rural economic development in Pakistan [7]. Mihai and Dona pointed that human resource structure was the most important factor of production to achieve economic growth [8]. Effective development of rural human resources could promote the development of the rural economy, thereby promoting the optimization and upgrading of social structure [9]. Stimulating the internal power of rural talents is an important force to promote rural revitalization. Only by grasping the "bull nose" of talent revitalization and giving full play to the "multiplier effect" of talents, can we truly cultivate new business forms of rural industry and enhance the development power of rural revitalization [10, 11]. Sun et al. believed that strengthening the construction of rural talent teams was of great significance to enhancing the cohesion of rural grassroots teams [12].

Academic circles have not reached a consensus on the definition and classification standard of rural talents, and foreign scholars mostly use "human resources" or "human capital" to define talents [13]. Bernal and Mantilla believed that the formation of human capital includes three necessary conditions: training, experience, and organizational culture [14]. Zhang and Zhang called those who lived and worked in rural areas for a long time and engage in production, management, culture, education, technology, and other activities rural talents [15]. Han and Gi believed that rural talents were the "pillar" of rural revitalization, including rural management talents, new-type professional farmers, professional talents, and local talents [16]. Combined with scholars' point of view, this paper defines rural talents as those who are active in rural areas, can carry out creative work with their own skills, and play a role in promoting rural economic development. The number of talents needed in a region will eventually be reflected in employment, and the number of employed people needed for each industry development is the number of talents needed in this field [17]. Referring to the scholars' classification standards of rural human resource, according to the work nature of rural employees in the three industries, rural talents are divided into five types, production-oriented talents, service-oriented talents, business-oriented talents, management-oriented talents, and skilled talents. Among them, production-oriented talents refer to those engaged in agriculture, forestry, animal husbandry, fishery, and other industries. Service-oriented talents refer to those engaged in leasing services, resident services, and other industries. Business-oriented talents refer to those engaged in wholesale and retail, catering, and other industries. Management-oriented talents refer to those engaged in water conservancy, environment, and public facilities management. Skilled talents refer to those engaged in science and technology research and development, technical training, and software development.

In terms of the talent prediction method, Yan and Shang used the Markov model to predict the supply of human resources in Liaoning coastal economic belt from 2012 to 2020 and concluded that the supply of human resources in this region would exceed the demand [18]. Wang and Liu predicted the human resource demand of a power company through the grey BP neural network model and found that the human resource demand of company a would gradually increase [19]. Liu and Liu used the queue element method to predict China's population size from 2018 to 2100, and the results showed that the complete two child policy would increase the peak population by about 1.55% [20]. Jiang and Yang used regression analysis to predict knowledge innovation talents and found that most of the high-level talents in the next decade would come from universities [21]. Yun and Xue used GM (1,1) model to predict the number of health workers in Inner Mongolia and found that the number of health workers in Inner Mongolia would increase from 2019 to 2022, but the imbalance of the proportion of health workers between urban and rural areas needs to be improved [22]. Markov model, grey BP neural network model, queue element method, regression analysis method, and grey prediction model can be used for prediction, but different prediction methods have their own scope of application. The calculation of matrix in Markov model is more complex, which is mostly used by professionals. The grey BP neural network model has higher requirements for parameters, which is difficult to obtain the optimal solution. In order to get the optimal solution, the queue factor method needs to understand the cause and nature of the problem, and regression analysis is more suitable for the analysis of linear relationship and the prediction of talent scale is mostly nonlinear, which affects the accuracy of the prediction results [23]. The GM (1,1) model is to analyze and predict the development law of things through a small amount of irregular original data. It is easy to operate, and the prediction results are more accurate.

3. Data Sources and Research Methods

3.1. Data Sources. In this paper, the data from the "Hebei Rural Statistical Yearbook" compiled by the general office of Hebei Provincial People's government and Hebei Provincial Bureau of statistics from 2011 to 2020.

3.2. Research Methods. As the number of rural talents is affected by many factors, its connotation and denotation are not easy to define, and there is a nonlinear relationship between them. In the case of uncertain influencing factors of

rural talents and incomplete original data information, the data show grey characteristics [24, 25]. The GM (1,1) model is to find out its inherent laws by establishing the grey differential equation in the "poor information" and "irregular" system and predict the development law of things. Therefore, using the GM (1,1) model to predict the scale of rural talents in Hebei Province from 2020 to 2025 can reduce the adverse impact of uncertain factors on the prediction results [26]. At the same time, the grey relational analysis principle is used to analyze the influencing factors of the scale of rural talents. The correlation degree reflects the closeness between the influencing factors and rural talents. That is, the greater the correlation degree is, the closer the relationship between the factors and rural talents is, and the more important the influence is. On the contrary, the relationship is not close, and the influence is weak [24].

3.2.1. Calculation Method and Formula of the GM (1,1) Model. (i) Set the original time series to

$$X^{(0)}(k) = \left(x^{(0)}(1), x^{(0)}(2), \ldots, x^{(0)}(k)\right), \quad k = 1, 2, 3, \ldots, n. \tag{1}$$

(ii) The feasibility of the model was judged by the grade ratio test:

$$\delta(k) = \frac{x^{(0)}(k-1)}{x^{(0)}(k)} \in \left(e^{-2/n+1}, e^{2/n+1}\right). \tag{2}$$

(iii) Modeling: a new sequence is obtained by accumulating the original sequence:

$$X^{(1)}(k) = \left(x^{(1)}(1), x^{(1)}(2), \ldots, x^{(1)}(k)\right), \quad k = 1, 2, 3, \ldots, n. \tag{3}$$

The weighted average of adjacent values of equation (3) is obtained:

$$Z^{(1)}(k) = \left(z^{(1)}(2), z^{(1)}(3), \ldots, z^{(1)}(k)\right), \quad k = 1, 2, 3, \ldots, n, \tag{4}$$

$$z^{(1)}(k) = \frac{1}{2}\left(X^{(1)}(k+1) + X^{(1)}(k)\right). \tag{5}$$

The whitening equation is established and the matrix is constructed:

$$\frac{\mathrm{d}x^{(1)}}{\mathrm{d}t} + ax^{(1)} = u, \tag{6}$$

$$B = \begin{pmatrix} -z^{(1)}(2) & 1 \\ -z^{(1)}(3) & 1 \\ \vdots & \vdots \\ -z^{(1)}(k) & 1 \end{pmatrix}, \quad Y = \begin{pmatrix} x^{(0)} & (2) \\ x^{(0)} & (3) \\ \vdots & \vdots \\ x^{(0)} & (k) \end{pmatrix}. \tag{7}$$

The least square method is used to find the parameter sequence:

$$P = (a, u)^T = \left(B^T B\right)^{-1} B^T Y, \text{ parameter } a, u. \tag{8}$$

The GM (1,1) model can be obtained by establishing the time response function and solving the differential equation:

$$\hat{x}^{(1)}(k+1) = \left(x^{(0)}(1) - \frac{u}{a}\right)e^{-ak} + \frac{u}{a}, \quad k = 1, 2, 3, \ldots, n. \tag{9}$$

Restore value is

$$\hat{x}^{(0)}(k+1) = x^{(1)}(k) - x^{(1)}(k-1) = \left(1 - e^{a}\right)\left(x^{(0)}(1) - \frac{u}{a}\right)e^{-ak}. \tag{10}$$

3.2.2. The Calculation Method and Formula of Grey Relational Analysis

(i) Determine the reference sequence and comparison sequence $X_i(k)$.

(ii) Each sequence is dimensionless

$$x_i(k) = \frac{X_i(k)}{X_i(1)}, \quad i = 1, 2, \ldots, 12. \tag{11}$$

(iii) Find the correlation coefficient

$$\varepsilon_i(k) = \frac{\min_k \min_i \left|x_0(k) - x_i(k)\right| + \rho \max_k \max_i \left|x_0(k) - x_i(k)\right|}{\left|x_0(k) - x_i(k)\right| + \rho \max_k \max_i \left|x_0(k) - x_i(k)\right|}, \tag{12}$$

where $\rho = 0.5$ is called resolution coefficient.

(iv) Find the degree of correlation

$$r_i(k) = \frac{1}{n}\sum \varepsilon_i(k). \tag{13}$$

4. Prediction of Rural Talent Scale in Hebei Province

The sample length of rural talent demand data in Hebei Province is set to 10. According to the data of Hebei Rural

Statistical Yearbook from 2011 to 2020, all kinds of talent data are calculated. The number of rural talents in Hebei Province from 2010 to 2019 is used to form the original sequence.

$$X^{(0)}(k) = \left(x^{(0)}(1), x^{(0)}(2), \ldots, x^{(0)}(10)\right), \quad k = 1, 2, 3, \ldots, 10. \tag{14}$$

Taking the data of skilled talents as an example, the GM (1,1) model is constructed, and the calculation method of other types of talents is the same.

4.1. Prediction Results and Accuracy Test of the GM (1,1) Model from 2010 to 2019. This paper tests the original number series of skilled talents from 2010 to 2019, showing that $\delta(k) = \{0.97, 0.97, 0.95, 0.98, 0.97, 0.98, 0.97, 0.99, 0.99\} \in (0.83, 1.20)$. It meets the modeling conditions of the grey prediction model. According to the calculation steps of GM (1,1) model, the GM (1,1) model is established. The time response function of skilled talents in rural talent scale of Hebei Province is as follows.

$$\hat{x}^{(1)}(k+1) = 2389.445e^{0.024k} - 2333.03. \tag{15}$$

The reduction value of skilled talents in rural talent scale of Hebei Province is as follows:

$$\hat{x}^{(0)}(k+1) = 57.611e^{0.024k}. \tag{16}$$

Using the actual value of skilled talents from 2010 to 2019 to test the model, the results show that the average relative error of skilled talents is 0.95%, the accuracy of the model is 99.05%, and the small error probability is 1.00, indicating that the prediction result is excellent. Similarly, using the same method to predict other types of talents, the development coefficients α of production-oriented talents, service-oriented talents, business-oriented talents, management-oriented talents, and skilled talents are 0.0083, −0.0060, −0.0235, −0.0095, and −0.0244, respectively. When $-\alpha \leq 0.3$, medium and long-term prediction can be made. It can be seen from the above results that all kinds of talent prediction models can carry out medium and long-term prediction. The actual and predicted values of all kinds of rural talents from 2010 to 2019 are shown in Tables 1 and 2.

According to the prediction results, the accuracy test is carried out, as shown in Table3.

It can be seen from Table 3 that the accuracy of all kinds of talent models is greater than 95%, and the small error probability is greater than 0.8. According to the model accuracy evaluation standard and the precision grade table of posterior error test, the model has good accuracy and can be used for prediction.

4.2. Forecast of Rural Talent Scale in Hebei Province from 2020 to 2025. The scale of rural talents in Hebei Province in 2020–2025 is predicted by using the GM (1,1) model. The forecast results are shown in Table 4.

It can be seen from Table 4 that the scale of production-oriented talents is decreasing year by year from 13.25 million in 2020 to 12.71 million in 2025. The service-oriented, business-oriented, management-oriented, and skilled talents all show varying degrees of growth trends. Among them, the growth rate of service-oriented talents and management-oriented talents are gentle, with an average annual growth rate of 0.60% and 0.95%, respectively. The business-oriented and skilled talents are obvious, with an average annual growth rate of 2.38% and 2.47%, respectively.

5. Analysis of the Influencing Factors of Rural Talents Scale in Hebei Province

5.1. Index Selection. Wu found that the scale of human resources was related to the level of rural economic development, traffic conditions, health care level, and rural policy system [27]. Michael et al. believed that the level of rural infrastructure, living environment constraints, and urban-rural income gap would affect the development choice of rural talents [28]. Arowolo et al. found that education level, financing difficulty, income level, salary, and career development potential were closely related to the scale of rural talents [29]. Latif et al., Pham et al., and Yue et al. pointed out that education, health, rural electrification, infrastructure construction, and other factors would affect the scale of rural talents [30–32]. Zeng and Li used the logistic analysis method to analyze Western Chongqing and found that rural work attraction includes psychology, organizational behavior, management, economics, and other fields. Infrastructure, working environment, family environment, and quality of life were important factors to measure the scale of rural talents [33].

Drawing on the analysis of scholars on the influencing factors of rural talent development, this paper summarizes the influencing factors of rural talent development in Hebei Province into six factors, economy, environment, education, government, medical care, and policy. The expression, name, and meaning of each index are shown in Table 5.

5.2. Result Analysis. According to the data of Hebei Rural Statistical Yearbook from 2011 to 2020, this paper sorts out the original data of each influencing factor, uses the grey relational analysis method, takes the number of all kinds of talents from 2010 to 2019 as the reference sequence, and takes the above six influencing factors as the comparison sequence for grey relational analysis, so as to explore the influence degree of each factor on the development of rural talents, taking the correlation degree between production-oriented talents and various influencing factors as an example to calculate.

In order to eliminate the influence of dimension, the initial value processing is carried out to make the data of production-oriented talents comparable with the influencing factors. Then, the correlation coefficient between the data of production-oriented talents and the influencing factors is calculated. Finally, the importance of the influencing factors to the development of production-oriented talents is judged according to the correlation degree. The calculation process is as follows.

Table 1: The actual value of rural talent in Hebei from 2010–2019. Unit: 10000 person.

Year	Production-oriented talents	Service-oriented talents	Business-oriented talents	Management-oriented talents	Skilled talents
2010	1458.33	871.68	248.91	206.71	56.41
2011	1433.17	898.08	259.52	216.37	58.20
2012	1419.85	919.13	264.39	221.73	59.77
2013	1397.22	926.57	290.13	219.98	62.77
2014	1389.29	940.85	296.78	222.61	63.88
2015	1371.37	951.04	302.83	229.49	65.59
2016	1369.28	959.57	308.58	233.13	67.02
2017	1354.71	963.31	311.98	233.13	69.12
2018	1354.33	928.34	310.71	225.28	70.05
2019	1338.01	953.14	317.21	236.83	70.58

Table 2: The predicted value of rural talent in Hebei from 2010–2019. Unit: 10000 person.

Year	Production-oriented talents	Service-oriented talents	Business-oriented talents	Management-oriented talents	Skilled talents
2010	1458.33	871.68	248.91	206.71	56.41
2011	1426.83	915.49	268.77	218.01	59.03
2012	1415.10	920.99	275.16	220.09	60.49
2013	1403.47	926.51	281.70	222.18	61.99
2014	1391.93	932.07	288.40	224.30	63.52
2015	1380.48	937.67	295.26	226.44	65.09
2016	1369.13	943.30	302.28	228.59	66.70
2017	1357.87	948.96	309.47	230.77	68.34
2018	1346.71	954.65	316.83	232.97	70.03
2019	1335.63	960.38	324.36	235.19	71.76

Table 3: GM (1,1) model accuracy test.

	Average relative error $(1/n-1)\varepsilon(\text{avg})\sum_{k=2}^{n}\lvert\varepsilon(k)\rvert$	Model accuracy, P^0 (%)	Posterior error, C	Small error probability, P
Production-oriented talents	0.0034	99.66	0.14	1.00
Service-oriented talents	0.0125	98.75	0.48	0.90
Business-oriented talents	0.0255	97.45	0.31	1.00
Management-oriented talents	0.0129	98.71	0.39	0.90
Skilled talents	0.0095	99.05	0.14	1.00

Table 4: Forecast value of rural talents in Hebei Province from 2020 to 2025. Unit: 10000 person.

Year	Production-oriented talents	Service-oriented talents	Business-oriented talents	Management-oriented talents	Skilled talents
2020	1324.65	966.15	332.07	237.43	73.54
2021	1313.76	971.95	339.97	239.69	75.35
2022	1302.96	977.78	348.05	241.97	77.22
2023	1292.24	983.65	356.33	244.28	79.12
2024	1281.62	989.55	364.80	246.60	81.08
2025	1271.08	995.49	373.48	248.95	83.08

Table 5: Index selection of influencing factors of rural talent development.

Type	Expression	Index name and unit	Meaning
---	X_1~X_5	Production-oriented, service-oriented, business-oriented, management-oriented, and skilled talents (10000 person)	People who promote the development of rural economy in Hebei Province
Economic factors	X_6	Agricultural industrialization operation rate (%)	Economic development level
	X_7	Per capita GDP of residents (yuan)	
	X_8	Wage income (yuan)	
	X_9	Per capita disposable income of rural residents (yuan)	
Environmental factor	X_{10}	Investment in power, network, and transportation (unit)	Infrastructure investment

Table 5: Continued.

Type	Expression	Index name and unit	Meaning
Educational factors	X_{11}	Number of rural primary and secondary schools (unit)	Education development level
	X_{12}	Number of full-time teachers in rural primary and secondary schools (10000 person)	
Government factors	X_{13}	Financial investment (10000 yuan)	Government investment level
Medical factors	X_{14}	Health technicians in township hospitals (person)	Medical and health conditions
Policy factors	X_{15}	Number of insured persons (10000 person)	Insurance policy

(i) Initialization

$$\begin{aligned}
X_1' &= (1.00, 0.98, 0.97, 0.96, 0.95, 0.94, 0.94, 0.93, 0.93, 0.92),\\
X_6' &= (1.00, 1.02, 1.05, 1.08, 1.10, 1.12, 1.10, 1.14, 1.12, 1.15),\\
X_7' &= (1.00, 1.08, 1.25, 1.32, 1.39, 1.38, 1.84, 1.55, 1.62, 1.64),\\
X_8' &= (1.00, 1.06, 1.11, 1.17, 1.28, 1.39, 1.51, 1.64, 1.77, 1.79),\\
X_9' &= (1.00, 1.00, 1.01, 1.04, 1.05, 1.07, 1.18, 1.30, 1.32, 1.35),\\
X_{10}' &= (1.00, 1.00, 0.92, 0.93, 0.87, 0.90, 0.91, 0.92, 0.95, 0.96),\\
X_{11}' &= (1.00, 0.77, 0.71, 0.69, 0.69, 0.66, 0.64, 0.61, 0.59, 0.58),\\
X_{12}' &= (1.00, 0.74, 0.67, 0.67, 0.68, 0.67.0.68, 0.68, 0.68, 0.68),\\
X_{13}' &= (1.00, 0.42, 1.67, 1.49, 0.78, 0.63, 1.16, 0.55, 0.55, 0.56),\\
X_{14}' &= (1.00, 1.02, 1.02, 1.02, 1.01, 1.02, 1.03, 1.05, 1.03, 1.06),\\
X_{15}' &= (1.00, 1.19, 1.36, 1.54, 1.71, 1.85, 2.00, 2.16, 2.35, 2.58).
\end{aligned} \tag{17}$$

(ii) To find the correlation coefficient

$$\begin{aligned}
&\min_k \min_i \left|x_0(k) - x_i(k)\right| = 0,\\
&\max_k \max_i \left|x_0(k) - x_i(k)\right| = 1.66,\\
&\varepsilon_{1,i}(k) = \frac{\min_k \min_i \left|x_0(k) - x_i(k)\right| + \rho \max_k \max_i \left|x_0(k) - x_i(k)\right|}{\left|x_0(k) - x_i(k)\right| + \rho \max_k \max_i \left|x_0(k) - x_i(k)\right|},
\end{aligned} \tag{18}$$

where $k = 1, 2, \ldots, 10$, $i = 6, 7, \ldots, 15$, $\rho = 0.5$.

$$\begin{aligned}
&\varepsilon_{1,6}(1) = 1.00,\ \varepsilon_{1,6}(2) = 0.95,\ \varepsilon_{1,6}(3) = 0.92, \varepsilon_{1,6}(4) = 0.88,\\
&\varepsilon_{1,6}(5) = 0.85, \varepsilon_{1,6}(6) = 0.82,\ \varepsilon_{1,6}(7) = 0.83, \varepsilon_{1,6}(8) = 0.80,\\
&\varepsilon_{1,6}(9) = 0.81,\ \varepsilon_{1,6}(10) = 0.79,\\
&\qquad \ldots\\
&\varepsilon_{1,15}(1) = 1.00,\ \varepsilon_{1,15}(2) = 0.80,\ \varepsilon_{1,15}(3) = 0.68, \varepsilon_{1,15}(4) = 0.59,\\
&\varepsilon_{1,15}(5) = 0.52, \varepsilon_{1,15}(6) = 0.48,\ \varepsilon_{1,15}(7) = 0.44, \varepsilon_{1,15}(8) = 0.40,\\
&\varepsilon_{1,15}(9) = 0.37, \varepsilon_{1,15}(10) = 0.33.
\end{aligned} \tag{19}$$

(iii) Find the degree of correlation

Table 6: Grey relational analysis of rural talent development in Hebei Province.

Influence factor/types of talents	Production-oriented (X_1)	Service-oriented (X_2)	Business-oriented (X_3)	Management-oriented (X_4)	Skilled talents (X_5)
X_6	0.87	0.98	0.89	0.98	0.93
X_7	0.70	0.73	0.76	0.72	0.74
X_8	0.73	0.78	0.79	0.76	0.78
X_9	0.86	0.92	0.90	0.90	0.92
X_{10}	0.96	0.85	0.75	0.83	0.78
X_{11}	0.78	0.69	0.60	0.66	0.62
X_{12}	0.78	0.69	0.61	0.67	0.63
X_{13}	0.72	0.68	0.62	0.67	0.63
X_{14}	0.93	0.95	0.83	0.92	0.86
X_{15}	0.59	0.60	0.58	0.57	0.57

$$\begin{aligned} &r_{1,i}(k) = \frac{1}{10}\sum \varepsilon_{1,i}(k), \\ &r_{1,6}(k) = 0.87,\ r_{1,7}(k) = 0.70, r_{1,8}(k) = 0.73, r_{1,9}(k) = 0.86, \\ &r_{1,10}(k) = 0.96,\ r_{1,11}(k) = 0.78, \gamma_{1,12}(k) = 0.78, \gamma_{1,13}(k) = 0.72, \\ &\gamma_{1,14}(k) = 0.93, \gamma_{1,15}(k) = 0.59. \end{aligned} \tag{20}$$

Similarly, according to the above method, the correlation between each type of talent and its influencing factors is calculated, and the results are shown in Table 6.

(1) For production-oriented talents, infrastructure and medical and health conditions have the strongest impact on them, and the correlation degree is more than 0.90. The correlation among the operation rate of agricultural industrialization, per capita GDP, wage income, the comparison of urban and rural income levels, the number of primary and secondary schools, and the number of teachers and government investment is also relatively high, and the correlation degree is above 0.70. Economic factors will have an important impact on its scale. Productive talents are mainly engaged in agricultural production activities. The important factors to be considered are the backward development level of productive infrastructure, the guarantee of children's education, and the sound medical and health conditions.

(2) For service-oriented talents, agricultural industrialization operation rate, per capita GDP, wage income, comparison of urban and rural income levels, and infrastructure and health care are the main factors affecting the scale of service-oriented talents, and the correlation degree is more than 0.70. Among them, the correlation degree between agricultural industrialization operation rate and comparison of urban and rural income levels and health care is even more than 0.90. The purpose of service-oriented talents is to enable farmers to get satisfactory services. With the increase of agricultural industrialization operation rate, agricultural added value will also increase, so as to improve farmers' income, increase their satisfaction with production and life, and reduce the work pressure of service-oriented talents. Therefore, regional industrial development is an important factor for service-oriented talents, and its development level directly affects the scale of service-oriented talents.

(3) For business-oriented talents, management-oriented talents and skilled talents, urban-rural income level, agricultural industrialization rate, and medical and health conditions ranked the top three, and the correlation degree is above 0.80. The income level directly affects the development scale of talents. The better the economic development, the higher the agricultural industrialization operation rate, the more confident the talents have in the development of the region, the larger the scale of the talents. In addition, the sound medical conditions can effectively guarantee the health rights and interest of people. With the development of economy and society, people's demand for basic medical and health service level is also gradually improving. It is very important for rural talents to improve the medical and health conditions in rural areas and solve the problem of "difficult and expensive to see doctors."

(4) The impact of education development level, government investment, and insurance policy on all rural talents is generally the same, and the correlation degree is between 0.57 and 0.78. No matter what the nature of rural talents is, they will focus on the regional economic development level and educational ability when choosing a career.

6. Conclusion and Discussion

According to 2010–2019 rural talents and related data in Hebei Province, this study uses the GM (1,1) model to predict the scale of rural talents in Hebei Province from 2020 to 2025 and explores the main influencing factors of the scale and draws the following conclusions:

(1) The overall scale of rural talents in Hebei Province shows an upward trend, but the scale of production-oriented talents is gradually declining, and the scale of service-oriented, business-oriented, management-oriented, and skilled talents is gradually expanding.

(2) There is a close relationship between the level of economic development and the scale of rural talents. The income level of urban-rural areas has the greatest impact on the service-oriented talents, business-oriented talents, management-oriented talents, and skilled talents.

(3) Infrastructure is an important factor to measure the scale of rural talents, and production-oriented talents are most strongly affected by water conservancy, transportation, and other infrastructure.

(4) Medical and health conditions are one of the main concerns of rural talents, and the number of rural doctors and village health centers is the focus of production-oriented talents and service-oriented talents.

(5) The level of education development and government investment have the strongest impact on production-oriented talents, and teachers are very necessary for rural development.

(6) Insurance policy does not play a significant role in promoting the development of all kinds of talents. The scale of talents is weakly affected by insurance policies such as basic medical care and endowment insurance.

According to the research conclusions, the following policy recommendations are put forward.

All regions of Hebei Province should adapt measures to local conditions and create an environment conducive to the development of all kinds of talents:

(1) For production-oriented talents, the first step is to increase policy support, optimize the agricultural and rural development environment, increase investment in irrigation and water conservancy projects, optimize irrigation and water-saving technology, increase the coverage of rural power grid, and accelerate the construction of rural roads. Secondly, strengthen the construction standards of rural public schools, improve the teaching conditions of teachers, increase the treatment of rural teachers, encourage graduates of normal universities to teach in rural areas, strengthen the exchange of urban-rural teachers, and constantly improve the quality of rural schools. Thirdly, we should strengthen the rural vocational skills training, guide the rural grassroots cadres and the broad masses of farmers to actively participate in the training, and cultivate a group of professional farmers with strong comprehensive quality who understand agricultural production and are good at management.

(2) For service-oriented talents, we should accelerate the improvement of urban-rural income level, accelerate the equalization of urban and rural public services, narrow the development gap between urban and rural areas, promote the rational flow of resource elements between urban and rural areas, improve the service-oriented talents' sense of identity with public basic services, improve rural medical and health conditions, and strengthen the management of rural medical practitioners. Strictly enforce the professional standards of rural doctors and increase the investment in rural social security.

(3) For business-oriented, management-oriented and skilled talents, we should improve the pattern of income distribution, introduce policies to optimize the working environment of talents, provide guarantee for rural development from financial, cultural, resource and technical aspects, and create a good entrepreneurial environment. Let the excellent projects incline to the countryside, allow the farmers who settle down in the city to transfer their homestead and housing to the entrepreneurs, let the talents who are willing to start a business in the countryside start a business smoothly, and drive the development of more farmers.

(4) Government investment should be inclined to rural areas and increase investment in rural economic development. Firstly, invest in high-quality development projects of modern agriculture and develop characteristic agricultural industrial parks and characteristic agricultural vegetable gardens to promote the development of rural characteristic industries. Secondly, invest in agricultural products processing projects to ensure the safety and efficiency of the whole process of agricultural products production, storage, and circulation. Thirdly, invest in the construction of training bases for rural talents, optimize the talent service environment, and provide technical guidance and service items to improve the quality of talent training.

(5) Strengthen policy incentives and improve the development treatment of rural talents. Firstly, we should strengthen work guidance and life care, provide guarantee for rural talents, and reduce the anxiety about the development after the work expires. Secondly, reduce the threshold of entrepreneurship access in the rural market, simplify the relevant procedures such as project approval and financing guarantee, and reduce the cost of entrepreneurship as much as possible. The third is to plan the introduction standards of rural talents, allocate rural jobs, so that rural talents can give full play to their skills, establish an open, transparent, scientific, fair and pragmatic reward and punishment system, and make more talents realize that rural development is also promising.

Data Availability

All data are included within this paper. However, the reader may contact the corresponding author for more details of the data.

Conflicts of Interest

The authors declare that they have no conflicts of interest.

Acknowledgments

This paper was supported by the National Social Science Fund Project, Research on Deepening Characteristics, Behavior Mechanism and Quality Improvement Path of Farmers' Professional Differentiation in the New Development Stage (no. 21BGL173).

References

[1] H. Shi, "Who will revitalize the countryside? -Construction of human resource support system for rural revitalization," *Governance Research*, vol. 35, no. 6, pp. 115–121, 2019.

[2] People's Network. There Are 103600 New Professional Farmers in Hebei Province [EB/OL]. http://he.people.com.cn/n2/2018/0205/c192235-31221129.html.

[3] P. Drucker, *The Practice of Management*, China Machine Press, Beijing, China, 2006.

[4] Li Bo, "Talent revitalization and its promotion Path in rural revitalization: based on the internal logic between different talents and rural revitalization," *Yunnan Social Sciences*, vol. 4, pp. 137–143, 2020.

[5] B. R. Biobele, "Human resource development research as a route to sustainable development in Nigeria," *Journal of Economics and Sustainable Development*, vol. 5, 2014.

[6] W. Houkai, L. Gao, and K. Cui, "Ideas and policies for promoting rural revitalization during the 14th five-year plan period," *Rural Economy*, vol. 8, pp. 1–11, 2020.

[7] A.-u. Haq, "Human resource development in Pakistan: evolution, trends and challenges," *Human Resource Development International*, vol. 18, no. 1, 2015.

[8] D. Mihai and I. Dona, "The efficiency forecast of rural human resources use by the data envelopment analysis approach," *Scientific Papers Series: Management, Economic Engineering in Agriculture and Rural Development*, vol. 14, no. 4, 2014.

[9] X. C. Gao and C. L. Xian, "Study of human resources development of underdeveloped areas of western China: case study of Liangzhou," *Inquiry into Economic Issues*, vol. 12, pp. 79–83, 2012.

[10] W. Wang, "Reflections on promoting the revitalization of rural talents through institutional innovation," *Rural Economy*, vol. 10, pp. 22–29, 2019.

[11] Z. Cao, "Building talent engine to help rural revitalization," *People's Forum*, vol. 23, pp. 70-71, 2019.

[12] J. Sun, Y. Ma, and Z. Wang, "New rural social relationship structure and promotion Path from the perspective of integration of agriculture and tourism: a case study of Chenjie village in Jinhua, Zhejiang province," *Geographical Research*, vol. 39, no. 3, pp. 696–708, 2020.

[13] S. Tian and D. Wang, "Core driven model and policy enlightenment of rural talent revitalization: an empirical study of policy texts based on grounded theory," *Jianghuai Forum*, vol. 1, pp. 10–17, 2020.

[14] C. E. T. Bernal and S. M. S. Mantilla, "General aspects of the concept of "human capital"," *Criterio Libre*, vol. 9, no. 14, 2011.

[15] M. Zhang and X. Zhang, "Invigorating rural areas with talents," *Cooperative Economy and Technology*, vol. 4, pp. 109–111, 2019.

[16] X. Han and T. Ge, "Countermeasures to speed up the construction of rural talent team-taking rudong county as an example," *Jiangnan Forum*, vol. 4, pp. 52-53, 2019.

[17] Y. Zhang, T. Zhang, and S. Li, "Research on economic and population demand of Shanxi Province under the background of economic transformation and Reform," *Economic Issues*, vol. 9, pp. 126–128, 2012.

[18] Y. Yan and H. Shang, "Application of Markov model in the prediction of human resource supply in liaoning coastal economic zone," *China Population, Resources and Environment*, vol. 24, no. S1, pp. 196–198, 2014.

[19] B. Wang and Y. Liu, "Human resource demand forecasting method based on grey BP neural network model," *Statistics & Decisions*, vol. 34, no. 16, pp. 181–184, 2018.

[20] Q. Liu and X. Liu, "Prediction of China's population size and structure from 2018 to 2100 under the background of fertility policy adjustment," *Practice and Understanding of Mathematics*, vol. 48, no. 8, pp. 180–188, 2018.

[21] L. Jiang and J. Yang, "Prediction of high-level knowledge innovation talents in Chinese universities in the next 10 years-based on the research perspective of highly cited scientists," *Research on Science and Technology Management*, vol. 31, no. 22, pp. 133–136, 2011.

[22] C. Yun and Q. Xue, "Prediction and analysis of health human resources in inner Mongolia based on GM (1,1) model," *Medicine in Society*, vol. 32, no. 9, pp. 20–23, 2019.

[23] L. Wu, Y. Liang, and C. Wen, "GM (0, N) model for predicting the development cost of complex equipment," *China Management Science*, vol. 27, no. 7, pp. 203–207, 2019.

[24] J. Deng, *Basis of Grey Theory*, Huazhong University of Science and Technology Press, Wuhan, China, 2002.

[25] Z. Zhang, L. Wu, and Y. Chen, "Forecasting PM2.5 and PM10 concentrations using GMCN(1, N) model with the similar meteorological condition: case of Shijiazhuang in China," *Ecological Indicators*, vol. 119, Article ID 106871, 2020.

[26] J. Yao, H. Liu, and J. Liu, "Research on regional demand trend of scientific and technological innovation talents-prediction and comparative analysis of Sichuan, Shaanxi and Shanghai," *Scientific and technological progress and countermeasures*, vol. 36, no. 14, pp. 46–52, 2019.

[27] B. Wu, "Research on the influential factors of rural human resources development of tianjin in the context of new-type urbanization," *Chinese Journal of Urban and Environmental Studies*, vol. 3, no. 4, 2015.

[28] O. Michael, E. Kwasie, and K. Alam, "Towards understanding digital divide in rural partnerships and development: a framework and evidence from rural Australia," *Journal of Rural Studies*, vol. 43, 2016.

[29] A. O. Arowolo, X. Deng, O. A. Olatunji, and A. E. Obayelu, "Assessing changes in the value of ecosystem services in response to land-use/land-cover dynamics in Nigeria," *The Science of the Total Environment*, vol. 636, 2018.

[30] A. Latif, M. S. Nazar, T. M. Khan, and F. M. Shaikh, "Human resource development: strategies for sustainable rural development," *Asian Social Science*, vol. 7, 2011.

[31] P. D. N. Tien and T. T. T. Ha, "Rethinking education and training in vietnam rural areas," *US-China Education Review B*, vol. 5, no. 6, 2015.

[32] S. Yue, D. Xu, Y. Liu, and S. Liu, "The influence of human capital and social capital on the gendered division of labor in peasant family in Sichuan, China," *Social Indicators Research*, vol. 155, 2021.

[33] S. Zeng and X. Li, "An empirical study on the influencing factors of talent attraction under the background of rural revitalization-based on the survey data of western chongqing," *China Agricultural Machinery Chemical Journal*, vol. 40, no. 8, pp. 214–220, 2019.

Hindawi
Journal of Mathematics
Volume 2021, Article ID 7765325, 9 pages
https://doi.org/10.1155/2021/7765325

Research Article

An Empirical Analysis of the Price Volatility Characteristics of China's Soybean Futures Market Based on ARIMA-GJR-GARCH Model

Yang Xu,[1] **Zhihao Xia**,[2] **Chuanhui Wang**,[2] **Weifeng Gong**,[2,3] **Xia Liu**,[2] **and Xiaodi Su**[2]

[1]*Management College, Ocean University of China, Qingdao 266100, China*
[2]*School of Economics, Qufu Normal University, Rizhao 276826, China*
[3]*School of Economics and Management, Nanjing University of Aeronautics and Astronautics, Nanjing 211006, China*

Correspondence should be addressed to Chuanhui Wang; chhwang001@163.com

Received 15 June 2021; Accepted 6 October 2021; Published 5 November 2021

Academic Editor: Niansheng Tang

As the main force in the futures market, agricultural product futures occupy an important position in the China's market. Taking the representative soybean futures in Dalian Commodity Futures Market of China as the research object, the relationship between price fluctuation characteristics and trading volume and open position was studied. The empirical results show that the price volatility of China's soybean futures market has a "leverage effect." The trading volume and open interest are divided into expected parts and unexpected parts, which are added to the conditional variance equation. The expected trading volume coefficient is estimated. Also, the estimated value of the expected open interest coefficient is, respectively, smaller than the estimated value of the unexpected trading volume coefficient and the estimated value of the unexpected open interest coefficient. Therefore, the impact of expected trading volume on the price fluctuation of China's soybean futures market is less than that of unexpected trading volume on the price of soybean futures market. This paper adds transaction volume as an information flow to the variance of the conditional equation innovatively and also observes transaction volume as the relationship between conditional variance and price fluctuations.

1. Introduction

In bulk commodity trade, soybean is one of the agricultural products with large demand in China, and its price fluctuation is more prominent. China's soybean import is at a disadvantage, and China has become the world's largest importer. Due to the further opening of the soybean market, the price fluctuation of domestic soybean futures is affected by many factors at home and abroad, which has aroused wide attention in China. Since 1996, China has become the world's major soybean importer. In order to optimize the soybean supply structure, the Chinese government has implemented the "reduction of corn and the beans" since 2016. With the Sino-US trade frictions intensified in 2018, the United States increased import tariffs by 25% and import costs rose. Russia and Canada have thrown out olive branches to increase exports to China. In 2019, the Ministry of Agriculture and Rural Affairs decided to implement the Soybean Revitalization Plan and put forward six subsidy policies to support the development of soybean. In 2020, the No. 1 document of the Chinese government central committee pointed out increasing support for high-yielding soybean varieties and the promotion of new agronomic techniques for intercropping corn and soybean. The reason that China imports more soybeans is mainly reflected in the large domestic supply and demand gap, the inadequate genetic modification technology, and low tariffs. China has a high degree of dependence on international imports of soybeans. Therefore, there is a large price fluctuation of China's soybeans.

The classical theory often assumes that the return is subject to conditional or unconditional normal distribution, so its volatility is stable. However, the return of financial assets has more complex volatility in the actual market transactions. FAMA [1] studies show that although the volatility of financial asset prices is similar in the similar time periods, there is volatility aggregation effect. The change of the return rate appears a form of peak and thick tail, which does not conform to the simple normal distribution. The return rate is more likely to fall in the limit value region, which has high risk. Foster [2] studied the international crude oil pickup market and found that trading volume has a significant positive impact on futures price volatility. Liu and Wei [3] also found that there was a significant positive correlation between trading volume and futures price volatility. Wang et al. [4] used the ARCH (autoregressive conditional heteroscedasticity) model to analyze the price fluctuation of soybean futures daily trading price data from 2006 to 2011. The research shows that the yield of soybean futures has a second-order arch process, and its price fluctuation has volatility clustering, in which trading volume has a positive role in promoting price fluctuation. Tang et al. [5] took soybean futures and wheat futures in agricultural futures as examples to analyze the long-term correlation of futures price fluctuations and found that the agricultural futures market has state continuity and volatility aggregation. Hua and Zhong [6]; Zhou and Qi [7]; and Cai [8], respectively, used daily trading data of high-frequency data to analyze the characteristics of futures price fluctuations from different perspectives when studying different futures. Based on the EGARCH (exponential generalized autoregressive conditional heteroscedasticity) model, Li et al. [9] studied the relationship among the depth, liquidity, and volatility of CSI 300 Index futures market, which showed that stock index futures can improve the structure of capital market and deepen the reform of capital market. In the research on the price fluctuation of China and American soybean futures market, experts and scholars believe that the price of American soybean futures plays a major role in the transmission of information, and there is fluctuation spillover effect between the two markets [10–16]. Macroeconomic regulation and control may affect commodity price volatility, and some studies show that there is volatility spillover effect from energy market to agricultural product market [17–19]. Jiang and Zhang [20] established a stochastic volatility model by using the non-parametric Bayesian method and studied the data characteristics of the SSE 50 Index, so as to provide suggestions for preventing financial risks. Chen et al. [21] predicted the volatility of Brent crude oil futures market by introducing the hidden Markov model. They believed that the pseudo-structure mutation might occur in this state, and they corrected it by using the ICSS (intra-cranial self-stimulation) model to make the results more accurate. Liu et al. [22] conducted modeling and prediction based on three types of high-frequency extreme volatility data, demonstrating the significance and effectiveness of high-frequency data. Dan et al. [23] constructed a copper futures price fluctuation prediction model based on symbolic high-frequency time series, which shows that K-NN (k-nearest neighbors) algorithm is more accurate. Cai and Liao [24] predicted the volatility of the GEM market and measured the risk by constructing the dynamic higher moment realized EGARCH model and improved the prediction accuracy and risk measurement accuracy.

The futures price fluctuates frequently, which can reflect the market information sensitively. Domestic and foreign scholars mostly use daily high-frequency data to analyze the relationship between trading volume and price fluctuation. It is of great significance to change the perspective to analyze the characteristics of futures price fluctuation. In the soybean futures market, most scholars study the impact of volatility agglomeration effect, spillover effect, and information symmetry on volatility, while there are few studies on price volatility using yield to express the degree of price volatility. It is more to take the trading volume as an explanatory variable and add it into the model, but it is less to introduce the conditional variance equation and use the related models to divide the forecast.

In this paper, the soybean futures of Dalian Commodity Exchange will be researched. The trading volume and position as information flow will be innovatively added to the variance of conditional equation. The relationship between trading volume as conditional variance and price fluctuation will be analyzed. The ARIMA-GJR-GARCH combination model will be constructed. The relationship between trading volume and price fluctuation will be studied, and the relationship between open positions and price fluctuation will also be studied. The relationship between trading volume and open positions is mainly divided into expected trading volume and open positions and unexpected trading volume and open positions. The relationship between trading volume and price fluctuations can be analyzed.

2. Methods

2.1. The Established Model. In China's soybean futures market, trading volume and open position are two important variables. Trading volume is mainly used to describe the amount of market information, and open position mainly reflects the depth of the market. They can reflect the role of asymmetric information and the activity of market trading. Trading volume and open position can also describe the different responses of speculators to price changes under the condition of information asymmetry. In the futures market, the time series of trading volume and open position are significantly correlated. Therefore, by entering the prediction model, the trading volume and open position are divided into expected and unexpected to forecast.

In the financial market, AR, MA, ARMA, and ARIMA models are usually used to predict the transaction price or volatility of the in-sample and out-of-sample markets. ARMA and ARIMA models are established on the basis of AR and MA and can be more comprehensively predicted. The paper will choose both expected and unexpected volume and open interest on the fluctuation of prices, which can only be applicable to the stationary time series ARMA model. The model for the seasonal time series has no direct model, so the paper chooses the ARIMA model.

In order to deeply and comprehensively describe the volatility characteristics of China's soybean futures price, an ARIMA-GJR-GARCH model will be constructed. Taking into account the trading volume and open interest, the relationship between expected and unexpected trading volume and open interest and the price volatility of China's soybean futures will be comprehensively analyzed.

A "leverage effect" of the financial time series often exists. The characteristic of "leverage effect" is that the price fluctuations caused by bad news or negative shocks are greater than the price fluctuations caused by good news or positive shocks. Therefore, an asymmetric ARCH model needs to be established. The trading volume and open interest are divided into expected and unexpected parts, and the ARIMA-GJR-GARCH model is constructed to analyze the characteristics of price fluctuations. For such non-stationary and seasonal sequences, a model can be established as follows:

$$\phi_p(L)\Phi_p(L)(1-L)^d\left(1-L^S\right)^D y_t = \theta_q(L)\,\Theta_Q(L)\varepsilon_t, \quad (1)$$

where p represents the order of the seasonal autoregressive process SAR; Q represents the order of the seasonal moving average process SMA; p, q, respectively, represent the order of the non-seasonal autoregressive process AR and the order of the non-seasonal moving average process MA; d, Q, respectively, represent the order of the non-seasonal and seasonal difference of the sequence y_t; $\phi_p(L), \Phi_p(L)$, respectively, represent the lag operator polynomial of the non-seasonal autoregressive process AR and the seasonal autoregressive process SAR; $(1-L^d), (1-L^S)^D$, respectively, represent the order of the non-seasonal difference and the seasonal difference lag operator of the sequence; S is the step size of the seasonal difference; and $\theta_q(L), \Theta_q(L)$, respectively, represent the lag operator polynomial of the non-seasonal moving average process MA and the seasonal autoregressive process SMA.

The constructed model form is as follows:

$$\begin{aligned} R_t &= \alpha + \sum_{j=1}^{n}\gamma_j R_{t-j} + \sum_{j=1}^{n}\pi_j\widehat{\sigma}_{t-j} + U_t, \\ \widehat{\sigma}_t &= \delta + \sum_{j=1}^{n}\omega_j\widehat{U}_{t-j} + \sum_{k=1}^{m}\mu_k A_k + \sum_{j=1}^{n}\beta_j\widehat{\sigma}_{t-j} + e_t, \\ \widehat{\sigma}_t &= \alpha + \mu_1\mathrm{ETV}_t + \mu_2\mathrm{UTV}_t + \rho_1\mathrm{EOI}_t \\ &\quad + \rho_2\mathrm{UOI}_t + \sum_{j=1}^{n}\beta_j\widehat{\sigma}_{t-j} + e_t, \end{aligned} \quad (2)$$

where t stands for time; R_t is the price return variable on the day t; ETV_t represents the expected trading volume on the day t; UTV_t represents the unexpected trading volume on the day t; EOI_t is the expected position on day t; UOI_t is the unexpected position on day t; and α, γ_j, π_j, δ, ω_j, μ_k, and β_j are the coefficients of the relevant variables in the above models.

2.2. Data Collection and Selection. In recent years, China's soybean futures contracts have been active on the Dalian Commodity Exchange, so the paper chooses the soybean futures contract of Dalian Commodity Exchange for research. The volatility of soybean futures market in China is mainly caused by the fluctuation of price and yield rate, so this paper chooses soybean futures market price as the research object. Two problems should be noted in the selection of data. Firstly, unlike the stock market, futures contracts have a continuous time series of stock prices. Futures contracts are discontinuous, which means that they will be liquidated and stopped trading after the future trading date. Secondly, because there are multiple contracts of different delivery months on the same trading day, there will be different trading prices for the same futures product on the same trading day. Because a number of contracts with different delivery months will participate in the trading on the same trading day, the same futures product has different trading prices on the same trading day. Therefore, in the selection of data, both the discontinuity of futures market prices and the price of futures contracts should be taken into account. This paper selects data of Dalian Commodity Exchange, which are from the database of China Stock Market & Accounting Research Database (CSMAR). In order to make the transaction data more representative and more convincing, the contracts with large settlement price, volume, and position in the transaction contract are selected. If two contracts are included in a day, the contract with large volume of trading volume and large position is selected. The main contract of China's soybean futures market will be constituted according to the above selection. The settlement price of the contract is selected as the transaction data to form a continuous time series. Soybean futures that can be delivered in Dalian Commodity Exchange include soybean No. 1 and soybean No. 2. As a non-genetically modified soybean, soybean No. 1 is a good representative in the study of price fluctuation in Chinese soybean futures market. Therefore, the main contract of soybean No. 1 is selected as the research object. A total of 1219 sample data from December 31, 2014, to December 31, 2019, were selected.

Through logarithmic processing of the settlement price data of China's soybean futures, the return rate series data were obtained and the statistical characteristics were analyzed. The formula for calculating the return rate was as follows:

$$R_t = \ln\frac{P_t}{P_{t-1}}, \quad (3)$$

where R_t represents the return rate of the day, P_t represents the settlement price of the day, and P_{t-1} represents the settlement price of the previous day. Thus, the time series of return rate can be obtained and analyzed.

3. Empirical Analysis

3.1. The Statistical Characteristics of China's Soybean Futures Market

3.1.1. Statistical Characteristics of Return Rate. Through logarithmic processing of sample data, the basic statistical results are obtained. A linear chart of daily yield fluctuation of China's soybean futures main contract is obtained as shown in Figure 1.

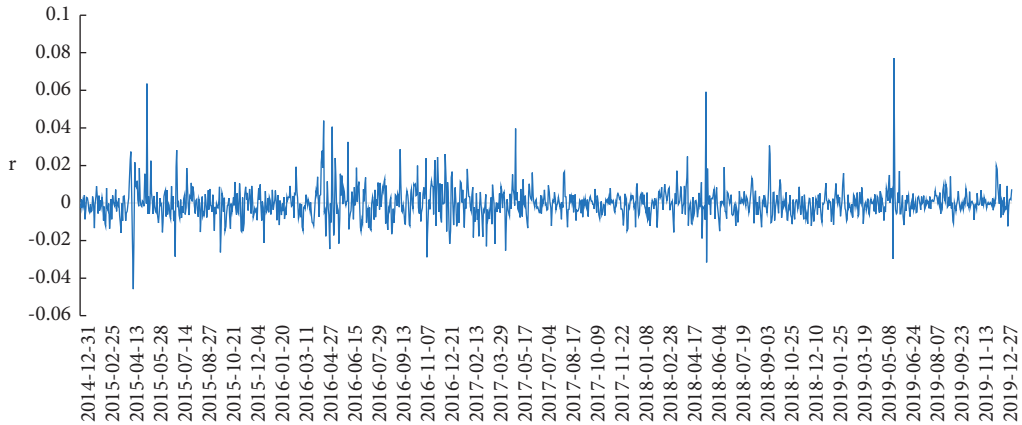

Figure 1: Line chart of daily yield fluctuation in Chinese soybean futures market.

Table 1: Statistics of the daily return rate sequence of the main continuous contracts of China's soybean futures.

Statistics	Standard deviation	Skewness	Kurtosis	J-B statistics	p value
Soybean futures daily return sequence	0.0086258	1.436	14.74	7417	≤0.001

The fluctuation curve of yield rate directly shows the fluctuation degree of yield in China soybean futures market. It can be seen from Figure 1 that the yield sequence of China's soybean futures market has a volatility agglomeration effect, that is, when the volatility is large, it will continue to fluctuate significantly for a period of time, and when the volatility is small for a period of time, it will continue to fluctuate to a smaller extent, and the appearance of volatility agglomeration effect often means that there will be an ARCH effect in the sequence of returns. The emergence of volatility aggregation effect usually represents the ARCH effect of return series.

The statistical test of the return rate sequence of China's soybean futures market is carried out. Standard deviation is mainly used to reflect the degree of dispersion between individuals of data within the group. Skewness is used as the skewness direction and degree of statistical data. Kurtosis is a statistic used to describe the steep degree of distribution of all values in the overall data. When the data are normally distributed, K equals 3.3. It has a high and thin shape and a thick tail, that is, a sharp peak and a thick tail. Most financial sequences have a sharp peak and a thick tail and are asymmetrically distributed. J-B test statistics are used to test whether the sample sequence obeys normal distribution and study the fluctuation information of return rate. These statistics can best reflect it. The histogram and statistical table of the daily return rate sequence of China's soybean futures continuous contract are shown in Table 1.

From the statistical results in Table 1, it can be seen that the skewness of the daily yield series of China's soybean futures is 1.436. It means that the distribution is skewed to the right relative to the normal distribution, and the rate of return series has a right trailing phenomenon. Kurtosis K equals 14.74, which is greater than the kurtosis value 3 in the normal distribution. It means that the yield series have the characteristics of sharp peaks. Therefore, the yield series of China's soybean futures show the characteristics of sharp peaks and thick tails. The J-B statistic is 7417, and the corresponding p value is not more than 0.001, so the null hypothesis should be rejected. It means that the yield series do not obey the standard normal distribution. Considering that financial time series generally have heteroscedasticity, an ARCH model is considered to solve the problem. Therefore, stationarity test and autocorrelation test are also needed for sample time return series.

3.1.2. Stability Test and Partial Autocorrelation Test of Return Rate. Before establishing a model for the rate of return data, it needs to be tested for stationarity, autocorrelation and partial autocorrelation, and ARCH effect. It has been determined that the model to be established subsequently has practical significance.

There is no unit root in the daily yield series of China' soybean futures, which is a stationary series. The autocorrelation and partial autocorrelation tests on the yield data of China's soybean futures market are shown in Table 2.

As can be seen from Table 2, various order sequence correlation values are two times the standard deviation of the set range. It means that China's soybean futures have no obvious yield sequence truncation and trailing phenomenon. Sample sequence lag order autocorrelation and partial autocorrelation coefficient is close to zero. The sample sequence rejects the non-autocorrelation hypothesis under the condition of 5% confidence level. Therefore, there are autocorrelation and partial autocorrelation in the yield series of China's soybean futures market.

3.1.3. ARCH Effect Test. This paper chooses the Lagrange multiplier test to verify whether the residual series has the ARCH effect. Engle and Granger [25] proposed a Lagrange multiplier test to test whether the residual sequence has the ARCH effect. The ARCH LM test results of the residual sequence are shown in Table 3.

Table 2: The autocorrelation and partial autocorrelation tests on the yield data of China's soybean futures market.

Lag	AC	PAC	Q	Prob > Q
1	0.1433	0.1433	25.077	≤0.0000
2	0.0361	0.0159	26.673	≤0.0000
3	0.0384	0.0317	28.476	≤0.0000
4	0.0078	−0.0026	28.55	≤0.0000
5	0.0401	0.0387	30.525	≤0.0000
6	0.0163	0.0042	30.852	≤0.0000
7	0.0086	0.0041	30.942	0.0001
8	0.0112	0.0066	31.096	0.0001
9	−0.011	−0.0147	31.245	0.0003
10	0.0127	0.0145	31.444	0.0005

Table 3: The ARCH LM test of residual sequence.

Lags(p)	Chi2	Df	Prob > chi2
1	24.996	1	≤0.001
2	25.293	2	≤0.001
3	26.459	3	≤0.001
4	26.457	4	≤0.001
5	28.198	5	≤0.001

According to Table 3, it can be obtained that the p value corresponding to each statistic of the residual squared lag of order from 1 to 5 is no more than 0.001. It means that all the lagging residual squares are jointly significant, and the p value of the ARCH effect test is also not more than 0.001, so the null hypothesis is rejected. The residual sequence has conditional heteroscedasticity and has an ARCH effect.

3.2. Volatility Characteristics of China's Soybean Futures Price. A volatility curve between trading volume and open interest and yield is drawn, as shown in Figure 2.

According to Figure 2, it can be seen that the volatility of trading volume is relatively large. The range of change between open interest and trading volume is basically the same. The range of change in the rate of return is relatively small.

Firstly, the ARIMA model is used to predict the volume and open interest in the sample. The predictable part is called the expected volume and the open interest, which are recorded as ETV_t and EOV_t, respectively. The relative error of the difference between the actual value and the predicted value is called the unexpected transaction. The volume and open interest are recorded as UTV_t and UOV_t, respectively. Then, the above two variables are added to the conditional variance equations of the GJR-GARCH (2, 1) model to explore the empirical analysis of the impact of soybean futures price fluctuations.

The regression analysis results are shown in Tables 4 and 5.

As can be seen from Tables 4 and 5, c represents the coefficient of the constant term, which is greater than zero. μ_1 represents the estimated value of the expected trading volume coefficient. μ_2 represents the estimated value of the unexpected trading volume coefficient. ρ_1 represents the expected open position coefficient, and ρ_2 represents the unexpected open position coefficient.

According to Tables 4 and 5, the following conclusions can be drawn.

The estimated value μ_1 of expected trading volume coefficient and the estimated value μ_2 of unexpected trading volume coefficient are more than 0, respectively. The results are significant, which indicates that there is a positive correlation between expected trading volume and unexpected trading volume and price fluctuation in China's soybean futures market. The estimated values of the expected position coefficient ρ_1 and the unexpected position coefficient ρ_2 are not more than 0.001, and the results are significant, indicating that there is a negative correlation between the expected position and the unexpected position and the price fluctuation in China's soybean futures market. Increasing a certain number of positions will reduce the impact of price fluctuation caused by the increase of trading volume.

From the perspective of the relationship between current trading volume and open interest, soybean futures price fluctuations have a deeper level. The newly opened trades are far less than the impact of closing trades and handover transactions on price fluctuations from the perspective of trader behavior. Set the marginal impact of current trading volume on price fluctuations as M_μ and the marginal impact of current holdings on price fluctuations as M_ρ. At the beginning of the new position trading, it has an impact on the current trading volume. The current trading volume will increase, but the change of the current position is uncertain. If the new transaction is a new open position futures contract, then the current trading volume and position will have the same amount of increase. At this time, the impact on the price fluctuation in the soybean futures market is the sum of the marginal impact of the current trading volume on the price fluctuation and the marginal impact of the current position on the price fluctuation, which is recorded as $M_\mu + M_\rho$. If the new transaction is a soybean futures contract with closed trading units, the impact on the current trading volume and position is that when the trading volume increases by a certain amount, the position will decrease by a certain amount. At this time, the impact on price fluctuation in soybean futures market is the marginal impact of current trading volume on price fluctuation minus the marginal impact of current position on price fluctuation, which is recorded as $M_\mu - M_\rho$. If the new transaction is to change the number of trading units of soybean futures contract, the impact on the current trading volume and position is that the trading volume will have a certain amount of increase, and the position will remain unchanged. At this time, the impact on the price fluctuation in the soybean futures market is the marginal impact of the current trading volume on the price fluctuation, which is recorded as M_μ. In the soybean futures market, there is such a relationship: $M_\mu > 0$, $M_\rho < 0$; then, $M_\mu - M_\rho > M_\mu > M_\mu + M_\rho$. When the soybean futures market rises unilaterally, the trading parties establish new transactions. The market participants will increase their interests in the new trading contract, so that a large number of funds will enter the new trading futures contract, and the market depth will continue to increase. Thus, it can reduce the impact of current trading volume changes on price fluctuations.

The estimated value of the expected trading volume coefficient μ_1 is less than the estimated value of the unexpected trading volume coefficient μ_2, and the estimated value

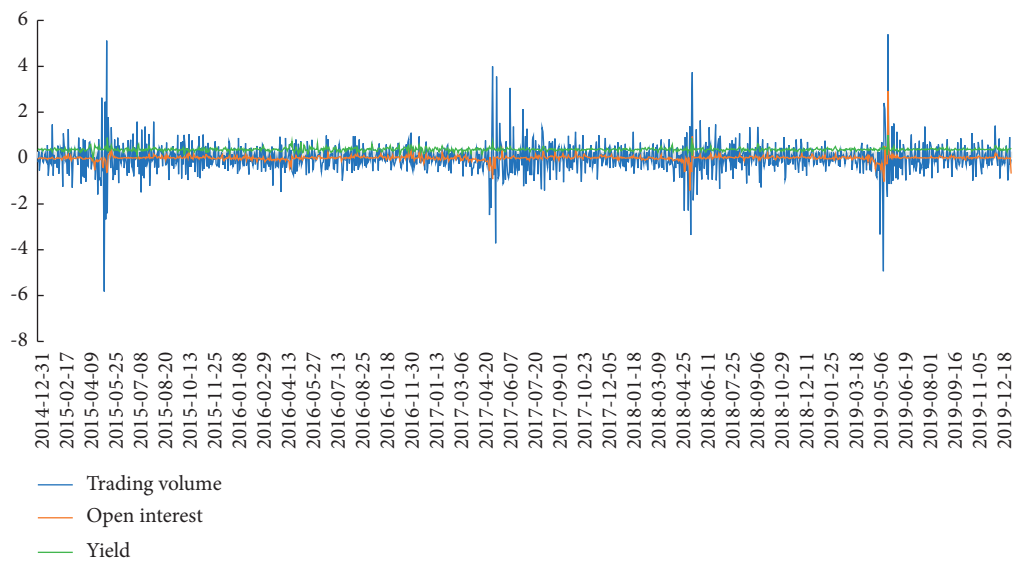

Figure 2: The volatility curve of trading volume, open interest, and yield.

of the expected position coefficient ρ_1 is less than the estimated value of the unexpected trading volume coefficient ρ_2. Therefore, the impact of the expected trading volume on the price fluctuation of China's soybean futures market is less than the impact of the unexpected trading volume on the price fluctuation of China's soybean futures market. This phenomenon can be explained as follows: in China's soybean futures market, when new information appears, there will be transactions caused by information asymmetry and liquidity demand difference. The emergence of new information will lead to the emergence of transactions to a certain extent. In China's soybean futures market, the expected trading volume and position are not generated by new information, but mainly by market participants through changing liquidity demand or adjusting positions. The unexpected trading volume and position are mainly generated by the arrival of new information in the soybean futures market, which contains more information. Therefore, the impact of unexpected trading volume and position on the price fluctuation of China's soybean futures market is stronger than that of the expected trading volume and position on the price fluctuation of China's soybean futures market.

3.3. The Influence of Trading Volume and Open Position on ARIMA-GJR-GARCH Model. The influence of trading volume and open position on ARIMA-GJR-GARCH model is further analyzed. The trading volume is introduced into the conditional variance equation based on the ARIMA-GJR-GARCH model as information flow. The results are shown in Table 6.

The coefficient of current trading volume is greater than zero and significant at the significance level of 5% in Table 6. It means that there is a positive correlation between trading volume and price volatility. After the current trading volume is added into the conditional variance equation, the GARCH term coefficient changes from the previous 0.9615618 to 0.1830656, which decreases significantly. The result is still significant at the significance level of 5%, indicating that the GARCH effect in the model is obviously weakened, but the GARCH effect still exists.

However, the coefficient of ARIMA-GJR-GARCH term changed from −0.0453458 to 0.2090938, and the result was significant at the significance level of 5%. The coefficient changed from negative to positive, indicating that the model no longer had asymmetry after adding volume. It means that volume absorbs part of the persistence and asymmetry of price fluctuations, indicating that volume has a strong ability to explain price fluctuations. In the mixed distribution hypothesis (MDH), there is a positive correlation between the volatility variance of asset prices and information variables after the introduction of information variables. The conditional expected value of trading volume mainly depends on information variables, so there is a positive correlation between trading volume and price volatility in the futures market. Through the empirical analysis of China's soybean futures market, the mixed distribution hypothesis is proved. Adding the current soybean futures trading volume into the model as a substitute index of mixed variables has a strong ability to explain price fluctuations.

Open positions are introduced into the conditional variance equation based on ARIMA-GJR-GARCH model as information flow. The results are shown in Table 7.

In Table 7, the coefficient of open position in the current period is less than zero and significant at the significance level of 5%, indicating that there is a negative correlation between open position and price volatility, and open position has a strong explanatory power on the variance of price volatility. After adding the current open position into the conditional variance equation, the GARCH term coefficient decreases slightly, and the GARCH effect exists. It means that the current open position has little influence on the persistence of soybean futures price volatility, and the volatility variance of soybean futures price still has a strong persistence. The coefficient of ARIMA-GJR-GARCH term changes from −0.0453458 to 0.0158608, and the result is not

Table 4: The relationship between expected trading volume and open interest and price fluctuations in China's soybean futures market.

	Coefficient	Standard error	z value	p value	2.5% quantile	97.5% quantile
C	0.3687882	0.0017501	214.39	≤0.001	0.3654168	0.3721596
μ_1	0.9586294	0.1421858	6.74	≤0.001	0.6799503	1.2373090
ρ_1	−15.59571	0.7651638	−20.38	≤0.001	−17.09541	−14.096020
α_1	0.1640964	0.0397881	4.12	≤0.001	0.0861133	0.2420796
α_2	−0.0977562	0.0355365	−2.75	0.006	−0.1674065	0.0281059
γ	0.0745078	0.029619	2.52	0.012	0.0164555	0.1325600
β_1	0.7738417	0.025848	29.94	≤0.001	0.7231805	0.8245029

Table 5: The relationship between unexpected trading volume and open interest and price fluctuations in China's soybean futures market.

	Coefficient	Standard error	z value	p value	2.5% quantile	97.5% quantile
c	0.3687889	0.0014382	256.43	≤0.001	0.3659701	0.3716077
μ_2	1.681456	0.0767077	21.92	≤0.001	1.531108	1.831797
ρ_2	−1.179658	0.1932675	−6.10	≤0.001	−1.558455	−0.8008604
α_1	0.1919649	0.0284119	6.76	≤0.001	0.1362786	0.2476511
α_2	−0.004453	0.0235912	−0.19	0.850	−0.0506908	0.0417848
γ	0.1492003	0.057995	2.57	0.010	0.0355234	0.2628773
β_1	0.2068837	0.0231923	8.92	≤0.001	0.1614275	0.2523398

Table 6: The relationship between trading volume and China's soybean futures price volatility.

		α_1	α_2	β_1	γ_1	μ
Untraded model	Coefficient estimation	0.4193364	−0.3562949	0.9615618	−0.0453458	
	Z	13.24	−10.82	153.91	−5.38	
	P	0.000	0.000	0.000	0.000	
Traded model	Coefficient estimation	0.2300784	−0.026109	0.1830656	0.2090938	1.317224
	Z	7.08	−1.1	6.87	3.42	15.65
	P	0.000	0.272	0.000	0.001	0.000

Table 7: The relationship between open position holding and price fluctuation of China's soybean futures market.

		α_1	α_2	β_1	γ_1	μ
Untraded model	Coefficient estimation	0.4193364	−0.3562949	0.9615618	−0.0453458	
	Z	13.24	−10.82	153.91	−5.38	
	P	0.000	0.000	0.000	0.000	
Traded model	Coefficient estimation	0.2467478	−0.1721645	0.8575355	0.0158608	−3.950086
	Z	7.03	−5.42	51.40	0.81	−20.16
	P	0.000	0.000	0.000	0.420	0.000

significant at the significance level of 5%. The coefficient changes from negative to positive, indicating that the model is no longer asymmetric after the addition of position. Therefore, open position has a strong explanatory power on price fluctuations.

4. Conclusion

This paper analyzes the price fluctuation characteristics of China's soybean futures market by constructing an ARIMA-GJR-GARCH model and draws the following conclusions:

(1) The price volatility of China's soybean futures is stable. The impact of the previous shock on the variance of the subsequent conditions is long lasting and will act on future volatility for a long time. Therefore, the volatility and market risk are relatively high. The main reason is that China's soybeans are mainly derived from imports and changes in the international political situation will have a huge impact on China's soybean futures market. Secondly, China's soybean futures price fluctuations have a leverage effect. The impact of negative news is greater than the impact of positive news. Exogenous interference will affect China's soybeans. Fluctuations in futures prices have an impact.

(2) In this paper, the current trading volume and position of China's soybean futures contract are added to the conditional variance equation based on ARIMA-GJR-GARCH (2, 1) model, respectively, and the relationship between expected and unexpected trading volume and position and price fluctuation is studied. The results show that the estimated value of the expected trading volume coefficient and the estimated value of the expected

position coefficient are less than the estimated value of the unexpected trading volume coefficient and the estimated value of the unexpected trading volume coefficient, respectively. When the trading volume of the current soybean futures contract increases and the open interest decreases, the impact on the variance of price fluctuations is greater than that of the current increase in trading volume, and the open interest increases or remains unchanged. Therefore, the impact of the expected trading volume on the price fluctuation of China's soybean futures market is less than that of the unexpected trading volume on the price fluctuation of China's soybean futures market. The main reason is that the expression of new information is mainly realized by unexpected trading volume, and new information is an important factor affecting price volatility.

Data Availability

Previously reported data were used to support this study and are available at https://www.gtarsc.com/.

Conflicts of Interest

The authors declare that they have no conflicts of interest.

Acknowledgments

This paper benefited from years of thinking about these issues and discussion with many colleagues related to economics at that time. This research was supported by the Humanities and Social Sciences Youth Foundation of Ministry of Education of China under grant no. 19YJC790128.

References

[1] FAMA, "Efficient capital markets: a review of theory and empirical work," *The Journal of Finance*, vol. 25, no. 2, pp. 383–471, 1970.

[2] A. J. Foster, "Volume-volatility relations for crude oil futures markets," *Journal of Futures Markets*, vol. 15, no. 8, pp. 929–951, 1995.

[3] X. M. Liu and Z. X. Wei, "Discussion on the relationship between trading volume and income volatility in wheat futures market," *Financial Theory & Practice*, vol. 11, pp. 87–90, 2011.

[4] X. D. Wang, B. Liu, and Y. Yan, "Fluctuation analysis of China's soybean futures price based on arch model," *Journal of Agrotechnical Economics*, vol. 12, pp. 73–79, 2013.

[5] Y. W. Tang, G. Chen, and C. H. Zhang, "An empirical research on the long-term correlation of the price volatility of the agricultural products futures markets," *Systems Engineering*, vol. 12, pp. 79–84, 2005.

[6] R. H. Hua and W. J. Zhong, "An empirical analysis on the dynamic relationship between futures price fluctuation and trading volume and short offer volume in Chinese futures market," *The Journal of Quantitative & Technical Economics*, vol. 7, pp. 123–132, 2004.

[7] B. Zhou and Z. Y. Qi, "Empirical research on the volatility in two different stages of Chinese futures markets," *Journal of Applied Sport Management*, vol. 3, pp. 518–527, 2007.

[8] C. Cai, "Research on the price volatility of major commodity futures in this economic crisis," *Financial Theory & Practice*, vol. 2, pp. 64–69, 2010.

[9] J. L. Li, Y. Lei, and S. J. Li, "Market depth, liquidity and volatility: the impact of CSI 300 stock index futures on spot market," *Journal of Financial Research*, vol. 6, pp. 124–138, 2012.

[10] T. Xia and X. Y. Cheng, "Research on the dynamic relationship between domestic and foreign futures prices and domestic spot prices——based on the empirical analysis of DCE and CBOT soybean futures markets and domestic soybean markets," *Journal of Financial Research*, vol. 2, pp. 110–117, 2006.

[11] Y. H. Zhou and L. G. Zou, "Research on the price relationship between China's soybean futures market and international soybean futures market——an empirical analysis based on VAR model," *Journal of Agrotechnical Economics*, vol. 1, pp. 55–62, 2007.

[12] X. G. Li and Y. H. Zhou, "Research on volatility spillover effect among Chinese and international soybean future markets," *Journal of Technical Economics & Management*, vol. 6, pp. 103–107, 2014.

[13] L. Sun, K. K. Ni, and X. G. Li, "The dynamic correlation of food price between domestic and abroad: based on DCC-MGARCH model," *Journal of Nanjing Agricultural University (Social Sciences Edition)*, vol. 14, no. 2, pp. 65–72, 2014.

[14] J. Y. Zheng, "Effects of international genetically modified soybean on China's soybean industry and its futures market," *Asia-pacific Economic Review*, vol. 5, pp. 39–46, 2015.

[15] H. L. Wang and Y. F. Zhao, "An analysis on price relationship between China and US soybean futures markets: based on structural breaks viewpoint," *Journal of China Agricultural University*, vol. 21, no. 9, pp. 156–165, 2016.

[16] J. H. Liu, J. H. Tian, Y. B. Wang, and H. Z. Wu, "Volatility spillover effect between Chinese and American soybean futures markets based on variable structure copula function," *Soybean Science*, vol. 38, no. 3, pp. 469–476, 2019.

[17] X. Du, C. L. Yu, and D. J. Hayes, "Speculation and volatility spillover in the crude oil and agricultural commodity markets: a bayesian analysis," *Energy Economics*, vol. 33, no. 3, pp. 497–503, 2011.

[18] S. Nazlioglu and U. Soytas, "Oil price agricultural commodity prices and the dollar: a panel co-integration and causality analysis," *Energy Economics*, vol. 34, no. 4, pp. 1098–1104, 2012.

[19] Q. Ji and Y. Fan, "How does oil price volatility affect non-energy commodity markets?" *Applied Energy*, vol. 89, no. 1, pp. 273–280, 2012.

[20] Y. Y. Jiang and B. Zhang, "Non-parameter bayesian stochastic volatility model and its application in the financial markets," *Journal of Applied Sport Management*, vol. 38, no. 1, pp. 49–61, 2019.

[21] Z. Chen, Y. Lin, D. S. Huang, and Y. X. Chen, "Forecasting of structure breakthrough points in brent crude oil futures market," *Journal of Systems & Management*, vol. 28, no. 6, pp. 1095–1105, 2019.

[22] W. Y. Liu, H. Y. Jiang, T. W. Zhang, and W. Chen, "Volatility modeling and forecasting based on high frequency extreme value data," *Systems Engineering-Theory & Practice*, vol. 40, no. 12, pp. 3095–3111, 2020.

[23] W. Dan, B. Jbha, and B. Mrza, "Prediction of metal futures price volatility and empirical analysis based on symbolic time

series of high-frequency," *Transactions of Nonferrous Metals Society of China*, vol. 30, no. 6, pp. 1707–1716, 2020.

[24] G. H. Cai and Y. Q. Liao, "Dynamic higher moment realized EGARCH model and application based on structural breaks," *The Journal of Quantitative & Technical Economics*, vol. 38, no. 1, pp. 157–173, 2021.

[25] R. F. Engle and C. Granger, "Cointegration and error-correction: representation, estimation and testing," *Econometrica*, vol. 55, no. 2, pp. 251–276, 1987.

Hindawi
Journal of Mathematics
Volume 2021, Article ID 6178629, 13 pages
https://doi.org/10.1155/2021/6178629

Research Article

Forecasting the Cumulative Confirmed Cases with the FGM and Fractional-Order Buffer Operator in Different Stages of COVID-19

Yanhui Chen, Minglei Zhang, Kai Lisa Lo, and Jackson Jinhong Mi

School of Economics and Management, Shanghai Maritime University, Shanghai 201306, China

Correspondence should be addressed to Yanhui Chen; chenyh@shmtu.edu.cn and Kai Lisa Lo; kllo@shmtu.edu.cn

Received 16 June 2021; Accepted 30 September 2021; Published 26 October 2021

Academic Editor: Lifeng Wu

This study proposes to use the fractional-order accumulation grey model (FGM) combined with the fractional-order buffer operator to predict the cumulative confirmed cases in different stages of COVID-19. In the early stages of COVID-19 outbreak, when the cumulative confirmed cases increased rapidly, we used the strengthening buffer operator in the prediction process. After the government's prevention measures started to take effect, the growth rate of cumulative confirmed cases slows down. Therefore, the weakening buffer operator is applied in the prediction process. The fractional order of the buffer operator is derived from the historical data, which are more relevant. The empirical analysis of seven countries' data shows that the FGM with the fractional-order buffer operator achieves the best results for most cases. The fractional-order buffer operator improves the prediction accuracy of the FGM in this study. Our study also suggests a practical way for predicting the trend of epidemic diseases.

1. Introduction

Fractional-order system is a more extensive complex system than the integer-order system, which has attracted extensive attention from academia and industry in recent years. The fractional-order system is more flexible, which realizes the precise modeling of complex systems; compared with the traditional integer-order controller, additionally, the fractional-order controller has advantages in robustness and design freedom. Many valuable achievements have been made in numerical calculation [1], system modeling [2], stability analysis [3], and integrated control [4] under the concept of fractional-order systems.

In the predictions of complex systems, an inevitable problem is how to forecast the system in the early stage or with limited existing data. Under the condition of less data environment, the grey system theory makes full use of the known "minimum information" and gives priority to extract the more valuable "new information," realizing the modeling of the whole system. It can be used to predict the changing trend of the system in the future [5, 6]. One of the most useful methods under this theory is GM (1, 1), which is suitable to predict the data with an exponential growing trend. Researchers used GM (1, 1) to solve the prediction problems in consumption demand, pollutant emission, and energy utilization [7–10]. The advantage of GM (1, 1) is prediction with limited data; however, it is more suitable for the data with an exponential growing trend. In order to improve the prediction accuracy of limited data with nonexponential growth trends, many scholars derived more models from traditional GM (1, 1), such as the grey Verhulst model [11, 12], grey Bernoulli model [13, 14], and fractional-order accumulation grey model (FGM) [15]. Since the fractional-order accumulation grey model solves the problem that the GM (1, 1) model cannot be used to predict the data that do not follow the grey exponential law completely accurately, it has attracted researchers' attention widely, such as Liu et al. [16], Zeng [17], Wu et al. [18], and Liu et al. [19].

The predictions of complex systems also face another problem that is how to predict the future trend of the system changes accordingly when the development of the system is disturbed. The problem in forecasting at this time does not lie in the pros and cons of the model but in the fact that the information provided by the system cannot accurately reflect the future trend. It is difficult to use the information directly

to make an accurate prediction. In order to deal with this problem in system prediction, Liu [20] proposed the concept of buffer operator in the grey system prediction models. The operator which slows down the growth rate of the sequence is called the weakening buffer operator (WBO). The operator which speeds up the growth rate of the sequence is called the strengthening buffer operator (SBO). Many scholars have proposed a variety of buffer operators based on different data to accurately predict the system with disturbance [21–23]. Buffer operator of grey system theory combines the quantitative and empirical prediction (qualitative prediction) because in these literature studies, the researchers used their experiences to analyze the future trend qualitatively and proposed a new form of buffer operators. This means that the buffer operators they built may have the problem of poor versatility. Recently, Wu et al. [24] generalized the expression of weakening and strengthening buffer operators using the fractional order, which provides us a new choice to generate different buffer operators based on different fractional orders.

Infectious diseases have always been a major public health concern. Historically, the large-scale outbreaks of infectious diseases have brought great trauma to human society. Recently, relying on modern science and technology, we have found the causes of many infectious diseases, summarized the control methods, and found the effective treatment methods of most infectious diseases. Yet, the pathogens of infectious diseases are constantly mutating and evolving, and they have struggled with human beings for a long time. The outbreak of COVID-19 is just the case. This disease is caused by SARs-CoV-2 which is a variant coronavirus. It has similar symptoms to cold and flu if the symptoms are mild, but this new coronavirus has stronger concealment and infectivity. Patients often develop symptoms long after they are infected with the virus. In addition to droplet transmission, the virus can also be transmitted through contact, aerosol transmission. Patients in the incubation period also have strong infectious power. Besides attacking our lungs, the virus can also damage other organs. Severe patients often lose their lives due to multiple organ failure, but at the very beginning, when COVID-19 broke out in Wuhan, China, the doctors knew nothing about this virus. A lot of people were infected. Doctors and scientists had to gradually deepen their understanding of the virus during the treatment of patients. We now know the nature of the coronavirus, and face masks can protect us from infection. Keeping social distance and home quarantine can slow down the spread of the virus. Although some governments did not take effective epidemic control measures in the very beginning, after the number of infected people in their own countries soared, these countries began to adopt strict control measures.

Ever since the outbreak of COVID-19, the prediction of the number of confirmed cases has attracted the attention of researchers. Generally speaking, three types of methods are mainly adopted in the literature. The first type is the time series regression model, in which ARMA/ARIMA is a commonly employed model. Perone [25] constructed the ARIMA model to predict the number of confirmed cases at the national and regional levels in Italy. Sharma et al. [26] and Ilie et al. [27] also used this method for prediction. The second uses machine learning. Tameng et al. [28] predicted the confirmed cases and deaths in India, the United States, France, and the United Kingdom through the curve fitting technique based on the artificial neural network (ANN). Hazarika and Gupta [29] predicted the COVID-19 spread in five worst-hit countries by combining the random vector function chain network (RVFL) method with wavelet transform. Chimmula and Zhang [30] used the LSTM neural network to predict the confirmed cases in Canada. The third type is the epidemic dynamic model-SIR (susceptible-infection-recovered). Based on this model, the researchers extended their model according to the particularity of COVID-19. Khajanchi and Sarkar constructed a new SAIUQR model to predict the numbers of daily and cumulative confirmed cases in four states in India [31]. Cooper et al. augmented the classic SIR model with the ability to accommodate surges in the number of susceptible individuals to predict the community confirmed cases in five countries [32].

Grey system methods have their advantage of predicting the COVID-19 epidemic as it is shown that they are effective for predicting exponential growth data. Liu et al. predicted the number of early confirmed cases in China by the fractional grey model [19]. However, with the development of the epidemic situation, it has been proved that the epidemic control measures, such as lockdown/quarantine, have effectively slowed down the rise in the number of infected people [33, 34]. Exponential growth is no longer appropriate to describe the increase in COVID-19's cumulative number of confirmed cases. Besides, according to the stage of the epidemic, it is necessary to choose the forecasting methods. This paper proposes to use different fractional-order buffer operators integrated with the FGM to forecast the trend of COVID-19.

In this paper, we name the order of the generalized strengthening and weakening buffer operator as the buffer level. By using the generalized strengthening and weakening buffer operator, the researchers need not build a new buffer operator in their research studies; all they need is to decide an order according to their experiences or generate an order based on similar cases. In the empirical analysis, this paper uses the prediction of COVID-19 cumulative confirmed cases in the early stage and after the governments' epidemic control measures were in effect to demonstrate the use of the fractional-order buffer operator in the grey system model. Our main contribution is threefold. Firstly, this study introduces different kinds of buffer operators in different stages of the epidemic. Secondly, different from previous studies in which the fractional order of the buffer operator is determined based on the experts' experiences, this paper uses the historical data to estimate the fractional order of the buffer operator and proposes an applicable prediction process (see the last paragraphs in Sections 3.1 and 3.2). Thirdly, this paper takes into account both government control measures and public responses in predicting cumulative confirmed cases.

The following of the paper includes three sections. Section 2 introduces the method, Section 3 demonstrates the empirical results, and Section 4 concludes the paper briefly.

2. Methodology

2.1. Fractional-Order Accumulation Grey Model. GM (1, 1) is the most classical and basic model in grey system theory. Driven by practice, academic research on GM (1, 1) has been very active over the past three decades. Scholars derive many models from traditional GM (1, 1) to improve the forecast precision and apply them to more new fields. Fractional-order accumulation grey model (FGM) is one of these derived models. It uses the fractional accumulate order to make the historical data in the weighted form. The order is very important in the FGM. The larger the order is, the larger the weight of old data is. Increasing the order can increase the weight of old data, which puts less emphasis on the newer data, and vice versa. As a result, it can extract the pivotal information of the historical data and make accurate prediction. A standard FGM (1, 1) is established as follows.

Definition 1. It is assumed that the original sequence is

$$X^{(0)} = \left(x^{(0)}(1), x^{(0)}(2), \ldots, x^{(0)}(n)\right). \tag{1}$$

$X^{(0)}$ is a nonnegative sequence, while the r-AGO $(0 < r < 1)$ sequence of $X^{(0)}$ is

$$X^{(r)} = \left(x^{(r)}(1), x^{(r)}(2), \ldots, x^{(r)}(n)\right), \tag{2}$$

where

$$x^{(r)}(k) = \sum_{i=1}^{k} C_{k-i+r-1}^{k-i} x^{(0)}(i), \quad k = 1, 2, \ldots, n. \tag{3}$$

According to the definition of the gamma function, $X^{(r)}$ can be rewritten in the form of gamma function as follows:

$$x^{(r)}(k) = \sum_{i=1}^{k} \frac{\Gamma(k-i+r)}{\Gamma(k-i+1)\cdot\Gamma(r)} x^{(0)}(i), \quad k = 1, 2, \ldots, n. \tag{4}$$

$Z^{(r)}$ represents the generated mean sequence of consecutive neighbors of $X^{(r)}$.

$$Z^{(r)} = \left(z^{(r)}(1), z^{(r)}(2), \ldots, z^{(r)}(n)\right), \tag{5}$$

where

$$Z^{(r)}(k) = \frac{\left(x^{(r)}(k) + x^{(r)}(k+1)\right)}{2}, \quad k = 1, 2, \ldots, n-1. \tag{6}$$

Definition 2. If $X^{(0)}$, $X^{(r)}$, and $Z^{(r)}$ are described as Definition 1, the following formula is obtained:

$$x^{(r)}(k) - x^{(r)}(k-1) + az^{(r)}(k) = u. \tag{7}$$

This formula is the original form of FGM (1, 1), and

$$\frac{\mathrm{d}x^{(r)}}{\mathrm{d}t} + ax^{(r)} = u \tag{8}$$

is the whitening equation of FGM (1, 1).

Theorem 1. *If $X^{(0)}$ and $X^{(r)}$ are described as Definition 1, the parameter vector $\hat{a} = [a, u]T$ can be estimated by the least square method as follows:*

$$\hat{a} = \left(B^T B\right)^{-1} B^T Y, \tag{9}$$

where

$$B = \begin{bmatrix} -\dfrac{x^{(r)}(1) + x^{(r)}(2)}{2} & 1 \\ -\dfrac{x^{(r)}(2) + x^{(r)}(3)}{2} & 1 \\ \vdots & \vdots \\ -\dfrac{x^{(r)}(n-1) + x^{(r)}(n)}{2} & 1 \end{bmatrix},$$
$$Y = \begin{bmatrix} x^{(r)}(2) - x^{(r)}(1) \\ x^{(r)}(3) - x^{(r)}(2) \\ \vdots \\ x^{(r)}(n) - x^{(r)}(n-1) \end{bmatrix}. \tag{10}$$

The solution to the whitening equation of FGM (1, 1) is shown as follows:

$$\hat{x}^{(r)}(k) = \left(x^{(0)}(1) - \frac{u}{a}\right)e^{-a(k-1)} + \frac{u}{a}. \tag{11}$$

By substituting the parameter vector $\hat{a} = [a, u]T$ into formula (11), the fitting value sequence $\hat{X}^{(r)}$ can be obtained. The fitting value sequence $\hat{X}^{(0)}$ can be calculated by the r-order inverse accumulation.

$$\begin{aligned} \hat{X}^{(1)} &= \left(\hat{x}^{(1)}(1), \hat{x}^{(1)}(2), \ldots, \hat{x}^{(1)}(n+1), \ldots\right) \\ &= \left(\hat{x}^{(r)(1-r)}(1), \hat{x}^{(r)(1-r)}(2), \ldots, \hat{x}^{(r)(1-r)}(n+1), \ldots\right), \\ \hat{x}^{(0)}(k) &= \hat{x}^{(1)}(k+1) - \hat{x}^{(1)}(k), \\ \hat{X}^{(0)} &= \left(\hat{x}^{(0)}(1), \hat{x}^{(0)}(2), \ldots, \hat{x}^{(0)}(n+1), \cdots\right). \end{aligned} \tag{12}$$

2.2. Buffer Operator with the Fractional Order. When a system is affected by a shock, the existing data cannot reflect the law of the system truthfully. In this case, buffer operator of the grey system was proposed to revise the future trend. It combines quantitative and judgmental forecast (qualitative analysis). Recently, several buffer operators have been proposed and used in many fields successfully [35–37]. The basic idea of using the buffer operator in the prediction

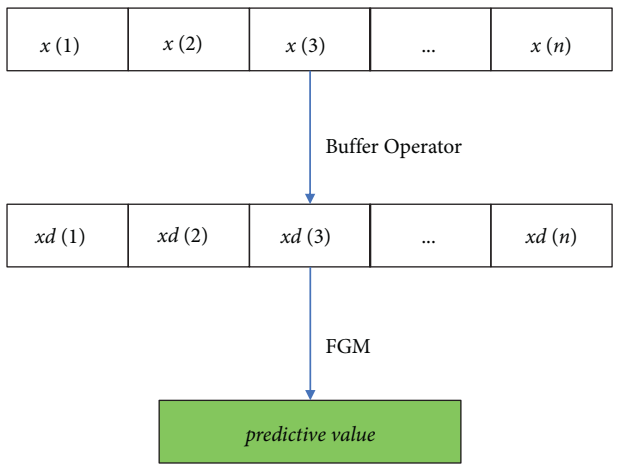

Figure 1: The basic idea of prediction with the buffer operator.

models is the trend of the original data which is modified by the buffer operator. Through the strengthening buffer effect, the original data turn into a new dataset, which shows more rapid growth. Through the weakening buffer effect, the original data turn into a new dataset with slower growth. As the prediction should be based on the historical data, it is necessary to modify the historical data which are more convenient for prediction modeling. Buffer operator is used to adjust the historical data to make it consistent with the future possible development trend which will show more rapid or slower growth according to the experience and expert's judgement. This transform would be conducive to accurate prediction. Wu et al. [24] extended the traditional integer-order buffer operator to the fractional-order one.

Definition 3. Assume that the raw data sequence is $X = x(1), x(2), \ldots, x(n)$.

$$D = \begin{bmatrix} \frac{1}{n} & 0 & \cdots & 0 \\ \frac{1}{n} & \frac{1}{n-1} & \cdots & 0 \\ \vdots & \vdots & \ddots & \vdots \\ \frac{1}{n} & \frac{1}{n-1} & \cdots & 1 \end{bmatrix}. \tag{13}$$

Then, p/q order of the weakening buffer operator is

$$XD^{p/q} = X \begin{bmatrix} \frac{1}{n} & 0 & \cdots & 0 \\ \frac{1}{n} & \frac{1}{n-1} & \cdots & 0 \\ \vdots & \vdots & \ddots & \vdots \\ \frac{1}{n} & \frac{1}{n-1} & \cdots & 1 \end{bmatrix}^{p/q}. \tag{14}$$

Definition 4. For original data $X = x(1), x(2), \ldots, x(n)$, the p/q order of the strengthening buffer operator is

$$\begin{aligned} XD^{-(p/q)} &= X \begin{bmatrix} \frac{1}{n} & 0 & \cdots & 0 \\ \frac{1}{n} & \frac{1}{n-1} & \cdots & 0 \\ \vdots & \vdots & \ddots & \vdots \\ \frac{1}{n} & \frac{1}{n-1} & \cdots & 1 \end{bmatrix}^{-(p/q)} \\ &= X \begin{bmatrix} n & 0 & 0 & \cdots & 0 \\ -(n-1) & n-1 & 0 & \cdots & 0 \\ 0 & -(n-2) & n-2 & \cdots & 0 \\ \vdots & \vdots & \vdots & \ddots & \vdots \\ 0 & 0 & 0 & \cdots & 1 \end{bmatrix}^{p/q}. \end{aligned} \tag{15}$$

The value of p/q is noted as the buffer level in the following sections. The prediction procedure is demonstrated briefly in Figure 1.

3. Empirical Analysis

3.1. The Prediction of COVID-19 Confirmed Cases in the Early Stage. Since the outbreak of COVID-19, the prediction of confirmed cases has become a hot topic. Accurate prediction of confirmed cases can help the government to arrange appropriate preventive measures and allocate medical resources scientifically (For the same reason, forecasting the trend of other epidemics accurately is also important. This method can be used to predict the confirmed cases of other epidemic diseases.). The increase of cumulative confirmed cases just meets the requirements of the FGM and buffer operator. To be specific, in the early stage, the number of confirmed cases is increasing rapidly, and there is the possibility of outbreak at any time. Therefore, this study uses the strengthening buffer operator to simulate this increasing mechanism. In the empirical analysis, we choose the data of Italy, Spain, the United Kingdom, Japan, the United States, and the Republic of South Africa to demonstrate improved prediction accuracy. The data of cumulative confirmed cases

Table 1: The buffer levels of the strengthening buffer operator for different countries.

	ITA	ESP	GBR	JPN	USA	RSA	CHN
SBO	0.25	0.41	0.43	0.1	0.2	0.62	0

ITA, EPS, GBR, JPN, USA, RSA, and CHN indicate Italy, Spain, the United Kingdom, Japan, the United States, the Republic of South Africa, and mainland China separately.

Table 2: The prediction performance.

	FGM		FGM + SBO		GM (1, 1)	
	MAPE (%)	RMSE	MAPE (%)	RMSE	MAPE (%)	RMSE
ITA	11.981	1205.576	3.494	271.156	25.601	1845.407
ESP	40.725	2543.256	15.663	837.511	55.579	2940.273
GBR	23.465	370.812	11.868	168.288	30.117	377.849
JPN	2.339	7.204	2.353	6.804	9.244	23.669
USA	38.152	1806.701	31.574	1503.262	52.140	2229.252
RSA	46.091	497.059	29.366	303.475	48.347	491.166
CHN	7.179	611.061	7.179	611.061	26.316	2267.579

ITA, EPS, GBR, JPN, USA, RSA, and CHN indicate Italy, Spain, the United Kingdom, Japan, the United States, the Republic of South Africa, and mainland China separately.

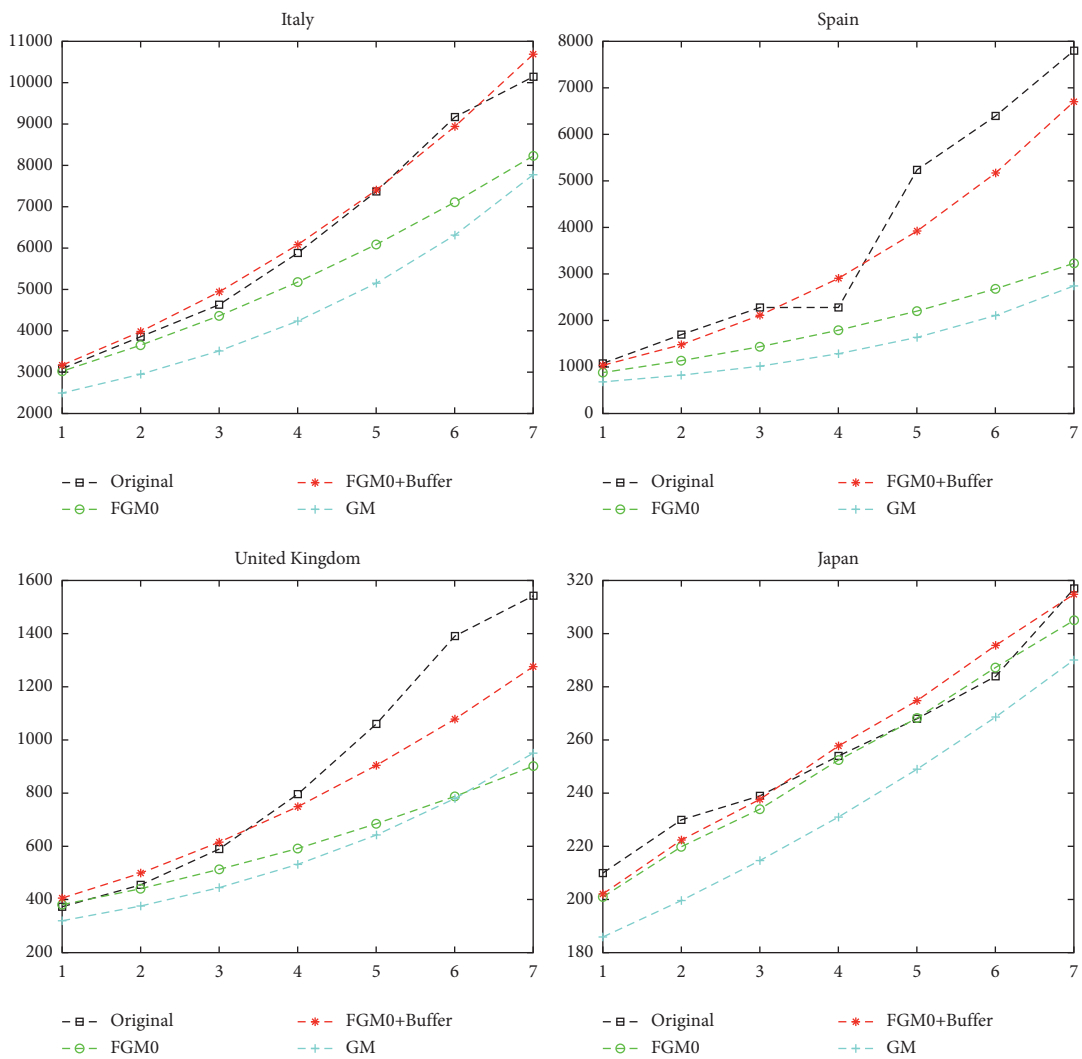

Figure 2: The prediction performance in the early stage (part 1).

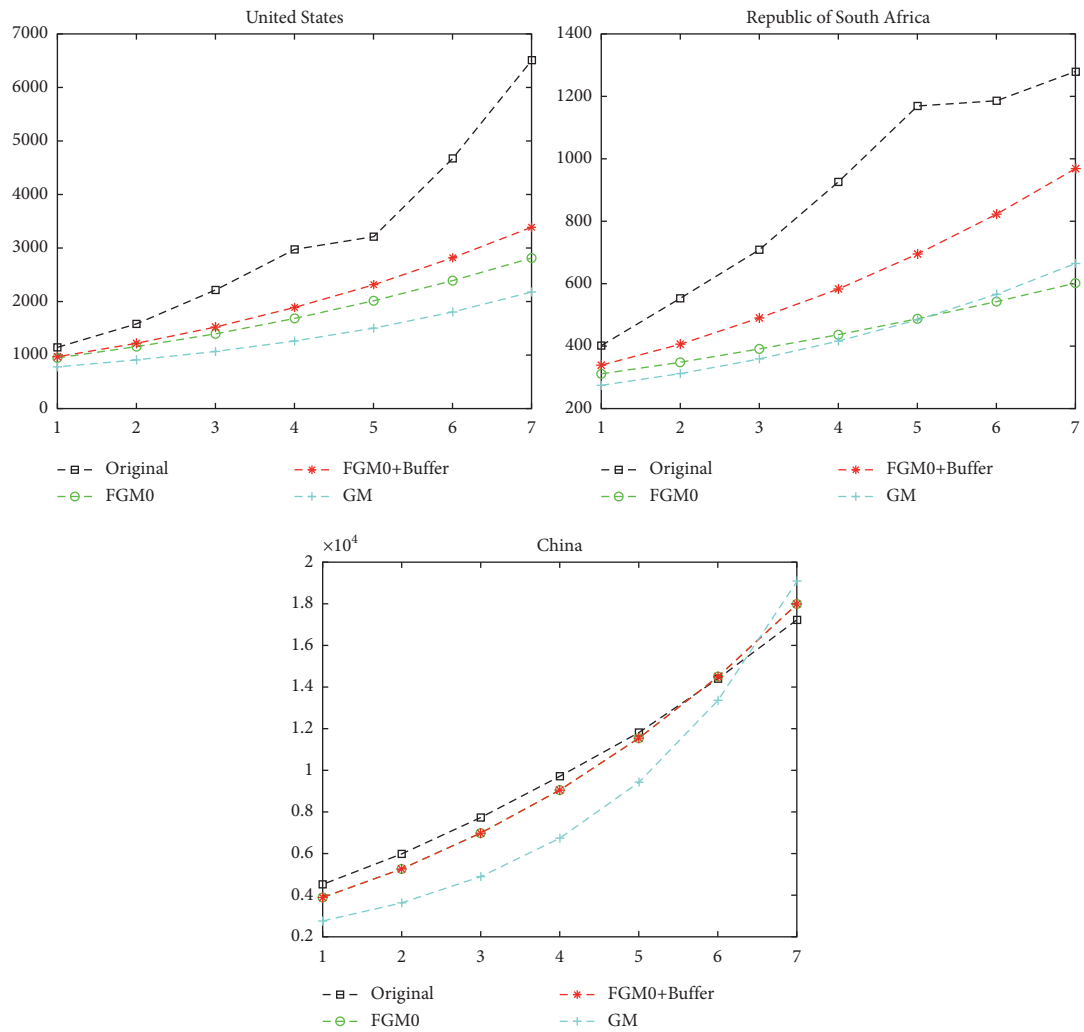

Figure 3: The prediction performance in the early stage (part 2).

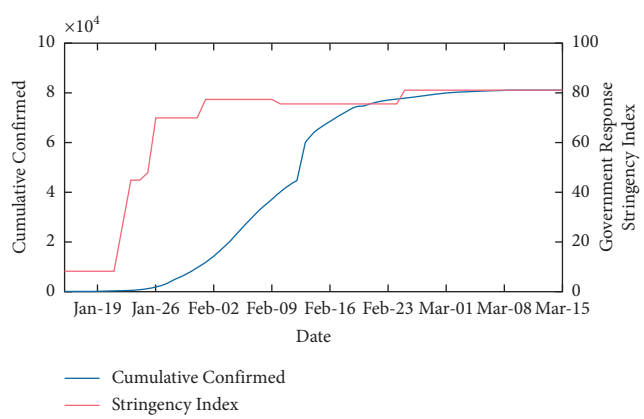

Figure 4: China cumulative confirmed cases and stringency index (January 15, 2020–March 15, 2020).

are collected from the Center for Systems Science and Engineering (CSSE) at Johns Hopkins University. This study chooses the first 12 days when the cumulative confirmed cases increase continuously as the training set to achieve the orders of the strengthening buffer operator. The training set can be divided into two parts.

The first part only includes the first five observations, the minimum requirement for GM modeling. The other part,

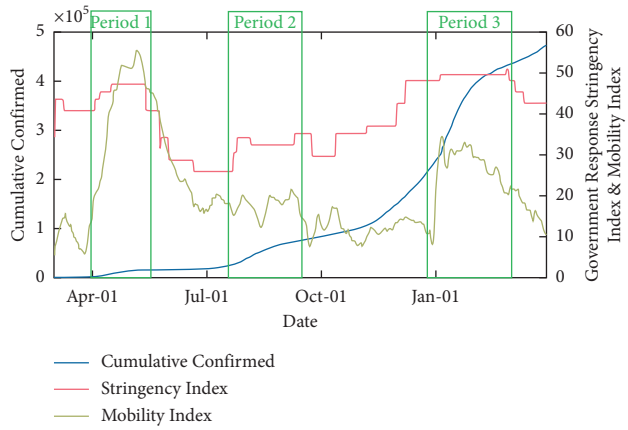

Figure 5: Japan cumulative confirmed cases, stringency index, and mobility index (March 1, 2020–March 31, 2020).

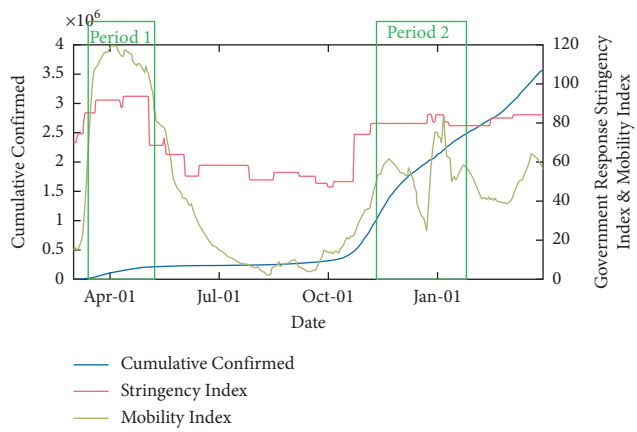

Figure 6: Italy cumulative confirmed cases, stringency index, and mobility index (March 1, 2020–March 31, 2020).

which includes other seven observations, is used to compare the prediction accuracy so that the buffer level (or fractional order) can be determined. The buffer levels of the strengthening buffer operator for the sample countries are shown in Table 1. With the data buffered by the strengthening buffer operator, this paper predicts with the FGM. Every time the model predicts a new value, we take the new value as the given value and achieve a new order for the FGM. Consequently, the order of the FGM is not fixed.

Then, this paper selects the last five data in the training set as the in-sample data to predict the next seven days' cumulative confirmed cases. The benchmark models include the FGM without the strengthening buffer operator and GM (1, 1). Both of them are suitable for the prediction based on small sample data. The criteria include mean absolute percentage error (MAPE) and root mean square error (RMSE), two most widely used criteria in prediction performance comparison. The results are shown in Table 2.

The results in Table 2 show that the FGM achieves smaller MAPE and RMSE than GM (1, 1) for all seven countries. FGM with the strengthening buffer operator always performs better than the FGM in RMSE. FGM with the strengthening buffer operator also achieves smaller MAPE when it predicts the cumulative confirmed cases of Italy, Spain, the United Kingdom, the United States, and the Republic of South Africa. Figures 2 and 3 indicate the prediction results provided by the FGM with the strengthening buffer operator which are more consistent with the true values. As a result, in the early stage of the epidemic, the prediction accuracy can be improved by considering the strengthening buffer operator and modeling with the FGM. The practitioners can continuously add new data and use this method to predict the future cumulative confirmed cases continually when the scientists and doctors do not find the effective way to prevent the epidemic.

3.2. The Prediction of COVID-19 Confirmed Cases after the Prevention Measures Work. After the outbreak of COVID-19 for a period of time, the public knows and adopts the prevention method. Consequently, the growth of the confirmed cases is slowing down. As a result, the weakening buffer operator should be utilized to predict the cumulative confirmed cases after the governments issue prevention measures, and the public respond positively to them. The severity of the governments' prevention and control measures can be evaluated by the Oxford COVID-19 Government Response Tracker Stringency Index which is collected

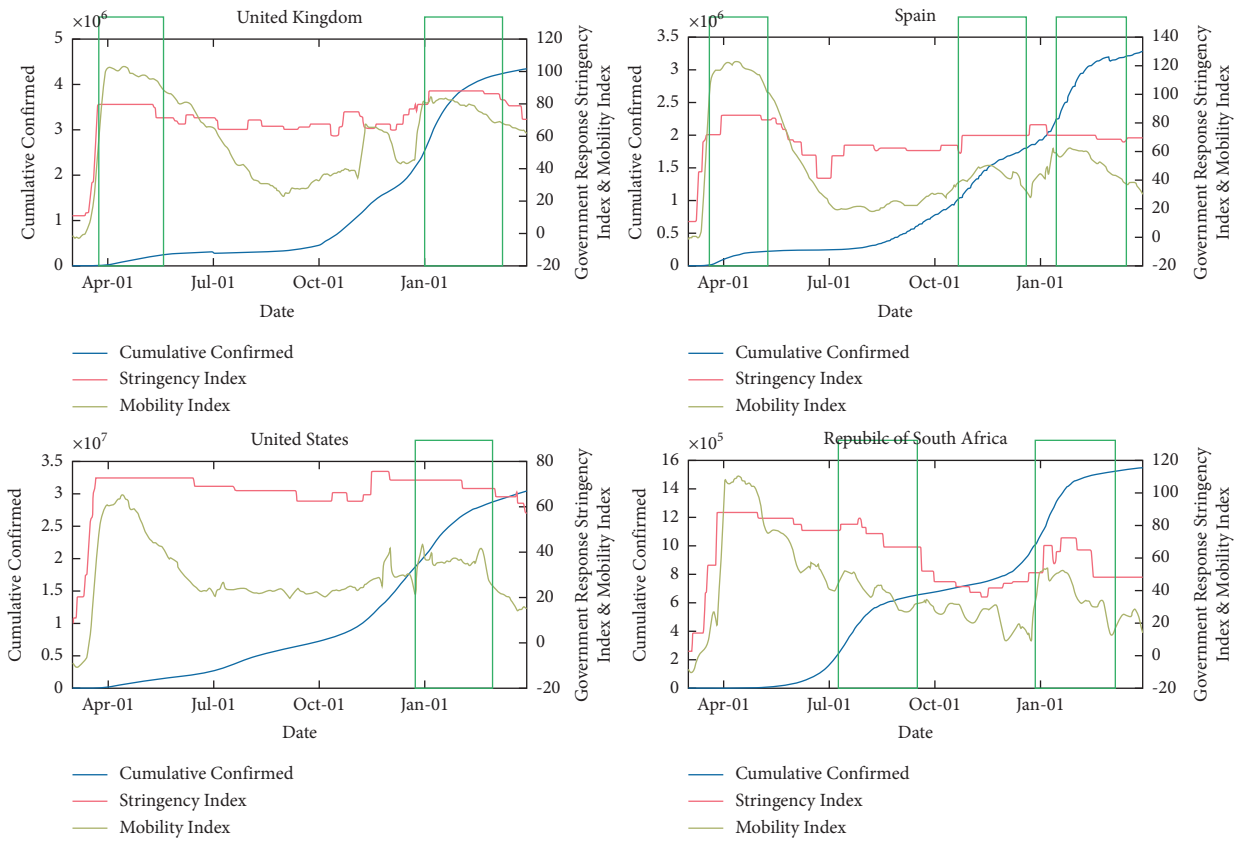

Figure 7: Cumulative confirmed cases, stringency index, and mobility index in the United Kingdom, Spain, the United States, and the Republic of South Africa (March 1, 2020–March 31, 2020).

Table 3: The buffer levels of the weakening buffer operator for different countries.

	ITA	ESP	GBR	JPN	USA	RSA	CHN
SBO	0.08	0.17	0	0.11	0.01	0.15	1.09

ITA, EPS, GBR, JPN, USA, RSA, and CHN indicate Italy, Spain, the United Kingdom, Japan, the United States, the Republic of South Africa, and mainland China separately.

Table 4: The prediction performance.

	FGM		FGM + WBO		GM (1, 1)	
	MAPE (%)	RMSE	MAPE (%)	RMSE	MAPE (%)	RMSE
ITA	0.938	1941.600	0.724	1056.425	3.314	4421.660
ESP	0.527	1195.532	0.114	262.480	0.867	2332.846
GBR	1.380	1912.883	1.380	1912.883	4.836	6042.056
JPN	1.370	198.692	0.572	84.863	3.201	576.989
USA	0.453	4070.153	0.464	3822.088	3.932	27981.766
RSA	1.534	9100.926	1.430	8387.564	1.539	9069.371
CHN	0.757	763.740	0.354	303.324	0.576	536.375

ITA, EPS, GBR, JPN, USA, RSA, and CHN indicate Italy, Spain, the United Kingdom, Japan, the United States, the Republic of South Africa, and mainland China separately.

from publicly available sources such as news articles and government press releases. COVID-19 Community Mobility Reports published by Google are considered to measure the effect of each government's control measures. The Community Mobility Report dataset is presented by location and highlights the percent change in visits to places such as retail and recreation places, grocery and pharmacy stores, parks within a geographic area, and staying at residence. Consider grocery and pharmacy stores are very necessary in daily life, and the visits to parks also depend on the weather, for example, the public go to parks more often in summer than in winter. Moreover, the most important prevention

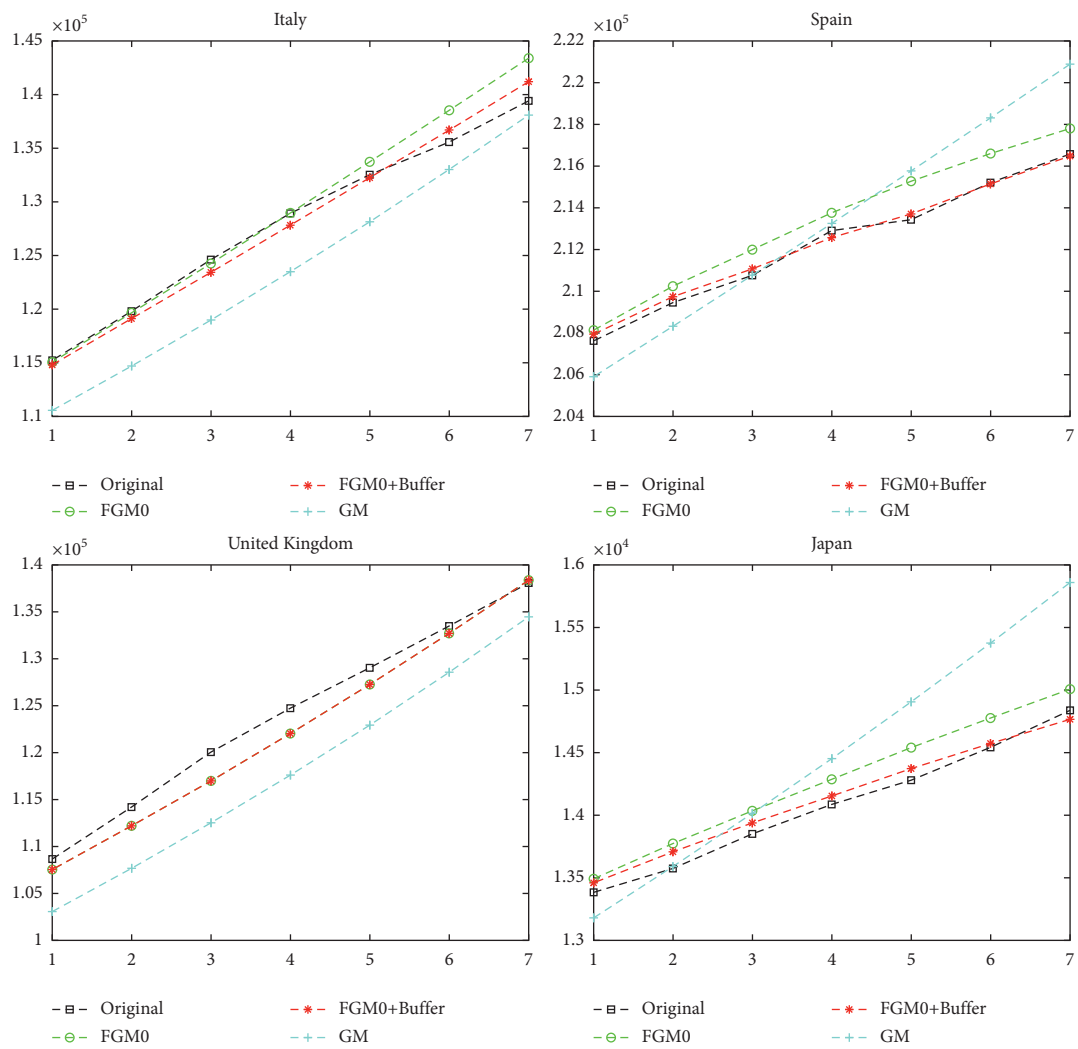

Figure 8: The prediction performance after the government's control measures took effect (part 1).

measure is home quarantine order. This paper only considers the percent change in visits to places such as retail and recreation and staying at residence. Due to the home quarantine order, people reduce unnecessary visits. The percentage change in visits to places such as retail and recreation is negative, and the percentage change in staying at home is positive. This paper considers the absolute percentage change. Because people visit retail and recreation places more frequently in the weekend than in the workdays, the seven-day moving average is also applied in processing the data. This paper uses the seven-day moving average of the summation of the absolute percentage changes in visits to retail and recreation places and staying at home to measure the level that the public comply with the government's prevention measures.

Mainland China was the first region which controlled the spread of COVID-19 well because the Chinese government took strong prevention measures, and the public actively cooperated. Figure 4 shows the stringency index and the cumulative confirmed cases in China from January 15, 2020, to March 15, 2020 (Because Google has no business in mainland China, Community Mobility Reports do not contain any data about mainland China.). It can be found that, about twenty days (from January 26 to February 16) after the stringency index increased dramatically, the daily confirmed cases began to decrease (There was a sharp increase on February 12 because the clinically diagnosed cases were included into the confirmed cases. The detection ability of nucleic acid in the early stage is limited, and there are errors in nucleic acid detection. This measure enabled patients to receive intensive treatment earlier while reducing the risk of community transmission.). Figure 5 illustrates the cumulative confirmed cases, stringency index, and mobility index of Japan. It can be found that there are three periods in that the growth rate of cumulative confirmed cases slowed down. Period 1 is in the early spring, and period 3 is in the winter. Both seasons are easy to break out for COVID-19. However, due to the strict prevention of the government (measured by the stringency index) and the active cooperation of people (measured by the mobility index), the number of confirmed cases has changed from rapid growth to low growth. Part of the reasons for the slow growth in period 2 is summer is not the high-incidence season. Refer to Italy; there are two periods in that the growth rate of

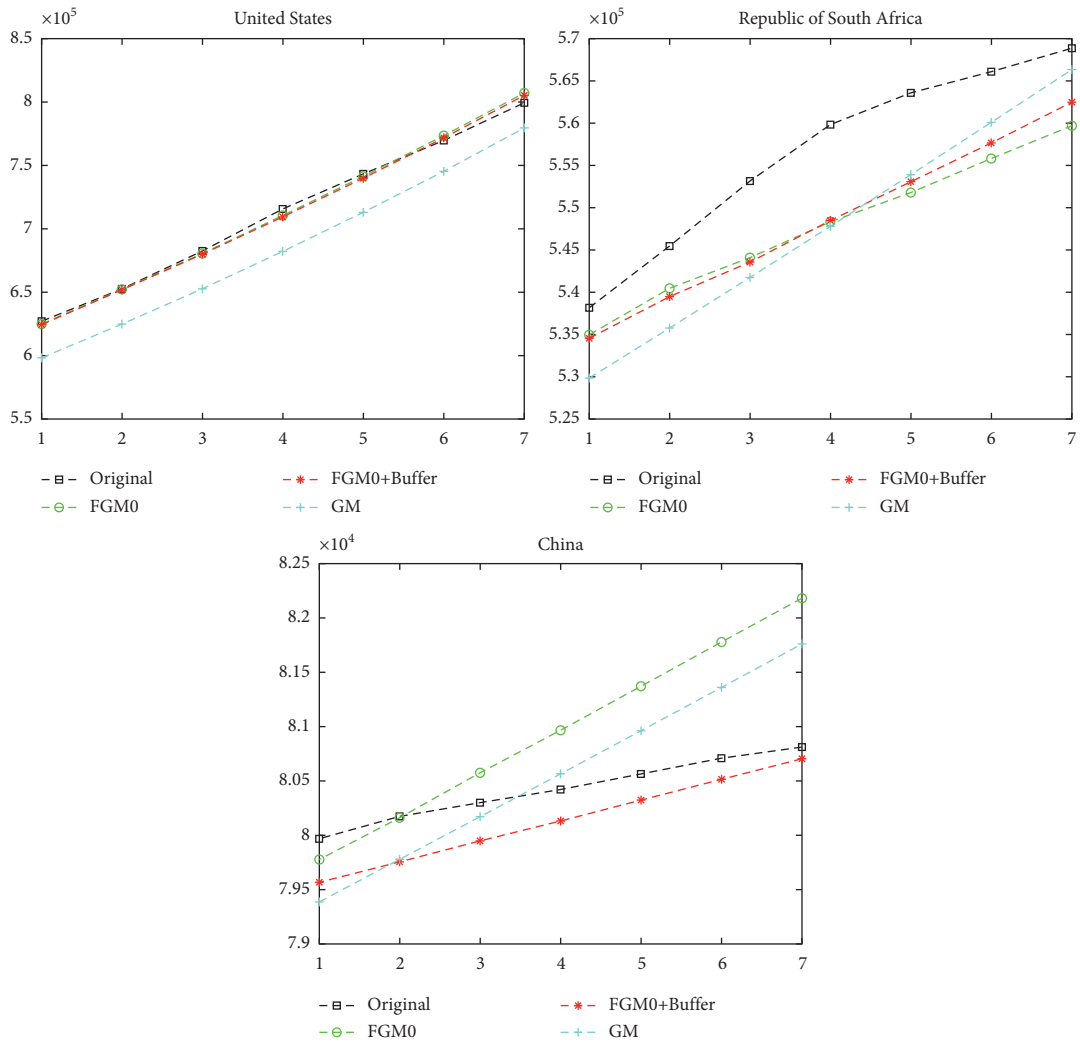

Figure 9: The prediction performance after the government's control measures took effect (part 2).

Table 5: The prediction performance in the second outbreak.

	FGM		FGM + WBO		GM (1, 1)	
	MAPE (%)	RMSE	MAPE (%)	RMSE	MAPE (%)	RMSE
ITA	2.166	29078.137	1.314	16297.286	4.490	43236.182
ESP	1.153	15756.608	1.246	16753.955	1.307	15307.242
GBR	0.285	4627.756	0.285	4627.756	1.697	20850.792
JPN	0.788	3496.378	0.716	2499.642	2.190	7388.862
USA	1.045	185861.267	1.012	180634.907	1.925	290226.135
RSA	0.488	8024.826	0.457	6444.510	2.375	29474.302

(1) ITA, EPS, GBR, JPN, USA, and RSA indicate Italy, Spain, the United Kingdom, Japan, the United States, and the Republic of South Africa separately. (2) Since there is no large-scale outbreak in China at the end of 2020, this paper did not analyze China's data here.

cumulative confirmed cases decreased (shown in Figure 6). In both periods, the stringency index and the mobility index increased. Especially in the first half of the second period, there was an obvious turning point in the growth of the cumulative confirmed cases. However, due to the impact of Christmas and New Year holidays, the mobility index dropped sharply, which did not further reduce the growth rate of confirmed cases. From the growth chart of confirmed cases in China, Japan, and Italy, we found a similar rule: the government's strict prevention and control measures and the public's cooperation (such as reducing aggregation and home isolation) can slow down the growth rate of confirmed cases. The growths of confirmed cases in the United Kingdom, Spain, the United States, and the Republic of South Africa also show this rule (see Figure 7).

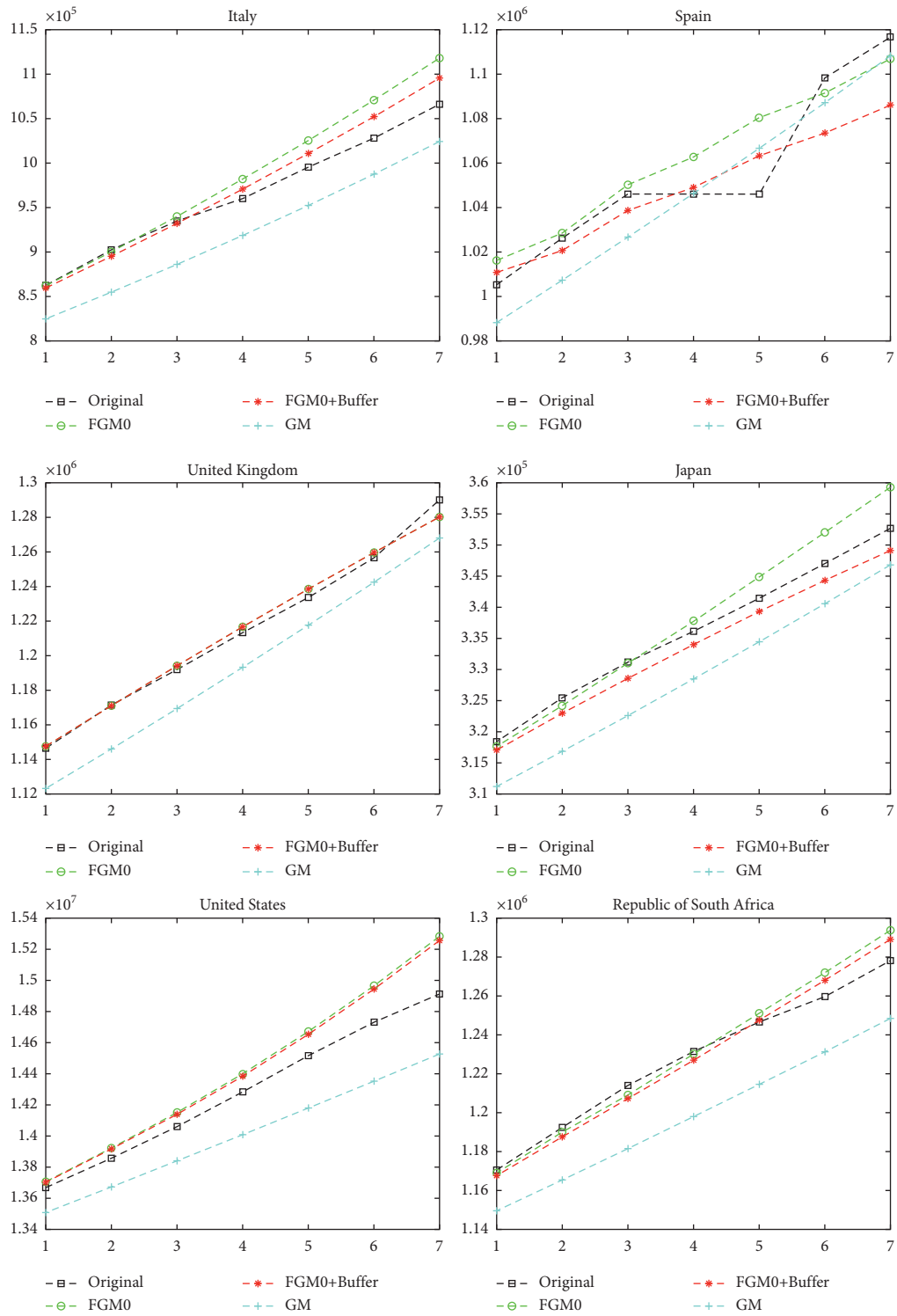

Figure 10: The prediction performance after the government's control measures took effect in the second outbreak of COVID-19.

Because the government's strict prevention and control and the public's cooperation can slow down the growth rate of confirmed cases, it is necessary to bring in the weakening buffer operator. Since the maximum incubation period of COVID-19 is 14 days proposed by both the WHO and European Center for Disease Prevention and Control [38], the growth rate of cumulative confirmed cases slowed down from the fourteenth day after the stringency index and mobility index increased. With the same method of estimating the strengthening buffer operator, the starting point of the training set is the 10th day after the stringency index and mobility index increased in the first outbreak (for the Northern Hemisphere countries, the first outbreak started from March). The orders of weakening buffer operators for

the sample countries are shown in Table 3. Because the buffer operator is used together with the FGM and FGM is suitable for the prediction of nonexponential growth, the order of the weakening buffer operator is zero for the United Kingdom.

Then, this paper used the last five data of the training set as the in-sample data to predict the next seven data. The results indicate that the FGM with the weakening buffer operator has the smallest RMSE for all the countries. It also has the smallest MAPE for Italy, Spain, the United Kingdom, Japan, the Republic of South Africa, and China, except the United States (Table 4). The prediction results are also displayed in Figures 8 and 9.

In the end of 2020, COVID-19 broke out twice in a lot of countries. When the governments realized the second outbreak of the epidemic, they raised the level of government prevention and control again. At the same time, residents reduced unnecessary travel and increased the time of home isolation. So, this paper used the same fractional order of the weakening buffer operator and the first five data after the government stringency index and mobility index both increased for ten days to test the reliability. The results are indicated in Table 5. It can be found that, except Spain, the FGM with the fractional weakening buffer operator performs better than other two models. Although the FGM with the fractional weakening buffer operator does not achieve the smallest MAPE and RMSE, it beats GM (1, 1) with Spain's data, and it has similar results to the FGM (shown in Figure 10). Also, the FGM with the fractional weakening buffer operator and the FGM have similar prediction accuracy.

Some of the characteristics of COVID-19 have been mastered by scientists; however, because of its strong variability and high contagion, COVID-19 is still not defeated by human beings. With the improvement of vaccination rate and public awareness of self-protection, the number of newly diagnosed patients in most countries is no longer increasing exponentially. The practitioners can use the FGM with the weakening buffer operator to predict the trend of the epidemic through continuously adding new data to estimate the appropriate buffer levels. Because the FGM is suitable for predicting nonexponential growth [18, 39] and the weakening buffer operator reflects the effect of government prevention measures and vaccination, the combination of the FGM and weakening buffer operator through the rolling mechanism is suitable in the future. However, when a more infectious mutation appears, the strengthening buffer operator should be considered.

4. Conclusion

In this study, we use the FGM combined with the fractional-order buffer operator to predict the cumulative confirmed cases of COVID-19. FGM is one of the forefront methods in grey system modeling. It makes full use of known information under the condition of less data environment and has an excellent performance in predicting the future trend. Combining the fractional-order buffer operator with the FGM in an appropriate way can improve the forecasting accuracy. By analyzing the characteristics of the epidemic in different stages, this study proposes to introduce different buffer operators in the prediction process. The examples of Italy, Spain, the United Kingdom, Japan, the USA, the Republic of South Africa, and China show that the FGM combined with the fractional-order buffer operator can improve the prediction accuracy.

In practice, this paper finds that only when government pandemic control measures are in place and people respond actively to these measures, the spread of COVID-19 is deterred. Appropriate use of the buffer level according to government stringency and mobility can improve the predictive accuracy. Buffer levels are obtained from countries' historical data.

Data Availability

The data on cumulative confirmed cases are collected from the Center for Systems Science and Engineering (CSSE) at Johns Hopkins University (https://coronavirus.jhu.edu/map.html). The data on the stringency index are provided by the Oxford COVID-19 Government Response Tracker (http://www.bsg.ox.ac.uk/covidtracker). The data on the mobility index are based on the COVID-19 Community Mobility Reports published by Google. The stringency index and the number of cumulative confirmed cases are available at https://covid19datahub.io/. The COVID-19 Community Mobility Reports are downloaded from https://www.google.com/covid19/mobility/. The data used to support the findings of this study are also available from the corresponding author upon request.

Conflicts of Interest

The authors declare that there are no conflicts of interest regarding the publication of this article.

Acknowledgments

This work was supported by the National Natural Science Foundation of China (71701127, 42176217, and 72073086) and National Statistical Science Research (2020LY048).

References

[1] K. M. Furati, I. O. Sarumi, and A. Q. M. Khaliq, "Fractional model for the spread of covid-19 subject to government intervention and public perception," *Applied Mathematical Modelling*, vol. 95, no. 89–105, pp. 89–105, 2021.

[2] A. E. Aboanber, A. A. Nahla, and S. M. Aljawazneh, "Fractional two energy groups matrix representation for nuclear reactor dynamics with an external source," *Annals of Nuclear Energy*, vol. 153, 2021.

[3] C. Xu, Z. Liu, M. Liao, P. Li, Q. Xiao, and S. Yuan, "Fractional-order bidirectional associate memory (BAM) neural networks with multiple delays: the case of HOPF bifurcation," *Mathematics and Computers in Simulation*, vol. 182, pp. 471–494, 2021.

[4] P. Li, L. Xiong, Z. Wang, M. Ma, and J. Wang, "Fractional-order sliding mode control for damping of subsynchronous

control interaction in DFIG-based wind farms," *Wind Energy*, vol. 23, no. 3, pp. 749–762, 2020.

[5] J. L. Deng, "Control problems of grey systems," *Systems & Control Letters*, vol. 1, no. 5, pp. 288–294, 1982.

[6] S. Liu and Y. Lin, *Grey Information: Theory and Practical Applications*, Springer-Verlag, London, UK, 2006.

[7] T. H. M. El-Fouly, E. F. El-Saadany, M. M. A. Salama, F. E. Salama, and M. Ma, "Improved grey predictor rolling models for wind power prediction," *IET Generation, Transmission & Distribution*, vol. 1, no. 6, pp. 928–937, 2007.

[8] T.-Y. Pai, "Gray and neural network prediction of effluent from the wastewater treatment plant of industrial park using influent quality," *Environmental Engineering Science*, vol. 25, no. 5, pp. 757–766, 2008.

[9] R.-C. Tsaur, "Forecasting analysis by using fuzzy grey regression model for solving limited time series data," *Soft Computing*, vol. 12, no. 11, pp. 1105–1113, 2008.

[10] L. Tu and Y. Chen, "An unequal adjacent grey forecasting air pollution urban model," *Applied Mathematical Modelling*, vol. 99, pp. 260–275, 2021.

[11] J. Deng, *The Basis of Grey Theory*, Press of Huazhong University of Science & Technology, Wuhan, China, 2002.

[12] Z.-X. Wang, Y.-G. Dang, and S.-F. Liu, "Unbiased grey verhulst model and its application," *Systems Engineering-Theory & Practice*, vol. 29, no. 10, pp. 138–144, 2009.

[13] C.-I. Chen, "Application of the novel nonlinear grey Bernoulli model for forecasting unemployment rate," *Chaos, Solitons & Fractals*, vol. 37, no. 1, pp. 278–287, 2008.

[14] Z.-X. Wang, K. W. Hipel, Q. Wang, and S.-W. He, "An optimized NGBM (1, 1) model for forecasting the qualified discharge rate of industrial wastewater in China," *Applied Mathematical Modelling*, vol. 35, no. 12, pp. 5524–5532, 2011.

[15] L. Wu, S. Liu, L. Yao, S. Yan, and D. Liu, "Grey system model with the fractional order accumulation," *Communications in Nonlinear Science and Numerical Simulation*, vol. 18, no. 7, pp. 1775–1785, 2013.

[16] F. Liu, W. Guo, R. Li, and J. Liu, "Improved load forecasting model based on two-stage optimization of gray model with fractional order accumulation and Markov chain," *Communications in Statistics-Theory and Methods*, vol. 50, pp. 1–15, 2019.

[17] L. Zeng, "Analysing the high-tech industry with a multivariable grey forecasting model based on fractional order accumulation," *Kybernetes*, vol. 48, no. 6, pp. 1158–1174, 2019.

[18] W. Wu, X. Ma, B. Zeng, Y. Wang, and W. Cai, "Application of the novel fractional grey model FAGMO (1, 1, k) to predict China's nuclear energy consumption," *Energy*, vol. 165, no. B, pp. 223–234, 2018.

[19] L. Liu, Y. Chen, and L. Wu, "Forecasting confirmed cases, deaths, and recoveries from covid-19 in China during the early stage," *Mathematical Problems in Engineering*, vol. 2020, Article ID 1405764, 4 pages, 2020.

[20] S. Liu, "The three axioms of buffer operator and their application," *Journal of Grey System*, vol. 3, no. 1, pp. 39–48, 1991.

[21] Y. Dang, S. Liu, B. Liu, and X. Tang, "Study on the buffer weakening operator," *Chinese Journal of Management Science*, vol. 12, no. 2, pp. 109–112, 2004.

[22] Y. Dang, S. Liu, and C. Mi, "Study on characteristics of the strengthening buffer operators," *Control and Decision*, vol. 22, no. 7, pp. 730–734, 2007.

[23] Z. Wang, Y. Dang, and S. Liu, "Study on buffer operators with variable weights and their effect strength to original sequence," *Control and Decision*, vol. 24, no. 8, pp. 1218–1222, 2007.

[24] L. Wu, S. Liu, and Y. Yang, "Using the fractional order method to generalize strengthening buffer operator and weakening buffer operator," *IEEE/CAA Journal of Automatica Sinica*, vol. 5, no. 6, pp. 1074–1078, 2018.

[25] G. Perone, *An ARIMA Model to Forecast the Spread and the Final Size of Covid-2019 Epidemic in Italy*, HEDG-WP University of York, London, UK, 2020.

[26] S. K. Sharma, S. Bhardwaj, R. Bhardwaj, and M. Alowaidi, "Nonlinear time series analysis of pathogenesis of covid-19 pandemic spread in Saudi Arabia," *CMC-Computers Materials & Continua*, vol. 66, no. 1, pp. 805–825, 2021.

[27] O. D. Ilie, R. O. Cojocariu, A. Ciobica, S. I. Timofte, I. Mavroudis, and B. Doroftei, "Forecasting the spreading of covid-19 across nine countries from Europe, Asia, and the American continents using the ARIMA models," *Microorganisms*, vol. 8, no. 8, 2020.

[28] S. K. Tamang, P. D. Singh, and B. Datta, "Forecasting of covid-19 cases based on prediction using artificial neural network curve fitting technique," *Global Journal of Environmental Science and Management*, vol. 6, pp. 53–64, 2020.

[29] B. B. Hazarika and D. Gupta, "Modelling and forecasting of covid-19 spread using wavelet-coupled random vector functional link networks," *Applied Soft Computing*, vol. 96, 2020.

[30] V. K. R. Chimmula and L. Zhang, "Time series forecasting of covid-19 transmission in Canada using lstm networks," *Chaos, Solitons & Fractals*, vol. 135, 2020.

[31] S. Khajanchi and K. Sarkar, "Forecasting the daily and cumulative number of cases for the covid-19 pandemic in India," *Chaos*, vol. 30, no. 7, p. 71101, 2020.

[32] I. Cooper, A. Mondal, and C. G. Antonopoulos, "A sir model assumption for the spread of covid-19 in different communities," *Chaos, Solitons, and Fractals*, vol. 139, Article ID 110057, 2020.

[33] F. G. Santeramo, M. Tappi, and E. Lamonaca, "On the management of covid-19 pandemic in Italy," *Health Policy*, vol. 125, no. 8, pp. 995–1001, 2021.

[34] Y. Tsori and R. Granek, "Epidemiological model for the inhomogeneous spatial spreading of covid-19 and other diseases," *PLoS One*, vol. 16, no. 2, 2021.

[35] J. Chen and Z. Wu, "A positive real order weakening buffer operator and its applications in grey prediction model," *Applied Soft Computing*, vol. 99, 2021.

[36] X. H. Gao and L. Wu, "Using fractional order weakening buffer operator to forecast the main indices of online shopping in China," *Grey Systems: Theory and Application*, vol. 9, no. 1, pp. 128–140, 2019.

[37] W. Li and X. Han, "Geometrical variable weights buffer GM (1, 1) model and its application in forecasting of China's energy consumption," *Journal of Applied Mathematics*, vol. 2014, Article ID 131432, 6 pages, 2014.

[38] N. Zaki and E. A. Mohamed, "The estimations of the COVID-19 incubation period: a scoping reviews of the literature," *Journal of Infection and Public Health*, vol. 14, no. 5, pp. 638–646, 2021.

[39] M. Gao, S. Mao, X. Yan, and J. Wen, "Estimation of Chinese CO_2 emission based on a discrete fractional accumulation grey model," *Journal of Grey System*, vol. 27, no. 4, pp. 114–130, 2015.

Hindawi
Journal of Mathematics
Volume 2021, Article ID 4562392, 9 pages
https://doi.org/10.1155/2021/4562392

Research Article

Sliding Mode Matrix-Projective Synchronization for Fractional-Order Neural Networks

Jinman He,[1,2] **Tengfei Lei**,[3] **and Limin Jiang**[1]

[1]*College of Science, Zhongyuan University of Technology, Zhengzhou 451191, China*
[2]*College of Mathematics and Statistics, Zhengzhou University, Zhengzhou 450000, China*
[3]*School of Mechanical and Electrical Engineering, Qilu Institute of Technology, Jinan 250200, China*

Correspondence should be addressed to Jinman He; hejinman1026@163.com and Tengfei Lei; leitengfeicanhe@126.com

Received 29 May 2021; Accepted 1 September 2021; Published 20 September 2021

Academic Editor: Lifeng Wu

This work generalizes the projection scaling factor to a general constant matrix and proposes the matrix-projection synchronization (MPS) for fractional-order neural networks (FNNs) based on sliding mode control firstly. This kind of scaling factor is far more complex than the constant scaling factor, and it is highly variable and difficult to predict in the process of realizing the synchronization for the driving and response systems, which can ensure high security and strong confidentiality. Then, the fractional-order integral sliding surface and sliding mode controller for FNNs are designed. Furthermore, the criterion for realizing MPS is proved, and the reachability and stability of the synchronization error system are analyzed, so that the global MPS is realized for FNNs. Finally, a numerical application is given to demonstrate the feasibility of theory analysis. MPS is more general, so it is reduced to antisynchronization, complete synchronization, projective synchronization (PS), and modified PS when selecting different projective matrices. This work will enrich the synchronization theory of FNNs and provide a feasible method to study the MPS of other fractional-order dynamical models.

1. Introduction

Neural network is an important part of artificial intelligence, which is composed of a large number of highly connected neurons. It is a mathematical model based on the preliminary understanding of the physiological structure and activity mechanism of the brain. The neural network has the unique knowledge representation structure and can process information, learn, and adapt to the unknown system efficiently and quickly, which provide new research ideas for control problems and intelligent information processing. Integer order differential equations cannot describe the memory properties of neurons and the dependence on past history, but the fractional-order calculus [1–4], which has strong memory and hereditary characteristic, contains all of the information from the start point to the current moment and can describe the memory properties and dynamical behaviors of neurons more accurately. Therefore, FNNs can improve the computational ability of neurons, speed up the information transmission of neurons, and solve the problem of parameter identification effectively. With the development of fractional-order calculus, FNNs are becoming more and more popular and their dynamical behaviors have been widely investigated, such as stability [5–8], bifurcations [9], chaos and hyperchaos [10], and synchronization [11–14].

Two systems are called PS when the drive and response systems are synchronized to a scaling factor. Recently, scholars have researched the PS of FNNs and achieved a lot of valuable results. In [15–17], by using different control methods, the authors have researched the PS for FNNs. In [18], Zhang et al. have used the adaptive control method to achieve the PS of FNNs in quaternion field. In [19–21], researchers have explored the PS for fractional-order memristive neural networks with different characters. In [22–24], the authors extend the FNNs to the complex domain and study their PS and quasiprojective synchronization by using different control strategies. In [25], Ding and Shen constructed the fractional-order integral sliding mode

surface, designed fractional-order sliding mode controller, and realized PS for two FNNs with different structures. In [26, 27], by means of the fractional Lyapunov-like method, the authors realized PS in finite-time and mixed $H\infty$/passive projective synchronization for nonidentical FNNs via a new sliding mode controller. In [28], by using sliding mode control, Wu et al. realized the finite-time interlayer PS of fractional-order two-layer networks based on Caputo derivates.

To the best of our knowledge, the scaling factor of PS in most research studies is a diagonal matrix or a fixed constant, but in fact this kind of scaling factor may not ensure high security of communication. Our work will generalize the proportion factor to a general constant matrix, which is far more complex than the constant scaling factor. Also, it is highly variable and difficult to predict in the process of realizing the synchronization for the driving and response systems, which can ensure the high security and strong confidentiality. Based on the characteristics of matrix scaling factor, our work presents a new kind of MPS for FNNs, whose complexity and unpredictability can effectively increase the difficulty for hackers to track the right path, improve the antiattack capability of the system, and enhance the confidentiality of secure communication.

As everyone knows, synchronization of FNNs can be reached via various control methods. Especially, sliding mode control strategy has many important and special advantages, which include low sensitivity to the parameter perturbation and external disturbance, implementation simplicity, and fast response. In our work, because of the complexity of the MPS and nonidentical FNNs, it greatly increases the difficulty of control in actual operation. Hence, it is extremely necessary to use fractional-order sliding mode control strategy to research the global MPS.

According to the above discussion and main research content, our work is divided into the following chapters. Section 2 introduces some lemmas and establishes the FNNs. In Section 3, by using the fractional-order sliding mode control method, MPS is defined and sufficient criterion is proved. As applications, a numerical application is given to demonstrate theory analysis in Section 4. Section 5 concludes the whole work.

2. Preliminaries

Definition 1 (see [1]). Fractional integral for function $f\colon [t_0, +\infty) \longrightarrow R$ is

$$ {}_{t_0}I_t^{\alpha} f(t) = \frac{1}{\Gamma(\alpha)} \int_{t_0}^{t} (t-\xi)^{\alpha-1} f(\xi)\mathrm{d}\xi, \quad (\alpha > 0, t \geq t_0), \tag{1} $$

where $\Gamma(\alpha) = \int_0^{+\infty} e^{-t} t^{\alpha-1}\mathrm{d}t$ is gamma function.

Definition 2 (see [1]). Caputo derivative for a function $f(t) \in C^n([t_0, +\infty), R)$ is defined as

$$ {}_{t_0}^{C}D_t^{\alpha} f(t) = \frac{1}{\Gamma(n-\alpha)} \int_{t_0}^{t} \frac{f^n(\xi)}{(t-\xi)^{\alpha-n+1}}\mathrm{d}\xi, \quad (\alpha > 0, t \geq t_0), \tag{2} $$

where n is the positive integer satisfying $n-1 < \alpha < n$, $f^{(n)}$ is the n-th-order derivative of $f(x)$, and $C^n([t_0, +\infty), R)$ is the space which is composed of n order continuous differentiable functions from $[t_0, +\infty)$ to R. In particular, when $0 < \alpha < 1$, ${}_{t_0}^{C}D_t^{\alpha} f(t) = (1/\Gamma(1-\alpha)) \int_{t_0}^{t} (f'(\xi)/(t-\xi)^{\alpha})\mathrm{d}\xi$; when $\alpha = 1$, the Caputo derivative operation ${}_{t_0}^{C}D_t^{\alpha} f(t)$ is identified with integer order ones $(\mathrm{d}f(t)/\mathrm{d}t)$.

Lemma 1. *If Caputo derivative ${}_{t_0}^{C}D_t^{\alpha} f(t)$ is integrable, then*

$$ {}_{t_0}^{C}I_t^{\alpha}\left({}_{t_0}^{C}D_t^{\alpha} f(t)\right) = f(t) - \sum_{k=0}^{n-1} \frac{f^{(k)}(t_0)}{k!}(t-t_0)^k. \tag{3} $$

Especially, for $0 < \alpha < 1$, one can obtain ${}_{t_0}^{C}I_t^{\alpha}({}_{t_0}^{C}D_t^{\alpha} f(t)) = f(t) - f(t_0)$.

Lemma 2. *For Caputo derivative ${}_{t_0}^{C}D_t^{\alpha} f(t)$, the following equality holds:*

$$ {}_{t_0}^{C}D_t^{1-\alpha}\,{}_{t_0}^{C}D_t^{\alpha} f(t) = {}_{t_0}^{C}D_t^{1} f(t) = \frac{\mathrm{d}f(t)}{\mathrm{d}t}. \tag{4} $$

Lemma 3. *If the constant $C \neq 0$, then ${}_{t_0}^{C}D_t^{\alpha} C = 0$.*

Lemma 4. *If function $f(t) \in L^{\infty}(t_0, t)$, for $\alpha > 0$ and $\beta > 0$, then*

$$ {}_{t_0}^{C}D_t^{\alpha}\,{}_{t_0}^{C}I_t^{\beta} f(t) = {}_{t_0}^{C}D_t^{\alpha-\beta} f(t), \tag{5} $$

when $\alpha = \beta$,

$$ {}_{t_0}^{C}D_t^{\alpha}\left({}_{t_0}^{C}I_t^{\alpha} f(t)\right) = f(t). \tag{6} $$

Lemma 5 (see [2]). *For any time instant $t \geq 0$, if $x(t) \in R$ is continuously differentiable, then the inequality $(1/2)\,{}_a^{C}D_t^{\alpha}[x^2(t)] \leq x(t)\,{}_a^{C}D_t^{\alpha} x(t)\,(0 < \alpha < 1)$ holds; if $x(t) \in R^n$, the inequality $(1/2)\,{}_a^{C}D_t^{\alpha} x^T(t) x(t) \leq x^T(t)\,{}_a^{C}D_t^{\alpha} x(t)$ also holds.*

Lemma 6 (see [6]). *If $f(t) \in C^1([0, +\infty), R)$ is a continuously differentiable function, the inequality*

$$ {}_0^{C}D_t^{\alpha}\left|f(t^+)\right|^{\text{a.e.}} \leq \operatorname{sgn}(f(t))\,{}_0^{C}D_t^{\alpha} f(t), \tag{7} $$

holds almost everywhere, where $0 < \alpha < 1$ and $f(t^+) \overset{\Delta}{=} \lim_{\tau \longrightarrow t^+} f(\tau)$.

Consider two nonidentical FNNs as the drive and response system:

$$\begin{cases} {}_0^C D_t^\alpha x(t) = -Cx(t) + Af(x(t)), \\ z(t) = Px(t), \end{cases} \tag{8}$$

$$\begin{cases} {}_0^C D_t^\alpha y(t) = -Dy(t) + Bg(y(t)) + u(t), \\ \hat{z}(t) = Py(t), \quad (0 < \alpha < 1), \end{cases} \tag{9}$$

where $x(t) = (x_1(t), x_2(t), \ldots, x_n(t))^T \in R^n$ and $y(t) = (y_1(t), y_2(t), \ldots, y_n(t))^T \in R^n$ denote the state variables and $z(t)$ and $\hat{z}(t)$ are the outputs. $f(x(t)) = (f_1(x_1(t)), f_2(x_2(t)), \ldots, f_n(x_n(t)))^T \in R^n$ and $g(y(t)) = (g_1(y_1(t)), g_2(y_2(t)), \ldots, g_n(y_n(t)))^T \in R^n$ are neuron activation functions at time t. n is the number of units. $C = \mathrm{diag}(C_1, C_2, \ldots, C_n)$ and $D = \mathrm{diag}(D_1, D_2, \ldots, D_n)$ are self-regulating parameters of neurons. $A = (A_{ij})_{n\times n}$ and $B = (B_{ij})_{n\times n}$ denote synaptic connection weight matrices. $u(t)$ is the controller to be designed later.

Assumption 1. The continuous neuron activation functions f and g meet Lipschitz condition

$$\begin{aligned} &|f(\phi) - f(\varphi)| < F|\phi - \varphi|, \\ &|g(\phi) - g(\varphi)| < G|\phi - \varphi|, \quad (\phi, \varphi \in R), \end{aligned} \tag{10}$$

where $F, G > 0$ are Lipschitz constants.

3. Main Results

In this part, based on the fractional sliding mode control method, the sliding mode controllers will be designed to research the MPS between systems (8) and (9).

The error function of MPS is

$$e(t) = y(t) - \Lambda x(t), \tag{11}$$

where $e = (e_1, e_2, \ldots, e_n)^T$ and $\Lambda = (\Lambda_{ij})_{n\times n}$ is a general constant matrix.

Definition 3. If any two solutions $x(t)$ and $y(t)$ with initial values $x(0)$ and $y(0)$ meet

$$\lim_{t\longrightarrow+\infty} \|e(t)\|_1 = \lim_{t\longrightarrow+\infty} \|y(t) - \Lambda x(t)\| = 0, \tag{12}$$

systems (8) and (9) are said to be MPS, where $_1 = \sum_{i=1}^n$ denotes the Euclidean norm.

Taking Caputo derivative of both sides of error function $e(t) = y(t) - \Lambda x(t)$ and substituting into (8) and (9), the error system can be obtained as

$$\begin{aligned} {}_0^C D_t^\alpha e(t) &= {}_0^C D_t^\alpha y(t) - \Lambda {}_0^C D_t^\alpha x(t) \\ &= -Dy(t) + Bg(y(t)) + u(t) - \Lambda(-Cx(t) + Af(x(t))) \\ &= -D(y(t) - \Lambda x(t)) - D\Lambda x(t) + B(g(y(t)) - g(\Lambda x(t))) + Bg(\Lambda x(t)) + u(t) \\ &\quad - \Lambda(-Cx(t) + Af(x(t))) \\ &= -De(t) + B(g(y(t)) - g(\Lambda x(t))) - D\Lambda x(t) + Bg(\Lambda x(t)) \\ &\quad - \Lambda(-Cx(t) + Af(x(t))) + u(t), \end{aligned} \tag{13}$$

$$\bar{z}(t) = Pe(t). \tag{14}$$

3.1. Sliding Mode Controller Design. The design principle of sliding mode control is usually to design a suitable sliding surface as required and then construct a controller to force the system to move on the sliding surface and stay on it forever. First, the fractional integral sliding surface is designed as

$$S(t) = e(t) + {}_0^C I_t^\alpha [(C + KP)e(t) - B(g(y(t)) - g(\Lambda x(t)))], \tag{15}$$

where $K \in R^{n\times n}$ is the gain matrix. Integrate system (13) from 0 to t, and using Lemma 1, we have

$$\begin{aligned} {}_0^C I_t^\alpha \left({}_0^C D_t^\alpha e(t)\right) &= e(t) - e(0) \\ &= {}_0^C I_t^\alpha [-De(t) + B(g(y(t)) - g(\Lambda x(t))) - D\Lambda x(t) + Bg(\Lambda x(t)) \\ &\quad - \Lambda(-Cx(t) + Af(x(t))) + u(t)], \end{aligned} \tag{16}$$

then

$$e(t) = e(0) + {}_0^C I_t^\alpha [-De(t) + B(g(y(t)) - g(\Lambda x(t))) - D\Lambda x(t) + Bg(\Lambda x(t)) - \Lambda(-Cx(t) + Af(x(t))) + u(t)]. \tag{17}$$

Next, from equations (15) and (17), we have

$$S(t) = e(0) + {}_0 I_t^\alpha [(C - D + KP)e(t) - D\Lambda x(t) + Bg(\Lambda x(t)) - \Lambda(-Cx(t) + Af(x(t))) + u(t)], \tag{18}$$

and sliding surface (18) and (15) are equivalent. Based on the sliding mode control method, when error system (13) moves on sliding surface, the formulas $S(t) = 0$ and $\dot{S}(t) = 0$ have to be satisfied. Then, one can obtain $\dot{S}(t) = {}_0^C D_t^{1-\alpha} {}_0^C D_t^\alpha S(t) = 0$ by using Lemma 2, which means ${}_0^C D_t^\alpha S(t) = 0$. Using (18) and Lemmas 3 and 4, we obtain

$$\begin{aligned} {}_0^C D_t^\alpha S(t) &= {}_0^C D_t^\alpha e(0) + {}_0^C D_t^\alpha {}_0 I_t^\alpha [(C - D + KP)e(t) - D\Lambda x(t) + Bg(\Lambda x(t)) \\ &\quad - \Lambda(-Cx(t) + Af(x(t))) + u(t)] \\ &= (C - D + KP)e(t) - D\Lambda x(t) + Bg(\Lambda x(t)) - \Lambda(-Cx(t) + Af(x(t))) + u(t) = 0. \end{aligned} \tag{19}$$

From equation (19), the equivalent sliding mode controller is designed as

$$u_{\text{eq}}(t) = -(C - D + KP)e(t) + D\Lambda x(t) - Bg(\Lambda x(t)) + \Lambda(-Cx(t) + Af(x(t))). \tag{20}$$

Substituting controller (20) into (13), the sliding mode error system is described as

$${}_0^C D_t^\alpha e(t) = -(C + KP)e(t) + B(g(y(t)) - g(\Lambda x(t))). \tag{21}$$

Obviously, $e(t) = 0$ is an equilibrium point of (21). In order to make the trajectories of the system reach the sliding surface more efficiently and faster, the reaching law is selected as

$$u_r(t) = -k^* \operatorname{sgn}(S(t)), \tag{22}$$

where the switching gain is $k^* > 0$ and $\operatorname{sgn}(S(t)) = \begin{cases} -1 & S(t) < 0 \\ 0 & S(t) = 0 \\ 1 & S(t) > 0 \end{cases}$. Then, the sliding mode control $u(t)$ is denoted by

$$\begin{aligned} u(t) &= u_{\text{eq}}(t) + u_r(t) \\ &= -(C - D + KP)e(t) + D\Lambda x(t) - Bg(\Lambda x(t)) + \Lambda(-Cx(t) + Af(x(t))) - k^* \operatorname{sgn}(S(t)). \end{aligned} \tag{23}$$

Theorem 1. *According to sliding switching surface (15) and sliding mode controller (23), synchronization error trajectories (13) asymptotically reach sliding surface $S(t) = 0$.*

Proof. Construct a Lyapunov function as

$$V(t) = \frac{1}{2} S^T(t) S(t), \tag{24}$$

taking Caputo derivative of (24) with respect to time t and based on Lemma 5, we obtain

$$\begin{aligned} {}_0^C D_t^\alpha V(t) &\le S^T(t) {}_0^C D_t^\alpha S(t) \\ &= S^T(t)[(C - D + KP)e(t) - D\Lambda x(t) + Bg(\Lambda x(t)) - \Lambda(-Cx(t) + Af(x(t))) + u(t)] \\ &= S^T(t)[-k^* \operatorname{sgn}(S(t))] \\ &= -k^* \|S(t)\|. \end{aligned} \tag{25}$$

As $k^* > 0$, system trajectories asymptotically converge to $S(t) = 0$, which means synchronization error trajectories (21) reach the predetermined sliding surface globally and stay on it forever. □

3.2. Stability Analysis

Theorem 2. *If Assumption 1 and the inequality*

$$C_i > \sum_{j=1}^{n}\left(\sum_{l=1}^{n}\left|k_{jl}P_{li}\right|\right) + \sum_{j=1}^{n}\left(\left|b_{ji}\right|m_i\right), \tag{26}$$

hold, then the drive system (8) and response system (9) can realize MPS based on controller (23).

Proof. First, error system (21) is converted as

$$\begin{aligned}{}_0^C D_t^\alpha e_i(t) &= -C_i e_i(t) - \sum_{j=1}^{n}\left(\sum_{l=1}^{n} k_{il}p_{lj}\right)e_j(t) \\ &\quad + \sum_{j=1}^{n} b_{ij}\left(g_j\left(y_j(t)\right) - tg_j n\left(\sum_{i=1}^{n}\Lambda_{ji}x_i(t)\right)\right).\end{aligned} \tag{27}$$

Next, design Lyapunov function $V(t) = \|e(t)\|_1 = \sum_{i=1}^{n}|e_i(t)|$, according to Assumption 1 and Lemma 6, taking Caputo derivative of Lyapunov function $V(t)$ along error trajectories (21), then

$$\begin{aligned}{}_0^C D_t^\alpha V(t) &= {}_0^C D_t^\alpha\left(\sum_{i=1}^{n}\left|e_i(t)\right|\right) = \sum_{i=1}^{n}{}_0^C D_t^\alpha\left|e_i(t)\right| \le \sum_{i=1}^{n}\operatorname{sgn}\left(e_i(t)\right){}_0^C D_t^\alpha e_i(t) \\ &= \sum_{i=1}^{n}\operatorname{sgn}\left(e_i(t)\right)\left(-C_i e_i(t) - \sum_{j=1}^{n}\left(\sum_{l=1}^{n}k_{il}p_{lj}\right)e_j(t) + \sum_{j=1}^{n}b_{ij}\left(g_j\left(y_j(t)\right) - g_j\left(\sum_{i=1}^{n}\Lambda_{ji}x_i(t)\right)\right)\right) \\ &= \sum_{i=1}^{n}\operatorname{sgn}\left(e_i(t)\right)\left(-C_i e_i(t)\right) - \sum_{i=1}^{n}\operatorname{sgn}\left(e_i(t)\right)\left(\sum_{j=1}^{n}\left(\sum_{l=1}^{n}k_{il}p_{lj}\right)e_j(t)\right) \\ &\quad + \sum_{i=1}^{n}\operatorname{sgn}\left(e_i(t)\right)\left(\sum_{j=1}^{n}b_{ij}\left(g_j\left(y_j(t)\right) - g_j\left(\sum_{i=1}^{n}\Lambda_{ji}x_i(t)\right)\right)\right) \\ &\le \sum_{i=1}^{n}\left[-C_i\left|e_i(t)\right| + \sum_{j=1}^{n}\left(\sum_{l=1}^{n}\left|k_{il}p_{lj}\right|\right)\left|e_j(t)\right| + \sum_{j=1}^{n}\left|b_{ij}\right|G_j\left|e_j(t)\right|\right] \\ &= \sum_{i=1}^{n}\left[-C_i\left|e_i(t)\right| + \sum_{j=1}^{n}\left(\sum_{l=1}^{n}\left|k_{jl}p_{li}\right|\right)\left|e_i(t)\right| + \sum_{j=1}^{n}\left|b_{ji}\right|G_i\left|e_i(t)\right|\right] \\ &= -\sum_{i=1}^{n}\left[C_i - \sum_{j=1}^{n}\left(\sum_{l=1}^{n}\left|k_{jl}p_{li}\right|\right) - \sum_{j=1}^{n}\left|b_{ji}\right|G_i\right]\left|e_i(t)\right|.\end{aligned} \tag{28}$$

Let $\lambda_i = C_i - \sum_{j=1}^{n}\left(\sum_{l=1}^{n}|k_{jl}p_{li}|\right) - \sum_{j=1}^{n}|b_{ji}|G_i$, and we can obtain

$$\lambda = \min_{1\le i\le n}\lambda_i = \min_{1\le i\le n}\left(C_i - \sum_{j=1}^{n}\left(\sum_{l=1}^{n}\left|k_{jl}p_{li}\right|\right) - \sum_{j=1}^{n}\left|b_{ji}\right|G_i\right) > 0, \tag{29}$$

then

$${}_0^C D_t^\alpha V(t) \le -\lambda V(t) = -\lambda\|e(t)\|_1 \le 0, \quad (t \ge 0), \tag{30}$$

and $V(t)$ is monotonously nonincreasing. Hence, $V(t) \le V(0)\,(t \ge 0)$ and $e_i(t)$ is bounded on $t \ge 0$ from the definition of $V(t)$. There exists a positive constant satisfying $|{}^C D^\alpha\|e(t)\|_1| \le M$; then, we claim that $\lim_{t\longrightarrow\infty}\|e(t)\|_1 = 0$ whose proof is similar to Theorem 1 in [16]. Therefore, error system (21) is globally asymptotically stable and MPS between systems (8) and (9) is realized based on controller (23). □

Remark 1. When activating controller (23), response system (9) converts to

$$\begin{aligned}{}_0^C D_t^\alpha y(t) &= -(C + KP)y(t) + (C\Lambda - \Lambda C)x(t) + kp\Lambda x(t) \\ &\quad + Bg(y(t)) - Bg(\Lambda x(t)) + \Lambda A f(x(t)),\end{aligned} \tag{31}$$

and then based on drive system (8), controlled response system (31), and error system (27), the MPS behaviors between systems (8) and (9) can be analyzed furthermore.

Remark 2. Theorems 1 and 2 are still true and new for $\alpha = 1$.

In particular, the MPS is a kind of more general synchronization. Selecting different projection matrices and controllers, it degenerates to some special synchronization types as Remark 3.

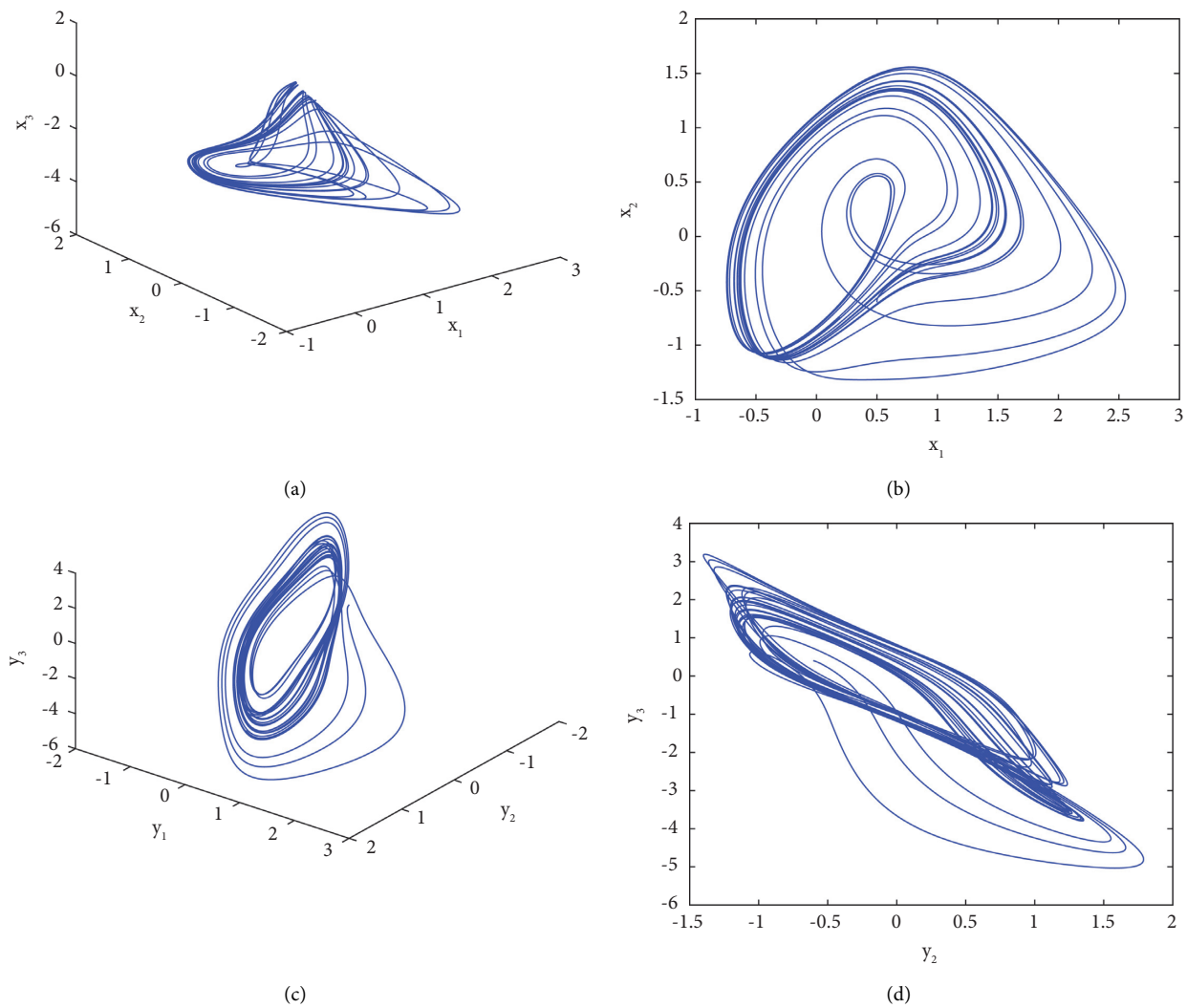

Figure 1: Chaotic behaviors of systems (34) and (35) at $\alpha = 0.98$. (a) $x_1 - x_2 - x_3$ phase portrait of system (34). (b) $x_1 - x_2$ phase portrait of system (34). (c) $y_2 - y_1 - y_3$ phase portrait of system (35). (d) $y_2 - y_3$ phase portrait of system (35).

Remark 3

(1) If $\Lambda = I$, the sliding mode controller becomes

$$\begin{aligned} u(t) &= u_{eq}(t) + u_r(t) \\ &= -(C - D + KP)y(t) + KPx(t) \\ &\quad - Bg(x(t)) + Af(x(t)) - k^* \operatorname{sgn}(S(t)), \end{aligned} \tag{32}$$

where sliding surface $S(t)$ is given by (15), and then systems (8) and (9) can achieve complete synchronization.

(2) If $\Lambda = -I$, based on sliding surface (15), the sliding mode controller becomes

$$\begin{aligned} u(t) &= u_{eq}(t) + u_r(t) \\ &= -(C - D + KP)y(t) - Bg(-x(t)) \\ &\quad - KPx(t) - Af(x(t)) - k^* \operatorname{sgn}(S(t)), \end{aligned} \tag{33}$$

and then systems (8) and (9) can realize antisynchronization.

(3) If $\Lambda = cI$ ($c = \text{const}$ and $c \neq \pm 1$), the sliding mode controller is similar to (23) and sliding surface $S(t)$ is given by (15), and then systems (8) and (9) can achieve the PS.

(4) If $\Lambda = \operatorname{diag}(c_1, c_2, \ldots, c_n)$ ($c_i = \text{const}, i = 1, 2, \ldots, n$) and at least two c_i of them are unequal, the sliding mode controller is similar to (23) and sliding surface $S(t)$ is given by (15), and then systems (8) and (9) can achieve the modified PS.

4. Numerical Application

Two nonidentical drive and response systems are considered as

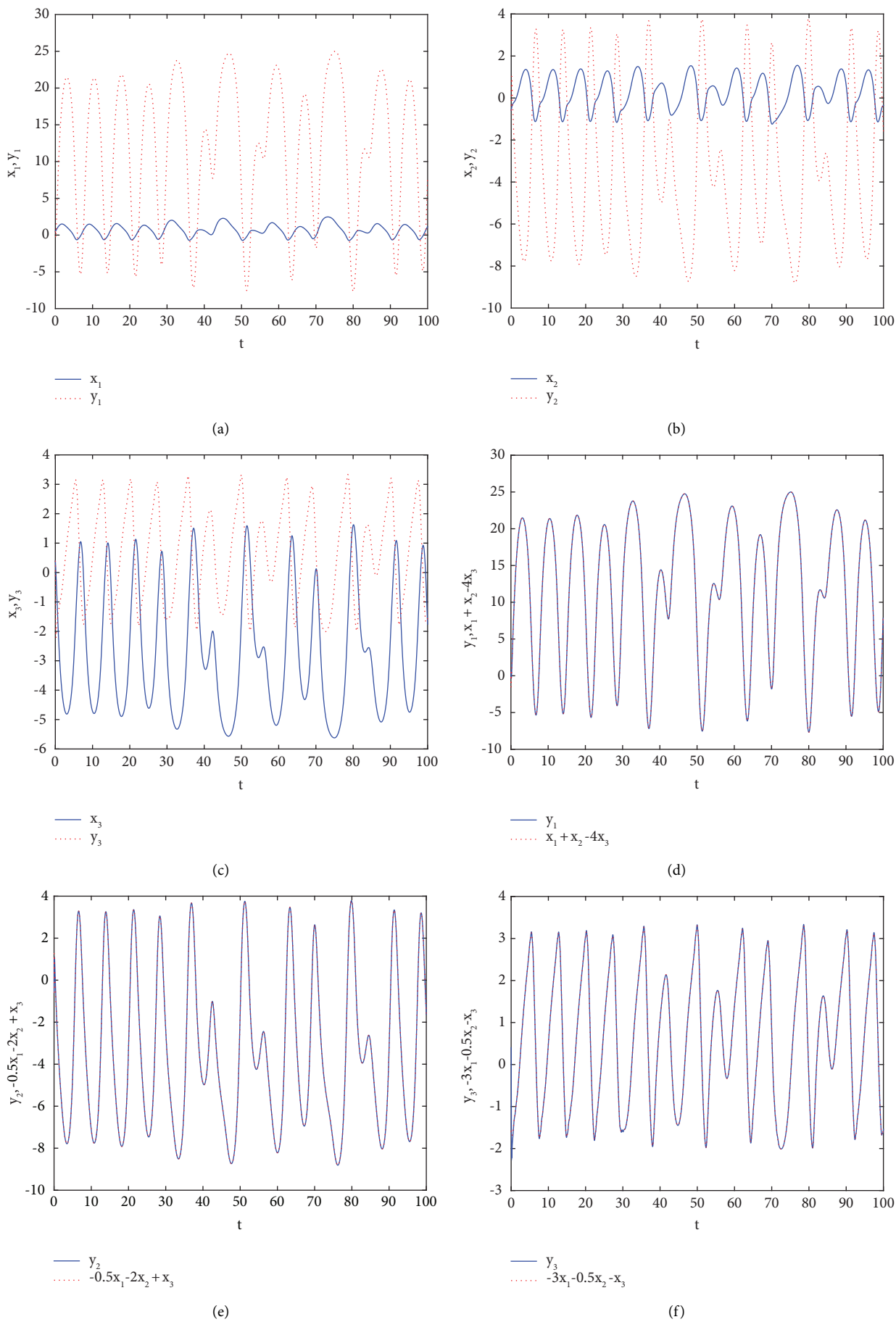

Figure 2: MPS behaviors between systems (34) and (35). Time history of (a) x_1, y_1; (b) x_2, y_2; (c) x_3, y_3; (d) $x_1 + x_2 - 4x_3, y_1$; (e) $-0.5x_1 - 2x_2 + x_3, y_2$; and (f) $-3x_1 - 0.5x_2 - x_3, y_3$.

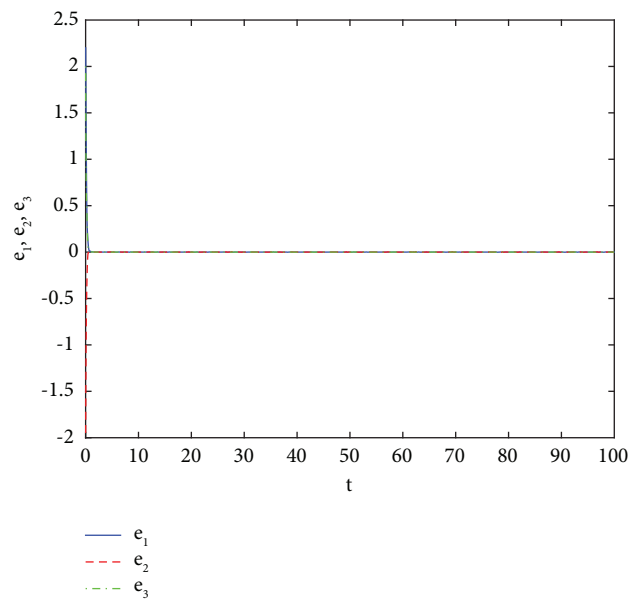

Figure 3: Trajectories of synchronization errors e_1, e_2, and e_3.

$$\begin{cases} {}_0^C D_t^\alpha x(t) = -Cx(t) + Af(x(t)), \\ z(t) = Px(t), \end{cases} \tag{34}$$

$$\begin{cases} {}_0^C D_t^\alpha y(t) = -Dy(t) + Bg(y(t)) + u(t), \\ \hat{z}(t) = Py(t), \end{cases} \tag{35}$$

where $C = D = \begin{pmatrix} 1 & 0 & 0 \\ 0 & 1 & 0 \\ 0 & 0 & 1 \end{pmatrix}$, $A = \begin{pmatrix} 2 & -1.2 & 0 \\ 1.8 & 1.71 & 1.15 \\ -4.75 & 0 & 1.1 \end{pmatrix}$, $B = \begin{pmatrix} 2.5 & -1.5 & 0 \\ 2 & 1.7 & 1.2 \\ -4.7 & 0 & 1 \end{pmatrix}$, $P = \begin{pmatrix} 1 & 0 & 0 \\ 0 & 1 & 0 \\ 0 & 0 & 1 \end{pmatrix}$, $f(x(t)) = \tanh(x(t))$, $g(y(t)) = \tanh(y(t))$, and $u(t)$ is the controller. In order to analyze chaotic synchronization for systems (34) and (35), the value of derivative order is chosen as $\alpha = 0.98$, which causes the two systems to exhibit chaotic behaviors described in Figures 1(a)–1(d) with initial conditions $[x_1(0), x_2(0), x_3(0)] = [y_1(0), y_2(0), y_3(0)] = [0.5, -0.6, 0.4]$.

Projection matrix Λ is chosen as

$$\Lambda = \begin{pmatrix} 1 & 1 & -4 \\ -0.5 & -2 & 1 \\ -3 & -0.5 & -1 \end{pmatrix}, \tag{36}$$

and then error functions are calculated as

$$\begin{aligned} e_1 &= y_1 - \sum_{j=1}^{3} \Lambda_{1j} x_j = y_1 - (x_1 + x_2 - 4x_3), \\ e_2 &= y_2 - \sum_{j=1}^{3} \Lambda_{2j} x_j = y_2 - (-0.5x_1 - 2x_2 + x_3), \\ e_3 &= y_3 - \sum_{j=1}^{3} \Lambda_{3j} x_j = y_3 - (-3x_1 - 0.5x_2 - x_3). \end{aligned} \tag{37}$$

Next, choosing $k_1 = 5, k_2 = 5, k_3 = 5$, and $k^* = 20$ and according to Theorems 1 and 2, the MPS between systems (34) and (35) is realized.

Figures 2(a)–2(c) depict the time trajectories of variables $x_1 \sim y_1$, $x_2 \sim y_2$, and $x_3 \sim y_3$. Simultaneously, it is clearly seen that variables $x_1 + x_2 - 4x_3 \sim y_1$, $-0.5x_1 - 2x_2 + x_3 \sim y_2$, and $-3x_1 - 0.5x_2 - x_3 \sim y_3$ realize the complete synchronization as depicted in Figures 2(d)–2(f). Figure 3 describes that the synchronization error trajectories converge to zero asymptotically for drive system (34) and response system (35). These numerical simulations and figures clearly indicate the applicability and effectiveness of the sliding controller for MPS.

5. Conclusions

For general FNNs, the paper comes up with the global MPS, constructs the fractional-order sliding surface, designs a sliding mode controller, establishes and proves the sufficient condition, and then realizes the global MPS. Our theory analysis provides important theoretical basis and technical support for enhancing signal security by using MPS of FNNs and contributes to the development of artificial intelligence. In future works, we will extend the MPS to the fractional-order memristive neural networks and consider applying them into secret communication.

Data Availability

The data used to support the findings of this study are included within the article.

Conflicts of Interest

The authors declare that there are no conflicts of interest regarding the publication of this paper.

Acknowledgments

This work was supported by the National Natural Science Foundation of China (12102492).

References

[1] A. K. Anatoly, *Theory and Applications of Fractional Differential Equations*, Elsevier, Netherlands, 2006.

[2] N. Aguila-Camacho, M. A. Duarte-Mermoud, and J. A. Gallegos, "Lyapunov functions for fractional order systems," *Communications in Nonlinear Science and Numerical Simulation*, vol. 19, no. 9, pp. 2951–2957, 2014.

[3] L. Wu, S. Liu, and Y. Yang, "Using the fractional order method to generalize strengthening buffer operator and weakening buffer operator," *IEEE/CAA Journal of Automatica Sinica*, vol. 5, no. 6, pp. 1074–1078, 2018.

[4] Y. Chen, L. F. Wu, L. Y. Liu, and K. Zhang, "Fractional Hausdorff grey model and its properties," *Chaos, Solitons & Fractals*, vol. 138, Article ID 109915, 2020.

[5] S. Liang, R. Wu, and L. Chen, "Comparison principles and stability of nonlinear fractional-order cellular neural networks with multiple time delays," *Neurocomputing*, vol. 168, pp. 618–625, 2015.

[6] S. Zhang, Y. Yu, and H. Wang, "Mittag-Leffler stability of fractional-order Hopfield neural networks," *Nonlinear Analysis: Hybrid Systems*, vol. 16, pp. 104–121, 2015.

[7] L. Zhang, Q. Song, and Z. Zhao, "Stability analysis of fractional-order complex-valued neural networks with both leakage and discrete delays," *Applied Mathematics and Computation*, vol. 298, pp. 296–309, 2017.

[8] L.-L. Huang, J. H. Park, G.-C. Wu, and Z.-W. Mo, "Variable-order fractional discrete-time recurrent neural networks," *Journal of Computational and Applied Mathematics*, vol. 370, Article ID 112633, 2020.

[9] C. Huang, J. Cao, M. Xiao, A. Alsaedi, and T. Hayat, "Bifurcations in a delayed fractional complex-valued neural network," *Applied Mathematics and Computation*, vol. 292, pp. 210–227, 2017.

[10] X. Huang, Z. Zhao, Z. Wang, and Y. Li, "Chaos and hyperchaos in fractional-order cellular neural networks," *Neurocomputing*, vol. 94, pp. 13–21, 2012.

[11] H.-L. Li, L. Zhang, C. Hu, H. Jiang, and J. Cao, "Global Mittag-Leffler synchronization of fractional-order delayed quaternion-valued neural networks: direct quaternion approach," *Applied Mathematics and Computation*, vol. 373, Article ID 125020, 2020.

[12] J. He, F. Chen, T. Lei, and Q. Bi, "Global adaptive matrix-projective synchronization of delayed fractional-order competitive neural network with different time scales," *Neural Computing & Applications*, vol. 32, no. 16, pp. 12813–12826, 2020.

[13] X. Huang, Y. Fan, J. Jia, Z. Wang, and Y. Li, "Quasi-synchronisation of fractional-order memristor-based neural networks with parameter mismatches," *IET Control Theory & Applications*, vol. 11, no. 14, pp. 2317–2327, 2017.

[14] J. M. He, F. Q. Chen, and Q. S. Bi, "Quasi-matrix and quasi-inverse-matrix projective synchronization for delayed and disturbed fractional order neural network," *Complexity*, vol. 2019, Article ID 4823709, 15 pages, 2019.

[15] H. Q. Wu, L. F. Wang, Y. Wang, P. F. Niu, and B. L. Fang, "Global Mittag-Leffler projective synchronization for fractional-order neural networks: an LMI-based approach," *Advances in Difference Equations*, vol. 132, 2016.

[16] J. Yu, C. Hu, H. Jiang, and X. Fan, "Projective synchronization for fractional neural networks," *Neural Networks*, vol. 49, pp. 87–95, 2014.

[17] J. Yu, C. Hu, and H. Jiang, "Corrigendum to "Projective synchronization for fractional neural networks"," *Neural Networks*, vol. 67, pp. 152–154, 2015.

[18] W. Zhang, C. Sha, J. Cao, G. Wang, and Y. Wang, "Adaptive quaternion projective synchronization of fractional order delayed neural networks in quaternion field," *Applied Mathematics and Computation*, vol. 400, Article ID 126045, 2021.

[19] S. Yang, C. Hu, J. Yu, and H. Jiang, "Projective synchronization in finite-time for fully quaternion-valued memristive networks with fractional-order," *Chaos, Solitons & Fractals*, vol. 147, Article ID 110911, 2021.

[20] H.-B. Bao and J.-D. Cao, "Projective synchronization of fractional-order memristor-based neural networks," *Neural Networks*, vol. 63, pp. 1–9, 2015.

[21] L. Zhang, Y. Yang, and F. Wang, "Projective synchronization of fractional-order memristive neural networks with switching jumps mismatch," *Physica A: Statistical Mechanics and Its Applications*, vol. 471, pp. 402–415, 2017.

[22] Q. Xu, X. Xu, S. Zhuang, J. Xiao, C. Song, and C. Che, "New complex projective synchronization strategies for drive-response networks with fractional complex-variable dynamics," *Applied Mathematics and Computation*, vol. 338, pp. 552–566, 2018.

[23] S. Yang, J. Yu, C. Hu, and H. Jiang, "Quasi-projective synchronization of fractional-order complex-valued recurrent neural networks," *Neural Networks*, vol. 104, pp. 104–113, 2018.

[24] H. Du, "Modified function projective synchronization between two fractional-order complex dynamical networks with unknown parameters and unknown bounded external disturbances," *Physica A: Statistical Mechanics and Its Applications*, vol. 526, Article ID 120997, 2019.

[25] Z. Ding and Y. Shen, "Projective synchronization of nonidentical fractional-order neural networks based on sliding mode controller," *Neural Networks*, vol. 76, pp. 97–105, 2016.

[26] H. Wu, L. Wang, P. Niu, and Y. Wang, "Global projective synchronization in finite time of nonidentical fractional-order neural networks based on sliding mode control strategy," *Neurocomputing*, vol. 235, pp. 264–273, 2017.

[27] S. Song, X. N. Song, and I. T. Balsera, "Mixed $H\infty$/passive projective synchronization for nonidentical uncertain fractional-order neural networks based on adaptive sliding mode control," *Neural Processing Letters*, vol. 47, pp. 443–462, 2018.

[28] X. Wu, H. Bao, and J. Cao, "Finite-time inter-layer projective synchronization of Caputo fractional-order two-layer networks by sliding mode control," *Journal of the Franklin Institute*, vol. 358, no. 1, pp. 1002–1020, 2021.

Hindawi
Journal of Mathematics
Volume 2021, Article ID 3793522, 13 pages
https://doi.org/10.1155/2021/3793522

Research Article

Regional Heterogeneity of Carbon Emissions and Peaking Path of Carbon Emissions in the Bohai Rim Region

Chuanhui Wang,[1] **Mengzhen Zhao**,[1] **Weifeng Gong**,[1,2] **Zhenyue Fan**,[1] **and Wenwen Li**[1,2]

[1]*School of Economics, Qufu Normal University, Rizhao 276826, China*
[2]*School of Economics and Management, Nanjing University of Aeronautics and Astronautics, Nanjing 211006, China*

Correspondence should be addressed to Weifeng Gong; gongweifeng0539@163.com

Received 8 June 2021; Accepted 24 July 2021; Published 7 September 2021

Academic Editor: Lifeng Wu

Taking the Bohai Rim region as the research object and based on the relevant data of energy consumption, GDP, and energy structure from 2000 to 2019, the total carbon emissions of the provinces and cities from 2020 to 2050 were predicted. The carbon peak situation of each province and municipality in the Bohai Rim region was also analyzed. A comparative analysis of the peaks among the provinces and cities has been carried out. The results show the following: (1) it is predicted that Beijing will reach its carbon peak before 2025. Tianjin is predicted to reach its carbon peak before 2030. Renewable energy development and utilization technologies in the two municipalities are crucial to achieving carbon peaks when energy intensity is already low. (2) Shandong and Shanxi have a heavy energy structure, are coal-minded, and have high energy intensity, while the replacement rate of renewable energy is relatively low. Shandong and Shanxi are predicted to reach carbon peaks around 2030. Liaoning also has the problem of heavy industrial structure, and it is predicted to reach the carbon peak before 2027. (3) Hebei itself relies on Beijing, and its renewable energy utilization technology is relatively advanced. It is predicted to reach the carbon peak before 2026. The energy intensity of Inner Mongolia has decreased rapidly, and it is predicted to reach the carbon peak before 2029. Therefore, according to the forecast results and the analysis of the similarities and differences among the provinces and cities, some specific suggestions for the optimization of the energy structure and the development of renewable energy in each province and city have been proposed in order to promote the comprehensive realization of the regional carbon peak goal in the Bohai Rim region.

1. Introduction

China is the world's second largest economy and one of the world's largest energy consumers. For a long time, one of the important reasons for China's severe carbon emission problem is the energy consumption structure dominated by coal. China's commitment to carbon peaks and carbon emission reductions has brought huge transformation pressures and challenges to the domestic energy structure. On September 22, 2020, the Chinese government delivered an important speech at the general debate of the 75th UN General Assembly. The Chinese government pointed out that "China will increase its nationally determined contributions and adopt more powerful policies and measures. Carbon dioxide emissions will strive to reach a peak before 2030 and strive to achieve carbon neutrality by 2060." The adjustment of the energy structure is a huge practical problem facing China, including the coordinated development of economy, energy, and technology. The improvement of China's energy structure, the effective replacement of traditional energy by new energy, the technical requirements for energy structure adjustment, and the direction of economic development all directly affect the target of peak carbon emissions.

The Bohai Rim region is an important coastal economic circle in China. The land area accounts for about 60% of China's total area, and the gross national product accounts for about 40% of the country. After 2015, the energy consumption in the Bohai Rim region accounted for about 43%

of China's total, and carbon emissions accounted for about 52% of China's total carbon emissions. The development of this region directly affects China's overall economic growth, energy consumption, and technological development. The coordinated development of the Bohai Rim region has promoted the rapid development of China's economy. There are also some practical problems, such as dependence on traditional industries and insufficient energy structure. All these seriously affect China's target of peak carbon emissions in 2030. This paper takes the Bohai Rim region as the research object and uses the basic model of carbon emission prediction to analyze the peak carbon situation of the provinces and municipalities in the Bohai Rim region.

With the increasing public attention to global warming issues, scholars have also conducted comprehensive and in-depth research and analysis on the peaking of carbon emissions in various countries. The research view of most scholars is that most developed countries have already passed the peak of carbon emissions because of their early industrialization. China is the largest developing country and is still in the stage of industrialization and modernization and has not yet reached the peak of carbon emissions. A large number of domestic scholars use different mathematical and economic methods to predict China's future carbon emissions. Some scholars directly use the system model to predict the total amount of carbon emissions in the future. The main methods include the grey prediction model and computable general equilibrium (CGE) model. The grey model was originally used to predict energy consumption demand and supply. Later, the grey model was used to predict carbon emissions. Pao et al. [1] used the nonlinear grey Bernoulli model (NGBM) to predict the three indicators of carbon emissions, energy consumption, and actual output. The forecast results show that, between 2011 and 2020, China's average annual compound emissions, energy consumption, and GDP growth are set to 4.47%, −0.06%, and 6.67%, respectively. Wang and Ye [2] used a nonlinear grey multivariate model to predict the carbon emissions of China's fossil energy consumption. Huang et al. [3] explored sixteen potential factors affecting carbon emissions and used grey correlation analysis to identify factors closely related to carbon emissions. Ye et al. [4] proposed a novel time-delay multivariate grey model to measure the CO_2 emissions' accumulating impact of China's transportation sector. Zhu and Ling [5] used to calculate the general equilibrium theory, construct a dynamic CGE model, and draw the conclusions of carbon emission reduction policies to promote industrial structure optimization. Li et al. [6] used the generalized dividing index method to find that GDP has the highest cumulative contribution rate to carbon emissions in my country's construction industry.

In addition, Grossman and Krueger [7] discussed the environmental Kuznets curve (abbreviation for the "EKC") between environmental conditions and economic growth. Debdatta and Subrata [8] studied the cointegration relationship between carbon dioxide emissions and economic activity and tested the environmental Kuznets curve (EKC) hypothesis. Lin and Jiang [9] used a traditional EKC model simulation and carbon dioxide emission prediction and comparative research and prediction of China's carbon dioxide emissions. Jiang et al. [10] used the environmental Kuznets curve to quantitatively study the relationship between coal consumption, economic development, and carbon emissions, and the results showed that China has not yet reached the "inflection point."

However, most scholars decompose and analyze the influencing factors of carbon emissions and then use scenario analysis to predict future carbon emissions. The main models used to decompose the influencing factors of carbon emissions include the one proposed by Ehrlich and Holdren [11], the model that environment (I) is equal to the product of population (P), affluence (A), and technology (T) (abbreviation for the "IPAT"). The model of stochastic impacts by regression on population, affluence, and technology is abbreviated to the "STIRPAT". The logarithmic mean Divisia index (abbreviation for the "LMDI") decomposition method of carbon dioxide emission driving factors was proposed by Ang et al. [12]. Qu and Guo [13] used the STIRPAT model to predict the peak of China's carbon emissions in the future and proposed that if the economic and social development keeps a reasonable decline in carbon emission intensity, the peak time for China should be between 2020 and 2045. Wang et al. [14] used the extended STIRPAT model based on the classic IPAT identity to determine the main drivers of energy-related carbon emissions in Xinjiang. Lin et al. [15] focused on the impact of the extended STIRPAT model on carbon dioxide emissions from urbanization and economic development in non-high-income countries. Chang et al. [16] used the STIRPAT model to study the regional differences in the impact of population size, GDP per capita, energy structure, energy intensity, urbanization level, and industrialization level on CO_2 emissions. Quan et al. [17] uses the LMDI decomposition model to decompose the factors affecting carbon emissions of the logistics industry. Chai and Xu [18] conducted an in-depth analysis of the four paths and scenarios for China to achieve total emission control and peak emissions based on the IAMC model, carefully tested the relevant conditions, and put forward reasonable target recommendations at this stage. Li et al. [19] established an assessment framework of provincial carbon emission drivers using system dynamics modelling. Part of the research will also directly use scenario analysis to predict future carbon emissions [20–24].

2. Model Construction, Parameter Determination, and Data Source

2.1. Decomposition of Comprehensive Carbon Emission Coefficient Based on the IPAT Model. The research methods of carbon emission prediction mainly include the IPAT model, Kaya identity, STIRPAT model, and LEAP model. The reasonably optimized IPAT equation has the potential for carbon emission prediction. The IPAT equation was first proposed by Ehrlich et al. in 1971. It systematically reflects the relationship between population, economy, technology, and environment. The model can decompose and analyze the influencing factors according to the actual situation and can clarify which factors have the greatest impact on the

environment. The impact is the greatest, and the general form of the equation is as follows:

$$\mathrm{I} = \mathrm{P} \times \mathrm{A} \times \mathrm{T}. \tag{1}$$

Among them, I (impact) represents the impact of the population on the environment, P (population) represents the total population of the study area, A (affluence) represents per capita output, and T (technology) represents the impact of unit economic output on the environment, which is determined by the level of technological progress. When studying the effects of the population on the environment, we use emissions, GDP levels, and energy consumption per unit of GDP to replace I, A, and T. The formula is shown as follows:

$$C = P \times \frac{G}{P} \times \frac{C}{G}. \tag{2}$$

In addition, considering the impact of the energy structure on emissions, Kaya [25] proposed the Kaya equation, which decomposes the influencing factors by constructing a chain product to further increase the accuracy of the result. The calculation formula is as follows:

$$C = P \times \frac{G}{P} \times \frac{E}{G} \times \frac{C}{E}. \tag{3}$$

Among them, E represents the total energy consumption, $E = \sum S_i \times R_i$, S_i represents the carbon emission coefficient of the ith energy, $R_i$indicates the consumption of type i energy, and C/Eindicates the energy structure. In addition, when using the IPAT model to make predictions, the population changes in the future period must be predicted first. This is also a factor that causes large differences in the prediction results. Therefore, formula (3) is simplified:

$$C = G \times \frac{E}{G} \times \frac{C}{E}. \tag{4}$$

From formula (4), we know that the changes in carbon emissions in the short term are only affected by economic aggregates, energy intensity, and energy structure. Suppose that the annual growth rate of GDP is represented by r and g is the reduction rate of energy consumption per unit of GDP. Let v represent the comprehensive carbon emission coefficient of energy structure adjustment, that is, the optimization coefficient of the energy structure. Based on the improvement of the model by Zhu et al. [26] combined with the definition of the reduction rate of energy consumption per unit of GDP, the relationship between the energy consumption per unit of GDP in the current period and the energy consumption per unit of GDP in period t can be expressed as

$$\frac{E_t}{G_t} = \frac{E_0}{G_0}(1-g)^t = \frac{E_t}{G_0(1+r)^t}. \tag{5}$$

That is, $E_t = E_0(1-g)^t(1+r)^t$.

Therefore, carbon dioxide emissions can be expressed as

$$C^0 = \frac{44}{12} \times E_0 \times v_0, \tag{6}$$

$$C^t = \frac{44}{12} \times E_t \times v_t. \tag{7}$$

From (5) to (7), the relationship between the current carbon dioxide emissions and the carbon dioxide emissions during t can be derived:

$$C^t = C^0(1+r)^t(1-g)^t(1-e)^t. \tag{8}$$

In formula (8), we introduce e as the rate of change in the comprehensive carbon emission coefficient brought about by the optimization of the energy structure. Among them, $v_t = v_0(1-e)^t$, v_t represents the comprehensive carbon emission coefficient for the t period, v_0 represents the comprehensive carbon emission coefficient for the base period, C^t represents the total carbon dioxide emissions during the t period, and C^0 represents the total carbon dioxide emissions during the base period.

Under the current technological level and technological development, considering the driving factors of energy structure optimization, the replacement of renewable energy is the most important factor. Due to the nonrenewability of traditional energy, the development of alternative energy and the development and utilization of new energy have become the focus of research. Bastianoni et al. [27] used renewable energy and nonrenewable energy to build a model and concluded that the only way to achieve sustainable economic and social development is to use traditional nonrenewable energy while increasing investment in alternative renewable energy. Sustainable development is realized by improving the energy structure. Therefore, the optimization of the energy structure is, on the one hand, the optimal allocation of traditional energy sources such as coal and oil and, on the other hand, the increase in the replacement rate of renewable energy sources. We decompose the comprehensive carbon emission coefficient change ratio e brought about by the optimization of the energy structure into the sum of two effects, namely,

$$e = \alpha_t + \beta_t, \tag{9}$$

$$\begin{aligned} \alpha_t &= \frac{\sum\left(R_{it} - R_{i(t-1)}\right)}{R_{i(t-1)}}, \\ \beta_t &= \frac{\left((N_t/E_t) - (N_{t-1}/E_{t-1})\right)}{N_{t-1}/E_{t-1}}. \end{aligned} \tag{10}$$

Among them, N represents the total consumption of renewable energy in primary energy consumption, including clean energy such as hydropower, bioenergy, solar energy, and nuclear energy, β represents the change rate of the carbon emission coefficient affected by the change in the replacement rate of renewable energy, and then α indicates the change ratio of the carbon emission coefficient of the optimal allocation of coal, oil, and other traditional energy

sources on the energy structure. The carbon dioxide emissions during t are finally expressed as

$$C^t = C^0 (1 + r)^t (1 - g)^t (1 - \alpha - \beta)^t. \quad (11)$$

2.2. Data Sources and Parameter Prediction

2.2.1. Data Sources. The carbon dioxide emissions produced by human activities mainly come from energy consumption. In a large number of previous studies, scholars have used the carbon dioxide emissions of total energy consumption to represent the total carbon emissions of a certain area. In this paper, the carbon emissions of provinces around the Bohai Sea are also calculated in this way, and the actual carbon emissions of each province are calculated by the energy consumption cost of each province and its corresponding carbon emission coefficient. The actual carbon emissions of the provinces and cities in the Bohai Sea Rim from 2000 to 2018 are calculated based on the consumption of various major energy sources and the corresponding carbon emission indexes. The major energy sources include coal, oil, and natural gas, the consumption of which is based on the relevant data in the Statistical Yearbook (2001–2020) of all provinces in the Bohai Rim region. The national carbon dioxide emissions are calculated using the carbon emission coefficient method. The carbon emission coefficient of coal, oil, and natural gas is 0.7476 kg carbon/kg standard coal, 0.5825 kg carbon/kg standard coal, and 0.4435 kg carbon/kg standard coal, respectively, and the relevant data released by the Energy Research Institute of the National Development and Reform Commission are adopted to calculate the national carbon emissions.

Figure 1 shows the calculated changes in actual carbon emissions of the provinces in the Bohai Sea Rim from 2000 to 2018. The calculation results show that Shandong and Shanxi provinces are large in population and energy, and the total carbon emissions of Shandong and Shanxi provinces are more than other provinces in the region, and the overall trend is increasing year by year. The total carbon emissions in Shandong province dropped significantly in 2013. In this year, the Shandong Provincial Party Committee and the Provincial Government attached great importance to the prevention and control of air pollution and successively implemented the Shandong Province 2013–2020 Air Pollution Prevention and Control Plan, and the Air Pollution Prevention and Control Plan Phase I (2013–2015) Action Plan has achieved certain results. Due to geographical factors, its own climate, and industrial development, the total carbon emissions in Hebei province are relatively high, while those in Inner Mongolia and Liaoning are slightly lower. Beijing and Tianjin, as the two major municipalities in the Beijing-Tianjin-Hebei region, have lower total carbon emissions than other provinces in the region, but the overall trend is slowly increasing.

Figure 2 shows the actual carbon emission change rate of the provinces in the Bohai Rim region from 2000 to 2019. It can be seen that the overall carbon emission growth rate in the Bohai Rim region is declining year by year. Shanxi province and Shandong province experienced negative growth in total carbon emissions in 2014 and 2015, respectively. Liaoning province and Inner Mongolia also experienced negative growth in total carbon emissions in 2013. The growth rate of carbon emissions in Beijing has been at a relatively low level. In 2020, Beijing's carbon intensity was expected to drop by more than 23% in 2015, exceeding the goal of the 13th Five-Year Plan. Carbon emissions are the lowest in the provinces of the country. Beijing is one of the first provinces and cities in the country to carry out carbon emission trading pilot projects. In 2013, the carbon market was officially launched. As of the end of 2020, there were 843 key carbon emission units incorporated into the Beijing pilot carbon market management, covering 8 industries including electricity, heating, and aviation. The overall growth rate of carbon emissions in Tianjin has shown a downward trend year by year and achieved negative growth in 2017.

2.2.2. Parameter Prediction

(1) Gross Domestic Product. This paper uses the quadratic parabolic model $y_t = a + bt + ct^2$ to predict GDP. From the new normal stage to the high-quality development stage, the GDP growth rate in the Bohai Rim region has hovered around 6%. In recent years, the average GDP growth rates of Shandong province, Liaoning province, Hebei province, Shanxi province, Inner Mongolia, Beijing, and Tianjin are around 7.3%, 4.5%, 7.1%, 6.5%, 5.6%, 7.2%, and 6.1%, respectively. Using the quadratic parabola method of GDP and time to forecast, with three scenarios from 2000 to 2020, 2005 to 2020, and 2010 to 2020, the GDP from 2021 to 2050 (constant prices in 2005) is predicted. The annual growth rate of GDP in the three base periods is calculated from the predicted GDP of each province, as shown in Tables 1 and 2.

(2) Energy Intensity. This paper uses an improved GM (1, 1) model to predict the energy intensity of each province. The GM (1, 1) with fractional Hausdorff accumulation model is a univariate first-order differential equation. A nonnegative sequence is $X^{(0)} = \{x^{(0)}(1), x^{(0)}(2), \ldots, x^{(0)}(n)\}$. This article refers to the grey model method with the fractional Hausdorff derivative proposed by Yan et al. [28], which improves the prediction accuracy of the traditional grey model. There are large differences in energy intensity and its changes in various provinces due to the influence of factors such as population, geographical environment, and economic and social development level. Three scenarios with 2000–2020, 2005–2020, and 2010–2020 as the base years are used to predict the energy intensity of each province from 2021 to 2050. Other provinces are also treated in the same way, and the annual average decline rate of energy intensity in each province under the three scenarios is calculated as shown in Table 3.

According to the energy intensity forecasts of various provinces, it can be seen that Shanxi province is rich in mineral resources, with reserves of 276.785 billion tons of coal. The total energy consumption is relatively large. From 2000 to 2010, the average annual energy intensity reached

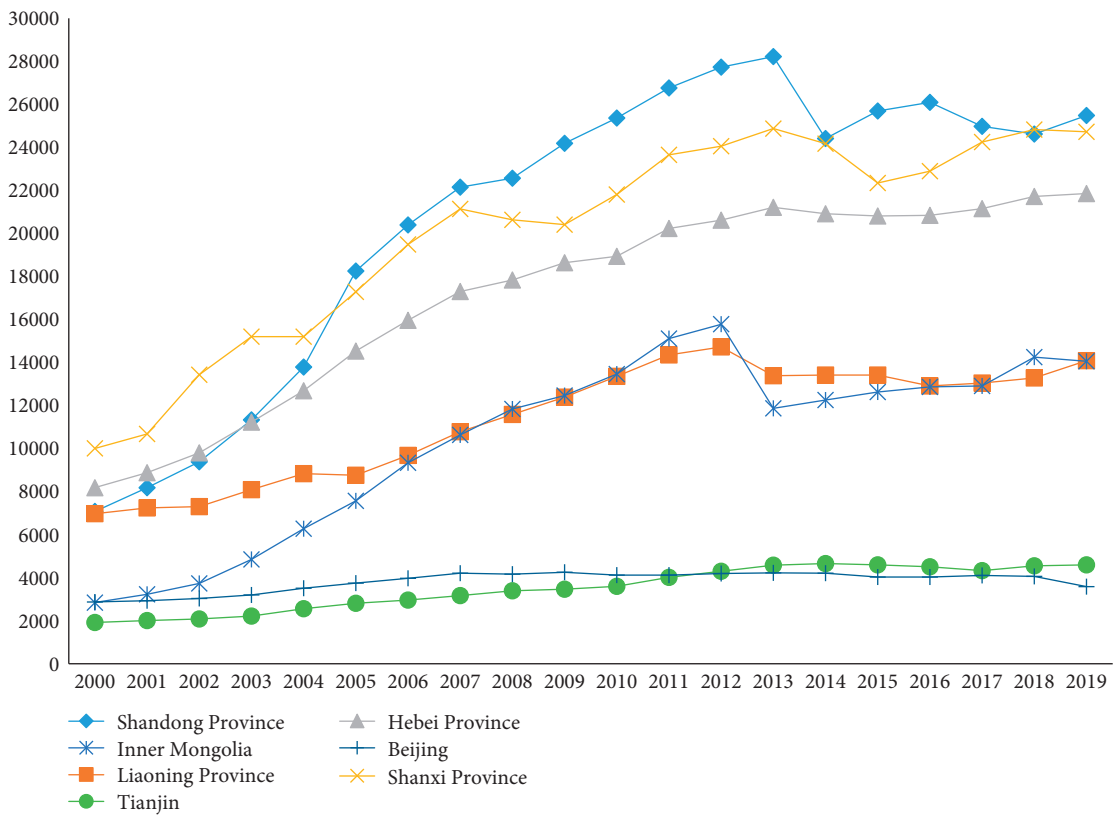

Figure 1: Total carbon emissions of provinces in the Bohai Rim region (unit: 10,000 tons).

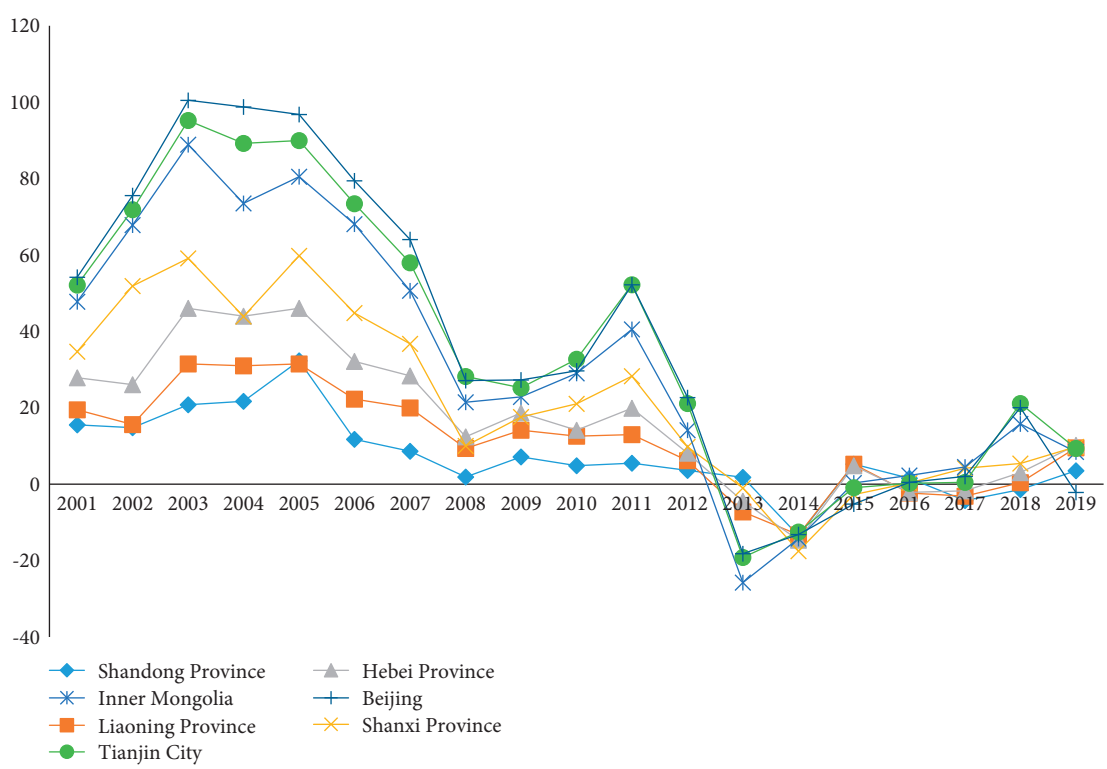

Figure 2: The rate of change of carbon emissions by provinces in the Bohai Rim region (unit: %).

Table 1: Prediction of annual growth rate of GDP of Shandong, Liaoning, Hebei, and Shanxi from 2021 to 2050 (unit: %).

PR	Shandong			Liaoning			Hebei			Shanxi		
Base period	2000	2005	2010	2000	2005	2010	2000	2005	2010	2000	2005	2010
2021	6.69	6.08	5.81	5.60	4.89	4.13	5.72	7.04	6.09	5.01	6.73	7.51
2022	6.47	5.85	5.56	5.30	4.72	4.04	5.55	6.77	5.75	4.86	6.53	7.59
2023	6.27	5.64	5.33	5.25	4.63	3.96	5.38	6.53	5.45	4.71	6.34	7.62
2024	6.08	5.44	5.12	5.21	4.57	3.88	5.23	6.30	5.18	4.57	6.16	7.60
2025	5.89	5.26	4.92	5.17	4.51	3.81	5.09	6.09	4.93	4.45	6.00	7.55
2026	5.72	5.09	4.75	5.12	4.46	3.74	4.96	5.90	4.70	4.32	5.85	7.47
2027	5.56	4.93	4.58	5.09	4.40	3.68	4.83	5.72	4.50	4.21	5.71	7.37
2028	5.41	4.78	4.43	5.05	4.38	3.61	4.71	5.55	4.31	4.10	5.58	7.26
2029	5.27	4.65	4.29	4.98	4.32	3.56	4.60	5.38	4.13	4.00	5.46	7.13
2030	5.13	4.52	4.16	4.83	4.27	3.50	4.49	5.23	3.97	3.91	5.34	7.00
2031	5.00	4.40	4.04	4.75	4.22	3.44	4.38	5.09	3.82	3.82	5.24	6.86
2032	4.88	4.28	3.92	4.61	4.18	3.39	4.29	4.96	3.68	3.73	5.13	6.72
2033	4.76	4.17	3.81	4.58	4.13	3.34	4.19	4.83	3.54	3.65	5.04	6.57
2034	4.65	4.07	3.71	4.45	4.06	3.30	4.10	4.71	3.42	3.57	4.94	6.43
2035	4.54	3.98	3.62	4.32	4.00	3.25	4.02	4.60	3.30	3.50	4.86	6.29
2036	4.44	3.88	3.53	4.28	3.96	3.21	3.93	4.49	3.19	3.43	4.77	6.15
2037	4.34	3.80	3.44	4.17	3.94	3.17	3.85	4.38	3.09	3.36	4.69	6.01
2038	4.25	3.71	3.36	4.04	3.90	3.12	3.78	4.29	2.99	3.29	4.62	5.87
2039	4.16	3.63	3.28	3.89	3.87	3.09	3.71	4.19	2.90	3.23	4.54	5.74
2040	4.08	3.56	3.21	3.74	3.85	3.05	3.64	4.10	2.81	3.17	4.47	5.61
2041	3.99	3.49	3.14	3.62	3.82	3.01	3.57	4.02	2.73	3.11	1.41	5.49
2042	3.92	3.42	3.07	3.51	3.79	2.98	3.50	3.93	2.64	3.06	4.34	5.37
2043	3.84	3.35	3.01	3.47	3.76	2.95	3.44	3.85	2.57	3.00	4.28	5.25
2044	3.77	3.29	2.95	3.34	3.72	2.91	3.38	3.78	2.49	2.95	4.22	5.14
2045	3.70	3.23	2.89	3.21	3.70	2.88	3.32	3.71	2.42	2.90	4.16	5.03
2046	3.63	3.17	2.84	3.16	3.67	2.85	3.27	3.64	2.35	2.86	4.11	4.92
2047	3.56	3.11	2.79	3.03	3.63	1.82	3.21	3.57	2.29	2.81	4.05	4.82
2048	3.50	3.06	2.73	2.97	3.61	2.80	3.16	3.50	2.22	2.77	4.00	4.72
2049	3.44	3.01	2.69	2.82	3.58	2.77	3.11	3.44	2.16	2.72	3.95	4.63
2050	3.38	2.96	2.64	2.76	3.55	2.74	3.06	3.38	2.10	2.68	3.90	4.53

96,000 tons of standard coal per 100 million yuan, making it the province with the highest energy intensity in the Bohai Rim. The main reason is that Shanxi province is in a period of vigorously developing heavy industry, and the heavy-duty economy has brought high energy consumption, which has led to a rapid increase in energy consumption. However, energy intensity basically shows a downward trend year by year. After 2010, Shanxi province's National Resource-Based Economy Transformation Comprehensive Supporting Reform Pilot Zone was officially approved. During the "Thirteenth Five-Year Plan" period, with the improvement of energy utilization efficiency and the continuous adjustment of the industrial structure in Shanxi province, the trend of energy intensity decline is obvious.

Since 2000, the energy intensity of Shandong province, Beijing city, and Tianjin city has not exceeded 20,000 tons of standard coal per 100 million yuan. They have maintained a relatively stable downward trend. In particular, Beijing reached 21,000 tons of standard coal per 100 million yuan in 2019. In recent years, Beijing has continued to promote industrial structure optimization and clean energy transformation. Vigorous efforts have been made to relieve noncapital functions, and coal consumption has dropped drastically. As one of the first pilot provinces and cities to carry out carbon emission trading in the country, Beijing has officially launched the carbon market since 2013. A total of 843 key carbon emission units have been incorporated into Beijing's pilot carbon market management. By the end of 2020, Beijing's carbon intensity was expected to drop by more than 23% in 2015, exceeding the goal of the "Thirteenth Five-Year Plan." The successful pilot in Beijing has provided certain experience for the Bohai Rim provinces. The development of carbon emission trading has effectively promoted the reduction of energy intensity, thereby further conducting research on special plans for carbon emission reduction based on the vision of carbon neutrality.

The energy intensities of the Inner Mongolia Autonomous Region, Liaoning province, and Hebei province are all falling steadily in the range of 8,000 to 25,000 tons of standard coal per 100 million yuan. They are relatively lagging behind Hebei province in terms of geographical factors and technological development. However, in recent years, the energy structure of the Inner Mongolia Autonomous Region has been further optimized, and green coal mines account for 1/3 of production coal mines. Liaoning province has joined universities and other research institutions to continuously explore scientific and technological innovation in the energy field to improve energy utilization

Table 2: Prediction of annual growth rate of GDP of Inner Mongolia, Beijing, Tianjin from 2021 to 2050 (unit: %).

PR	Inner Mongolia			Beijing			Tianjin		
Base period	2000	2005	2010	2000	2005	2010	2000	2005	2010
2021	5.72	7.04	6.09	5.25	5.29	5.62	6.46	5.51	7.56
2022	5.55	6.77	5.75	5.09	5.13	5.48	6.24	5.27	7.24
2023	5.38	6.53	5.45	4.95	4.98	5.34	6.03	5.04	6.94
2024	5.23	6.3	5.18	4.81	4.84	5.21	5.84	4.83	6.67
2025	5.09	6.09	4.93	4.68	4.71	5.09	5.66	4.65	6.43
2026	4.96	5.90	4.70	4.55	4.59	4.97	5.50	4.47	6.20
2027	4.83	5.72	4.50	4.44	4.47	4.85	5.34	4.31	5.98
2028	4.71	5.55	4.31	4.33	4.36	4.74	5.19	4.16	5.75
2029	4.60	5.38	4.13	4.22	4.25	4.64	5.05	4.03	5.37
2030	4.49	5.23	3.97	4.12	4.15	4.54	4.92	3.90	5.16
2031	4.38	5.09	3.82	4.03	4.06	4.44	4.79	3.78	4.73
2032	4.29	4.96	3.68	3.94	3.97	4.35	4.68	3.66	4.65
2033	4.19	4.83	3.54	3.85	3.88	4.26	4.56	3.56	4.37
2034	4.10	4.71	3.42	3.77	3.8	4.17	4.46	3.46	4.25
2035	4.02	4.60	3.30	3.70	3.72	4.09	4.36	3.36	4.10
2036	3.93	4.49	3.19	3.62	3.65	4.01	4.26	3.28	3.97
2037	3.85	4.38	3.09	3.55	3.58	3.94	4.17	3.19	3.82
2038	3.78	4.29	2.99	3.48	3.51	3.86	4.08	3.11	3.68
2039	3.71	4.19	2.90	3.42	3.44	3.79	3.99	3.04	3.54
2040	3.64	4.10	2.81	3.35	3.38	3.72	3.91	2.96	3.42
2041	3.57	4.02	2.73	3.29	3.32	3.66	3.83	2.90	3.30
2042	3.50	3.93	2.64	3.23	3.26	3.59	3.76	2.83	3.19
2043	3.44	3.85	2.57	3.18	3.2	3.53	3.69	2.77	3.09
2044	3.38	3.78	2.49	3.12	3.15	3.47	3.62	2.71	2.99
2045	3.32	3.71	2.42	3.07	3.09	3.41	3.55	2.65	2.90
2046	3.27	3.64	2.35	3.02	3.04	3.36	3.49	2.60	2.81
2047	3.21	3.57	2.29	2.97	2.99	3.30	3.43	2.54	2.73
2048	3.16	3.50	2.22	2.93	2.95	3.25	3.37	2.49	2.64
2049	3.11	3.44	2.16	2.88	2.90	3.20	3.31	2.44	2.57
2050	3.06	3.38	2.10	2.84	2.86	3.15	3.25	2.40	2.49

Table 3: Forecast value of annual energy intensity reduction in each province.

Province	2000–2020 (%)	2005–2020 (%)	2010–2020 (%)	Annual average (%)
Shandong	4.25	5.80	7.12	5.72
Liaoning	5.24	4.14	1.02	3.47
Hebei	6.12	6.42	3.99	5.51
Shanxi	5.39	4.10	2.93	4.14
Inner Mongolia	6.91	4.70	1.74	4.45
Beijing	9.56	6.44	2.72	6.24
Tianjin	7.10	4.20	1.83	4.38

efficiency. In recent years, the energy intensity of Liaoning province has declined slightly. Energy intensity in 2019 has increased compared with 2018.

Comparing the annual reduction rate of energy intensity of each province in the comparison table, it can be found that Shandong province has a relatively high reduction rate in recent years, and the reduction rate of other provinces in recent years is lower than in previous years. Beijing had a high rate of energy intensity reduction before 2010, and it has maintained a steady downward trend in recent years. Liaoning province has the lowest energy intensity reduction rate in the Bohai Rim region after 2010. The other provinces and cities in the descending order are Inner Mongolia, Tianjin, Beijing, Shanxi, Hebei, and Shandong. Liaoning province and the Inner Mongolia Autonomous Region have low rates of energy intensity reduction due to geographical factors and relatively backward technological development. As municipalities directly under the Central Government, Tianjin and Beijing have relatively low energy intensity, and the degree of decline has been slowed. Shanxi province and Hebei province rely on the adjustment of the energy structure and the upgrading of industries, and their energy intensity has fallen to a relatively high level. Shandong province is rich in energy resources, emphasizes the industrial structure, and has prominent problems such as a high proportion of coal consumption. However, during the "13th Five-Year Plan" period, Shandong province seized the opportunity to rapidly promote the construction of new energy and renewable energy projects. Significant

achievements have been made in the transition to a green and low-carbon energy structure. Since 2020, the province's installed capacities of photovoltaic power generation and biological power generation have both ranked first in the country, and the energy intensity has fallen sharply.

(3) Setting the Replacement Rate of Renewable Energy and Other Parameters. On the basis of calculating the number of renewable energy replacement rates of 2000–2020, 2005–2020, and 2010–2020, according to the prediction of energy intensity under three scenarios, the change ratio β of the carbon emission coefficient affected by the replacement rate of renewable energy and the change ratio α of the carbon emission coefficient affected by the optimal allocation of traditional energy such as coal and oil on the energy structure were set under the three scenarios, as shown in Table 4 (α) and Table 5 (β).

3. The Prediction of Carbon Emissions of Various Provinces in the Bohai Rim Region

The aforementioned domestic product, energy intensity, renewable energy replacement rate change ratio, and coal, oil, and other traditional energy optimization configurations affect the rate of the energy structure of the carbon emission coefficient of the carbon emission factor belt in formula (11). The total amount of carbon emissions in the provinces under three scenarios and the peak of carbon emissions in various provinces are shown in Figures 3–5.

Based on the above prediction results, the following results can be drawn:

(1) After 2020, the total carbon emission forecasts of the provinces and cities in the Bohai Rim are from high to bottom: Shanxi province, Shandong province, Hebei province, Liaoning province, Inner Mongolia, Tianjin, and Beijing. Although there are differences in the growth of total carbon emissions among provinces and cities, the proportion of overall emissions in the Bohai Rim region has not changed much. Shandong province and Shanxi province, as the most populous provinces and energy provinces, have higher overall carbon emissions than other provinces in the region. The pressure to reduce emissions will be relatively greater in the future. Beijing and Tianjin are municipalities directly under the Central Government, and their total carbon emissions are lower than other provinces in the region. In the next few years, priority should be given to achieving "carbon neutrality" as a strategic goal. Beijing has also established the country's first "carbon neutral" park to form a benchmark experience of "carbon neutral" as soon as possible, providing a reference for further emission reductions in other regions around the Bohai Sea.

(2) On the premise that all provinces and cities in the Bohai Rim region continue to promote and maintain high-quality development, all provinces and cities can reach their peak carbon emissions around 2030 under the three prediction scenarios. However, there are obvious differences in the peak situation of each province.

(3) Beijing predicts that it will reach its carbon peak in 2025. If under the background of the base period in 2000, Beijing could reach its carbon peak in 2021. In recent years, Beijing has continued to promote the optimization of the industrial structure and the transition to clean energy, and the amount of coal burned has dropped significantly. In this case, the replacement of renewable energy sources and the development of renewable energy sources are critical to achieving peak carbon. Tianjin and Beijing are very similar in terms of peaking carbon emissions,

Table 4: Prediction of α parameter under three scenarios.

Province	Years	2000–2020	2005–2020	2010–2020
Shandong	2021–2025	−0.009	−0.040	−0.090
	2026–2030	−0.006	−0.037	−0.087
	2031–2035	−0.003	−0.034	−0.084
	2036–2040	0	−0.031	−0.081
	2041–2045	0.003	−0.029	−0.079
	2046–2050	0.006	−0.026	−0.076
Liaoning	2021–2025	−0.008	−0.004	0.008
	2026–2030	−0.004	0	0.012
	2031–2035	0	0.004	0.016
	2036–2040	0.004	0.008	0.02
	2041–2045	0.008	0.012	0.022
	2046–2050	0.012	0.016	0.024
Hebei	2021–2025	−0.004	0.001	0.001
	2026–2030	−0.002	0.003	0.003
	2031–2035	0	0.005	0.005
	2036–2040	0.002	0.007	0.007
	2041–2045	0.004	0.009	0.009
	2046–2050	0.006	0.011	0.011
Shanxi	2021–2025	−0.008	−0.001	0.001
	2026–2030	−0.005	0.002	0.002
	2031–2035	−0.002	0.005	0.003
	2036–2040	0.001	0.008	0.004
	2041–2045	0.004	0.011	0.005
	2046–2050	0.007	0.014	0.006
Inner Mongolia	2021–2025	−0.003	−0.002	−0.008
	2026–2030	−0.001	0	−0.006
	2031–2035	0.001	0.002	−0.004
	2036–2040	0.003	0.004	−0.002
	2041–2045	0.005	0.006	0
	2046–2050	0.007	0.008	0.002
Beijing	2021–2025	0.006	0.006	0.01
	2026–2030	0.007	0.007	0.011
	2031–2035	0.008	0.008	0.012
	2036–2040	0.009	0.009	0.013
	2041–2045	0.010	0.010	0.014
	2046–2050	0.011	0.011	0.015
Tianjin	2021–2025	−0.001	−0.002	−0.002
	2026–2030	0	−0.001	0
	2031–2035	0.001	0	0.002
	2036–2040	0.002	0.001	0.004
	2041–2045	0.003	0.002	0.006
	2046–2050	0.004	0.003	0.008

Table 5: Prediction of β parameter under three scenarios.

Province	Years	2000–2020	2005–2020	2010–2020
Shandong	2021–2025	0.020	0.030	0.040
	2026–2030	0.022	0.032	0.045
	2031–2035	0.024	0.034	0.050
	2036–2040	0.026	0.036	0.055
	2041–2045	0.028	0.038	0.060
	2046–2050	0.030	0.040	0.065
Liaoning	2021–2025	−0.001	0.001	0.001
	2026–2030	0	0.003	0.003
	2031–2035	0.001	0.005	0.005
	2036–2040	0.002	0.007	0.007
	2041–2045	0.003	0.009	0.009
	2046–2050	0.004	0.011	0.011
Hebei	2021–2025	0.002	0.007	0.010
	2026–2030	0.004	0.008	0.012
	2031–2035	0.006	0.009	0.014
	2036–2040	0.008	0.010	0.016
	2041–2045	0.010	0.011	0.018
	2046–2050	0.012	0.012	0.020
Shanxi	2021–2025	−0.008	0.010	0.010
	2026–2030	−0.006	0.012	0.020
	2031–2035	−0.004	0.014	0.030
	2036–2040	−0.002	0.016	0.040
	2041–2045	0	0.018	0.050
	2046–2050	0.002	0.02	0.060
Inner Mongolia	2021–2025	0.010	0.015	0.020
	2026–2030	0.015	0.020	0.025
	2031–2035	0.020	0.025	0.030
	2036–2040	0.025	0.030	0.035
	2041–2045	0.030	0.035	0.040
	2046–2050	0.035	0.040	0.045
Beijing	2021–2025	0.003	0.004	0.002
	2026–2030	0.005	0.006	0.005
	2031–2035	0.007	0.008	0.008
	2036–2040	0.009	0.010	0.011
	2041–2045	0.011	0.012	0.014
	2046–2050	0.013	0.014	0.017
Tianjin	2021–2025	0	0.010	0.014
	2026–2030	0.005	0.012	0.016
	2031–2035	0.010	0.014	0.018
	2036–2040	0.015	0.016	0.020
	2041–2045	0.020	0.018	0.022
	2046–2050	0.025	0.020	0.024

and they are expected to peak in 2024. If 2010 is the base period, it will reach its peak in 2030. Faced with the goal of carbon peaking, Tianjin city still has considerable pressure and challenges.

(4) Shandong province is expected to reach its carbon peak before 2028. If in the context of the 2010 base period, the peak goal will be achieved in 2031. Shandong province itself is a big energy-consuming province, and it is also a big coal-consuming province. The energy structure is biased towards coal, the energy intensity is too high, and the replacement rate of renewable energy is relatively low. The peaking process still needs to actively reduce energy intensity and, at the same time, develop renewable energy. Shanxi province and Shandong province have similar problems. Shanxi province is predicted to reach its peak in 2027 or even 2030. As a large industrial province, Liaoning province also has problems with its industrial structure and high energy intensity. It is predicted that the carbon peak will be reached in 2027.

(5) As an important province to relieve Beijing's non-capital pressure, Hebei province is under pressure to reduce emissions. However, relying on Beijing itself, renewable energy utilization technology is relatively advanced. In recent years, the industrial structure has been continuously optimized, and energy intensity has declined rapidly. It is predicted that the

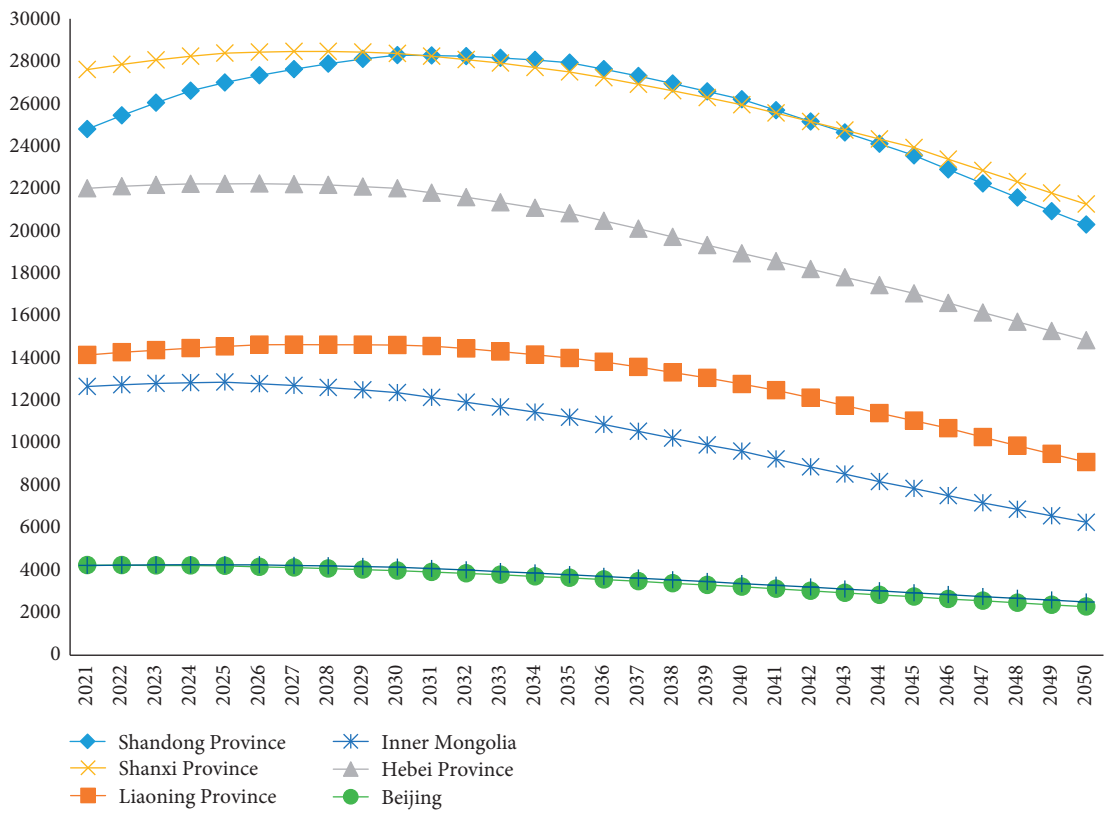

Figure 3: Carbon emissions of each province and city under the 2000–2020 scenario (unit: 10,000 tons).

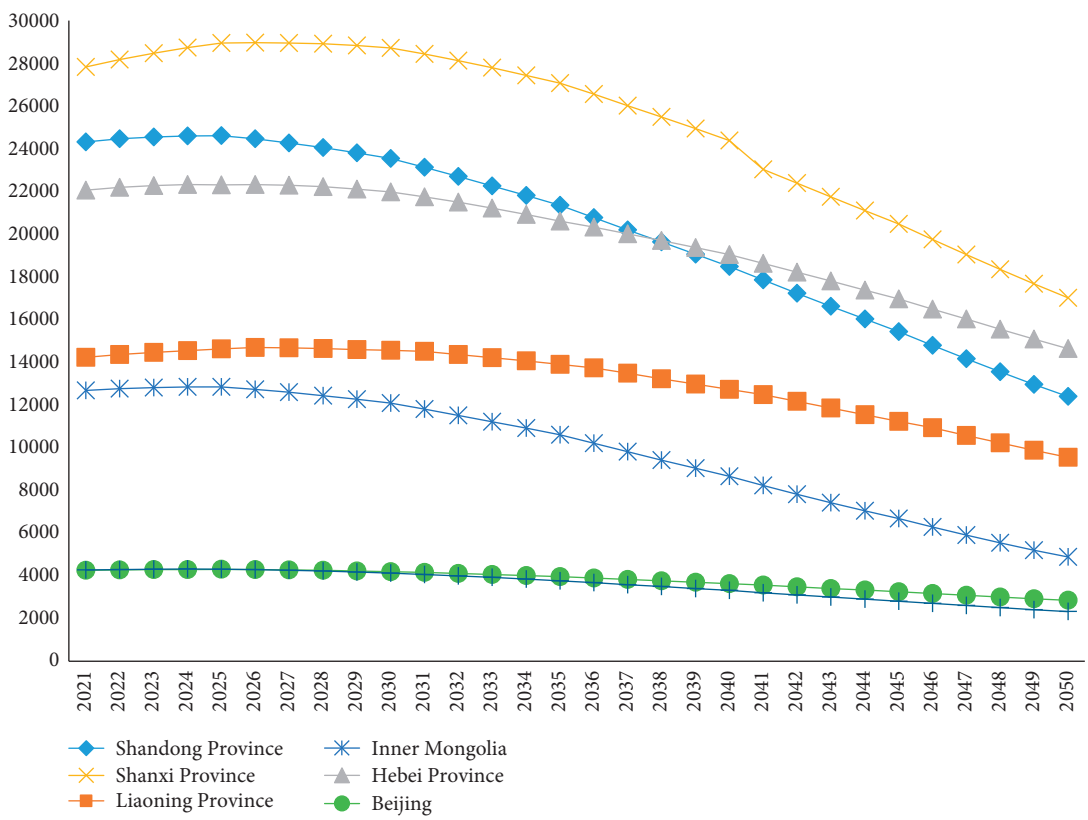

Figure 4: Carbon emissions of each province and city under the 2005–2020 scenario (unit: 10,000 tons).

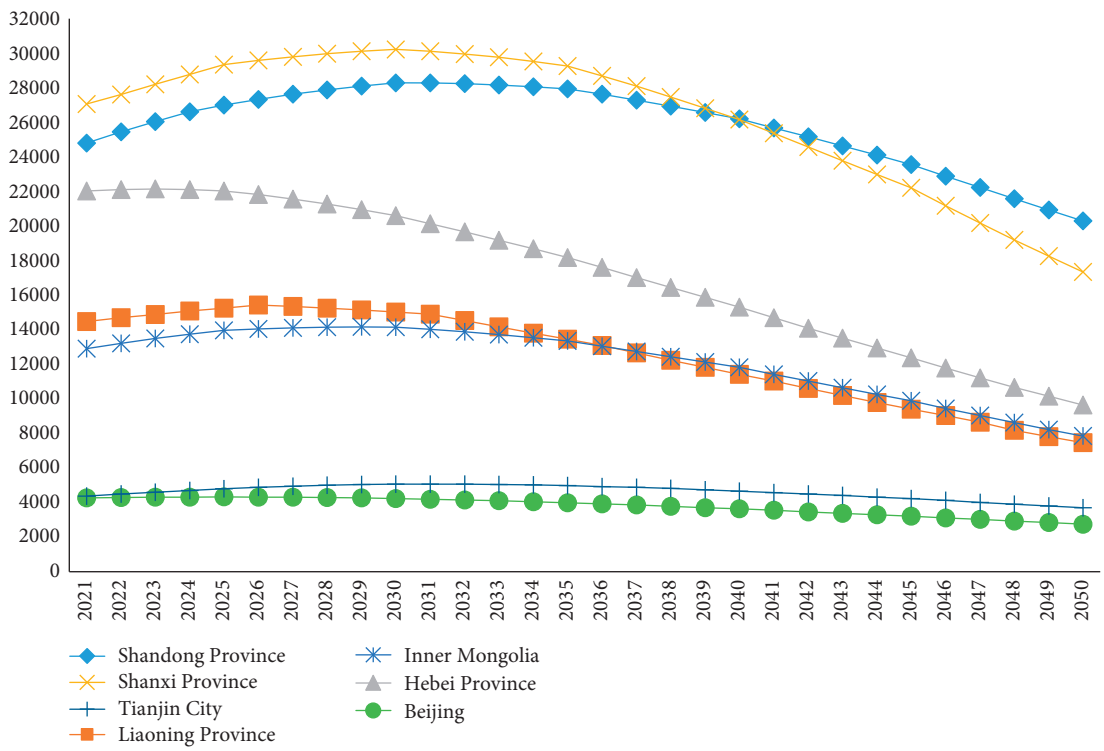

Figure 5: Carbon emissions of each province and city under the 2010–2020 scenario (unit: 10,000 tons).

carbon peak will be reached before 2026. The Inner Mongolia Autonomous Region predicts that the carbon peak will be reached in 2025. However, under the scenario of 2010 as the base period, the carbon peak is expected to be reached in 2029. Energy intensity has decreased rapidly, but the utilization rate of renewable energy has increased slowly.

4. Conclusions and Recommendations

Based on the analysis of the above prediction results and comparing the carbon emissions of the provinces and cities around the Bohai Sea, this article puts forward the following suggestions:

(1) In recent years, Beijing has continued to promote the optimization of the industrial structure and the transition to clean energy. The amount of coal burned has dropped significantly, and the energy intensity is relatively low. The carbon intensity of Beijing has dropped significantly since the pilot work of carbon emission trading was launched. In 2020, Beijing's carbon intensity was expected to drop by more than 23% in 2015. The successful pilot in Beijing has provided certain experience for the Bohai Rim provinces. The development of carbon emission trading has effectively promoted the reduction of carbon intensity. Beijing has also established the country's first "carbon neutral" park to form a benchmark experience of "carbon neutral" as soon as possible, providing a reference for further emission reductions in other regions around the Bohai Sea. Therefore, we will further carry out research on the special plan of carbon emission reduction based on the vision of carbon neutrality and prioritize the realization of "carbon neutrality" as a strategic goal.

(2) Based on the measures taken by Beijing, Tianjin should combine the peaking target with the "14th Five-Year Plan" outline, the energy consumption "dual control" target, and major engineering projects. Tianjin should perfect the scientific research index system and form a complete action plan. We must do a good job not only in the addition of renewable energy but also do a good job in the "subtraction" of reducing coal consumption. Pay close attention to key areas of high energy consumption and provide a good development environment for environmental protection industries such as photovoltaics, hydrogen energy, and green energy conservation. Hebei province should firmly grasp high-tech and use artificial intelligence and big data platforms to actively promote the construction of carbon-inclusive pilots and enrich the low-carbon reward mechanism.

(3) Shandong province, as a major energy-consuming province, faces certain challenges in reaching the peak goal. However, in recent years, it has established the energy structure adjustment target of coal power, new energy and renewable energy, and electricity from outside the province. This provides the basis for further adjustment of the energy structure of Shandong province. Haiyang of Shandong province has become the country's first "zero-carbon" heating city using nuclear energy technology. Therefore,

Shandong should accelerate the comprehensive utilization of nuclear energy as soon as possible and regard the development of nuclear energy as an important starting point for promoting energy structure optimization and ensuring energy security. Shanxi province and Shandong province have similar problems. Shanxi province should also vigorously develop clean energy, promote the transformation of "three counties and one city" clean heating according to local conditions, and accelerate the access of key coal mining enterprises to special railway lines. Shanxi should pay more attention to emission reduction in key areas of high energy consumption, find out the source of emissions, and provide special emission reduction guidance to key enterprises in key industries.

(4) Liaoning province is a major industrial province in the northeast. Energy consumption focuses on coal, and the industrial structure is uneven. The task of peaking carbon is very difficult. It is necessary to further understand the current status of carbon emissions and formulate specific action plans. Low-carbon transformation and upgrading in energy, industry, construction, agriculture, and forestry should be coordinated and promoted. Resolutely curb the blind development of energy-intensive and high-emission projects. Actively carry out the creation of low-carbon pilot demonstrations. Promote the construction of zero-carbon emission demonstration projects and carbon neutral demonstration zones. Provide a model for Liaoning province to reach the peak as soon as possible.

(5) The Inner Mongolia Autonomous Region should actively learn from Beijing's relevant measures. Encourage enterprises to accelerate the implementation of carbon emission management and actively participate in the upcoming carbon emission market transactions. Strengthen the professional training of relevant carbon emission management personnel at different levels and stages, and reduce the total amount of carbon emissions starting from the enterprise industry. There are certain challenges in achieving the goal of achieving carbon peaks in the Bohai Rim as a whole. It should be advanced to drive the backward, focusing on the three provinces of Shandong, Shanxi, and Liaoning that are difficult to reach the peak. Actively try to implement measures to form an effective emission reduction model that can be replicated so as to fully realize the regional emission reduction target in the Bohai Rim.

Data Availability

Previously reported data were used to support this study and are available at http://tjj.shandong.gov.cn/col/col6279/index.html, http://tjj.hebei.gov.cn/hetj/tjsj/jjnj/, http://tjj.beijing.gov.cn/tjsj_31433/, http://stats.tj.gov.cn/tjsj_52032/tjnj/, http://tjj.ln.gov.cn/tjsj/sjcx/ndsj/, http://tjj.shanxi.gov.cn/tjsj/tjnj/, and http://tj.nmg.gov.cn/datashow/index.htm.

Ethical Approval

Not Applicable.

Consent

Not Applicable.

Conflicts of Interest

The authors declare that they have no conflicts of interest.

Authors' Contributions

Chuanhui Wang conceptualized the study, developed the methodology, wrote the original draft, and contributed to funding acquisition. Mengzhen Zhao investigated the study, administered the project, and performed formal analysis. Weifeng Gong performed formal analysis and reviewed and edited the article. Zhenyue Fan and Wenwen Li jointly collected and collated data.

Acknowledgments

This research was supported by the Humanities and Social Sciences Youth Foundation of Ministry of Education of China (Grant nos. 18YJCZH034).

References

[1] H. T. Pao, H. C. Fu, and C. L. Tseng, "Forecasting of CO_2 emissions, energy consumption and economic growth in China using an improved grey model," *Energy*, vol. 40, no. 01, pp. 400–409, 2012.

[2] Z. X. Wang and D. J. Ye, "Forecasting Chinese carbon emissions from fossil energy consumption using non-linear grey multivariable models," *Journal of Cleaner Production*, vol. 142, no. P2, pp. 600–612, 2016.

[3] Y. Huang, L. Shen, and H. Liu, "Grey relational analysis, principal component analysis and forecasting of carbon emissions based on long short-term memory in China," *Journal of Cleaner Production*, vol. 209, pp. 415–423, 2019.

[4] L. Ye, N. Xie, and A. Hu, "A novel time-delay multivariate grey model for impact analysis of CO_2 emissions from China's transportation sectors," *Applied Mathematical Modelling*, vol. 91, pp. 493–507, 2021.

[5] P. Y. Zhu and W. Ling, "The impact of different carbon emission peak scenarios on the industrial structure: an analysis based on the dynamic CGE model," *Finance and Economics Theory and Practice*, vol. 41, no. 05, pp. 110–118, 2020.

[6] B. Li, S. Han, Y. Wang, Y. Wang, J. Li, and Y. Wang, "Feasibility assessment of the carbon emissions peak in China's construction industry: factor decomposition and peak forecast," *The Science of the Total Environment*, vol. 706, Article ID 135716, 2020.

[7] G. M. Grossman and A. B. Krueger, *Environmental Impacts of a North American Free Trade Agreement*, p. 3914, National Bureau of Economic Research Working Paper, Cambridge, MA, USA, 1991.

[8] P. Debdatta and K. M. Subrata, "The environmental Kuznets curve for carbon dioxide in India and China: Growth and

pollution at crossroad," *Journal of Policy Modeling*, vol. 39, no. 02, pp. 371–385, 2017.

[9] B. Q. Lin and Z. J. Jiang, "Environmental Kuznets curve forecast of China's carbon dioxide and analysis of influencing factors," *Management World*, vol. 04, pp. 27–36, 2009.

[10] P. Jiang, H. Yang, and X. Ma, "Coal production and consumption analysis, and forecasting of related carbon emission: Evidence from China," *Carbon Management*, vol. 10, no. 2, pp. 189–208, 2019.

[11] P. R. Ehrlich and J. P. Holdren, "Impact of population Growth," *Science*, vol. 171, no. 3977, pp. 1212–1217, 1971.

[12] B. W. Ang, F. Q. Zhang, and K. H. Choi, "Factorizing changes in energy and environmental indicators through decomposition," *Energy*, vol. 23, no. 6, pp. 489–495, 1980.

[13] S. N. Qu and C. X. Guo, "Study on China's peak carbon emission prediction based on STIRPAT model," *China Population· Resources and Environment*, vol. 20, no. 12, pp. 10–15, 2010.

[14] C. Wang, F. Wang, X. Zhang et al., "Examining the driving factors of energy related carbon emissions using the extended STIRPAT model based on IPAT identity in Xinjiang," *Renewable and Sustainable Energy Reviews*, vol. 67, pp. 51–61, 2017.

[15] S. Lin, S. Wang, D. Marinova, D. Zhao, and J. Hong, "Impacts of urbanization and real economic development on CO_2 emissions in non-high income countries: Empirical research based on the extended STIRPAT model," *Journal of Cleaner Production*, vol. 166, pp. 952–966, 2017.

[16] K. Chang, Z. Du, G. Chen, Y. Zhang, and L. Sui, "Panel estimation for the impact factors on carbon dioxide emissions: a new regional classification perspective in China," *Journal of Cleaner Production*, vol. 279, Article ID 123637, 2021.

[17] C. Quan, X. Cheng, S. Yu, and X. Ye, "Analysis on the influencing factors of carbon emission in China's logistics industry based on LMDI method," *The Science of the Total Environment*, vol. 734, Article ID 138473, 2020.

[18] Q. M. Chai and H. Q. Xu, "Research on the path to achieve China's peak carbon emission target based on the IAMC model," *China Population· Resources and Environment*, vol. 25, no. 06, pp. 37–46, 2015.

[19] W. Li, C. An, and C. Lu, "The assessment framework of provincial carbon emission driving factors: an empirical analysis of Hebei Province," *The Science of the Total Environment*, vol. 637-638, pp. 91–103, 2018.

[20] D. Guan, K. Hubacek, C. L. Weber, G. P. Peters, and D. M. Reiner, "The drivers of Chinese CO_2 emissions from 1980 to 2030," *Global Environmental Change*, vol. 18, no. 4, pp. 626–634, 2008.

[21] D. Liu and B. Xiao, "Can China achieve its carbon emission peaking? A scenario analysis based on STIRPAT and system dynamics model," *Ecological Indicators*, vol. 93, pp. 647–657, 2018.

[22] G. X. Zhang and Z. X. Su, "Decomposition and scenario prediction of influencing factors of transportation carbon emissions in the Yellow River Basin," *Management Review*, vol. 32, no. 12, pp. 283–294, 2020.

[23] X. Liu, Y. Hang, Q. Wang, and D. Zhou, "Flying into the future: a scenario-based analysis of carbon emissions from China's civil aviation," *Journal of Air Transport Management*, vol. 85, Article ID 101793, 2020.

[24] P. P. Wang, Y. P. Li, G. H. Huang, S. G. Wang, C. Suo, and Y. Ma, "A multi-scenario factorial analysis and multi-regional input-output model for analyzing CO_2 emission reduction path in Jing-Jin-Ji region," *Journal of Cleaner Production*, vol. 300, Article ID 126782, 2021.

[25] Y. Kaya, "Impact of carbon dioxide emission on GNP growth: interpretation of scenarios," Energy and Industry Subgroup, Response Strategies Group IPCC, Paris, France, 1989.

[26] Y. E. Zhu, L. F. Li, S. S. He, H. Li, and Y. Wang, "Peak year prediction of Shanxi Province's carbon emissions based on IPAT modeling and scenario analysis," *Resources Science*, vol. 38, no. 12, pp. 2316–2325, 2016.

[27] S. Bastianoni, R. M. Pulselli, and F. M. Pulselli, "Models of withdrawing renewable and non-renewable resources based on Odum's energy systems theory and Daly's quasi-sustainability principle," *Ecological Modelling*, vol. 220, no. 16, pp. 1926–1930, 2009.

[28] C. Yan, L. F. Wu, L. Y. Liu, and K. Zhang, "Fractional Hausdorff grey model and its properties," *Chaos, Solitons and Fractals: The Interdisciplinary Journal of Nonlinear Science, and Nonequilibrium and Complex Phenomena*, vol. 138, Article ID 109915, 2020.

Hindawi
Journal of Mathematics
Volume 2021, Article ID 5406547, 10 pages
https://doi.org/10.1155/2021/5406547

Research Article

Fractional Order Accumulation NGM (1, 1, *k*) Model with Optimized Background Value and Its Application

Jun Zhang,[1] **Yanping Qin**,[2] **Xinyu Zhang**,[1] **Bing Wang**,[3] **Dongxue Su**,[1] **and Huaqiong Duo**[2]

[1]*College of Science, Inner Mongolia Agricultural University, Hohhot 010018, China*
[2]*College of Material Science and Art Design, Inner Mongolia Agricultural University, Hohhot 010018, China*
[3]*Water Conservancy and Civil Engineering College, Inner Mongolia Agricultural University, Hohhot 010018, China*

Correspondence should be addressed to Jun Zhang; zj325328333@163.com and Huaqiong Duo; duohuaqiong@163.com

Received 18 June 2021; Revised 30 June 2021; Accepted 10 August 2021; Published 3 September 2021

Academic Editor: Lifeng Wu

Aiming at the problem of unstable prediction accuracy of the classic NGM (1, 1, *k*) model, the modeling principle and parameter estimation method of this model are deeply analyzed in this study. Taking the minimum mean absolute percentage error as the objective function, the model is improved from the two perspectives of the construction method of the background value and the fractional order accumulation generation. The fractional order accumulation NGM (1, 1, *k*) model based on the optimal background value (short for the FBNGM (1, 1, *k*) model) is proposed in the study. The particle swarm optimization algorithm is used to estimate the parameters of the proposed model. Taking two actual cases with economic significance as examples, empirical analysis of the proposed model is conducted. The simulation and prediction results show the practicality and efficiency of the FBNGM (1, 1, *k*) model proposed in this study, which further broadens the application scope of the grey prediction model.

1. Introduction

The grey forecasting model has the advantages of no special requirements on the distribution of modeling data and easily understood modeling mechanism. So it is used in many fields such as environment [1, 2], agriculture [3], industry [4], energy [5, 6], economy [7, 8], and so on. The GM (1, 1) model plays an important role in the grey forecasting model. In order to improve the prediction accuracy of the GM (1, 1) model, some scholars have made a series of improvements from the perspectives of the background value [8], cumulative order [9], and discretization [10]. But the prediction accuracy of the improved model for nonhomogeneous exponential series is still not ideal, so the NGM (1, 1, *k*) model came into being [11].

In order to expand the application scope of the NGM (1, 1, *k*) model, the researchers further optimized the grey differential equation of the NGM (1, 1, *k*) model in practical applications and proposed the NHGM (1, 1, *k*) model [12] and the grey prediction model with time power term [13]. In order to eliminate the inherent bias caused by the mismatch problem, Wang and Gong [14] proposed the intensional NGM (1, 1, *k*) model based on the classic NGM (1, 1, *k*) model. In order to compensate the lack of accuracy of GM (1, 1) in simulating nonhomogeneous exponential growth series, Cui et al. [11] constructed the NGM (1, 1, *k*) model to approximate the characteristics of nonhomogeneous exponential growth series by using the grey differential equation of GM (1, 1) as a deductive reasoning tool. Tong et al. [15] proposed the BNGM (1, 1, *k*) model with optimized grey differential equation by analyzing the cause of parameter estimation error in the classic NGM (1, 1, *k*) model. However, the single optimized NGM (1, 1, *k*) model has limited effect in improving the accuracy of model prediction. Based on fractional order accumulation, Wu et al. [16] proposed the discrete grey model with the fractional order. Zeng et al. [17] proposed the idea of multiple optimizations and verified the prediction accuracy of the dual optimized GM (1, 1) model based on function transformation, and background value reconstruction is much higher than the single optimized GM (1, 1) model through actual application examples. This shows that multiple optimizations could

complement each other through different optimization measures. It makes up for the limitations of single optimization and further improves the accuracy of the grey prediction model.

The main contributions of this study are as follows:

(1) Based on the previous scholars' research, referring to the fractional order accumulation generation technology and the idea of optimizing the background value, the fractional order accumulation NGM (1, 1, k) model based on the optimal background value (short for FBNGM (1, 1, k) model) is constructed in this study.

(2) Based on the actual application cases of China's electricity consumption and agricultural output value, the proposed FBNGM (1, 1, k) model is compared with the NGM (1, 1, k) model and two single optimization model in simulation and prediction accuracy. The results show that the FBNGM (1, 1, k) model has better performance in improving model accuracy than the other models, which verifies the practicality and efficiency of the proposed model.

The remainder of this study is organized as follows: the second part introduces the basic model and accuracy measure indicator; the third part introduces the FBNGM (1, 1, k) model and its parameter solution in detail; the fourth part is the empirical study, based on two actual application cases of predicting China's electricity consumption and agricultural output value; the fifth part is the conclusion.

2. Preliminary Knowledge

This section presents the fractional order accumulation and inverse accumulation generation technology of modeling sequence, the related concepts of the NGM (1, 1, k) model, and the accuracy measure indicator of the model.

2.1. Fractional Order Accumulation and Inverse Accumulation Generation Technology [17]

(1) Assuming $X^{(0)} = \{x^{(0)}(1), x^{(0)}(2), \ldots, x^{(0)}(n)\}$is a nonnegative original sequence, so $X^{(r)} = \{x^{(r)}(1), x^{(r)}(2), \ldots, x^{(r)}(n)\}$, $r \in R^{+}$ is called the rth order accumulation generation sequence of $X^{(0)}$, where

$$x^{(r)}(k) = \sum_{i=1}^{k} \frac{\Gamma(r+k-i)}{\Gamma(k-i+1)\Gamma(r)} x^{(0)}(i), \quad k = 1, 2, \ldots, n. \tag{1}$$

(2) Assuming$X^{(0)} = \{x^{(0)}(1), x^{(0)}(2), \ldots, x^{(0)}(n)\}$ is a nonnegative original sequence, so $X^{(-r)} = \{x^{(-r)}(1), x^{(-r)}(2), \ldots, x^{(-r)}(n)\}$,$r \in R^{+}$ is called the rth order inverse accumulation generation sequence of $X^{(0)}$, where

$$x^{(-r)}(k) = \sum_{i=0}^{k-1} (-1)^{i} \frac{\Gamma(r+1)}{\Gamma(i+1)\Gamma(r-i+1)} x^{(0)}(k-i), \quad k = 1, 2, \ldots, n. \tag{2}$$

2.2. NGM (1, 1, k) Model [15]. $X^{(1)} = \{x^{(1)}(1), x^{(1)}(2), \ldots, x^{(1)}(n)\}$ is the first-order accumulation generation sequence of $X^{(0)}$ and $Z^{(1)} = \{z^{(1)}(2), z^{(1)}(3), \ldots, z^{(1)}(n)\}$, $z^{(1)}(k) = 0.5x^{(1)}(k) + 0.5x^{(1)}(k-1), k = 2, 3, \ldots, n,$ is the mean generation sequence of $X^{(1)}$, so

$$x^{(0)}(k) + az^{(1)}(k) = b\frac{2k-1}{2} + c \tag{3}$$

is called the grey differential equation form of the NGM (1, 1, k) model, where $z^{(1)}(k)$ is called the background value, a is called the development coefficient, $b(2k-1)/2 + c$ is named the grey action or driving term, and the least squares estimates of the parameter a, b, c is

$$\hat{P} = (\hat{a}, \hat{b}, \hat{c})^{T} = \left(B^{T}B\right)^{-1} B^{T}Y, \tag{4}$$

where

$$B = \begin{pmatrix} -z^{(1)}(2) & \frac{3}{2} & 1 \\ -z^{(1)}(3) & \frac{5}{2} & 1 \\ \vdots & \vdots & \vdots \\ -z^{(1)}(n) & \frac{(2n-1)}{2} & 1 \end{pmatrix}, \quad Y = \begin{pmatrix} x^{(0)}(2) \\ x^{(0)}(3) \\ \vdots \\ x^{(0)}(n) \end{pmatrix}. \tag{5}$$

Finally,

$$\frac{\mathrm{d}x^{(1)}(t)}{\mathrm{d}t} + ax^{(1)}(t) = bt + c \tag{6}$$

is called whitened differential equation form of the NGM (1, 1, k) model.

Under the initial condition $\hat{x}^{(1)}(1) = x^{(1)}(1)$, the time response function of the NGM (1, 1, k) model is

$$\hat{x}^{(1)}(k) = \left[x^{(1)}(1) - \frac{\hat{b}}{\hat{a}} - \frac{\hat{c}}{\hat{a}} + \frac{\hat{b}}{\hat{a}^{2}}\right)\right] e^{-\hat{a}(k-1)} + \frac{\hat{b}}{\hat{a}}k + \frac{\hat{c}}{\hat{a}} - \frac{\hat{b}}{\hat{a}^{2}}, \quad k = 2, 3, \ldots, n. \tag{7}$$

The simulated and predicted values of the NGM (1, 1, k) model for the original sequence $X^{(0)}$ are

$$\begin{cases} \hat{x}^{(0)}(k) = \hat{x}^{(1)}(k) - \hat{x}^{(1)}(k), & k = 2, 3, \ldots, \\ \hat{x}^{(0)}(1) = x^{(0)}(1). \end{cases} \tag{8}$$

2.3. Accuracy Measure Indicator. In grey system theory, the absolute percentage error (APE) of each point, the mean absolute percentage error (MAPE) of all points, and the root mean square error (RMSE) of all points are usually used to measure the simulation and prediction accuracy of the grey prediction model [6].

The absolute percentage error of each point is

$$\mathrm{APE}(k) = \frac{\left|\hat{x}^{(0)}(k) - x^{(0)}(k)\right|}{x^{(0)}(k)} \times 100\%, \quad k = 1, 2, \ldots. \tag{9}$$

The mean absolute percentage error of all points is

$$\mathrm{MAPE} = \frac{1}{n-1} \sum_{k=2}^{n} \frac{\left|\hat{x}^{(0)}(k) - x^{(0)}(k)\right|}{x^{(0)}(k)} \times 100\%. \tag{10}$$

The root mean square error of all points is

$$\mathrm{RMSE} = \sqrt{\frac{1}{n-1} \sum_{k=2}^{n} \left[\hat{x}^{(0)}(k) - x^{(0)}(k)\right]^2}. \tag{11}$$

3. Fractional Order Accumulation NGM (1, 1, k) Model with Optimal Background Value

3.1. FBNGM (1, 1, k) Model. Assuming $X^{(r)} = \{x^{(r)}(1), x^{(r)}(2), \ldots, x^{(r)}(n)\}$, $r \in R^+$ is the rth order accumulation generation sequence of the nonnegative original sequence $X^{(0)} = \{x^{(0)}(1), x^{(0)}(2), \ldots, x^{(0)}(n)\}$, and $Z^{(r)} = \{z^{(r)}(2), z^{(r)}(3), \ldots, z^{(r)}(n)\}$ is the optimized background value sequence of $X^{(r)}$, among them, $z^{(r)}(k) = wx^{(1)}(k) + (1-w)x^{(1)}(k-1)$, $0 < r < 1$, $0 < w < 1$, $k = 2, 3, \ldots, n$, so

$$x^{(r-1)}(k) + az^{(r)}(k) = b\frac{2k-1}{2} + c \tag{12}$$

is called the grey differential equation form of the NGM (1, 1, k) model with the fractional order and optimized background value, denoted as the FBNGM (1, 1, k) model. Where a is called development coefficient, $z^{(r)}(k)$ is named the optimized background value, w is named the optimized background value weight, and the least squares estimate of the three parameters a, b, c is

$$\hat{P} = (\hat{a}, \hat{b}, \hat{c})^T = \left(B^T B\right)^{-1} B^T Y, \tag{13}$$

where

$$B = \begin{pmatrix} -z^{(r)}(2) & \frac{3}{2} & 1 \\ -z^{(r)}(3) & \frac{5}{2} & 1 \\ \vdots & \vdots & \vdots \\ -z^{(r)}(n) & \frac{(2n-1)}{2} & 1 \end{pmatrix}, \quad Y = \begin{pmatrix} x^{(r-1)}(2) \\ x^{(r-1)}(3) \\ \vdots \\ x^{(r-1)}(n) \end{pmatrix}. \tag{14}$$

Thus,

$$\frac{\mathrm{d}x^{(r)}(t)}{\mathrm{d}t} + ax^{(r)}(t) = bt + c \tag{15}$$

is called the whitened differential equation form of the FBNGM (1, 1, k) model.

Under initial condition $\hat{x}^{(r)}(1) = x^{(r)}(1)$, the time response function of the FBNGM (1, 1, k) model is

$$\hat{x}^{(r)}(k) = \left[x^{(r)}(1) - \frac{\hat{b}}{\hat{a}} - \frac{\hat{c}}{\hat{a}} + \frac{\hat{b}}{\hat{a}^2}\right)\right] e^{-\hat{a}(k-1)} + \frac{\hat{b}}{\hat{a}}k + \frac{\hat{c}}{\hat{a}} - \frac{\hat{b}}{\hat{a}^2}, \quad k = 2, 3, \ldots, n. \tag{16}$$

The simulated and predicted values of the FBNGM (1, 1, k) model for the original sequence $X^{(0)}$ are

$$\begin{cases} \hat{x}^{(0)}(k) = \left[\hat{x}^{(r)}\right]^{(-r)}(k) = \sum_{i=0}^{k-1} (-1)^i \frac{\Gamma(r+1)}{\Gamma(i+1)\Gamma(r-i+1)} \hat{x}^{(r)}(k-i), & k = 2, 3, \ldots, \\ \hat{x}^{(0)}(1) = x^{(0)}(1). \end{cases} \tag{17}$$

3.2. Parameter Solution of the FBNGM (1, 1, k) Model. The proposed FBNGM (1, 1, k) model described above is established based on unknown parameters r and w. In order to find the best fitness for the FBNGM (1, 1, k) model, MAPE is taken as the objective function, the relationship between model parameters is taken as constraint condition, and the nonlinear programming model is conducted as follows:

$$\min f(r,w) = \frac{1}{n-1}\sum_{k=2}^{n}\left|\frac{\hat{x}^{(0)}(k) - x^{(0)}(k)}{x^{(0)}(k)}\right| \times 100\%,$$

$$\text{s.t.}\begin{cases} 0 < r < 1, 0 < w < 1, \\ \hat{P} = [\hat{a}, \hat{b}, \hat{c}]^T = \left(B^T B\right)^{-1} B^T Y, \\ B = \begin{pmatrix} -z^{(r)}(2) & \frac{3}{2} & 1 \\ -z^{(r)}(3) & \frac{5}{2} & 1 \\ \vdots & \vdots & \vdots \\ -z^{(r)}(n) & \frac{(2n-1)}{2} & 1 \end{pmatrix}, Y = \begin{pmatrix} x^{(r-1)}(2) \\ x^{(r-1)}(3) \\ \vdots \\ x^{(r-1)}(n) \end{pmatrix}, \\ z^{(r)}(k) = wx^{(r)}(k) + (1-w)x^{(r)}(k-1), \quad k = 2,3,\ldots,n, \\ \hat{x}^{(r)}(k) = \left[x^{(r)}(1) - \left(\frac{\hat{b}}{\hat{a}} - \frac{\hat{c}}{\hat{a}} + \frac{\hat{b}}{\hat{a}^2}\right)\right]e^{-\hat{a}(k-1)} + \frac{\hat{b}}{\hat{a}}k + \frac{\hat{c}}{\hat{a}} - \frac{\hat{b}}{\hat{a}^2}, \quad k = 2,3,\ldots,n, \\ \hat{x}^{(0)}(k) = \left[\hat{x}^{(r)}\right]^{(-r)}(k) = \sum_{i=0}^{k-1}(-1)^i \frac{\Gamma(r+1)}{\Gamma(i+1)\Gamma(r-i+1)}\hat{x}^{(r)}(k-i), \quad k = 2,3,\ldots, \\ \hat{x}^{(0)}(1) = x^{(0)}(1). \end{cases} \tag{18}$$

For the abovementioned nonlinear programming model, the particle swarm optimization algorithm [18] (PSO) is used to solve the best parameters of the proposed FBNGM (1, 1, k) model in this study.

3.3. Modeling Procedure of the FBNGM (1, 1, k) Model. The modeling procedure of the FBNGM (1, 1, k) model is presented clearly in Figure 1.

4. Empirical Applications

In this section, two cases will be used to verify the feasibility and effectiveness of the proposed FBNGM (1, 1, k) model.

4.1. Case 1. China is the most electricity consuming country in the world, accounting for 27.5% of global electricity consumption. The shortage of power supply will have a serious negative impact on the stable development of China's economy. Therefore, the ability to reasonably predict China's electricity consumption plays an important role in formulating the Chinese government's energy policy. The national electricity consumption data from 2010 to 2016 are used for modeling in this study (http://www.stats.gov.cn/tjsj/ndsj/2020/indexch.htm), while the data from 2017 to 2020 are used to measure the accuracy of the model. In order to illustrate the superiority of the FBNGM (1, 1, k) model in simulation and prediction, the NGM (1, 1, k) model (abbreviated as NGM), BNGM (1, 1, k) model (abbreviated as BNGM), FNGM (1, 1, k) model (abbreviated as FNGM), and FBNGM (1, 1, k) model (abbreviated as FBNGM) together are used to simulate and predict the electricity consumption in China. The selection or optimization results of hyperparameters as well as estimation results of system parameters for all models are given in Table 1. The seeking process of hyperparameters based on PSO is shown in Figure 2. The

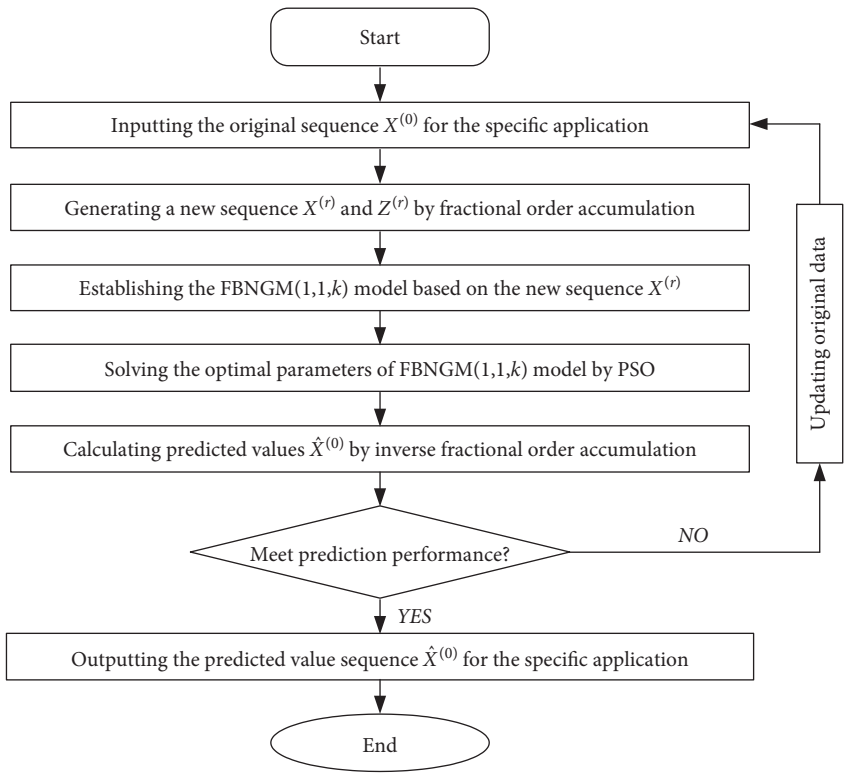

Figure 1: Modeling procedure of the FBNGM (1, 1, k) model.

Table 1: The parameters for all models in Case 1.

Model	Parameter				
	r	w	a	b	c
NGM	1.0000	0.5000	0.0041	3.0516	4.2635
BNGM	1.0000	0.4620	0.0043	3.0669	4.2623
FNGM	0.2091	0.5000	0.9109	6.3085	4.8645
FBNGM	0.8986	0.5017	−0.2269	−8.9817	4.1691

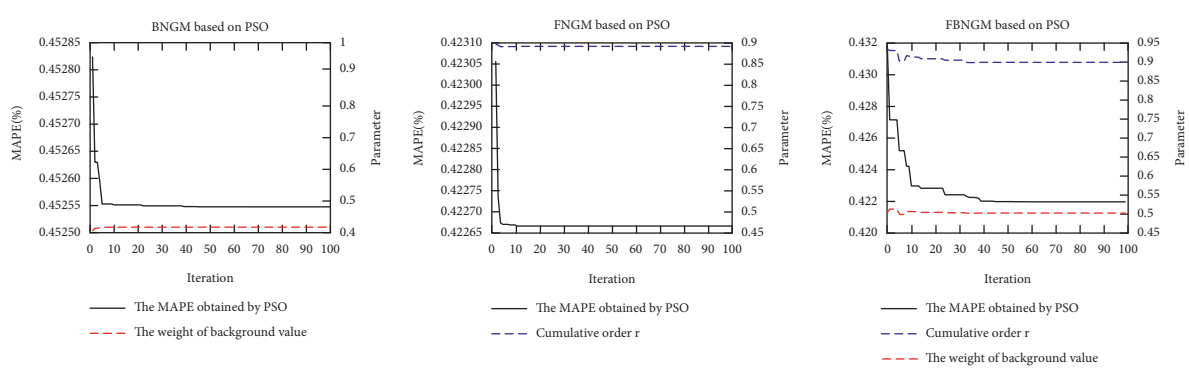

Figure 2: Track of the seeking process of PSO algorithms for the three models in Case 1.

simulation and prediction results of all models are given in Table 2 and Figures 3 and 4.

In the case, the estimation results and search process of the unknown parameters of the models are given in Table 1 and Figure 2. From Table 2 and Figures 3 and 4, it is easy to see that the simulation accuracy of the FBNGM (1, 1, k) model is higher than that of the other three prediction models, and the prediction accuracy of the FBNGM (1, 1, k) model is higher than that of the NGM (1, 1, k) model and the BNGM (1, 1, k) model. According to the accuracy measure

Table 2: Simulation and prediction results of China's electricity consumption (billion kilowatt hours).

Year	Actual value	NGM		BNGM		FNGM		FBNGM	
		Forecasting value	APE (%)	Forecasting value	APE (%)	Forecasting value	APE (%)	Forecasting value	APE (%)
2010	4192	4192	0.00	4192	0.00	4192	0.00	4192	0.00
2011	4693	4695	0.04	4693	0.00	4680	0.28	4680	0.28
2012	4959	4980	0.43	4979	0.39	5000	0.82	4995	0.73
2013	5322	5265	1.08	5263	1.11	5269	1.00	5265	1.08
2014	5523	5548	0.45	5546	0.42	5530	0.12	5527	0.06
2015	5802	5830	0.49	5828	0.45	5804	0.04	5802	0.00
2016	6130	6111	0.30	6109	0.34	6112	0.29	6107	0.38
Modeling period (2010–2016)									
MAPE (%)		0.4653		0.4599		0.5393		0.4220	
RMSE (10^{-2})		0.3032		0.3033		0.3337		0.2981	
Testing period (2017–2020)									
2017	6482	6391	1.40	6388	1.45	6473	0.14	6456	0.40
2018	7151	6670	6.73	6666	6.78	6909	3.39	6867	3.97
2019	7285	6947	4.64	6942	4.71	7447	2.22	7360	1.02
2020	7511	7224	3.82	7218	3.91	8122	8.14	7957	5.94
MAPE (%)		4.1485		4.1768		3.1238		2.8328	
RMSE (10^{-2})		3.3029		3.3219		2.6123		2.6727	

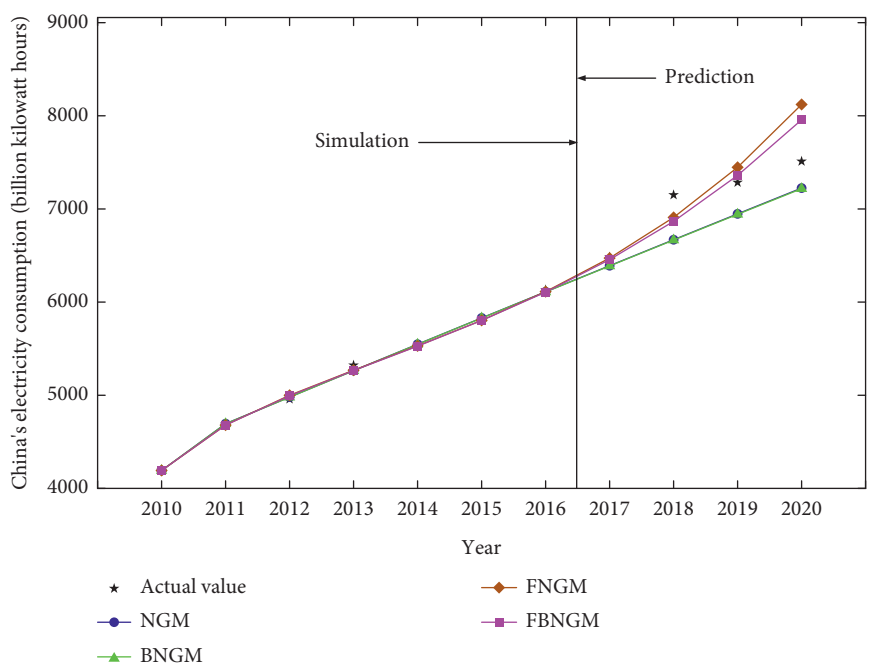

Figure 3: Simulation and prediction results for the four grey models in Case 1.

indicator, the proposed FBNGM (1, 1, k) model has good performance in simulation and prediction, which shows that the FBNGM (1, 1, k) model is suitable and effective for predicting China's electricity consumption.

4.2. Case 2. Agriculture is the basic industry to support the construction and development of national economy, and accurately predicting the development trend of agricultural production is the premise and foundation for formulating national economic plan and social development strategy. China is a large population country; its agriculture is related to national livelihood and social stability and has a fundamental position and role in the national economy. In the study, country agriculture gross output value data in 2007–2014 (http://data.stats.gov.cn/easyquery.htm) is used to establish the model, and the data in 2015–2018 is used to test the prediction accuracy. In order to illustrate the superiority of the FBNGM (1, 1, k) model in simulation and prediction, the NGM (1, 1, k) model (abbreviated as NGM), BNGM (1, 1, k) model (abbreviated as BNGM), FNGM (1, 1, k) model (abbreviated as FNGM), and FBNGM (1, 1, k) model (abbreviated as FBNGM) together are used to simulate and predict the agriculture gross output value in China.

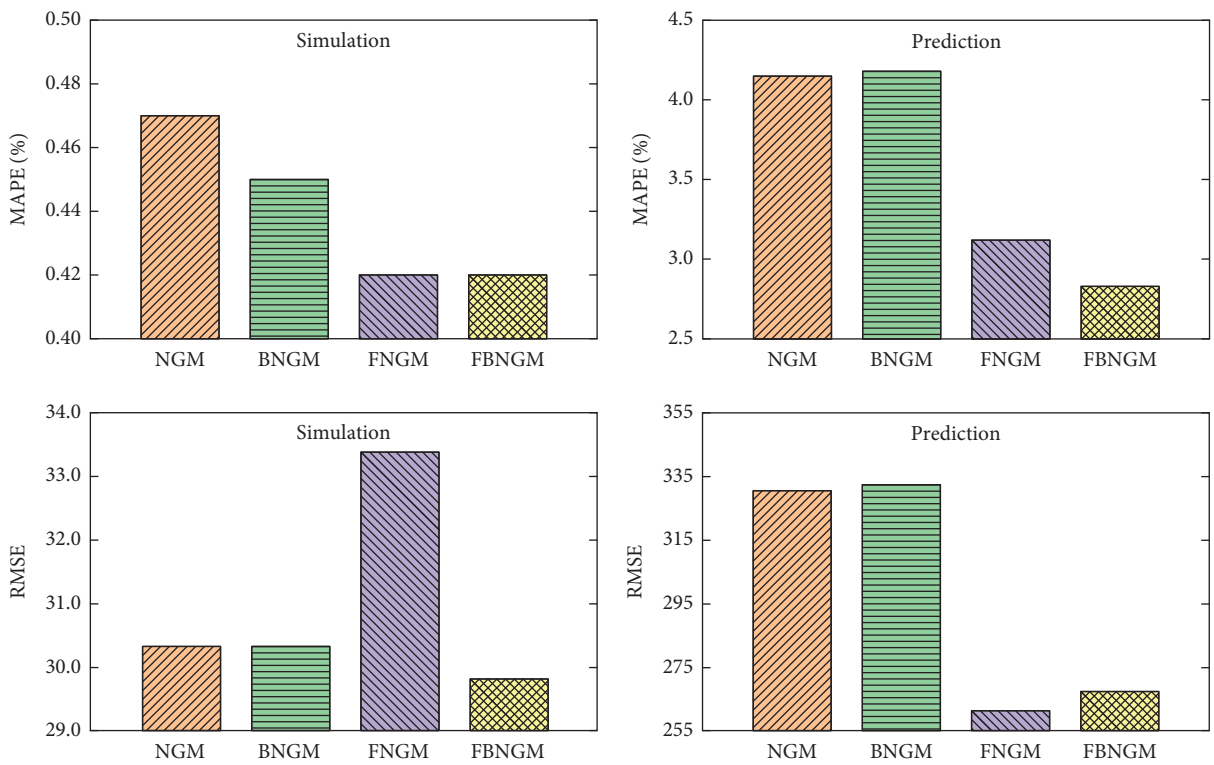

Figure 4: Comparison of simulation and prediction accuracy for the four grey models in Case 1.

Table 3: The parameters for all models in Case 2.

Model	Parameter				
	r	w	a	b	c
NGM	1.0000	0.5000	0.0059	4.5083	2.4532
BNGM	1.0000	0.6232	0.0032	4.3929	2.4631
FNGM	0.1230	0.5000	−0.2754	−1.9803	1.2934
FBNGM	0.1041	0.5017	−0.2749	−1.8595	7.7389

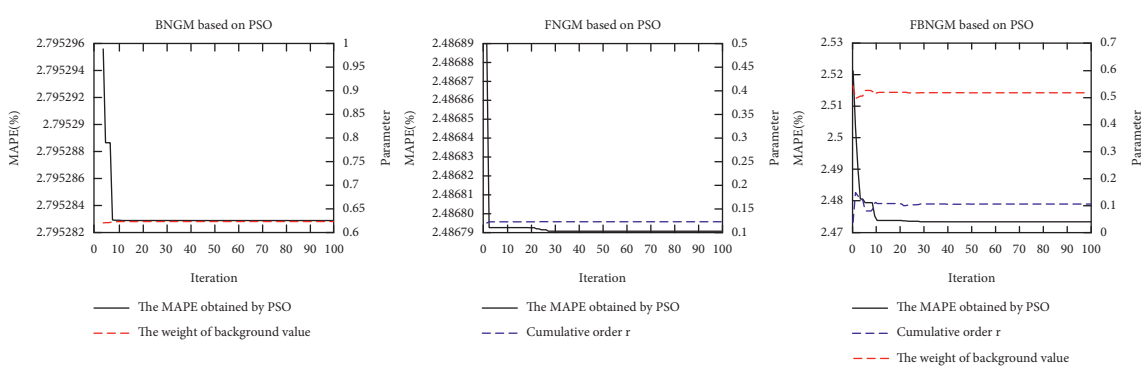

Figure 5: Track of the seeking process of PSO algorithms for the three models in Case 2.

The selection or optimization results of hyperparameters as well as estimation results of system parameters for all models are given in Table 3. The seeking process of hyperparameters based on PSO is shown in Figure 5. The simulation and prediction results of all models are given in Table 4 and Figures 6 and 7.

Table 4: Simulation and prediction results of agriculture gross output value in China (100 million yuan).

Year	Actual value	NGM		BNGM		FNGM		FBNGM	
		Forecasting value	APE (%)	Forecasting value	APE (%)	Forecasting value	APE (%)	Forecasting value	APE (%)
2007	27674	27674	0.00	27674	0.00	27674	0.00	27674	0.00
2008	32464	31044	4.38	31083	5.32	31166	4.00	31242	3.76
2009	33584	35357	5.28	35369	3.15	35627	6.09	35658	6.18
2010	38431	39646	3.16	39642	1.96	40163	4.51	40155	4.49
2011	44781	43909	1.95	43902	1.91	44586	0.44	44559	0.49
2012	49085	48147	1.91	48148	1.22	48807	0.56	48777	0.62
2013	53028	52361	1.26	52380	1.75	52756	0.51	52722	0.58
2014	55626	56550	1.66	56599	4.25	56351	1.30	56286	1.19
Modeling period (2007–2014)									
MAPE (%)		2.7990		2.7953		2.4868		2.4885	
RMSE (10^{-2})		11.6963		11.6997		11.6974		11.8765	
Testing period (2015–2018)									
2015	57774	60714	5.09	60804	5.24	59493	2.97	59324	2.68
2016	60139	64854	7.84	64996	8.08	62053	3.18	61634	2.49
2017	62099	68970	11.06	69175	11.39	63860	2.84	62929	1.34
2018	64734	73062	12.87	73340	13.30	64691	0.07	62808	2.97
MAPE (%)		9.2150		9.5027		2.2649		2.7201	
RMSE (10^{-2})		60.7154		62.6322		15.5892		17.7565	

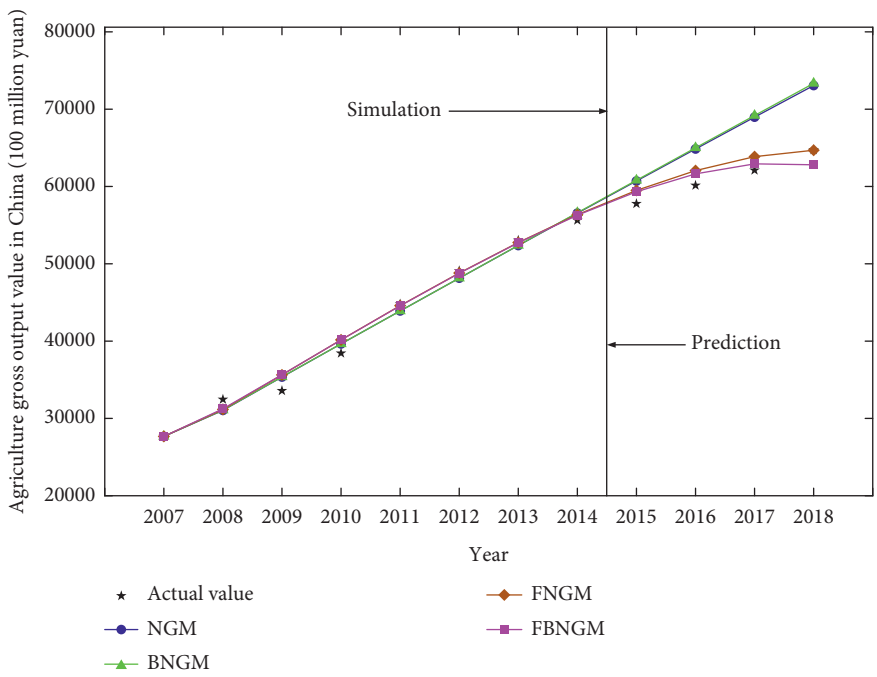

Figure 6: Simulation and prediction results for the four grey models in Case 2.

In the case, the estimation results and search process of the unknown parameters of the models are given in Table 3 and Figure 5. From Table 4 and Figures 6 and 7, it is easy to see that the simulation accuracy of the FBNGM (1, 1, k) model is higher than that of the other three prediction models, and the prediction accuracy of the FBNGM (1, 1, k) model is higher than that of the NGM (1, 1, k) model and the BNGM (1, 1, k) model. According to the accuracy measure indicator, the proposed FBNGM (1, 1, k) model has good performance in simulation and prediction, which shows that the FBNGM (1, 1, k) model is suitable and effective for predicting the agriculture gross output value in China.

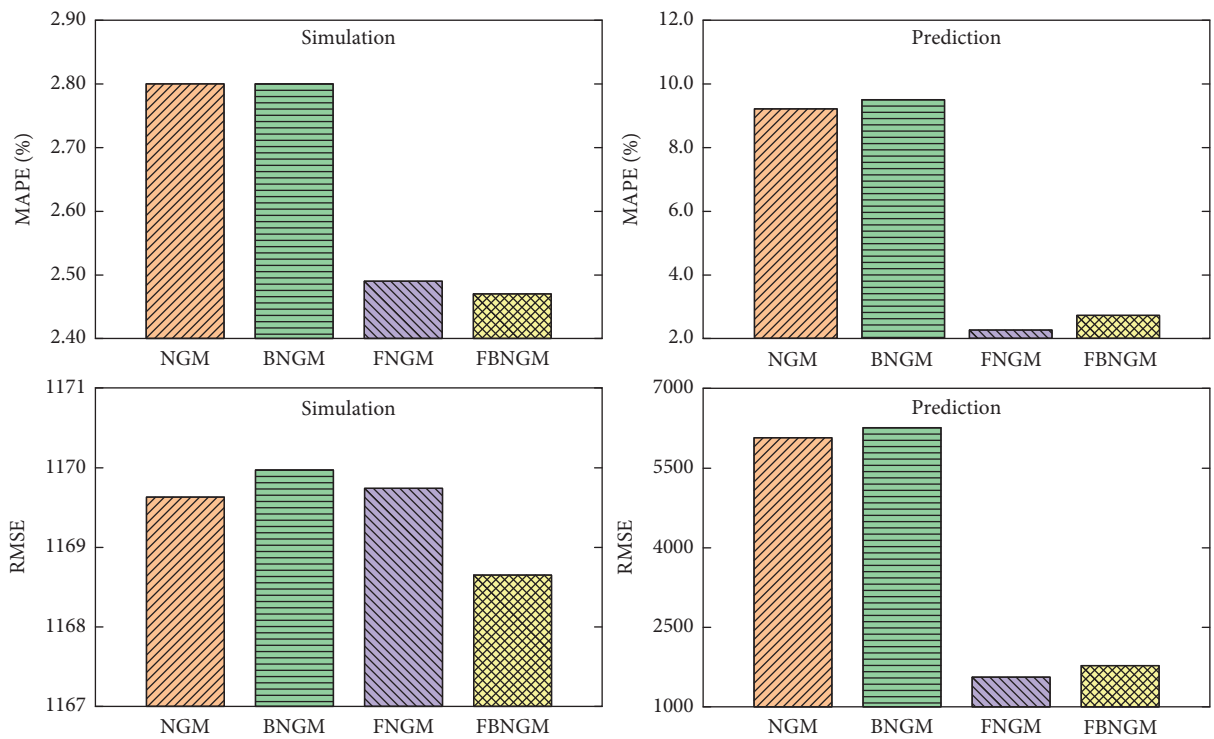

Figure 7: Comparison of simulation and prediction accuracy for the four grey models in Case 2.

5. Conclusion

In order to further improve the prediction accuracy of the NGM (1, 1, k) model, this study optimizes the model from the weight of the background value and fractional order accumulation generation. Then, the parameter solution and modeling process of the proposed FBNGM (1, 1, k) model is described in detail. In order to verify the feasibility and effectiveness of the FBNGM (1, 1, k) model proposed in this study, the novel model and other three grey forecasting models together are applied to the two actual cases with economic significance. It is obvious from the empirical results of the application examples that the simulation and prediction accuracy of the FBNGM (1, 1, k) model are higher than NGM (1, 1, k) and BNGM (1, 1, k) models. It confirms that the proposed FBNGM (1, 1, k) model has certain effectiveness in improving prediction accuracy. Therefore, the thought of optimizing the NGM (1, 1, k) model proposed in the study based on the weight of the background value and fractional order accumulation generation has a certain application value in the prediction of electricity consumption and agriculture gross output value.

Data Availability

The data used to support the findings of this study are available at http://data.stats.gov.cn/easyquery.htm.

Conflicts of Interest

The authors declare that they have no conflicts of interest.

Authors' Contributions

Jun Zhang wrote the original draft and developed the methodology. Yanping Qin developed software and involved in visualization. Xinyu Zhang involved in modification. Bing Wang wrote the review. Dongxue Su validated the study. Huaqiong Duo updated the draft.

Acknowledgments

The relevant works conducted were supported by National Natural Science Foundation of China (32160332), Inner Mongolia Agricultural University High-Level Talents Scientific Research Project (NDYB2019-35), Key Project of the Study of Statistical Science from Statistics Bureau of Inner Mongolia Autonomous Region (TJXHKT202001), and the first batch of Industry-University Cooperative Education Project of the Ministry of Education in 2019 (201901148037).

References

[1] E. Cui, L. Ren, and H. Sun, "Analysis of energy-related CO2 emissions and driving factors in five major energy consumption sectors in China," *Environmental Science and Pollution Research*, vol. 23, no. 19, pp. 19667–19674, 2016.

[2] L. Tu and Y. Chen, "An unequal adjacent grey forecasting air pollution urban model," *Applied Mathematical Modelling*, vol. 99, pp. 260–275, 2021.

[3] B. Zeng, H. Li, and X. Ma, "A novel multi-variable grey forecasting model and its application in forecasting the grain production in China," *Computers & Industrial Engineering*, vol. 150, Article ID 106915, 2020.

[4] B. Zeng, M. Zhou, X. Liu, and Z. Zhang, "Application of a new grey prediction model and grey average weakening buffer operator to forecast China's shale gas output," *Energy Report*, vol. 6, pp. 1608–1618, 2020.

[5] C. Liu, W.-Z. Wu, W. Xie, and J. Zhang, "Application of a novel fractional grey prediction model with time power term to predict the electricity consumption of India and China," *Chaos, Solitons & Fractals*, vol. 141, Article ID 110429, 2020.

[6] J. Zhang, Y. Qin, and H. Duo, "The development trend of China's natural gas consumption: a forecasting viewpoint based on grey forecasting model," *Energy Reports*, vol. 7, pp. 4308–4324, 2021.

[7] C. Liu, W. Xie, W.-Z. Wu, and H. Zhu, "Predicting Chinese total retail sales of consumer goods by employing an extended discrete grey polynomial model," *Engineering Applications of Artificial Intelligence*, vol. 102, no. 3, Article ID 104261, 2021.

[8] P. F. Zu, W. Y. Zhou, W. Xie et al., "The application of GM (1,1) model based on the optimization of background value to the GDP Prediction in Mudanjiang," *Mathematics in Practice and Theory*, vol. 48, no. 1, pp. 1–7, 2018.

[9] L. Wu, S. Liu, L. Yao, S. Yan, and D. Liu, "Grey system model with the fractional order accumulation," *Communications in Nonlinear Science and Numerical Simulation*, vol. 18, no. 7, pp. 1775–1785, 2013.

[10] N.-M. Xie and S.-F. Liu, "Discrete grey forecasting model and its optimization," *Applied Mathematical Modelling*, vol. 33, no. 2, pp. 1173–1186, 2009.

[11] J. Cui, Y. G. Dang, and S. F. Liu, "Novel grey forecasting model and its modeling mechanism," *Control and Decision*, vol. 24, no. 11, pp. 1702–1706, 2009.

[12] L. Q. Zhan and H. J. Shi, "Methods and model of grey modeling for approximation non-homogenous exponential data," *Systems Engineering-Theory and Practice*, vol. 33, no. 3, pp. 659–694, 2013.

[13] J. Cui, S. F. Liu, and H. Y. Ma, "Morbid property of grey prediction model with time-power," *Control and Decision*, vol. 31, no. 5, pp. 953–956, 2016.

[14] H. T. Wang and L. Gong, "Extended NGM (1,1,k) prediction model and its application in oil spectrum analysis," *Lubrication Engineering*, vol. 46, no. 5, pp. 113–117, 2021.

[15] M. Y. Tong, X. H. Zhou, and B. Zeng, "Optimization of background value in grey NGM (1,1,k) model," *Control and Decision*, vol. 32, no. 3, pp. 507–514, 2017.

[16] L. F. Wu, S. F. Liu, and L. G. Yao, "Discrete grey model based on fractional order accumulate," *Systems Engineering Theory and Practice*, vol. 34, no. 7, pp. 1822–1827, 2014.

[17] B. Zeng and S. Liu, "A self-adaptive intelligence gray prediction model with the optimal fractional order accumulating operator and its application," *Mathematical Methods in the Applied Sciences*, vol. 40, no. 18, pp. 7843–7857, 2017.

[18] Y. L. Zhao, N. Hua, and Z. H. Yu, "Improved particle swarm optimization algorithm based on twice search," *Journal of Computer Applications*, vol. 37, no. 9, pp. 2541–2546, 2017.

Hindawi
Journal of Mathematics
Volume 2021, Article ID 9200560, 14 pages
https://doi.org/10.1155/2021/9200560

Research Article

Forecasting Chinese Wind Power Installed Capacity Using a Novel Grey Model with Parameters Combination Optimization

Xiaoshuang Luo,[1] **Bo Zeng**,[2] **Hui Li**,[2] **and Wenhao Zhou**[3]

[1]*School of International Business, Chongqing Finance and Economics College, Chongqing 401320, China*
[2]*School of Management Science and Engineering, Chongqing Technology and Business University, Chongqing 400067, China*
[3]*College of Business Administration, Huaqiao University, Quanzhou, 362021, China*

Correspondence should be addressed to Bo Zeng; bozeng@ctbu.edu.cn

Received 17 June 2021; Accepted 3 August 2021; Published 17 August 2021

Academic Editor: Lifeng Wu

The intermittent and uncertain characteristics of wind generation have brought new challenges for the hosting capacity and the integration of large-scale wind power into the power system. Consequently, reasonable forecasting wind power installed capacity (WPIC) is the most effective and applicable solution to meet this challenge. However, the single parameter optimization of the conventional grey model has some limitations in improving its modeling ability. To this end, a novel grey prediction model with parameters combination optimization is proposed in this paper. Firstly, considering the modeling mechanism and process, the order of accumulation generation of the grey prediction model is optimized by Particle Swarm Optimization (PSO) Algorithm. Secondly, as different orders of accumulation generation correspond to different parameter matrixes, the background value coefficient of the grey prediction model is optimized based on the optimal accumulation order. Finally, the novel model of combinational optimization is employed to simulate and forecast Chinese WPIC, and the comprehensive error of the novel model is only 1.34%, which is superior to the other three grey prediction models (2.82%, 1.68%, and 2.60%, respectively). The forecast shows that China's WPIC will keep growing in the next five years, and some reasonable suggestions are put forward from the standpoint of the practitioners and governments.

1. Introduction

With the development of China's manufacturing, the rapid growth of energy consumption has become a major bottleneck affecting China's sustainable development of the economy. As a typical representative of green and environment-friendly energy, wind power is driven by international policies and led by the global development trend. It is of great significance to develop new power energy and to solve the shortage of power supply and consumption [1]. Wind turbines use installed capacity to describe how much electricity may be generated by a turbine in optimal wind conditions, describing how many watts of electricity the turbine hardware can possibly produce—generally measured in megawatts or kilowatts. The US Energy Information Administration (EIA) refers to capacity as the maximum output of electricity that a generator can produce under ideal conditions.

Although China's wind power industry started late, it has achieved extremely rapid development since 2005, with the installed capacity of wind power (WPIC) doubling for five consecutive years. Wind generation is characterized by intermittency and volatility, which requires coordination and cooperation after large-scale access to the power grid, especially the continuous improvement of adaptability and stability [2].

However, the rapid development of China's wind power market does not make the grid connection improved on a par. The characteristics of reverse peak regulation and uneven distribution and the fluctuation of wind power have a significant impact on the safe operation and power quality of the power system. Unsuccessful grid-connected operation of

wind farms will result in a negative impact on the following aspects: the power quality, the voltage stability, the power grid security, etc. [3]. With the continuous expansion of the scale of wind farms, the impact of wind power's characteristics on the operation of conventional power systems is becoming more and more significant. The power grid security and risks have become serious constraints to energy supply and demand structure, even seriously wind abandoning phenomenon occurs, which will be resulting in a great waste of resources [4, 5].

As reported by National Energy Administration (NEA) 2019, China's wind power cumulative installed capacity reached 210.05 million kW, accounting for about 32.29% of the global total, and wind abandoning power was 16.9 billion kW. Especially in the following provinces (region) with more than 5% abandonment rate: Xinjiang province (14.0% abandonment rate, 6.61 billion kW), Gansu province (7.6% abandonment rate, 1.88 billion kW), and Inner Mongolia (7.1% abandonment rate, 5.12 billion kW). The abandoned wind power of these provinces (regions) totaled 13.6 billion kW, accounting for 81% of the abandoned wind power in the country. Therefore, accurate forecasting tools and scientific evaluation methods are necessary to support these environmental protection policies. The policy executors need more reliable predictive and assessment tools to predict and analyze installed capacity.

Considering that the development of the wind power industry in China is relatively short, the data available is relatively limited, and there are many factors affecting wind power generation. As a consequence, the prediction of wind power generation is essentially an uncertainty prediction problem based on the characteristics of a small sample and poor data. So far, there are many scholars who have carried out extensive research on prediction aspects of wind generation problems, such as the conventional grey prediction model, the ARMA model, the neural networks (including BP neural network and artificial network), the support vector machine (SVM) method, etc., these methods are presented as follows:

1.1. Grey Prediction Model in Wind Power in Wind Power Industry Forecasting. Ma et al. defined a new information priority accumulated grey model with time power to predict short-term wind turbine capacity [6]. Yang et al. put forward a method to enhance the prediction accuracy and robustness of the grey prediction model by introducing multisource information into traditional grey models [7]. Wu and Cong propose a novel method for short-term wind power forecasting, which combines the wavelet transform, particle swarm optimization dynamic grey model, and Lyapunov exponent prediction method [8]. Zhang et al. proposed a novel power-driven fractional accumulated grey model (PFAGM) to solve the wind energy consumption prediction problem. A heuristic intelligent algorithm WOA was used to search the optimal order and the least-square method to estimate linear parameters of the PFAGM model [9]. Qian and Wang proposed a seasonal GM (1, 1) method based on the HP filter for forecasting wind power generation in China [10]. Duman et al. using optimized multivariate grey models to estimate the electronic waste [11].

1.2. Application of SVM in Wind Power Industry Forecasting. Vinothkumar and Deeba employ long short-term memory network model and variants of SVM models to predict the wind speed for the considered locations where the windmill has been installed [12]. Li et al. present a novel backward bat algorithm (BBA) for the parameter tuning of the SVM to forecast solar power and wind speed [13]. Yeh et al. built a long cycle maintenance of wind turbine predictive model based on the convolutional neural network and support vector machine [14]. Agasthian et al. nominate a method to decide the parameters for support vector machine (SVM) in wind turbine, called Cuckoo search optimization (CSO). They found that the CSO model based on the SVM algorithm accomplishes the most accurate fault detection than the past models [15].

1.3. ARMA Model in Wind Power Industry Forecasting. In order to address the static voltage stability issue and suppress the voltage fluctuation caused by the increasing integration of wind farms and solar photovoltaic (PV) power plants, Lu et al. proposed a two-tier reactive power and voltage control strategy based on ARMA power forecasting models for wind and solar plants [16]. Ergin and Shi proposed four approaches based on the autoregressive moving average (ARMA) method to forecasting short-term wind speed and direction tuple [17]. Chen et al. proposed a stochastic wind power model based on an autoregressive integrated moving average (ARIMA) process. This model takes into account the nonstationary and physical limits of stochastic wind power generation [18].

1.4. Neural Networks in Wind Power Industry Forecasting. Luo et al. proposed a novel fault prediction method that is combined based on BP neural network and Pair-Copula model [19]. An artificial neural network (ANN) based model is investigated for short-term forecasting of the hourly wind speed, solar radiation, and electrical power demand [20]. In order to enhance the accuracy of short-term wind speed prediction, Wang et al. constructed an improved small-world BP neural (SWBP) based on the MI algorithm to predict short-term wind power [21]. Jahangir et al. proposed a short-term wind speed prediction framework based on Artificial neural networks [22]. Zhang et al. use the similar day data preprocess and unprocessed as the input of back propagation neural network optimized by genetic algorithm (GA-BP neural network) [23].

1.5. Other Predictive Models. In addition to the above research methods, scholars have adopted other predictive methods in the field of wind power. For instance, Tan et al. explored and developed the Salp Swarm Algorithm in the iterative process to optimize the input weight matrix and hidden layer deviation of the Extreme Learning Machine (ELM), in order to improve the adaptability and accuracy of

the prediction model [24]. Wang et al. build a hybrid PSO-SVM-ARMA prediction model for wind power prediction, and the covariance minimization method and PSO are employed to find the optimal weights [25]. Wang et al. designed a novel deep learning network stacked by independent recurrent autoencoder (IRAE) which, according to the characteristics of ultrashort-term wind power data, hereafter called SIRAE (staked independently recurrent autoencoder). This approach accommodates a sheer volume of data in the smart energy era and overcomes the effects of random changes in the natural environment [26]. Wang et al. proposed a hybrid model known as SAM–ESM–RBFN, which is used for capturing these different patterns and obtaining better prediction performance. This model is based on the seasonal adjustment method (SAM), exponential smoothing method (ESM), and radial basis function neural network (RBFN) [27].

The above research results are of great value to realize the scientific prediction of wind power installed capacity in China and to provide solutions for the healthy development of the wind power industry. Because of the randomness, volatility, and intermittence of wind power systems, the data characteristics of wind power prediction and installed capacity are consistent with the grey model of "small samples, poor information." The techniques based on large samples, such as the SVM and neural network, are difficult to apply to the prediction of WPIC and the ARMA model is difficult to detect the complex nonlinear dynamic processes of power system and wind energy, so it can not accurately describe the real changes of a wind speed or wind farm power, which affects the performance of the prediction results. The artificial neural network forecasting model has a high predictive ability for nonlinear data, but it is difficult to search for the optimal solution so that it barely meets the accuracy requirements. The conventional grey prediction model has the advantages of small data modeling and can be used to predict the hosting capacity of wind power. However, the conventional GM (1, 1) model is the most primitive single variable grey model, and the limitation of the structure makes it difficult to meet the requirements of complex systems. As a consequence, the conventional GM (1, 1) model does not perform well in wind power industry. Another problem of the current grey model with the combination model is that no detailed optimization algorithm is used to seek the optimum solution of parameters [28–31]. Therefore, we establish an optimization model to search the parameters and use the PSO algorithm to determine the optimized values of the novel model. This paper intends to expand the structure and optimize the parameters of the conventional grey model, on the basis of which a more reasonable prediction model of wind power installed capacity is constructed.

The remainder of the paper is organized as follows: In Section 2, a new grey optimization model is proposed, which include optimization with background value and optimization with fractional order accumulation. In Section 3, we simulate China's WPIC from 2009 to 2016 by employing the WPICM (1, 1, r, ξ) model and compare its error with the other three conventional grey models. In Section 4, we use the WPICM (1, 1, r, ξ) model to forecast China's WPIC for 2020–2024. According to the forecast results, some suggestions are provided for the policy-making of the Chinese government. Conclusions are presented in Section 5. The paper structure is presented in Figure 1.

2. WPICM (1, 1, r, ξ) Model

This paper will study the predictive problem of the WPIC in China by using the combination grey prediction model. In order to construct a suitable grey forecast model for wind power installed capacity, we expand the structure of the traditional GM (1, 1) model and optimizes the model parameters. These will provide a methodological basis for forecasting the WPIC in China in Section 4.

2.1. Basic Form of the WPICM (1, 1) Model

Definition 1 (see [32]). Assume that a raw sequence is $W^{(0)} = (w^{(0)}(1), w^{(0)}(2), \ldots, w^{(0)}(n))$, where $w^{(0)}(k) \geq 0$, $k = 1, 2, \ldots, n$. $W^{(1)}$ is the 1-AGO sequence of $W^{(0)}$, that is,

$$W^{(1)} = \left(w^{(1)}(1), w^{(1)}(2), \ldots, w^{(1)}(n)\right), \tag{1}$$

where

$$W^{(1)} = \sum_{i=1}^{k} w^{(0)}, \quad k = 1, 2, \ldots, n, \tag{2}$$

and $Z^{(1)}$ is the mean sequence generated by consecutive neighbors of $W^{(1)}$, that is $Z^{(1)} = (z^{(1)}(1), z^{(1)}(2), \ldots, z^{(1)}(n))$, where $z^{(1)} = 0.5 \times [x^{(1)}(k) + x^{(1)}(k-1)]$, $k = 1, 2, \ldots, n$. Then,

$$w^{(0)} + az^{(r)}(k) = 0.5(2k-1)b + c \tag{3}$$

is the common form of the WPICM (1, 1) model.

Definition 2. Assuming that $W^{(0)}$, $W^{(1)}$, and $Z^{(1)}$ are given by Definition 1, we have the following equation:

$$\frac{\mathrm{d}w^{(1)}}{\mathrm{d}t} + aw^{(1)} = bt + c, \tag{4}$$

which is named the whitenization equation of grey model WPICM(1,1) for short [32].

In equation (3), we can estimate the parameter a and b using the least-square method, which is as follows:

$$\widehat{p} = (a, b, c)^T = \left(B^T B\right)^{-1} B^T Y, \tag{5}$$

where

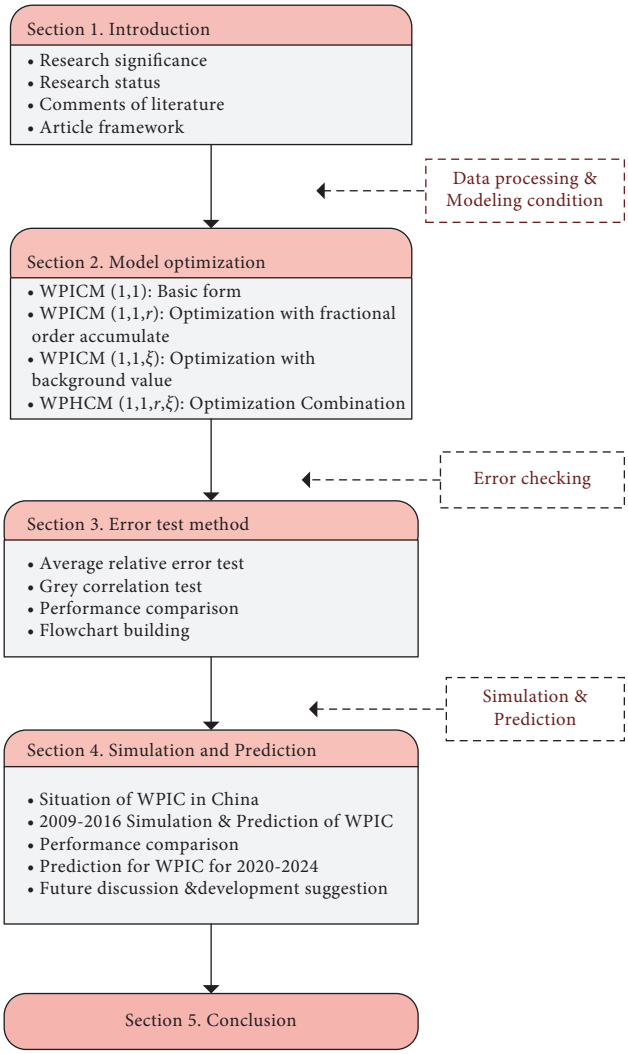

Figure 1: Paper structure.

$$Y = \begin{bmatrix} w^{(0)}(2) \\ w^{(0)}(3) \\ \vdots \\ w^{(0)}(n) \end{bmatrix},$$

$$B = \begin{bmatrix} -z^{(1)}(2) & \frac{3}{2} & 1 \\ -z^{(1)}(3) & \frac{5}{2} & 1 \\ \vdots & \vdots & \vdots \\ -z^{(1)}(n) & \frac{(2n-1)}{2} & 1 \end{bmatrix}. \tag{6}$$

Theorem 1 (see [32]). *Assuming that Y, B, and $\widehat{p}$ are the same as those Definition 2, one can obtain that the time response sequence of WPICM(1,1) is given by the following:*

$$\begin{aligned} \widehat{w}^{(0)}(t) &= \widehat{w}^{(1)}(t) - \widehat{w}^{(1)}(t-1) \\ &= \left(1-e^{a}\right)\left(w^{(0)}(1) - \frac{b}{a} + \frac{b}{a^2} - \frac{c}{a}\right)e^{-a(t-1)} + \frac{b}{a}. \end{aligned} \tag{7}$$

Let

$$\begin{aligned} \alpha &= \left(1-e^{a}\right)\left(w^{(0)}(1) - \frac{b}{a} + \frac{b}{a^2} - \frac{c}{a}\right), \\ \beta &= \frac{b}{a}. \end{aligned} \tag{8}$$

Equation (7) will be transformed as follows:

$$w^{(0)}(k) = \alpha e^{-a(k-1)} + \beta. \tag{9}$$

2.2. Optimization with Fractional Order Accumulate. In the process of constructing the grey prediction model, the fractional order accumulate r is an important tool to weaken the randomness of grey modeling sequence. Different orders have different effects on the performance of the grey prediction model. The traditional grey model is set $r = 1$, which largely limits the room for improving the performance of the model. In the actual modeling process, r can be accepted as a fraction, a negative number, or another integer [30, 33]. Hence, in this section, a new order optimization model r is discussed.

Definition 3. The raw sequence is proposed by Definition 1; $W^{(r)}$ is the r-AGO (Accumulating Generation Operator) sequence of $W^{(0)}$, that is,

$$W^{(r)} = \left(w^{(r)}(1), w^{(r)}(2), \ldots, w^{(r)}(n)\right), \tag{10}$$

where

$$w^{(r)}(k) = \sum_{i=1}^{k} \frac{\Gamma(r+k-i)}{\Gamma(k-i+1)\Gamma(r)} w^{(0)}(i), \quad k = 1, 2, \ldots, n. \tag{11}$$

Definition 4. Assuming that $W^{(0)}$ is given by Definition 1 and $W^{(r)}$ is given by Definition 3, $r \in R^{+}$, then, $Z^{(r)} = (z^{(r)}(1), z^{(r)}(2), \ldots, z^{(r)}(n))$ is called the mean sequence generated by consecutive neighbors of $W^{(r)}$, where

$$z^{(r)}(k) = \frac{w^{(r)}(k) + w^{(r)}(k-1)}{2}, \quad k = 2, 3, \ldots, n. \tag{12}$$

As the $W^{(0)}$, $W^{(r)}$, and $Z^{(r)}$ are known, then

$$w^{(r-1)} + a z^{(r)}(k) = 0.5(2k-1)b + c \tag{13}$$

is the basic form of WPICM (1, 1, r).

$\widehat{p} = (a, b, c)^T = (B^T B)^{-1} B^T Y$ is a sequence of parameters, and

$$Y = \begin{bmatrix} w^{(r-1)}(2) \\ w^{(r-1)}(3) \\ \vdots \\ w^{(r-1)}(n) \end{bmatrix},$$

$$B = \begin{bmatrix} -z^{(r)}(2) & \frac{3}{2} & 1 \\ -z^{(r)}(3) & \frac{5}{2} & 1 \\ \vdots & \vdots & \vdots \\ -z^{(r)}(n) & \frac{(2n-1)}{2} & 1 \end{bmatrix}. \tag{14}$$

The least squares estimate sequence of WPICM (1, 1, r) satisfied $\widehat{p} = (a, b, c)^T = (B^T B)^{-1} B^T Y$.

2.3. WPICM (1, 1, ξ) Model Optimization with Background Value. When constructed a grey prediction model, the generation of the immediate means is a smooth processing method to weaken the influence of the extreme value on the size of the grey action in the 1-ago sequence, and the background value is the main parameter for the weight allocation of the two adjacent elements in the immediate mean sequence.

In the conventional grey modeling process, it is a simplification to set the background value generally as 0.5 [32, 34], in which $z^{(1)}(k) = 0.5 \times w^{(1)}(k) + 0.5 \times w^{(1)}(k-1)$. Under the condition of minimizing the sum of squares of the average simulation error, we optimize the background value on the basis of the WPICM (1, 1) model, which improves the performance of the grey prediction model to some extent.

Definition 6. The sequence of $W^{(0)}$, $W^{(1)}$, and $Z^{(1)}$ is given in Definition 1, assuming that background value is ξ; then,

$$z_g^{(1)}(k) = \xi w^{(1)}(k) + (1-\xi) w^{(1)}(k-1) \tag{15}$$

and

$$w^{(0)}(k) + a\left(\xi w^{(1)}(k) + (1-\xi) w^{(1)}(k-1)\right) = 0.5(2k-1)b + c, \tag{16}$$

which is the basic form of WPICM (1, 1, ξ) model.

Theorem 2. *The sequence of $W^{(0)}$, $W^{(1)}$, and $Z^{(1)}$ is given in Definition 1, $\widehat{p} = (a, b, c)^T = (B^T B)^{-1} B^T Y$ is a sequence of parameters, and*

$$Y = \begin{bmatrix} w^{(0)}(2) \\ w^{(0)}(3) \\ \vdots \\ w^{(0)}(n) \end{bmatrix},$$

$$B = \begin{bmatrix} \left[-\xi w^{(1)}(2) + (1-\xi) w^{(1)}(1)\right] & \frac{3}{2} & 1 \\ \left[-\xi w^{(1)}(3) + (1-\xi) w^{(1)}(1)\right] & \frac{5}{2} & 1 \\ \vdots & \vdots & \vdots \\ \left[-\xi w^{(1)}(n) + (1-\xi) w^{(1)}(1)\right] & \frac{(2n-1)}{2} & 1 \end{bmatrix}. \tag{17}$$

The least squares estimate sequence of WPICM(1,1,ξ) satisfied $\widehat{p} = (a, b, c)^T = (B^T B)^{-1} B^T Y$.

The background value corresponds to different array distance B, and the undetermined value ξ in array distance B can be calculated by the PSO algorithm through MATLAB to obtain the optimal coefficient ξ. The calculation process is similar to the WPICM (1, 1, r) model and will not be repeated here.

2.4. WPICM (1, 1, r, ξ) Optimization Combination. From the perspective of parameter optimization, the three basic parameters a, b, and c of the grey prediction model are important metrics that affect its simulation and prediction accuracy. On the basis of the model structure optimized by the individual parameters, the fractional order accumulates r and the background value ξ have a direct influence on the parameters a, b, and c. Therefore, the fractional order accumulates and the background value can greatly improve the performance of the grey prediction model.

Definition 7. Assuming that $W^{(0)}$, $W^{(1)}$, and $Z^{(r)}$ are given by Definition 4, then sequence $W^{(0)} = (w^{(0)}(1), w^{(0)}(1), \ldots, w^{(0)}(n))$, which $w^{(0)}(k) \geq 0, k = 1, 2, \ldots, n$; $W^{(r)} = (w^{(r)}(1), w^{(r)}(2), \ldots, w^{(r)}(n))$ $r \in R^+$, where

$$w^{(r)}(k) = \sum_{i=1}^{k} \frac{\Gamma(r+k-i)}{\Gamma(k-i+1)\Gamma(r)} w^{(0)}(i), \quad k = 1, 2, \ldots, n, \tag{18}$$

$Z^{(r)} = (z^{(r)}(1), z^{(r)}(2), \ldots, z^{(r)}(n))$ is called the mean sequence generated by consecutive neighbors of $W^{(r)}$, where

$$z_g^{(r)}(k) = \xi w^{(r)}(k) + (1-\xi) w^{(r)}(k-1). \tag{19}$$

Then,

$$w^{(r-1)}(k) + a\left(\xi w^{(r)}(k) + (1-\xi) w^{(r)}(k-1)\right) = 0.5(2k-1)b + c \tag{20}$$

is the basic form of WPICM (1, 1, r, ξ).

We solve its whitening differential equation and the final restored expression can be formulated as follows:

$$\widehat{w}^{(0)}(t) = \widehat{w}^{(0)}(t) = \left(\widehat{w}^{(r)}(t)\right)^{(-r)} = \left(1 - e^{a}\right)\left(w^{(0)}(1) - \frac{b}{a} + \frac{b}{a^2} - \frac{c}{a}\right)e^{-a(t-1)} + \frac{b}{a}. \tag{21}$$

Let $\alpha = (1 - e^{a})(w^{(0)}(1) - (b/a) + (b/a^2) - (c/a))$, and $\beta = (b/a)$.

Then, the time response sequence of WPICM $(1, 1, r, \xi)$ is $\widehat{w}^{(0)}(k) = \alpha e^{-a(k-1)} + \beta$.

Theorem 3. *The sequence of $W^{(r-1)}$, $W^{(r)}$, and $Z_g^{(r)}$ is given in Definition 1, $\widehat{p} = (a, b, c)^T = (B^T B)^{-1} B^T Y$ is a sequence of parameters, and*

$$Y = \begin{bmatrix} w^{(r-1)}(2) \\ w^{(r-1)}(3) \\ \vdots \\ w^{(r-1)}(n) \end{bmatrix},$$

$$B = \begin{bmatrix} -\xi w^{(r)}(2) + (1-\xi)w^{(r)}(1) & \frac{3}{2} & 1 \\ -\xi w^{(r)}(3) + (1-\xi)w^{(r)}(1) & \frac{5}{2} & 1 \\ \vdots & \vdots & \vdots \\ -\xi w^{(r)}(n) + (1-\xi)w^{(r)}(1) & \frac{(2n-1)}{2} & 1 \end{bmatrix}. \tag{22}$$

The least squares estimate sequence of WPICM $(1, 1, r, \xi)$ satisfied $\widehat{p} = (a, b, c)^T = (B^T B)^{-1} B^T Y$.

3. Error Checking Method for WPICM (1,1,*r*,*ξ*)

In order to test whether a forecasting model could meet the prediction requirements of one system, we use the average relative error test and grey correlation test to examine the performance of the combinatorial optimization model. Usually, start with the relative percentage error. For giving a threshold value α, which is set according to the specific situation of a system, when $\overline{\Delta} < \alpha$ holds true, the grey model is said to be error-satisfactory. The relative average percentage error includes two parts: mean relative simulated percentage error and mean relative forecasted percentage error.

Definition 8. Assume a raw sequence $W^{(0)} = (w^{(0)}(1), w^{(0)}(2), \ldots, w^{(0)}(n), w^{(0)}(n+1), \ldots, w^{(0)}(n+t))$. Then, simulation sequence $\widehat{S}^{(0)}$ is as follows:

$$\widehat{S}^{(0)} = \left(\widehat{w}^{(0)}(1), \widehat{w}^{(0)}(2), \ldots, \widehat{w}^{(0)}(n)\right). \tag{23}$$

We use the WPICM $(1, 1, r, \xi)$ model to forecast the latter t-step data and the predictive sequence is as follows:

$$\widehat{F}^{(0)} = \left(\widehat{w}^{(0)}(n+1), \widehat{w}^{(0)}(n+2), \ldots, \widehat{w}^{(0)}(n+t)\right). \tag{24}$$

Definition 9. Assume that the residual sequence of $\widehat{S}^{(0)}$ and $\widehat{F}^{(0)}$ is ε_s and ε_F, respectively, which is as follows:

$$\begin{aligned} \varepsilon_s &= \left(\varepsilon_s(1), \varepsilon_s(2), \ldots, \varepsilon_s(n)\right), \\ \varepsilon_F &= \left(\varepsilon_F(n+1), \varepsilon_F(n+2), \ldots, \varepsilon_F(n+t)\right), \end{aligned} \tag{25}$$

then

$$\begin{aligned} \varepsilon_s(u) &= \left|x^{(0)}(u) - \widehat{x}^{(0)}(u)\right|, \quad u = 1, 2, \ldots, n, \\ \varepsilon_F(v) &= \left|x^{(0)}(v) - \widehat{x}^{(0)}(v)\right|, \quad v = n+1, n+2, \ldots, n+t. \end{aligned} \tag{26}$$

Definition 10. The relative simulated percentage error (RSPE) of the simulated sequence is Δ_S, and $\Delta_s = (\Delta_s(1), \Delta_s(2), \ldots, \Delta_s(n))$, where

$$\Delta_S(u) = \left|\frac{\varepsilon_s(u)}{x^{(0)}(u)} \times 100\%\right|, \quad u = 1, 2, \ldots, n. \tag{27}$$

The mean relative simulated percentage error (MRSPE) of the simulation sequence $\overline{\Delta}_S$ is as follows:

$$\overline{\Delta}_S = \frac{1}{n}\sum_{u=1}^{n} \Delta_s(u). \tag{28}$$

Definition 11. The relative forecasted percentage error (RFPE) of the forecasted sequence is Δ_F, and $\Delta_F = (\Delta_F(n+1), \Delta_F(n+2), \ldots, \Delta_F(n+t))$, where $\Delta_F(u) = |(\varepsilon_F(v)/x^{(0)}(v)) \times 100\%|$ and $v = n+1, n+2, \ldots, n+t$.

The mean relative simulation percentage error (MRSPE) of predicted sequence $\overline{\Delta}_F$ is as follows:

$$\overline{\Delta}_F = \frac{1}{t}\sum_{v=n+1}^{n+t} \Delta_F(v), \quad v = n+1, n+2, \ldots, n+t. \tag{29}$$

The comprehensive average relative percentage error of the model is recorded as Δ (CMRPE), where

$$\Delta = \frac{n \cdot \overline{\Delta}_s + t \cdot \overline{\Delta}_F}{n+t}. \tag{30}$$

The grey absolute correlation degree is an important tool to measure the degree of difference between different time series. When evaluating the error of the forecast model, it

can effectively check the degree of deviation of the original data before and after the modeling process. For giving a threshold value δ, in which the threshold is set according to the specific situation of a system. When $\delta_0 < \delta$ holds true, the grey model is said to be error satisfactory [29, 34, 35].

Definition 12 (see [35]). Assume that sequence $X^{(i)} = (x^{(i)}(1), x^{(i)}(2), \ldots, x^{(i)}(n))$, where $x^{(i)}(k)d = x^{(i)}(k) - x^{(i)}(1), k = 1, 2, \ldots, n$; then, $X_i D = X_i^0 = (x_i^0(1), x_i^0(2), \ldots, x_i^0(n))$ is the zero image of the starting point of X_i.

Definition 13 (see [29]). Let the sequence of X_i^0 and X_j^0 be equidistant and of the same length; then,

$$\varepsilon^{ji} = \frac{1 + |s_j| + |s_i|}{1 + |s_j| + |s_i| + |s_i - s_j|}, \tag{31}$$

which is called absolutely correlation degree of $x^{(j)}$ and $x^{(i)}$, where

$$\begin{aligned} |S_j| &= \left| \sum_{j=2}^{n-1} x_i^0(k) + \frac{1}{2} x_j^0(n) \right|, \\ |S_i| &= \left| \sum_{j=2}^{n-1} x_i^0(k) + \frac{1}{2} x_j^0(n) \right|. \end{aligned} \tag{32}$$

4. Forecasting with the WPICM (1, 1, ξ, r) Model

The data in the Statistical Communique of the People's Republic of China on Energy indicates that the growth rate of wind power generation is the highest, compared with hydropower, nuclear power, and solar photovoltaic power. Therefore, wind power has become one of the most popular clean energy sources, which effectively alleviates the energy supply pressure borne by fossil fuels [36].

On the basis of China's actual situation, it is of great practical significance to forecast the future wind power generation and clarify the seasonal characteristics of wind power generation evolution. On the one hand, it could reasonably allocate power resources, optimize the design of the power grid and power dispatching, and ensure the efficient use of power. On the other hand, it could accelerate the upgrading of energy consumption structure, reduce the use of fossil fuels, and finally achieve the coordinated development of the economy and environment. The data source of this paper is the original data (Table 1) of China's wind power installed capacity released by the Global Wind Energy Council (GWEC) in 2019.

As reported by China Renewable energy Association, the WPIC of China 2015 is 30.5 million kW. Affected by the reduction in the price of wind power benchmarking, there was a significant rush to install wind power projects. It increased by 31.5% compared with the same period last year, and the scale of new installed capacity is obvious. That is the reason in Figure 2 there is an inflection point in 2015, which slows down the WPIC in 2016–2017. Affected by the reduction in the price of wind power benchmarking, there was a significant rush to install wind power projects. It increased by 31.5% compared with the same period last year, and the scale of new installed capacity is obvious. Moreover, the structure of the application section is provided in Figure 3.

4.1. Simulation and Forecasting. Considered as an alternative to fossil fuels, wind energy has been highly valued as renewable energy around the world. However, due to the intermittency, fluctuant, and random probability, the wind power grid connection is limited, resulting in wind curtailment. Large-scale access leads to serious threats to the stability and security of the power system and inevitably affects the reliability of grid operation. Consequently, power quality is not guaranteed. To address this challenge, wind power installed capacity prediction, manual guidance of wind farm operation, and reasonable scheduling are valid methods to lessen the effect of wind power upon the grid when it is connected to the grid [37, 38].

We use the WPICM$(1, 1)$ model and its parameter optimization models WPICM$(1, 1, r)$, WPICM$(1, 1, \xi)$, WPICM$(1, 1, r, \xi)$ to predict and analyze China's wind power installed capacity. In the processing of data sets, $k = 1, 2, \ldots, 6$ are taken as in-sample data to test the simulation performance, and the data of the last two time points $k = 7$ are taken as out-of-sample data to test the prediction performance. The results are shown in Table 2. We find that the model with optimized order and background value simultaneously has better performance than the other two models with optimized parameters alone. Moreover, the flowchart of constructing the WPICM$(1, 1, r, \xi)$ combination model is presented in Figure 4.

We use MATLAB to find parameters for these four models. Corresponding parameters are shown in Table 3.

4.2. Performance Comparison. In order to compare these four models' simulated and forecasted performance, three metrics are selected, namely, MRSPE, MRFPE, RSPE, CRMPE. The model's performance evaluation metrics and meanings are shown in Table 4.

Table 2 shows the model WPICM(1,1,r,ξ)'s performance is better than the WPICM(1,1) model and the WPICM(1,1,ξ) model, in terms of simulation and prediction. In order to clearly compare the performance of the four models, we drew the simulation/prediction errors curves of the four models based on the data in Tables 2 and 3, and the results are plotted in Figure 5.

In order to test the simulation and prediction performance of different prediction models on the WPIC in China, the performance evaluation metrics in Table 4 is employed. The raw data and computational result are plotted in Figures 6 and 7 . It can be seen from the combination model, WPICM (1, 1, r, ξ) is better than no optimization WPICM (1, 1), or only optimizing a single parameter (WPICM (1, 1, ξ) and WPICM (1, 1, r)). Moreover, the results reveal that the combinatorial optimization model shows a more stable prediction performance. The simulation accuracy is 99.23%, the prediction accuracy is 97.26%. The grey absolute correlation is 0.9878%, $\varepsilon^{ji} = 0.9878 > 0.9$; the mean relative

Table 1: China's WPIC from 2009 to 2018 (ten thousand of kW).

Year	2009	2010	2011	2012	2013	2014	2015	2016	2017	2018
WPIC	25810	44730	62360	75320	91410	114610	145360	168730	188390	209533

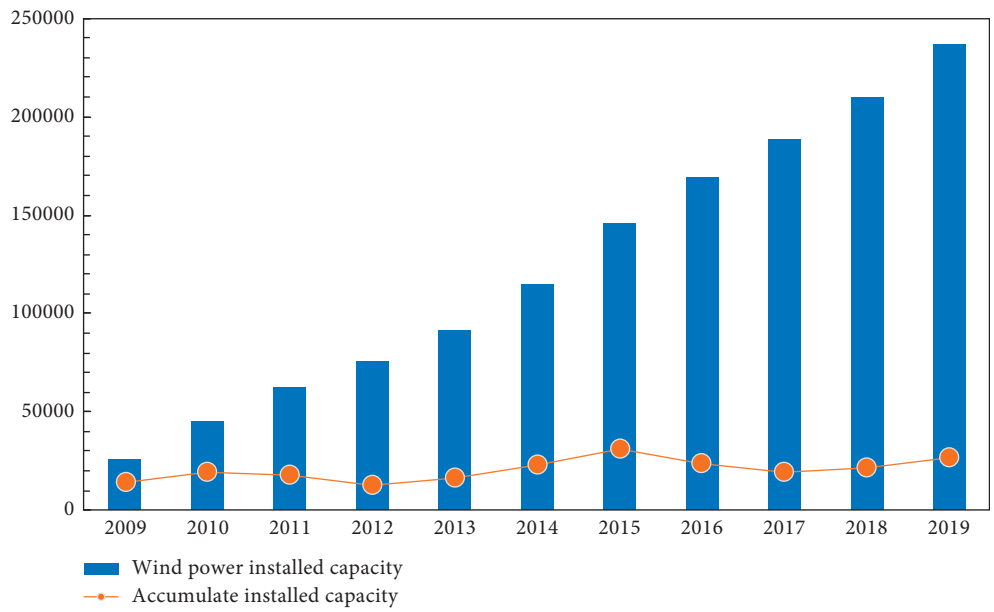

Figure 2: WPIC of China for 2009–2018 (ten thousand of kW).

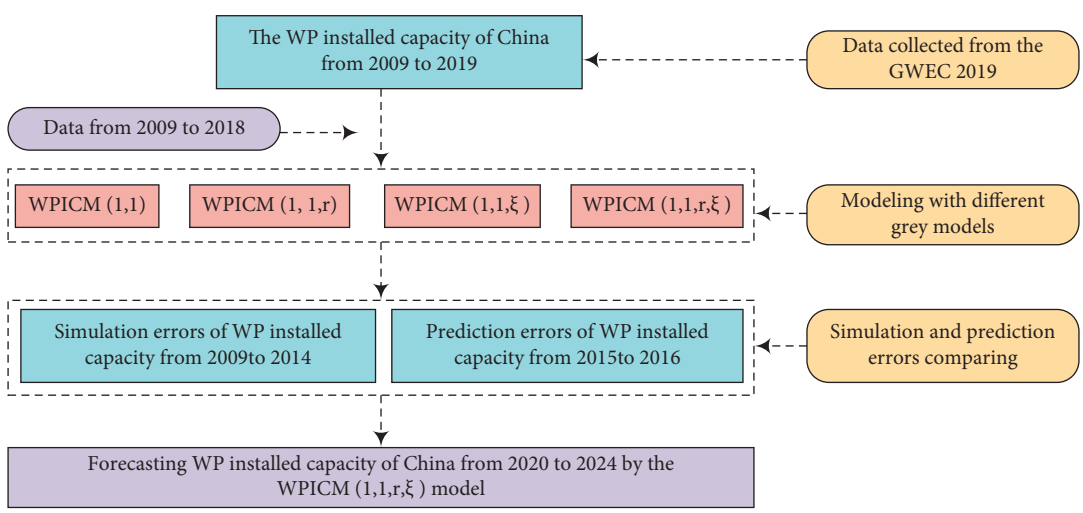

Figure 3: Structure chart of application.

simulated percentage error $\overline{\Delta}_S$ is 0.77%, $\overline{\Delta}_S = 0.77\% < 1\%$, which makes the WPICM (1, 1, r, ξ) model error satisfactory (Table 5).

4.3. Forecasting China's WPIC for 2020–2024. As can be seen from the earlier simulated and predicted results of China's WPIC, comparing to the conventional grey models, the novel WPICM (1, 1, r, ξ) model proposed in this paper has a relatively optimal simulation and prediction performance. Hence, in this section, we will use the WPICM (1, 1, r, ξ) model to forecast and analyze the WPIC for 2020 to 2024.

In this section, the WPICM (1, 1, r, ξ) combination model is built to forecast the demand of wind power capacity in China during 2020–2024, providing a picture of the demand conditions for the upcoming years. Based on this, the government can judge the status of supply and demand according to domestic output and take some preventive measures in advance to maintain the balance of supply and demand for WPIC.

Table 2: Simulated/forecast results of wind power installed capacity with different models.

Year	Raw data	WPICM(1, 1)		WPICM(1, 1, r)		WPICM(1, 1, ξ)		WPICM(1, 1, r, ξ)	
	$w^{(0)}(k)$	$\widehat{w}^{(0)}(k)$	RSPE (%)	$\widehat{w}^{(0)}(k)$	RSPE (%)	$\widehat{w}^{(0)}(k)$	RSPE (%)	$\widehat{w}^{(0)}(k)$	RSPE (%)
In-sample									
2009	25810	25810	0	25810	0	25810	0	25810	0
2010	44730	45935.00	2.69	44071.24	1.47	46297.13	3.50	44730.00	0.00
2011	62360	59636.23	4.37	61020.49	2.15	60183.19	3.49	61752.99	0.97
2012	75320	75249.90	0.09	74840.64	0.64	76010.17	0.91	75870.77	0.73
2013	91410	93042.95	1.79	91733.92	0.35	94049.37	2.89	93158.78	1.91
2014	114610	113319.57	1.13	112410.27	1.92	114610.00	2.01	114355.56	0.22
$\overline{\Delta}_S$			2.01		1.31		2.16		0.77
Out-sample									
2015	145360	136426.44	6.15	137726.78	5.25	138044.50	5.03	140354.90	3.44
2016	168730	162758.61	3.54	168729.99	0.00	164754.56	2.36	172250.14	2.09
$\overline{\Delta}_F$		4.84		2.63		3.69		2.76	
CRMPE		2.82		1.68		2.60		1.34	

Table 6 shows that with the support of existing policies, China's hosting capacity of wind power keeps expanding. By 2020, China's cumulative hosting capacity of wind power can reach 390,578.90 kW, and the total development target of wind power in the 13th Five-Year Plan can be achieved.

4.4. Future Discussion and Development Suggestion. Wind energy is one of the most important renewable resources in the world and plays a vital role in reducing carbon emission and solving the global warming problem. In order to promote the development of the wind energy industry, China has formulated corresponding energy policies based on the production, consumption, and distribution of wind energy.

In this paper, we focus on forecasting wind energy consumption from a macro perspective. From the above forecast trend, it can be seen that the WPIC will increase significantly from 2020 to 2024, and the installed capacity of wind power in China will reach 885,423.10 kW by 2024. On this basis, the following suggestions are made.

4.4.1. Strengthen the National Power Grid. According to the demand for economic development, power grid enterprises need to revise the existing power grid development plan. Power grid structures in remote areas, such as transmission, distribution, and energy storage facilities, should be built in a focused and step-by-step manner. They should create a larger regional electricity market. Through interprovincial and interregional power grid interconnection, so that the wind power consumption market can be found in the regional power grid and even outside the regional power grid.

4.4.2. Innovative Wind Power Grid Connection Technology and Application. The grid-connected technology of wind power in China still needs in-depth research and innovation to improve the consumption level of wind power to realize the efficient utilization of wind power. For this reason, the government should actively support the transmission investment needed for wind power development and integration into the power grid while maintaining the system's stability and reliability.

4.4.3. Strengthen Risk Control of Wind Power Project. National power regulatory authorities should pay attention to the mutual influence between wind farms and power grids. The International Development and Reform Commission should strictly approve and carefully examine and approve the application projects of large wind power. Authorities should unify planning and use it to avoid excessive wind power capacity caused by repeated construction.

4.4.4. Innovate the Utilization Mode of Wind Power. On the basis of focusing on solving the problem of wind power transmission in major development areas such as Inner Mongolia, Hebei province, Jilin province, and Gansu province, authorities should continue to develop heating and agricultural water-lifting irrigation to flexibly use electricity load. Through these ways, the government could promote the local consumption and utilization of wind power to ensure the sustained and healthy development of China's wind power industry.

4.4.5. Accelerate the Development of Green and Low Carbon. Relevant departments should strengthen land space planning and use control, implement space control boundaries such as ecological protection, basic farmland, and urban development, and reduce the occupation of natural space by human activities. The legislature should strengthen the legal and policy guarantee of green development, develop green finance, support green technological innovation, promote cleaner production, develop environmental protection industries, and promote the green transformation of key industries and important areas. Relevant departments should strengthen land space planning and use control, implement space control boundaries such as ecological protection, basic farmland, and urban development, and reduce the occupation of natural space by human activities. The legislature should strengthen the legal and policy guarantee of green development and promote the green transformation of key industries and important areas. The Chinese government should continue to promote clean, low-carbon, safe, and efficient use of energy.

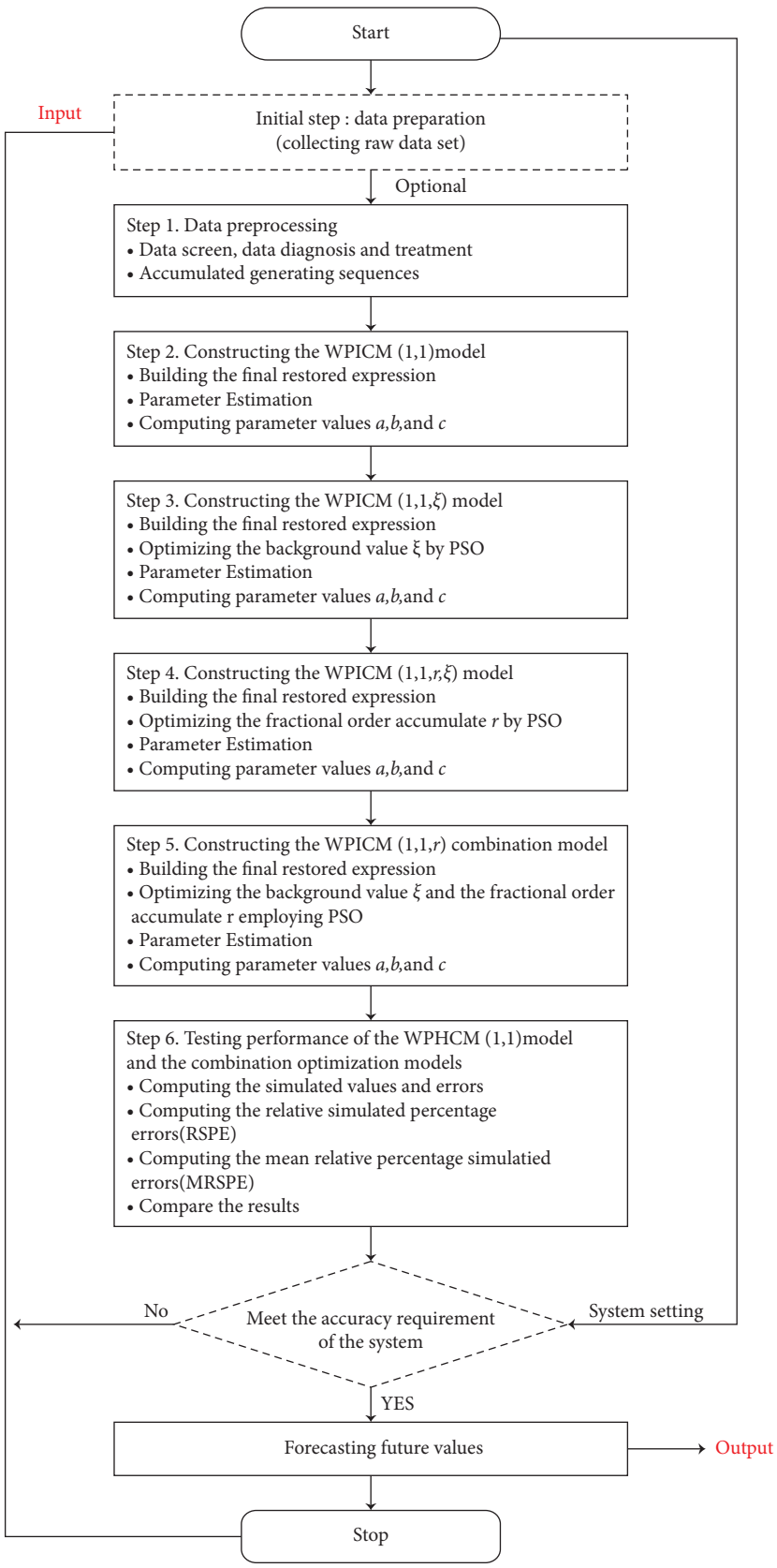

Figure 4: Flowchart of constructing the WPICM $(1, 1, r, \xi)$ combination model.

Table 3: Parameters of the prediction model.

Model	r	ξ	a	b	c	α	β
WPICM (1, 1)	1	0.5	−0.20282	40655.3559	−2604.1104	2.2060	−2.0044
WPICM (1, 1, r)	1.9955	0.5	−0.20283	40658.27	−2607.5377	2.2060	−2.0045
WPICM (1, 1, ξ)	1	0.44	−0.13083	6940.3893	29622.9115	8.7162	−5.3048
WPICM (1, 1, r, ξ)	1.9954	0.46	−0.20457	41006.4157	−2627.3167	2.20762	−20045

Table 4: Table model performance evaluation metrics.

Metrics	Symbol	Formula
MRPE	MRPE	$\mathrm{MRPE}(k) = \lvert(w^{(0)}(k) - \widehat{w}^{(0)}(k))/w^{(0)}(k)\rvert \times 100\%$
MRSPE	$\overline{\Delta}_S$	$\overline{\Delta}_S = (1/n)\sum_{u=1}^{n} \mathrm{MRPE}(k), k \text{ in in} - \text{sample}$
MRFPE	$\overline{\Delta}_F$	$\overline{\Delta}_F = (1/t)\sum_{k=n+1}^{n+t} \mathrm{MRPE}(k), k \text{ in out} - \text{sample}$
CRMPE	Δ	$\Delta = (n \cdot \overline{\Delta}_s + t \cdot \overline{\Delta}_F)/(n+t)$

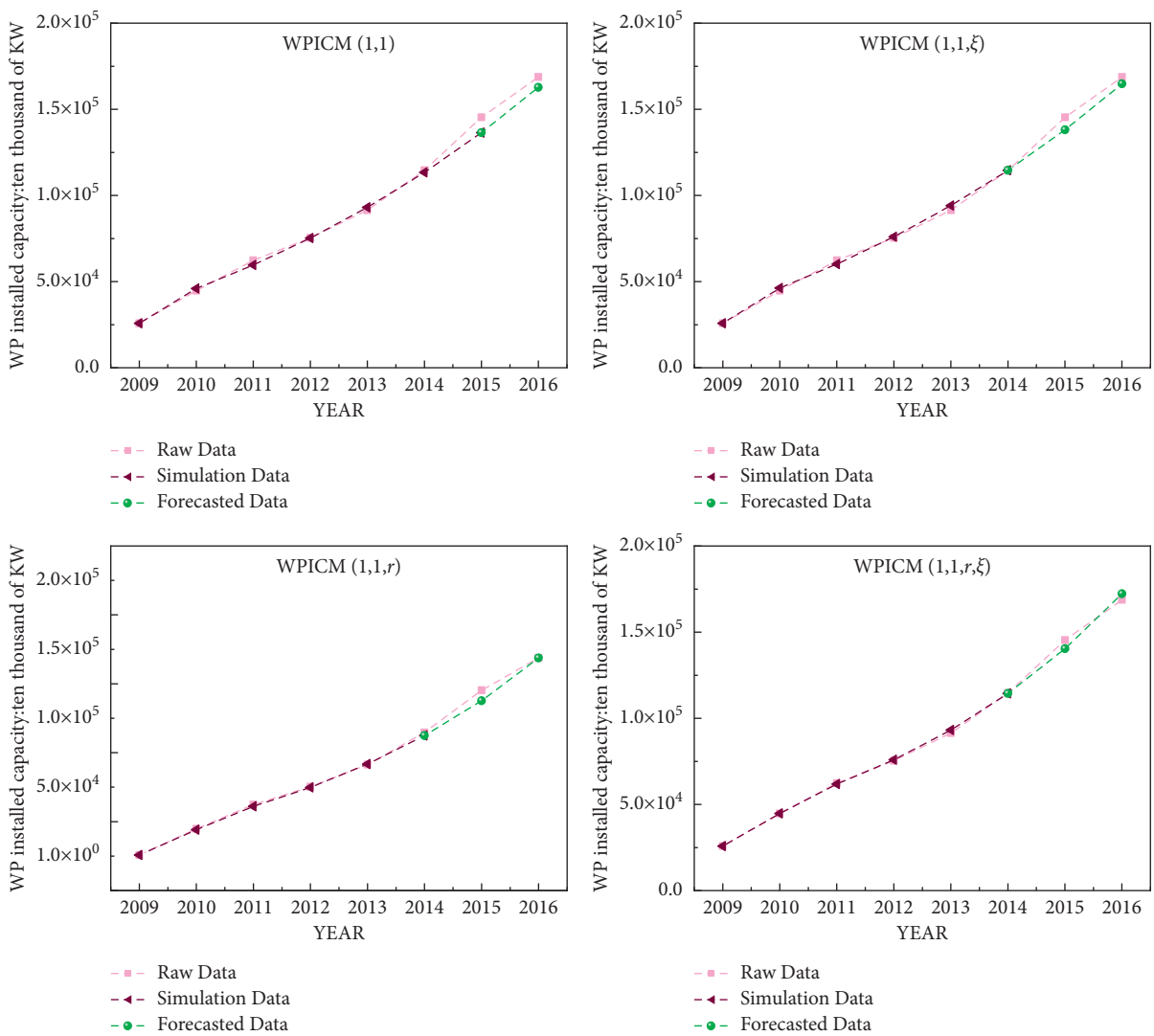

Figure 5: Performance comparison.

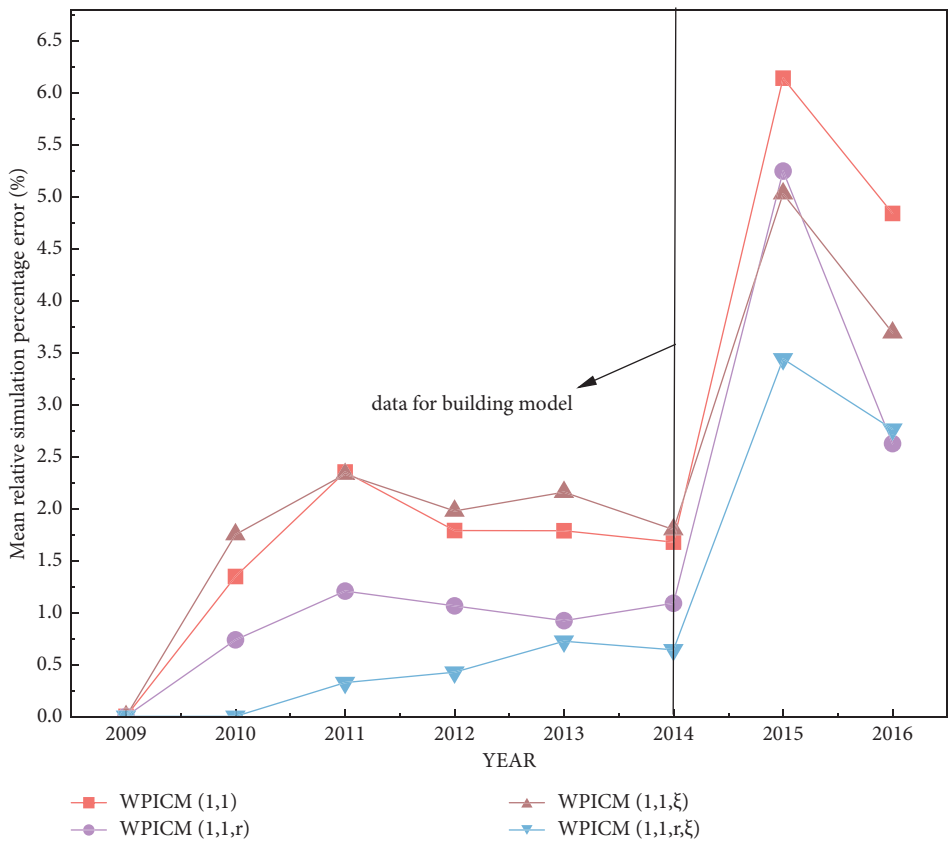

Figure 6: MRPE of model's performance.

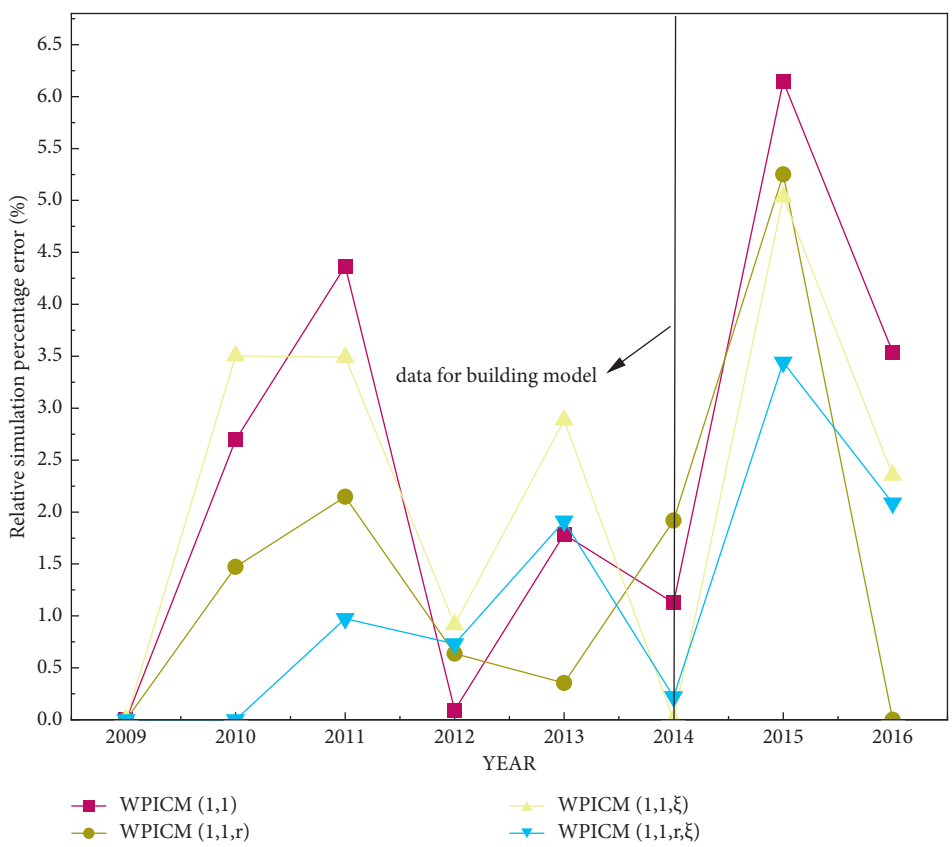

Figure 7: RSPE of model's performance.

Table 5: Error test.

Testing method	Average relative error test	Absolute grey correlation test
Testing results	$\overline{\Delta}_S = 0.77\% < 1\%$	$\varepsilon^{ji} = 0.9878 > 0.9$

Table 6: Prediction data of WPIC of China during 2018–2024 (ten thousand of kW).

Year	2018	2019	2020	2021	2022	2023	2024
WPIC(K)	259,392.73	318,300.48	390,578.90	479,263.68	588,079.56	721,596.80	885,423.10

These suggestions can contribute to the advance of the low carbon economy and achieve rapid development of clean energy production.

5. Conclusion

Wind power is fluctuant and intermittent, which has an impact on the power grid. Large-scale wind power is a serious threat to the stability and security of the power system. Accurate prediction of wind power installed capacity is significant to the safety of the power system.

In this paper, a new parameter combination optimization model WPICM$(1, 1, r, \xi)$ is proposed. Compared with the model that performs parameter optimization alone, the result shows the comprehensive performance of the proposed model WPICM$(1, 1, r, \xi)$. The MRPE is 1.34%, and the overall performance of the model is better than that of the conventional grey prediction model. By optimizing the performance parameters of the traditional grey model, improving the forecasting level of wind power installed capacity has important practical significance for the wind power industry.

The combination optimization model has some shortcomings, and there is a future study to be completed. For instance, the lack of processing methods for individual abnormal points in the data resulted in the abnormal points still affecting the prediction results. Other parameters may choose to be optimized, such as initial value. The data processing process needs to be improved. In the selecting variables process, correlation analysis focuses on wind power installed capacity. Future studies might involve other influencing factors.

Data Availability

The data that support the findings of this study are openly available in CWEA (Chinese Wind Energy Association) (https://www.cwea.org.cn/industry_data.html) and GWEC (Global Wind Energy Council) (https://gwec.net/green-recovery-data-analysis/).

Conflicts of Interest

The authors declare that they have no conflicts of interest.

Acknowledgments

This work was supported by the Chongqing Natural Science Foundation of China (Grant Nos. cstc2019jcyj-msxmX0003 and cstc2019jcyj-msxmX0767) and Key Project of Scientific and Technological Research of Chongqing Education Commission (Grant No. KJZD-K202000804).

References

[1] L. Adrian and R. Kristian, "Towards a policy model for climate change mitigation: China's experience with wind power development and lessons for developing countries," *Energy for Sustainable Development*, vol. 10, no. 4, pp. 5–13, 2006.

[2] J. Li, "Decarbonising power generation in China—is the answer blowing in the wind?," *Renewable and Sustainable Energy Reviews*, vol. 4, pp. 1154–1171, 2009.

[3] J. Li, C. Liu, P. F. Zhang, Y. F. Wang, and J. Rong, "Difference between grid connections of large-scale wind power and conventional synchronous generation," *Global Energy Interconnection*, vol. 3, no. 05, pp. 486–493, 2020.

[4] G. Wu, H. J. Wang, and Q. G. Wu, "Wind power development in the belt and road area of Xinjiang, China: problems and solutions," *Utilities Policy*, vol. 64, 2020.

[5] R. Zhang, M. Ni, G. Q. P. Shen, J. K. W. Wong, P. Shen, and J. K. W. Wong, "An analysis on the effectiveness and determinants of the wind power Feed-in-Tariff policy at China's national-level and regional-grid-level," *Sustainable Energy Technologies and Assessments*, vol. 34, pp. 87–96, 2019.

[6] J. Xia, X. Ma, W. Q. Wu, B. L. Huang, and W. P. Li, "Application of a new information priority accumulated grey model with time power to predict short-term wind turbine capacity," *Journal of Cleaner Production*, vol. 244, Article ID 118573, 2020.

[7] X. Yang, Z. Fang, Y. Yang, D. Mba, and X. Li, "A novel multi-information fusion grey model and its application in wear trend prediction of wind turbines," *Applied Mathematical Modelling*, vol. 71, pp. 543–557, 2019.

[8] D. H. Wu and C. Cong, "Short-term wind power generation forecasting based on the SVM-GM approach," *Electric Power Components and Systems*, vol. 46, no. 11-12, pp. 1250–1264, 2019.

[9] P. Zhang, X. Ma, and K. She, "A novel power-driven fractional accumulated grey model and its application in forecasting wind energy consumption of China," *PLoS One*, vol. 14, no. 12, Article ID e0225362, 2019.

[10] W. Y. Qian and J. Wang, "An improved seasonal GM (1, 1) model based on the HP filter for forecasting wind power generation in China," *Energy*, vol. 209, Article ID 118499, 2020.

[11] G. M. Duman, E. Kongar, and S. M. Gupta, "Predictive analysis of electronic waste for reverse logistics operations: a comparison of improved univariate grey models," *Soft Computing*, vol. 24, no. 20, pp. 1–16, 2020.

[12] T. Vinothkumar and K. Deeba, "Hybrid wind speed prediction model based on recurrent long short-term memory neural network and support vector machine models," *Soft Computing—A Fusion of Foundations, Methodologies and Applications*, vol. 24, no. 9, pp. 5345–5355, 2020.

[13] Z. L. Li, J. Xia, A. Liu, and P. Li, "States prediction for solar power and wind speed using BBA-SVM," *IET Renewable Power Generation*, vol. 13, no. 7, pp. 1115–1122, 2019.

[14] C. H. Yeh, M. H. Lin, C. H. Lin, C. E. Yu, and M. J. Chen, "Machine learning for long cycle maintenance prediction of wind turbine," *Sensors*, vol. 19, no. 7, Article ID 1671, 2019.

[15] A. Agasthian, R. Pamula, and L. A. Kumaraswamidhas, "Fault classification and detection in wind turbine using Cuckoo-optimized support vector machine," *Neural Computing and Applications*, vol. 31, no. 5, pp. 1503–1511, 2019.

[16] J. L. Lu, B. Wang, H Ren et al., "Two-tier reactive power and voltage control strategy based on ARMA renewable power forecasting models," *Energies*, vol. 10, pp. 1–13, 2017.

[17] E. Ergin and J. Shi, "ARMA based approaches for forecasting the tuple of wind speed and direction," *Applied Energy*, vol. 88, no. 4, pp. 1405–1444, 2010.

[18] P. Chen, T. Pedersen, B. Bak-Jensen, and Z. Chen, "ARIMA-based time series model of stochastic wind power generation," *IEEE Transactions on Power Systems*, vol. 25, no. 2, pp. 667–676, 2010.

[19] Z. Luo, C. Liu, and S. Liu, "A novel fault prediction method of wind turbine gearbox based on pair-copula construction and BP neural network," *IEEE Access*, vol. 8, pp. 91924–91939, 2020.

[20] A. Di Piazza, M. C. Di Piazza, G. La Tona, G. La Tona, and M. Luna, "An artificial neural network-based forecasting model of energy-related time series for electrical grid management," *Mathematics and Computers in Simulation*, vol. 184, pp. 294–305, 2021.

[21] S. X. Wang, M. Li, L. Zhao, and J. Chen, "Short-term wind power prediction based on improved small-world neural network," *Neural Computing & Applications*, vol. 31, pp. 73–85, 2019.

[22] H. Jahangir, A. Golkar Masoud, F. Alhameli, A. Mazouz, A. Ahmadian, and A. Elkamel, "Short-term wind speed forecasting framework based on stacked denoising auto-encoders with rough ANN," *Sustainable Energy Technologies and Assessments*, vol. 38, Article ID 100601, 2019.

[23] P. Zhang, Y. L. Wang, X. G. Yin, L. K. Liang, X. Li, and Q. T. Duan, "Short-term wind power prediction using GA-BP neural network based on DBSCAN algorithm outlier identification," *Processes*, vol. 8, no. 2, Article ID 157, 2020.

[24] L. Tan, J. Han, and H. Zhang, "Ultra-short-term wind power prediction by Salp swarm algorithm-based optimizing extreme learning machine," *IEEE Access*, vol. 8, pp. 44470–44484, 2020.

[25] Y. Wang, D. Wang, and Y. Tang, "Clustered hybrid wind power prediction model based on ARMA, PSO-SVM, and clustering methods," *IEEE Access*, vol. 8, pp. 17071–17079, 2020.

[26] L. Wang, R. Tao, H. Hu, and Y.-R. Zeng, "Effective wind power prediction using novel deep learning network: stacked independently recurrent autoencoder," *Renewable Energy*, vol. 164, pp. 642–655, 2021.

[27] J. Wang, W. Zhang, J. Wang, T. Han, and L. Kong, "A novel hybrid approach for wind speed prediction," *Information Sciences*, vol. 273, pp. 304–318, 2014.

[28] B. Zeng, H. M. Duan, and Y. F. Zhou, "A new multi variable grey prediction model with structure compatibility," *Applied Mathematical Modelling*, vol. 75, pp. 385–397, 2019.

[29] L. Tu and Y. Chen, "An unequal adjacent grey forecasting air pollution urban model," *Applied Mathematical Modelling*, vol. 99, pp. 260–275, 2021.

[30] B. Zeng and H. Li, "Prediction of coalbed methane production in China based on an optimized grey system model," *Energy & Fuels*, vol. 35, pp. 4333–4344, 2021.

[31] B. Zeng, M. Zhou, X. Z. Liu, and Z. W. Zhang, "Application of a new grey prediction model and grey average weakingning buffer operator to forecast China's shale gas output," *Energy Report*, vol. 6, pp. 1608–1618, 2020.

[32] B. Neeraj, F. Andrés, V. Daniel, and K. Kishore, "A novel and alternative approach for direct and indirect wind-power prediction methods," *Energies*, vol. 11, no. 11, Article ID 2923, 2018.

[33] B. Zeng, M. Y. Tong, and X. Ma, "A new structure grey Verhulst model: development and performance comparison," *Applied Mathematical Modelling*, vol. 81, no. 20, pp. 522–537, 2020.

[34] Z. Ming, P. Lilin, F. Qiannan, and Z. Yingjie, "Trans-regional electricity transmission in China: Status, issues and strategies," *Renewable and Sustainable Energy Reviews*, vol. 66, pp. 572–583, 2016.

[35] S. F. Liu and Y. Lin, *Grey Systems Theory and Applications*, Springer-Verlag, Berlin, Germany, 2010.

[36] B. Zeng, X. Ma, and J. J. Shi, "A new structure grey Verhulst model for China's tight gas production forecasting," *Applied Soft Computing*, vol. 96, Article ID 106600, 2020.

[37] C. Wang, S. Zhang, L. Xiao, and T. Fu, "Wind speed forecasting based on multi-objective grey wolf optimisation algorithm, weighted information criterion, and wind energy conversion system: a case study in Eastern China," *Energy Conversion and Management*, vol. 243, Article ID 114402, 2021.

[38] M. Kiaee, D. Infield, and A. Cruden, "Utilisation of alkaline electrolysers in existing distribution networks to increase the amount of integrated wind capacity," *Journal of Energy Storage*, vol. 16, no. 16, pp. 8–20, 2018.

Hindawi
Journal of Mathematics
Volume 2021, Article ID 8585238, 6 pages
https://doi.org/10.1155/2021/8585238

Research Article

Prediction of China's Express Business Volume Based on FGM (1, 1) Model

Chunyan Xiong [1] **and Liusan Wu** [1,2]

[1] *College of Information Management, Nanjing Agricultural University, Nanjing 210031, China*
[2] *School of Information Management, Nanjing University, Nanjing 210023, China*

Correspondence should be addressed to Liusan Wu; wuls@njau.edu.cn

Received 17 June 2021; Accepted 6 August 2021; Published 16 August 2021

Academic Editor: Lifeng Wu

With the continuous development of the economy, people's lifestyle has changed greatly, online shopping has become a better choice for many people, and the express business volume is also increasing. Forecasting express business volume is of benefit to the healthy development of the logistics industry. Based on the data of China's express business volume from 2015 to 2019, this paper uses the improved Particle Swarm Optimization algorithm to calculate the fractional-order r of the FGM (1, 1) model and forecasts China's express business volume from 2020 to 2023. The results indicate that in the next few years, China's express business volume will show a large growth trend, indicating that the express delivery industry still has a lot of room for development.

1. Introduction

Since the Internet has become widely available, people get accustomed to shopping online. Online shopping is convenient and time-saving, which has facilitated the development of China's express business volume in recent years. It can be predicted that the express business volume will continue to grow in the future. The following content will do specific research on the growth of China's express business volume. Figure 1 shows the data of China's express business volume from 2015 to 2019.

The rapid growth of express business volume brings about the development of the whole logistics industry. At the same time, the unreasonable allocation of various resources leads to the disorderly development of the logistics industry. Therefore, predicting the express business volume will help related personnel to make scientific decisions, and then promote the healthy development of the whole logistics industry. At present, some scholars have done relevant prediction research. Li and Zhang have established a support vector machine model based on trend adjustment and seasonal adjustment to predict and analyze the monthly express business volume [1]; Zhou Yang et al. used the *R* language software to establish a sliding window model and SARIMA model based on time series analysis. The residual of the model was fitted linearly, and then the daily express business volume of express enterprises was predicted [2]; Tang and Dengused GM (1, 1) model to forecast the express business volume [3].

Grey prediction is a systematic prediction method containing uncertainty, which identifies different degrees of development trends among system factors and then establishes corresponding differential equation models according to certain rules to predict the future development trend of things. GM (1, 1) model is the core model of grey prediction theory, which is often used in the prediction of short-term data [4]. After the model was put forward, scholars have studied the GM (1, 1) model from the perspectives of accumulation generation method, initial value optimization, background value optimization, parameter estimation method, model properties, and so on [5–8]. For the poor accuracy of GM (1, 1), Wu Lifeng et al. proposed the fractional-order FGM (1, 1) model [9, 10]. In FGM (1, 1) model, each sequence is multiplied by different fractional-order and then accumulated. At present, FGM (1, 1) model has been applied to predict solid waste treatment capacity,

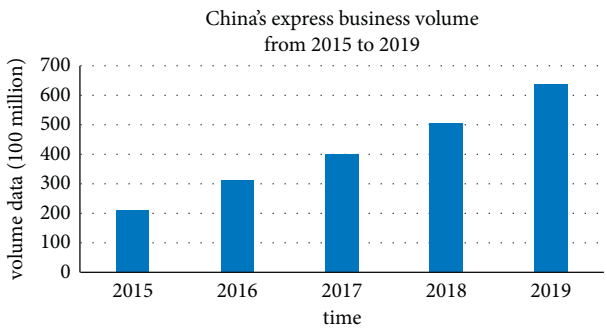

Figure 1: The data of China's express business volume from 2015 to 2019.

natural gas consumption, high-tech industrial added value, and so on [11–13].

Particle Swarm Optimization (PSO) algorithm has been proposed in 1995 by Kennedy and Eberhart [14, 15] based on the behavior of birds foraging, which is widely used in various calculations [16–18]. According to the data from China's express business from 2015-2019, this paper uses the improved particle swarm optimization algorithm to solve the fractional-order r of the FGM (1, 1) model and then predicts the express business volume of China in the coming years through the FGM (1, 1) model.

2. Modeling Process of FGM (1, 1) Model and Particle Swarm Optimization Algorithm

2.1. Modeling Process of FGM (1, 1) Model. For the deficiency of the traditional GM (1, 1) model, FGM (1, 1) model obtains more accurate results by selecting the appropriate cumulative order and reducing the relative error. The modeling process is as follows:

(1) The original sequence is given according to the original nonnegative data.

$$X^{(0)} = \left\{x^{(0)}(1), x^{(0)}(2), \ldots, x^{(0)}(n-1), x^{(0)}(n)\right\}. \tag{1}$$

(2) The r-order accumulation sequence is as follows:

$$X^{(r)} = \left\{x^{(r)}(1), x^{(r)}(2), \ldots, x^{(r)}(n)\right\}, \tag{2}$$

where $x^{(r)} = \sum_{i=1}^{k} C_{k-i+r-1}^{k-i} x^{(0)}(i)$, $C_{k-i+r-1}^{k-i} = (k-i+r-1)(k-i+r-2)\cdots(r+1)r/(k-i)!$, $C_{r-1}^{0} = 1$, $C_{k}^{k+1} = 0$.

(3) The whitening differential equation is as follows:

$$\frac{dx^{(r)}(t)}{dt} + ax^{(r)}(t) = b, \tag{3}$$

where "a" is called development grey number, "b" is called endogenous control grey number.

The solution of the equation is exponential as follows:

$$x^{(r)}(t+1) = \left[x^{(0)}(1) - \frac{b}{a}\right]e^{-at} + \frac{b}{a}. \tag{4}$$

Using the least square method, the following results can be obtained:

$$\begin{bmatrix} \hat{a} \\ \hat{b} \end{bmatrix} = \left(B^T B\right)^{-1} B^T Y, \tag{5}$$

where

$$B = \begin{bmatrix} -0.5\left(x^{(r)}(1) + x^{(r)}(2)\right. & 1 \\ -0.5\left(x^{(r)}(2) + x^{(r)}(3)\right. & 1 \\ \vdots & \vdots \\ -0.5\left(x^{(r)}(n-1) + x^{(r)}(n)\right. & 1 \end{bmatrix},$$
$$Y = \begin{bmatrix} x^{(r)}(2) - x^{(r)}(1) \\ x^{(r)}(3) - x^{(r)}(2) \\ \vdots \\ x^{(r)}(n) - x^{(r)}(n-1) \end{bmatrix}. \tag{6}$$

(4) The time response function is as follows:

$$\hat{x}^{(r)}(k+1) = \left[x^{(0)}(1) - \frac{\hat{b}}{\hat{a}}\right]e^{-\hat{a}k} + \frac{\hat{b}}{\hat{a}}, \tag{7}$$

where $\hat{x}^{(r)}(k+1)$ is the value of time $k+1$.

(5) The reduction sequence of $\hat{X}^{(r)} = \left\{\hat{x}^{(r)}(1), \hat{x}^{(r)}(2), \cdots, \hat{x}^{(r)}(n)\right\}$ is as follows:

$$\alpha^{(r)}\hat{X}^{(r)} = \left\{\alpha^{(1)}\hat{x}^{(r)(1-r)}(1), \alpha^{(1)}\hat{x}^{(r)(1-r)}(2), \ldots, \alpha^{(1)}\hat{x}^{(r)(1-r)}(n)\right\}, \tag{8}$$

where $\alpha^{(1)}\hat{x}^{(r)(1-r)}(k) = \hat{x}^{(r)(1-r)}(k) - \hat{x}^{(r)(1-r)}(k-1)$ so the predicted value is as follows:

$$\hat{X}^{(0)} = \left\{\hat{x}^{(0)}(1), \hat{x}^{(0)}(2), \ldots, \hat{x}^{(0)}(n)\right\}. \tag{9}$$

(6) Model test (mean absolute percentage error).

$$\text{MAPE} = 100\% \times \frac{1}{n}\sum_{k=1}^{n}\left|\frac{x^{(0)}(k) - \hat{x}^{(0)}(k)}{x^{(0)}(k)}\right|. \tag{10}$$

2.2. Particle Swarm Optimization Algorithm. The particle swarm optimization algorithm is an iterative-based optimization tool, where particles follow the optimal particle in the solution space to find the optimal solution. In each iteration, particles update themselves by tracking individual extremum (P_{Best}) and global extremum (G_{Best}). In addition, it is also possible to use only a part of the population instead of the whole population as the neighbors of the particle; then, the extremum in all the neighbors is the local extremum [14, 15].

Suppose there are N particles in a D-dimensional target search space to form a community, where the i-particle represents a vector of D dimensions, it is denoted by $X_i = (x_{i1}, x_{i2}, \ldots, x_{iD})$. A particle's velocity is also a vector of D dimensions, it is denoted by $V_i = (v_{i1}, v_{i2}, \ldots, v_{iD})$. The optimal position of the i-particle and the entire particle group searched so far are individual extreme value $P_{\text{Best}} = (p_{i1}, p_{i2}, \ldots, p_{iD})$ and global extreme value $G_{\text{Best}} = (g_{i1}, g_{i2}, \ldots, g_{iD})$, respectively.

The particles will update their velocity and position according to the following formula:

$$\begin{cases} v_{ij}(t+1) = wv_{ij}(t) + c_1 r_1(t)\left[p_{ij}(t) - x_{ij}(t)\right] + c_2 r_2(t)\left[g_{ij}(t) - x_{ij}(t)\right], \\ x_{ij}(t+1) = x_{ij}(t) + v_{ij}(t+1), \end{cases} \tag{11}$$

where c_1 and c_2 are the learning factors, w is the inertia factor, and $r_1(t)$ and $r_2(t)$ are uniform random numbers in [0, 1]. $v_{ij}(t+1)$ consists of three parts: the first part is the inertia or momentum part, which reflects the motion habit of particles and represents the tendency of particles to maintain their previous velocity; the second part is the cognitive part, which reflects the memory or recollection of the particle's own historical experience and represents that the particle tends to approach the best position in its own history; the third part is the social part, which reflects the historical experience of group cooperation and knowledge sharing among particles and represents the trend of particles approaching the best historical position of group or neighborhood.

2.3. Algorithm Design. The particle swarm optimization algorithm will be improved according to its characteristics. Let $c_1 = c_2 = 2$, $N = 50$, the maximum number of iterations is $t_{\max} = 100$, set the stop criterion to eps = 10^(−6), according to the concept of fractional-order, r is between 0 and 1. To avoid particles "oscillating" near the global optimal solution, let [19]

$$w = w_{\max} - t \times \frac{w_{\max} - w_{\min}}{t_{\max}}, \tag{12}$$

where t is the number of present iterations and w changes linearly between 0.1 and 0.9. The improved PSO algorithm flow chart is shown in Figure 2.

3. Empirical Research

In order to predict the express business volume in China, the FGM (1, 1) model is constructed. The original sequence of China's express business volume from 2015 to 2019 is $X^{(0)} = \{206.6637, 312.8315, 400.5592, 507.1043, 635.2291\}$ (unit: 100 million, data from China Statistical Yearbook). The particle swarm optimization algorithm is iterated by MATLAB, and the results are shown in the Figure 3. It is found that as the number of iterations increases, the fractional-order eventually tends to 0.8536.

The 0.8536 order cumulative sequence is as follows:

$$\begin{aligned} X^{(0.8536)} &= \left\{x^{(0.8536)}(1), x^{(0.8536)}(2), x^{(0.8536)}(3), x^{(0.8536)}(4), x^{(0.8536)}(5)\right\} \\ &= \{206.6637, 489.2396, 831.0872, 1252.024, 1770.216\}, \end{aligned} \tag{13}$$

$\hat{a}$ and $\hat{b}$ are obtained by the formula

$$\begin{bmatrix} \hat{a} \\ \hat{b} \end{bmatrix} = \left(B^T B\right)^{-1} B^T Y = \begin{bmatrix} -0.2033 \\ 209.8712 \end{bmatrix}, \tag{14}$$

where

$$B = \begin{bmatrix} -347.9517 & 1 \\ -660.1634 & 1 \\ -1041.556 & 1 \\ -1511.120 & 1 \end{bmatrix}, Y = \begin{bmatrix} 282.5759 \\ 341.8476 \\ 420.9370 \\ 518.1915 \end{bmatrix}. \tag{15}$$

Then the time series function is as follows:

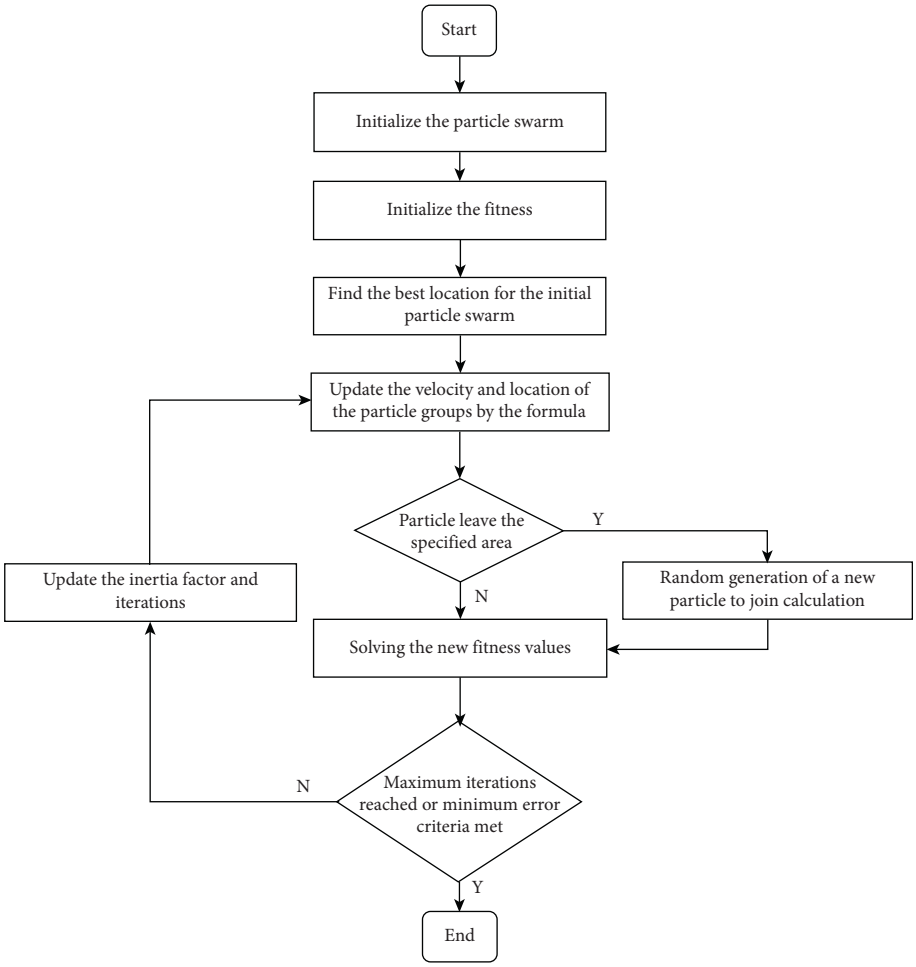

Figure 2: PSO flow chart.

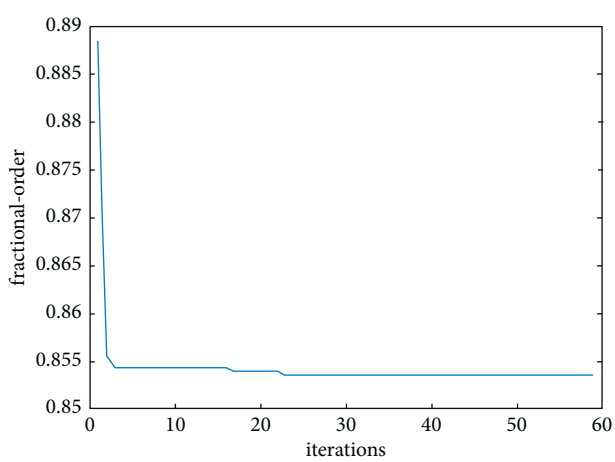

Figure 3: Fractional-order convergence process.

Table 1: The MAPE of GM (1, 1) model and FGM (1, 1) model (100 million pieces).

Year	Actual value	GM (1, 1)	FGM (1, 1) ($r = 0.8536$)
2015	206.6637	206.6637	206.6637
2016	312.8315	314.2032	309.5893
2017	400.5592	396.6401	400.5590
2018	507.1042	500.7057	505.4784
2019	635.2291	632.0748	630.7863
MAPE		0.64%	0.41%

Table 2: The prediction values of China's express business volume from 2020-2023 (100 million pieces).

Year	2020	2021	2022	2023
Prediction value	782.3501	966.7292	1191.693	1466.627
Growth rate (%)	24.03	23.57	23.27	23.07

$$\hat{x}^{(0.8536)}(k+1) = \left[206.6637 - \frac{209.8712}{-0.2033}\right]e^{0.2033k} + \frac{209.8712}{-0.2033}. \tag{16}$$

So

$$\begin{aligned}\hat{X}^{(0.8536)} &= \left\{\hat{x}^{(0.8536)}(1), \hat{x}^{(0.8536)}(2), \ldots, \hat{x}^{(0.8536)}(9)\right\} \\ &= \{206.6637, 485.9975, 828.3195, 1247.833, 1761.945, 2391.986, 3164.089, 4110.318, 5269.904\}.\end{aligned} \tag{17}$$

Accordingly, the reduction sequence is as follows:

$$\begin{aligned}\hat{X}^{(1)} &= \left\{\hat{x}^{(0.8536)(0.1464)}(1), \hat{x}^{(0.8536)(0.1464)}(2), \ldots, \hat{x}^{(0.8536)(0.1464)}(9)\right\} \\ &= \{206.6637, 516.2530, 916.8120, 1422.2904, 2053.0766, 2835.4267, 3802.1560, 4993.8488, 6460.4762\}.\end{aligned} \tag{18}$$

The predicted values are as follows:

$$\begin{aligned}\hat{X}^{(0)} &= \left\{\hat{x}^{(0)}(1), \hat{x}^{(0)}(2), \ldots, \hat{x}^{(0)}(9)\right\} \\ &= \{206.6637, 309.5893, 400.5590, 505.4784, 630.7863, 782.3501, 966.7292, 1191.693, 1466.627\}.\end{aligned} \tag{19}$$

The MAPE values of the GM (1, 1) model and FGM (1, 1) model are given in Table 1. According to Table 1, it can be found that both MAPE values of the FGM (1, 1) model and the GM (1, 1) model are small, which indicates that the simulation results are accurate. Meanwhile, the MAPE value of the FGM (1, 1) model is less than the GM (1, 1) model's, which verifies the superiority of the FGM (1, 1) model.

The prediction values of China's express business volume from 20202023 based on FGM (1, 1) model are shown in Table 2.

4. Conclusions

Compared with the traditional GM (1, 1) model, the FGM (1, 1) model can reduce the MAPE and better predict the data. In addition, it can be seen that China's express business volume is increasing year by year, and it will exceed 100 billion pieces in 2022. At the same time, although the growth rate is declining year by year, it is still maintained at more than 23% shortly, which indicates that there is still a lot of room for development in the express delivery industry. In the future work, other prediction models can be introduced to predict China's express business volume [20]. At the same time, the continuous growth of China's express business volume requires the continuous improvement of the logistics system, such as the site location of the logistics center, the optimization of distribution path, and so on.

Data Availability

No data were used to support this study.

Conflicts of Interest

The authors declare that they have no conflicts of interest.

Acknowledgments

This work was partially supported by China Postdoctoral Science Foundation (No. 2017M611785) and Jiangsu Planned Projects for Postdoctoral Research Funds (No. 1601091C).

References

[1] P. Li and R. Zhang, "Analysis and forecast of RBF-SVR monthly express business volume based on TSCI change," *Statistics & Decisions*, vol. 37, no. 5, pp. 184–188, 2021.

[2] Y. Zhou, L. Gan, and L. Jin, "Prediction of daily express business scale by R programming language-based SARIMA sliding window model," *Logistics Technology*, vol. 39, no. 10, pp. 103–108, 2020.

[3] S. Tang and G. Deng, "Based on the theory of grey system to forecast China's business volume of express services," *Modern Economy*, vol. 6, no. 2, pp. 283–288, 2015.

[4] J. Deng, "Properties of grey forecasting models GM (1, 1)," *Journal of Huazhong University of Science and Tedimelogy*, vol. 15, no. 5, pp. 1–6, 1987.

[5] Y. Wang, Z. Chen, Z. Gao et al., "A generalization of the GM (1, 1) direct modeling method with a step-by-step optimizing grey derivative's whiten values and its applications," *Kybernetes*, vol. 33, no. 2, pp. 382–389, 2004.

[6] Z.-X. Wang, Y.-G. Dang, and S.-F. Liu, "Optimization of background value in GM (1, 1) model," *Systems Engineering-Theory & Practice*, vol. 28, no. 2, pp. 61–67, 2008.

[7] J. Song and Y. Liu, "Prediction of polycyclic aromatic hydrocarbons from vehicle exhaust emission and coal combustion based on grey model GM (1, 1)," *Journal of Computational and Theoretical Nanoscience*, vol. 13, no. 9, pp. 6377–6381, 2016.

[8] Y. Wang, F. Wei, C. Sun, and Q. Li, "The research of improved grey GM (1, 1) model to predict the postprandial glucose in type 2 diabetes," *BioMed Research International*, vol. 2016, Article ID 6837052, 6 pages, 2016.

[9] L. Wu, *Fractional Order Grey Forecasting Models and Their Application*, Nanjing University of Aeronautics and Astronautics, Nanjing, Jiangsu, China, 2015.

[10] L. Wu, S. Liu, and L. Yao, "Discrete grey model based on fractional-order accumulates," *System Engineering-Theory & Practice*, vol. 34, no. 7, pp. 1822–1827, 2014.

[11] Y. Tong, Y. Chen, H. Chen et al., "Forecast of Tianjin municipal solid waste disposal volume based on FGM (1, 1) model," *Mathematics in Practice and Theory*, vol. 50, no. 8, pp. 67–72, 2020.

[12] Y. Tong, H. Chen, X. Zhang et al., "Forecast of Beijing natural gas consumption based on FGM (1, 1) model," *Mathematics in Practice and Theory*, vol. 50, no. 3, pp. 79–83, 2020.

[13] G. Zhao, Y. Tong, H. Chen et al., "Forecast of added value of high-tech industries in Hebei Province based on FGM (1, 1) model," *Mathematics in Practice and Theory*, vol. 51, no. 6, pp. 313–317, 2021.

[14] J. Kennedy and R. Eberhart, "Particle swarm optimization," in *Proceedings IEEE International Conference on Neural Networks*, pp. 1942–1948, Perth, WA, Australia, November 1995.

[15] R. Eberhart and J. Kennedy, "A new optimizer using particle swarm theory," in *Proceedings of the 6th International Symposium on Micro Machine and Human Science*, pp. 39–43, Nagoya, Japan, October 1995.

[16] J.-J. Shin and H. Bang, "UAV path planning under dynamic threats using an improved PSO algorithm," *International Journal of Aerospace Engineering*, vol. 2020, no. 10, 17 pages, Article ID 8820284, 2020.

[17] L. Guo, X. Yang, J. Wang et al., "Design of nonlinear observer of dynamic positioning based on particle swarm optimization algorithm," *Computing Technology and Automation*, vol. 39, no. 4, pp. 1–6, 2020.

[18] L. Yang, X. Hu, and K. Li, "A vector angles-based many-objective particle swarm optimization algorithm using archive," *Applied Soft Computing*, vol. 106, Article ID 107299, 2021.

[19] Z. Hou and Z. Lv, "Particle swarm optimization with application based on MATLAB," *Computer Simulation*, vol. 20, no. 10, pp. 68–70, 2003.

[20] L. Tu and Y. Chen, "An unequal adjacent grey forecasting air pollution urban model," *Applied Mathematical Modelling*, vol. 99, pp. 260–275, 2021.

Hindawi
Journal of Mathematics
Volume 2021, Article ID 7996776, 16 pages
https://doi.org/10.1155/2021/7996776

Review Article

A Bibliometric Analysis and Visualization of Fractional Order Research in China over Two Decades (2001–2020)

Yunfei Yang, Ke Lv, Jian Xue, and Xi Huang

School of Engineering Science, University of Chinese Academy of Sciences, Beijing 100049, China

Correspondence should be addressed to Jian Xue; xuejian@ucas.ac.cn

Received 15 June 2021; Accepted 28 July 2021; Published 13 August 2021

Academic Editor: Lifeng Wu

Fractional order research has interdisciplinary characteristics and has been widely used in the field of natural sciences. Therefore, fractional order research has become an important area of concern for scholars. This paper used 2854 literatures collected from China National Knowledge Infrastructure (CNKI) database from 2001 to 2020 as the data source and used bibliometrics and two visualization methods to conduct bibliometric analysis and visualization research on China's fractional order research. To begin with, this paper analyzed the time series distribution of publications, the distribution of research institutions, the author cooccurrence network, the distribution of important journals, and the distribution of important literature, which explained the research status of the fractional order. Furthermore, this paper used VOSviewer software to analyze the clustering and density distribution of the fractional order research keywords, which revealed the hotspots of the fractional order research. Finally, with the help of CiteSpace software, the burst keywords were analyzed to further explore the frontiers of fractional order research. This paper systematically reveals the research status, research hotspots, and research frontiers of China's fractional order research, which can provide certain theoretical and practical references for related follow-up researchers.

1. Introduction

The fractional calculus is a name for the theory of integrals and derivatives of arbitrary order, which unifies and generalizes the notions of integer-order differential and integral [1]. The idea of fractional calculus is known in developing regular calculation referring to Leibniz and L'hospital's work in 1695 [2]. Fractional calculus was introduced more than 300 years ago [3], and it was introduced by Leibniz in the scope of mathematics by the end of the 17th century [4]. The research on fractional calculus experienced its boom in the past decades [5], and recently this mathematical tool has found its way in various branches of science and engineering [6], such as electrical and electronic engineering [7, 8], automation control systems [9, 10], and computer science information systems [11, 12]. Therefore, the related research of fractional order has attracted the wide attention of international scholars.

In recent years, scholars have conducted reviews around the relevant topics of fractional order research and have achieved relatively rich research results, such as literatures [2–6]. In addition, other scholars focused on specific areas of fractional order research and reviewed them, such as the research field of fractional order control [13–15] and the research field of image processing [16, 17]. There is no doubt that the research results of the above scholars have contributed to the advancement of fractional order research and can also provide reference and support for subsequent scholars to further deepen the relevant research of fractional order. However, it is difficult to comprehensively extract the common elements and core points of the literature to a certain extent if the comprehensive analysis of the long term and a large amount of literature is conducted by combination, summary, and other methods. Furthermore, in this case, the researchers may find it difficult to avoid the subjective influence in the analysis process, so its scientificity is worth discussing.

Bibliometrics and visualization software are effective tools for analyzing mass literature [18]. VOSviewer is a software tool for constructing and visualizing bibliometric

networks [19], which can be used to construct maps of authors or journals based on cocitation data or to construct maps of keywords based on cooccurrence data [20]. Meanwhile, VOSviewer has an advanced graphic presentation capability that is suitable for large-scale data and locates key points and hotspots in scientific research using density view [21]. In addition, CiteSpace is a knowledge visualization tool developed by Dr. Chen Chaomei [22], which combines citation analysis and cocitation analysis to transform literature data from abstract data into visual and intuitive maps of scientific knowledge through information visualization, helping researchers find research hotspots, and frontiers in a scientific field [23].

In summary, regarding the related research of fractional literature review, many scholars reviewed the related research of fractional order from a micro perspective, that is, focusing on a specific area of the fractional order for exploration. However, there are few related research results of literature analysis on the overall fractional research from a macro perspective. At the same time, from the perspective of literature analysis methods, many scholars used methods such as combination and induction, but, with the help of visual analysis software, the findings of visual research on fractional research are rarely found.

Therefore, this paper collected the research data of China's fractional literature from 2001 to 2020 and used bibliometrics and two visualization research methods to analyze the literature of China's fractional order over two decades. The purpose of this paper is to analyze the research status and explore the hotspots and research frontiers of China's fractional order research. To be specific, this paper used the method of bibliometric analysis to explore the time series distribution of publications, the distribution of research institutions, the author cooccurrence network, the distribution of key journals, and the distribution of important literature, which clarified the research status of fractional order. Furthermore, it used VOSviewer to analyze the clustering and density distribution of the fractional research keyword network and used CiteSpace to analyze the fractional research burst keywords, which can reveal the hotspots and research frontiers of the fractional order research. This paper systematically analyzes and explores the research status, research hotspots, and frontier fields of fractional order research, which enriches the content system of fractional order research to a certain extent and can also provide some references for scholars to explore and further deepen the research on fractional order.

2. Research Methods and Data Sources

The research methods of this paper mainly include bibliometric analysis and visualization research methods. Firstly, this paper used the bibliometric analysis method to analyze the publications, research institutions, important journals, and important literature of fractional order research, which can explore the current status of fractional order research. Secondly, VOSviewer and CiteSpace software were used to visualize the fractional order research. To be specific, VOSviewer was used to analyze the author cooccurrence network, keyword network, keyword density, and so forth of fractional order research, thus revealing the author cooperation situation and research hotspots of fractional order research. Meanwhile, CiteSpace was used to analyze the burst keywords of fractional order research, thereby further exploring the frontiers of fractional order research.

The data of this paper came from China National Knowledge Infrastructure (CNKI). The literature retrieval conditions were as follows: set the title as fractional order, selected the categories of the sources as SCI source journals, EI source journals, core journals, CSSCI, and CSSCD, selected the period time from 2001 to 2020, and a total of 2854 literatures were retrieved. In view of this, 2854 literatures were retrieved as research data sources, and the retrieval date was May 18, 2021. It should be noted that the bibliometric data of this paper are all from CNKI statistics.

3. Research Status

This study focused on the perspective of the time series distribution of publications, the distribution of research institutions, the author cooccurrence network, the distribution of important journals, and the distribution of important literature and used the bibliometric analysis method to explore the research status of fractional order.

3.1. Time Series Distribution of Publications. The dynamic change of the publications with time evolution can effectively reveal the degree of concern in a certain research field. Therefore, this paper made a quantitative analysis on the time series distribution of 2854 papers on fractional order research in the CNKI database. The results are shown in Figure 1.

It can be seen from Figure 1 that the publications of fractional order research show an overall upward trend during the research period (2001–2020), but there are obvious differences in the distribution of publications in different time series phases. To be specific, the time series distribution of the publications of fractional order research can be divided into the four following phases: The first phase is from 2001 to 2010; the total number of publications in this phase is relatively small, accounting for about 15% of the total number of publications in the past 10 years, especially from 2001 to 2006, and the average annual number of publications in fractional order research is less than 20, so the first phase belongs to the slow development phase of fractional order research. The second phase is from 2010 to 2014; this phase belongs to the rapid growth phase of fractional order research. During this period, the publications of fractional order research continued to emerge, which indicates that Chinese scholars pay more and more attention to fractional order research. Especially in 2011, the number of publications in fractional order research increased by 68.13% compared with the previous year, and the number of publications in that year exceeded 100 for the first time. Therefore, it can be considered that 2011 is the transition period of fractional order research. The third phase is from 2014 to 2019; the average number of annual

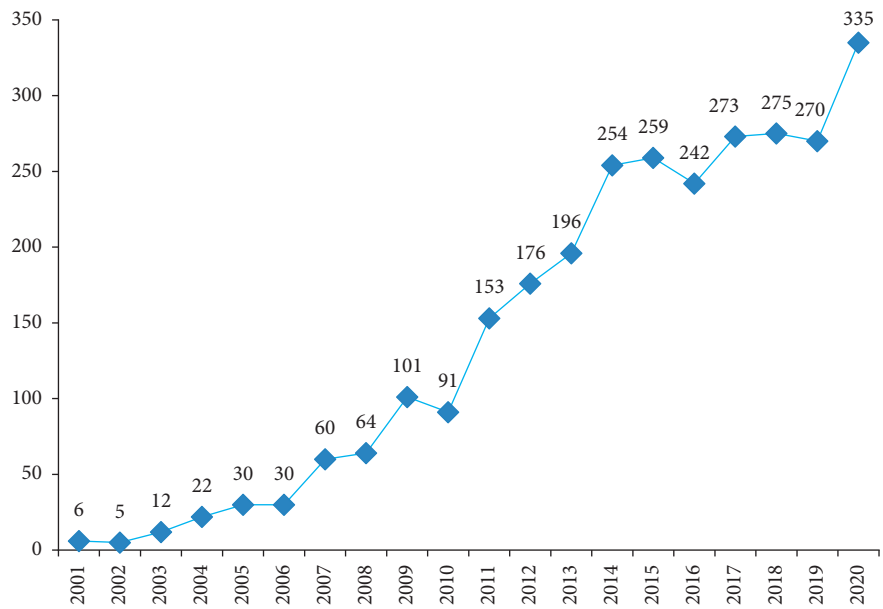

Figure 1: Time series distribution of publications.

publications in this phase is about 260, and there is a little difference in the number of publications each year, which indicates that the fractional order research has entered a phase of steady development. The fourth phase is from 2019 to 2020; the publications of fractional order research continued to grow, and the publications exceeded 300 for the first time in 2020. This phase belongs to the sustained growth phase of fractional order research, which shows that Chinese scholars' attention to fractional order research continues to advance.

3.2. Distribution of Research Institutions. In order to further explore the distribution of the main research power of fractional order, this paper made a quantitative analysis of the top 25 research institutions in the publications of fractional order research. The results are shown in Figure 2.

Figure 2 shows the distribution of the publications by the main research institutions. These research institutions are an important power of fractional order research and play an important role in promoting the development of fractional order research. Among them, Sichuan University has the largest number of publications on fractional order research, up to 95. Anhui University, Beijing Institute of Technology, Zhengzhou University of Aeronautics, and Yanshan University also published more papers; all of them have published more than 50 papers, which are 71, 66, 62, and 53, respectively. Therefore, it can be considered that these research institutions have an important influence on the development of fractional order research in China. In addition, according to the horizontal comparison of the publications by research institutions in Figure 2, we can see that the overall difference in the number of publications by research institutions is relatively small. Combined with data statistics, it can be seen that the average number of publications by the main research institutions in Figure 2 is about 45, which indicates that the distribution of fractional order research publications among research institutions is relatively balanced. Additionally, further analysis of the attributes of research institutions shows that the distribution of fractional order research institutions includes comprehensive universities, science, engineering universities, and military academy. In summary, the bibliometric analysis of the distribution of main research institutions in the fractional order can contribute to understanding the publications and attributes of research institutions for scholars.

3.3. Author Cooccurrence Network. This paper used VOSviewer to analyze the author cooccurrence network of fractional order research. The parameter options were set as follows: chose coauthorship for type of analysis, authors for unit of analysis, full counting for counting method, and 3 for the minimum number of documents of an author, thereby generating the author cooccurrence network visualization map, as shown in Figure 3.

Figure 3 shows the author cooccurrence network of fractional order research, in which the node size is related to the publications by authors, and the larger the node, the more publications by authors. The thickness of connecting lines and distance between nodes is significantly related to the cooperative relationship between authors. The thicker the connection and the closer the location between nodes, the closer the cooperation relationship between authors.

As can be seen from Figure 3, based on the global perspective analysis, it can be found that the author cooccurrence network nodes of fractional order research are relatively scattered, the overall connecting lines between nodes are relatively few, and the network distribution and connecting lines between nodes do not show obvious network cooperation relationship. Therefore, it can be considered that the overall cooperation intensity among authors

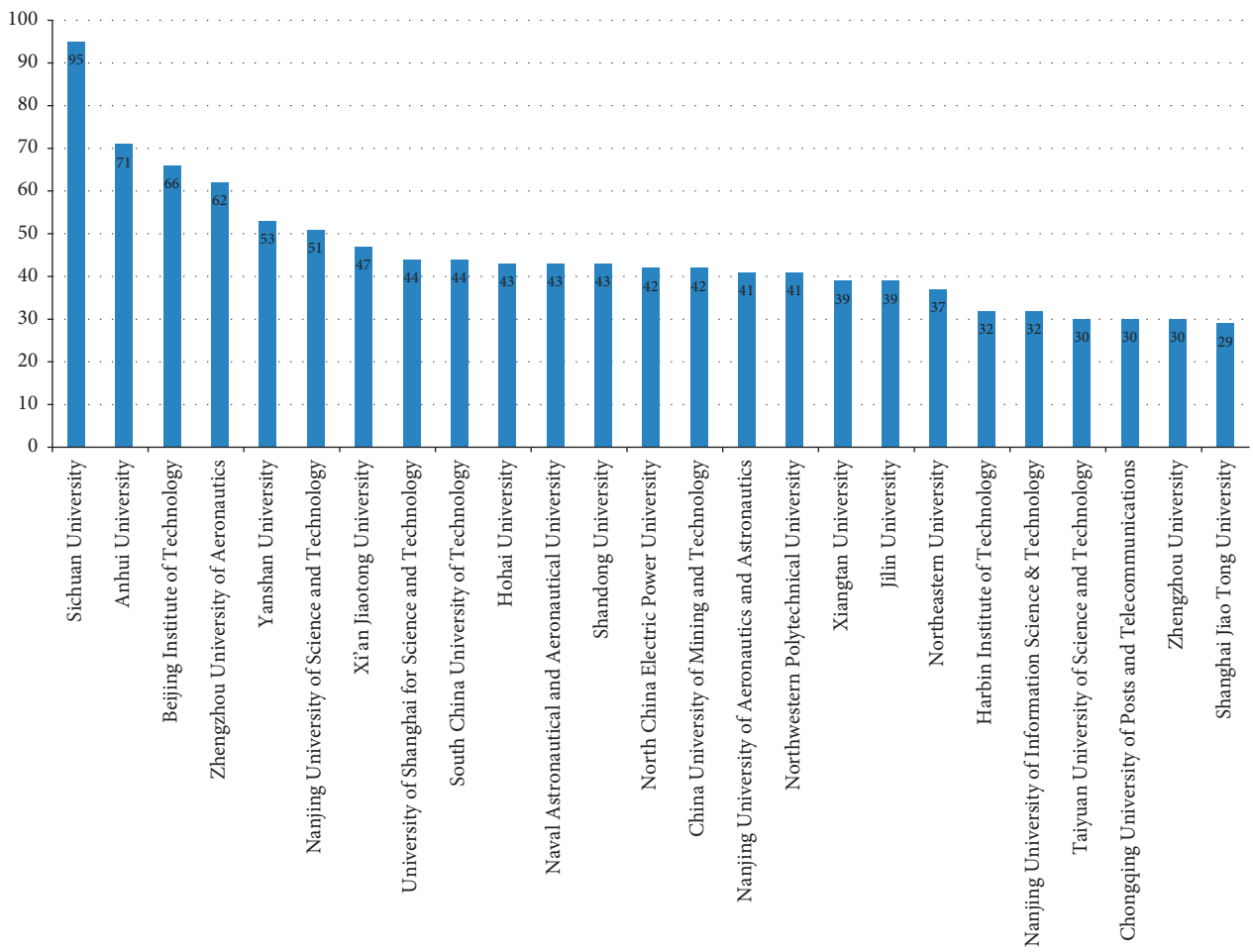

Figure 2: Distribution of main research institutions.

in fractional order is not high. However, based on the local perspective analysis, it can be found that some of the nodes are large and show a relatively close cooperative relationship, such as scholars Mao Beixing, Jiang Wei, Tao Ran, Pu Yifei, and Hu Weimin. These authors are in a relatively central position in the cooccurrence network and form a strong cooperative relationship with other scholars in the research group. Therefore, the global and local perspective analysis shows that the overall cooperation intensity of fractional order research is not high, but there are many research groups with a big number of publications and strong cooperation relationships.

3.4. Distribution of Important Journals. To a certain extent, the publications in a journal can reflect its influence in a certain research field. Statistics on the number of publications in a journal in fractional order research are also of great significance for revealing the distribution of fractional order research disciplines. In view of this, this paper made a quantitative analysis of the top 15 journals in terms of the publications of fractional order research. The results are shown in Table 1.

As can be seen from Table 1, regarding fractional research, *Acta Physica Sinica* has the largest number of publications, with 123 papers. Meanwhile, *Mathematics in Practice and Theory*, *Journal of Jilin University (Science Edition)*, *Mathematica Applicata*, and *Journal of Shandong University (Natural Science)* also have more publications, which show that these journals have an important influence in the field of fractional order research. From the number of publications and subject areas of journals, we can see that publications in mathematics are the largest, such as *Mathematics in Practice and Theory* and *Mathematica Applicata*. At same the time, some other journals also involve the research publications of mathematics, such as *Applied Mathematics and Mechanics* and *Acta Mathematica Scientia*. In addition, the publications of fractional order research are also involved in physics, computer, control engineering, and other fields, such as *Acta Physica Sinica*, *Computer Engineering and Applications*, and *Control Engineering of China*. Therefore, it indicates the interdisciplinary attribute of fractional order research.

3.5. Distribution of Important Literature. To further explore the highly cited literature of fractional order research, this paper made a bibliometric analysis on the top 10 cited literatures of fractional order research. The results are shown in Table 2.

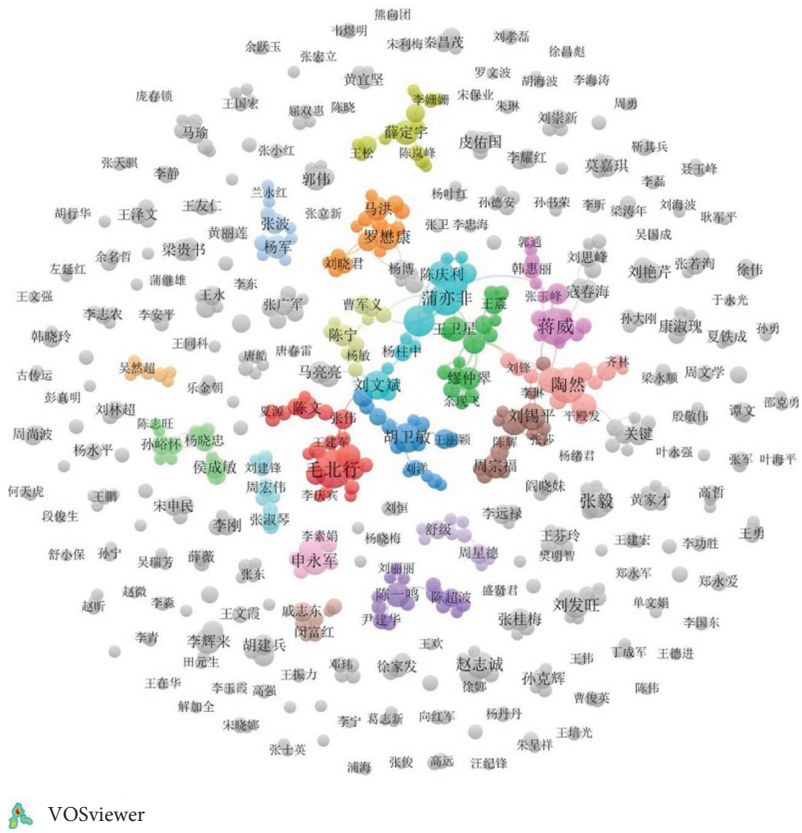

FIGURE 3: Author cooccurrence network. Note: due to the large number of authors in Figure 3 and limited space, this paper only translates the names of the following authors: 毛北行 = Mao Beixing; 蒋威 = Jiang Wei; 陶然 = Tao Ran; 蒲亦菲 = Pu Yifei; and 胡卫敏 = Hu Weimin.

TABLE 1: Statistics of the top 15 journals publications.

No.	Journal title	Publications
1	Acta Physica Sinica	123
2	Mathematics in Practice and Theory	119
3	Journal of Jilin University (Science Edition)	76
4	Mathematica Applicata	53
5	Journal of Shandong University (Natural Science)	50
6	Journal of Sichuan University (Natural Science Edition)	49
7	Computer Engineering and Applications	46
8	Control Engineering of China	39
9	Applied Mathematics and Mechanics	36
10	Acta Electronica Sinica	36
11	Acta Mathematica Scientia	35
12	Control Theory & Applications	34
13	Journal of Electronics & Information Technology	33
14	Science Technology and Engineering	33
15	Application Research of Computers	31

It can be seen from Table 2 that *Detection and parameter estimation of multi-component LFM signals based on fractional Fourier transform* is the most frequently cited literature in the fractional order research, and this paper proposed a method of multicomponent LFM signal detection and parameter estimation based on fractional Fourier transform [24]. Meanwhile, the frequently cited literatures in Table 2 such as *Dimensional normalization in the digital computation of the fractional Fourier transform* and *Research progress of fractional Fourier transform in the field of signal processing* are also related to the fractional Fourier transform, so this also reflects the importance of the fractional Fourier transform in the field of fractional order research. Based on the perspective of literature attribute analysis, there are many review literatures about fractional order, such as *Summary of research on fractional-order control*, *Research progress of fractional Fourier transform in the field of signal processing*, and *Summary of research on image processing*

Table 2: Statistics of top 10 important literatures cited in frequency.

No.	Literature	First author	Citation frequency	Year
1	Detection and parameter estimation of multi-component LFM signals based on fractional Fourier transform	Qi lin	358	2003
2	Design of fractional PID controller for fractional order system	Xue Dingyu	352	2007
3	Dimensional normalization in the digital computation of the fractional Fourier transform	Zhao Xinghao	263	2005
4	Summary of research on fractional-order control	Zhu Chengxiang	216	2009
5	Research progress of fractional Fourier transform in the field of signal processing	Tao Ran	182	2006
6	Image enhancement based on fractional differentials	Yang Zhuzhong	177	2008
7	Fractional order sliding-mode control for permanent magnet synchronous motor	Zhang Bitao	134	2012
8	Fractional differential masks of digital image and their numerical implementation algorithms	Pu Yifei	130	2007
9	Application of fractional differential approach to digital image processing	Pu Yifei	121	2007
10	Summary of research on image processing using fractional calculus	Huang Guo	117	2012

using fractional calculus. In addition, it can be seen from the year of publication that most of the highly cited literatures of fractional order research were published before 2010, while the highly cited literatures after 2010 were relatively few; both groups of literatures provide important support for the development of fractional order research.

4. Research Hotspots and Frontier Analysis

This study used VOSviewer to analyze the cooccurrence of the keywords, combined with CiteSpace to analyze the burst keywords, thereby revealing the hotspots and research frontiers of the fractional research.

4.1. Research Hotspots. The keyword is the core and essence of a document, which is a high-level summary of the content of the article [25]. After cluster analysis and words frequency count, topics and research hotspots can be known [26]. In view of this, this paper visually analyzed the cooccurrence of keywords in fractional order research using VOSviewer, which can explore the distribution of hotspots in fractional order research. To be specific, it selected type of analysis as cooccurrence, unit of analysis as keywords, and full counting as counting method and set minimum number of occurrences of a keyword to 18. Moreover, the keywords were merged and cleaned; that is, the different expressions of fractional Fourier transform were merged, and the repeated English keywords were cleaned. On this basis, by adjusting the clustering option and running the software to generate the keyword network and density visualization view, as shown in Figure 4 and Figure 5, respectively, it should be noted that this paper also tried to merge the keywords of fractional PID controller and fractional order $PI^{\lambda}D^{\mu}$ controller as well as fractional order and fractional calculus with the same method as above, but it was not successful. However, because fractional PID controller and fractional order $PI^{\lambda}D^{\mu}$ controller are distributed in the same cluster, there is only a slight difference in expression. Meanwhile, the fact that fractional order and fractional calculus are not merged has almost no effect on the cluster distribution, and the clustering distribution formed by software operation is still clear. Thus, the fact that these keywords were not merged has almost no effect on the analysis results.

In order to further explore the distribution of high-frequency keywords in fractional order research, the occurrences of the top 20 keywords were counted, as shown in Table 4.

According to Table 4, the most frequent keyword of fractional order research is fractional order (342), which is consistent with the retrieval method of this study. Meanwhile, the core keywords of fractional order theory, such as fractional differential equation, fractional Fourier transform, and fractional calculus, have high frequencies of 250, 243, and 228, respectively, which shows that these keywords are the key to the subject of fractional order research. In addition, fixed point theorem, positive solution, stability, chaos synchronization, sliding mode control, image enhancement, and so forth have a relatively high frequency of occurrence and involve multiple disciplines. Therefore, it can be also shown that the research of fractional order presents the characteristic of diversification.

Figure 4 shows the distribution of hot keywords in fractional order research, and different colors in the figure represent different clusters of research hotspots. Figure 4 is mainly composed of nodes and connecting lines. The larger the keyword node, the higher the frequency of occurrence, and the thicker the line between nodes, the higher the cooccurrence frequency. Moreover, the distribution of the distance between nodes is positively correlated with the relevance of keywords.

According to Figure 4, the research hotspots of fractional order are divided into four keyword clusters, and the different clusters represent the distribution of fractional order research in different fields.

Cluster 1 (red region) represents the research of fractional order in the field of mathematics. Cluster 1 has 25 keywords, including fractional differential equation, fixed point theorem, positive solution, boundary value problem, stability, and existence, and it is the largest cluster in the distribution of research hotspots of fractional order. According to the distribution of nodes, the high-frequency

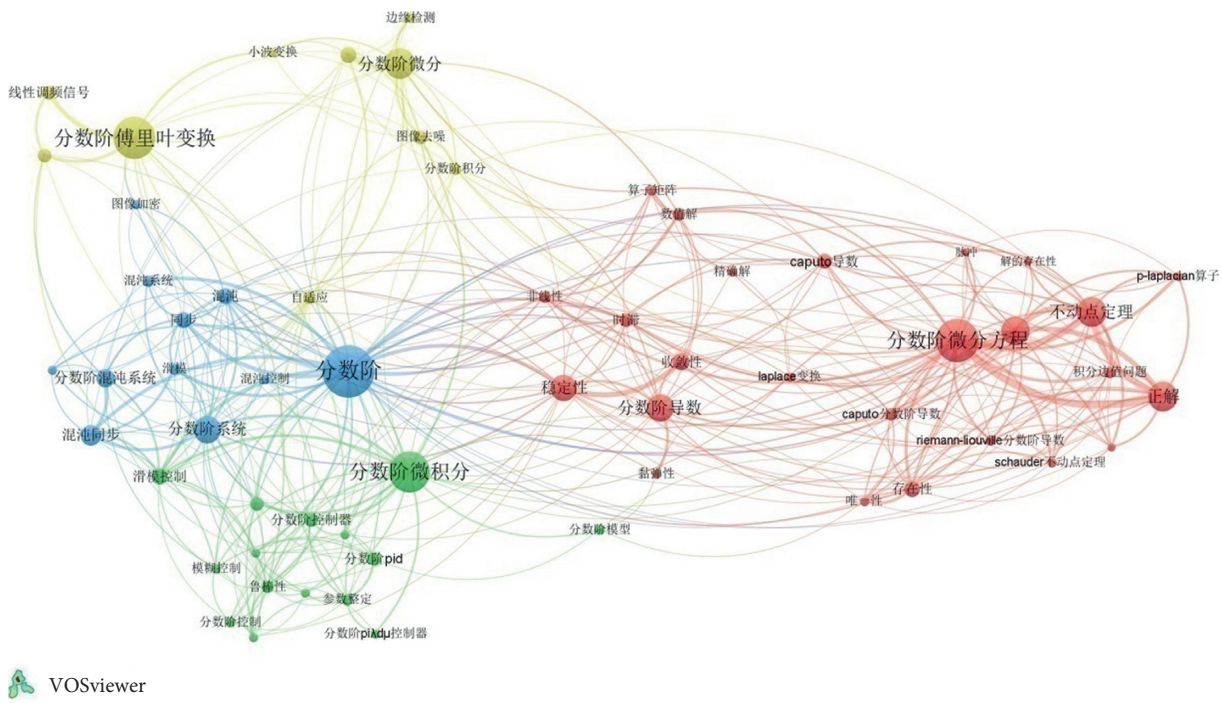

Figure 4: Keyword network visualization map. Note: the keywords translation in Figure 4 is shown in Table 3.

keywords are relatively close and the connecting lines are relatively thick, such as fractional differential equation, boundary value problem, fixed point theorem, and positive solution. Scholars took this kind of keyword as the mainline to carry out related research, such as using fixed point theorem to explore the positive solutions of boundary value problems of fractional differential equations with different properties [27–29]. There were also some scholars who proved, respectively, the existence of positive solutions for the boundary value problem of a class of nonlinear fractional different equations [30] and a class of fractional differential equations on the infinite interval [31] based on the fixed point theorem. Meanwhile, also some keywords have relatively high occurrence frequencies, such as fractional derivatives, stability, and convergence, which also represent the research hotspots of fractional orders in the field of mathematics. Especially for stability and convergence, their nodes are closer and lines are thicker, which means that the cooccurrence degree between them is high. Some scholars proposed a difference scheme for solving the fractional diffusion equation, such as a difference scheme for three-dimensional space fractional advection-diffusion equation [32] and a finite difference scheme for Riesz Space fractional diffusion equation [33]; the stability and convergence were proved by the matrix method. Furthermore, from the node distribution, it can be seen that the keywords in cluster 1 are scattered and compared with those in other clusters; this cluster involves the biggest number of keywords which indicates that the research of fractional order in the field of mathematics covers a wide range, and the research hotspots are relatively scattered.

Cluster 2 (green region) represents the research of fractional order in the field of control engineering. Cluster 2 has 15 keywords, including fractional calculus, sliding mode control, fractional order controller, fractional order PID, permanent magnet synchronous motor, sliding mode, and fractional order control. Compared with cluster 1, this cluster has a shorter distance between nodes, and the network connection is relatively close, which indicates that the research of fractional order in the field of control engineering is relatively concentrated. According to the distribution of keywords in cluster 2, the research hotspots of fractional order in the field of control engineering include the research of fractional order sliding mode control method and strategy and fractional order controller design, and so forth. Among them, regarding the research of fractional order sliding mode control method and strategy, some scholars put forward fractional order sliding mode control method and strategy based on the fractional order calculus theory and neural network, such as ANN-inversion system based fractional order sliding mode control scheme [34], fractional order sliding mode control scheme based on neural network and adaptive control algorithm [35], and fractional order sliding mode control algorithm based on radial basis function (RBF) neural network [36]. Regarding the research of fractional order controller design, it includes fractional order PID controller design [37–40], fractional order internal model controller design [41, 42], fractional order nonsingular terminal sliding mode controller [43], and fractional order PID improved autodisturbance rejection controller (FOPID-IADRC) [44]. In addition, the frequency of permanent magnet synchronous motor is relatively high, which is also one of the research hotspots in the field of fractional order control engineering. Zhou et al. studied the fractional order PI^{λ} controller parameters design method of permanent magnet synchronous generation wind

Table 3: Translation of keywords in Figures 4 and 5.

No.	The keywords	Translation
1	Caputo分数阶导数	Caputo fractional derivative
2	Caputo导数	Caputo derivative
3	Green函数	Green function
4	Laplace变换	Laplace transform
5	p-laplacian算子	p-Laplacian operator
6	Riemann-Liouville分数阶	Riemann-Liouville fractional order
7	Schauder不动点定理	Schauder fixed point theorem
8	不动点定理	Fixed point theorem
9	分数阶导数	Fractional derivative
10	分数阶微分方程	Fractional differential equation
11	唯一性	Uniqueness
12	存在性	Existence
13	收敛性	Convergence
14	数值解	Numerical solution
15	时滞	Time lag
16	正解	Positive solution
17	积分边值问题	Integral boundary value problem
18	稳定性	Stability
19	算子矩阵	Operator matrix
20	精确解	Exact solution
21	脉冲	Pulses per second
22	解的存在性	The existence of solutions
23	边值问题	Boundary value problem
24	非线性	Nonlinear
25	黏弹性	Viscoelasticity
26	内模控制	Internal model control
27	分数阶pid	Fractional order PID
28	分数阶pid控制器	Fractional order PID controller
29	分数阶$PI^{\lambda}D^{\mu}$控制器	Fractional order $PI^{\lambda}D^{\mu}$ controller
30	分数阶微积分	Fractional calculus
31	分数阶控制	Fractional order control
32	分数阶控制器	Fractional order controller
33	分数阶模型	Fractional order model
34	参数整定	Parameter tuning
35	模糊控制	Fuzzy control
36	永磁同步电机	Permanent magnet synchronous motor
37	滑模控制	Sliding mode control
38	神经网络	Neural networks
39	遗传算法	Genetic algorithm
40	鲁棒性	Robustness
41	分数阶	Fractional order
42	分数阶混沌系统	Fractional chaos system
43	分数阶系统	Fractional order system
44	参数辨识	Parameter identification
45	同步	Synchronization
46	图像加密	Image encryption
47	混沌	Chaos
48	混沌同步	Chaos synchronization
49	混沌控制	Chaos control
50	混沌系统	Chaotic system
51	滑模	Sliding mode
52	分数阶傅里叶变换	Fractional Fourier transform
53	分数阶微分	Fractional differential
54	分数阶积分	Fractional integral
55	参数估计	Parameter estimation
56	图像去噪	Image denoising
57	图像增强	Image enhancement
58	小波变换	Wavelet transform
59	线性调频信号	Linear frequency modulation signal
60	自适应	Self-adaptive
61	边缘检测	Edge detection

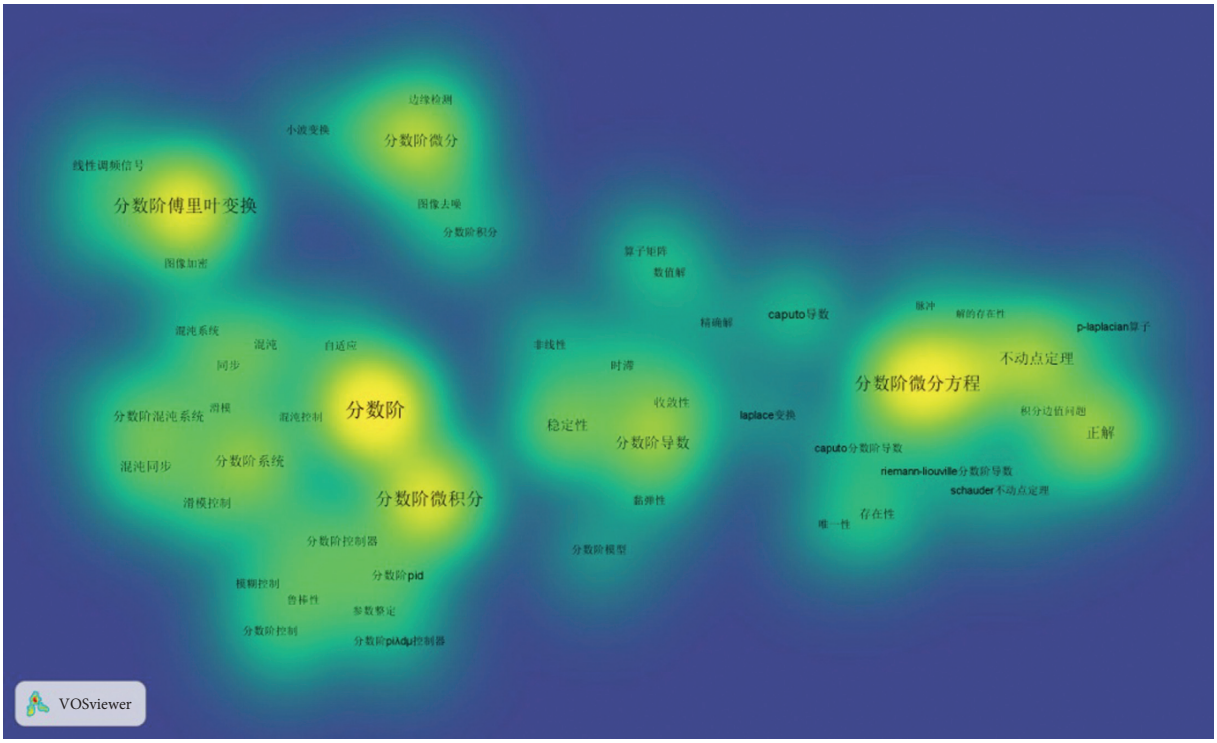

Figure 5: Visualization map of keyword density. Note: the keywords translation in Figure 5 is shown in Table 3.

Table 4: Occurrence distribution of the top 20 keywords.

No.	Keyword	Occurrence
1	Fractional order	342
2	Fractional differential equation	250
3	Fractional Fourier transform	243
4	Fractional calculus	228
5	Fractional differential	145
6	Fixed point theorem	138
7	Positive solution	135
8	Boundary value problem	123
9	Fractional derivative	119
10	Fractional order system	115
11	Stability	107
12	Chaos synchronization	72
13	Fractional chaos system	64
14	Convergence	56
15	Synchronization	52
16	Sliding mode control	52
17	Chaos	51
18	Image enhancement	51
19	Existence	47
20	Caputo derivative	45

turbine systems [45], Yu and Huang proposed the fuzzy RBF neural network based fractional order speed control system of permanent magnet synchronous motor [46], and so forth.

Cluster 3 (blue region) represents the research of fractional order in the field of physics. Cluster 3 has 11 keywords, including fractional order, fractional order system, chaos synchronization, fractional chaos system, synchronization, chaos, and sliding mode. Compared with other clusters, the nodes are relatively close in cluster 3, and the connecting lines between some nodes are relatively thick, such as the connecting lines between fractional order and synchronization, sliding mode, and chaos, as well as the connecting line between chaos synchronization and fractional order system and so forth, which indicates that the research of fractional order in the field of physics is more focused, and the connection of keywords is more closely related. Focusing on the distribution of keyword nodes in cluster 3, the research hotspots of fractional order in the field of physics are focused on the synchronization and control of fractional order chaotic systems and so forth. Regarding the research of synchronization and control of fractional order chaotic systems, some scholars combined Lyapunov stability theory to explore synchronization of fractional order chaotic systems [47–49], and some others studied the synchronization control of fractional order chaotic system [50, 51]. In addition, some scholars analyzed the synchronization and control of fractional order chaotic systems from the perspective of relative subdivision, such as adaptive synchronization or synchronization control of fractional order chaotic systems [52–54], sliding mode synchronization or synchronization control of fractional order chaotic system [55–57], and adaptive sliding mode synchronization or synchronization control of fractional order chaotic system [58–60].

Cluster 4 (yellow region) represents the research of fractional order in the field of computer and information communications. Cluster 4 has 10 keywords: fractional Fourier transform, fractional differential, fractional integral, image enhancement, image denoising, linear frequency modulation (LFM) signal, edge detection, parameter estimation, wavelet transform, and self-adaptive. Compared

with the first three clusters, the keywords around fractional differential and fractional Fourier transform in cluster 4 are relatively concentrated, but the distance between the keywords around them is far and the connecting lines are relatively less, such as LFM signal and image denoising, which indicates that the research hotspots of fractional order in the field of computer and information communication present the characteristics of partly concentration and general dispersion.

According to the distribution of nodes, there are some keyword node distribution forms clusters, such as the fractional differential, fractional integral, image denoising, image enhancement, edge detection, and self-adaptive, which reflects the application of fractional order in the computer field. Focusing on research field segmentation, we can find that image processing direction is the research hotspot of fractional order in the field of computers. To be specific, regarding the combination of fractional order and image enhancement, there are many research results related to image enhancement algorithm. Many scholars proposed fractional differential image enhancement algorithm, where there were relatively many findings related to adaptive fractional differential image enhancement algorithms, such as adaptive fractional differential MR image enhancement algorithm based on nonlocal means value [61], adaptive fractional order differential image enhancement algorithm based on 3 parameters related to an image texture, which were the local gradient of the image, the information entropy, and the variance [62], and image enhancement algorithm combining adaptive threshold fuzzy set enhancement and fractional differential [63]. Regarding the specific application of fractional differential in image enhancement, it includes medical image [64] and haze traffic image [65]. Regarding the combination of fractional order and image denoising, many scholars focused on the fractional integral theory to explore image denoising methods; for example, they studied image denoising based on fractional integral [66, 67] and proposed an improved fractional integration method for laser image denoising [68, 69]. Moreover, some scholars put forward image denoising method by combining fractional integral with wavelet transform [70], and some scholars introduced Gauss curvature into partial differential equation, and the image edge was detected by the image gradient, and they established adaptive image denoising model by combining Gauss curvature and fractional different operator [71]. Through further analysis, it can be found that the research on the application of fractional order in image enhancement focuses more on fractional differentiation, while the research on the application of fractional order in image denoising focuses more on fractional integral.

Combining with Figure 4, it can also be found that the distance between the fractional differential and the image enhancement node is closer, and the distance between the fractional integral and the image denoising node is closer, which indicates that the correlation between the nodes is strong, and the cooccurrence degree is high. Moreover, Huang et al. proposed that the applicable situations of the fractional differential equation, fractional integral equation, and fractional partial differential equation are image enhancement, image denoising, image enhancement, or denoising, respectively [72]. Therefore, it also provides further support and guidance for the above conclusions. According to the node distribution of cluster 4, some keywords form another cluster, such as fractional Fourier transform, LFM signal, and parameter estimation, which represents the application research of fractional order in the field of information and communication. Based on the perspective of research field segmentation, we can find that the direction of LFM signal detection and parameter estimation are the research hotspots of fractional order in the field of information and communication. To be specific, some scholars proposed joint parameter estimation method or signal detection and parameter estimation method of LFM signals based on Fourier transform, such as a novel method for joint parameter estimation of LFM signals in bistatic Multiple-Input Multiple-Output (MIMO) radar system [73], fast adaptive method of the multi-LFM signal detection, and parameter estimation based on fractional Fourier transform [74]. In addition, regarding the detection of the LFM signal or low parameter estimation accuracy of the LFM signal under low signal-to-noise ratio (SNR), some scholars proposed a concise fractional Fourier transform method for LFM signal detection under low SNR [75]. Some scholars aimed at the problem of low parameter estimation accuracy of LFM signal under low SNR, proposed a Rife interpolation short-time fractional Fourier transform-(STFRFT-) variable weight least square fitting (VWSF) algorithm [76]. Through further analysis, it can be found that the research findings of fractional order in the direction of LFM signal detection and parameter estimation focus more on the implementation based on the Fourier transform. Combining with the size of the nodes, it can also be found that the Fourier transform has the biggest nodes in this cluster, which means it has the highest frequency. Moreover, the connecting line between some keyword nodes and Fourier transform is relatively thick, such as LFM signal and parameter estimation, which can indicate that the correlation between these keywords is strong and the cooccurrence degree is high. Thus, it can be seen that fractional Fourier transform is an important method for the application of fractional order in information and communication.

Additionally, cluster 4 represents the research of fractional order in the computer and information communication field; the keywords belong to different disciplines, respectively, but they are distributed in the identical cluster because of the similar discipline direction and obvious cross characteristics. Furthermore, it can also be seen from the node distribution in Figure 4 that there are connecting lines among the keyword nodes of fractional order in the computer and information communication field, which further proves the rationality of their distribution in the identical cluster.

Figure 5 shows a visualization map of the keyword density of fractional order research, in which the keyword distribution shows a feature of a gradual change from the cold color region to the warm color region. Among them, the larger the keyword node and the more biased towards the

warm color series, the higher frequency of its occurrence. On the contrary, the smaller the keyword node and the more biased towards the cold color series, the lower frequency of its occurrence. It can be seen from Figure 5 that some keywords have large nodes and show the distribution characteristics of warm color series, such as fractional order, fractional differential equation, fractional calculus, fractional Fourier transform, fractional differential, fixed point theorem, and positive solution. Especially for the nodes of fractional order, fractional differential equation, fractional calculus, fractional Fourier transform, fractional differential, and so forth, their feature of warm color system is more obvious. Combined with the keyword node distribution in Figure 4, we can see that the keywords are centered on the important nodes such as fractional order, fractional differential equation, fractional calculus, fractional Fourier transform, and fractional differential and radiate to the surrounding keywords of their respective regions. Additionally, combined with the above cluster analysis, it can be seen that these keywords are key points or important methods and tools of fractional order research in the fields of mathematics, control engineering, physics, computer, information communication, and so forth. Therefore, keywords such as fractional order, fractional differential equation, fractional calculus, fractional Fourier transform, and fractional differential are the core points and important support of fractional order research.

In summary, this study analyzed the hotspots of fractional order research from the perspectives of keyword network and density analysis. In addition, it should be noted that some keywords are cross-related with other clusters in the four clusters. For instance, not only is the keyword stability distributed in the research of fractional order in the field of mathematics, but also it involves the fields of physics, control engineering, and so forth. Again, for instance, the keyword chaos not only belongs to the research of fractional order in the field of physics but also is distributed in the fields of mathematics and control engineering. Thus, this also reflects the interdisciplinary characteristics of fractional order research.

4.2. Research Frontiers. Keyword burst not only detects the focus of research on bursts but also realizes the research frontier [77]. Burst detection in CiteSpace is mainly based on the Kleinberg algorithm [78]; burst keyword analysis method shows keywords had rapidly changed in a short period of time or dramatically increased in number and emphasizes the abrupt change of keywords [79]. Therefore, CiteSpace was used to analyze the burst keywords of fractional order research, so as to explore the research frontier of fractional order. The relevant parameters of the software were set as follows: set the time slicing option to be from 2001 to 2020, set the years per slice option to 2, set the node types option to keyword, and use pathfinder to trim the keyword network and other options as default settings. By running the software, the cooccurrence distribution of the fractional research keywords was obtained. After a software trial run, it was found that there were repetitions in the expression of keywords about the fractional Fourier transform and LFM signals, so these keywords were merged. On this basis, the minimum duration in the burstness option was set to 3, and finally keywords with the strongest citation bursts of fractional order research were generated, as shown in Figure 6. It should be noted that the above keywords of fractional order and fractional calculus were not merged. In order to keep consistency with the above research, this paper also did not merge the two in this part. At the same time, combining with the analysis results in Figure 5, it can also be found that the burst keywords of fractional order and fractional calculus do not appear in Figure 5 at the same time; thus the fact that these two keywords were not merged has almost no effect on the overall results.

Figure 6 shows the top 26 keywords with the strongest citation bursts. To be specific, "Begin" represents the time when a certain keyword begins to burst, and "End" represents the burst end time for a certain keyword. In addition, the red and blue columns together constitute the time distribution (2001–2020) in the study period, and the red column represents the duration of a burst keyword. It can be seen from Figure 6 that the first burst keyword to appear in the research period is the LFM signal, and this keyword has the longest burst duration (2001–2012). According to the burst strength, the burst strength of fractional Fourier transform is the highest, and its burst value is 33.9667, which further reveals the importance of fractional Fourier transform in the field of fractional order research. Meanwhile, the burst value of the LFM signal is also relatively high, and its burst value is 15.3201. In addition, combined with the burst strength, it can also be found that the burst strength distribution of other burst keywords is relatively uniform, except for the significant burst strength of fractional Fourier transform and LFM signal, which is consistent with the multidisciplinary distribution characteristics of fractional order research.

Based on the time distribution of burst keywords and the subdivision of fractional order research, the distribution of fractional order burst keywords can be basically divided into the three following phases: The first phase is from 2001 to 2012; the burst keywords in this phase mainly include LFM signal, parameter estimation, information processing technology, fractional calculus, fractional Fourier transform, and edge detection. Through further analysis of burst keywords, it can be found that the research frontier of this phase focuses on the research of fractional order in the field of information communication and computer. Combined with the above clustering analysis, the keywords such as fractional Fourier transform, LFM signal, and parameter estimation form clusters, which indicates the research of fractional order in the field of information and communication, and the burst keywords such as edge detection and wavelet transform also represent the research of fractional order in the field of computer. Meanwhile, projective synchronization of burst keywords also appears in this phase, which mainly involves the application of fractional order in the field of physics, such as the study of projective synchronization in fractional order chaotic system [80, 81]. In addition, compared with the other two phases, the duration of

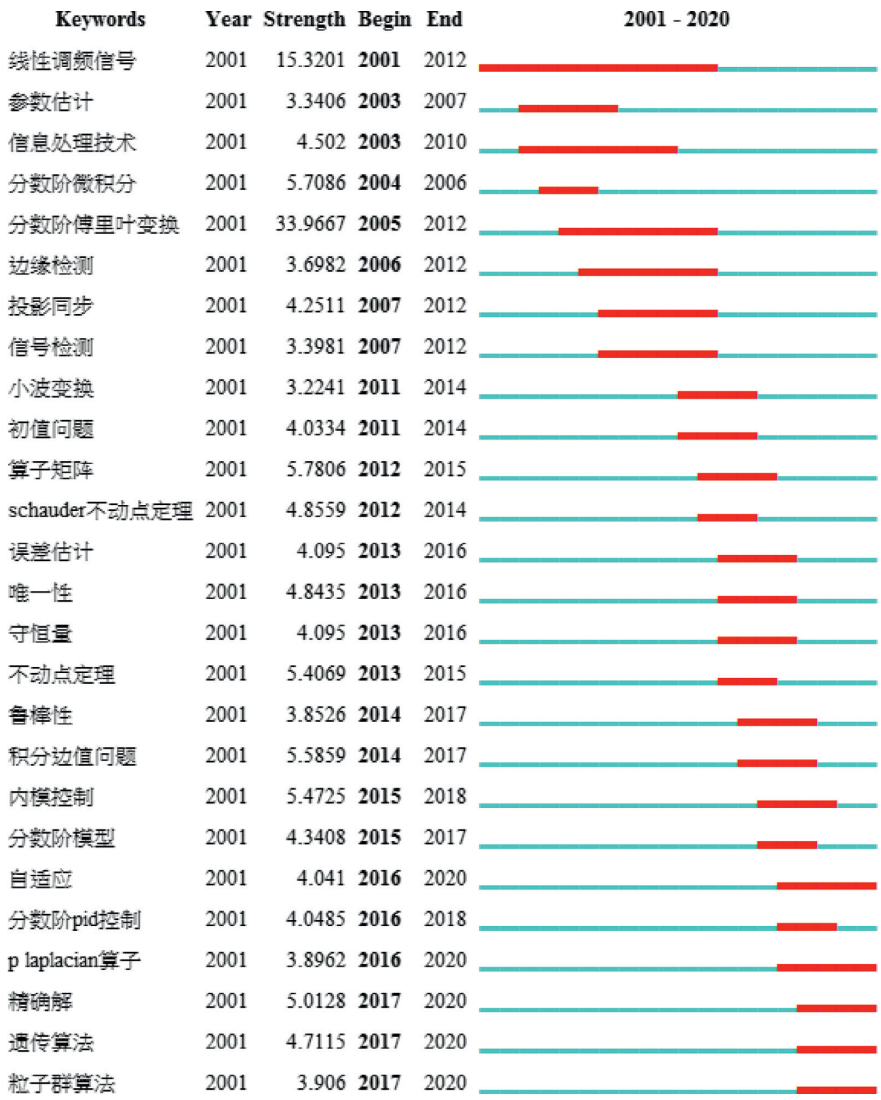

Figure 6: Top 26 keywords with the strongest citation bursts. Note: the keywords translation in Figure 6 is shown in Table 5.

burst keywords in this phase is longer, such as LFM signal, information processing technology, and fractional Fourier transform, which shows the importance of fractional order in information communication and computer fields. The second phase is from 2012 to 2017; this phase mainly covers burst keywords such as operator matrix, Schauder fixed point theorem, error estimation, uniqueness, fixed point theorem, and integral boundary value problem, which indicates that the research of fractional order in the field of mathematics has become the main frontier direction in this phase. Furthermore, compared with other phases, the number of burst keywords focusing on the identical frontier direction is the biggest in this phase, which further confirms the breadth of fractional order research in the field of mathematics. The third phase is from 2017 to 2020; new burst keywords appeared in 2017, such as exact solution, genetic algorithm, and particle swarm optimization. Among them, the exact solution mainly involves the research of fractional order in the field of mathematics, while genetic algorithm, particle swarm optimization, and so forth mainly involve the research of fractional order in the fields of automotive engineering, control engineering, and so forth. For example, some scholars used genetic algorithm to optimize the parameters of fractional order controller [82, 83] and particle swarm optimization to explore the optimal design of passive fractional order vehicle suspension parameters [84]. Also some scholars proposed a dynamic constriction factor based particle swarm optimization with fractional order velocity (DFFV-PSO) [85]. In addition, at the intersection of the second and third phases, there also appear some burst keywords, such as internal model control, fractional order PID control, and p-Laplacian operator. These burst keywords are mainly distributed around the fractional order in frontier fields such as control engineering and mathematics.

In conclusion, the priorities of the research frontier of fractional order are different in a different phase, which also reveals the law of the dynamic change of the research frontier of fractional order with time evolution. In particular, the burst time of burst keywords such as exact solution, genetic algorithm, and particle swarm

Table 5: Translation of keywords in Figure 6.

No.	The keywords	Translation
1	线性调频信号	Linear frequency modulation signal
2	参数估计	Parameter estimation
3	信息处理技术	Information processing technology
4	分数阶微积分	Fractional calculus
5	分数阶傅里叶变换	Fractional Fourier transform
6	边缘检测	Edge detection
7	投影同步	Projective synchronization
8	信号检测	Signal detection
9	小波变换	Wavelet transform
10	初值问题	Initial value problem
11	算子矩阵	Operator matrix
12	schauder不动点定理	Schauder fixed point theorem
13	误差估计	Error estimation
14	唯一性	Uniqueness
15	守恒量	Conserved quantity
16	不动点定理	Fixed point theorem
17	鲁棒性	Robustness
18	积分边值问题	Integral boundary value problem
19	内模控制	Internal model control
20	分数阶模型	Fractional order model
21	自适应	Self-adaptive
22	分数阶pid控制	Fractional order PID control
23	p-Laplacian算子	p-Laplacian operator
24	精确解	Exact solution
25	遗传算法	Genetic algorithm
26	粒子群算法	Particle swarm optimization

optimization lasted until the end of the research period (2020), so these burst keywords are to a large extent the frontier direction and method of fractional order research now and in the future.

5. Conclusion

This paper combined bibliometrics and visualization research methods to conduct a quantitative and visual analysis of the 2,854 Chinese fractional order research literatures collected by CNKI from 2001 to 2020, which explored the current status of China's fractional order research and also revealed the hotspots and frontier areas. The main research conclusions of this paper are as follows:

(1) Research current status aspect: China's fractional order research publications show an overall upward trend, but there are also obvious differences in the distribution of the number of publications in different time series; China's fractional order research publications are relatively evenly distributed among various research institutions, and the attributes of research institutions include comprehensive universities, universities of science and technology, and military academy. The overall intensity of cooperation among Chinese fractional order research authors is not high, but there are also many research groups with a high volume of publications and close cooperation relationships; China's fractional order research disciplines are distributed in a wide range, and the number of publications in the field of mathematics is the biggest, which had the characteristic of the multidisciplinary distribution.

(2) Research hotspot aspect: The research hotspots of fractional order in China are divided into 4 keyword clusters, which include the research of fractional order in the fields of mathematics, control engineering, physics, and computer and information communication. Meanwhile, keywords such as fractional order, fractional order differential equations, fractional calculus, fractional Fourier transform, and fractional differential are the core points and important supports of fractional order research in China.

(3) Research frontier aspect: The focus of China's fractional order research frontier is different at different stages, and it changes dynamically with the evolution of time. Meanwhile, burst keywords such as exact solution, genetic algorithm, and particle swarm optimization are likely to be the frontier directions and methods of China's fractional order research at present and in the future.

Data Availability

The data collected to support the findings of this study come from CNKI and are available from the corresponding author upon reasonable request.

Conflicts of Interest

The authors declare that they have no conflicts of interest.

Acknowledgments

This study was supported by the National Key R&D Program of China (2018AAA0100804) and the National Natural Science Foundation of China (62032022, 61972375, and 61929104).

References

[1] L. Wu, S. Liu, and Y. Yang, "Using the fractional order method to generalize strengthening buffer operator and weakening buffer operator," *IEEE/CAA Journal of Automatica Sinica*, vol. 5, no. 6, pp. 1074–1078, 2018.

[2] M. A. Balootaki, H. Rahmani, H. Moeinkhah, and A. Mohammadzadeh, "On the synchronization and stabilization of fractional-order chaotic systems: recent advances and future perspectives," *Physica a-Statistical Mechanics and ITS Applications*, vol. 551, Article ID 124203, 2020.

[3] H. Sun, Y. Zhang, D. Baleanu, W. Chen, and Y. Chen, "A new collection of real world applications of fractional calculus in science and engineering," *Communications in Nonlinear Science and Numerical Simulation*, vol. 64, pp. 213–231, 2018.

[4] A. M. Lopes and J. A. T. Machado, "A review of fractional order entropies," *Entropy*, vol. 22, no. 12, Article ID 1374, 2020.

[5] Z. Li, L. Liu, S. Dehghan, Y. Chen, and D. Xue, "A review and evaluation of numerical tools for fractional calculus and fractional order controls," *International Journal of Control*, vol. 90, no. 6, pp. 1165–1181, 2017.

[6] M. S. Tavazoei, "Fractional order chaotic systems: history, achievements, applications, and future challenges," *European Physical Journal-Special Topics*, vol. 229, no. 6-7, pp. 887–904, 2020.

[7] X. Sun, J. Ji, B. Ren, G. Chen, and Q. Zhang, "A novel online identification algorithm of lithium-ion battery parameters and model order based on a fractional order model," *IET Renewable Power Generation*, vol. 15, 2021.

[8] M. Al-Daloo, A. Soltan, and A. Yakovlev, "Advance interconnect circuit modeling design using fractional-order elements," *IEEE Transactions on Computer-Aided Design of Integrated Circuits and Systems*, vol. 39, no. 10, pp. 2722–2734, 2020.

[9] S. R. Sahoo and M. C. Ray, "Active control of nonlinear transient vibration of laminated composite beams using triangular SCLD treatment with fractional order derivative viscoelastic model," *Journal of Dynamic Systems Measurement and Control-Transactions of the Asme*, vol. 141, no. 11, Article ID 111014, 2019.

[10] E. Yumuk, M. Güzelkaya, and İ. Eksin, "Design of an integer order proportional-integral/proportional-integral-derivative controller based on model parameters of a certain class of fractional order systems," *Proceedings of the Institution of Mechanical Engineers, Part I: Journal of Systems and Control Engineering*, vol. 233, no. 3, pp. 320–334, 2019.

[11] H. Z. Lv, F. Wang, and R. Wang, "Robust active contour model using patch-based signed pressure force and optimized fractional-order edge," *IEEE Access*, vol. 9, pp. 8771–8785, 2021.

[12] W. Waseem, M. Sulaiman, A. Alhindi, and H. Alhakami, "A soft computing approach based on fractional order DPSO algorithm designed to solve the corneal model for eye surgery," *IEEE Access*, vol. 8, pp. 61576–61592, 2020.

[13] P. Warrier and P. Shah, "Fractional order control of power electronic converters in industrial drives and renewable energy systems: a review," *IEEE Access*, vol. 9, pp. 58982–59009, 2021.

[14] A. A. Dastjerdi, B. M. Vinagre, Y. Chen, and S. H. HosseinNia, "Linear fractional order controllers; A survey in the frequency domain," *Annual Reviews in Control*, vol. 47, pp. 51–70, 2019.

[15] C. Zhu and Y. Zou, "Summary of research on fractional-order control," *Control and Decision*, vol. 24, no. 2, pp. 161–169, 2009.

[16] Q. Yang, D. Chen, T. Zhao, and Y. Chen, "Fractional calculus in image processing: a review," *Fractional Calculus and Applied Analysis*, vol. 19, no. 5, pp. 1222–1249, 2016.

[17] Z. Gu, D. Yin, S. Nie et al., "Advances of image edge enhancement based on vortex filtering," *Infrared and Laser Engineering*, vol. 48, no. 6, pp. 244–257, 2019.

[18] H. Wang, Z. Chen, and R. Gong, "Mapping knowledge domains of industrial structure research in China: 1992-2015," *Journal of Discrete Mathematical Sciences & Cryptography*, vol. 20, no. 6-7, pp. 1393–1397, 2017.

[19] N. J. Van Eck and L. Waltman, "Citation-based clustering of publications using CitNetExplorer and VOSviewer," *Scientometrics*, vol. 111, no. 2, pp. 1053–1070, 2017.

[20] N. J. Van Eck and L. Waltman, "Software survey: VOSviewer, a computer program for bibliometric mapping," *Scientometrics*, vol. 84, no. 2, pp. 523–538, 2010.

[21] X. Lu, W. Peng, X. Huang, Q. Fu, and Q. Zhang, "Homestead management in China from the "separation of two rights" to the "separation of three rights": visualization and analysis of hot topics and trends by mapping knowledge domains of academic papers in China National Knowledge Infrastructure (CNKI)," *Land Use Policy*, vol. 97, Article ID 104670, 2020.

[22] B. Wang and Z. Wang, "Analysis of mapping knowledge domains of tennis teaching research in China," *Educational Sciences-Theory & Practice*, vol. 18, no. 6, pp. 2979–2988, 2018.

[23] H. Zeng, B. Shao, G. Bian, D. Song, and X. Li, "A survey of research progress and hot front of natural gas load forecasting from technical perspective," *IEEE Access*, vol. 8, pp. 222824–222840, 2020.

[24] L. Qi, R. Tao, S. Zhou, and Y. Wang, "The detection and parameter estimation for Multi-component LFM signals based on the fractional Fourier transforms," *Science in China (Series E)*, vol. 33, no. 8, pp. 749–759, 2003.

[25] W. Wang and C. Lu, "Visualization analysis of big data research based on Citespace," *Soft Computing*, vol. 24, no. 11, pp. 8173–8186, 2020.

[26] X. Zhou, T. Li, and X. Ma, "A bibliometric analysis of comparative research on the evolution of international and Chinese green supply chain research hotspots and frontiers," *Environmental Science and Pollution Research*, vol. 28, no. 6, pp. 6302–6323, 2021.

[27] F. Hu and W. Hu, "Multiple positive solutions for boundary value problems of fractional differential equations with p-Laplacian operator," *Journal of Northeast Normal University (Natural Science Edition)*, vol. 52, no. 3, pp. 62–67, 2020.

[28] Z. Peng, Y. Li, and Y. Xue, "Two positive solutions of boundary value problem for a class of coupled system of nonlinear fractional differential equations," *Journal of Jilin University (Science Edition)*, vol. 58, no. 4, pp. 775–781, 2020.

[29] X. Liang and Z. Zhou, "Positive solutions for a class of fractional differential equations with stieltjes integral boundary conditions," *Mathematica Applicata*, vol. 33, no. 4, pp. 826–835, 2020.

[30] J. Song, "Existence of positive solutions for boundary value problem of nonlinear fractional differential equation," *Acta Scientiarum Naturalium Universitatis Nankaiensis*, vol. 51, no. 5, pp. 79–84, 2018.

[31] X. Liao, Y. Wei, and C. Feng, "Existence of positive solutions for a class of boundary value problems of fractional differential equations on infinite interval," *Journal of Jilin University (Science Edition)*, vol. 56, no. 6, pp. 1299–1306, 2018.

[32] Y. Nie, J. Hu, and J. Wang, "Douglas-Gunn finite difference scheme for three-dimensional space fractional advection diffusion equation," *Journal of Zhengzhou University (Natural Science Edition)*, vol. 51, no. 1, pp. 44–50, 2019.

[33] J. Yang, Z. Li, and Y. Yan, "A new numerical method for solving riesz space-fractional diffusion equation," *Mathematica Numerica Sinica*, vol. 41, no. 2, pp. 170–190, 2019.

[34] Q. Xu, J. Huang, and L. Zhou, "ANN-inversion based fractional-order sliding control for the robot," *Modular Machine Tool & Automatic Manufacturing Technique*, vol. 12, pp. 49–52, 2015.

[35] B. Zhang, F. Gao, and K. Yao, "Neural network and adaptive algorithm-based fractional order sliding mode controller," *Control Theory & Applications*, vol. 33, no. 10, pp. 1373–1377, 2016.

[36] X. Wang and Y. Zhang, "Fractional-order sliding mode control based on RBF neural network for AUV path tracking," *Journal of Unmanned Undersea Systems*, vol. 28, no. 3, pp. 284–290, 2020.

[37] Y. Chen and T. Zhang, "Quadrotor aircraft control based on fractional order PID," *Journal of Tianjin Polytechnic University*, vol. 38, no. 4, pp. 58–63, 2019.

[38] Y. Yang, W. Zhang, J. Zhang, C. Li, and K. Li, "Controller design for electromechanical actuator servo system based on fractional-order," *Aero Weaponry*, no. 6, pp. 50–54, 2018.

[39] L. Guo, G. Dai, G. Li, and S. Pang, "Design and implementation of fractional order $PI^{\lambda}D^{\mu}$ controller based on FPGA," *Measurement & Control Technology*, vol. 37, no. 1, pp. 64–68, 2018.

[40] J. Yin, R. Wang, Q. Gao, and W. Zhang, "Fractional order PID of AC servo system based on neural network active disturbance rejection control," *Electronics Optics & Control*, vol. 26, no. 5, pp. 20–25, 2019.

[41] Y. Yu and P. Xu, "A design of fractional order controller based on internal model control," *Packaging Engineering*, vol. 39, no. 5, pp. 48–51, 2018.

[42] P. Liu, M. Wang, and M. Yao, "Design of optimized fractional order internal model controller for complex system," *Computer Engineering and Applications*, vol. 54, no. 21, pp. 224–229, 2018.

[43] Q. He, J. Niu, and W. Chen, "Application of fractional order terminal sliding mode controller in DTC system," *Fire Control & Command Control*, vol. 42, no. 9, pp. 74–78, 2017.

[44] R. Wang, B. Lu, R. Hou et al., "FOPID improved ADRC in AC servo systems," *China Mechanical Engineering*, vol. 30, no. 16, pp. 1989–1995, 2019.

[45] X. Zhou, X. Wang, T. Hoang, and G. Thu, "Direct-drive permanent magnet synchronous generator wind turbine system based on fractional-order controller," *Electric Machines & Control Application*, vol. 44, no. 7, pp. 92–97, 2017.

[46] X. Yu and H. Huang, "Optimization design of fractional-order sliding mode controller based on fuzzy RBF neural network," *Modern Electronics Technique*, vol. 41, no. 11, pp. 87–90, 2018.

[47] Z. Zhang, Y. Zhang, and Y. Wang, "Synchronization of fractional-order chaotic system with fractional-order controller," *Journal of Lanzhou University of Technology*, vol. 42, no. 4, pp. 152–158, 2016.

[48] Y. Chen, S. Li, and H. Liu, "Synchronization of fractional-order chaotic systems based on adaptive fuzzy control," *Acta Physica Sinica*, vol. 65, no. 17, pp. 258–268, 2016.

[49] X. Yan, T. Shang, and X. Zhao, "Synchronization of uncertain fractional-order chaotic systems based on the fractional-order sliding mode controller," *Acta Mathematicae Applicatae Sinica*, vol. 41, no. 6, pp. 765–776, 2018.

[50] M. Wu, M. Yu, and Y. Zhang, "Synchronization for fractional-order chaotic systems with limited gain and uncertain parameters," *Journal of University of Jinan (Science and Technology)*, vol. 31, no. 1, pp. 77–81, 2017.

[51] Y. Bai, Y. Yang, Q. Wei, J. Duan, and M. Fan, "Synchronization research and circuit implementation of fractional chaotic system," *Journal of Northwest Normal University (Natural Science)*, vol. 55, no. 6, pp. 47–52+73, 2019.

[52] D. Li, X. Zhang, Y. Hu, and Y. Yang, "Adaptive synchronization between two fractional-order chaotic systems with uncertain parameters," *Journal of Southwest University (Natural Science Edition)*, vol. 37, no. 11, pp. 69–76, 2015.

[53] F. Lin and Z. Zeng, "Synchronization of uncertain fractional-order chaotic systems with time delay based on adaptive neural network control," *Acta Physica Sinica*, vol. 66, no. 9, pp. 40–49, 2017.

[54] K. Shao, Z. Xu, X. Huang, T. Wang, and Y. Zhang, "RBF neural network adaptive synchronization control for fractional-order hyper-chaotic systems," *Journal of Yangzhou University (Natural Science Edition)*, vol. 23, no. 5, pp. 58–62, 2020.

[55] X. Wang, L. Shi, and B. Mao, "Sliding mode synchronization of fractional-order 4D memristive hyper chaotic systems," *Mathematics in Practice and Theory*, vol. 50, no. 15, pp. 189–194, 2020.

[56] M. Sun, Y. Hu, and J. Wei, "A novel sliding mode synchronization method of uncertain fractional-order chaotic systems," *Journal of University of electronic Science and Technology of China*, vol. 46, no. 3, pp. 555–561, 2017.

[57] X. Meng and B. Mao, "Sliding mode synchronization of fractional-order T chaotic systems with logarithmic," *Journal of Shandong University (Engineering Science)*, vol. 50, no. 5, pp. 7–12, 2020.

[58] J. Liu and B. Mao, "Self-adaptive sliding mode synchronization of fractional-order dual-exponential chaotic systems," *Mathematics in Practice and Theory*, vol. 50, no. 7, pp. 198–203, 2020.

[59] C. Cheng, J. Zhu, and D. Wang, "Adaptive synchronization of fractional-order four-wings chaotic systems with uncertainties based on sliding mode control," *Journal of Central China Normal University (Natural Sciences)*, vol. 52, no. 2, pp. 155–159, 2018.

[60] B. Mao and C. Cheng, "Self-adaptive sliding mode control of fractional-order Victor-Carmen chaotic systems," *Journal of Shandong University (Engineering Science)*, vol. 47, no. 4, pp. 31–36, 2017.

[61] N. Yang, Y. Feng, and Y. Wei, "Improved fractional differential algorithm for infant brain MR image enhancement," *Journal of Image and Graphics*, vol. 21, no. 12, pp. 1696–1706, 2016.

[62] X. Chen and L. Tan, "Medical image enhancement algorithm based on adaptive fractional order differentiation," *Application Research of Computers*, vol. 34, no. 12, pp. 3895–3898+3903, 2017.

[63] F. Sun, C. Kong, K. Zhang, Y. Jiang, and C. Cong, "DR Image enhancement of femoral head based on adaptive fuzzy set and fractional differential," *Computer Applications and Software*, vol. 37, no. 12, pp. 191–196, 2020.

[64] H. Liu, M. Zheng, X. Hou, B. Li, and J. Du, "Enhancement algorithm of fractional differential medical images based on local binary pattern variance," *Laser & Optoelectronics Progress*, vol. 56, no. 9, pp. 116–124, 2019.

[65] W. Wang and H. Zhao, "Haze traffic image enhancement based on improved retinex and adaptive fractional differential," *Optics and Precision Engineering*, vol. 28, no. 8, pp. 1820–1834, 2020.

[66] G. Huang, Y. Pu, Q. Chen, and J. Zhou, "Research on image denoising based on fractional order integral," *Systems Engineering and Electronics*, vol. 33, no. 4, pp. 925–932, 2011.

[67] X. Qin, M. Chen, W. Jia, J. He, and G. Zheng, "Research on OTC image denoising based on fractional integral algorithm," *Optical Technique*, vol. 45, no. 1, pp. 102–106, 2019.

[68] J. Cong and B. Zeng, "Laser image denoising based on improved fractional integral," *Laser Journal*, vol. 37, no. 2, pp. 69–72, 2016.

[69] T. Liu, "Research on laser image denoising based on improved fractional integral," *Journal of Inner Mongolia Normal University (Natural Science Edition)*, vol. 46, no. 2, pp. 216–218+222, 2017.

[70] C. Zhang, M. Chen, F. Wang, N. Gao, and G. Zheng, "Optical coherence tomography image denoising algorithm based on

wavelet transform and fractional integral," *Laser & Optoelectronics Progress*, vol. 56, no. 18, pp. 161–169, 2019.

[71] X. Zhou, M. Zhang, and T. Wu, "Adaptive image denoising based on fractional differential operator and Gauss curvature," *Modern Electronics Technique*, vol. 42, no. 15, pp. 54–58, 2019.

[72] G. Huang, L. Xu, and Y. Pu, "Summary of research on image processing using fractional calculus," *Application Research of Computers*, vol. 29, no. 2, pp. 414–420+426, 2012.

[73] L. Li and T. Qiu, "A novel method for joint parameter estimation of LFM signals in bistatic MIMO radar system based on FRFT," *Journal of Electronics & Information Technology*, vol. 34, no. 4, pp. 878–884, 2012.

[74] W. Shi and X. Xu, "Fast adaptive method of the multi-LFM signal detection and parameter estimation based on fractional fourier transform," *Science Technology and Engineering*, vol. 12, no. 7, pp. 1517–1521, 2012.

[75] Y. Chen, L. Guo, and Z. Gong, "The concise fractional fourier transform and its application in detection and parameter estimation of the linear frequency-modulated signal," *Acta Acustica*, vol. 40, no. 6, pp. 761–771, 2015.

[76] W. Cao, Z. Yao, W. Xia, and S. Yan, "Parameter estimation of linear frequency modulation signal based on interpolated short-time fractional fourier transform and variable weight least square fitting," *Acta Armamentarii*, vol. 41, no. 1, pp. 86–94, 2020.

[77] J. Wu, D. Jia, Z. Wei, and D. Xin, "Development trends and frontiers of ocean big data research based on CiteSpace," *Water*, vol. 12, no. 6, Article ID 1560, 2020.

[78] L. Meng, K. H. Wen, R. Brewin, and Q. Wu, "Knowledge atlas on the relationship between urban street space and residents' health—a bibliometric analysis based on VOSviewer and CiteSpace," *Sustainability*, vol. 12, no. 6, Article ID 2384, 2020.

[79] J. Wei, G. Liang, J. Alex, T. Zhang, and C. Ma, "Research progress of energy utilization of agricultural waste in China: bibliometric analysis by Citespace," *Sustainability*, vol. 12, no. 3, Article ID 812, 2020.

[80] X. Chen Xiang-Rong, C. Li Yong-Xun, and Y. Li, "Nonlinear observer based full-state projective synchronization for a class of fractional-order chaotic system," *Acta Physica Sinica*, vol. 57, no. 3, pp. 1453–1457, 2008.

[81] X. He Yi-Jie and Y. He, "Projective synchronization of the fractional order unified system," *Acta Physica Sinica*, vol. 57, no. 3, pp. 1485–1492, 2008.

[82] G. Gao, Q. Xu, and Z. Fang, "Fractional-order $PI^{\lambda}D^{\mu}$ control of hybrid mechanism for automobile electro-coating conveying," *Machinery Design & Manufacture*, vol. 2, pp. 70–74, 2019.

[83] Y. Chen, M. Yang, H. Xu, and J. Liu, "Vehicle ABS fractional PID control with parameter tuning using genetic algorithm," *Manufacturing Automation*, vol. 40, no. 1, pp. 24–27+39, 2018.

[84] H. You, Y. Shen, and S. Yang, "Parameters design for passive fractional-order vehicle suspension based on particle swarm optimization," *Journal of Vibration and Shock*, vol. 36, no. 16, pp. 224–228+254, 2017.

[85] Z. Zhai and S. Su, "A fractional-order particle swarm optimization with dynamic constriction factor," *Journal of Chongqing University of Technology (Natural Science)*, vol. 33, no. 7, pp. 94–101, 2019.

Hindawi
Journal of Mathematics
Volume 2021, Article ID 8877865, 9 pages
https://doi.org/10.1155/2021/8877865

Research Article

Container Throughput Forecasting of Tianjin-Hebei Port Group Based on Grey Combination Model

Chen He and Huipo Wang

School of Management Engineering and Business, Hebei University of Engineering, Handan 056038, China

Correspondence should be addressed to Huipo Wang; wanghuipo@hebeu.edu.cn

Received 15 June 2021; Accepted 30 July 2021; Published 11 August 2021

Academic Editor: Antonio Di Crescenzo

Container throughput forecasting plays an important role in port capacity planning and management. Regarding the issue of container throughput of Tianjin-Hebei Port Group, considering the container throughput is an incomplete grey information system affected by various factors, the effect is often unsatisfactory by adopting a single forecasting model. Therefore, this paper studies the issue by combining fractional GM (1, 1) and BP neural network. The comparison results show that the combination model performs better than other single models separately and has a higher level of forecasting accuracy. Furthermore, the combination model is adopted to forecast the container throughput of Tianjin-Hebei Port Group from 2021 to 2025, which would be a data reference for the future development optimization for the container operation of Tianjin-Hebei Port Group.

1. Introduction

Transportation by sea is the most important pattern of transportation in the international trade. 80%~90% of the total import and export goods in China are conducted by sea [1] in which container transport has most proportion. This is due to the development of container transportation, which not only makes the operation develop in the direction of aggregation and rationalization but also saves the packaging materials and miscellaneous costs, guarantees the cargo integrity, shortens the transport time, and thus reduces the transport cost. Tianjin-Hebei Port Group is located on the west bank of China's Bohai Economic Rim as in Figure 1, which is one of the shipping hubs in northern China, mainly including Tianjin Port, Tangshan Port, Qinhuangdao Port, and Huanghua Port. In the first quarter of 2021, Tianjin Port completed a container throughput of 4.469 million TEU, increasing 20.4% year on year, setting the record highest in the same period [2]. And Tangshan Port, Qinhuangdao Port, and Huanghua Port completed a total container throughput of 882,000 TEU, increasing by 31.9% in the first quarter of 2021 [3]. Under the background of international and domestic double circulation, the Tianjin-Hebei Port Group has become a primary support for the Beijing-Tianjin-Hebei region to participate in the international labor, cooperation, and competition and a key driving source for the economic development of the Beijing-Tianjin-Hebei region.

The structural arrangement of this paper is as follows: the second part reviews the relevant literature, the third part introduces the research methods, the fourth part gives the forecasting results and discusses the results, and the fifth part gives the research conclusions of this paper.

2. Literature Review

2.1. Importance of the Port Throughput Forecasting. Port throughput is a main scale index of port development and plays a crucial basic role in port planning and management. While the short-term forecasting of port throughput is for port enterprises in resource prescheduling and port intelligent scheduling, the long-term forecasting has an impact on the port strategic planning and national development strategy. The reasons that port throughput forecasting plays a particularly important role in port management are as follows. (1) Port infrastructure construction has a long technical life of indivisibles and irreversible nature of port

Figure 1: The geographical location of Tianjin-Hebei Port Group.

infrastructure investments [4]. Once the infrastructure is in place, the characteristics of the port are determined for a long period [5]. Furthermore, port planning processes may take 5–15 years from the initiation of the masterplan to its final approval [6] for which port capacity is critical to be determined with consideration of port throughput forecasting. (2) Port projects require capital and fixed investments having long payback periods. This necessitates the financial viability of investments based on projections of port throughput and commodity flows [7]. If the port throughput forecast is relatively accurate, it can provide valuable reference for the port investment and construction. Otherwise, it is likely to cause wrong port investment decisions and incalculable economic losses. (3) Under the "Belt and Road Initiative," the national sea strategy of China has been paid more and more attention, and the optimization of port construction has become the top priority. In order to make ports construction accurately serve the market demand in the future, it is of great practical significance to accurately forecast ports throughput for improving the port freight efficiency and raising economic benefits.

2.2. Influencing Factors and Various Methodologies on the Issue. Currently, many scholars have put up with extensive research studies on the issue of container throughput forecasting using different methods. There are 4 main factors dominating port container throughput: (1) the impact of the world economy; (2) the impact of port external environment; (3) the impact of port supply and demand; and (4) the impact of the port's own conditions. Moreover, the issue is also facing miscellaneous and volatile uncertainties. For example, the outbreak of the US-China trade war has been affecting the development process and pattern of global trade, leading to changes in the cost, circulation, and price of commodities and thus has an unpredictable impact on the shipping industry with demand of cargo transportation [8]; the outbreak of COVID-19 has been causing uncertainties to cargo flows, increasing the challenges of indecision-making in port development projects [9]. Chen et al. [10] noted that due to the various factors affecting the throughput, it is difficult to use a single linear or nonlinear model when the forecasted data fluctuates. Based on a large number of the literature, Xiao et al. [11] summarized the quantitative prediction methods of port throughput, mainly including the following:

(1) *Time Series Method.* This method establishes mathematical models based on historical throughput data, including autoregressive integrated mobile average (ARIMA) model, exponential smoothing, grey model (GM), and decomposition method (X-11). For examples, Rashed et al. [12] used the ARIMA intervention model to predict the container throughput in the Antwerp Port. Chen et al. [13] used the improved GM (1, 1) model to predict the Shanghai Port container throughput.

(2) *Causal Analysis Models.* This method examines the correlation between the port hinterland throughput and a series of economic indicators and establishes the port hinterland throughput forecast model according to the relevant economic indicators. Currently, these methods mainly include regression analysis and elastic coefficient method. For example, Rashed et al. [14] used the autoregressive distribution lag model combined with the economic scenario to analyze and predict the relationship between container throughput and the EU trade index of 19 countries.

(3) *Nonlinear Dynamics Forecasting Models.* The time series model and causal analysis models can obtain

satisfactory forecasting performance when the container throughput time series is linear or nearly linear. However, the factors affecting the container throughput are complex, and container throughput fluctuations often reveal high nonlinear dependencies. Therefore, using only these linear models may be very poor. Recently, some nonlinear dynamic prediction models are introduced in container throughput forecasting such as artificial neural network (ANN) and genetic planning (GP). For examples, Fang and Fang [15] used a port throughput prediction model based on the BP neural network algorithm. Chen and Chen [16] studied port container throughput prediction using the genetic planning-based approach. Eskafi et al. [17] predicted the port throughput using Bayesian estimation models taking epistemic uncertainty into account affecting macroeconomic variables to forecast the annual throughput of the multipurpose Port of Isafjordur in Iceland.

(4) *Combined Forecasting Method*. This method combines two or more prediction models to compensate for each other's defects and improve data processing so as to obtain more stable and accurate results. For examples, Fang and Fang [15] studied the issue of port throughput prediction in Guangdong Province using a multivariate combination model of the genetic algorithm (GA) and back propagation neural network (BPNN). Chen et al. [10] studied combination models of the pearl curve model, GM (1, 1), and double exponential smoothing models, which perform better by case study than any other single prediction model from the two or more.

These research studies have provided valuable reference for port throughput forecasting research, but some of the models consist of limits such as some lack of input data, limiting their performance, increasing uncertainty, and reducing the reliability of prediction results [18]; some models themselves have limited treatment of uncertainties, consider only internal factors, and ignore external factors [5];. Chen et al. [10] noted that a single model may cause inaccurate predictions due to numerous influencing factors.

2.3. Introduction to the Methodology in This Paper. In order to achieve better performance and more accurate results, considering the various factors entangling and the relevant research studies studied, we have decided to establish a combination model for the container throughput issue consisting of the fractional GM (1, 1) model and BP neural network model.

In 1981, Professor Deng [19] put forward and introduced [20] the concept of the grey system. In the last 3 decades, many scholars are having been studying and developing the new modified grey model to make up for the defects and increase the performance. Wu et al. [21, 22] firstly placed and improved the fractional accumulation on the grey system models which is of great innovation and dramatically improved the prediction precision of grey models. In recent years, new grey models have been put forward and relevant research studies have been carried out [23, 24] like mushrooms after a spring rain. Among the models, fractional order GM (1, 1) has been practically mature and extensively applied as well as BP neural network. BP neural network was proposed by scientists led by Rumelhart and McClelland in 1986. It is a multilayer feed-forward neural network trained according to the error back propagation algorithm, and it is the most widely used neural network [25]. For recent examples, Gao et al. [26] used the BP neural network to study the forecast of the short-term rainstorm; Deshwal et al. [27] has established a language recognition system using the BP neural network model; Duddu et al. [28] used the BP neural network model to predict visibility at the road connectivity level; Liu et al. [29] used fractional GM (1, 1) and BP neural network for power load forecasting and so on.

In this paper, we combine two models of the fractional GM (1, 1) model and BP neural network model, with the detailed data of Port Statistical Yearbook of China [30] and the officially published information from Ministry of Transport of China [3] and carry out a forecasting on the container throughput and provide a 5-year reference data for the port enterprises in resource prescheduling and port intelligent scheduling.

3. Methodologies

3.1. Modeling and Testing Method of FGM (1, 1) Model. The advantage of the GM (1, 1) model is that it can handle grey information and poor data, but the model also suffers with great errors in some cases and performs unstably. To improve the GM (1, 1) model, the fractional GM (1, 1) model selects the appropriate accumulation order, reduces the error, and can get better prediction results [21]. The basic process of the FGM (1, 1) model is given as follows:

(1) From the original nonnegative data, the original sequence is given as follows:

$$X^0 = \left(x^0(1), x^0(2), \ldots, x^0(n)\right). \tag{1}$$

(2) Based on the original nonnegative sequence, the order r accumulation sequence is as follows:

$$X^{(r)} = \left(x^{(r)}(1), x^{(r)}(2), \ldots, x^{(0)}(n)\right), \tag{2}$$

where

$$C_{r-1}^0 = 1, C_k^{k+1} = 0. \tag{3}$$

(3) The whitening differential equation was established as $(\mathrm{d}x^{(r)}t/\mathrm{d}t) + ax^{(r)}(t) = b$. The form of the solution is an exponential function as follows:

$$x^{(r)}(t+1) = \left[x^{(0)}(1) - \frac{b}{a}\right]e^{-at} + \frac{b}{a}, \tag{4}$$

solved by the least square method, for $\widehat{a}\widehat{b}$,

$$\begin{pmatrix} \hat{a} \\ \hat{b} \end{pmatrix} = \left(B^T B\right)^{-1} B^T Y, \tag{5}$$

where

$$B = \begin{pmatrix} -0.5\left(x^{(r)}(1) + x^{(r)}(2)\right) & 1 \\ -0.5\left(x^{(r)}(2) + x^{(r)}(3)\right) & 1 \\ \vdots & \vdots \\ -0.5\left(x^{(r)}(n-1) + x^{(r)}(n)\right) & 1 \end{pmatrix},$$
$$Y = \begin{pmatrix} x^{(r)}(2) - x^{(r)}(1) \\ x^{(r)}(3) - x^{(r)}(2) \\ \vdots \\ x^{(r)}(n) - x^{(r)}(n-1) \end{pmatrix}. \tag{6}$$

(4) Time response function solved is as follows: $\hat{x}^{(r)}(k+1) = [x^{(0)}(1) - (\hat{b}/\hat{a})]e^{-\hat{a}k} + (\hat{b}/\hat{a})$ while $\hat{x}^{(r)}(k+1)$ is the value of the time $k+1$.

(5) For the sequence $\hat{X}^{(r)} = \left\{\hat{x}^{(r)}(1), \hat{x}^{(r)}(2), \ldots, a^{(1)}\hat{x}^{(r)}(n)\right\}$, the reduction of the sequence is as folllows:

$$a^{(r)}\hat{X}^{(r)} = \left\{a^{(1)}\hat{x}^{(r)(1-r)}(1), a^{(1)}\hat{x}^{(r)(1-r)}(2), \ldots, a^{(1)}\hat{x}^{(r)(1-r)}(n)\right\}, \tag{7}$$

where $a^{(1)}\hat{x}^{(r)(1-r)}(k) = \hat{x}^{(r)(1-r)}(k) - \hat{x}^{(r)(1-r)}(k-1)$.

Through the b-b operation, the prediction sequence is as follows: $\left\{\hat{x}^{(0)}(1), \hat{x}^{(0)}(2), \ldots, \hat{x}^{(0)}(n)\right\}$.

(6) The model is evaluated using the mean absolute percentage error (MAPE), where

$$\text{MAPE} = \frac{1}{n} x \sum_{k=1}^{n} \left| \frac{x^{(0)}(k) - \hat{x}^{(0)}(k-1)}{x^{(0)}(k)} \right| \times 100\%. \tag{8}$$

When $r = 1$, the FGM (1, 1) model is the grey GM (1, 1) model.

3.2. Establishment Process of BP Neural Network Based on Layer Training. The BP neural network is a multilayer feed-forward neural network (MLFNN). The main features of BP neural network are the signal forward transmission and the error in back propagation. The input signal after the hidden processing is transmitted to the output layer. If the output layer node fails to reach the expected output, it will proceed to the back propagation phase of the error. The output error is returned in some subform to the input layer through the implicit layer and apportioned to the implicit layer nodes and the input layer nodes. Thus, the error signal of each layer unit is obtained as the basis for modifying the weights of each unit.

The BP algorithm only uses the mean square error function for first derivative (gradient) of weight and threshold, so the convergence rate of the algorithm is slow and easy to fall into local minimum. In order to solve this problem, Hinton and Salakhutdinov [31] proposed a unsupervised greedy layer-wise training algorithm, a machine learning method of deep neural network based on human brain learning thought, which brought hope to solving the optimization problem related to deep structure. The main idea of the layer-by-layer training algorithm is to train only one layer in the network each time, each layer training separately. It firstly trains a network with only one hidden layer and only then starts training a network with two hidden layers, and the rest can be done in the same manner (Figure 2). In each step, we fix the trained front $k-1$ layer and then add the layer k (that is to take the output of the prealready trained $k-1$ as input). The weights obtained by these layers trained individually are used to initialize all the weights of the BP neural network, putting all the layers together to optimize the training errors on the labeled training set.

BP neural network used in this paper is only capable for training normalized data ranging from [0, 1]; as in this paper, data from the FGM model must be normalized before being trained in the BP neural network.

The objective function of the BP neural network above is the mean relative error (MRE). BP neural network structure is shown in Figure 2:

$$\text{MRE} = \frac{1}{n} \sum_{i=1}^{n} \left| \frac{Y_i - \hat{Y}_i}{Y_i} \right|. \tag{9}$$

4. Testing, Forecasting, and Results

4.1. Comparing Test between Combination Model and Other FGM Models. This paper forecasts the container throughput of Tianjin-Hebei Port Group. The data from 2012–2020 come from the Port Statistical Yearbook of China and the official website of the Ministry of Transport, including Tianjin Port, Tangshan Port, Qinhuangdao Port, and Huanghua Port. We will firstly substitute the data of 2012–2017 into the model for operations, with the forecasted results of 2018–2020 against the actual figures of 2018–2020. Then, the forecasting accuracy of the combination model would thus be verified. The reason we only used six years of data is as follows. (1) The port group develops rapidly. The data base of each port is small, and the data change range is large. The earlier data have little influence on the current and future data. (2) The grey model has strong performance in processing small sample of data.

We substitute the container throughput data from 2012–2017 into GM (1, 1) and FGM (1, 1) models, respectively, when $r = 0.2$, $r = 0.5$, and $r = 0.8$ and obtain the simulation data for 2018–2020 (Tables 1–4).

As it can be seen from the above, different ports and total values are with different MAPE values. When $r = 1$ for Tianjin Port, $r = 0.2$ for Tangshan Port, $r = 0.2$ for Qinhuangdao Port, $r = 0.2$ for Huanghua Port, and $r = 0.8$ for the total, MAPE value is the minimum, respectively: 1.137%, 1.568%, 2.459%, 6.777% ,and 0.800%, as shown in Figure 3.

Particularly, the reason for the largest data MAPE in Huanghua Port is that it is an emerging port with the

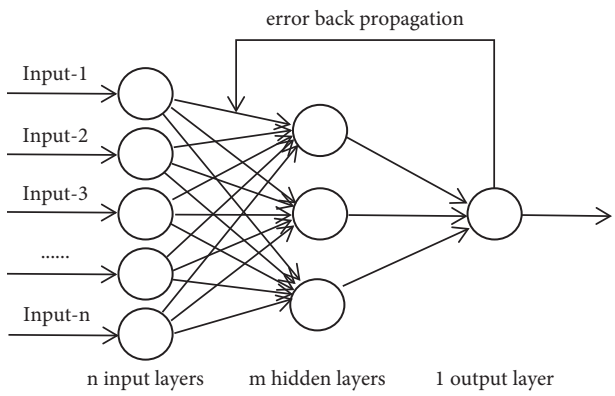

Figure 2: BP neural network structure.

Table 1: GM (1.1) container throughput of Tianjin-Hebei Port Group (unit: 10,000 TEU).

Year	Tianjin	Tangshan	Qinhuangdao	Huanghua	Total
2012	1230.00	46.00	34.00	10.00	1320.00
2013	1326.00	82.00	39.00	27.00	1461.00
2014	1369.00	109.00	43.00	35.00	1556.00
2015	1414.00	144.00	47.00	44.00	1658.00
2016	1460.00	191.00	52.00	55.00	1767.00
2017	1508.00	254.00	57.00	70.00	1882.00
2018	1557.00	337.00	62.00	88.00	2005.00
2019	1608.00	448.00	69.00	111.00	2136.00
2020	1661.00	594.00	75.00	140.00	2276.00
MAPE	1.076%	4.267%	2.532%	11.66%	0.936%

Table 2: FGM (1.1) when $r = 0.2$ container throughput of Tianjin-Hebei Port Group (unit: 10,000 TEU).

Year	Tianjin	Tangshan	Qinhuangdao	Huanghua	Total
2012	1230.00	46.00	34.00	10.00	1320.00
2013	1295.64	74.78	38.15	23.98	1423.81
2014	1379.54	108.93	43.33	35.76	1565.69
2015	1438.67	148.94	48.09	46.43	1688.93
2016	1475.14	196.06	52.31	56.34	1789.79
2017	1494.34	251.83	56.01	65.67	1870.48
2018	1500.97	318.02	59.24	74.53	1933.97
2019	1498.72	396.77	62.05	82.98	1983.07
2020	1490.33	490.59	64.50	91.08	2020.21
MAPE	1.337%	1.568%	2.459%	6.777%	1.248%

Table 3: FGM (1.1) when $r = 0.5$ container throughput of Tianjin-Hebei Port Group (unit: 10,000 TEU).

Year	Tianjin	Tangshan	Qinhuangdao	Huanghua	Total
2012	1230.00	46.00	34.00	10.00	1320.00
2013	1287.35	76.09	37.87	24.94	1415.10
2014	1386.36	109.48	43.47	35.70	1573.96
2015	1446.84	148.41	48.29	45.84	1697.91
2016	1477.09	195.01	52.41	56.07	1790.92
2017	1485.78	251.56	55.96	66.72	1859.62
2018	1479.24	320.70	59.05	78.02	1909.25
2019	1462.00	405.58	61.74	90.14	1943.75
2020	1437.32	510.07	64.11	103.24	1966.09
MAPE	1.624%	1.810%	2.640%	8.222%	1.502%

Table 4: FGM (1.1) when $r = 0.8$ container throughput of Tianjin-Hebei Port Group (unit: 10,000 TEU).

Year	Tianjin	Tangshan	Qinhuangdao	Huanghua	Total
2012	1230.00	46.00	34.00	10.00	1320.00
2013	1300.32	78.99	38.31	26.28	1443.97
2014	1383.14	109.48	43.35	35.26	1565.56
2015	1435.55	146.48	47.87	44.74	1672.60
2016	1469.36	193.05	52.12	55.58	1773.23
2017	1490.85	252.40	56.26	68.28	1871.10
2018	1503.62	328.45	60.38	83.34	1968.15
2019	1509.94	426.17	64.51	101.29	2065.56
2020	1511.33	551.91	68.71	122.76	2164.13
MAPE	1.137%	2.786%	2.491%	10.18%	0.800%

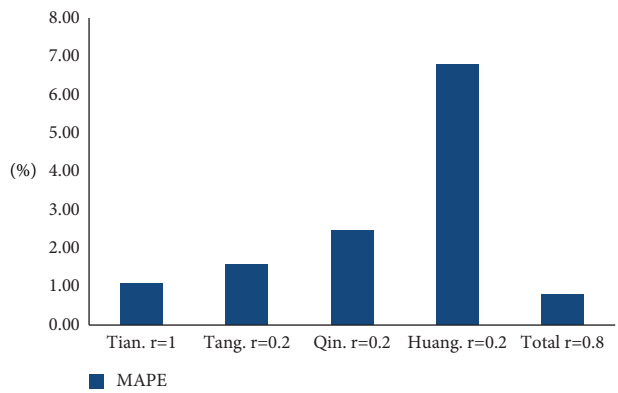

Figure 3: MAPE for the optimized orders of the FGM models.

smallest data and the most random factors and unpredictable influences. Regardlessly, we will proceed and test the BP neural network model with the output data.

As the FGM model is mainly suitable for small data modeling, while BPNN is more suitable for big data modeling, bootstrap has been applied in the process with which small data for FGM are transformed to big data for BPNN by random sampling. Because the BP neural network model can only deal with the normalized data ranging [0, 1], we normalize and substitute the original data into the BP neural network model for a test, error percentage calculated against the original data, as in Table 5.

From Table 5, we can see the data error after BPNN processing is very small, especially the recent 2020 data error is only −0.92% which is completely satisfactory for the forecasting. So as tested, the BPNN model is fully feasible for the combination model. Therefore, after normalization of the results of grey forecasting of the 4 ports in Table 6 ($r = 1$ Tianjin Port, $r = 0.2$ Tangshan Port, $r = 0.2$ Qinhuangdao Port, and $r = 0.2$ Huanghua Port), we substitute the optimized output data from FGM into the BP neural network for training, which is actually using the FGM (1, 1) and BP neural network combination model to process the data, and conclude in Table 6.

It can be seen that the data obtained by the FGM (1, 1) and BP neural network combination model had a low error compared with the original data and outperformed any other grey model in forecasting accuracy and stability as in Figure 4. Amazingly, the runner-up is the GM (1, 1) model as we mentioned before that it could perform unstably. On some level, it proves again that the grey model fits well with the container throughput forecasting.

4.2. Forecasting Process of the Grey Combination Model and Results. As the grey combination model is feasible for forecasting, we proceed with the actual figures to forecast for the next 5 years. Given that we used six years of data for testing, we also use six years of data in the forecasting. In the first step, we substitute the data from 4 ports and the total, respectively, into the FGM (1, 1) with optimized orders for processing. Results of the first step using FGM (1, 1) model are shown in Table 7.

In the sSecond step, we then normalize the output data which we would apply bootstrap to transform into big data and substitute into the BP neural network for training. Training error progress is shown in Figure 5.

As shown in Figure 5, in the progress of training, the error rapidly decreases and reaches the target error of 0.01 when the epoches reach nearly 2200. Thus, the forecasting normalized data of the combination model are obtained. After the antinormalizing processing, the forecasted results and the container throughput developing trend can be obtained, as shown in Table 8 and Figure 6.

Table 5: Comparison of BP neural network and the original data.

Year	Tian. original norm.	Tang. original norm.	Qin. original norm.	Huang. original norm.	Total original data norm.	Original data (unit: 10,000 TEU)	Total after BPNN training	Total data antinorm. (unit: 10,000 TEU)	Error
2012	0.01	0.01	0.01	0.01	0.01	1320	0.018	1320.00	0.00%
2013	0.10	0.10	0.15	0.19	0.11	1436	0.124	1446.95	0.76%
2014	0.24	0.22	0.20	0.31	0.24	1589	0.232	1576.69	−0.77%
2015	0.24	0.36	0.45	0.58	0.30	1663	0.331	1696.50	2.01%
2016	0.30	0.49	0.51	0.72	0.38	1758	0.396	1773.62	0.89%
2017	0.37	0.68	0.62	0.79	0.48	1881	0.442	1829.75	−2.72%
2018	0.49	0.82	0.67	0.89	0.60	2027	0.597	2016.10	−0.54%
2019	0.65	0.82	0.78	0.67	0.70	2143	0.659	2089.84	−2.48%
2020	0.79	0.88	0.78	0.90	0.82	2282	0.801	2261.02	−0.92%

Table 6: Comparison of the two data between the combination model and the original data.

Year	Tian. $r = 1$ norm.	Tang. $r = 0.2$ norm.	Qin. $r = 0.2$ norm.	Huang. $r = 0.2$ norm.	Total original data norm.	BPNN training results	Trained data antinorm. (unit:10,000 TEU)	Error
2012	0.01	0.01	0.01	0.01	0.01	0.019	1320.00	0.00%
2013	0.13	0.06	0.10	0.15	0.11	0.102	1426.34	−0.67%
2014	0.19	0.12	0.21	0.27	0.24	0.242	1605.71	1.05%
2015	0.25	0.19	0.31	0.37	0.30	0.32	1705.65	2.56%
2016	0.31	0.28	0.40	0.47	0.38	0.389	1794.05	2.05%
2017	0.37	0.38	0.48	0.56	0.48	0.426	1841.45	−2.10%
2018	0.43	0.50	0.55	0.65	0.60	0.601	2065.67	1.91%
2019	0.50	0.64	0.61	0.73	0.70	0.658	2138.70	−0.20%
2020	0.56	0.80	0.67	0.81	0.82	0.773	2286.04	0.18%

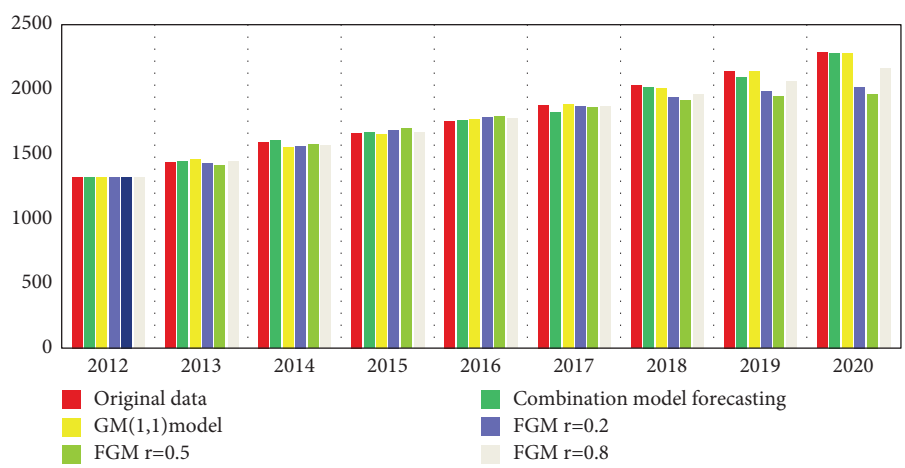

Figure 4: Comparison among original data, the grey combination model, and other grey models (unit: 10,000 TEU).

Table 7: The forecasting data of the first step using the optimized FGM (1, 1) model (unit: 10,000 TEU).

Year	Tian. $r = 1$	Tian. norm.	Tang. $r = 0.2$	Tang. norm.	Qin. $r = 0.2$	Qin. norm.	Huang. $r = 0.2$	Huang. norm.	Total $r = 0.8$	Total norm.
2015	1411.00	0.01	152.00	0.01	50.00	0.01	50.00	0.01	1663	0.01
2016	1432.00	0.03	205.99	0.23	52.15	0.08	59.50	0.32	1764.71	0.08
2017	1522.00	0.11	246.88	0.39	55.74	0.20	66.00	0.54	1882.89	0.15
2018	1618.00	0.20	276.80	0.51	58.64	0.30	69.81	0.66	2008.98	0.23
2019	1721.00	0.29	298.48	0.59	60.74	0.36	71.77	0.73	2143.51	0.32
2020	1829.00	0.39	313.97	0.66	62.18	0.41	72.54	0.75	2287.06	0.41

Table 7: Continued.

Year	Tian. $r = 1$	Tian. norm.	Tang. $r = 0.2$	Tang. norm.	Qin. $r = 0.2$	Qin. norm.	Huang. $r = 0.2$	Huang. norm.	Total $r = 0.8$	Total norm.
2021	1945.00	0.50	324.76	0.70	63.08	0.44	72.52	0.75	2440.22	0.51
2022	2068.00	0.61	331.97	0.73	63.58	0.46	72.03	0.74	2603.63	0.62
2023	2198.00	0.73	336.47	0.75	63.76	0.46	71.23	0.71	2777.99	0.73
2024	2337.00	0.85	338.90	0.76	63.71	0.46	70.28	0.68	2964.02	0.85
2025	2485.00	0.99	339.76	0.76	63.48	0.45	69.24	0.64	3162.51	0.98
MAPE	0.856%%		3.448%		0.835%		1.714%		0.323%	

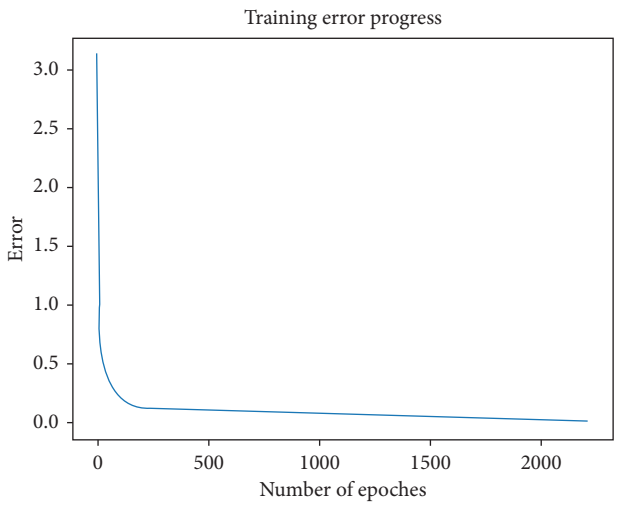

Figure 5: BP neural network training error process.

Table 8: The container throughput results of Tianjin-Hebei Port Group forecasted by the grey combination model.

Year	The grey combination model forecast (unit: 10,000 TEU)
2021	2477.59
2022	2578.05
2023	2760.45
2024	2851.25
2025	3106.66

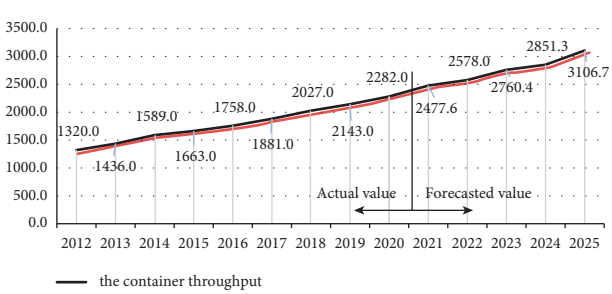

Figure 6: The container throughput developing trend (unit: 10,000 TEU).

5. Conclusion

Since the change of container throughput in Tianjin-Hebei Port Group is an incomplete information grey system affected by various factors, it is difficult to cover a variety of factors in the forecasting using a single forecasting model, which leads to the insufficient accuracy and stability of the forecast. The traditional GM (1, 1) model is suitable for the study of such grey systems, including the advantages of processing data from small samples, but the model has disadvantages such as high original sequence dependence and slow convergence. In this paper, we use the FGM model and BP neural network combination model that improves for the defects of each single model. The results show that the accuracy and stability of the combination model are better than those of any other grey model in data fitness and stability which meets the forecasting requirements of container throughput of Tianjin-Hebei Port Group. This paper forecasts the container throughput of Tianjin-Hebei Port Group in the next 5 years. The results show that the container throughput of Tianjin-Hebei Port Group remains increasing year by year in the next 5 years, which provides a data reference for the further exploitation of the ports' resources, shipping schedule planning, related infrastructure construction, and so on in dealing with the increasing container throughput.

Data Availability

The port throughput data from 2012-2017 that support the findings of this study are openly available in China Statistical Yearbook published by the National Bureau of Statistics of China. 2013-2018. The port throughput data from 2018-2020 that support the findings of this paper are openly available at Government Information Disclosure column, Comprehensive Planning Division, Official website of the Ministry of Transport of the People's Republic of China (https://xxgk.mot.gov.cn/jigou/zhghs/201905/t20190513_3198922.html, https://xxgk.mot.gov.cn/2020/jigou/zhghs/202006/t20200630_3321297.html, and https://xxgk.mot.gov.cn/2020/jigou/zhghs/202101/t20210121_3517383.html).

Conflicts of Interest

The authors declare that they have no conflicts of interest.

Acknowledgments

This work was partially supported by Handan Science and Technology Research and Development Program (19422303008-72), Handan Philosophy and Social Science Planning (2020030), Major Projects of China National Social Science Foundation (20 & zd129), and General Program of National Natural Science Foundation of China (72073018).

References

[1] X. Lin, *Logistics Procurement and Transportation Practice*, Central Radio and Television University Press, Beijing, China, 2013.

[2] China Government Network, *Official Website Information Disclosure Platform of Hebei Provincial Department of Transportation-Comprehensive Statistics and Analysis. Completion of Road Passenger and Cargo Transportation and Port Production in the Province in March 2021*, China Government Network, Beijing, China, 2021, http://jtt.hebei.gov.cn/jtyst/zwgk/jcxxgk/jttj/zhtjfx/101618311221855.html.

[3] Official Website of the Ministry of Transport of the People's Republic of China, "The government information disclosure column of the department of comprehensive planning," 2021, https://xxgk.mot.gov.cn/jigou/zhghs/201905/t20190513_3198922.htmlhttps://xxgk.mot.gov.cn/2020/jigou/zhghs/202006/t20200630_3320172.html.

[4] P. Taneja, H. Ligteringen, and M. V. Schuylenburg, "Dealing with uncertainty in design of port infrastructure systems," *Journal of Design Research*, vol. 8, no. 2, pp. 101–118, 2010.

[5] C. Van Dorsser, M. Wolters, and B. Van Wee, "A very long term forecast of the port throughput in the le havre-hamburg range up to 2100," *European Journal of Transport and Infrastructure Research*, vol. 12, no. 1, pp. 88–110, 2012.

[6] T. E. Notteboom, "Traffic inequality in seaport systems revisited," *Journal of Transport Geography*, vol. 14, no. 2, pp. 95–108, 2006.

[7] P. W. De Langen, J. Van Meijeren, and L. A. Tavasszy, "Combining models and commodity chain research for making long-term projections of port throughput: an application to the hamburg-le havre range," *European Journal of Transport and Infrastructure Research*, vol. 12, no. 3, pp. 310–331, 2012.

[8] X. Cui, "The impact of trade friction on shipping industry," *China Ocean Shipping*, vol. 24, no. 5, pp. 54–56, 2018.

[9] T. E. Notteboom and H. E. Haralambides, "Port management and governance in a post-COVID-19 era: quo vadis?" *Maritime Economics & Logistics*, vol. 22, no. 3, pp. 329–352, 2020.

[10] Z. Chen, Y. Chen, and T. Li, "Port cargo throughput forecasting based on combination model," in *Proceedings of the 2016 Joint International Information Technology, Mechanical and Electronic Engineering*, Xi'an, China, October 2016.

[11] J. Xiao, Y. Xiao, J. Fu, and K. K. Lai, "A transfer forecasting model for container throughput guided by discrete PSO," *Journal of Systems Science and Complexity*, vol. 27, no. 1, pp. 181–192, 2014.

[12] Y. Rashed, H. Meersman, E. Van de Voorde, and T. Vanelslander, "Short-term forecast of container throughout: an ARIMA-intervention model for the port of Antwerp," *Maritime Economics & Logistics*, vol. 19, no. 4, pp. 749–764, 2017.

[13] C. Chen, R. Dai, T. Yang, Z. Wu, and Q. Li, "Container throughput forecast of Shanghai port based on improved GM (1,1) model," *Ship & Ocean Engineering*, vol. 45, no. 4, pp. 153–156, 2016.

[14] Y. Rashed, H. Meersman, E. Van de Voorde et al., "A combined approach to forecast container throughput demand: scenarios for the hamburg-le havre range of ports," *Transportation Research Part A: Policy and Practice*, vol. 117, pp. 127–141, 2018.

[15] F. P. Fang and X. F. Fang, "Multivariant forecasting mode of Guangdong province port throughput with genetic algorithms and back propagation neural network," *Procedia-Social and Behavioral Sciences*, vol. 96, pp. 1165–1174, 2013.

[16] S. H. Chen and J. N. Chen, "Forecasting container throughputs at ports using genetic programming," *Expert Systems with Applications*, vol. 37, no. 3, pp. 2054–2058, 2010.

[17] M. Eskafi, M. Kowsari, A. Dastgheib et al., "A model for port throughput forecasting using Bayesian estimation," *Maritime Economics & Logistics*, vol. 23, pp. 348–368, 2021.

[18] F. Parola, G. Satta, T. E. Notteboom, and L. Persico, "Revisiting traffic forecasting by port authorities in the context of port planning and development," *Maritime Economics and Logistics*, 2020.

[19] J. Deng, "Control problems of grey systems," *Systems & Control Letters*, vol. 1, no. 5, pp. 288–294, 1982.

[20] J. L. Deng, "Introduction to grey system theory," *The Journal of Grey System*, vol. 1, pp. 1–24, 1989.

[21] L. Wu, S. Liu, L. Yao, S. Yan, and D. Liu, "Grey system model with the fractional order accumulation," *Communications in Nonlinear Science and Numerical Simulation*, vol. 18, no. 7, pp. 1775–1785, 2013.

[22] L. Wu, S. Liu, Z. Fang, and H. Xu, "Properties of the GM (1,1) with fractional order accumulation," *Applied Mathematics and Computation*, vol. 252, 2015.

[23] B. Zeng, X. Ma, and M. Zhou, "A new-structure grey Verhulst model for China's tight gas production forecasting," *Applied Soft Computing*, vol. 96, Article ID 106600, 2020.

[24] B. Zeng, H. Li, and X. Ma, "A novel multi-variable grey forecasting model and its application in forecasting the grain production in China," *Computers & Industrial Engineering*, vol. 150, Article ID 106915, 2020.

[25] X. Wen, X. W. Zhang, Y. P. Zhu, and X. Z. Li, *Intelligent Fault Diagnosis Technology: MATLAB Application*, Vol. 9, Press of Beijing University of Aeronautics and Astronautics, Beijing, China, 2015.

[26] G. Gao, Y. Li, J. Li, X. Zhou, and Z. Zhou, "A hybrid model for short-term rainstorm forecasting based on a back-propagation neural network and synoptic diagnosis," *Atmospheric and Oceanic Science Letters*, vol. 14, no. 5, 2021.

[27] D. Deshwal, P. Sangwan, and D. Kumar, "A language identification system using hybrid features and back-propagation neural network," *Applied Acoustics*, vol. 164, Article ID 107289, 2020.

[28] V. R. Duddu, S. Pulugurtha, A. Mane, and C. Godfrey, "Back-propagation neural network model to predict visibility at a road link-level," *Transportation Research Interdisciplinary Perspectives*, vol. 8, Article ID 100250, 2020.

[29] C. Liu and H. Zhao, H. Yan and J. Wang, Power load forecasting based on fractional GM (1,1) and BP neural network," *Mathematics in Practice and Theory*, vol. 48, no. 23, pp. 145–151, 2018.

[30] China Statistical Yearbook, *The National Bureau of Statistics*, China Statistics Press, Beijing, China, 2018.

[31] G. E. Hinton and R. Salakhutdinov, "Reducing the dimensionality of data with neural networks," *Science*, vol. 313, no. 5786, pp. 504–507, 2006.

Hindawi
Journal of Mathematics
Volume 2021, Article ID 2477964, 7 pages
https://doi.org/10.1155/2021/2477964

Research Article

Energy Consumption Predication in China Based on the Modified Fractional Grey Prediction Model

Jiefang Liu[1] **and Pumei Gao**[2]

[1]*School of Management and Economics, Tianjin University of Technology and Education, Tianjin 300222, China*
[2]*Department of Economics and Management, Tianjin Electronic Information College, Tianjin 300350, China*

Correspondence should be addressed to Jiefang Liu; liujf101@126.com

Received 10 May 2021; Revised 15 July 2021; Accepted 24 July 2021; Published 10 August 2021

Academic Editor: Shuhua Mao

China's increasing energy consumption poses challenges to economy and environment. How to predict the energy consumption accurately and regulate the future energy consumption production is a problem worth studying. In this paper, the fractional order cumulative linear time-varying parameter discrete grey prediction model (FTDGM (1, 1) model) is introduced. Firstly, the data are preprocessed by buffer operators, and then, the FTDGM (1, 1) model is established. In this paper, the parameter estimation method and the specific process of model establishment are presented. Finally, the models of energy consumption in China are built. The advantages and prediction accuracy of the model established in this paper are analyzed, and the data in the following years are effectively predicted, so as to provide theoretical support for the government to formulate reasonable energy policies.

1. Introduction

Grey system theory is a small sample modeling method proposed by Professor Deng Julong in 1982, which mainly includes grey prediction theory, grey correlation theory, grey decision theory, grey clustering theory, and grey game theory [1, 2]. Among them, the grey predication theory is an important part of grey system theory, for the reason that the grey prediction theory does not have strict requirements on data. For example, the data do not need to meet certain distribution rule, and the high precision model can be established based on a small amount of data. Therefore, since the model is put forward, it has been widely used in the fields of agriculture, energy, economy, medicine, and so on and has achieved fruitful achievements [3]. Compared with other uncertainty methods, the advantage of grey system theory is that it treats the modeling object as a system and uses the idea of system theory to build the model.

In recent years, many scholars have carried out extensive research studies on the grey prediction model [4–17], whose achievements have played a positive role in improving the grey prediction theory. The GM (1, 1) model requires the transformation of differential equation and difference equation, which will lead to systematic errors. Based on this, Xie and Liu constructed the DGM (1, 1) model and its extended form. The DGM (1, 1) model does not require the conversion of differential equation and difference equation, but directly uses the difference equation for parameter estimation and model solution, so as to effectively reduce the error source within the model [18]. The GM (1, 1) and DGM (1, 1) models construct prediction models by accumulating quasi-exponential rules of sequences. However, accumulative sequences contain linear laws as well as quasi-exponential laws. Based on this, Zhang and Liu proposed a discrete grey prediction model with linear time-varying parameters and discussed the properties of the model and the parameter solving method, and the model has a completely error-free simulation accuracy for sequences with linear laws and exponential laws [19]. Wu et al. constructed time-varying parameters of the GM (1, 1) model by introducing a polynomial function of time [20]. Accumulation is the basis of grey prediction, through which the sequence regularity can be highlighted. Traditional accumulation is a kind of first-order accumulation, so the importance of data

has not been differentiated. In view of this, Wu Lifeng puts forward a fractional accumulative grey predication model and discussed the modeling process and parameter-solving method [21, 22].

Time series are generally affected by the shock disturbance of the system. When the shock disturbance exists in the system, there will be relatively large modeling errors in the modeling of time series, and the inconsistency between the qualitative analysis and quantitative calculation will occur. This paper proposes a discrete grey prediction model based on the weakening buffer operator and fractional order accumulation of linear time-varying parameters. Firstly, the buffer operators are used to weaken the impact disturbance of the system, and then, the prediction model is constructed. In this paper, the structure is as follows. Section 2 introduces the differences between existing accumulative methods, the advantages of the fractional order accumulation and its calculation method, and the parameter-solving method. In Section 3, the modeling process of the fractional order accumulative linear time-varying discrete grey prediction model is described. In Section 4, two practical examples are given, and the feasibility and practicability of the proposed method is verified. The conclusion is drawn in Section 5.

2. Construction of Fractional Discrete Grey Models

The grey prediction model is established based on the accumulation sequence, which can effectively reduce the randomness of the system and show the development law of the system. For example, for an original data sequence $X^{(0)} = (1, 4, 2, 5, 2, 3)$, its first-order accumulation sequence is $X^{(1)} = (1, 5, 7, 12, 14, 17)$, as shown in Figure 1.

It can be seen from Figure 1 that the generation of first-order accumulation can transform the oscillation sequence with no obvious regularity into a monotonic increasing sequence, thus highlighting the change law of data and making a good preliminary preparation for the establishment of the grey prediction model.

The disadvantages of the integer order cumulative grey prediction model are analyzed by taking DGM (1, 1) as an example. For a sequence $X^{(0)} = (1, 2, 6, 10, 14, 19)$, the first-order cumulative DGM (1, 1) model is established. And, we can calculate the parameters as follows: $\beta_1 = 1.49$ and $\beta_2 = 3.85$. The simulation sequence is $\widehat{X}^{(0)} = (1.00, 4.34, 6.46, 9.61, 14.31, 21.30)$, and the average relative error is 23.78%. In comparison, if the 0.2 order cumulative DGM (1, 1) model is established, then we can get $\beta_1 = 1.27$ and $\beta_2 = 2.51$, the simulation sequence $\widehat{X}^{(0)} = (3.00, 4.85, 7.38, 10.71, 15.11, 20.93, 28.64)$, and the average relative error is 3.07%.

Assume that the original value of the sequence is changed, and there is a sequence $X^{(0)} = (3, 2, 6, 10, 14, 19)$; then, there are $\beta_1 = 1.49$ and $\beta_2 = 2.87$, the simulation sequence = (3.00, 4.34, 6.46, 9.61, 14.31, 21.30), and the average relative error remains 23.78%. In comparison, when the 0.2-order cumulative DGM (1, 1) model is established, we can get $\beta_1 = 1.27$ and $\beta_2 = 2.51$, the simulation sequence $\widehat{X}^{(0)} = (1.00, 3.58, 6.46, 9.94, 14.24, 19.61, 26.34)$, and the average relative error changes to 10.38%.

It can be seen from the above results that, for an integer order accumulation at the DGM (1, 1) model, the change of the original value will not influence the modeling results of the sequence, which means that the first value has not been effective utilized, which is a serious waste for small sample modeling. As to the fractional order accumulation at the DGM (1, 1) model, the change of the original value can lead to sequence change and the corresponding change of simulation precision, which means that fractional-order accumulation can effectively use the original value. Moreover, with the adjustment of the order, the fractional-order cumulative DGM (1, 1) model can obtain better modeling accuracy than the integer order cumulative DGM (1, 1) model. The same conclusion can be reached for other grey prediction models.

3. Construction of Novel Fractional Discrete Grey Model

For the series with disturbance information if the grey prediction model is established based on the original data, the simulation and prediction results obtained will be quite different from the actual trend of the system. This paper uses a classical weakening buffer operator to preprocess the data.

Definition 1. Assume a nonnegative sequence $X^{(1)} = \{x^{(1)}(1), x^{(1)}(2), \ldots, x^{(1)}(n)\}$ is the first-order accumulative sequence of $X^{(0)}$, where

$$x^{(1)}(k) = \sum_{i=1}^{k} x^{(0)}(i), \quad k = 1, 2, \ldots, n. \tag{1}$$

Then,

$$x^{(1)}(k+1) = \beta_1 x^{(1)}(k) + \beta_2, \quad k = 1, 2, \ldots, n-1, \tag{2}$$

is called the discrete grey prediction model (DGM (1, 1) model).

Theorem 1. *The parameters of the DGM (1, 1) model can be solved by using the following least squares estimation:*

$$\begin{bmatrix} \beta_1 \\ \beta_2 \end{bmatrix} = \left(B^T B\right)^{-1} B^T Y. \tag{3}$$

Among them

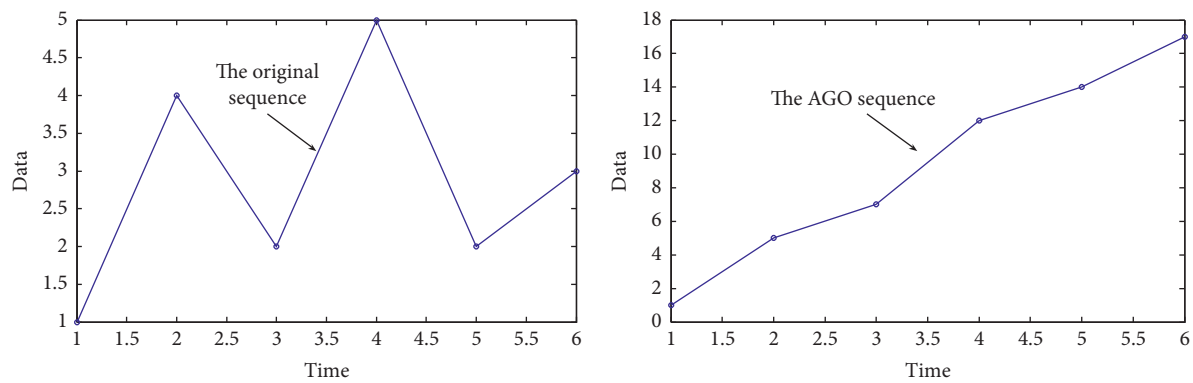

(a) (b)

Figure 1: Comparison between the original data sequence and its first-order accumulation.

$$B = \begin{bmatrix} x^{(1)}(1) & 1 \\ x^{(1)}(2) & 1 \\ \vdots & \vdots \\ x^{(1)}(n-2) & 1 \\ x^{(1)}(n-1) & 1 \end{bmatrix}, \quad Y = \begin{bmatrix} x^{(1)}(2) \\ x^{(1)}(3) \\ \vdots \\ x^{(1)}(n-1) \\ x^{(1)}(n) \end{bmatrix}. \tag{4}$$

The time response formula is as follows:

$$x^{(1)}(k+1) = \beta_1^k x^{(0)}(1) + \frac{1-\beta_1^k}{1-\beta_1}\beta_2, \quad k = 1, 2, \ldots, n-1. \tag{5}$$

From the above modeling, it can be seen that the DGM (1, 1) model avoids the transformation from differential equation to check score equation, so it can reduce the system error. The DGM (1, 1) model is an exponential model, which reflects the exponential law generated by accumulation. After accumulating, the sequence has both a trend of index and a linear trend. The linear time-varying parameters' discrete grey prediction model is inclusive for its complete linear specification. One of the problems for a linear time-varying discrete grey prediction model lies in ineffective use of the original value. Based on this, this paper carried out modeling by the fractional-order cumulative linear time-varying parameter discrete grey prediction model.

Definition 2. Assume the nonnegative sequence is $X^{(0)} = \{x^{(0)}(1), x^{(0)}(2), \ldots, x^{(0)}(n)\}$. $X^{(1)} = \{x^{(1)}(1), x^{(1)}(2), \ldots, x^{(1)}(n)\}$ is the first-order accumulative sequence of $X^{(0)}$.

Among them

$$x^{(1)}(k) = \sum_{i=1}^{k} x^{(0)}(i), \quad k = 1, 2, \ldots, n. \tag{6}$$

The equation,

$$x^{(1)}(k+1) = (\beta_1 k + \beta_2) x^{(1)}(k) + \beta_3 k + \beta_4, \quad k = 1, 2, \ldots, n-1, \tag{7}$$

is called linear time-varying parameters' discrete grey model TDGM (1,1) model.

Theorem 2. *The parameters of the TDGM (1, 1) model can be solved by using the following least squares estimation:*

$$\begin{bmatrix} \beta_1 \\ \beta_2 \\ \beta_3 \\ \beta_4 \end{bmatrix} = \left(C^T C\right)^{-1} C^T Y. \tag{8}$$

Among them

$$C = \begin{bmatrix} x^{(1)}(1) & x^{(1)}(1) & 1 & 1 \\ 2x^{(1)}(2) & x^{(1)}(2) & 2 & 1 \\ \vdots & \vdots & \vdots & \vdots \\ (n-2)x^{(1)}(n-2) & x^{(1)}(n-2) & n-2 & 1 \\ (n-1)x^{(1)}(n-1) & x^{(1)}(n-1) & n-1 & 1 \end{bmatrix}, \quad Y = \begin{bmatrix} x^{(1)}(2) \\ x^{(1)}(3) \\ \vdots \\ x^{(1)}(n-1) \\ x^{(1)}(n) \end{bmatrix}. \tag{9}$$

The time response formula is

$$\hat{x}^{(1)}(k+1) = (\beta_1 k + \beta_2)\hat{x}^{(1)}(k) + \beta_3 k + \beta_4, \quad k = 1, 2, \ldots, n-1. \tag{10}$$

Theorem 3. *For sequence $y = ab^k$, parameters $\beta_1 = \beta_3 = 0$, and the TDGM (1, 1) model is degraded to the DGM (1, 1) model. For the sequence $y = ax + b$, parameter $\beta_1 = 0$, and the TDGM (1, 1) model was degraded to the NDGM (1, 1) model. For sequence $y = ab^k + c$, parameter $\beta_1 = 0$, and the TDGM (1, 1) model was degraded to the NDGM (1, 1) model.*

It can be seen from Theorem 2 that the DGM (1, 1) model and NDGM (1, 1) model are uniform special cases of the TDGM (1, 1) model.

Definition 3 (see [20–22]). Assume the nonnegative sequence is $X^{(0)} = \{x^{(0)}(1), x^{(0)}(2), \ldots, x^{(0)}(n)\}$. $X^{(r)} = \{x^{(r)}(1), x^{(r)}(2), \ldots, x^{(r)}(n)\}$ is called the fractional-order accumulative sequence of $X^{(0)}$

Among them

$$x^{(r)}(k) = \sum_{i=1}^{k} C_{k-i+r-1}^{k-i} x^{(0)}(i), C_{r-1}^{0} = 1, C_{k-1}^{k} = 0, \quad k = 1, 2, \ldots, n. \tag{11}$$

Definition 4 (see [23]). Assume the nonnegative sequence $X^{(0)}$, $X^{(r)}$ is defined as Definition 3. The equation

$$x^{(r)}(k+1) = (\beta_1 k + \beta_2) x^{(r)}(k) + \beta_3 k + \beta_4, \quad k = 1, 2, \ldots, n-1, \tag{12}$$

is called the fractional-order accumulative linear time-varying parameters' discrete grey model FTDGM (1,1) model.

Theorem 4. *The parameters of the FTDGM (1, 1) model can be solved by using the following least squares estimation:*

$$\begin{bmatrix} \beta_1 \\ \beta_2 \\ \beta_3 \\ \beta_4 \end{bmatrix} = \left(D^T D\right)^{-1} D^T W. \tag{13}$$

Among them

$$D = \begin{bmatrix} x^{(r)}(1) & x^{(r)}(1) & 1 & 1 \\ 2x^{(r)}(2) & x^{(r)}(2) & 2 & 1 \\ \vdots & \vdots & \vdots & \vdots \\ (n-2)x^{(r)}(n-2) & x^{(r)}(n-2) & n-2 & 1 \\ (n-1)x^{(r)}(n-1) & x^{(r)}(n-1) & n-1 & 1 \end{bmatrix},$$
$$W = \begin{bmatrix} x^{(r)}(2) \\ x^{(r)}(3) \\ \vdots \\ x^{(r)}(n-1) \\ x^{(r)}(n) \end{bmatrix}. \tag{14}$$

The predicted value of the FTDGM (1, 1) model is as follows:

$$\hat{x}^{(r)}(k+1) = (\beta_1 k + \beta_2) \hat{x}^{(r)}(k) + \beta_3 k + \beta_4. \tag{15}$$

According to the calculation formula of fractional order accumulation, it is not difficult to calculate the reduced value of the predicted sequence as follows:

$$\hat{x}^{(0)}(k) = \hat{x}^{(r)}(k) - \sum_{i=1}^{k} C_{k-i+r-1}^{k-i} \hat{x}^{(r)}(i), \quad k = 1, 2, \ldots, n. \tag{16}$$

It can be seen from the modeling process that the FTDGM (1, 1) model can better reflect the change rule of the system through the adjustment and optimization of the cumulative order. The model not only has a good modeling effect for practice series with exponential trend but also has a good trend tracking ability for time series with linear trend and nonlinear trend superposition. The optimal parameters can be determined by intelligent optimization algorithm, and genetic optimization algorithm is adopted in this paper.

For the time series with system impact disturbance, the modeling results of the model become very poor, and even the qualitative analysis and the theorem analysis are inconsistent. Professor Liu Sifeng deeply analyzed this phenomenon and believed that it was not due to the choice of model, but due to the impact disturbance of the system, which made the data series unable to show the real change rule of the system. Therefore, it was necessary to restore the real face of the system. Based on this, Professor Liu Sifeng put forward the concept of buffer operator, analyzed its properties, and carried out a lot of applications.

In reality, the system is relatively complex, and many systems can be regarded as complex systems with shock disturbance. For such a system, the first step of modeling is to present the real rules of the system and then build the model. In this paper, the weakening buffer operator proposed by Professor Liu Sifeng is selected for data preprocessing. The definition of the weakening buffer operator is as follows.

Table 1: China's total energy consumption between 2009 and 2019 (10000 tce).

Year	2009	2010	2011	2012	2013	2014	2015	2016	2017	2018	2019
Consumption	336126	360648	387043	402138	416913	428334	434113	441492	455827	471925	487000

Table 2: Results from different grey predication models.

Original value	DGM (1, 1) predication	Predication error (%)	FTDGM (1, 1) predicated value ($r = 0.88$)	Predication value (%)	B-FTDGM (1, 1) predicated value ($r = 0.11$)	Predication error (%)
441492	457233.2	3.57	444420.4	0.66	444771.5	0.74
455827	473641.2	3.91	451907.1	0.86	461055.2	1.15
471925	490637.9	3.97	458769.2	2.79	455037.9	3.58
487000	508244.7	4.36	465125.7	4.49	486801.3	0.04
MAPE		3.95		2.20		1.38

MAPE (mean absolute percentage error) = $100\% (1/n) \sum_{k=1}^{n} |(x(k) - \hat{x}(k)/x(k))|$.

Table 3: Per capita consumption of domestic electricity in Beijing from 2011 to 2019.

Year	2011	2012	2013	2014	2015	2016	2017	2018	2019
Consumption	727.2	791.8	750.6	793.5	808.7	899.9	1004	1185.5	1168.1

Definition 5. Assume $X^{(0)} = (x^{(0)}(1), x^{(0)}(2), \ldots, x^{(0)}(n))$ is the original sequence and $X^{(0)}d_1$ is the buffered sequence and where

$$x^{(0)}(k)d_1 = \frac{x^{(0)}(k) + x^{(0)}(k+1) + \cdots + x^{(0)}(n)}{n-k+1}. \quad (17)$$

Then, $X^{(0)}d$ is called the average weakening buffer operator.

Definition 6. Assume $X^{(0)} = (x^{(0)}(1), x^{(0)}(2), \ldots, x^{(0)}(n))$ is the original sequence, $X^{(0)}d_2$ is the buffered sequence and $X^{(0)}d_2 = (x^{(0)}(1)d_2, x^{(0)}(2)d_2, \ldots, x^{(0)}(n)d_2)$, where

$$x^{(0)}(k)d_2 = \frac{(n-k+1)x^{(0)}(k)}{x^{(0)}k + x^{(0)}(k+1) + \cdots + x^{(0)}n} x^{(0)}k. \quad (18)$$

Then, $X^{(0)}d_2$ is called the average strengthening buffer operator.

Weakening buffer operator can be used for real time series with fast change in the front and slow change in the back, while strengthening buffer operator can be used for real time series with slow change in the front and fast change in the back. $X^{(0)}d_1$ and $X^{(0)}d_2$ are the most commonly used buffer operators.

Therefore, the modeling ideas proposed in this paper are as follows. Firstly, the system data are buffered to restore the real law of the system. Then, the FTDGM (1, 1) model was established to calculate and optimize the parameters. In order to illustrate the practicability and effectiveness of the new model, two case studies are is carried out as follows.

4. Case Study

Case 1: In recent years, with the development of society and economy, China's total energy consumption grows rapidly, which poses higher requirements to energy production and natural environment. Accurate predictions for China's energy consumption can help the government and enterprises take reasonable measures to cope with the situation. Therefore, energy consumption prediction in China is of great value. China's total energy consumption between 2009 and 2019 is shown in Table 1.

We take the data from 2009 to 2015 as the modeling data and the data from 2016 to 2019 as the prediction data to test the prediction effect of different grey prediction models. Among them, genetic algorithm is used to determine the optimal order, and MATLAB software is used for programming calculation.

It can be seen from Table 2 that the prediction error of the B-FTDGM (1, 1) model has been effectively reduced. There is no obvious phenomenon that the error increases with the increase of step size. Thus, it can overcome the problem that the traditional grey prediction model can only be used for short-term prediction.

Case 2: In recent years, with the progress of China's industrialization, electricity, as a very important energy source, become the foundation of economic development. Therefore, it become of great significance to forecast power consumption timely and accurately for economic and social development. The per capita consumption of domestic electricity in Beijing from 2011 to 2019 is shown in Table 3.

Data from 2011 to 2017 are used as modeling data, and data from 2018 to 2019 are used as prediction data to test the prediction effect of different gray prediction models. Calculation results of different grey prediction models are shown in Table 4.

As can be seen from Table 4, due to the impact disturbance of the system, the prediction accuracy of DGM

Table 4: Predication results of different grey predication models.

Original value	DGM (1, 1) predication	Predication error (%)	FTDGM (1, 1) predication ($r = 1.21$)	Predication error (%)	B-FTDGM (1, 1) predication ($r = 0.43$)	Predication error (%)
1185.5	1010.14	14.79	1095.63	7.58	1087.62	8.26
1168.1	1065.65	8.77	1226.11	4.97	1168.16	0.00
MAPE		11.78		6.27		4.13

(1, 1) is not high, while the accuracy of the FTDGM (1, 1) model is improved to some extent. The 2-step average prediction error can be further reduced by using the sequence strengthened by the strengthening operator for modeling.

5. Conclusion

In this paper, a discrete grey prediction model of linear time-varying combination of buffering operator and fractional-order accumulation is constructed, and its properties, parameter-solving method, and modeling process are discussed. The model is applied to the prediction of energy consumption and per capita electricity consumption in China, and high prediction accuracies are obtained, showing the obvious superiority of the model. The discussion of other time-varying parameter grey prediction models and multivariable time-varying parameter grey prediction models is a direction that needs to be further studied in the future.

Data Availability

The data used to support the findings of this study have been deposited in http://www.stats.gov.cn/tjsj/ndsj and http://tjj.beijing.gov.cn.

Conflicts of Interest

The authors declare that they have no conflicts of interest.

Acknowledgments

This research was supported by the Project of Chinese Postdoctoral Science Foundation (2018M632777), Henan Provincial Department of Education the Generally Project of Humanities and Social Science (2017-ZZJH-180), Henan Province Backbone Young Teachers Program (2018GGJS115), Key Scientific Research Projects of Colleges and Universities in Henan province (20A790012), and General Program of Humanities and Social Sciences from Ministry of Education (20YJC630083).

References

[1] J. L. Deng, "Introduction to grey system theory," *Journal of Grey System*, vol. 1, no. 1, pp. 1–24, 1989.

[2] S. F. Liu and Y. Lin, *Grey Information*, Springer, London, UK, 2006.

[3] S. F. Liu, J. Forrest, and R. Valle, "Emergence and development of grey systems theory," *Kybernetes*, vol. 38, no. 39, pp. 1246–1256, 2009.

[4] X. Xiao, J. Yang, S. Mao et al., "An improved seasonal rolling grey forecasting model using a cycle truncation accumulated generating operation for traffic flow," *Applied Mathematical Modelling*, vol. 1, no. 51, pp. 386–404, 2017.

[5] X. Ma and Z. B. Liu, "Application of a novel time-delayed polynomial grey model to predict the natural gas consumption in China," *Journal of Computational and Applied Mathematics*, vol. 324, pp. 17–24, 2007.

[6] S. Ding, "A novel self-adapting intelligent grey model for forecasting China's natural-gas demand," *Energy*, vol. 16, pp. 393–407, 2018.

[7] S. Ding, R. J. Li, S. Wu, and W. J. Zhou, "Application of a novel structure-adaptative grey model with adjustable time power item for nuclear energy consumption forecasting," *Applied Energy*, vol. 298, pp. 1–20, Article ID 117114, 2021.

[8] S. Ding, R. J. Li, and Z. Tao, "A novel adaptive discrete grey model with time-varying parameters for long-term photovoltaic power generation forecasting," *Energy Conversion and Management*, vol. 227, pp. 1–15, Article ID 113644, 2021.

[9] S. Ding and R. J. Li, "Forecasting the sales and stock of electric vehicles using a novel self-adaptive optimized grey model engineering," *Applications of Artificial Intelligence*, vol. 100, pp. 1–13, Article ID 104148, 2021.

[10] S. Ding, R. J. Li, S. Wu, and W. J. Zhou, "A novel composite forecasting framework by adaptive data preprocessing and optimized nonlinear grey bernoulli model for new energy vehicles sales," *Communications in Nonlinear Science and Numerical Simulation*, vol. 99, pp. 1–21, Article ID 105847, 2021.

[11] M. L. Cheng and G. J. Shi, "Modeling and application of grey model GM (2, 1) based on linear difference equation," *Journal of Grey System*, vol. 31, no. 2, pp. 37–50, 2019.

[12] X. J. Shen, M. H. Yue, P. F. Duan et al., "Application of grey prediction model to the prediction of medical consumables consumption," *Grey Systems: Theory and Application*, vol. 9, pp. 213–223, 2019.

[13] B. Zeng and C. Li, "Improved multi-variable grey forecasting model with a dynamic background-value coefficient and its application," *Computers & Industrial Engineering*, vol. 118, pp. 278–290, 2018.

[14] J. Ye, Y. G. Dang, and B. J. Li, "Grey-markov prediction model based on background value optimization and central-point triangular whitenization weight function," *Communications in Nonlinear Science and Numerical Simulation*, vol. 54, pp. 320–330, 2018.

[15] J. Cui, S. F. Liu, B. Zeng, and N. M. Xie, "A novel grey forecasting model and its optimization," *Applied Mathematical Modelling*, vol. 37, pp. 4399–4406, 2013.

[16] Z. X. Wang and P. Hao, "An improved grey multivariable model for predicting industrial energy consumption in China," *Applied Mathematical Modelling*, vol. 40, pp. 5745–5758, 2016.

[17] M. L. Cheng and M. Y. Xiang, "Generalized GM (1, 1)model and its application," *Journal of Grey System*, vol. 29, no. 3, pp. 110–122, 2017.

[18] N. M. Xie and S. F. Liu, "Discrete grey forecasting model and its optimization," *Applied Mathematical Modelling*, vol. 33, pp. 173–1186, 2009.

[19] K. Zhang and S. F. Liu, "Linear time-varying parameters discrete grey forecasting model," *Systems Engineering- Theory & Practice*, vol. 30, pp. 1650–1657, 2010.

[20] L. F. Wu, S. F. Liu, and L. G. Yao, "Discrete grey model based on fractional order accumulate," *System Engineering-Theory& Practice*, vol. 34, pp. 1822–1827, 2014.

[21] L. P. Tu and Y. Chen, "An unequal adjacent grey forecasting air pollution urban model," *Applied Mathematical Modelling*, vol. 99, pp. 260–275, 2021.

[22] L. F. Wu, S. F. Liu, W. Cui, D. L. Liu, and T. X. Yao, "Non-homogenous discrete grey model with fractional-order accumulation," *Neural Computing and Applications*, vol. 25, no. 5, pp. 1215–1221, 2014.

[23] P. M. Gao, J. Zhan, and J. F. Liu, "Fractional-order accumulative linear time-varying parameters discrete grey forecasting model," *Mathematical Problems in Engineering*, vol. 63, pp. 1–12, 2019.

Hindawi
Journal of Mathematics
Volume 2021, Article ID 3153731, 13 pages
https://doi.org/10.1155/2021/3153731

Research Article

A Predictive Analysis of the Business Environment of Economies along the Belt and Road Using the Fractional-Order Grey Model

Lingling Pei [1] **and Jun Liu** [2]

[1] *School of Business Administration, Zhejiang University of Finance and Economics, Hangzhou 310018, China*
[2] *School of Economics, Zhejiang University of Finance and Economics, Hangzhou 310018, China*

Correspondence should be addressed to Jun Liu; liujunzjcj@163.com

Received 17 June 2021; Accepted 28 July 2021; Published 3 August 2021

Academic Editor: Lifeng Wu

This paper determined the optimal order of FGM (1, 1) model through particle swarm optimization algorithm and combined with the World Bank business environment data to predict and analyze the business environment of economies along the Belt and Road. The empirical results show that the FGM (1, 1) model has a good predicting effect on the business environment. In terms of prediction accuracy, the FGM (1, 1) model based on particle swarm optimization algorithm to determine the optimal order is significantly better than the traditional GM (1, 1) model. The predict results show that the business environment level of economies along the Belt and Road will increase year by year from 2021 to 2022, but the overall level is still relatively low. The main innovation of this paper lies in the introduction of the fractional-order grey model into the predictive analysis of the business environment, which is of great significance to the extension and application of fractional-order models in management and economic systems.

1. Introduction

In 2013, the Chinese government put forward the Belt and Road initiative, aiming to promote the reasonable flow of factors and effective allocation of resources in the economies along the Belt and Road, improve the level of regional trade and investment facilitation, and explore a new model of international and regional economic cooperation [1]. The Belt and Road initiative has effectively promoted the investment and cooperation between China and countries along the Belt and Road [2]. Lv [3] used the DID method to comprehensively evaluate the investment promotion effect of the Belt and Road initiative and found that the implementation of the Belt and Road initiative significantly promoted the growth of Chinese enterprises' foreign greenfield investment. Previous studies have shown that transnational investment activities of enterprises can bring about multiple effects such as reverse technology spillover, industrial upgrading, and economic growth [4–7]. From the perspective of investment risk, some scholars also pointed out that enterprises face many challenges in the host country's politics, economy, investment policies, and other aspects when carrying out transnational investment activities [8, 9]. Due to the significant differences in the development stages, cultural backgrounds, historical traditions, and institutional conditions of the economies along the Belt and Road, when enterprises conduct transnational investment activities in economies along the Belt and Road, they not only face the challenges of political, economic, and other macrolevel risks but also face the test of the host country's business environment.

The term "Business Environment" is derived from the survey of the "Doing Business" project of the International Finance Corporation of the World Bank Group [10]. As an important indicator to measure the quality of different

business environments, the Business Environment Report issued by the World Bank provides an important reference for investors of various countries to make transnational investment decisions [11]. In view of the importance of the business environment in transnational investment activities, scholars have studied the relationship between the business environment and transnational investment from different perspectives. Corcoran and Gillanders [12] analyzed whether there is any correlation between FDI inflow and the business environment in a country. The empirical results show that there is a strong positive correlation between FDI inflow and the business environment. Based on the panel data of 123 economies in the world from 2009 to 2018, Zhang and Liu [13] empirically analyzed the impact of the business environment on foreign direct investment. The results show that there is a significant positive correlation between the improvement of the host country's business environment and foreign direct investment. Some scholars have also conducted research on the business environment of the economies along the Belt and Road. Based on the OFDI data of Chinese enterprises in 49 representative countries along the Belt and Road from 2007 to 2017, Wang and Zhou [14] investigated the impact of the business environment of the countries along the Belt and Road on the OFDI of Chinese enterprises. It is found that the OFDI with different investment motivations has a heterogeneous preference for the host country's business environment. At present, the existing literature has made a relatively comprehensive exploration on the relationship between the business environment of the host country and FDI, but no scholars have explored the prediction of the business environment. As a supplement to the macroindicators of the institutional environment, the business environment objectively measures the business laws and regulations of various countries and their implementation, which will have a direct impact on the transnational business activities of enterprises. Therefore, using scientific methods to predict the business environment of the economies along the Belt and Road is of great significance for enterprises to reduce the risk of transnational investment and better carry out transnational investment activities.

The grey system theory and prediction model originally proposed by professor Deng can accurately predict the future development trend with "small sample and poor information" data in the real world, which has been widely applied in many fields such as energy, economy, and environment [15]. Several scholars use grey prediction models to predict product sales, customer demand, and development trend in the economic field. For example, Xia and Wong [16] established a seasonal discrete grey prediction model based on cycle truncation accumulation in order to accurately predict inventory data in the apparel retail industry. The problem of seasonality of inventory data and data missing is solved effectively. Nguyen and Tran [17] used GM (1, 1), DGM (1, 1), DGM (2, 1), and Verhulst models to forecast the tourism demand of Vietnam's tourism industry and put forward corresponding policy suggestions to the government. Mao et al. [18], based on the relationship between Chinese commercial banks and third-party online payment systems, used the Grey Lotka–Volterra model to quantitatively analyze and predict the impact of commercial banks' online payment systems on the development of third-party online payment systems. Xiao et al. [19] proposed a new grey multivariable coupling model, CFGM (1, N), to evaluate the coordination degree of China's R & D system and economic system under the condition of limited information. The results show that this model has better convergence and interpretability. On the basis of unequal accumulation, Tu and Chen [20] proposed an unequal adjacent discrete multivariable grey model. Compared with other models, this model has good predictive performance and algorithm efficiency. Rajesh et al. [21] used the grey prediction model and Markov model based on movement probability to predict the retail elasticity level of the urban retail system and then proposed policies to improve the elasticity level of the urban center. In addition to its application in the economic field, due to its simple modeling results and excellent performance, the grey prediction model is currently widely used in energy and environment fields, such as wind power [22], power consumption [23, 24], high-tech industry [25], natural gas consumption [26, 27], and pollution emission [28, 29].

The advantage of the GM (1, 1) model is that it can deal with grey information and poor data, but the model is mainly applicable to the sequence with strong exponential law and can only describe the monotone change process, and it has a big error in some specific fields. In view of the shortcomings of the traditional GM (1, 1) model, Wu et al. [30] first proposed the fractional-order cumulative GM (1, 1) model (FGM (1, 1)). The matrix perturbation theory was used to explain that the traditional integer-order cumulative generating operator violated the new information priority principle of grey system theory and proved that the smaller the cumulative order, the higher the priority of new information. Through accumulation, the characteristics and laws of integration hidden in the original data can be fully revealed. Later, many scholars used the FGM (1, 1) model and the extended model to predict the time series data in different fields, and the error could be effectively reduced by selecting the appropriate fractional order. A large number of examples showed that the prediction accuracy of the FGM (1, 1) model and its extended model was significantly higher than that of the traditional grey prediction model [31–37]. Wu et al. [38] established a new fractional-order prediction model and introduced a fractional cumulative generation matrix to analyze the properties of the model. Yan et al. [39] proposed a grey model with fractionalized Hausdorff derivative to improve the prediction accuracy of the traditional grey model and analyzed the model. The results showed that the model would not be affected by the initial value, and more consideration was given to the principle of new information first. Zhu et al. [40] optimized the initial conditions by introducing the fractional-order weighting

coefficient. Compared with the old initial conditions in the traditional grey model, the newly optimized initial conditions had a flexible structure and could more effectively capture the dynamic characteristics of the time series data. In addition, in order to further improve the prediction accuracy, the particle swarm optimization algorithm (PSO) is used to estimate the adjustable fractional weighting coefficient and the corresponding time parameters of the initial conditions. Liu et al. [41] established a generalized discrete grey prediction model to predict the total retail sales of consumer goods in China by introducing weighted fractional-order accumulation and discretization errors.

By combining the relevant literature, it can be found that the existing literature has made a relatively comprehensive study on the relationship between the business environment and transnational investment, but no scholars have discussed the prediction of the business environment. In terms of prediction theory and model, the existing grey model for environmental prediction research mainly focuses on the fields of pollution emission and energy consumption and has not involved the prediction research on the business environment. Based on this, this paper makes use of the transnational panel data of the World Bank on the business environment from 2014 to 2020 and uses the FGM (1, 1) model to predict and analyze the business environment of 52 economies along the Belt and Road. The innovation lies in the application of the fractional-order grey model in the field of business environment, which broadens the research field of the fractional-order grey model and is of great significance for the expansion of fractional-order models in the field of economic management. The research conclusions are conducive to a clearer understanding of the business environment and future trend of economies along the Belt and Road and provide a reference for enterprises to conduct transnational investment activities in the economies along the Belt and Road.

The rest of this paper is structured as follows: The second part introduces the method of the fractional-order grey model. The third part is the empirical analysis and the discussion of the results, including the determination of the optimal order of the FGM (1, 1) model, the comparison of the prediction accuracy between the GM (1, 1) model and FGM (1, 1) model, and the prediction results of the FGM (1, 1) model. The fourth part is the conclusion.

2. Methods

2.1. A Brief Introduction to the Basic Fractional-Order Grey Model

Definition 1. assume the nonnegative sequence

$$X^{(0)} = \left(x^{(0)}(1), x^{(0)}(2), \ldots, x^{(0)}(n)\right) \tag{1}$$

as the original sequence and let

$$X^{(r)}(k) = \sum_{i=1}^{k} \binom{k-i+r-1}{k-i} x^{(0)}(i), \quad k = 1, 2, \ldots, n \tag{2}$$

be the $r\,(0 < r < 1)$-order accumulated generating operator $(r - AGO)$. We set $\binom{r-1}{0} = 1$, $\binom{k-1}{k} = 0$, $k = 1, 2, \ldots, n$, and

$$\binom{k-i+r-1}{k-i} = \frac{(r+k-i-1)(r+k-i-2), \ldots, (r+1)r}{(k-i)!}, \tag{3}$$

where $X^{(r)} = (x^{(r)}(1), x^{(r)}(2), \ldots, x^{(r)}(n))$ is the $r\,(0 < r < 1)$-order accumulated generation sequence.

Definition 2. Let the nonnegative sequence

$$X^{(0)} = \left(x^{(0)}(1), x^{(0)}(2), \ldots, x^{(0)}(n)\right). \tag{4}$$

Then, let

$$\alpha^{(1)} x^{(1-r)}(k) = x^{(1-r)}(k) - x^{(1-r)}(k-1) \tag{5}$$

be the $r\,(0 < r < 1)$-order inverse accumulated generating operator $(r - \mathrm{IAGO})$, and

$$\begin{aligned} \alpha^{(r)} X^{(0)} &= \alpha^{(1)} X^{(1-r)} \\ &= \left(\alpha^{(1)} x^{(1-r)}(1), \alpha^{(1)} x^{(1-r)}(2), \ldots, \alpha^{(1)} x^{(1-r)}(n)\right) \end{aligned} \tag{6}$$

is the r-order inverse accumulated generation sequence.

Definition 3. Let the nonnegative sequence

$$X^{(0)} = \left(x^{(0)}(1), x^{(0)}(2), \ldots, x^{(0)}(n)\right). \tag{7}$$

The $r\,(0 < r < 1)$-order accumulated generation sequence is

$$X^{(r)} = \left(x^{(r)}(1), x^{(r)}(2), \ldots, x^{(r)}(n)\right). \tag{8}$$

Thus,

$$x^{(r)}(k) - x^{(r)}(k-1) + a z^{(r)}(k) = b \tag{9}$$

is the basic form of the fractional-order GM (1, 1) model (FGM model), where $z^{(r)}(k) = (x^{(r)}(k) + x^{(r)}(k-1))/2, k = 2, 3, \ldots, n$, when $r = 1$, and it transforms into the traditional GM (1, 1) model.

The least square method is used to estimate the parameters of equation (9):

$$\begin{bmatrix} \hat{a} \\ \hat{b} \end{bmatrix} = \left(B^T B\right)^{-1} B^T Y, \tag{10}$$

where

$$Y = \begin{bmatrix} x^{(r)}(2) - x^{(r)}(1) \\ x^{(r)}(3) - x^{(r)}(2) \\ \vdots \\ x^{(r)}(n) - x^{(r)}(n-1) \end{bmatrix}, \quad B = \begin{bmatrix} -z^{(r)}(2) & 1 \\ -z^{(r)}(3) & 1 \\ \vdots & \vdots \\ -z^{(r)}(n) & 1 \end{bmatrix}. \tag{11}$$

According to equation (9), the corresponding whitening equation is

$$\frac{\mathrm{d}x^{(r)}(t)}{\mathrm{d}t} + ax^{(r)}(t) = b. \tag{12}$$

The time response formula of the abovementioned equation is

$$\hat{x}^{(r)}(k+1) = \left[x^{(0)}(1) - \frac{\hat{b}}{\hat{a}}\right]e^{-\hat{a}k} + \frac{\hat{b}}{\hat{a}}, \quad k = 1, 2, \ldots, n. \tag{13}$$

2.2. Optimization of the Fractional Order r Based on Particle Swarm Optimization (PSO) Algorithm. In this paper, particle swarm optimization algorithm is used to optimize the order of the FGM (1, 1) model, in order to minimize the error. Mean Percentage Error (MAPE) is generally used as the main criterion. This algorithm was first proposed by Kennedy and Eberhart [42] in 1995 and originated from the study of simulating the random hunting and predation behavior of birds. The main steps of particle swarm optimization are as follows:

(1) The particle swarm was initialized. The population size was $m = 50$ particles, the search space was D dimension, the learning factor $c_1 = c_2 = 1.2$ was set, and the inertia weight was $w = 0.8$. The particle dimension of the FGM (1, 1) model is set as 1 dimension, which represents the solving parameter r. The positions and velocities of the particles in the initialized particle swarm are as follows:

$$\mathbf{X} = \left(x_1, x_2, \ldots, x_j\right), \quad \mathbf{V} = \left(v_1, v_2, \ldots, v_j\right), \quad j = 1, 2, \ldots, m. \tag{14}$$

(2) calculate the fitness value of each particle according to the fitness algorithm. In this paper, the goal is to minimize the MAPE value, and the mathematical form is expressed as

$$\mathrm{MAPE}_{r\ \min} = \underset{r}{\mathrm{Min}}(F(r)) = \frac{1}{n}\sum_{i=1}^{n}\left|\frac{x^{(0)}(j) - \hat{x}^{(0)}(j)}{x^{(0)}(j)}\right| \times 100\%, \tag{15}$$

$$\text{s.t.}\begin{cases} [\hat{a}\,\hat{b}] = \left(B^T B\right)^{-1} B^T Y, \\ Y = \begin{bmatrix} x^{(r)}(2) - x^{(r)}(1) \\ x^{(r)}(3) - x^{(r)}(2) \\ \vdots \\ x^{(r)}(n) - x^{(r)}(n-1) \end{bmatrix}, \\ B = \begin{bmatrix} -z^{(r)}(2) & 1 \\ -z^{(r)}(3) & 1 \\ \vdots & \vdots \\ -z^{(r)}(n) & 1 \end{bmatrix}, \\ \hat{x}^{(r)}(k+1) = \left[x^{(0)}(1) - \frac{\hat{b}}{\hat{a}}\right]e^{-\hat{a}k} + \frac{\hat{b}}{\hat{a}}, \quad k = 1, 2, \ldots, n, \\ \hat{x}^{(0)}(k) = \left\{\left[\hat{x}^{(r)}(1)\right]^{(-r)}, \left[\hat{x}^{(r)}(1)\right]^{(-r)}, \ldots, \left[\hat{x}^{(r)}(1)\right]^{(-r)}\right\}. \end{cases} \tag{16}$$

(3) use equation (15) to calculate the fitness value of each particle. We compare the current fitness value of each particle with the fitness value of the optimal position p_{best} experienced by the individual and the global optimal position g_{best} and update p_{best} and g_{best}.

(4) optimize the velocity and position, update the velocity and position of the particle according to equations (17) and (18), and limit the velocity within $V_{\max}$.

$$v_{j+1} = wv_j^d + c_1 r_1\left(p_{\text{best}} - x_j^d\right) + c_2 r_2\left(g_{\text{best}} - x_j^d\right), \tag{17}$$

$$x_{j+1}^d = x_j^d + v_j^d, \tag{18}$$

where $j = 1, 2, \ldots, m$, $d = 1, 2, \ldots, D$: r_1, r_2 are random numbers; x_j^d, v_j^d are the current position and velocity of the j_{th} particle, respectively; and p_{best} and g_{best} are, respectively, the optimal position experienced by the j_{th} particle and the optimal position experienced by the whole population.

(5) Judging the termination condition: if the termination condition (MAPE value is small enough or

reaches the maximum number of cycles) is met, we set the maximum number of iterations $T_{\max}$= 500 to terminate the algorithm; otherwise, we return to step 2.

2.3. The Modelling Steps of the FGM (1, 1) Based on PSO Algorithm. The modeling steps of the r-order accumulated grey prediction model based on PSO algorithm are as follows:

Step 1: the r-order accumulated generation sequence is calculated $X^{(r)} = (x^{(r)}(1), x^{(r)}(2), \ldots, x^{(r)}(n))$

Step 2: the least square method is used to estimate the parameters $\begin{bmatrix} \hat{a} \\ \hat{b} \end{bmatrix}$

Step 3: the optimal order r_{best} is obtained based on particle swarm optimization algorithm

Step 4: the predicted value is obtained according to the time response formula of the FGM (1, 1) model

Step 5: finally, the abovepredicted value is reduced to r order to get the final predicted value $\hat{X}^{(0)}$

The specific flow chart is shown in Figure 1.

In order to compare the accuracy of the model and verify the validity and reliability of the model, the MAPE value is selected in this paper to calculate the prediction error [23, 26, 43]. The smaller the MAPE value is, the higher the accuracy of the model is, which can be found using the following formula:

$$\text{MAPE} = \frac{1}{n}\sum_{i=1}^{n}\left|\frac{e(i)}{x^{(0)}(i)}\right| \times 100\%. \tag{19}$$

In formula (19), $e(i) = x^{(0)}(i) - \hat{x}^{(0)}(i)$, $x^{(0)}(i)$ and $\hat{x}^{(0)}(i)$ represent the actual value and predicted value, respectively.

3. Empirical Analysis

3.1. Data Collection. The Belt and Road is an open international regional economic cooperation initiative, taking the Eurasian continent as the main region and gradually extending to relevant countries and regions, without defining clear geographical boundaries. Referring to the research of Guo et al. [44] and combined with data availability, the research objects set in this paper include 52 countries along the Belt and Road. In terms of data on the environment of doing business, the World Bank has issued a yearly report on the environment of doing business since the end of 2003. The latest edition is "Doing Business 2020," which was released in October 2019. Starting from different stages of daily business operations, the report makes a comprehensive evaluation and horizontal comparison of the level of business environment within each economy, which has gained widespread attention worldwide. The ranking of ease of doing business and the reform suggestions put forward by the World Bank's Doing Business Report have not only become an important reference tool for many countries to force domestic reforms, attract capital inflows, and promote economic development but also provide a reference for enterprises to make decisions on transnational investment activities. Because some sample countries lack business environment data before 2014, this paper obtained the original data of the business environment scores of 52 countries along the Belt and Road from 2014 to 2020 by referring to the World Bank's Doing Business database (https://www.doingbusiness.org/) and conducted empirical modeling analysis.

3.2. The Optimal Order Value of the FGM (1, 1) Model. The main advantage of the FGM (1, 1) model is that it can effectively reduce the prediction error by selecting appropriate fractional order, so as to obtain more accurate prediction results. In this paper, particle swarm optimization algorithm is used to solve the optimal order of the FGM (1, 1) model to minimize the prediction error. The calculation results of the optimal order of the FGM (1, 1) model based on particle swarm optimization algorithm are shown in Table 1.

According to the particle swarm optimization given in Sections 2.2 and 2.3 and the optimization steps of the fractional-order grey model based on this algorithm, we take Poland as an example to observe the convergence process of particle swarm optimization. The specific convergence of MAPE is shown in Figure 2. For comparison, the cases of r = 0.1, 0.2, 0.3, 0.4, 0.5, 0.6, 0.7, 0.8, 0.9, and 1 are listed. The actual and predicted values are shown in Table 2, and the error comparison is shown in Table 3. It can be seen that the particle swarm optimization algorithm can quickly find the optimal solution and the optimal parameters of fractional order, so as to effectively reduce the prediction error and improve the prediction accuracy of the model, which indicates that the FGM (1, 1) model based on particle swarm optimization algorithm has good reliability and stability.

3.3. Comparison of Prediction Accuracy between the GM (1, 1) Model and FGM (1, 1) Model. In the process of empirical analysis, this paper divides the original data of the business environment scores of 52 countries along the Belt and Road from 2014 to 2020 into the training set and the testing set. Among them, the business environment score data from 2014 to 2019 are used as the training set and the business environment score data from 2020 are used as the testing set. According to the MAPE value of the GM (1, 1) model and FGM (1, 1) model in the training set and testing set, the prediction ability of the two models in the business environment was compared. The specific MAPE values calculated by the GM (1, 1) model and FGM (1, 1) model in the training set and testing set are shown in Tables 4 and 5. Figures 3 and 4 visually show the difference in accuracy between the GM (1, 1) model and the FGM (1, 1) model in predicting the business environment.

According to the empirical results in Tables 4 and 5, it can be found that, in the training stage, the maximum value of MAPE of the GM (1, 1) model is 5.37%, the minimum value is 0.2%, and the average value is 1.46%. The maximum value of MAPE in the FGM (1, 1) model was 5.26%, the minimum value was 0.11%, and the average value was 0.96%.

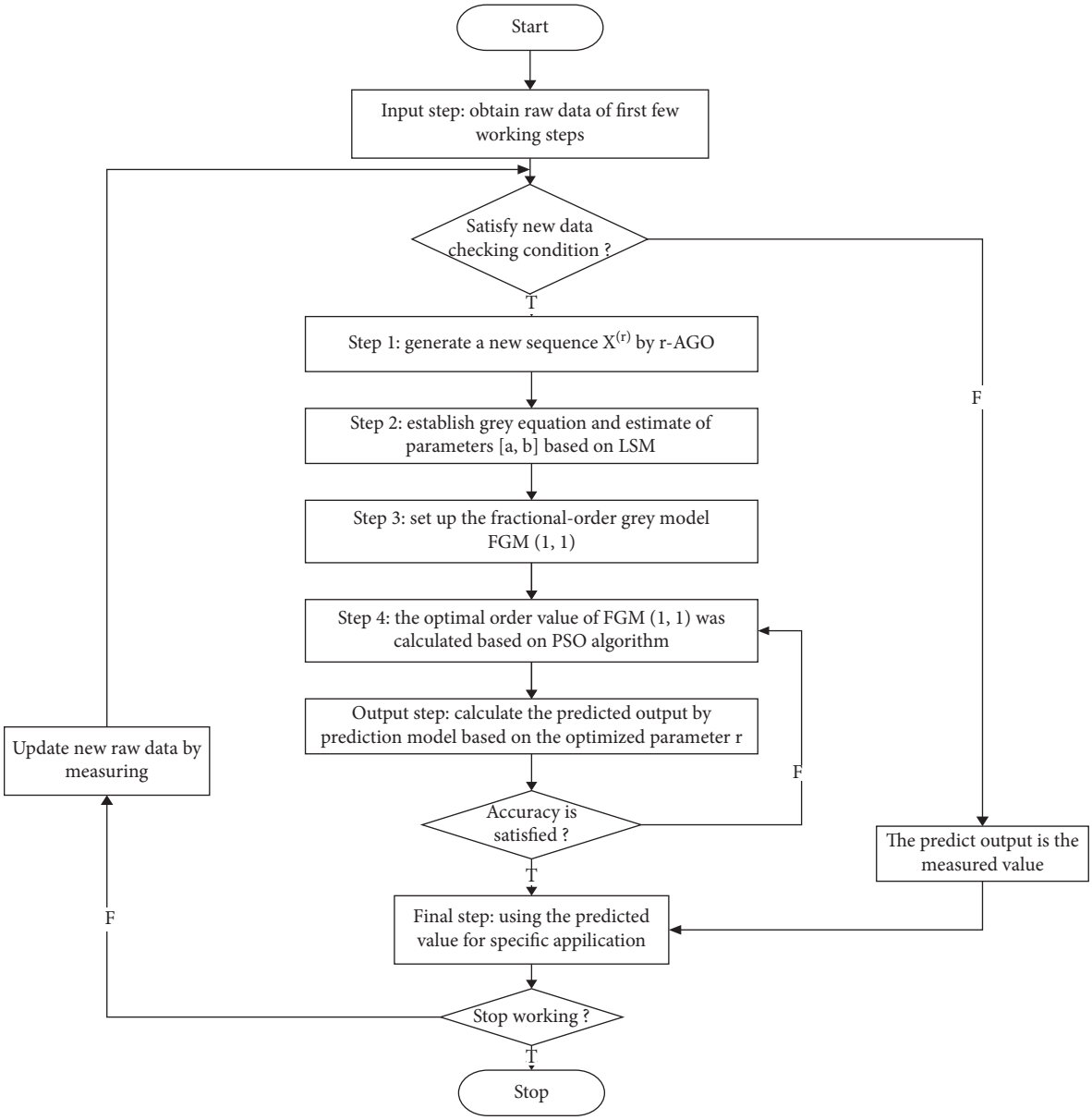

Figure 1: The calculation steps of the FGM (1, 1) model based on PSO algorithm.

Table 1: Optimal order value of FGM (1, 1).

Country	r
Singapore	0.01
Georgia	0.03
Latvia	0.09
Estonia	0.92
Lithuania	0.86
Poland	0.79
Macedonia	0.15
Czech	0.92
Israel	0.02
Slovakia	0.85
Bulgaria	0.06
Slovenia	0.75
Turkey	0.04

Table 1: Continued.

Country	r
Russia	0.83
Qatar	0.01
Hungary	0.88
Montenegro	0.09
Oman	0.06
Bahrain	0.94
Romania	0.19
Croatia	0.86
Armenia	0.94
Belarus	0.25
Mongolia	0.95
Serbia	0.55
Moldova	0.72
Vietnam	0.08
Kazakhstan	0.53
Kuwait	0.01
Indonesia	0.003
Bosnia	0.84
China	1.00
Sri Lanka	0.02
Ukraine	0.99
Egypt	0.08
Lebanon	0.05
Nepal	0.20
Kyrgyzstan	0.03
Brunei	0.07
Jordan	0.02
Albania	0.02
Maldives	0.05
Iran	0.05
Cambodia	0.01
Uzbekistan	0.44
Iraq	0.05
Syria	0.08
Bangladesh	0.05
Lao PDR	0.93
East Timor	0.06
Myanmar	1.00
Afghanistan	0.13

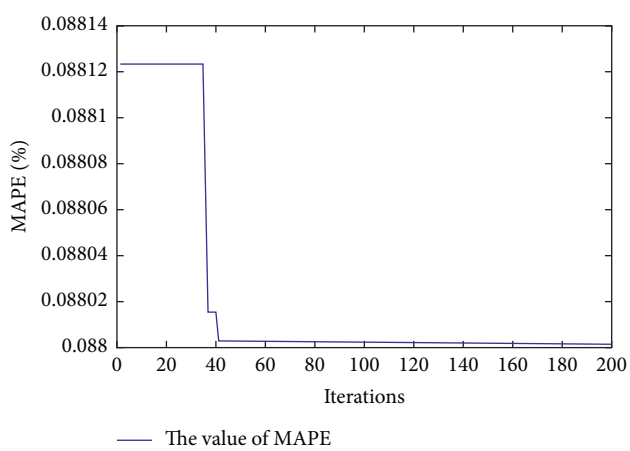

Figure 2: Optimization process of FGM (1, 1) based on PSO algorithm (an example of Poland).

Table 2: Actual values and predicted values (an example of Poland).

Time	Actual value	$r = 0.1$	$r = 0.2$	$r = 0.3$	$r = 0.4$	$r = 0.5$	$r = 0.6$	$r = 0.7$	$r = 0.8$	$r = 0.9$	$r = 1$
2014	73.60	73.60	73.60	73.60	73.60	73.60	73.60	73.60	73.60	73.60	73.60
2015	74.10	74.63	74.29	73.99	73.77	73.65	73.66	73.82	74.15	74.67	75.40
2016	76.90	76.22	76.43	76.62	76.79	76.92	76.98	76.95	76.81	76.52	76.04
2017	77.70	77.08	77.46	77.78	78.02	78.16	78.17	78.05	77.77	77.32	76.69
2018	77.90	77.35	77.53	77.69	77.81	77.87	77.87	77.81	77.70	77.54	77.35
2019	76.90	77.21	76.98	76.79	76.66	76.59	76.61	76.73	76.98	77.40	78.01

Table 3: Error comparison (an example of Poland).

APE (%)	r									
	$r = 0.1$	$r = 0.2$	$r = 0.3$	$r = 0.4$	$r = 0.5$	$r = 0.6$	$r = 0.7$	$r = 0.8$	$r = 0.9$	$r = 1$
	0.00	0.00	0.00	0.00	0.00	0.00	0.00	0.00	0.00	0.00
	0.72	0.25	0.15	0.45	0.60	0.59	0.38	0.06	0.76	1.75
	0.89	0.61	0.36	0.14	0.02	0.10	0.06	0.12	0.50	1.11
MAPE (%)	0.79	0.31	0.10	0.41	0.59	0.61	0.45	0.09	0.49	1.29
	0.71	0.47	0.27	0.12	0.04	0.03	0.11	0.26	0.46	0.71
	0.41	0.10	0.14	0.32	0.40	0.38	0.22	0.11	0.65	1.44
	0.70	0.35	0.20	0.29	0.33	0.29	0.24	0.13	0.57	1.26

Table 4: MAPE values of the training set.

	Training set	
Model Country	GM (1, 1) MAPE (%)	FGM (1, 1) MAPE (%)
Singapore	0.55	0.37
Georgia	1.21	0.96
Latvia	0.53	0.26
Estonia	0.67	0.21
Lithuania	0.82	0.38
Poland	1.26	0.09
Macedonia	1.03	0.31
Czech	0.64	0.13
Israel	0.22	0.19
Slovakia	1.29	0.51
Bulgaria	0.78	0.58
Slovenia	1.60	0.44
Turkey	1.48	1.30
Russia	1.36	0.45
Qatar	0.82	0.68
Hungary	0.79	0.37
Montenegro	0.82	0.51
Oman	0.57	0.50
Bahrain	0.69	0.62
Romania	1.46	0.35
Croatia	1.15	0.33
Armenia	0.45	0.21
Belarus	1.17	0.40
Mongolia	0.43	0.19
Serbia	3.08	1.47
Moldova	1.78	0.52
Vietnam	0.52	0.45
Kazakhstan	2.82	1.14
Kuwait	0.74	0.48
Indonesia	0.61	0.53
Bosnia	1.23	0.32
China	2.49	2.49
Sri Lanka	1.45	0.96

Table 4: Continued.

	Training set	
Model Country	GM (1, 1) MAPE (%)	FGM (1, 1) MAPE (%)
Ukraine	0.40	0.38
Egypt	3.33	1.98
Lebanon	2.04	1.66
Nepal	1.00	0.99
Kyrgyzstan	1.15	1.04
Brunei	1.68	1.40
Jordan	1.64	1.07
Albania	2.66	2.57
Maldives	2.36	1.79
Iran	1.98	1.44
Cambodia	0.34	0.22
Uzbekistan	3.02	1.76
Iraq	2.39	1.73
Syria	1.98	1.50
Bangladesh	2.64	1.76
Lao PDR	0.70	0.28
East Timor	4.49	4.07
Myanmar	0.20	0.20
Afghanistan	5.37	5.26

In the testing stage, the maximum value of MAPE of the GM (1, 1) model was 10.64%, the minimum value was 0.05%, and the average value was 3.19%. The maximum value of MAPE in the FGM (1, 1) model was 8.41%, the minimum value was 0.05%, and the average value was 1.95%. The empirical results show that both the GM (1, 1) model and FGM (1, 1) model have good applicability and accuracy in predicting the business environment, but the FGM (1, 1) model is more accurate in predicting results. The MAPE value of the FGM (1, 1) model was less than 10%, and the average MAPE value of the FGM (1, 1) model was lower than that of the GM (1, 1) model in both the training stage and the testing stage.

Table 5: MAPE values of the testing set.

Model Country	Testing set GM (1, 1) MAPE (%)	FGM (1, 1) MAPE (%)
Singapore	0.99	0.68
Georgia	0.81	1.97
Latvia	1.19	0.52
Estonia	1.51	0.13
Lithuania	1.52	1.10
Poland	2.98	0.93
Macedonia	2.85	0.71
Czech	1.17	0.51
Israel	1.40	1.89
Slovakia	2.08	0.79
Bulgaria	0.55	0.58
Slovenia	3.34	0.84
Turkey	1.94	2.44
Russia	2.61	0.59
Qatar	4.24	0.32
Hungary	2.08	0.28
Montenegro	2.82	0.31
Oman	0.47	1.40
Bahrain	7.02	5.96
Romania	1.30	2.45
Croatia	1.78	1.10
Armenia	0.54	0.80
Belarus	4.79	0.45
Mongolia	1.94	0.81
Serbia	4.23	1.49
Moldova	1.82	2.99
Vietnam	0.95	0.33
Kazakhstan	5.55	0.17
Kuwait	6.92	4.38
Indonesia	0.86	0.19
Bosnia	2.71	0.37
China	4.58	4.58
Sri Lanka	1.28	8.41
Ukraine	1.40	1.33
Egypt	6.36	0.37
Lebanon	3.57	0.05
Nepal	6.03	4.11
Kyrgyzstan	1.65	1.65
Brunei	5.58	5.37
Jordan	10.64	6.97
Albania	2.54	3.35
Maldives	3.06	2.21
Iran	1.83	3.12
Cambodia	0.05	0.78
Uzbekistan	4.94	1.70
Iraq	2.15	1.62
Syria	5.92	1.90
Bangladesh	8.67	0.44
Lao PDR	0.52	1.61
East Timor	7.48	0.89
Myanmar	6.32	6.16
Afghanistan	6.75	5.60

Figures 3 and 4 visually show the difference in prediction accuracy between the GM (1, 1) model and the FGM (1, 1) model. Compared with the traditional GM (1, 1) model, the FGM (1, 1) model has better prediction ability in terms of business environment. Therefore, this paper chooses to predict and analyze the business environment of 52 economies along the Belt and Road based on the FGM (1, 1) model.

3.4. The Predicted Results of the FGM (1, 1) Model. According to the abovementioned empirical results, the FGM (1, 1) model has a good prediction effect in both the training set and the testing set. Based on this, this paper uses the FGM (1, 1) model to predict the business environment scores and rankings of 52 economies along the Belt and Road in 2021 and 2022. The specific predicted results are shown in Tables 6 and 7.

As can be seen from the predicted values of the business environment in Tables 6 and 7, the business environment level of economies along the "Belt and Road" is uneven, and there are great differences among different economies. Specific analysis can be carried out from the following aspects:

(1) In terms of the specific score of the business environment, according to the prediction results of the FGM (1, 1) model, among the 52 economies along the Belt and Road, countries with a score of business environment above 80 in 2021 include Georgia, Singapore, Turkey, Lithuania, and Estonia and countries with scores below 60 include Nepal, Cambodia, Lebanon, Maldives, Laos, Afghanistan, Iraq, Myanmar, Bangladesh, Syria, and Timor, while the scores of other countries were between 60 and 80. Business environment score was over 80 in 2022, including Georgia, Turkey, Singapore, Brunei, and China, and below 60 points, including Cambodia, Afghanistan, Maldives, Lebanon, Laos, Bangladesh, Iraq, Brunei, East Timor, and Syria, and the rest is between 60 to 80 points. According to the World Bank's Doing Business 2020 report, the No. 1 economy is New Zealand, with a score of 86.8. Among the 52 economies along the Belt and Road, most of the sample countries' business environment scores are between 60 and 80 points, indicating that their overall level needs to be improved. In terms of business environment ranking, according to the prediction results of the FGM (1, 1) model, among the 52 economies along the Belt and Road, the top five economies in 2021 are Georgia, Singapore, Turkey, Lithuania, and Estonia and the bottom five economies are Iraq, Myanmar, Bangladesh, Syria, and East Timor. The top five economies in 2022 are Georgia, Turkey, Singapore, Brunei, and China, while the bottom five are Iraq, Bangladesh, Myanmar, East Timor, and Syria.

(2) In terms of changes in the overall level of the business environment, according to the predicted results of the FGM (1, 1) model, the average level of the business environment in 52 economies along the Belt and Road will increase year by year from 2021 to 2022, but the increase is slow and the overall level is still low. The forecast average score for 2021 and

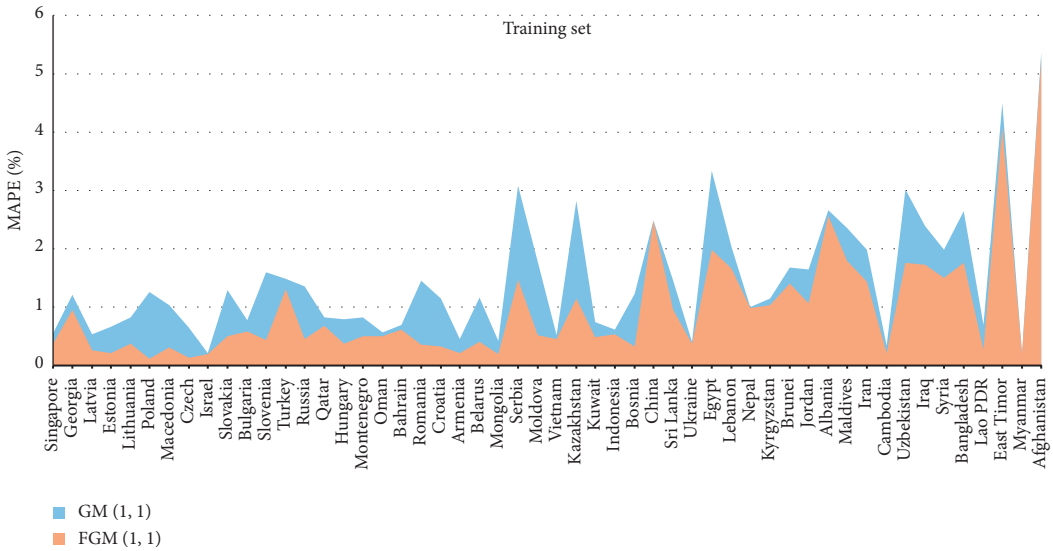

Figure 3: MAPE comparison between GM (1, 1) and FGM (1, 1) in the training set.

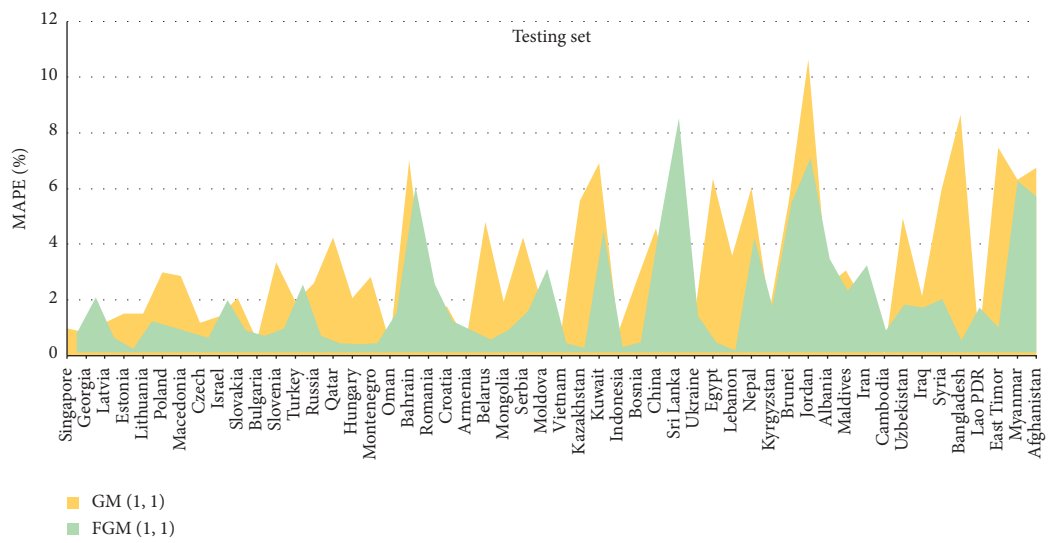

Figure 4: MAPE comparison between GM (1, 1) and FGM (1, 1) in the testing set.

2022 is 68.30 and 69.17, respectively. According to the prediction results of the FGM (1, 1) model, among the 52 economies along the Belt and Road, economies with an upward trend in business environment scores in 2021 and 2022 include Georgia, Turkey, Singapore, Brunei, Armenia, Indonesia, Ukraine, Kyrgyzstan, Vietnam, Qatar, Albania, Mongolia, Sri Lanka, Egypt, Iran, Cambodia, Afghanistan, Maldives, Iraq, and East Timor and economies with a downward trend in business environment scores in 2021 and 2022 include Lithuania, Estonia, Latvia, Macedonia, Russia, Czech, Slovakia, Slovenia, Serbia, Hungary, Poland, Croatia, Romania, Bulgaria, Moldova, Uzbekistan, Bosnia, Lebanon, and Syria. Brunei, Turkey, Afghanistan, Iran, and Georgia are the top five countries in terms of improvement in the business environment in 2021. The top five countries with a decline in the level of the business environment in 2021 are Moldova, Bahrain, Nepal, Romania, and Myanmar. Jordan, Turkey, Brunei, Afghanistan, and Kuwait are the top five countries in terms of improvement in the business environment in 2022. The top five countries with a decline in the level of the business environment in 2021 are Poland, Moldova, Romania, Slovenia, and Serbia.

Table 6: Predicted score and ranking for 2021.

Ranking	Country	Score
1	Georgia	86.99
2	Singapore	86.90
3	Turkey	83.25
4	Lithuania	80.32
5	Estonia	80.06
6	Macedonia	79.78
7	Kazakhstan	79.70
8	Latvia	79.64
9	Brunei	78.03
10	Russia	77.78
11	China	77.50
12	Israel	75.97
13	Czech	75.39
14	Slovenia	74.97
15	Armenia	74.82
16	Belarus	74.48
17	Slovakia	74.37
18	Poland	74.23
19	Montenegro	74.17
20	Serbia	74.10
21	Hungary	73.11
22	Ukraine	72.98
23	Indonesia	72.70
24	Bahrain	72.68
25	Croatia	72.38
26	Vietnam	71.42
27	Bulgaria	71.25
28	Moldova	71.07
29	Kyrgyzstan	70.41
30	Romania	70.37
31	Oman	69.26
32	Uzbekistan	68.99
33	Albania	68.98
34	Mongolia	68.84
35	Qatar	68.76
36	Jordan	68.33
37	Kuwait	67.27
38	Bosnia	64.67
39	Sri Lanka	64.35
40	Egypt	62.55
41	Iran	62.44
42	Nepal	59.91
43	Cambodia	54.60
44	Lebanon	53.92
45	Maldives	53.60
46	Lao PDR	50.46
47	Afghanistan	50.32
48	Iraq	45.99
49	Myanmar	44.25
50	Bangladesh	44.04
51	Syria	39.77
52	East Timor	39.65

Table 7: Predicted score and ranking for 2022.

Ranking	Country	Score
1	Georgia	89.04
2	Turkey	88.99
3	Singapore	87.88
4	Brunei	82.63
5	China	80.81
6	Lithuania	79.78
7	Kazakhstan	79.58
8	Estonia	79.51
9	Latvia	79.19
10	Macedonia	79.04
11	Russia	77.62
12	Israel	76.38
13	Armenia	75.62
14	Indonesia	75.31
15	Ukraine	74.88
16	Czech	74.78
17	Bahrain	74.39
18	Jordan	74.25
19	Montenegro	74.11
20	Belarus	73.98
21	Slovenia	73.81
22	Slovakia	73.56
23	Kyrgyzstan	73.30
24	Serbia	73.25
25	Hungary	72.88
26	Vietnam	72.60
27	Poland	72.52
28	Croatia	71.80
29	Kuwait	71.36
30	Qatar	71.01
31	Bulgaria	70.90
32	Albania	69.69
33	Moldova	69.68
34	Oman	69.33
35	Mongolia	69.26
36	Romania	69.17
37	Uzbekistan	68.82
38	Sri Lanka	66.23
39	Egypt	66.09
40	Iran	65.17
41	Bosnia	64.03
42	Nepal	60.02
43	Cambodia	55.15
44	Afghanistan	54.73
45	Maldives	53.87
46	Lebanon	53.75
47	Lao PDR	50.58
48	Iraq	47.02
49	Bangladesh	45.63
50	Myanmar	44.65
51	East Timor	39.70
52	Syria	39.37

4. Conclusions

Based on the fractional-order grey model, this paper makes a predict analysis on the business environment of 52 economies along the Belt and Road by using the business environment data of the World Bank from 2014 to 2020. The main conclusions are as follows:

(1) The GM (1, 1) model and FGM (1, 1) model both have good applicability and accuracy in predicting the business environment, but the FGM (1, 1) model is more accurate in predicting results. The empirical results show that the MAPE values of the FGM (1, 1) model in both the training set and the testing set are less than 10%, indicating that the prediction results of the business environment of economies along the Belt and Road based on the FGM (1, 1) model have good robustness. Meanwhile, the average MAPE values of the FGM (1, 1) model is lower than that of the GM (1, 1) model, indicating that the FGM (1, 1) model has better predictive ability in terms of business environment compared with the traditional GM (1, 1) model.

(2) There are significant differences in the level of business environment among different economies along the Belt and Road. Countries such as Georgia, Singapore, Turkey, Lithuania, and Estonia are at the forefront of the world's business environment, while Nepal, Cambodia, Lebanon, Maldives, and Laos have much room for improvement. Most other countries are in the middle. The overall level of the business environment of the economies along the Belt and Road is still low, but it will improve year by year. There are significant differences in the trend and degree of change of the business environment in different economies along the Belt and Road. In terms of changing trends, the economies showing an upward trend in the business environment in 2021 and 2022 include Georgia, Turkey, and Singapore, while the economies showing a downward trend include Lithuania, Estonia, and Latvia. In terms of the range of change, countries with big increases in the level of the business environment in 2021 include Brunei, Turkey, and Afghanistan. Countries with big declines in the level of the business environment in 2021 include Moldova, Bahrain, and Nepal. Countries with big increases in the level of the business environment in 2022 include Jordan, Turkey, and Brunei. Countries with big declines in the level of the business environment in 2022 include Poland, Moldova, and Romania.

Data Availability

The business environment score data used to support the findings of this study are available through the World Bank Doing Business database (https://www.doingbusiness.org/).

Conflicts of Interest

The authors declare that the research was conducted in the absence of any conflicts of interest.

Acknowledgments

This research was supported by the Humanities and Social Science Research Fund of the Ministry of Education of China (Grant no. 18YJC630130).

References

[1] R. Z. Yang and Q. Wei, "Research on international direct investment rules and China's plan under the belt and road initiative," *Intertrade*, vol. 4, pp. 38–44, 2018.

[2] K. P. B. Cullinane, P. T.-W. Lee, Z. Yang, and Z.-H. Hu, "Editorial: China's belt and road initiative," *Transportation Research Part E: Logistics and Transportation Review*, vol. 117, pp. 1–4, 2018.

[3] Y. Lv, Y. Lu, S. B. Wu, and Y. Wang, "The effect of the belt and road initiative on firms' OFDI: evidence from China's greenfield investment," *Economic Research Journal*, vol. 54, no. 9, pp. 187–201, 2019.

[4] L. Branstetter, "Is foreign direct investment a channel of knowledge spillovers? evidence from Japan's FDI in the United States," *Journal of International Economics*, vol. 68, no. 2, pp. 325–344, 2006.

[5] A. J. Hijzen, I. Tomohiko, and T. Yasuyuki, *The Effects of Multinational Production on Domestic Performance: Evidence from Japanese Firms*, Research Institute of Economy, Trade and Industry (RIETI), Tokyo, Japan, 2007.

[6] J. E. Haskel, S. C. Pereira, and M. J. Slaughter, "Does inward foreign direct investment boost the productivity of domestic firms?" *Review of Economics and Statistics*, vol. 89, no. 3, pp. 482–496, 2007.

[7] L.-S. Lau, C.-K. Choong, and Y.-K. Eng, "Investigation of the environmental kuznets curve for carbon emissions in Malaysia: do foreign direct investment and trade matter?" *Energy Policy*, vol. 68, pp. 490–497, 2014.

[8] P. J. Buckley, L. J. Clegg, A. R. Cross, X. Liu, H. Voss, and P. Zheng, "The determinants of Chinese outward foreign direct investment," *Journal of International Business Studies*, vol. 38, no. 4, pp. 499–518, 2007.

[9] K. Hayakawa, F. Kimura, and H.-H. Lee, "How does country risk matter for foreign direct investment?" *The Developing Economies*, vol. 51, no. 1, pp. 60–78, 2013.

[10] P. X. Luo, *The World Bank's Doing Business Assessment: Methodology, Rules and Case*sp. 1, 1st edition, Yilin Press, Nanjing, China, 2020.

[11] Z.-X. Wang, W.-Q. Lou, and L.-L. Pei, "Evaluation of the business environment of participating countries of the Belt and Road Initiative," *Technological and Economic Development of Economy*, vol. 26, no. 6, pp. 1339–1365, 2020.

[12] A. Corcoran and R. Gillanders, "Foreign direct investment and the ease of doing business," *Review of World Economics*, vol. 151, no. 1, pp. 103–126, 2015.

[13] Y. W. Zhang and L. B. Liu, "Does the improvement of business environment promote foreign direct investment?" *International Business*, vol. 1, pp. 59–68, 2020.

[14] Z. X. Wang and Q. Zhou, "How business environment affects Chinese enterprises' OFDI to countries along "the belt and road"," *Collected Essays on Finance and Economics*, vol. 9, pp. 42–52, 2019.

[15] S. Liu, Y. Yang, N. Xie, and J. Forrest, "New progress of grey system theory in the new millennium," *Grey Systems: Theory and Application*, vol. 6, no. 1, pp. 2–31, 2016.

[16] M. Xia and W. K. Wong, "A seasonal discrete grey forecasting model for fashion retailing," *Knowledge-Based Systems*, vol. 57, pp. 119–126, 2014.

[17] N. T. Nguyen and T. T. Tran, "Optimizing mathematical parameters of grey system theory: an empirical forecasting case of Vietnamese tourism," *Neural Computing and Applications*, vol. 31, no. 2, pp. 1075–1089, 2017.

[18] S. H. Mao, M. Zhu, X. P. Wang, and X. P. Xiao, "Grey–Lotka–Volterra model for the competition and cooperation between third-party online payment systems and online banking in china," *Applied Soft Computing*, vol. 95, 2020.

[19] Q. Xiao, M. Shan, M. Gao, X. Xiao, and H. Guo, "Evaluation of the coordination between China's technology and economy using a grey multivariate coupling model," *Technological and Economic Development of Economy*, vol. 27, no. 1, pp. 24–44, 2020.

[20] L. Tu and Y. Chen, "An unequal adjacent grey forecasting air pollution urban model," *Applied Mathematical Modelling*, vol. 99, pp. 260–275, 2021.

[21] R. Rajesh, A. K. Agariya, and C. Rajendran, "Predicting resilience in retailing using grey theory and moving probability based markov models," *Journal of Retailing and Consumer Services*, vol. 62, 2021.

[22] J. Xia, X. Ma, W. Q. Wu, B. L. Huang, and W. P. Li, "Application of a new information priority accumulated grey model with time power to predict short-term wind turbine capacity," *Journal of Cleaner Production*, vol. 244, 2020.

[23] S. Ding, K. W. Hipel, and Y.-G. Dang, "Forecasting China's electricity consumption using a new grey prediction model," *Energy*, vol. 149, pp. 314–328, 2018.

[24] Z.-X. Wang, Q. Li, and L.-L. Pei, "A seasonal GM(1,1) model for forecasting the electricity consumption of the primary economic sectors," *Energy*, vol. 154, pp. 522–534, 2018.

[25] H.-H. Zheng, Q. Li, and Z.-X. Wang, "Predicting the capital intensity of the new energy industry in China using a new hybrid grey model," *Computers & Industrial Engineering*, vol. 126, pp. 507–515, 2018.

[26] W. Wu, X. Ma, B. Zeng, W. Lv, Y. Wang, and W. Li, "A novel Grey Bernoulli model for short-term natural gas consumption forecasting," *Applied Mathematical Modelling*, vol. 84, pp. 393–404, 2020.

[27] Z.-X. Wang and Q. Li, "Modelling the nonlinear relationship between CO_2 emissions and economic growth using a PSO algorithm-based grey verhulst model," *Journal of Cleaner Production*, vol. 207, pp. 214–224, 2019.

[28] Z. X. Wang and Y. Q. Jv, "A non-linear systematic grey model for forecasting the industrial economy-energy-environment system," *Technological Forecasting and Social Change*, vol. 167, 2021.

[29] P.-P. Xiong, W.-J. Yan, G.-Z. Wang, and L.-L. Pei, "Grey extended prediction model based on IRLS and its application on smog pollution," *Applied Soft Computing*, vol. 80, pp. 797–809, 2019.

[30] L. Wu, S. Liu, L. Yao, S. Yan, and D. Liu, "Grey system model with the fractional order accumulation," *Communications in Nonlinear Science and Numerical Simulation*, vol. 18, no. 7, pp. 1775–1785, 2013.

[31] L. Wu, N. Li, and Y. Yang, "Prediction of air quality indicators for the Beijing-Tianjin-Hebei region," *Journal of Cleaner Production*, vol. 196, pp. 682–687, 2018.

[32] H. J. Chen, Y. Z. Tong, and L. F. Wu, "Forecast of energy consumption based on FGM (1, 1) model," *Mathematical Problems in Engineering*, vol. 43, 2021.

[33] S. H. Mao, Y. X. Kang, Y. H. Zhang, X. P. Xiao, and H. M. Zhu, "Fractional grey model based on non-singular exponential kernel and its application in the prediction of electronic waste precious metal content," *ISA Transactions*, vol. 43, 2020.

[34] W. L. Xie, C. X. Liu, W. Z. Wu, W. D. Li, and C. Liu, "Continuous grey model with conformable fractional derivative," *Chaos, Solitons & Fractals*, vol. 139, 2020.

[35] C. L. Zheng, W. Z. Wu, W. L. Xie, and Q. Li, "A MFO-based conformable fractional nonhomogeneous grey bernoulli model for natural gas production and consumption forecasting," *Applied Soft Computing*, vol. 99, 2021.

[36] N. Li, J. L. Wang, L. F. Wu, and Y. M. Bentley, "Predicting monthly natural gas production in china using a novel grey seasonal model with particle swarm optimization," *Energy*, vol. 215, 2021.

[37] C. Liu, W. Z. Wu, W. L. Xie, and J. Zhang, "Application of a novel fractional grey prediction model with time power term to predict the electricity consumption of India and China," *Chaos, Solitons & Fractals*, vol. 141, 2020.

[38] W. Q. Wu, X. Ma, B. Zeng, Y. Wang, and W. Cai, "Application of the novel fractional grey model FAGMO(1,1) k) to predict China's nuclear energy consumption," *Energy*, vol. 165, pp. 223–234, 2018.

[39] C. Yan, L. F. Wu, L. Y. Liu, and Z. Kai, "Fractional Hausdorff grey model and its properties," *Chaos, Solitons & Fractals*, vol. 138, 2020.

[40] X. Y. Zhu, Y. G. Dang, and S. Ding, "Using a self-adaptive grey fractional weighted model to forecast jiangsu's electricity consumption in China," *Energy*, vol. 190, 2020.

[41] C. Liu, W. L. Xie, W. Z. Wu, and H. Zhu, "Predicting Chinese total retail sales of consumer goods by employing an extended discrete grey polynomial model," *Engineering Applications of Artificial Intelligence*, vol. 102, 2021.

[42] J. Kennedy and R. Eberhart, "Particle-swarm-optimization," in *Proceedings of IEEE International Conference on Neural Networks*, pp. 1942–1948, Perth, Australia, December 1995.

[43] C. D. Lewis, *Industrial and Business Forecasting Methods*, Butterworth scientific, London, UK, 1982.

[44] Y. Guo and C. S. Xu, "Meetings between high-ranking officials and kroute," *Journal of International Trade*, vol. 2, pp. 26–36, 2016.

Hindawi
Journal of Mathematics
Volume 2021, Article ID 5098378, 9 pages
https://doi.org/10.1155/2021/5098378

Research Article

Electric Vehicle Charging Station Location Decision Analysis for a Two-Stage Optimization Model Based on Shapley Function

Lifeng Yang,[1] **Zhongwei Cheng**,[1] **Baojie Zhang**,[2] **and Fengyun Ma**[3]

[1]*School of Economics, Fuyang Normal University, Fuyang 236037, China*
[2]*School of Business, Fuyang Normal University, Fuyang 236037, China*
[3]*Hebei North Diesel Engine Co., Ltd., Zhongshan West Road 198, Shijiazhuang 050081, China*

Correspondence should be addressed to Zhongwei Cheng; 2019111061@stu.fynu.edu.cn and Baojie Zhang; 19210501@stu.fynu.edu.cn

Received 30 May 2021; Accepted 23 July 2021; Published 2 August 2021

Academic Editor: Kenan Yildirim

The promotion of electric vehicles and their charging facilities to achieve carbon emission reduction is a research hotspot in the field of transportation. Aiming at the comprehensive decision of electric vehicle charging station (EVCS) location, this paper constructs an EVCS location evaluation index system that includes five indexes of grid load, traffic facilities, user preference, construction cost, and service radius. Firstly, we convert the exact number into interval judgment matrix, introduce Shapley fuzzy measure to calculate the weight of factors, and use the two-stage optimization model to further optimize the weight. Then, we combine the multiple criteria decision-making (MCDM) method in the Pythagorean fuzzy environment with partitioned normalized weighted Bonferroni mean (PFPNWBM) operator, and calculate the optimal ranking of alternatives according to the performance function and the accuracy function. Finally, a numerical example is used to analyze the difference between first-order linear optimization and two-stage optimization in alternative scheme evaluation, and the practical value of using model to evaluate EVCS location is verified.

1. Introduction

Under the pressure of carbon emission reduction and carbon neutrality, the promotion and use of new energy vehicles represented by electric vehicles are becoming increasingly popular. The location and construction of EVCS have attracted extensive attention in the academic community [1]. EVCS location is affected by many objective and subjective factors such as service radius [2], electric vehicle (EV) mileage [3], and user preference [4]. There is great uncertainty in the decision-making process [5], and it becomes increasingly impossible to assign accurate values in the evaluation scheme [6]. Fuzzy set theory [7] and MCDM model [8], which rely on subjective judgment data selection, are often used in the scheme selection of such problems [9].

The evaluation form of ordinary fuzzy sets cannot adequately describe the actual situation related to a large number of fuzziness and uncertainties [10]. To cope with this challenge, Zeng et al. [11] proposed the concepts of weighted double hesitation fuzzy set (WDHFS) and weighted double hesitation fuzzy element (WDHFE) and applied them to group decision-making. Fan and Xiao [12] proposed a two-dimensional intuitionistic fuzzy set (TDIFS) model to integrate the uncertainty and reliability expression of intuitionistic fuzzy set (IFS), which can carry more information than simple indexes. In order to accurately reflect the relative relationship between alternatives, Tao et al. [13] extended the classical alternative queuing method (AQM) by using fuzzy preference relation (FPR). However, since IFS can only describe the case where the sum of membership and non-membership does not exceed 1 [14], Yager and Abbasov [15] successfully extended IFS to Pythagorean fuzzy set (PFS), which allows a larger space to describe certain, uncertain, and hesitant information. PFS method is used in the selection of electric bicycle sharing recycling suppliers [16], on-site evaluation of household waste processing plants [17],

and other optimization scheme selection decisions. Due to the uncertainty of the reality in the Pythagorean fuzzy environment, the choice of weight is often restricted by objective constraints. Based on this, Nie et al. [18] defined the constraints of incomplete known weights and built a linear programming model with the maximum performance value of the alternatives schemes as the optimal goal. The weight acquisition process of Shapley fuzzy metric was optimized.

In addition, Wang et al. [19] developed a rapid charging facility planning model by considering battery deterioration and vehicle heterogeneity within the driving range. The corresponding MCDM conceptual framework is also widely used in location decisions. Ni et al. [20], in the framework of MCDM, proposed a comprehensive model to characterize vaccination decision-making process influenced by society. Gao et al. [21] suggested a MCDM method based on probabilistic language term set and regret theory. For the significance of Shapley fuzzy measure method in measuring the importance of elements and the interaction characteristics of combinations between elements, Tan et al. [22] used Shapley comprehensive authorization benefit distribution method to analyze the energy storage and charging pile project. And this method is often used in conjunction with MCDM to study program decision-making problems. Jing et al. [23] proposed a decision-making method of integrated product conceptual scheme based on Shapley value method and fuzzy logic model.

Yang and Ma [24] believed that, with the increase of the order of the judgment matrix, the granularity of the scale is not meticulous enough, which limits the consistency of the judgment matrix. There is a trade-off between simplicity and precision when choosing a digital scale. Pasman and Rogers [25] proposed that expert opinions are enveloped in uncertainty, which includes accidental uncertainty (lack of accuracy and precision observation means) and cognitive uncertainty (quantity and quality of data). Xu and Hua [26] found that, in view of the differences in professional knowledge, problem familiarity, social background, and other aspects of the evaluation team members, they are more inclined to represent the evaluation situation by their own preferred information forms, so that the evaluation results often present a complex situation where multiple types of information coexisted. Due to the difficulty and contradiction of subjective judgment, as well as the time pressure, incomplete relative information of factors in the decision-making process, limitations of experts' expertise, and other reasons [27], Teng and Liu [28] proposed a new large group decision method in probabilistic language to analyze the interaction between interest subgroups and the relationship between criteria. Li [29] believed that because different quantitative attributes have different physical dimensions, normalization processing is needed to transform the exact number into an interval fuzzy number with membership degree and nonmembership degree.

In Section 2, we briefly review the concepts of PFS and Shapley fuzzy measure on the basis of existing research results. In Section 3, based on the review of relevant research literature, a systematic and complete evaluation index system of EVCS is constructed, and then an empirical study is conducted on 5 regions with large charging demand. In Section 4, we establish a two-stage optimization model to identify the optimal Shapley fuzzy measure under the background that incomplete weight information is known, which is the basis for determining the standard weight. Then, based on the PFPNWBM operator, performance, and accuracy function, the comprehensive performance value of each alternative scheme is calculated, so as to determine the optimal scheme ranking. Section 5 provides detailed resolution steps. Section 6 illustrates the availability of the proposed method through an example. Finally, Section 7 compares the differences between the optimal Shapley fuzzy measure identified by the two-stage dynamic optimization model and the first-order linear optimization model through a numerical example. The research proves that the evaluation index system and the evaluation method have good practicability, accuracy, and flexibility.

In summary, from the perspective of EVCS location decision analysis, this paper constructs a comprehensive and systematic EVCS location evaluation index system that includes five indexes of grid load, traffic facilities, user preference, construction cost, and service radius. And the heterogeneity of experts and the incomplete information of the weights in the evaluation are well dealt with by establishing a two-stage optimization model to identify the optimal Shapley fuzzy measure, which provides some theoretical support and practical methods for EVCS location construction.

2. Preliminaries

In this section, some basic concepts and theoretical methods are introduced, which conclude IFS, PFS, and Shapley function.

2.1. Intuitionistic Fuzzy Set

Definition 1 (see [30]). Let X be a finite universe of discourse. $A = \{\langle x, \mu_A(x), \nu_A(x) | x \in X\rangle\}$ is defined as an IFS with the condition:

$$\begin{aligned} &\mu_A(x), \nu_A(x)\colon X \longrightarrow [0,1], \\ &0 \le \mu_A(x) + \nu_A(x) \le 1. \end{aligned} \tag{1}$$

The $\mu_A(x)$, $\nu_A(x)$ is the membership degree of $x \in X$ indicating the degree of support and unsupported.

2.2. Pythagorean Fuzzy Set

Definition 2 (see [31]). Let X be the domain of argument. $A = \{\langle x, A(\mu_A(x), \nu_A(x))\rangle, | x \in X\}$ is a PFS on X, where $\mu_A(x), \nu_A(x)\colon X \longrightarrow [0,1]$ represents the membership and nonmembership of element X to A and $0 \le (\mu_A(x))^2 + (\nu_A(x))^2 \le 1$, respectively. The degree of indeterminacy $\pi_A(x)$ is expressed by $\pi_A(x) = \sqrt{1 - (\mu_A(x))^2 - (\nu_A(x))^2}$.

Definition 3 (see [32]). Let $a = A(\mu_a, v_a)$ be a PFN, and its score function and accuracy function are defined as follows:

$$\begin{aligned} S(a) &= \mu_a^2 - v_a^2, \\ H(a) &= \mu_a^2 + v_a^2, \quad \text{where } S(a), H(a) \in [0,1]. \end{aligned} \tag{2}$$

Definition 4 (see [33]). Let $a_1 = A(\mu_{a_1}, v_{a_1})$ and $a_2 = A(\mu_{a_2}, v_{a_2})$ be two PFNs. Then, the distance between a_1 and $a_2$is expressed as

$$d(a_1, a_2) = \sqrt{\frac{1}{2}\left[\left(\left(\mu_{a_1}\right)^2 - \left(\mu_{a_2}\right)^2\right)^2 + \left(\left(v_{a_1}\right)^2 - \left(v_{a_2}\right)^2\right)^2 + \left(\left(\pi_{a_1}\right)^2 - \left(\pi_{a_2}\right)^2\right)^2\right]}. \tag{3}$$

As shown in Figure 1, the applicable scope of PFS and IFS is 1/4 circle and right triangle in the first quadrant of the plane Cartesian coordinate system, respectively. Obviously, the use range of PFS is larger than that of IFS, so PFS has a wider computing space.

2.3. Shapley Function

Definition 5 (see [34]). Let X be a finite set, and $P(x)$ is the power set of X. The fuzzy measure μ defined on X: $P(x) \longrightarrow [0,1]$ satisfies the following conditions:

(1) $\mu(\Phi) = 0, \mu(X) = 1$

(2) If $A, B \in P(x)$ and $A \subseteq B$, then $\mu(A) \subseteq \mu(B)$

Shapley function is used to measure the income distribution of each member alliance in the game. With respect to the fuzzy measure $\mu(A)$ on the finite set defined as above, it can be expressed as

$$\varphi_i(\mu, N) = \mu(i) = \sum_{S \subseteq N/i} \frac{(n-s-1)!s!}{n!} (\mu(S \cup i) - \mu(i)), \quad \forall i \in N. \tag{4}$$

3. The Evaluation Index System of EVCS Location

With the rapid development of EV technology, EV has become a major participant in the future development of new energy vehicles. However, due to the limited number of fast chargers and the increase of residents' charging demands, EV charging operation may encounter the problems of increased queuing delay and increased charging operation costs [35]. To this end, governments around the world are promoting the use of EV in possible ways and issuing various preferential policies to encourage EV enterprises to cooperate with energy companies to build EVCS [4]. Therefore, establishing a comprehensive and complete EVCS location evaluation index system is the most effective way to promote the popularization of EV and solve the contradiction between supply and demand. Based on relevant literature review and analysis, we select the following five indicators from 10 indicators, such as grid load, traffic facilities, user preference, construction cost, service radius, EV ownership, driving mileage, policy support, regional service level, and elastic demand [2–4, 35–37].

3.1. Grid Load. Strong grid load capacity is the basic requirement of EVCS construction. Grid load refers to the ability of regional grid to withstand voltage load. The simultaneous charging of many vehicles in a fixed station by quick charging technology may produce huge additional demands on the power grid and may lead to power loss, which is bound to have certain requirements on the bearing capacity and supply level of grid.

3.2. Traffic Facilities. The location of EVCS directly affects the cost of driving on the road for vehicle owners (time and energy consumption on the way to the charging station). Electric vehicle users will give priority to EVCS with short travel distance and convenient road passage, so as to reduce driving costs. Therefore, the perfection of regional traffic facilities, namely, the minimization of customer travel costs is an important factor affecting EVCS location.

3.3. User Preference. User preference is mainly for users themselves, that is, drivers may form the habit of charging battery electric vehicle (BEV) after daily travel, including the battery capacity of the purchased electric vehicles, the acceptable charging time, the familiarity with public charging stations and travel mode (total travel duration of the next travel day, day interval between the start of the next travel and the start of the current charging event), etc.

3.4. Construction Cost. EVCS location should minimize the total cost and network loss cost of the charging station during the planning period as the goal of the optimal planning of the charging station [38]. The construction cost of charging station

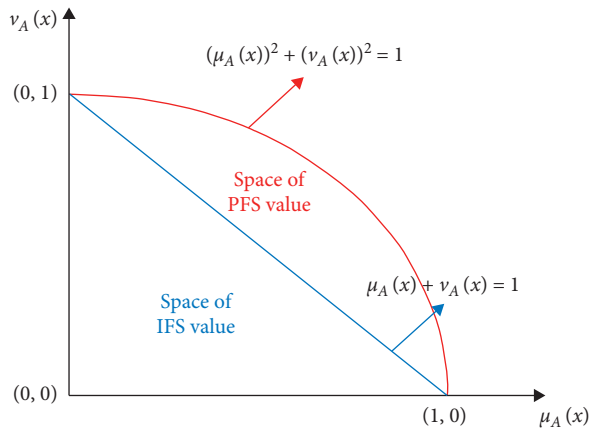

Figure 1: IFS and PFS applicable scope comparison.

location includes investment cost, operating cost, and maintenance cost. Among them, investment cost refers to the investment cost per unit capacity of transformers and charging equipment, investment cost per unit capacity of other equipment except transformers and charging equipment, and land use cost. Operating cost includes charging cost, electric energy consumption cost of electrical equipment, filtering compensation cost of charging station, and labor cost. Maintenance cost refers to the maintenance cost per unit capacity of transformers and charging equipment and the maintenance cost per unit capacity of other equipment except transformers and charging equipment.

3.5. Service Radius. When the number of charging station is large, the smaller the Voronoi diagram area of the service area of the corresponding charging stations is, the lower the driving cost of the vehicle owner will be. In order to maximize EV battery cycle life and EVCS resources, on the premise of satisfying users' charging needs, the service radius of charging station should be less than the actual distance between two adjacent charging stations under the premise of meeting the charging needs of the user and at most equal to the reasonable continuous driving distance of electric vehicle at a constant speed.

4. EVCS Location Evaluation Method

4.1. Conversion of Exact Numbers. Comparison scale refers to the pairwise comparison of the relative importance of the indicators and gives the exact number judgment result according to one's own preference. We use the 1–9 scale: the range of a_{ij} is going to be in the range $1, 2, \ldots, 9$. When making qualitative pairwise comparisons, people usually have five distinct levels in mind. Assume that m schemes comprise scheme set $X = \{x_1, x_2, \ldots, x_m\}$ and n evaluation indicators are divided into index set $C = \{c_1, c_2, \ldots, c_n\}$, and then the exact scoring value of the j evaluation object given by experts on the i indicator performance is a_{ij}. It can be transformed into an intuitionistic fuzzy set by the following formula:

$$\mu_{ij} = \begin{cases} \alpha_i \dfrac{a_{ij}}{a_i^{\max}}, & i \in \Omega_b, \\ \delta_i \dfrac{a_i^{\min}}{a_{ij}}, & i \in \Omega_c, a_i^{\min} \neq 0, \\ \delta_i \left(1 - \dfrac{a_{ij}}{a_i^{\max}}\right) & i \in \Omega_c, a_i^{\min} = 0, \end{cases}$$
$$v_{ij} = \begin{cases} \beta_i \dfrac{a_{ij}}{a_i^{\max}}, & i \in \Omega_b, \\ \gamma_i \dfrac{a_i^{\min}}{a_{ij}}, & i \in \Omega_c, a_i^{\min} \neq 0, \\ \gamma_i \left(1 - \dfrac{a_{ij}}{a_i^{\max}}\right), & i \in \Omega_c, a_i^{\min} = 0, \end{cases} \tag{5}$$

where Ω_b and Ω_c represent the set of cost-type and benefit-type indicators, respectively. The determination method of $a_i^{\min}$ and $a_i^{\max}$ is as follows:

$$a_i^{\min} = \min_{1 \le j \le n} \{a_{ij}\},$$
$$a_i^{\max} = \min_{1 \le j \le n} \{a_{ij}\}. \tag{6}$$

α_i, β_i, γ_i, and δ_i are four adjustment parameters, which are given by the actual decision-making environment and decision-maker's experience [29]. Their values are all between 0 and 1, and they meet $0 \le \alpha_i + \beta_i \le 1$ and $0 \le \alpha_i + \beta_i \le 1$. Accordingly, the exact number a_{ij} can be transformed into an interval fuzzy number $A_{ij} = (\mu_{ij}, v_{ij})$.

4.2. Identifying the Optimal Shapley Fuzzy Measure. In practical MCDM issues, the weights of the attributes and decision makers (DM) are always partially known or completely unknown. To overcome this limitation, Wang et al. [39] developed the maximized deviation method

(MDM) to handle more complex decision applications. It is well known that it is easier to choose better alternatives by ranking the fusion value, so as to more clearly reflect the differences between all alternatives. The main principle of MDM is that when an attribute has a significant impact on the ranking priority results, it is obvious that the attribute should be given greater weight in influencing the decision results. Conversely, if an attribute causes only a small change in the order of alternatives, it means that the attribute has less impact on the decision process and should be given less weight.

Set the scheme set $X = \{x_1, x_2, \ldots, x_m\}$, n evaluation index set $C = \{c_1, c_2, \ldots, c_n\}$, and weighted vector set $w = \{w_1, w_2, \ldots, w_n\}$. Under the same criteria, the set of deviation values of the pairwise alternatives is $d(a_{ij}, a_{kj})$. Then we can calculate the degree of difference between each alternative through MDM. The calculation formula of deviation is as follows:

$$D_j(\varphi) = \sum_{i=1}^{m} D_{ij}(\varphi) = \sum_{i=1}^{m}\sum_{k=1}^{m} d\left(a_{ij}, a_{kj}\right)\varphi_j(\mu, P_h), \quad j = 1, 2, \ldots, n. \tag{7}$$

In order to determine the optimal Shapley fuzzy measure, this paper establishes a two-stage dynamic programming model, which aims to achieve the maximum deviation of all standards.

$$\max D(\varphi) = \sum_{j=1}^{n}\sum_{i=1}^{m}\sum_{k=1}^{m} d\left(a_{ij}, a_{kj}\right)\varphi_j(\mu, P_h)$$
$$\text{s.t.} \quad \begin{cases} \mu(P_h) = 1, \\ \mu(S) \le \mu(T), \quad \forall S, T \subseteq P_h, S \subseteq T, \\ \mu(j) \in U_j, \quad \forall j \in P_h. \end{cases} \tag{8}$$

4.3. Calculating the Comprehensive Performance Value. Let $r, q \ge 0, a_i = A(\mu_{ai}, v_{ai})\,(i = 1, 2, \ldots, m)$ be a collection of PFNs, the aggregated results derived by PFPNWBM [18] operator are still a PFN, and it is expressed as

$$\text{PFPNWBM}(a_1, a_2, \ldots, a_m) = \left(\sqrt{1 - \left(\prod_{h=1}^{d}\left(1 - \left(1 - \left(1 - \mu_{a_i}^{2r}\mu_{a_j}^{2q}\right)^{\left(\varphi_{i,h}(\mu,P_h)\varphi_{j,h}(\mu,P_h)/\left(1-\varphi_{i,h}(\mu,P_h)\right)\right)}\right)^{(1/(r+q))}\right)\right)}\right)^{(1/d)},$$
$$\prod_{h=1}^{d}\left(\sqrt{1 - \left(1 - \prod_{\substack{i,j \in P_h \\ i \ne j}}\left(1 - \left(1 - v_{a_i}^2\right)^r\left(1 - v_{a_j}^2\right)\right)^{\left(\varphi_{i,h}(\mu,P_h)\varphi_{j,h}(\mu,P_h)/\left(1-\varphi_{i,h}(\mu,P_h)\right)\right)}\right)^{(1/(r+q))}}\right)^{(1/d)}\right). \tag{9}$$

5. The Decision Steps and the Characteristics

In this section, the detailed steps of the evaluation index system of EVCS location are provided:

Step 1: establish a normalized judgment matrix.

We adopt a 1–9 comparative scale and invited experts to give an exact score of a_{ij} for the performance of the J_{th} evaluation object under the I_{th} indicator according to their preferences. If there are cost criteria, the decision matrix $A = (a_{ij})_{m\times n}$ need to be normalized by the following equations [18]:

$$\widetilde{a_{ij}} = \begin{cases} a_{ij}, & \text{for benefit criteria}, \\ \left(a_{ij}\right)^c = (v_a, u_a), & \text{for cost criteria}. \end{cases} \tag{10}$$

Step 2: calculate the distance of each alternative.

The distance between the alternative scheme I and k under the standard j can be calculated by the formula.

Step 3: determine the optimal Shapley fuzzy measure.

Using the above distance value and formula (7), the linear programming model is solved and the optimal Shapley fuzzy measure is obtained.

Step 4: use formula (9) to calculate the comprehensive performance value of each alternative.

Step 5: use formula (2) to calculate the value of score and accuracy function.

The decision frame is shown in Figure 2.

6. An Illustrative Example

To test the practicality of the EVCS location evaluation index system, we select five optional areas $X = \{x_1, x_2, x_3, x_4, x_5\}$: electric refueling area x_1, high-speed service area x_2, user residential area x_3, commercial shopping area x_4, and civic work area x_5. The index set consists of five evaluation indicators: grid load C_1, traffic facilities C_2, user preference C_3, construction cost C_4, and service radius C_5. Based on the correlation pattern, it is assumed that the criteria are divided into two categories $P_1 = \{c_1, c_2, c_3\}$ and $P_2 = \{c_4, c_5\}$. The above potential alternatives are evaluated by experts

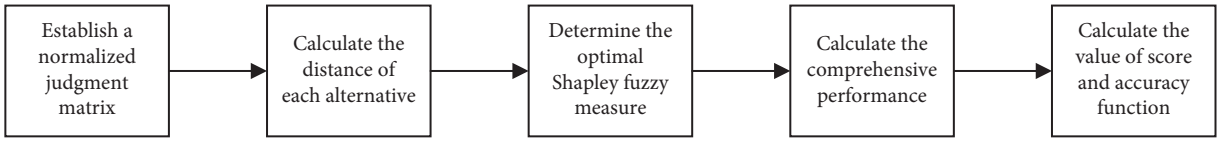

Figure 2: EVCS site selection decision diagram.

according to these criteria using Pythagorean fuzzy information. This assessment provides incomplete information on importance weights:

$$\begin{aligned} U_1 &= [0.25, 0.4], \\ U_2 &= [0.4, 0.5], \\ U_3 &= [0.35, 0.4], \\ U_4 &= [0.45, 0.6], \\ U_5 &= [0.3, 0.5]. \end{aligned} \tag{11}$$

Now the method in the paper can be used to solve the problem. The detailed decision steps are shown as follows :

Step 1: establish the normalized judgment matrix.

The exact quantitative evaluation matrix given by experts is shown in Table 1, which is converted into Table 2 by formula (10). As the cost types, they should be normalized into Table 3 by formula (5).

Step 2: calculate the distance of the alternative.

Under the same criteria, the distance values of pairwise schemes obtained by using the formula (3) are shown in Table 4.

Step 3: determine the optimal Shapley fuzzy measure.

The indexes are divided into p_1 and p_2, and their Shapley fuzzy measure is calculated, respectively.

Table 1: Accurate number rating.

	c_1	c_2	c_3	c_4	c_5
x_1	8	4	3	6	7
x_2	4	5	6	2	7
x_3	3	4	2	6	5
x_4	7	7	8	9	9
x_5	2	1	4	3	5

Table 2: Interval fuzzy number rating.

	c_1	c_2	c_3	c_4	c_5
x_1	(0.26, 0.17)	(0.20, 0.13)	(0.12, 0.80)	(0.43, 0.29)	(0.60, 0.40)
x_2	(0.33, 0.22)	(0.33, 0.22)	(0.60, 0.40)	(0.33, 0.22)	(0.43, 0.29)
x_3	(0.20, 0.13)	(0.20, 0.13)	(0.30, 0.20)	(0.60, 0.40)	(0.60, 0.40)
x_4	(0.12, 0.08)	(0.12, 0.08)	(0.12, 0.08)	(0.60, 0.40)	(0.30, 0.20)
x_5	(0.12, 0.08)	(0.12, 0.08)	(0.60, 0.40)	(0.60, 0.40)	(0.60, 0.40)

Taking the criteria in the first category p_1 as an example, Shapley fuzzy measure of each criterion can be obtained from equation (4)

:

$$\begin{aligned} \varphi_1(\mu, P_h) &= \frac{1}{3}\mu(c_1) + \frac{1}{6}(\mu(c_1, c_2) - \mu(c_2) + \mu(c_1, c_3) - \mu(c_3)) + \frac{1}{3}(1 - (\mu(c_2, c_3))), \\ \varphi_2(\mu, P_h) &= \frac{1}{3}\mu(c_2) + \frac{1}{6}(\mu(c_1, c_2) - \mu(c_1) + \mu(c_2, c_3) - \mu(c_3)) + \frac{1}{3}(1 - (\mu(c_1, c_3))), \\ \varphi_3(\mu, P_h) &= \frac{1}{3}\mu(c_3) + \frac{1}{6}(\mu(c_1, c_3) - \mu(c_1) + \mu(c_2, c_3) - \mu(c_2)) + \frac{1}{3}(1 - (\mu(c_1, c_2))). \end{aligned} \tag{12}$$

Based on the above derivation, a linear programming model can be established as follows:

$$\max[-0.4165\mu(c_1) - 0.0775\mu(c_2) + 0.4939\mu(c_3) - 0.4939\mu(c_1, c_2) + 0.0775\mu(c_1, c_3) + 0.4165\mu(c_2, c_3) + 1.4758]$$

$$\text{s.t.} \begin{cases} \mu(1, 2, 3) = 1, \\ \mu(1) \le \mu(1, 2), \mu(1) \le \mu(1, 2), \mu(1) \le \mu(1, 3), \\ \mu(2) \le \mu(1, 3), \mu(2) \le \mu(2, 3), \mu(3) \le \mu(2, 3), \\ \mu(1) \in [0.25, 0.4], \mu(2) \in [0.4, 0.5], \mu(3) \in [0.35, 0.4]. \end{cases} \tag{13}$$

Table 3: Normalized rating.

	c_1	c_2	c_3	c_4	c_5
x_1	(0.17, 0.26)	(0.40, 0.60)	(0.12, 0.80)	(0.29, 0.43)	(0.60, 0.40)
x_2	(0.22, 0.33)	(0.40, 0.60)	(0.60, 0.40)	(0.22, 0.33)	(0.43, 0.29)
x_3	(0.13, 0.20)	(0.27, 0.41)	(0.30, 0.20)	(0.40, 0.60)	(0.60, 0.40)
x_4	(0.08, 0.12)	(0.32, 0.48)	(0.12, 0.08)	(0.40, 0.60)	(0.30, 0.20)
x_5	(0.08, 0.12)	(0.40, 0.60)	(0.60, 0.40)	(0.40, 0.60)	(0.60, 0.40)

Table 4: The same standard pairwise alternative distance.

	c_1	c_2	c_3	c_4	c_5
$d(a_{1j}, a_{2j})$	0.0723	0.0000	0.4429	0.1181	0.2230
$d(a_{1j}, a_{3j})$	0.0352	0.2472	0.0969	0.2230	0.0000
$d(a_{1j}, a_{4j})$	0.0673	0.1661	0.4429	0.2230	0.3460
$d(a_{1j}, a_{5j})$	0.0673	0.0000	0.4429	0.2230	0.0000
$d(a_{2j}, a_{3j})$	0.0965	0.2472	0.3460	0.3218	0.2230
$d(a_{2j}, a_{4j})$	0.1231	0.1661	0.0000	0.3218	0.1230
$d(a_{2j}, a_{5j})$	0.1231	0.0000	0.0000	0.3218	0.2230
$d(a_{3j}, a_{4j})$	0.0322	0.0811	0.3460	0.0000	0.3460
$d(a_{3j}, a_{5j})$	0.0322	0.2472	0.3460	0.0000	0.0000
$d(a_{4j}, a_{5j})$	0.0000	0.1661	0.0000	0.0000	0.3460

By solving the model, we can obtain

$$\begin{aligned} \mu(1) &= 0.25, \\ \mu(2) &= 0.4, \\ \mu(3) &= 0.35, \\ \mu(1,2) &= 0.5, \\ \mu(1,3) &= \mu(2,3) = 1. \end{aligned} \tag{14}$$

After a round of anonymous ratings by experts, the proceeds of the collaboration are returned to all parties. $\mu(1) + \mu(2) \geq \mu(1,2)$ is found, which means that the profit value after the two cooperation is lower than the value created separately. So they will choose the final cooperation. In order to guarantee the firmness and reliability of alliance cooperation, the benefits of all parties after cooperation should be at least greater than or equal to the sum of the benefits of all parties without cooperation. Therefore, on the basis of the original linear programming, we add constraint conditions:

$$\mu(S_m) + \mu(S_n) \leq \mu(T), \quad \forall S_m, S_n, T \subseteq P_h, S_m, S_n \subseteq T. \tag{15}$$

We can obtain $\mu(1) = 0.25, \mu(2) = 0.4, \mu(3) = 0.35, \mu(1,2) = 1, \mu(1,3) = 0.6$, and $\mu(2,3) = 1$.

According to formula (4), the Shapley fuzzy measure is calculated as $\varphi_1(\mu, P_h) = 0.2083, \varphi_2 \ (\mu, P_h) = 0.2833$, and $\varphi_3(\mu, P_h) = 0.5084$.

Similar to the processing procedure of the criteria in p_1, for Shapley's fuzzy measure of C_3 and C_4 in p_2, we can get

$$\begin{aligned} \varphi_4(\mu, P_h) &= 0.2, \\ \varphi_5(\mu, P_h) &= 0.3. \end{aligned} \tag{16}$$

Step 4: use formula (9) to calculate the comprehensive performance value of each alternative.

When $r = q = 1$, the comprehensive performance value of each alternative can be calculated as

$$\begin{aligned} a_1 &= [0.1609, 0.4738], \\ a_2 &= [0.1065, 0.7398], \\ a_3 &= [0.0354, 0.6870], \\ a_4 &= [0.1628, 0.5836], \\ a_5 &= [0.0941, 0.7273]. \end{aligned} \tag{17}$$

Step 5: the score and accuracy function values are calculated using equation (2).

Performance function and accuracy function are shown in Table 5.

7. Comparison and Analysis

The application case shows that the constructed EVCS location evaluation system and evaluation method can prioritize the final alternatives and can better deal with problems such as the heterogeneity of experts and the incomplete information of the weights in the evaluation.

From the point of view of indicator weight, the importance of the five indicators of "grid load C_1, traffic facilities C_2, user preference C_3, construction cost C_4, and service radius C_5" in EVCS location evaluation system is significantly different. The importance is ranked as follows:

Table 5: Score and accuracy ranking.

	$S(a_i)$	$H(a_i)$	Ranking
x_1	−0.1986	0.2504	2
x_2	−0.0566	0.2181	4
x_3	−0.6227	0.6273	1
x_4	−0.3141	0.3671	5
x_5	−0.4425	0.4750	3

$C_4 \prec C_1 \prec C_2 \prec C_5 \prec C_3$. It can be seen that, for government EVCS location, understanding the charging preference and travel modes of regional users is the key to EVCS obtaining maximum profits. The service radius ranks second in importance, showing that regional charging demand is the basic requirement for EVCS to perform its service functions.

Judging from the evaluation results, the location of the 5 EVCS areas obtained by the two-stage optimization planning model is relatively good, especially the expressway, which has perfect infrastructure, convenient transportation, and huge passenger flow. Only through the first stage of decision-making, we get the comprehensive performance value of the five alternatives:

$$\begin{aligned} a_1 &= [0.2705, 0.8107], \\ a_2 &= [0.1065, 0.7398], \\ a_3 &= [0.0354, 0.6870], \\ a_4 &= [0.1326, 0.6541], \\ a_5 &= [0.0941, 0.7273]. \end{aligned} \tag{18}$$

The optimal ranking is $x_3 \prec x_5 \prec x_4 \prec x_1 \prec x_2$.

The results show that, due to the special complexity of the decision state, the two-stage optimization modifies the Shapley fuzzy measure, changes the original weight value, and then affects the optimal ranking of the final alternative. This supports the EVCS location evaluation method constructed by this research.

8. Conclusions

Using scientific methods to evaluate EVCS location is of great significance for improving the design, development, promotion, and application of EV. This paper builds a systematic EVCS location evaluation index system on the basis of comprehensive domestic and foreign research results on EV evaluation and various charging station location evaluation.

First of all, in order to better deal with the heterogeneity, fuzziness, and uncertainty of expert evaluation information, this study introduces 1–9 evaluation scale for qualitative paired comparison and constructs interval fuzzy quantitative evaluation matrix by converting the exact number into the intuitionistic fuzzy set and other relevant theoretical results. Moreover, a two-stage optimization model to identify the optimal Shapley fuzzy measure is established by fully considering the incomplete knowledge of weights in the actual decision-making environment. And five representative EVCS locations are taken as the research objects for empirical application. Finally, the practicability, effectiveness, and flexibility of the evaluation index system and evaluation method are verified by analyzing the difference of the evaluation results between the first-order linear optimization and the two-stage optimization.

Admittedly, this study also has some limitations, such as relatively small selection of research samples, insufficient geographical coverage, relatively small number of evaluators, and sample data collected. Although the heterogeneity of expert groups in the evaluation process has been considered, the diversity of evaluation criteria and the multi-granularity of decision-making information have not been considered. In follow-up research, we will further expand research objects, enrich sample data, optimize research methods, and consider researching EVCS construction issues from the perspective of consumer experience, so as to enhance consumer experience and make it better to use charging services.

Data Availability

The data came from expert ratings.

Conflicts of Interest

The authors declare that they have no conflicts of interest.

Acknowledgments

This work was supported by Anhui Province Philosophy and Social Science Planning General Project (no. AHSKY2017D70).

References

[1] A. Pal, B. Aniruddha, and A. C. Kumar, "Allocation of electric vehicle charging station considering uncertainties," *Sustainable Energy, Grids and Networks*, vol. 25, Article ID 100422, 2021.

[2] Z. P. Liu, F. Wen, Y. S. Xue, and J. B. Xin, "The optimal location and determination of the electric vehicle charging station," *Automation of Electric Systems*, vol. 36, no. 3, pp. 54–59, 2012.

[3] S. Q. Zhao, Z. W. Li, and D. Lei, "Optimal location and capacity of electric vehicle charging station based on urban traffic network information," *Electrical Automation Equipment*, vol. 36, no. 10, pp. 8–15, 2016.

[4] M. Xu, Q. Meng, K. Liu, and T. Yamamoto, "Joint charging mode and location choice model for battery electric vehicle users," *Transportation Research Part B: Methodological*, vol. 103, pp. 68–86, 2017.

[5] Z. P. Chen and W. Yang, "An MAGDM based on constrained FAHP and FTOPSIS and its application to supplier selection," *Mathematical and Computer Modelling*, vol. 54, no. 11, pp. 2802–2815, 2011.

[6] A. Sotoudeh-Anvari, "A critical review on theoretical drawbacks and mathematical incorrect assumptions in fuzzy OR methods: review from 2010 to 2020," *Applied Soft Computing*, vol. 93, Article ID 106354, 2020.

[7] L. A. Zadeh, "Fuzzy sets," *Information and Control*, vol. 8, no. 3, pp. 338–353, 1965.

[8] C. Fu, M. Xue, W. Y. Liu, D. L. Xu, and J. B. Yang, "Data-driven preference learning in multiple criteria decision

making in the evidential reasoning context," *Applied Soft Computing*, vol. 102, Article ID 107109, 2021.

[9] P. P. Ghaebi, M. Bornapour, R. Hemmati, and M. J. Guerrero, "Charging station stochastic programming for hydrogen/battery electric buses using multi-criteria crow search algorithm," *Renewable and Sustainable Energy Reviews*, vol. 144, Article ID 111046, 2021.

[10] M. Krawczak and G. Szkatuła, "On matching of intuitionistic fuzzy sets," *Information Sciences*, vol. 517, pp. 254–274, 2020.

[11] W. Y. Zeng, Y. Xi, Q. Yin, and P. Guo, "Weighted dual hesitant fuzzy set and its application in group decision making," *Neurocomputing*, 2020.

[12] Y. Fan and F. Y. Xiao, "TDIFS: two dimensional intuitionistic fuzzy sets," *Engineering Applications of Artificial Intelligence*, vol. 95, Article ID 103882, 2020.

[13] R. Tao, Z. Liu, R. Cai, and K. H. Cheong, "A dynamic group MCDM model with intuitionistic fuzzy set: perspective of alternative queuing method," *Information Sciences*, vol. 555, pp. 85–103, 2021.

[14] W. F. Liu and H. Xia, "Pythagoras hesitates the fuzzy set," *Fuzzy System and Mathematics*, vol. 30, no. 4, pp. 107–115, 2016.

[15] R. R. Yager and A. M. Abbasov, "Pythagorean membership grades in multicriteria decision making," *IEEE Transactions of Fuzzy Systems*, vol. 22, no. 4, pp. 958–965, 2014.

[16] Y. Tang and Y. Yang, "Sustainable e-bike sharing recycling supplier selection: an interval-valued pythagorean fuzzy MAGDM method based on preference information technology," *Journal of Cleaner Production*, vol. 287, Article ID 125530, 2021.

[17] C. H. Zhang, Q. Q. Hu, S. Z. Zeng, and W. H. Su, "IOWLAD-based MCDM model for the site assessment of a household waste processing plant under a pythagorean fuzzy environment," *Environmental Impact Assessment Review*, vol. 89, Article ID 106579, 2021.

[18] R. X. Nie, Z. P. Tian, J. Q. Wang, and J. H. Hu, "Pythagorean fuzzy multiple criteria decision analysis based on shapley fuzzy measures and partitioned normalized weighted bonferroni mean operator," *International Journal of Intelligent Systems*, vol. 34, no. 5, pp. 1–28, 2018.

[19] H. Wang, D. Zhao, Y. T. Cai, Q. Meng, and P. O. Ghim, "Taxi trajectory data based fast-charging facility planning for urban electric taxi systems," *Applied Energy*, vol. 286, Article ID 116515, 2021.

[20] L. Ni, Y.-W. Chen, and O. de Brujin, "Towards understanding socially influenced vaccination decision making: an integrated model of multiple criteria belief modelling and social network analysis," *European Journal of Operational Research*, vol. 293, no. 1, pp. 276–289, 2021.

[21] J. W. Gao, H. J. Men, F. J. Guo et al., "A multi-criteria decision-making framework for compressed air energy storage power site selection based on the probabilistic language term sets and regret theory," *Journal of Energy Storage*, vol. 37, Article ID 102473, 2021.

[22] Q. Tan, P. Wu, W. Tang et al., "Benefit allocation model of distributed photovoltaic power generation vehicle shed and energy storage charging pile based on integrated weighting-shapley method," *Global Energy Interconnection*, vol. 3, no. 4, pp. 375–384, 2020.

[23] L. Jing, Y. Zhan, Q. Li et al., "An integrated product conceptual scheme decision approach based on shapley value method and fuzzy logic for economic-technical objectives trade-off under uncertainty," *Computers & Industrial Engineering*, vol. 156, Article ID 107281, 2021.

[24] H. T. Yang and D. T. Ma, "Research on consistency of judgment matrix in analytic hierarchy process," *Modern Electronic Technology*, vol. 19, pp. 46–48, 2007.

[25] H. J. Pasman and W. J. Rogers, "How to treat expert judgment? with certainty it contains uncertainty," *Journal of Loss Prevention in the Process Industries*, vol. 66, Article ID 104200, 2020.

[26] X. K. Xu and S. Z. Hua, "Evaluation of government APP under the background of "internet + government service" based on intuitionistic fuzzy analytic hierarchy process," *Journal of Information*, vol. 39, no. 3, pp. 198–207, 2020.

[27] R. Şahin and P. Liu, "Correlation coefficient of single-valued neutrosophic hesitant fuzzy sets and its applications in decision making," *Neural Computing & Applications*, vol. 28, no. 6, pp. 1387–1395, 2017.

[28] F. Teng and P. D. Liu, "A large group decision-making method based on a generalized shapley probabilistic linguistic choquet average operator and the TODIM method," *Computers & Industrial Engineering*, vol. 151, Article ID 106971, 2021.

[29] D. F. Li, *Intuitionistic Fuzzy Set Decision Making and Game Analysis*, National Defense Industry Press, Beijing, China, 2012.

[30] K. T. Atanassov, "Intuitionistic fuzzy sets," *Fuzzy Sets and Systems*, vol. 20, pp. 87–96, 1986.

[31] R. R. Yager, "Pythagorean fuzzy subsets," in *Proceedings of the 2013 Joint P1 IFSA World Congress and NAFIPS Annual Meeting*, Edmonton, Canada, June 2013.

[32] X. Yager and Y. Yang, "Some results for pythagorean fuzzy sets," *International Journal of Intelligent Systems*, vol. 30, no. 11, pp. 1133–1160, 2015.

[33] P. Ren, Z. X, and X. Gou, "Pythagorean fuzzy TODIM approach to multi-criteria decision making," *Applied Soft Computing*, vol. 42, pp. 246–259, 2016.

[34] L. S. Shapley, *A Value for n-Person Game*, Princeton University Press, Princeton, NJ, USA, 1953.

[35] Y. Mu, J. Wu, N. Jenkins, H. Jia, and C. Wang, "A spatial-temporal model for grid impact analysis of plug-in electric vehicles," *Applied Energy*, vol. 114, pp. 456–465, 2014.

[36] X. Huang and J. Ge, "Electric vehicle development in Beijing: an analysis of consumer purchase intention," *Journal of Cleaner Production*, vol. 216, pp. 361–372, 2019.

[37] C. Csiszár, C. Bálint, D. Földes, E. Wirth, and L. Amás, "Location optimisation method for fast-charging stations along national roads," *Journal of Transport Geography*, vol. 88, Article ID 102833, 2020.

[38] Z. P. Liu, F. S. Wen, and Y. S. Xue, "Optimalsiting and sizing of distributed generators considering plug-inelectric vehicles," *Automation of Electric Power Systems*, vol. 35, no. 18, pp. 11–16, 2011.

[39] J. Wang, G.-W. Wei, C. Wei, and J. Wu, "Maximizing deviation method for multiple attribute decision making under q-rung orthopair fuzzy environment," *Defence Technology*, vol. 16, no. 5, pp. 1073–1087, 2020.

Hindawi
Journal of Mathematics
Volume 2021, Article ID 5242414, 18 pages
https://doi.org/10.1155/2021/5242414

Research Article

Does Industrial Agglomeration Promote Carbon Efficiency? A Spatial Econometric Analysis and Fractional-Order Grey Forecasting

Zuoren Sun [1] **and Yi Liu** [1,2]

[1] *Business School, Shandong University, No. 180 West of Wenhua Road, Weihai, Shandong 264209, China*
[2] *Tianjin Central Sub-branch, The People's Bank of China, Economic and Technological Development Zone, No. 59 East of Xincheng Road, Tianjin 300450, China*

Correspondence should be addressed to Zuoren Sun; sunzuoren@sdu.edu.cn

Received 11 June 2021; Accepted 17 July 2021; Published 31 July 2021

Academic Editor: Lifeng Wu

In theory, the industrial agglomeration is a double-edged sword as there are both positive and negative externalities. China's cities, with great disparities on degrees of the industrial agglomeration, often face different energy and carbon dioxide emission problems, which raise the question whether the industrial agglomeration promotes or inhibits energy efficiency and carbon dioxide emission. This paper explored the effects of the industrial agglomeration on carbon efficiency in China. Spatial econometric methods were implemented using panel data (2007–2016) of 285 cities above the prefecture level. The results revealed that industrial agglomerations have significant impacts on the urban carbon efficiency with significant spatial spillover effects. The agglomerations of the manufacturing and high-end productive service industries take positive effects on carbon efficiency while the low-end productive and living service industries take negative effects. As a comparison, we found that the agglomeration effects at the level of the megalopolis are greater than those at the national level, especially for the living services industry, in which the higher levels of agglomeration make the effects on carbon efficiency change from negative to positive. The divisions of labor for the central and common cities in the megalopolises are integrated into the industrial agglomeration. Furthermore, the fractional-order grey forecasting model is used in this paper. By the virtue of its advantage in dealing with small sample data which lack statistical rules, this paper makes an out-of-sample prediction of carbon efficiency and industrial agglomeration degree of Chinese cities. By adding the predicted results to the spatial correlation test, new evidence on the spatial correlation of carbon efficiency and spatial division of labor between cities is obtained. Based on the empirical results of the present study, we have proposed some policy recommendations.

1. Introduction

Since its reform and opening up, China's rapid urbanization process has brought about a significant increase in energy consumption and CO_2 emissions. During 1980–2014, China's average annual growth rate of CO_2 emissions was as much as 9.2%. The International Energy Agency (IEA) reported that China has, since 2007, far exceeded the CO_2 emissions of the European Union and the United States [1]. At present, according to statistics from the World Bank, China's CO_2 emissions had reached 10.29 billion tons, accounting for 28% of global CO_2 emissions in 2014. In comparison, in 2014, the CO_2 emissions of the European Union and the United States were only 3.24 and 5.25 billion tons, respectively [2]. There is no doubt that the Chinese government faces an increasing amount of international and domestic pressure while keeping economic development stable. The Chinese government has made a list of commitments for reducing carbon emissions and to curb global climate change. In 2014, the Chinese government announced, in the "Sino US joint statement on climate change," that it plans to reach the peak of CO_2 emissions by

2030. At the 2015 Paris Climate Conference, the Chinese government committed to CO_2 emissions per unit of GDP being 60–65% lower in 2030 than the level in 2005. Accordingly, China has enhanced a series of restrictions on CO_2 emissions. For instance, China has controlled the expansion of the production capacity of the manufacturing industry because this industry produces high levels of pollution, consumes a large amount of energy, and is responsible for high CO_2 emissions. China has intentionally reduced its reliance on the manufacturing industry to achieve industrial upgrading. However, the implementation of restrictions on the manufacturing industry is bound to slow down economic growth.

In the process of economic development, cities are regarded as carriers of economic activities and also account for about 85% of China's CO_2 emissions [3]. The rapid urbanization increases not only massive CO_2 emissions but also the level of total factor productivity (TFP) with the accumulation of the population, economic factors, and activities in the cities [4]. An improvement of the TFP plays an essential role in promoting economic growth and transformation [5, 6], as well as improving efforts to reduce energy consumption and CO_2 emissions [7, 8]. Therefore, the economies of scale and technology spillover effects will inevitably affect the quantity and efficiency of CO_2 emission. In this sense, the effective use of urban industrial agglomeration effects is conducive to not only reducing CO_2 emissions but also promoting economic growth.

Many scholars studied how urbanization improves carbon efficiency from the perspective of agglomeration economies. Most scholars identified that the driving factors for improving carbon efficiency are the aggregation of the population, technological progress, and industrial structure. For example, Li et al. studied the efficiency of CO_2 emissions of China's 31 manufacturing industries, from 2012 to 2016, and found that the high-tech industry ranked at the top of the list of industries with different levels of technology [9]. Wang et al. discovered that the energy structure, technological level, and rate of urbanization all have significant impacts on carbon efficiency [10]. Sun et al. evaluated the carbon efficiency and the global value chain (GVC) position index. They highlighted that, compared with the labor-intensive and resource-intensive manufacturing industries, the technology-intensive manufacturing industry in the GVC is most effective in improving carbon efficiency [11]. Zhang et al. indicated that enterprise size is a crucial factor for improving carbon efficiency [12]. Wang and Ma determined that the level of urbanization, the structure of energy consumption, and the level of industrialization are the main driving factors of CO_2 emissions [13]. Wang et al. found that the gradual improvement of the level of technology is the main driving force for the improvement of the efficiency of CO_2 emissions [14, 15]. Wang et al. found that the production technology shows heterogeneities at the level of region [16] and sector [17].

In general, technological progress, economies of scale, and the aggregation of the population will significantly affect the carbon efficiency. However, these studies did not discuss the agglomeration of the segmented service industries. Thus, it is unknown that how the impact of the spatial agglomeration of economic activity on carbon efficiency is derived from the agglomeration of services. Besides, according to the China Megalopolises Development Report 2010, megalopolises cover 21.13% of the national land area, accounting for 48.99% of the total population, 51.41% of the urban population, and 46.7% of the urban members. In addition, they create 81.94% of the added value of the second industry and 83.5% of the added value of the third industry. The megalopolis is an advanced form of spatial organization with a concentration of economic actions resulting from highly developed industrialization and urbanization [18]. The spatial characteristics of a megalopolis contribute to providing transportation, communication, information, and other infrastructures, as well as market conditions, which further stimulate the agglomeration of industries natively. However, few scholars have studied the relationship between industrial agglomeration and carbon efficiency in megalopolises.

Compared to the extant research, the present study makes three major contributions: (1) the present study built a spatial Durbin model to study the effects of the heterogeneity of the industrial agglomeration on carbon efficiency at the national level and at the level of the megalopolis; (2) we explored the different impacts from various service industry agglomerations on urban carbon efficiency and identified specific impacts in megalopolises; (3) comparisons between the manufacturing and segmented service industries were made, and finally, we sought the optimal development path of cities for the dual goals of economic development and the reduction of CO_2 emissions.

2. Theoretical Frameworks and Research Hypotheses

At present, most urban-related studies focused on the relationship between different types of industrial agglomeration and the labor productivity of a single city, but no consistent conclusions could be drawn. First, some studies showed that industrial agglomeration has caused serious environmental pollution along with the expansion of enterprise-scale and large-scale use of energy from fossil fuels. Virkanen found that industrial agglomeration in southern Finland caused heavy metal pollution of the local water resources and atmosphere [19]. Verhoef and Nijkamp found that industrial agglomeration harms the quality of the environment, leading to the aggravation of environmental pollution [20]. Frank et al. showed that industrial agglomeration worsens air quality in sampled cities in the European Union [21]. Duc et al. surveyed industrial companies on both sides of the Vietnamese river and found that industrial agglomeration caused river pollution [22]. In contrast to mentioned above, some scholars further discovered that industrial agglomeration is conducive to the progress and diffusion of environmental protection technology, promoting production and energy

efficiencies, and reducing environmental pollution [23–27]. Han et al. analyzed the impact of Marshall's agglomeration, such as labor concentration effects, economies of scale of intermediate inputs, and space spillover effects, on industrial energy efficiency. They pointed out that the space availability of intermediate inputs and space technology spillover effects significantly increase industrial energy efficiency [28]. Furthermore, Han et al. constructed a spatial Durbin model to explore the effects of industrial specialization and diversified agglomerations of manufacturing on CO_2 emissions. They provided an evidence that both of them can reduce CO_2 emissions locally and in surrounding cities through the agglomeration of economic externalities [29]. Zhang et al. analyzed data from 18 cities in Henan Province and proposed that industrial agglomeration reduces CO_2 emissions in the surrounding areas and that there is a negative impact on the intensity of CO_2 emissions [30]. Shen et al. used a dynamic spatial panel model and demonstrated that the agglomeration of the productive service industries has a significant positive space spillover effect on energy efficiency in surrounding areas [31]. Jacobs et al. found that diversified agglomeration is available for the high-end productive service industry in central cities, such as large and international cities. They found that the industries of these cities have the characteristics of high added value within products, a large service radius, and a small transaction frequency, thus affecting the surrounding areas with significant spatial spillover effects of improvements in energy efficiency [32]. However, in the existing literature, there is an absence of research on the low-end productive services and living services. In addition, there are no comparative studies between the manufacturing and service industries, or with the inter-heterogeneity in the subdivided service industries, regarding the effects of industrial agglomeration on urban carbon efficiency. Therefore, we propose Hypothesis 1.

Hypothesis 1. The agglomeration effects of various industries show heterogeneity, and their impacts on urban carbon efficiency have diversity spatially.

The urban area provides transportation, communication, information, and other infrastructures as well as market conditions and stimulates the agglomeration of industries. The development of industrial agglomeration is part of the trend of urbanization, resulting in the industries being close to the source of innovation of the central city to obtain advanced technology. When the urbanization is in different stages, the internal industrial agglomeration pattern has different characteristics. The expansion of cities promotes the diffusion and re-agglomeration of industries. The second industry cluster is dominant in the developing stage of urbanization, while the third industry cluster is evident in the developed stage. The coordinated development of regional industrial agglomeration and urbanization promotes the overall development of the regional economy. Therefore, cities of different scales and grades are adjacent to each other or cities of the same scale and grade in space. This will form a megalopolis through strengthening the division of labor and cooperation between cities. Huang et al. argued that the development of a megalopolis is beneficial to the improvement of urban ecological efficiency and that the degree of improvement is affected by the city level [33]. Yue et al. found that the impact of an industrial structural adjustment on the energy intensity of cities in the Pearl River Delta is not apparent [34]. Chen et al. found that the transfer of high energy-consuming industries, which are led by capital-intensive industries, from the developed region to the developing region, can effectively reduce CO_2 emissions in the developed regions [35]. Li et al. indicated that industrial transfer between any two cities within a megalopolis would bring about a decline in energy intensity [36]. Xiao et al. revealed that the performance of the total-factor CO_2 emissions of the tertiary industry is better than that of the secondary industry. However, prospects for the low-carbon development of the tertiary industry, in the Yangtze River Delta, are not optimistic [37]. Therefore, we propose Hypothesis 2.

Hypothesis 2. The diversified characteristics of the industrial agglomeration of a megalopolis in space result in its effects on carbon efficiency being different.

The structural optimization effect is the driving force for improving carbon efficiency in a megalopolis. First, the development of megalopolises improves the proportion of production service industries and promotes the diversification of production in central cities. Second, the development of megalopolises promotes their industrialization progress and the specialization of production in common cities. Henderson pointed out that there is an inverted *U*-shaped relationship between urban scale and industrial agglomeration. With the expansion of the urban scale, the competition for urban public resources, the rise of factor costs, the congestion of transportation, and other factors will accelerate the industrial diffusion. Simultaneously, some industries leapfrog to the same level or to a low gradient city, namely, Friedman's "centre-periphery" mode, which leads to the initial formation of megalopolises [38, 39]. In recent years, megalopolises have played an essential role in China's new urbanization process [40]. In the Yangtze River Delta, the development of the service industry in Shanghai far exceeds other industries, but the manufacturing industry still leads and plays a decisive role in Jiangsu and Zhejiang [41]. The Pearl River Delta has entered the post-industrialization period and has developed with the promotion of the agglomeration of the service industry and manufacturing diffusion [35]. In the Circum-Bohai Sea Economic Zone, the heavy industry accounts for too large a share of the overall economy, which restricts the division of labor between the cities [42]. Yu et al. found that there is a negative correlation between the size of a city and carbon emissions and further demonstrated that a megalopolis is more efficient with regard to carbon emissions [43]. Liu et al. deemed that the social, land, population, and economic urbanization are all related to urbanization and conducted an assessment of the multiple effects of these components of urbanization on CO_2 emissions in the Pearl River Delta [44–46]. Zheng et al. predicted that the energy consumption of the Yangtze River

Delta would continue to rise, and the main source of energy consumption will be manufacturing. They also suggested that the government should update its methods and concepts related to sustainable development and limit the development of energy-intensive industries [41]. Ouyang et al. found that GDP per capita, environmental regulation strength, factor input structure, foreign direct investment, local government spending, and the degree of openness have positive impacts on the industrial total-factor energy efficiency in the Pearl River Delta [47]. Li et al. argued that socioeconomic factors, such as the industrial structure, economic level, carbon intensity, and other spatial factors, play significant roles in decreasing carbon intensity in the Yangtze River Delta [48]. Therefore, the development of megalopolises improves the proportion of the tertiary industry in central cities and also promotes the progress of both industrialization and specialized production in common cities. The development of megalopolises decentralizes the diseconomy of agglomeration of central cities and promotes the flow of the elements of production to common cities. However, although the aforementioned studies have contributed to the theoretical discussion on the mechanism by which industrial agglomeration influences economic development of megalopolis, they still lack empirical support. On the basis of these studies, we propose the following.

Hypothesis 3. On the internal side of a megalopolis, the division of labor between central and common cities is coupled with industrial agglomeration for improving carbon efficiency.

3. Data and Methodology

Limited by the availability of data, the present study selected panel data (2007–2016) for 285 cities in China. The original data sources were the China City Statistical Yearbook, China Energy Statistics Yearbook, and Beijing Shu Huitong Environmental Technology Research Institute Data Service Network (http://www.3edata.com). To ensure the consistency and comparability of the statistical data, the present study used the relatively stable statistical caliber of the city.

3.1. Measurement of CO_2 Emissions at Prefecture-Level Cities. Given the availability of data sources, we selected four forms of energy consumption, electricity, natural gas, liquefied petroleum gas, and transportation industries, to measure CO_2 emissions [49].

To better reflect the actual situation in China, the reference coefficient of coal for various energy conversions and the average low calorific value were adopted from the Chinese National Standard GB/T2589-2008. The data of the unit calorific value of the carbon content and the oxidation rate used to calculate the CO_2 emission coefficient were obtained from the "2006 IPCC National Greenhouse Gas Emission Inventory Guide." The formula used to calculate the CO_2 emissions is as follows:

$$C = \sum C_{ij} = \sum E_{ij} \times f_{ij}, \tag{1}$$

where C denotes the CO_2 emissions, i is the i-th energy, j is the j-th city (region), C_{ij} denotes the CO_2 emissions generated by the i-th energy consumption in city j, and E_{ij} is the consumption of the i-th energy in city j, and f_{ij} represents the CO_2 emission coefficient of the i-th energy in city j.

The average low calorific value, carbon content per unit calorific value, carbon oxidation rates of the principal energies, and calculated CO_2 emission factors are shown in Table 1.

Data on the electricity consumption of the whole society were collected from the China City Statistical Yearbook. Glaeser and Kahn argued that there is an independent CO_2 emission coefficient in each regional power grid [50]. Accordingly, we divide China into six regions: North China, Northeast China, East China, Central China, Northwest China, and South China. The CO_2 emission coefficient for electricity was measured according to the baseline emission coefficient in the regional grid, which was issued by the China Certified Emission Reduction Exchange Information Platform.

The data on the supplies of natural gas and liquefied petroleum gas in a region were obtained from the data service network of the Beijing Shu Huitong Environmental Technology Research Institute. The CO_2 emission coefficient of natural gas is 0.2666 kg/m^3, and the CO_2 emission coefficient of liquefied petroleum gas is 3.1013 kg/m^3.

Due to differences between the regions of China and incomplete statistical data, it was difficult to obtain data such as mileage travelled by vehicle, the fuel used per mile for different types of motor vehicles, etc. According to public data, it is less accurate to use the "bottom-up" method to calculate CO_2 emissions from transportation. In the present study, we use a "top-down" algorithm to calculate the CO_2 emissions by transportation in various cities in China. The CO_2 emissions from transportation mainly come from direct emissions from the combustion of fossil fuels. In contrast, the indirect emissions of CO_2 from electricity and heat consumption are less. Therefore, in the present study, the calculations of CO_2 emissions by transportation included only the direct emissions from the consumption of fossil fuels.

At the provincial level, the Regional Energy Balance Sheet contains the energy consumed by transportation, warehousing, and postal industries. The present study excluded the energy consumption of the warehousing and postal industries. This was achieved by using the income ratios of transportation, warehousing, and postal industries in the "China Economic Census Yearbook" to estimate energy consumption and calculate CO_2 emissions for the transportation industry only. Then, referring to Li et al. [51], we obtained the values of the passenger and freight turnovers from the China Economic Network Statistics Database and the energy intensity data in the Transportation Energy Data Book (TEDB). These were used to calculate the ratio of CO_2 emissions between passenger and freight transport. According to this ratio, we divided the CO_2 emissions by the transport activities for passenger and freight at the provincial level. At the city level, we calculated the proportion of the volume of the passenger transport of each city and that of

Table 1: The CO_2 emission coefficients of the principal energy sources.

Energy	Average low calorific value	Carbon content per unit calorific value	Carbon oxidation rates	CO_2 emission factors
Raw coal	20908 kJ/kg	26.37	0.94	1.9002 kg/kg
Washed coal	26344 kJ/kg	25.41	0.94	2.3072 kg/kg
Other coal washing	8363 kJ/kg	25.41	0.94	0.7324 kg/kg
Briquette	1589 kJ/kg	33.56	0.9	0.1762 kg/kg
Coke	28435 kJ/kg	29.42	0.93	2.8604 kg/kg
Coke oven gas	173535 kJ/m^3	12.1	0.98	7.5452 kg/m^3
Blast furnace gas	3763 kJ/m^3	70.8	0.99	0.9671 kg/m^3
Converter gas	5227 kJ/m^3	49.6	0.99	0.9411 kg/m^3
Crude	41816 kJ/kg	20.08	0.98	3.0202 kg/kg
Gasoline	41070 kJ/kg	18.9	0.98	2.9251 kg/kg
Kerosene	43070 kJ/kg	19.6	0.98	3.0334 kg/kg
Diesel	42652 kJ/kg	20.2	0.98	3.0959 kg/kg
Fuel oil	41816 kJ/kg	20.1	0.98	3.1705 kg/kg
Liquefied petroleum gas	50179 kJ/m^3	17.2	0.98	3.1013 kg/m^3
Refinery dry gas	46055 kJ/m^3	18.2	0.98	3.0119 kg/m^3
Other petroleum products	40200 kJ/kg	20	0.98	2.889 kg/kg
Natural gas	4800 kJ/m^3	15.32	0.99	0.2666 kg/m^3
Liquified natural gas	44200 kJ/m^3	17.2	0.98	2.7318 kg/m^3

the freight transport of each city in a province. We then divided the provincial CO_2 emissions into the city level in terms of each calculated proportion. Finally, we aggregated the CO_2 emissions data of the passenger and freight transports as the total emissions for the transportation industry of the prefecture-level cities.

According to Figure 1, from 2007 to 2016, the total CO_2 emissions of China's prefecture-level cities increased from 2022.77 to 3499.70 million tons, with an average annual growth rate of 6.31%. The CO_2 emissions of cities in megalopolises increased from 1065.89 to 1741.97 million tons, with an average annual growth rate of 5.63%. The CO_2 emissions of other cities increased from 956.89 to 1757.72 million tons, and the average growth rate was 7.04%. There has been an annual decrease in the proportion of CO_2 emissions in megalopolises. During 2007–2016, the 70 cities in three megalopolises contributed an average of 50.37% of the total CO_2 emissions among 285 above prefecture-level cities across the country. This means that the megalopolises are still the main sources of China's CO_2 emissions.

3.2. Spatial Distribution of CO_2 Emissions. According to Tobler's first law, everything is related to other things, and similar things are more closely related to each other. This means that spatial data can interact with each other due to geographical location. We explored the spatial distribution of CO_2 emissions in 2007, 2011, and 2016 in above prefecture-level cities. As shown in Figure 2, CO_2 emissions show distinct spatial agglomeration characteristics. CO_2 emissions decreased gradually along the east, central, and west areas. The Pearl River Delta, Yangtze River Delta, Beijing-Tianjin-Hebei Economic Zone, and Chengdu-Chongqing Economic Zone, which are the largest and most developed areas in China, showed higher levels of emissions. Shandong and Liaoning Provinces showed significantly high concentrations of emissions, which combined with the Tianjin-Hebei Economic Zone form the Circum-Bohai Sea Economic Zone.

3.3. Measurement of the Agglomeration of the Service and Manufacturing. As for the measurement of industrial agglomeration, a series of measurement methods are available, such as market concentration, location entropy, Herfindahl index, spatial Gini coefficient, geographic concentration index, and MS index. Each of them has its own focus. The location entropy measures industrial agglomeration through industrial specialization, which is conducive to indicating the advantageous industries in the region. The Herfindahl index reflects the concentration of enterprises in the industry, and the spatial Gini coefficient reflects the regional agglomeration of the industry. The geographic concentration index comprehensively evaluates the degree and structure of industrial agglomeration. Accordingly, to find the dominant industries and leading industries in different cities, the present research concentrated on evaluating the impacts of different industrial agglomerations, in different regions, on the local and surrounding carbon efficiencies. The number of employees for each industry was obtained from public data. Therefore, we used the location entropy to measure the level of urban industrial agglomeration. The formula for calculating the industrial agglomeration level is

$$LQ_{ij} = \frac{e_{ij}/e_j}{E_i/E}, \tag{2}$$

where e_{ij} indicates the number of employees in industry i in city j, e_j indicates the total number of employees in city j, E_i indicates the total number of employees in industry i in the country, and E indicates the total number of employees in the country. The larger the value of LQ_{ij}, the more obvious

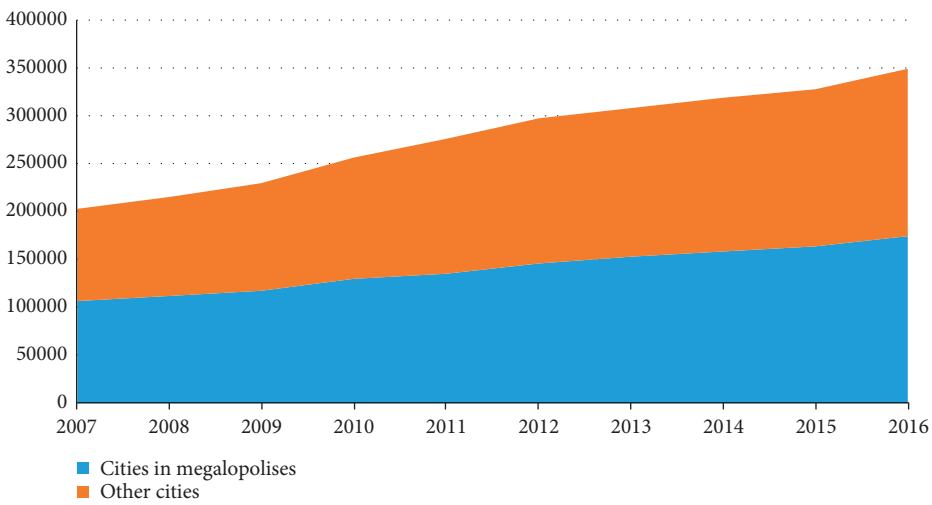

Figure 1: The CO_2 emissions in megalopolises and other cities from 2007 to 2016 (unit: 10,000 ton).

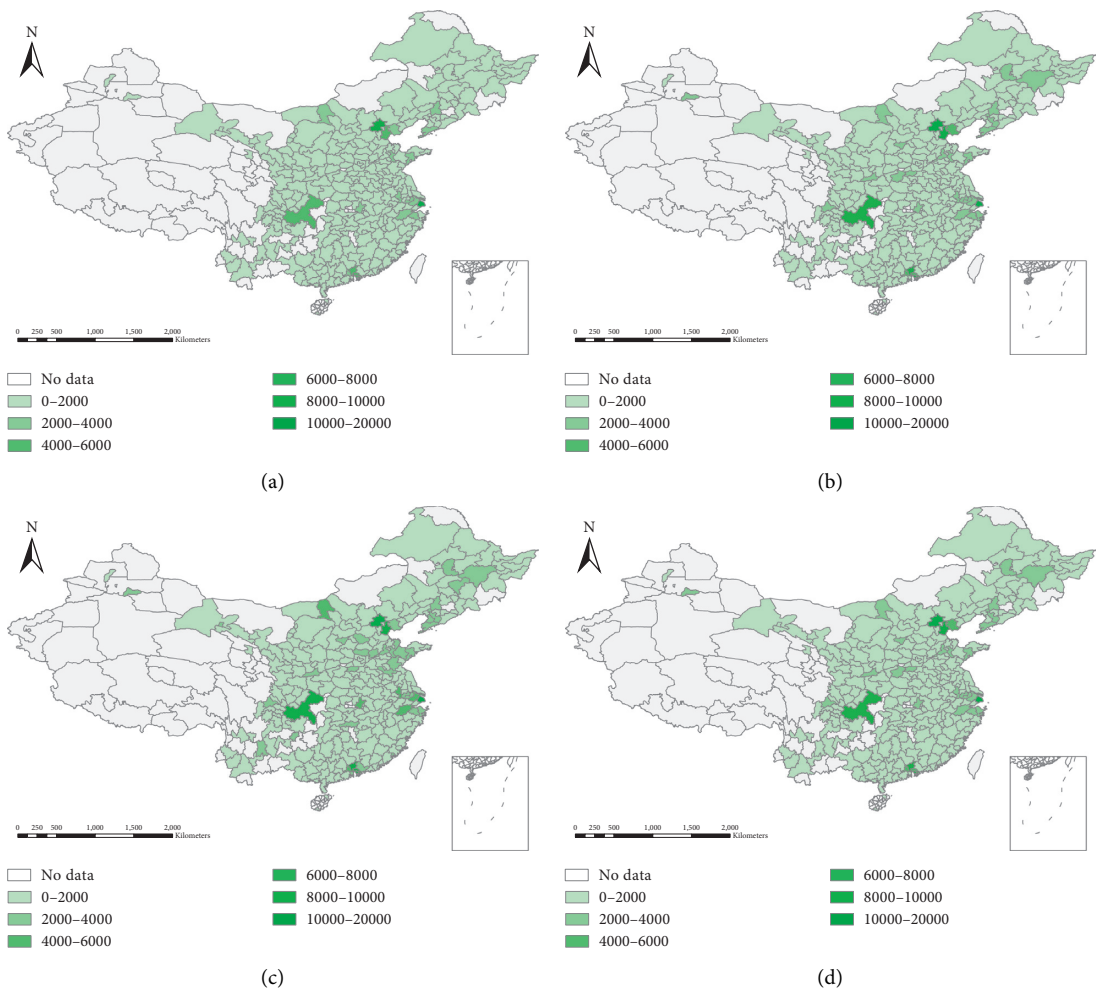

Figure 2: The spatial distribution of CO_2 emissions at the city level in China. (a) CO_2 emissions in 2007. (b) CO_2 emissions in 2011. (c) CO_2 emissions in 2016. (d) Average of CO_2 emissions from 2007 to 2016.

the agglomeration advantage. When $LQ_{ij} > 1$, it indicates that the development intensity of the industry in the region is higher than the national average for similar industries; when $LQ_{ij} > 1.5$, it indicates that the development intensity of the industry in the region has a significant comparative advantage.

In the manufacturing sector, due to the lack of complete classification statistics for the above prefecture-level city, the preset study analyzed it as a whole and could not discuss the segmented manufacturing industries any further. In 2011, China established classification standards for the 15 sub-industries of the service sector. Complete employment statistics were available at the city level, and the preset study categorized them accordingly. In the classification of the service industries, referring to Li and Li [52] and Lu [53], we divided the service sector into three categories: (1) the productive service industries whose service targets are the manufacturers of industrial goods; (2) the living service industries who serve to the final consumer; and (3) the public service industries whose providers are governments. The public administrations determine the size of the public service industry, and it was not discussed in the present study. In terms of the intensity of knowledge accumulation in the productive service industry, there exist high-end productive service industries with strong knowledge accumulation and low-end productive service industries with low knowledge accumulation [54]. Accordingly, this paper focused on the specific industries within manufacturing, productive services (high-end and low-end), and living services (see Table 2).

Based on the original data of employees in 285 above prefecture-level cities in China, the location entropy calculation formula was used to measure the average annual value of agglomeration level of each industry in various cities (Figure 3). Figure 4 shows the average location entropy in the different areas.

As shown in Figure 3, manufacturing showed a significant aggregation in space, especially in the eastern coastal areas. However, there were no apparent spatial agglomerations in the distributions of the service industries. In Figure 4, the average degree of the manufacturing agglomeration of each megalopolis was higher than that at the national level. The levels of manufacturing agglomeration decreased in the order of the Pearl River Delta, Yangtze River Delta, and Circum-Bohai Sea Economic Zone, respectively. The average concentrations of all kinds of service industries in the Circum-Bohai Sea Economic Zone were higher than those in the Pearl River Delta and the Yangtze River Delta. The concentration of the productive service industry in the Pearl River Delta was the lowest of the three megalopolises.

3.4. Fractional-Order Grey Forecasting Model. At present, there are two popular methods to make forecasting: (1) the white box models, commonly used as the differential equations, and (2) the black box models, such as the machine learning models. The grey models take the merits of above models. Especially, the grey models are good at modeling time series forecasting in small sample [55]. The grey model is between the black model and the white model. It contains both unknown information and known information. At the same time, the factors in the system have uncertain relations, and the biggest characteristic is that the accumulation process can reflect the regularity of the data. This model has been applied well in many fields since its establishment [56]. The old grey models all are integer derivative models, which belong to ideal memory models and are not suitable for describing some irregular phenomena. In fact, the grey model is usually fractional. For example, the weather is the derivative of fractional order of climate, so it is the bridge between cause and effect in the complex system. Moreover, when the objects with fractional characteristics are described by fractional order, the essential characteristics and behaviors of the objects can be better revealed [57]. Therefore, this method is capable to describe dynamic behavior of the processes and systems with high accuracy and concise models. The economic phenomena are the activities of multiagent social system, so fractional-order grey forecasting is capable for addressing our topic.

Referring to Wu [55], this paper used the fractional-order grey forecasting model to forecast the carbon efficiency and industrial agglomeration degree of each prefecture-level city from 2017 to 2021. The modeling steps are as follows.

Step 1. The cumulative sequence of order (p/q) was calculated:

$$X^{(p/q)} = \left(x^{(p/q)}(1), x^{(p/q)}(2), \ldots, x^{(p/q)}(n)\right). \tag{3}$$

Step 2. A non-negative sequence, $X^{(0)} = (x^0(1), x^0(2), \ldots, x^0(n))$, should be an accumulation operator of order $p/q\,(0 < (p/q) < 1)$. Stipulate $C^0_{(p/q)-1} = 1, C^{k+1}_k = 0$, $k = 0, 1, \ldots, n-1, C^{k-i}_{k-i+(p/q)-1} = (((k-i+(p/q)-1)(k-i+(p/q)-2), \ldots, ((p/q)+1)(p/q))/(k-i)!)$, and it is called a cumulative sequence of order $(p/q)\,(0 < (p/q) < 1)$.

Step 3. Substituting $x^{p/q}(k)\,(k = 1, 2, \ldots, n)$ into Step 2, the least square method is used to estimate parameter $\begin{bmatrix} \widehat{\beta}_2 \\ \widehat{\beta}_1 \end{bmatrix}$.

Step 4. Using $x^{(p/q)}(k) = (x^0(1) - (\widehat{\beta}_2/(1-\widehat{\beta}_1)))\widehat{\beta}_1^{(k-1)} + (\widehat{\beta}_2/(1-\widehat{\beta}_1))$ to predict $\widehat{x}^{(p/q)}(1), \widehat{x}^{(p/q)}(2), \ldots,$.

Step 5. Decrease $X^{(p/q)} = (\widehat{x}^{(p/q)}(1), \widehat{x}^{(p/q)}(2), \ldots, \widehat{x}^{(p/q)}(n), \ldots,)$ by order (p/q). That is,

$$\alpha^{(p/q)}X^{(0)} = \left(\alpha^{(1)}\widehat{x}^{1-(p/q)}(1), \alpha^{(1)}\widehat{x}^{1-(p/q)}(2), \ldots, \alpha^{(1)}\widehat{x}^{1-(p/q)}(n), \alpha^{(1)}\widehat{x}^{1-(p/q)}(n+1), \ldots,\right). \tag{4}$$

Table 2: A classification of the service industries.

Name	Industry category
High-end productive services	Information transmission, computer services, and software; finance; scientific research, technical services, and geological prospecting
Low-end productive services	Transportation, warehousing, and postal services; leasing and business services
Living services	Wholesale and retail trade; accommodation and catering; resident services and other services; culture, sports, and entertainment; real estate

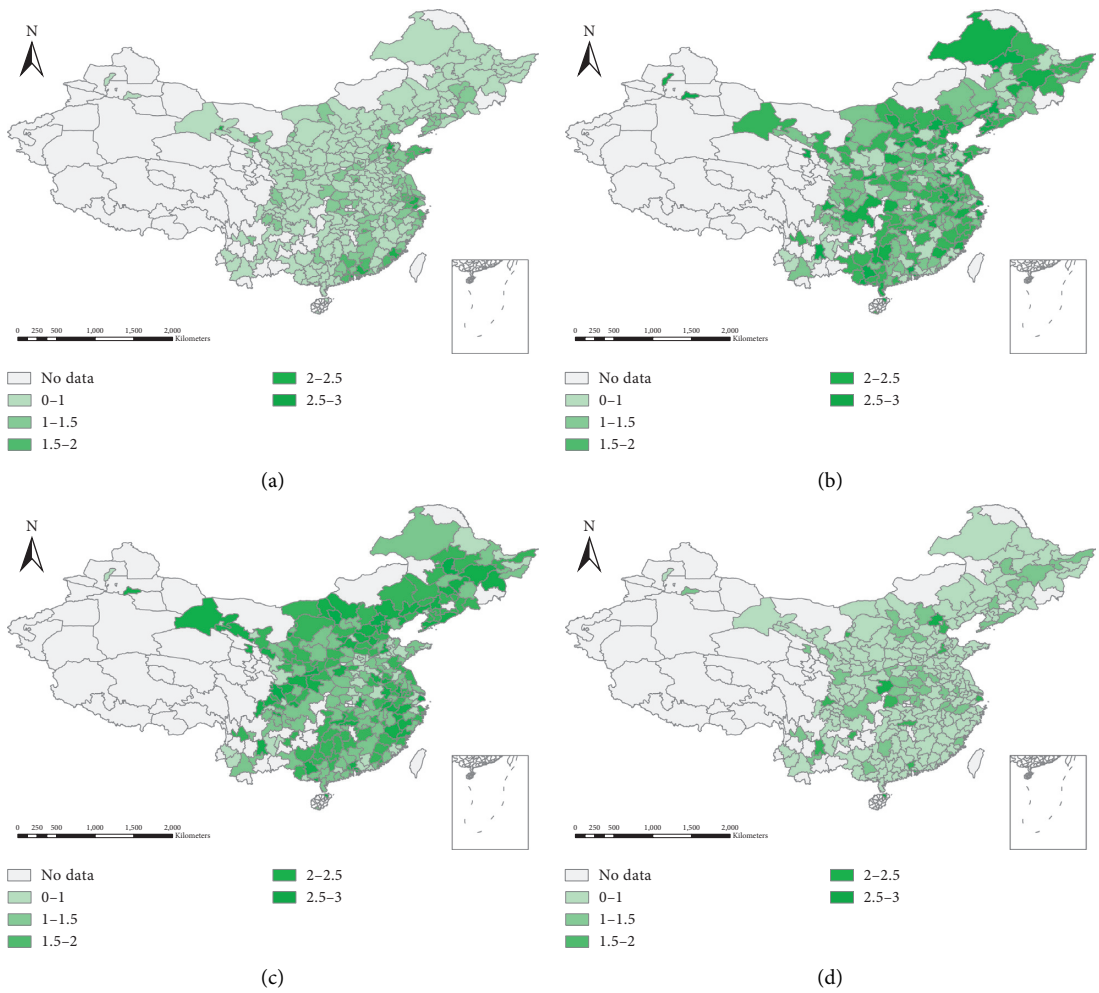

Figure 3: The spatial distribution of the average annual value (2007–2016) of the location entropy of each industry at city level. (a) Manufacturing industry. (b) Low-end productive service industry. (c) High-end productive service industry. (d) Living service industry.

4. Econometric Models and Main Results

4.1. Basic Model. Referring to Griliches [58], we assumed that the Cobb–Douglas function can manifest the production function of city i at period t:

$$Y_{it} = A\left(L_{it}^{\alpha}\right)\left(K_{it}^{\phi}\right)\left(E_{it}^{\varphi}\right)e^{\varepsilon_{it}}, \quad \alpha + \phi + \varphi = 1, \tag{5}$$

where Y_{it} is the desirable output, L_{it}, K_{it}, and E_{it} are the labor, capital, and energy consumption for urban production, respectively, A denotes the total factor productivity, which is related to economies of economy, technology change, technology spillover, and institutional arrangements, α, ϕ, and φ are the production elasticities, and ε is the error term. Divide both sides of equation (5) by C (CO_2 emission):

$$\mathrm{YC}_{it} = A\left(\mathrm{LC}_{it}^{\alpha}\right)\left(\mathrm{KC}_{it}^{\phi}\right)\left(\mathrm{EC}_{it}^{\varphi}\right)e^{\varepsilon_{it}}, \tag{6}$$

where $\mathrm{YC}_{it} = (Y_{it}/C_{it})$ is the desirable output per unit of CO_2 emissions, denoting the carbon efficiency. $\mathrm{LC}_{it} = (L_{it}/C_{it})$, $\mathrm{KC}_{it} = (K_{it}/C_{it})$, and $\mathrm{EC}_{it} = (E_{it}/C_{it})$ are input factor-carbon ratios including labor, capital, and energy consumption, describing the efficiencies of input

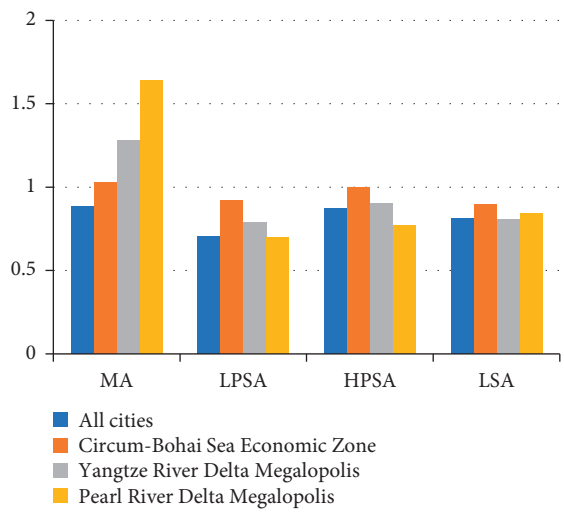

Figure 4: Averages of the location entropy in different areas (2007–2016).

factors. Therefore, the efficiencies of input factors are the decompositions of carbon efficiency. Take the logarithm form of equation (6) as follows:

$$\ln \mathrm{YC}_{it} = a + \alpha \ln \mathrm{LC}_{it} + \phi \ln \mathrm{KC}_{it} + \varphi \ln \mathrm{EC}_{it} + \varepsilon_{it}, \quad (7)$$

where $a = \ln A$. Also, we take government intervention (GOV) [59] and foreign direct investment (FDI) [60] as control variables in equation (7). The controlled model is

$$\begin{aligned} \ln \mathrm{YC}_{it} = a + \alpha \ln \mathrm{LC}_{it} + \phi \ln \mathrm{KC}_{it} + \varphi \ln \mathrm{EC}_{it} \\ + \lambda_1 \ln \mathrm{GOV}_{it} + \lambda_2 \ln \mathrm{FDI}_{it} + \varepsilon_{it}, \end{aligned} \quad (8)$$

where λ_1 and λ_2 are the elasticities of the control variables. Transform equation (8) into a matrix form:

$$\mathbf{YC} = \mathbf{A} + \alpha(\mathbf{LC}) + \phi(\mathbf{KC}) + \varphi(\mathbf{EC}) + \lambda_1 \mathbf{GOV} + \lambda_2 \mathbf{F\ DI} + \boldsymbol{\varepsilon}. \quad (9)$$

In equation (9), **A**, **LC**, **KC**, **EC**, **GOV**, and **F DI** are the $N \times 1$ vectors of the logarithms of independent variables and ε is the $N \times 1$ vector of error terms.

Moreover, the improvement of total factor productivity brought about by technological progress is another important way to improve carbon efficiency, other than improving the efficiency of input factors. The technology spillover and economies of scale, based on the theory of agglomeration economies, are two main driving forces promoting the total factor productivity [61, 62], which also will further strengthen carbon efficiency. Moreover, the effects of agglomeration not only affect the carbon efficiency in the local area but also affect surrounding cities [61, 63]. Therefore, we composed total factor productivity with the industrial agglomerations of native and surrounding cities. Accordingly, A_{it} can be set as

$$\begin{aligned} A_{it} = \theta_0 \left(\mathrm{MA}_{it}^{\theta_1}\right)\left(\mathrm{LPSA}_{it}^{\theta_2}\right)\left(\mathrm{HPSA}_{it}^{\theta_3}\right)\left(\mathrm{LSA}_{it}^{\theta_4}\right), \\ \prod_{j \neq i}^{N} \left(\mathrm{MA}_{jt}^{\vartheta_1 w_{ij}}\right)\left(\mathrm{LPSA}_{jt}^{\vartheta_2 w_{ij}}\right)\left(\mathrm{HPSA}_{jt}^{\vartheta_3 w_{ij}}\right)\left(\mathrm{LSA}_{jt}^{\vartheta_4 w_{ij}}\right) A_{jt}^{\delta w_{ij}}, \end{aligned} \quad (10)$$

where θ_0 is the exogenous variable noting an advanced technology for all cities national-wide; MA_{it}, LPSA_{it}, HPSA_{it}, and LSA_{it} are manufacturing, low-end productive service, high-end productive service, and living service agglomerations for city i at time t, respectively; $\theta_1, \theta_2, \theta_3$, and θ_4 indicate the elasticities of the four kinds of industrial agglomeration; and $\mathrm{MA}_{jt}^{\vartheta_1 w_{ij}}$, $\mathrm{LPSA}_{jt}^{\vartheta_2 w_{ij}}$, $\mathrm{HPSA}_{jt}^{\vartheta_3 w_{ij}}$, $\mathrm{LSA}_{jt}^{\vartheta_4 w_{ij}}$, and $A_{jt}^{\delta w_{ij}}$ are geometrically weighted values of the agglomerations of manufacturing, low-end productive service, high-end productive service, living service, and the total factor productivity of neighboring cities. The degree of effects of industrial agglomeration among cities is described by identical ϑ_1, ϑ_2, ϑ_3, ϑ_4, and δ, respectively. However, the net effects of these effects are dominated by the connectivity between each city, which can be described with the exogenous friction terms w_{ij}, where $j = 1, \ldots, N$ and $j \neq i$. The closer the connectivity exists, the higher the value w_{ij} takes. We took the logarithm of equation (10) and transformed it into a matrix form:

$$\begin{aligned} \mathbf{A} = \boldsymbol{\theta}_0 + \theta_1 \mathbf{MA} + \theta_2 \mathbf{LPSA} + \theta_3 \mathbf{HPSA} + \theta_4 \mathbf{LSA} \\ + \vartheta_1 \mathbf{WMA} + \vartheta_2 \mathbf{WLPSA} + \vartheta_3 \mathbf{WHPSA} + \vartheta_4 \mathbf{WLSA} + \delta \mathbf{WA}, \end{aligned} \quad (11)$$

where **MA**, **LPSA**, **HPSA**, and **LSA** are the $N \times 1$ vectors of the logarithms of industrial agglomeration and **W** is the $N \times N$ matrix of the friction term w_{ij}. If $\vartheta_1 \neq 0$, $\vartheta_2 \neq 0$, $\vartheta_3 \neq 0$, $\vartheta_4 \neq 0$, and $\delta \neq 0$ and if $(1/\vartheta_1)$, $(1/\vartheta_2)$, $(1/\vartheta_3)$, $(1/\vartheta_4)$, and $(1/\delta)$ are not eigenvalues of **W**, equation (11) can be transformed to

$$\begin{aligned} A = (\mathbf{I} - \delta \mathbf{W})^{-1} \boldsymbol{\theta}_0 + \theta_1 (\mathbf{I} - \delta \mathbf{W})^{-1} \mathbf{MA} + \theta_2 (\mathbf{I} - \delta \mathbf{W})^{-1} \mathbf{LPSA} \\ + \theta_3 (\mathbf{I} - \delta \mathbf{W})^{-1} \mathbf{HPSA} + \theta_4 (\mathbf{I} - \delta \mathbf{W})^{-1} \mathbf{LSA} + \vartheta_1 (\mathbf{I} - \delta \mathbf{W})^{-1} \mathbf{WMA} \\ + \vartheta_2 (\mathbf{I} - \delta \mathbf{W})^{-1} \mathbf{WLPSA} + \vartheta_3 (\mathbf{I} - \delta \mathbf{W})^{-1} \mathbf{WHPSA} + \vartheta_4 (I - \delta \mathbf{W})^{-1} \mathbf{WLSA}. \end{aligned} \quad (12)$$

Substitute equation (12) into equation (9) and multiply equation (9) by $(\mathbf{I} - \delta\mathbf{W})$ on both sides:

$$\begin{aligned}\mathbf{YC} = {} & \boldsymbol{\theta}_0 + \delta\mathbf{WYC} + \theta_1\mathbf{MA} + \theta_2\mathbf{LPSA} + \theta_3\mathbf{HPSA} + \theta_4\mathbf{LSA} + \alpha\mathbf{LC} + \varphi\mathbf{KC} \\ & + \phi\mathbf{EC} + \lambda_1\mathbf{GOV} + \lambda_2\mathbf{F\ DI} + \vartheta_1\mathbf{WMA} + \vartheta_2\mathbf{WLPSA} + \vartheta_3\mathbf{WHPSA} \\ & + \vartheta_4\mathbf{WLSA} + \vartheta_5\mathbf{WLC} + \vartheta_6\mathbf{WKC} + \vartheta_7\mathbf{WEC} + \vartheta_8\mathbf{WGOV} + \vartheta_9\mathbf{WF\ DI} + \zeta,\end{aligned} \tag{13}$$

where $\vartheta_5 = -\alpha\delta$, $\vartheta_6 = -\phi\delta$, $\vartheta_7 = -\varphi\delta$, $\vartheta_8 = -\lambda_1\delta$, $\vartheta_9 = -\lambda_2\delta$, and $\xi = \varepsilon - \delta W\varepsilon$. Describe equation (13) with the subscript i and obtain the carbon efficiency of city i:

$$\begin{aligned}\ln \mathrm{YC}_{it} = {} & \ln \theta_0 + \delta \sum_{j \neq i}^{N} w_{ij}\mathrm{YC}_{it} + \theta_1 \ln \mathrm{MA}_{it} + \theta_2 \ln \mathrm{LPSA}_{it} + \theta_3 \ln \mathrm{HPSA}_{it} \\ & + \theta_4 \ln \mathrm{LSA}_{it} + \alpha \ln \mathrm{LC} + \varphi \ln \mathrm{KC} + \phi \ln \mathrm{EC} + \lambda_1 \ln \mathrm{GOV} + \lambda_2 \ln \mathrm{FDI} \\ & + \vartheta_1 \sum_{j \neq i}^{N} w_{ij} \ln \mathrm{MA}_{it} + \vartheta_2 \sum_{j \neq i}^{N} w_{ij} \ln \mathrm{LPSA}_{it} + \vartheta_3 \sum_{j \neq i}^{N} w_{ij} \ln \mathrm{HPSA}_{it} \\ & + \vartheta_4 \sum_{j \neq i}^{N} w_{ij} \ln \mathrm{LSA}_{it} + \vartheta_5 \sum_{j \neq i}^{N} w_{ij} \ln LC_{it} + \vartheta_6 \sum_{j \neq i}^{N} w_{ij} \ln KC_{it} \\ & + \vartheta_7 \sum_{j \neq i}^{N} w_{ij} \ln \mathrm{EC}_{it} + \vartheta_8 \sum_{j \neq i}^{N} w_{ij} \ln \mathrm{GOV}_{it} + \vartheta_9 \sum_{j \neq i}^{N} w_{ij} \ln \mathrm{FDI}_{it} + \zeta_{it}.\end{aligned} \tag{14}$$

Equation (14), which includes both local effects and spatial effects, is called a spatial Durbin model. The descriptive statistics for the above variables are shown in Table 3. The original data sources were the China City Statistical Yearbook, China Energy Statistics Yearbook, and Beijing Shu Huitong Environmental Technology Research Institute Data Service Network (http://www.3edata.com).

4.2. Spatial Weighted Matrix and Spatial Correlation Analysis. Based on the availability of data sources, we constructed and standardized the weighted spatial matrix with a geographical distance matrix, where the sum of elements of each row is equal to one:

$$W_{ij} = \frac{1}{d_{ij}^2}, \quad i \neq j, \tag{15}$$

where d_{ij} is the distance between each pair of cities based on latitudinal and longitudinal data, where $i \neq j$. The geographical attenuation parameter takes the value of 2. On the basis of W_{ij}, the present study used Moran's I index to measure the autocorrelation in the geographical distribution of the explained variables and the core explanatory variables:

$$I = \frac{n}{\sum_{i=1}^{n}\sum_{j=1}^{n} W_{ij}} \times \frac{\sum_{i=1}^{n}\sum_{j=1}^{n} W_{ij}\left(X_i - \overline{X}\right)\left(X_j - \overline{X}\right)}{\sum_{i=1}^{n}\left(X_i - \overline{X}\right)^2}, \tag{16}$$

where X_i is the value of the variable for region i. Moran's I index takes a value within [-1, 1]. A positive value indicates that the distribution of the spatial agglomeration of the variable of interest is in a specific region with similar values; otherwise, it will follow the discrete distribution. If Moran's I value is close to zero, observed values are randomly distributed and have no relationship in space. As shown in Table 4, Moran's I values of carbon efficiency, manufacturing agglomeration, and high-end productive service agglomeration all meet the significance test at the 1% level, indicating that these variables have significant spatial dependencies. The low-end productive service passed the significance test for most years, but a small part of the living service industrial agglomeration degree passed the significance test. Therefore, the results showed that it is necessary to consider the spatial effects of industrial agglomeration on carbon efficiency.

In order to make up the lag of the released data in the official statistics and also to make the division of functional space between cities more convincing, in this part, we use the data from 2007 to 2016 and the fractional-order grey prediction model to forecast the data of the urban carbon efficiency and industrial agglomeration degree from 2017 to 2021 and measure the Moran value according to the prediction results (i.e., all the predictions for Moran's I index were calculated again based on the predicted data). The results show that the spatial correlation of carbon efficiency is expected to stabilize at a high level during 2017–2021 after experiencing the "high-low-high-low" fluctuation. For the

Table 3: Sample statistics of carbon efficiency and other variables of Chinese cities.

Variables	Mean	Std. dev.	Min.	Max.
YC (GDP-carbon ratio, yuan/ton, 2010 price)	23574.30	14808.54	1161.51	174833.01
MA (manufacturing agglomeration)	0.8870	0.4917	0.0219	2.9114
LPSA (low-end productive service agglomeration)	0.7066	0.3766	0.1065	2.7629
HPSA (high-end productive service agglomeration)	0.8706	0.3262	0.2452	3.0570
LSA (living service agglomeration)	0.8150	0.4335	0.1554	4.9674
LC (labor-carbon ratio, person/10,000 ton)	762.92	549.61	34.83	6558.53
KC (capital-carbon ratio, yuan/ton, 2010 price)	69842.46	55213.73	2733.59	722772.70
EC (energy-carbon ratio, kW·h/ton)	786.00	336.84	118.30	9881.44
GOV (public finance income-GDP ratio, %)	7.2893	3.8857	0.4208	120.6395
FDI (foreign direct investment, 10,000 yuan, 2010 price)	501408.20	1211010.00	106.28	20475308.20

Table 4: Moran's I values.

Year	YC	MA	LPSA	HPSA	LSA
2007	0.025***	0.102***	0.013***	0.012***	0.003
2008	0.020***	0.104***	0.009**	0.013***	0.003
2009	0.017***	0.105***	0.005*	0.015***	0.001
2010	0.022***	0.109***	0.005*	0.022***	0.005*
2011	0.023***	0.100***	0.008**	0.021***	0.002
2012	0.014***	0.112***	0.010**	0.021***	0.007**
2013	0.009***	0.129***	0.001	0.025***	0.006*
2014	0.012***	0.133***	−0.003	0.031***	−0.001
2015	0.016***	0.134***	0.000	0.036***	0.002
2016	0.014***	0.133***	−0.003	0.034***	0.009**
2017	0.021***	0.128***	−0.001	0.033***	0.005*
2018	0.020***	0.120***	−0.001	0.033***	0.007**
2019	0.020***	0.111***	0.001	0.031***	0.008**
2020	0.019***	0.100***	0.002	0.030***	0.010**
2021	0.019***	0.089***	0.003	0.029***	0.010***

Note. The symbols *, **, and *** represent significance levels at 10%, 5%, and 1%, respectively.

manufacturing and high-end productive service, which are of representative significance in the spatial division of urban labor, their Moran's I value continued to rise from 2007 to 2014. After reaching the maximum value in 2015, both of them showed a decreasing trend in the following year. According to the results of fractional-order grey prediction, their spatial correlation decreased year by year from 2017 to 2021, which also well confirmed the changing trend. It is worth noting that the spatial correlation of the living service industry in each city gradually emerged, and its spatial correlation showed a stable upward trend from 2017 to 2021. The results give us the following implications. (1) In terms of the spatial correlation of carbon efficiency, except for carbon dioxide due to its natural characteristics, the economic correlation between cities is increasingly close. The carbon efficiency presents a "high-high" agglomeration trend in space, and the spatial correlation degree expressed by Moran's I values remains at a high level in the predicted years. (2) The essence of the spatial division of labor in urban agglomerations discussed above is that cities of different levels focus on the development of different industries. According to the Moran value of the predicted values, it can be found that the pattern of urban functional spatial division of labor still exists at the national level. Especially for manufacturing and high-end productive service, local government should choose industries with comparative advantages according to their development status and resource endowment, to form "staggered peak" development among cities. China's overall economic development will continue to advance in this development direction. (3) As a living service industry whose main function is to meet a number of necessary needs in residents' life, the development of this industry is highly correlated with urban economic conditions and residents' wealth. The increasing degree of spatial correlation of this industry year by year also proves that economic development among cities is more closely correlated.

4.3. Determination of Spatial Econometric Model. In order to accurately reflect the degree of spatial effects and the reasons for the spatial dependence, it is necessary to select a suitable spatial econometric model before doing the regression analysis. Referring to Elhorst [64], the method of "specific to general" was used in the preset study to identify the spatial econometric model (Table 5). First, the Lagrange multiplier (LM) tests were used to choose the spatial autoregressive model (SAR) or the spatial error model (SEM). If both LM_lag and R-LM_lag fail the significance test, we choose the SAR. If both LM_err and R_LM_err fail the significance test, we choose the SEM. In the present study, we rejected the SEM because both LM_err and R_LM_err passed the

Table 5: Tests of the spatial econometric model.

Contents	Methods	Statistic value	*P* value
SAR and SEM	LM_lag test	138.865	≤0.01
	LM_err test	3274.995	≤0.01
	R-LM_lag test	0.372	0.542
	R-LM_err test	3136.502	≤0.01
Hausman test of SDM	Hausman test	5266.850	≤0.01
	Wald test	333.270	≤0.01
		173.850	≤0.01
Simplified test of SDM	LR test for SDM or SAR	307.100	≤0.01
	LR test for SDM or SEM	60.130	≤0.01

significance tests. However, we could not choose the SAR on the condition that the LM_lag passed the significance test and the R-LM_lag failed the significance test. We need to determine whether the spatial Durbin model (SDM) could degenerate into SAR and SEM through performing the LR test and Wald test. Because both of these results significantly rejected the null hypothesis, we chose the SDM for the spatial econometric regression. Then, we performed a Hausman test to determine whether the model uses fixed or random effects. However, when calculating the variance inflation factor (VIF), we found that the addition of urban fixed effects would produce multicollinearity problem (VIF>10) among the explanatory variables (Table 6). Since the result of the Hausman test significantly rejected the null hypothesis, we used the time fixed spatial Durbin model.

Table 6: Test of the fixed effects.

Variables	Fixed individual dummy variable	Fixed time dummy variable
	VIF value	VIF value
lnMA	11.68	1.60
lnLPSA	5.40	1.63
lnHPSA	5.98	1.48
lnLSA	5.53	1.40
lnLC	8.39	3.42
lnKC	4.96	3.98
lnEC	3.06	1.19
lnGOV	3.56	1.34
lnFDI	8.88	1.77

4.4. Estimated Results of Spatial Econometric Model. According to Table 5, we chose the SDM with the time fixed effect to estimate equation (14). To take the robustness test, we also estimated OLS, SAR, SEM, and SLX with the time fixed effect (Table 7). Most explanatory variables passed the significance test, which indicated that the empirical data support the theoretical model and variables. Also, urban carbon efficiency is affected by both the endogenous and exogenous spatial interaction effects.

The spatial econometric model includes the interaction terms between the spatial weight matrix and the explained variables. It also includes the interaction terms between the spatial weight matrix and the explanatory variables. Consequently, the total effect includes two parts: the direct effect of the local area and the indirect effect caused by other areas (also known as spatial spillover effect). As the spatial spillover effect, the change of explanatory variables will cause the change of the carbon efficiency both in the local area and surrounding areas. Therefore, the change of carbon efficiency in surrounding areas will eventually cause the change of carbon efficiency in the local area owing to the feedback effect [65]. In other words, the change of the explanatory variables of city i at time t will not only have a direct impact on the explained variable of the city itself but also have an indirect impact on the explained variable of other cities (i.e., the adjacent areas of the city) and will eventually affect the area in turn (because for other areas, the area is also the "other area"). Therefore, considering the global effect in the spatial Durbin model, the coefficients of the explanatory variables only represent the direction and significance of their influences on the explained variable in the SDM model but do not reflect their actual marginal effects, which was raised as an issue by LeSage and Pace [66]. Accordingly, to solve the problem of the coefficients in the spatial econometric model being difficult to explain, we further separated the direct and indirect effects (Table 8). The direct effects contain the pure direct effects and the feedback effects on local carbon efficiency. The indirect effects contain the spatial impact of the explanatory variables from the surrounding areas on the local carbon efficiency, reflecting the spatial spillover effect.

As shown in Table 8, we found that the agglomeration effects of various industries showed significant heterogeneity. Thus, Hypothesis 1 is validated. The agglomeration of manufacturing industry and the agglomeration of high-end productive services have significant impacts on the urban carbon efficiency. In addition, the impact of the high-end productive service is greater than that of the manufacturing industry, while the low-end productive services and living services have negative impacts on the urban carbon efficiency. Li et al. indicated that the greater demand for energy from fossil fuels of the manufacturing industry results in more CO_2 emissions than other industries [67]. However, in the process of manufacturing industry agglomeration, the knowledge spillover, economies of scale of intermediate inputs, the information exchange among enterprises, and the multiple infrastructure construction will further promote carbon efficiency [29, 30, 68]. The impacts of segmented service industries showed significant heterogeneity. In the high-end

Table 7: Estimation results of the spatial econometrics.

Variables	OLS	SAR	SEM	SLX	SDM
lnMA	0.0642***	0.0636***	0.0558***	0.0413***	0.0449***
	(8.67)	(8.56)	(7.46)	(5.29)	(5.86)
lnLPSA	−0.0168	−0.0166	−0.0217	−0.0192*	−0.0168*
	(−1.64)	(−1.63)	(−2.18)	(−1.93)	(−1.72)
lnHPSA	0.0771***	0.0779***	0.0841***	0.0917***	0.0954***
	(6.22)	(6.26)	(6.86)	(7.39)	(7.86)
lnLSA	−0.0489***	−0.0491***	−0.0453***	−0.0324***	−0.0323***
	(−4.71)	(−4.73)	(−4.38)	(−3.25)	(−3.10)
lnLC	0.3102***	0.3098***	0.3011***	0.3067***	0.2888***
	(30.48)	(30.44)	(29.34)	(29.37)	(27.27)
lnKC	0.5845***	0.5839***	0.5980***	0.5846***	0.6056***
	(58.92)	(58.31)	(59.34)	(57.24)	(57.75)
lnEC	0.0168	0.0156	0.0110	0.0171	0.0166
	(1.47)	(1.35)	(0.98)	(1.51)	(1.50)
lnGOV	−0.1449***	−0.1449***	−0.1424***	−0.1459***	−0.1328***
	(−13.78)	(−13.78)	(−13.47)	(−13.48)	(−12.16)
lnFDI	0.0431***	0.0430***	0.0379***	0.0247***	0.0243***
	(16.71)	(16.64)	(13.97)	(8.15)	(8.16)
W*lnYC		0.0280	0.8810***		0.7410***
		(0.65)	(34.07)		(22.95)
W*lnMA				0.2622***	0.1604***
				(4.52)	(2.58)
W*lnLPSA				0.0929	0.2920**
				(0.93)	(2.48)
W*lnHPSA				−0.0475	0.1181
				(−0.64)	(0.88)
W*lnLSA				−0.0936	−0.0918
				(−1.00)	(0.84)
W*lnL*C*				−0.0775*	0.1160
				(−1.88)	(1.23)
W*lnKC				−0.1404***	−0.9061***
				(−4.81)	(−10.66)
W*lnEC				0.2639***	0.4451***
				(3.07)	(3.73)
W*lnGOV				−0.3234***	−0.3823***
				(−4.16)	(−3.36)
W*lnFDI				0.0900***	0.0620***
				(5.49)	(3.39)
log-lik	563.3508	563.5052	630.6464	663.2215	715.5981
R^2	0.8942	0.8976	0.8970	0.9045	0.9092
Observation	2850	2850	2850	2850	2850

Note. The symbols *, **, and *** represent significance levels at 10%, 5%, and 1%, respectively; the values in parentheses are *t* statistics; log-lik is log-likelihood.

productive service industry, the learning effect of knowledge spillover among enterprises, with the high added value of products, has brought significant improvements in efficiency. On the contrary, the agglomeration of the low-end productive service industries, such as transportation, warehousing and postal industry, and leasing and business service industry, cause an increase in direct energy consumption and "crowding effect" as bad as urban congestion and resource waste to worsen the urban carbon efficiency. Therefore, in order to achieve low-carbon development, priority should be given to the high-end productive service industry with the characteristics of knowledge- and capital-intensiveness.

The impacts of industrial agglomerations on carbon efficiency from neighboring areas, that is, the spatial spillover effect brought by urban industrial agglomeration, showed that all industries will have positive impacts on carbon efficiency. The impact of the high-end productive service industry is not significant, which shows that China is still in the early stage of industrial transformation. The high-end productive service industry with a large service radius and small transaction frequency has not shown significant spatial spillover effects. The impact of the living service industry is not significant either, which indicated that the living service industry has the characteristic of a native service.

As for other explanatory variables, the direct effect coefficients of labor-carbon ratio, capital-carbon ratio, and energy-carbon ratio are significantly positive, noting that the improvement of efficiencies of input factors has significant positive effects on the improvement of carbon efficiency. The direct and indirect effects of FDI are both significantly

Table 8: Direct and indirect effects of the SDM model.

Explanatory variables	Effects	
	Direct effects	Indirect effects
lnMA	0.0477***	0.7610***
	(6.05)	(3.05)
lnLPSA	−0.0128	1.0955**
	(−1.27)	(2.30)
lnHPSA	0.0980***	0.7468
	(8.06)	(1.39)
lnLSA	−0.0316***	0.2567
	(−3.15)	(0.59)
lnLC	0.2931***	1.2854***
	(27.87)	(3.32)
lnKC	0.5997***	−1.7800***
	(57.50)	(−4.71)
lnEC	0.0224**	1.7800***
	(2.06)	(3.41)
lnGOV	−0.1393***	−1.8826***
	(−12.99)	(−3.79)
lnFDI	0.0255***	0.3102***
	(8.69)	(4.11)

Note. The symbols *, **, and *** represent significance levels at 10%, 5%, and 1%, respectively; the values in parentheses are t statistics; log-lik is log-likelihood.

positive, which shows that FDI plays a positive role in promoting China's economic development and shows that the "pollution heaven hypothesis" is not currently available for China [67]. The coefficient of lnGOV is significantly negative, which indicates that the government should not interfere too much in the economy. Otherwise, it will lead to an inefficiency of resource allocation and the "race to the bottom" in energy utilization, which will not be conducive to improving urban carbon efficiency.

4.5. The Effects of Industrial Agglomeration on Carbon Efficiency in a Megalopolis. At the level of the megalopolis, the agglomerations of manufacturing, high-end productive service, and living service industries all play important roles in promoting the urban carbon efficiency (Table 9), while the low-end productive service industry mainly has a negative impact on the carbon efficiency. Compared with the estimated results at the national level (Table 8), the manufacturing industry and the high-end industry have the same impact direction, but the degree of industrial agglomeration in promoting carbon efficiency in the megalopolis is significantly higher than that at the national level. The reason is that the spatial concentration of industries and population in a megalopolis improve the frequencies of knowledge spillover between manufacturing and service enterprises and reduce the transportation cost of goods exchanged between enterprises. They ultimately improve the efficiency of the economic operation and the efficiency of the energy utilization of the whole region. As far as the control variables are concerned, the direct effects of labor-carbon ratio, capital-carbon ratio, and energy-carbon ratio are significantly positive, while the direct effect of lnGOV is negative. This indicates that at both the national or level of the megalopolis, too much policy intervention will reduce carbon efficiency.

Comparing three large megalopolises, the direct effect of manufacturing agglomeration in the Yangtze River Delta is the largest, and the positive spatial spillover effect of manufacturing agglomeration in the Pearl River Delta is significantly greater than that in other megalopolises. In terms of the segmented service industry, the low-end productive service industry has no significant impact in the Circum-Bohai Sea Economic Zone. The direct effect in the Yangtze River Delta city group is significantly negative, and the indirect effect in the Pearl River Delta city group is significantly negative. The high-end productive service industry has a significant positive impact in each megalopolis, and the impact degrees are arranged by the Pearl River Delta, the Yangtze River Delta, and the Circum-Bohai Sea Economic Zone from large to small. All of the above are consistent with Hypothesis 2. It is worth noting that the spatial effect of high-end productive service agglomeration in the Pearl River Delta megalopolis is far greater than other megalopolises, which provides a good example for the development of megalopolis.

We know that the manufacturing industry is inclined to be located near to the cities with productive services [69], while there also exists a "crowding out" effect between the manufacturing and service industries [70]. We further analyzed the trend of the ratio of the employment number in central cities (municipalities, subprovincial cities, and provincial capital cities) in megalopolises to measure the level of the division of labor. As shown in Figure 5, the employment proportion of high-end productive service increased in the central cities but that of manufacturing and low-end productive service decreased year by year, which partially confirm Hypothesis 3. Therefore, the central cities tend to cultivate the high-end productive service industry and gradually become "technology pools" and "market areas" for improving carbon efficiency of themselves and surrounding areas.

Table 9: Direct and indirect effects of the SDM model in three megalopolises.

Explanatory variables	Circum-Bohai Sea Economic Zone		Yangtze River Delta Megalopolis		Pearl River Delta Megalopolis	
	Direct effect	Indirect effect	Direct effect	Indirect effect	Direct effect	Indirect effect
lnMA	0.0824***	0.3533***	0.1700***	0.9558**	0.0540	2.4513***
	(4.21)	(3.53)	(3.96)	(2.13)	(0.81)	(3.85)
lnLPSA	0.0090	−0.0819	−0.0699**	−0.2967	−0.0554	−0.7830**
	(0.49)	(−0.87)	(-2.10)	(−1.09)	(−1.15)	(−2.88)
lnHPSA	0.0747***	0.0118	0.1978***	−0.4740	0.4088***	2.2624***
	(2.84)	(0.10)	(3.60)	(−0.79)	(5.04)	(4.88)
lnLSA	0.0570*	0.2721**	0.0329	0.9612*	0.0880**	0.6404**
	(1.93)	(2.62)	(0.70)	(2.05)	(2.31)	(2.82)
lnLC	0.2555***	−0.6340***	0.4077***	0.9400***	0.3041***	0.5630**
	(8.39)	(−3.54)	(11.30)	(2.91)	(6.29)	(2.45)
lnKC	0.5859***	0.3367**	0.5403***	0.1373	0.6311***	0.7830**
	(22.81)	(2.53)	(14.26)	(0.57)	(14.04)	(2.73)
lnEC	0.1922***	0.6959***	0.1319***	1.0999***	0.1133**	−1.7118***
	(3.89)	(3.17)	(3.42)	(3.32)	(2.52)	(−4.79)
lnGOV	−0.1336***	0.2348***	−0.2877***	0.0798	−0.3571***	−0.0075
	(−4.65)	(2.76)	(−4.78)	(0.15)	(−6.47)	(−0.02)
lnFDI	0.0137**	−0.0188	0.0188	−0.1689	0.1440***	0.3523***
	(2.28)	(−1.17)	(1.45)	(−1.37)	(10.65)	(3.04)

Note. The symbols *, **, and *** represent significance levels at 10%, 5%, and 1%, respectively; the values in parentheses are t statistics; log-lik is log-likelihood.

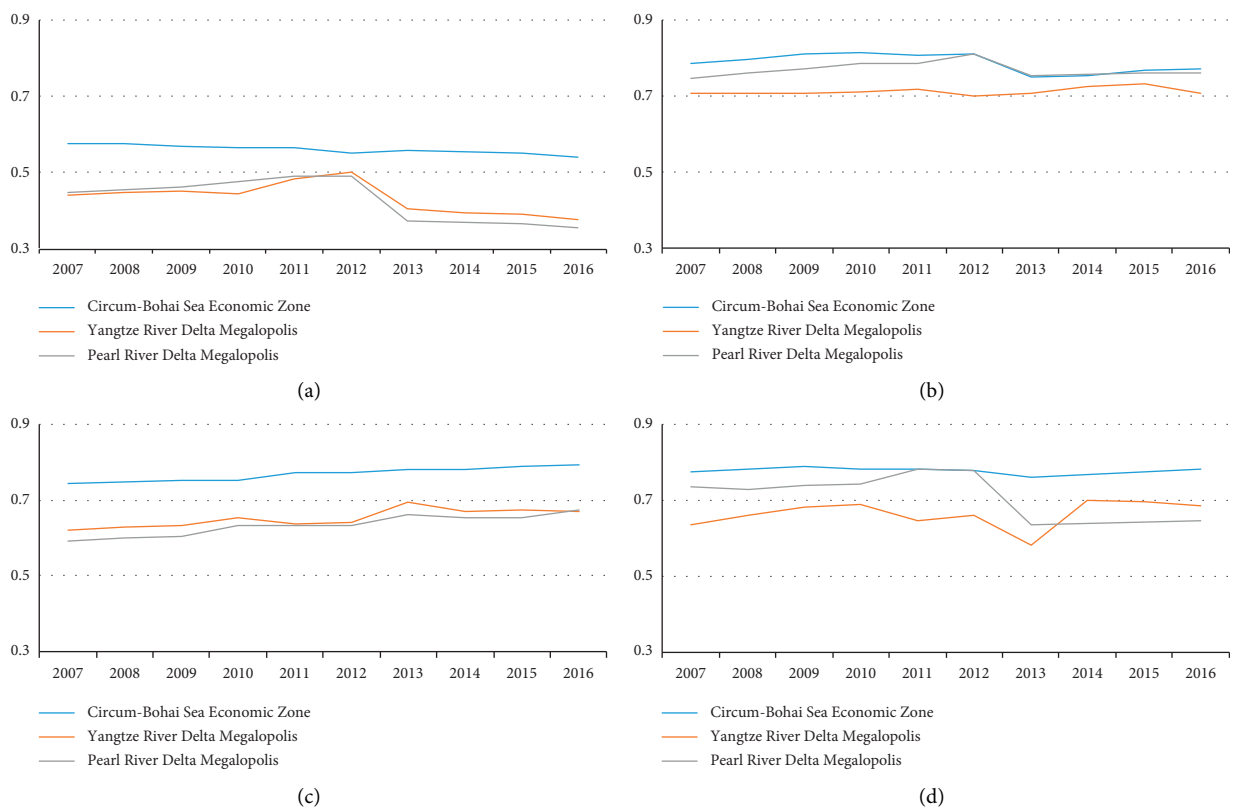

Figure 5: The ratio of employees of central cities to other cities in three megalopolises from 2007 to 2016. (a) Manufacturing industry. (b) Low-end productive service industry. (c) High-end productive service industry. (d) Living service industry.

The common cities are inclined to develop their manufacturing industry with complementary functions for neighboring areas. Therefore, the divisions of labor for central and common cities in the megalopolis are coupled with the industrial agglomeration for improving carbon efficiency.

5. Conclusion

There are two constraints on China's economic development: economic growth and the control of CO_2 emissions. In the present study, we used the spatial econometric method to explore the impact of industrial agglomeration on carbon efficiency with panel data of 285 cities above prefecture level and three megalopolises in China, for the period 2007–2016. The results showed the following. (1) At the national level, all industrial agglomerations, except the living service industry, take positive roles in improving the urban carbon efficiency, and the impact from low-end productive service agglomeration mainly comes from the spatial spillover effect. (2) Comparing the industrial agglomerations of the whole country and the megalopolises, we found that manufacturing industry, high-end productive service industry, and living service industry of each megalopolis have significant influences on the urban carbon efficiency, and the influences are greater than the average national level. (3) In the three megalopolises, manufacturing agglomeration, high-end productive service agglomeration, and living service agglomeration all significantly improve carbon efficiency. The impacts of manufacturing agglomeration and high-end productive service agglomeration on carbon efficiency are ranked from large to small in the order of the Pearl River Delta, the Yangtze River Delta, and the Circum-Bohai Sea Economic Zone. The low-end productive service agglomerations in the Yangtze River Delta and Pearl River Delta have negative effects on carbon efficiency with the crowding effect.

Accordingly, we propose several policy implications.

The empirical examination showed that manufacturing agglomeration and high-end productive service agglomeration improve carbon efficiency in the city itself and surrounding cities. With the purpose of keeping stable economic growth and reducing CO_2 emissions, the Chinese government should "unbound" the factor market and establish a "common market" between cities and release the "institutional dividend" through breaking down administrative barriers and regional trade protectionism. According to the heterogeneity of the industrial agglomeration effects, the government should accord priority to specific industries from the perspective of regional comparative advantages. It should avoid the excessive pursuit of industrial advancement in the competition of cities, especially the "comparison and pursuit" for the development of high-end productive service industry among cities.

At the level of megalopolises, compared with the national level, the agglomerations of manufacturing and high-end productive service have greater impacts on carbon efficiency. The central cities have more chances to obtain institutional and policy priority and should cultivate diversified high-end productive service industries as well as become the "technology pool" and "market area" for improving carbon efficiency in native and surrounding areas. Since the manufacturing and low-end productive service industries are more dependent on savings on production costs and improvement of transaction efficiency, the common cities should form complementary functions for central cities and make the coordinated development of manufacturing and low-end productive services.

Data Availability

The original data sources were the China City Statistical Yearbook, China Energy Statistics Yearbook, and Beijing Shu Huitong Environmental Technology Research Institute Data Service Network (http://www.3edata.com).

Conflicts of Interest

The authors declare that they have no conflicts of interest.

Acknowledgments

This study was supported by the National Natural Science Foundation of China (grant no. 71704095) (a study on regional air pollutant emission reduction target, step-by-step benchmark path and technical prediction based on environmental production technology) and Young Scholars Program of Shandong University, Weihai.

References

[1] IEA, *World Energy Outlook 2008,* https://www.iea.org/reports/world-energy-outlook-2008, International Energy Agency, Paris, France, 2008, https://www.iea.org/reports/world-energy-outlook-2008.

[2] World Bank, *Carbon Dioxide Emission Open Data 2014,* World Bank Group, Washington D.C., USA, 2014, https://data.worldbank.org/indicator/EN.ATM.CO2E.KT?view=chart.

[3] Z. Mi, Y. Zhang, D. Guan et al., "Consumption-based emission accounting for Chinese cities," *Applied Energy*, vol. 184, no. 12, pp. 1073–1081, 2016.

[4] H.-L. Lin, H.-Y. Li, and C.-H. Yang, "Agglomeration and productivity: Firm-level evidence from China's textile industry," *China Economic Review*, vol. 22, no. 3, pp. 313–329, 2011.

[5] B. B. Yu, "Economic growth effects of industrial restructuring and productivity improvement——analysis of dynamic spatial panel model with Chinese city data," *China Industrial Economics*, vol. 34, no. 12, pp. 83–98, 2015.

[6] Y. M. Liang and M. J. Dong, "Sources of China's economic growth: an analysis based on nonparametric accounting method," *China Economist*, vol. 12, no. 3, pp. 78–93, 2017.

[7] M. A. Cole, R. J. R. Elliott, and S. Wu, "Industrial activity and the environment in China: an industry-level analysis," *China Economic Review*, vol. 19, no. 3, pp. 393–408, 2008.

[8] A. Otsuka, M. Goto, and T. Sueyoshi, "Energy efficiency and agglomeration economies: the case of Japanese manufacturing industries," *Regional Science Policy & Practice*, vol. 6, no. 2, pp. 195–212, 2014.

[9] J. Li and Z. Cheng, "Study on total-factor carbon emission efficiency of China's manufacturing industry when considering technology heterogeneity," *Journal of Cleaner Production*, vol. 260, no. 7, Article ID 121021, 2020.

[10] G. Wang, X. Deng, J. Wang, F. Zhang, and S. Liang, "Carbon emission efficiency in China: a spatial panel data analysis," *China Economic Review*, vol. 56, Article ID 101313, 2019.

[11] C. Sun, Z. Li, T. Ma, and R. He, "Carbon efficiency and international specialization position: evidence from global value

chain position index of manufacture," *Energy Policy*, vol. 128, pp. 235–242, 2019.

[12] N. Zhang, F. Kong, Y. Choi, and P. Zhou, "The effect of size-control policy on unified energy and carbon efficiency for Chinese fossil fuel power plants," *Energy Policy*, vol. 70, pp. 193–200, 2014.

[13] S. Wang and Y. Ma, "Influencing factors and regional discrepancies of the efficiency of carbon dioxide emissions in Jiangsu, China," *Ecological Indicators*, vol. 90, pp. 460–468, 2018.

[14] Y. Wang, F. Duan, X. Ma, and L. He, "Carbon emissions efficiency in China: key facts from regional and industrial sector," *Journal of Cleaner Production*, vol. 206, pp. 850–869, 2019.

[15] F. Zhang, X. Deng, F. Phillips, C. Fang, and C. Wang, "Impacts of industrial structure and technical progress on carbon emission intensity: evidence from 281 cities in China," *Technological Forecasting and Social Change*, vol. 154, p. 119949, 2020.

[16] Q. Wang, B. Su, P. Zhou, and C.-R. Chiu, "Measuring total-factor CO_2 emission performance and technology gaps using a non-radial directional distance function: A modified approach," *Energy Economics*, vol. 56, no. 5, pp. 475–482, 2016.

[17] Q. Wang, Y. Hang, J.-L. Hu, and C.-R. Chiu, "An alternative metafrontier framework for measuring the heterogeneity of technology," *Naval Research Logistics (NRL)*, vol. 65, no. 5, pp. 427–445, 2018.

[18] C. L. Fang and D. Yu, *China's New Urbanization: Developmental Paths, Blueprints and Patterns*, Science Press, Beijing, China, 2016.

[19] J. Virkanen, "Effect of urbanization on metal deposition in the bay of Töölönlahti, Southern Finland," *Marine Pollution Bulletin*, vol. 36, no. 9, pp. 729–738, 1998.

[20] E. Verhoef and P. Nijkamp, "Urban environmental externalities, agglomeration forces, and the technological "Deus ex Machina"," *Environment and Planning A: Economy and Space*, vol. 40, no. 4, pp. 928–947, 2008.

[21] A. Frank, N. Moussiopoulos, P. Sahm et al., "Urban air quality in larger conurbations in the European Union," *Environmental Modelling & Software*, vol. 16, no. 4, pp. 399–414, 2001.

[22] T. A. Duc, G. Vachaud, M. P. Bonnet et al., "Experimental investigation and modelling approach of the impact of urban wastewater on a tropical river: a case study of the Nhue River, Hanoi, Viet Nam," *Journal of Hydrology*, vol. 334, no. 3, pp. 347–358, 2007.

[23] M. E. Poter, "Clusters and the new economics of competition," *Harvard Business Review*, vol. 11, pp. 77–90, 1998.

[24] P. Krugman, "Space: The final frontier," *Journal of Economic Perspectives*, vol. 12, no. 2, pp. 161–174, 1998.

[25] M. Fujita and J. F. Thisse, *Economics of Agglomeration: Cities, Industrial Location, and Regional Growth*, Cambridge University Press, Cambridge, UK, 2002.

[26] M. Hosoe and T. Naito, "Trans-boundary pollution transmission and regional agglomeration effects∗," *Papers in Regional Science*, vol. 85, no. 1, pp. 99–120, 2006.

[27] Q. Su, "The effect of population density, road network density, and congestion on household gasoline consumption in U.S. urban areas," *Energy Economics*, vol. 33, no. 3, pp. 445–452, 2011.

[28] F. Han, P. Feng, and L. G. Yang, "Spatial agglomeration effects of China's cities and industrial energy efficiency," *China Population Resources and Environment*, vol. 24, no. 05, pp. 72–79, 2014.

[29] F. Han, R. Xie, Y. Lu et al., "The effects of urban agglomeration economies on carbon emissions: evidence from Chinese cities," *Journal of Cleaner Production*, vol. 172, pp. 1096–1110, 2018.

[30] L. J. Zhang, P. J. Rong, Y. C. Qin et al., "Does industrial agglomeration mitigate fossil CO_2 emissions? an empirical study with spatial panel regression model," *Energy Procedia*, vol. 152, pp. 731–737, 2018.

[31] N. Shen, R. M. Deng, and Q. W. Wang, "Influence of agglomeration of manufacturing and the producer service sector on energy efficiency," *Polish Journal of Environmental Studies*, vol. 28, no. 5, pp. 14–31, 2019.

[32] W. Jacobs, H. R. A. Koster, and F. Van Oort, "Co-agglomeration of knowledge-intensive business services and multinational enterprises," *Journal of Economic Geography*, vol. 14, no. 2, pp. 443–476, 2014.

[33] Y. Huang, L. Li, and Y. T. Yu, "Does urban cluster promote the increase of urban eco-efficiency? evidence from Chinese cities," *Journal of Cleaner Production*, vol. 197, pp. 957–971, 2018.

[34] W. C. Yue, Y. P. Cai, Z. F. Yang et al., "Structural optimization for industrial sectors to achieve the targets of energy intensity mitigation in the urban cluster of the Pearl River Delta," *Ecological Indicators*, vol. 95, pp. 673–686, 2018.

[35] L. Chen, L. Y. Xu, and Z. F. Yang, "Accounting carbon emission changes under regional industrial transfer in an urban agglomeration in China's Pearl River Delta," *Journal of Cleaner Production*, vol. 167, pp. 110–119, 2017.

[36] Y. M. Li, L. Y. Sun, H. L. Zhang et al., "Does industrial transfer within urban agglomerations promote dual control of total energy consumption and energy intensity?" *Journal of Cleaner Production*, vol. 204, pp. 607–617, 2018.

[37] H. J. Xiao, Y. L. Shan, N. Zhang et al., "Comparisons of CO_2 emission performance between secondary and service industries in Yangtze River Delta cities," *Journal of Environmental Management*, vol. 252, pp. 109–136, 2019.

[38] J. Friedman, *Regional Development Policy: A Case Study of Venezuel*, MIT Press, Cambridge, UK, 1966.

[39] J. V. Henderson, "The sizes and types of cities," *American Economic Review*, vol. 64, no. 4, pp. 55–69, 1974.

[40] X. Deng, J. Huang, S. Rozelle et al., "Economic growth and the expansion of urban land in China," *Urban Studies*, vol. 47, no. 4, pp. 813–843, 2010.

[41] J. J. Zheng, P. Jiang, W. Qiao et al., "Analysis of air pollution reduction and climate change mitigation in the industry sector of Yangtze River Delta in China," *Journal of Cleaner Production*, vol. 114, pp. 314–322, 2016.

[42] Q. M. Yuan and A. Z. Zhang, "Research on the present situation of coordinated development and the innovation path of Beijing-Tianjin-Hebei industry," in *Proceedings of the 2015 3rd International Conference on Education, Management, Arts, Economics and Social Science*, pp. 1358–1361, Atlantis Press, Paris, France, July 2016.

[43] X. Yu, Z. Y. Wu, H. R. Zheng et al., "How urban agglomeration improve the emission efficiency? a spatial econometric analysis of the Yangtze River Delta urban agglomeration in China," *Journal of Environmental Management*, vol. 260, pp. 110–132, 2020.

[44] B. Q. Liu, C. Tian, Y. Q. Li et al., "Research on the effects of urbanization on carbon emissions efficiency of urban agglomerations in China," *Journal of Cleaner Production*, vol. 197, pp. 1374–1381, 2018.

[45] S. J. Wang, J. Y. Zeng, Y. Y. Huang et al., "The effects of urbanization on CO_2 emissions in the Pearl River Delta: a

comprehensive assessment and panel data analysis," *Applied Energy*, vol. 228, pp. 1693–1706, 2018.

[46] Q. Xu, Y. X. Dong, and R. Yang, "Urbanization impact on carbon emissions in the Pearl River Delta region: Kuznets curve relationships," *Journal of Cleaner Production*, vol. 180, pp. 514–523, 2018.

[47] X. L. Ouyang, X. Y. Mao, C. W. Sun et al., "Industrial energy efficiency and driving forces behind efficiency improvement: evidence from the Pearl River Delta urban agglomeration in China," *Journal of Cleaner Production*, vol. 220, pp. 899–909, 2019.

[48] J. B. Li, X. J. Huang, H. Yang et al., "Convergence of carbon intensity in the Yangtze River Delta, China," *Habitat International*, vol. 60, pp. 58–68, 2017.

[49] R. Xie, J. R. Fang, and C. J. Liu, "The effects of transportation infrastructure on urban carbon emissions," *Applied Energy*, vol. 196, pp. 199–207, 2017.

[50] E. L. Glaeser and M. E. Kahn, "The greenness of cities: carbon dioxide emissions and urban development," *Journal of Urban Economics*, vol. 67, no. 3, pp. 404–418, 2010.

[51] H. Q. Li, Y. Lu, J. Zhang et al., "Trends in road freight transportation carbon dioxide emissions and policies in China," *Energy Policy*, vol. 57, pp. 99–106, 2013.

[52] S. T. Li and H. X. Li, "On the characteristics and evolution trends of the distribution pattern of service industries," *Industrial Economics Research*, vol. 5, pp. 1–10, 2014.

[53] H. Y. Lu, *Research on the Development Mode and Supply Policy of Service Industry from the Perspective of Dual Upgrading of Industry and Consumption*, China Commerce and Trade Press, Beijing, China, 2016.

[54] Y. Xuan and Y. Z. Yu, "Hierarchical division of productive service industry and manufacturing efficiency—empirical study based on 38 cities in Yangtze River Delta region," *Industrial Economics Research*, vol. 3, pp. 1–10, 2014.

[55] L. F. Wu, S. Liu, L. Yao et al., "Grey system model with the fractional order accumulation," *Communications in Nonlinear Science Numerical Simulation*, vol. 18, no. 7, pp. 1775–1785, 2013.

[56] M. S. Yin and H. Tang, "On the fit and forecasting performance of grey prediction models for China's labor formation," *Mathematical and Computer Modelling*, vol. 57, no. 3-4, pp. 357–365, 2013.

[57] C. Yan, L. F. Wu, L. Y. Liu et al., "Fractional Hausdorff grey model and its properties," *Chaos, Solitons & Fractals*, vol. 138, no. 9, Article ID 109915, 2020.

[58] Z. Griliches, "Issues in assessing the contribution of research and development to productivity growth," *Bell Journal Economy*, vol. 10, pp. 92–116, 1979.

[59] F. Shi and K. R. Shen, "Government intervention, economic agglomeration and energy efficiency," *Management World*, vol. 10, pp. 6–18, 2013.

[60] F. Han, R. Xie, and J. Y. Fang, "Urban agglomeration economies and industrial energy efficiency," *Energy*, vol. 162, pp. 45–59, 2018.

[61] S. Z. Ke, "Agglomeration, productivity, and spatial spillovers across Chinese cities," *The Annals of Regional Science*, vol. 45, no. 1, pp. 157–179, 2010.

[62] F. Han and S. Ke, "The effects of factor proximity and market potential on urban manufacturing output," *China Economic Review*, vol. 39, pp. 31–45, 2016.

[63] C. Ertur and K. W. Growth, "Growth, technological interdependence and spatial externalities: theory and evidence," *Applied Economic*, vol. 22, no. 6, pp. 1033–1062, 2007.

[64] J. P. Elhorst, "Matlab software for spatial panels," *International Regional Science Review*, vol. 37, no. 1, pp. 197–206, 2014.

[65] S. Shao, X. Li, J. H. Cao et al., "The choice of economic policy for haze pollution control in China—based on the perspective of spatial spillover effect," *Economic Research*, vol. 51, no. 9, pp. 73–88, 2016.

[66] J. Lesage and R. K. Pace, *Introduction to Spatial Econometrics*, Chapman and Hall/CRC, London, UK, 2009.

[67] L. Li, Y. L. Lei, S. M. Wu et al., "Impacts of city size change and industrial structure change on CO_2 emissions in Chinese cities," *Journal of Cleaner Production*, vol. 195, pp. 831–838, 2018.

[68] D. K. Chen, S. Y. Chen, and H. Jin, "Industrial agglomeration and CO_2 emissions: evidence from 187 Chinese prefecture-level cities over 2005–2013," *Journal of Cleaner Production*, vol. 172, pp. 993–1003, 2018.

[69] S. Z. Ke, M. He, and C. H. Yuan, "Synergy and co-agglomeration of producer services and manufacturing: a panel data analysis of Chinese cities," *Regional Studies: The Journal of the Regional Studies Association*, vol. 48, no. 11, pp. 1829–1841, 2014.

[70] F. Tregenna, "The contributions of manufacturing and services to employment creation and growth in South Africa," *South African Journal of Economics*, vol. 76, p. 175, 2008.

Hindawi
Journal of Mathematics
Volume 2021, Article ID 7725125, 11 pages
https://doi.org/10.1155/2021/7725125

Research Article

Predicting the Population Growth and Structure of China Based on Grey Fractional-Order Models

Xiaojun Guo,[1,2] **Rui Zhang**,[1] **Naiming Xie**,[2] **and Jingliang Jin**[1,2]

[1]*School of Science, Nantong University, Nantong 226019, China*
[2]*College of Economics and Management, Nanjing University of Aeronautics and Astronautics, Nanjing 211106, China*

Correspondence should be addressed to Xiaojun Guo; guoxj159@163.com and Jingliang Jin; chinajjl@ntu.edu.cn

Received 29 April 2021; Accepted 3 July 2021; Published 21 July 2021

Academic Editor: Lifeng Wu

Scientific prediction and accurate grasp of the future trend of population change are conducive to the formulation of different population policies at different stages, so as to alleviate the adverse effects of the aging population on society and provide scientific theoretical reference for controlling the population size and making policy. Considering that the population system is affected by many complex factors and the structural relationship among these factors is complex, it can be regarded as a typical dynamic grey system. In this paper, the fractional-order GM (1, 1) model and the fractional-order Verhulst model are established, respectively, based on the statistical data of China's population indices from 2015 to 2019 to forecast the population size and the change trend of population structure of China from 2015 to 2050 in the short-term and medium- to long-term. The forecast results show that China's population will grow in an inverse S shape from 2015 to 2050, when the total population will reach 1.43 billion. Moreover, during this period, the birth rate and natural growth rate of population will decrease year by year, and the proportion of aging population and the dependency ratio of population will increase year by year. Besides, the problem of aging population is going to become increasingly serious. The application of grey system method to population prediction can mine the complex information contained in the population number series. Meanwhile, the fractional-order accumulation can weaken the randomness of the original data series and reduce the influence of external disturbance factors, so it is a simple and effective population prediction method.

1. Introduction

China is the country with the largest population in the world. From the perspective of the process of population development, China's population grew at a relatively high speed from the early years after the founding of the People's Republic of China to the end of the 1970s. After the reform and opening up, despite the implementation of a strong family planning policy and efforts to control population growth, the growth rate was still relatively fast in the early 1980s due to the large population base and the effect of growth inertia. As time goes on, the growth rate of population slows down and the natural growth rate slowly decreases. By 2018, the natural growth rate of China's population has been below 4‰, achieving the target of low population growth, and the population growth is in an important period of transition to a low rate of birth, death, and growth. The number and structure of the population can reflect the level of economic development of a region, and it is also the indicator to measure social progress. The change of population will affect the formulation of basic state policies, the arrangement of employment, the development of social welfare, and even the standardization of national economic and social development strategies. Only by correctly dealing with the relationship between population, resources, and economy can we promote the sustainable development of society and construct a harmonious society. Population prediction is to infer the future population development process; its purpose is to be able to predict the future population development trend, and put forward the corresponding solutions and effective suggestions. It is of great significance to the formulation of population planning

and policies, the strengthening of population management, and the formulation of national economic and social development plans.

The method of population prediction is to establish a mathematical model on the basis of understanding the objective law of population development and change, the characteristics of population variables, and their internal relations. Many scholars usually use Leslie model [1, 2], Markov model [3, 4], combination model [5], random prediction [6], and other model methods to predict and analyze the population size and structure. However, since the index parameters of the model are set on the basis of various assumptions and conjectures, the combined operation will bring cumulative errors to the prediction inevitably, resulting in a decline in the prediction accuracy. At the same time, there are many factors affecting the population system, including social and economic factors, natural environment factors, traditional customs, and thinking mode factors. The structural relationship among these factors is quite complex and in dynamic change, and its operation mechanism, change rule, and effect on population change cannot be accurately expressed, which is exactly the difficulty of population prediction. However, the grey system theory holds that the population system is a grey system containing both many known information and many unknown or uncertain information [7]. The quantity which is affected by many factors and cannot be accurately determined is called grey quantity. The grey system method is to dig and find its change rule from the time series of the grey quantity itself. The dynamic change of population time series data is the result of the interaction between the main, secondary, direct, indirect, known, unknown, obvious, and implicit factors. The interaction of these factors with known information and unknown information determines the actual grey quantity, i.e., the total population.

Grey system theory is a borderline subject with large cross-section, strong permeability, and wide application. It takes the uncertain system with small samples and poor information with "partial information known and partial information unknown" as the research object, mainly through the generation and development of some known information to extract valuable information, achieving the effective control on the system operation law [8, 9]. The essence of the core grey GM (1, 1) model is an exponential model, while the economic system, ecological system, and agricultural system can all be regarded as a generalized energy system, and the accumulation and release of energy generally have an exponential rule [10–14]. Population growth in a certain period of time in line with the exponential growth law, so the use of GM (1, 1) model for short-term prediction under the condition of low development coefficient has the higher prediction accuracy. However, the limitation of living resources and space, as well as the competition and conflict between people, will restrict the population growth, so the population growth is not an exponential model in the long run. Dutch scientist Verhulst put forward the Logistic Curve for the study of population development. The Verhulst model took into account the finiteness of the total population growth and proposed the law of the total population growth: the population growth rate gradually decreases with the total population growth, so it is applicable to the long-term population prediction [15, 16].

However, the traditional grey prediction models are all integer-order derivative models and belong to ideal memory models. The actual phenomenon is often irregular. Based on the idea of "in between," the fractional order is usually used to replace the integer order. There must be a fractional order between the 0 order and the 1 order. The order of magnitude between the accumulations can be adjusted accurately through the fractional order, and the target sequence can be generated by adjusting the order to improve the fitting accuracy of the prediction model. As an important branch of the grey system theory, Wu proposed the fractional-order accumulation grey model for the first time, which transformed the traditional first-order accumulation into fractional-order accumulation, and used the data after fractional-order accumulation to make predictions [17, 18]. It is proved that fractional-order accumulation can not only weaken the randomness of the original data series, but also make the perturbation bound of the solution of the grey prediction model smaller, which improves the priority of new information to a certain extent and indeed enhances the prediction stability of the model, thus achieving fruitful research results in many fields.

Fang proposed FGM (1, 1) to predict the maintenance cost of weapon system with small sample and improved the prediction performance [19]. Wu proposed a novel nonlinear grey Bernoulli model with fractional-order accumulation (FANGBM (1, 1)) to forecast short-term renewable energy consumption of China during the 13th Five-Year Plan [20]. Yan put forward fractional Hausdorff grey model to predict natural gas consumption, quarterly hydropower production, etc. [21]. Şahin proposed a novel optimized fractional nonlinear grey Bernoulli model (OFANGBM (1, 1)) to forecast the gross final energy consumption, energy consumption of renewable energy sources, and its share in France, Germany, Italy, Spain, Turkey, and the United Kingdom [22]. Liu developed a novel fractional grey polynomial model with time power term (FPGM (1, 1, t^{α})) for forecasting electricity consumption of India and China [23]. Based on the grey prediction model GM (1, 1), Meng proposed a novel fractional-order grey prediction model and systematically studied its modeling error [24].

The paper is organized as follows. Section 2 provides an overview on modeling process of fractional-order GM (1, 1) model, fractional-order Verhulst model, and particle swarm optimization algorithm. In Section 3, the fractional-order accumulation grey prediction models are adopted to forecast not only the total population of China, but also the birth rate, death rate, natural growth rate, and the changing trend of the age structure of the population. Finally, some conclusions are drawn and suggestions proposed in Section 4.

2. Modeling Methodologies

In fractional-order accumulation grey model, the traditional first-order accumulation is transferred into fractional-order

accumulation. And the data after fractional-order accumulation are used to forecast. This method can weaken randomness of the original data sequence, making smaller disturbance of solution of grey prediction model, and to some extent improve the priority of the new information to gain higher prediction precision.

2.1. Fractional-Order GM (1, 1) Model. The modeling process of fractional-order GM (1, 1) model (abbreviated as FGM (1, 1)) is as follows:

Step 1: set the nonnegative sequence of the original data as $X^{(0)} = \{x^{(0)}(1), x^{(0)}(2), \ldots, x^{(0)}(n)\}$, $r \in R^{+}$, and the corresponding r-order cumulative generation sequence is $X^{(r)} = \{x^{(r)}(1), x^{(r)}(2), \ldots, x^{(r)}(n)\}$, where

$$x^{(r)}(k) = \sum_{i=1}^{k} \frac{\Gamma(r+k-i)}{\Gamma(k-i+1)\Gamma(r)} x^{(0)}(i), \quad k = 1, 2, \ldots, n. \tag{1}$$

Also, $\Gamma(r+k-i) = (r+k-i-1)!$ and $\Gamma(k-i+1) = (k-i)!$, $\Gamma(r) = (r-1)!$. For background value generation of $X^{(r)}$, the sequence adjacent to the mean value generation is $Z^{(r)} = \{z^{(r)}(2), z^{(r)}(3), \ldots, z^{(r)}(n)\}$, where

$$z^{(r)}(k) = \frac{x^{(r)}(k) + x^{(r)}(k-1)}{2}, \quad k = 2, 3, \ldots, n. \tag{2}$$

Step 2: let $X^{(0)}$, $X^{(r)}$, and $Z^{(r)}$ be as described in Step 1, and r be nonnegative real numbers; then the grey differential equation of the r-order cumulative grey GM (1, 1) model (abbreviated as FGM (1, 1)) is

$$x^{(r)}(k) - x^{(r)}(k-1) + az^{(r)}(k) = b. \tag{3}$$

Here, a is the development coefficient and b is the grey action. The whitening differential equation can be expressed as

$$\frac{\mathrm{d}x^{(r)}(t)}{\mathrm{d}t} + ax^{(r)}(t) = b. \tag{4}$$

Solve differential equation (4), and the time response function can be obtained as

$$x^{(r)}(k+1) = \left(x^{(0)}(1) - \frac{b}{a}\right)e^{-ak} + \frac{b}{a}. \tag{5}$$

Step 3: set parameters a, b as described in Step 2, the parameter sequence $\begin{bmatrix} \hat{a} \\ \hat{b} \end{bmatrix}$ of FGM (1, 1) model can be based on the principle of minimum error sum of squares, and be obtained by using the least squares estimation method

$$\begin{bmatrix} \hat{a} \\ \hat{b} \end{bmatrix} = \left(B^{T}B\right)^{-1}B^{T}Y. \tag{6}$$

Here, $Y = \begin{bmatrix} x^{(r-1)}(2) \\ x^{(r-1)}(3) \\ \vdots \\ x^{(r-1)}(n) \end{bmatrix}$, $B = \begin{bmatrix} -z^{(r)}(2) & 1 \\ -z^{(r)}(3) & 1 \\ \vdots & \vdots \\ -z^{(r)}(n) & 1 \end{bmatrix}$.

Step 4: substitute the parameters $\hat{a}$ and $\hat{b}$ into the time response function (5), and set $\hat{x}^{(r)}(1) = x^{(r)}(1)$ to obtain the time response function of the original sequence

$$\hat{x}^{(r)}(k+1) = \left(x^{(0)}(1) - \frac{\hat{b}}{\hat{a}}\right)e^{-\hat{a}k} + \frac{\hat{b}}{\hat{a}}. \tag{7}$$

Here, $k = 1, 2, \ldots, n, \ldots$, $\hat{x}^{(r)}(k+1)$ is the fitting value at the time-point $k+1$, and the sequence is obtained as

$$\hat{X}^{(r)} = \left\{\hat{x}^{(r)}(1), \hat{x}^{(r)}(2), \ldots, \hat{x}^{(r)}(n), \ldots\right\}. \tag{8}$$

Step 5: r-order reduction is made for sequence $\hat{X}^{(r)}$, and the fitting sequence of original data can be obtained as $\hat{X}^{(0)} = \left\{\hat{x}^{(0)}(1), \hat{x}^{(0)}(2), \ldots, \hat{x}^{(0)}(n)\right\}$, where the reducing value is $\hat{x}^{(0)}(1) = x^{(0)}(1)$, and

$$\hat{x}^{(0)}(k) = \left(\hat{x}^{(r)}\right)^{(-r)}(k) = \sum_{i=0}^{k-1} (-1)^{i} \frac{\Gamma(r+1)}{\Gamma(i+1)\Gamma(r-i+1)} \hat{x}^{(r)}(k-i), \quad k = 2, 3, \ldots, n, \tag{9}$$

where $\Gamma(r+1) = r!$, $\Gamma(i+1) = i!$, $\Gamma(r-i+1) = (r-i)!$. And the predicted value is $\hat{x}^{(0)}(n+1)$, $\hat{x}^{(0)}(n+2)$, ….

2.2. Fractional-Order Verhulst Model. The modeling process of fractional-order Verhulst model (abbreviated as FVGM) is as follows:

Step 1: let the nonnegative sequence of the original data be $X^{(0)} = \{x^{(0)}(1), x^{(0)}(2), \ldots, x^{(0)}(n)\}$, $r \in R^{+}$, and the corresponding r-order cumulative generation sequence $X^{(r)} = \{x^{(r)}(1), x^{(r)}(2), \ldots, x^{(r)}(n)\}$ and the sequence adjacent to the mean value generation $Z^{(r)} = \{z^{(r)}(2), z^{(r)}(3), \ldots, z^{(r)}(n)\}$ are the same as Step 1 in Section 2.1.

Step 2: suppose $X^{(0)}$, $X^{(r)}$, and $Z^{(r)}$ as described in Step 1, and r is a nonnegative real number; then the grey differential equation of the r-order accumulation grey Verhulst model (abbreviated as FVGM) is

$$x^{(r)}(k) - x^{(r)}(k-1) + az^{(r)}(k) = b\left(z^{(r)}(k)\right)^{2}. \tag{10}$$

Here, a is the development coefficient and b is the gray action. The whitening differential equation can be expressed as

$$\frac{\mathrm{d}x^{(r)}(t)}{\mathrm{d}t} + ax^{(r)}(t) = b\left(x^{(r)}(t)\right)^2. \tag{11}$$

Solve differential equation (11), and the time response function can be obtained as

$$x^{(r)}(k+1) = \frac{ax^{(0)}(1)}{bx^{(0)}(1) + \left(a - bx^{(0)}(1)\right)e^{ak}}. \tag{12}$$

Step 3: same as Step 3 in Section 2.1; the parameter sequence $\begin{bmatrix} \hat{a} \\ \hat{b} \end{bmatrix}$ of FVGM model is obtained by least square estimation, where $Y = \begin{bmatrix} x^{(r-1)}(2) \\ x^{(r-1)}(3) \\ \vdots \\ x^{(r-1)}(n) \end{bmatrix}$ and $B = \begin{bmatrix} -z^{(r)}(2) & (z^{(r)}(2))^2 \\ -z^{(r)}(3) & (z^{(r)}(3))^2 \\ \vdots & \vdots \\ -z^{(r)}(n) & (z^{(r)}(n))^2 \end{bmatrix}$.

Step 4: substitute the parameters $\hat{a}$ and $\hat{b}$ into the time response function (12), and let $\hat{x}^{(r)}(1) = x^{(r)}(1)$; the time response function of the original sequence can be obtained as

$$\hat{x}^{(r)}(k+1) = \frac{\hat{a}x^{(0)}(1)}{\hat{b}x^{(0)}(1) + \left(\hat{a} - \hat{b}x^{(0)}(1)\right)e^{\hat{a}k}}, \tag{13}$$

Here, $k = 1, 2, \ldots, n, \ldots$, $\hat{x}^{(r)}(k+1)$ is the fitting value at the $k+1$ time-point, thus obtaining the sequence $\hat{X}^{(r)}$.

Step 5: same as Step 5 in Section 2.1; r-order reduction is made for sequence $\hat{X}^{(r)}$. Thus, the fitting sequence of the original data is $\hat{X}^{(0)} = \left\{\hat{x}^{(0)}(1), \hat{x}^{(0)}(2), \ldots, \hat{x}^{(0)}(n)\right\}$, and predicted values are $\hat{x}^{(0)}(n+1)$, $\hat{x}^{(0)}(n+2)$, ….

2.3. Particle Swarm Optimization Algorithm. For fractional-order grey prediction model, the value of order r has a great influence on the prediction accuracy of the model, and the results of the model are also different with the different value of r. The main idea of finding the optimal value of order r is to minimize the error of the prediction model, which is generally expressed by the mean absolute relative error (MAPE):

$$\mathrm{MAPE} = \frac{1}{n}\sum_{k=1}^{n}\left|\frac{\hat{x}^{(0)}(k) - x^{(0)}(k)}{x^{(0)}(k)}\right| \times 100\%. \tag{14}$$

To determine the optimal order r, a number of operations need to be repeated. It is difficult to achieve that by using the traditional method, but the particle swarm optimization algorithm can provide a good way for the determination of the optimal order r. Particle swarm optimization (abbreviated as PSO) was proposed by Dr. Kennedy and Dr. Eberhart in 1995 [25], which is a simulation of a simple social model. It originates from the artificial life theory and the clustering phenomenon of birds and fish and is mainly inspired by the behavior of animals.

The basic process of PSO algorithm is to assume that there are m particles in a D-dimensional target search space, and the position of each particle represents a potential solution. The position vector of the i particle is $X_i = (x_i^1, x_i^2, \ldots, x_i^D)$, the velocity vector is $V_i = (v_i^1, v_i^2, \ldots, v_i^D)$, and the best position it passes through is the individual extreme value denoted by p_{best}, and the optimal position searched by the whole particle swarm so far is denoted by g_{best}. In each iteration, the velocity of the particle is updated by the individual extremum and the global extremum, and the formula for calculating the change in the velocity of the particle is

$$V_{i+1} = wv_i^d = c_1r_1\left(p_i^d - x_i^d\right) + c_2r_2\left(p_g^d - x_i^d\right). \tag{15}$$

where V_{i+1} is the velocity of the updated particle, w is the inertial vector, r_1 and r_2 are the random numbers that vary within the range $[0, 1]$, c_1 and c_2 are the acceleration constants (usually $c_1 = c_2 = 2$), and v_i is limited by a maximum velocity $v_{\max}$. In each iteration, the position of each particle is modified by the velocity vector plus the position vector, and the formula to determine the position of the particle is

$$x_{i+1} = x_i + v_i, \tag{16}$$

where x_{i+1} is the position of the updated particle.

The termination condition of iteration is determined according to the specific problem. It is generally selected as the best position found by the particle swarm so far, satisfying the preset minimum adaptive threshold or reaching the maximum number of iterations.

2.4. Model Verification. Error analysis is an important criterion to judge the prediction model. Before extrapolation and application, the prediction model must be verified, so as to judge the reliability and robustness of the prediction model. In practice, a variety of error analysis methods can be used to verify the model. Considering the typical grey uncertainty features of grey fractional-order prediction model, this paper uses residual, relative error, average relative error, posterior error ratio, and small error probability to verify the model [9].

Let the original data sequence be $X^{(0)} = \{x^{(0)}(k)\}$, $k = 1, 2, \ldots, n$, and its corresponding fitting sequence be $\hat{X}^{(0)} = \left\{\hat{x}^{(0)}(k)\right\}$, $k = 1, 2, \ldots, n$:

Error criterion 1: calculate the residual $e(k)$, relative error Δ_k and average relative error $\overline{\Delta}$ between the original value $x^{(0)}(k)$ and the fitting value $\hat{x}^{(0)}(k)$ at the time-point k, as follows:

$$e(k) = x^{(0)}(k) - \hat{x}^{(0)}(k),$$

$$\Delta_k = \left|\frac{e(k)}{x^{(0)}(k)}\right|, \qquad \Delta_k. \tag{17}$$

$$\overline{\Delta} = \frac{1}{n}\sum_{k=2}^{n}$$

Error criterion 2: calculate the mean value $\overline{x}$ and the mean residual $\overline{e}$ of the original data series $X^{(0)}$ as follows:

$$\overline{x} = \frac{1}{n}\sum_{k=1}^{n} x^{(0)}(k),$$
$$\overline{e} = \frac{1}{n-1}\sum_{k=2}^{n} e^{(0)}(k). \tag{18}$$

Error criterion 3: calculate the posterior error ratio C between variance S_1^2 and residual variance S_2^2 of the original data series $X^{(0)}$, and the small error probability P as follows:

$$S_1^2 = \frac{1}{n}\sum_{k=1}^{n}\left[x^{(0)}(k) - \overline{x}\right]^2,$$
$$S_2^2 = \frac{1}{n-1}\sum_{k=2}^{n}\left[e^{(0)}(k) - \overline{e}\right]^2,$$
$$C = \frac{S_2}{S_1},$$
$$P = P\left\{\left|e^{(0)}(k) - \overline{e}\right| < 0.6745S_1\right\}. \tag{19}$$

In general, the smaller the value of residual $e(k)$, relative error Δ_k, average relative error $\overline{\Delta}$ and posterior error ratio C is, the larger the value of small error probability P is, and the higher the prediction accuracy of the model is. If $\Delta_k < 0.01$, and $\overline{\Delta} < 0.01$, $C < 0.35$, $P > 0.95$, then the prediction accuracy of the model is first-level. According to the grey system theory, when the development coefficient is $a \in (-2, 2)$ and $a \geq -0.3$, the grey fractional-order model can be used for medium- to long-term prediction.

3. Population Forecasting and Empirical Analysis

According to the statistical data of population indicators from 2015 to 2019 in China Statistical Yearbook 2020 (shown in Table 1) [26], the grey fractional-order models are used to predict the total population, the factors of population change, and the age structure of the population, respectively, in the short-term and medium- to long-term. Among them, the FGM (1, 1) model is used for the short-term prediction in the period of 2020–2025, while the FVGM model is used for the medium- to long-term prediction in the period of 2026–2050.

The calculation is performed as mentioned above with the help of MATLAB software. And the modeling flowsheet of FGM (1, 1) model for population prediction is taken as an example to illustrate (shown in Figure 1).

3.1. Predicting Gross Population. Based on the statistical data of China's total population from 2015 to 2019, a 5-dimensional grey dynamic prediction model is established. The short-term prediction of the total population from 2020 to 2025 is firstly made by using the 5-year data. The FGM (1, 1) model of the total population is

$$\hat{x}^{(r)}(k+1) = \left(x^{(0)}(1) + \frac{13.689211}{0.001180}\right)e^{0.001180k} + \frac{13.689211}{0.001180}, \tag{20}$$

where the optimal value of the accumulation order r determined by the PSO algorithm is $r = 0.9917$. Through the model test, the values of the corresponding relative error Δ_k and average relative error $\overline{\Delta}$ are all <0.01, and posteriori error ratio, $C < 0.35$, small error probability $P > 0.95$; the model meets the first-level accuracy requirements, so it can be used for short-term prediction. The medium- to long-term prediction takes 5 years as the interval, and the FVGM model is established as

$$\hat{x}^{(r)}(k+1) = \frac{-0.146298x^{(0)}(1)}{-0.010206x^{(0)}(1) + \left(-0.146298 + 0.010206x^{(0)}(1)\right)e^{-0.146298k}}, \tag{21}$$

where the order r is determined by the PSO algorithm and its optimal value is $r = 1.0292e-07$. The prediction results of total population and gender composition of China are shown in Table 2.

As can be seen from Table 2, the total population of China will reach 1.42 billion in 2025 and 1.433 billion in the middle of this century. However, the gender ratio of males to females will continue to decrease since 2015 and will be as low as 1.0134 in 2050. In addition, it can be seen from Figure 2 that the growth trend of China's total population from 2015 to 2050 is in the shape of an anti-S curve.

3.2. Predicting Indexes of Population Change Factor. Birth rate and death rate are the main indicators to directly measure the population change. If we only know the general trend of population change, it is far from enough to grasp the specific situation of the population change in a country or region. Therefore, the change situation of birth rate and death rate must be analyzed accordingly.

According to the statistical data of birth rate from 2015 to 2019, a 5-dimensional grey dynamic prediction model was established, and a FGM (1, 1) model for short-term prediction of birth rate was established as

Table 1: Demographic indicators statistics.

Population indicators		2015	2016	2017	2018	2019
Population size and composition (unit: 10^8people)	Gross population	13.7462	13.8271	13.9008	13.9538	14.0005
	Male population	7.0414	7.0815	7.1137	7.1351	7.1527
	Female population	6.7048	6.7456	6.7871	6.8187	6.8478
Birth rate, death rate, and natural growth rate (unit: ‰)	Birth rate	12.07	12.95	12.43	10.94	10.48
	Death rate	7.11	7.09	7.11	7.13	7.14
	Natural growth rate	4.96	5.86	5.32	3.81	3.34
Population age structure (unit: ‰)	Proportion of aged 0–14	16.5	16.7	16.8	16.9	16.8
	Proportion of aged 15–64	73.0	72.5	71.8	71.2	70.6
	Proportion of age over 65	10.5	10.8	11.4	11.9	12.6

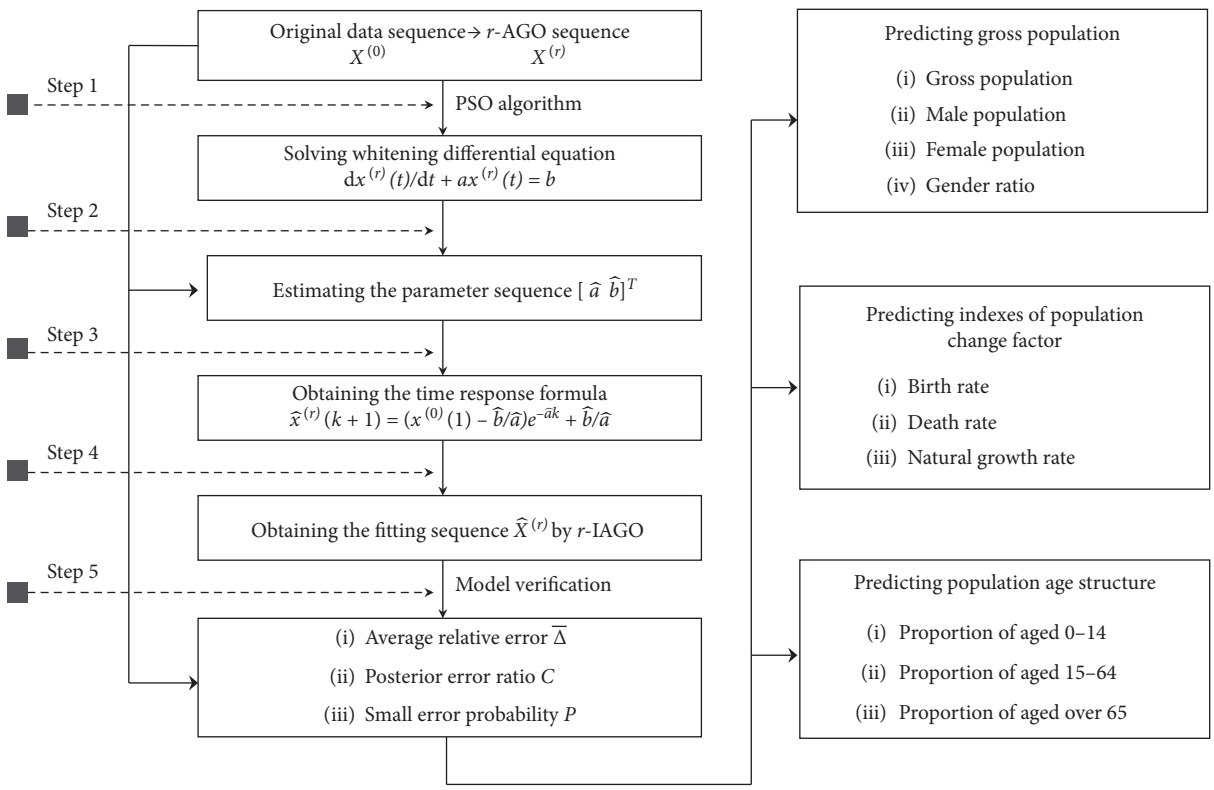

Figure 1: Modeling flowsheet of FGM (1, 1) model for population prediction.

$$\hat{x}^{(r)}(k+1) = \left(x^{(0)}(1) - \frac{13.940994}{0.147828}\right)e^{-0.147828k} + \frac{13.940994}{0.147828}, \tag{22}$$

where the optimal accumulation order is $r = 0.8636$. Through the model test, all values of error criteria $\Delta_k, \overline{\Delta}, C, P$ all meet the first-level accuracy requirements. Then the FVGM model for medium- to long-term prediction was established with the interval of 5 years as

$$\hat{x}^{(r)}(k+1) = \frac{-0.777432x^{(0)}(1)}{-0.025749x^{(0)}(1) + \left(-0.777432 + 0.025749x^{(0)}(1)\right)e^{-0.777432k}}, \tag{23}$$

where the optimal accumulation order is $r = 0.5019$. The same forecasting method can be used to forecast the death rate and natural growth rate in the short-term and medium- to long-term. The predicted results of the corresponding

Table 2: Predictions of population size and gender composition.

	Year	Gross population predicted values (unit: 10^8people)	Male population predicted values (unit: 10^8people)	Female population predicted values (unit: 10^8people)	Gender ratio
The fitting samples area	2015	13.7462	7.0414	6.7048	1.0502
	2016	13.8271	7.0815	6.7456	1.0498
	2017	13.9003	7.1135	6.7868	1.0481
	2018	13.9548	7.1355	6.8193	1.0464
	2019	14.0000	7.1525	6.8475	1.0445
Short-term forecast area	2020	14.0395	7.1665	6.8731	1.0427
	2021	14.0753	7.1784	6.8970	1.0408
	2022	14.1084	7.1889	6.9196	1.0389
	2023	14.1395	7.1983	6.9414	1.0370
	2024	14.1691	7.2069	6.9624	1.0351
	2025	14.1974	7.2147	6.9829	1.0332
Medium- to long-term forecast area	2030	14.2669	7.2260	7.0482	1.0252
	2035	14.3022	7.2304	7.0886	1.0200
	2040	14.3192	7.2319	7.1131	1.0167
	2045	14.3274	7.2323	7.1279	1.0146
	2050	14.3314	7.2325	7.1369	1.0134

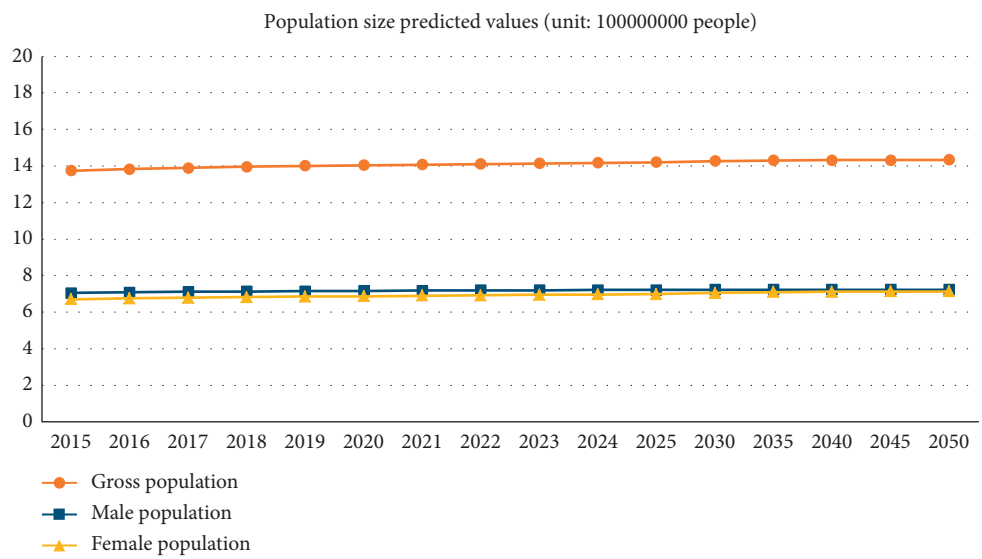

Figure 2: Predicted trend curves of total population and sex composition.

factors of population change are shown in Table 3, and the predicted trend curves of birth rate, death rate, and natural growth rate are shown in Figure 3.

3.2.1. Birth Rate Prediction. The changes in China's birth rate during the forecast period are as follows: the birth rate has been decreasing year by year. In 2015, the birth rate was 12.07‰. It is predicted to drop to 5.65‰ in 2025, below 5‰ in 2030 and 2.90‰ in 2050. Due to China's long-term implementation of family planning policy after the 1970s, and with the continuous improvement of the population quality and the change in fertility attitudes, the birth rate in China has declined accordingly.

3.2.2. Death Rate Prediction. China's death rate will remain between 7.10‰ and 7.20‰ from 2015 to 2050. This is because living standards and living environment have been relatively stable during this period, so the death rate has not changed much. However, from 2040, there will be a small decrease in the death rate because of demographic changes, especially the increase in the aged population, which will lead to a slow decline in the death rate.

3.2.3. Natural Growth Rate Prediction. During the forecast period, the natural growth rate will be on a downward trend due to a decline in the birth rate and little change in the death rate. The natural growth rate reached the peak of 5.86‰ in 2016 and will drop to 1.60‰ in 2025 and 1.06‰ in 2035. By 2040, the natural population growth rate will be below 1.00‰, which means that the death rate will be far greater than the birth rate, and the total population will tend to decrease in the future.

3.3. Predicting Population Age Structure. Population age structure refers to the proportion of the population of each age group in the whole population at a certain point in time

Table 3: Predictions of birth rate, death rate and natural growth rate.

	Year	Birth rate predicted values (unit: ‰)	Death rate predicted values (unit: ‰)	Natural growth rate predicted values (unit: ‰)
The fitting samples area	2015	12.07	7.11	4.96
	2016	12.95	7.09	5.86
	2017	12.22	7.11	4.96
	2018	11.28	7.13	4.05
	2019	10.30	7.14	3.34
Short-term forecast area	2020	9.36	7.15	2.81
	2021	8.47	7.16	2.42
	2022	7.66	7.18	2.13
	2023	6.92	7.19	1.91
	2024	6.25	7.19	1.74
	2025	5.65	7.20	1.60
Medium- to long-term forecast area	2030	4.59	7.21	1.27
	2035	3.91	7.20	1.06
	2040	3.47	7.19	0.93
	2045	3.15	7.18	0.83
	2050	2.90	7.17	0.76

and in a certain area, which is one of the important indicators of population research. It is the result of the combined effect of past and present birth, death, and migration changes on population development. The age structure of population has a great influence on the type, speed, and trend of future population development, so the prediction of its development trend plays a very important role in the formulation of population policy.

According to the statistical data of different population age groups from 2015 to 2019, a 5-dimensional grey dynamic prediction model was established, and a FGM (1, 1) model was established for short-term prediction of the proportion of 0–14-year-old population as

$$\hat{x}^{(r)}(k+1) = \left(x^{(0)}(1) - \frac{10.839485}{0.605343}\right)e^{-0.605343k} + \frac{10.839485}{0.605343}, \tag{24}$$

where the optimal accumulation order is $r = 0.0273$. Through the model test, all values of error criteria Δ_k, $\overline{\Delta}$, C, and P are in line with the first-level accuracy requirements. Then, the FVGM model for medium- to long-term prediction of the proportion of 0–14-year-old population was established with the interval of 5 years as

$$\hat{x}^{(r)}(k+1) = \frac{-0.615838x^{(0)}(1)}{-0.034323x^{(0)}(1) + \left(-0.615838 + 0.034323x^{(0)}(1)\right)e^{-0.615838k}}, \tag{25}$$

where the optimal accumulation order is $r = 0.0281$. The same forecasting method can be used to predict the proportion of the population aged 15–64 and over 65 in the short-term and medium- to long-term. The prediction results of the proportion of the population of different age groups are shown in Table 4, and the column chart of the prediction of the population age structure is shown in Figure 4.

3.3.1. Population Ageing Trend. It can be seen from Table 4 that the aged population in China is on the rise from 2015 to 2050. In 2015, the aged population has exceeded 10%, and China has entered the stage of aging society. Especially in 2030, the pace of aging has accelerated significantly. By 2050, the proportion of the aged population will reach 24.83%; that is, about one in every four people will be aged. The problem of population aging is very serious, and it will bring a series of social and economic problems.

3.3.2. Change Trend of Labor Force. The labor population is an important part of the population age structure, and the scale of the labor population will have a crucial impact on the social and economic development. During the period of 2015–2025, the overall change of China's labor population will fluctuate little, but during the period of 2025–2050, the labor population will show a rapid decline trend, mainly due to the serious aging problem.

3.3.3. Dependency Ratio Analysis. According to the above analysis data, from 2015 to 2025, China's population dependency ratio will rise slowly year by year, but will continue to grow rapidly in the next 25 years, which is largely related to China's aging population and will bring great pressure to the society and family.

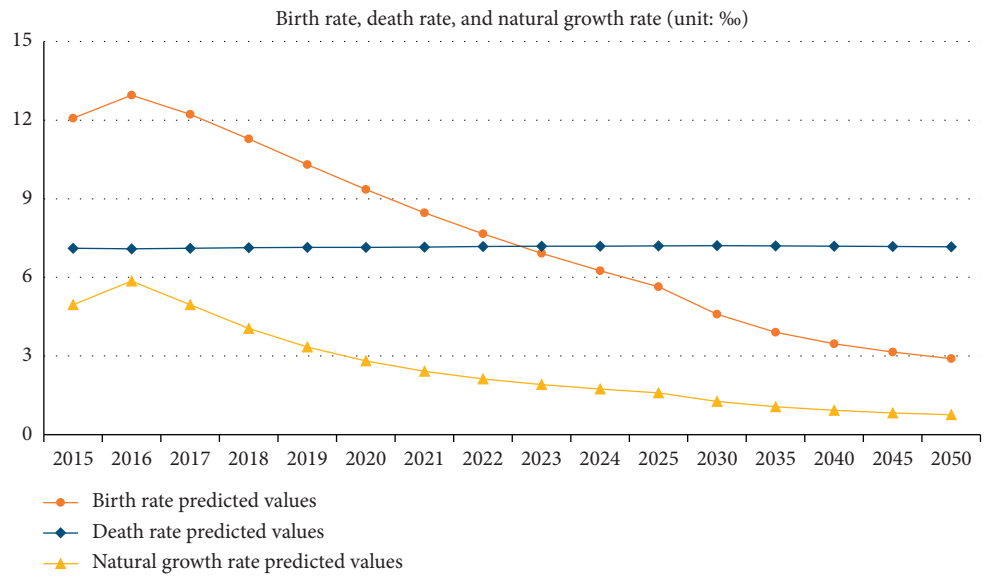

Figure 3: Predicted trend curves of birth rate, death rate, and natural growth rate.

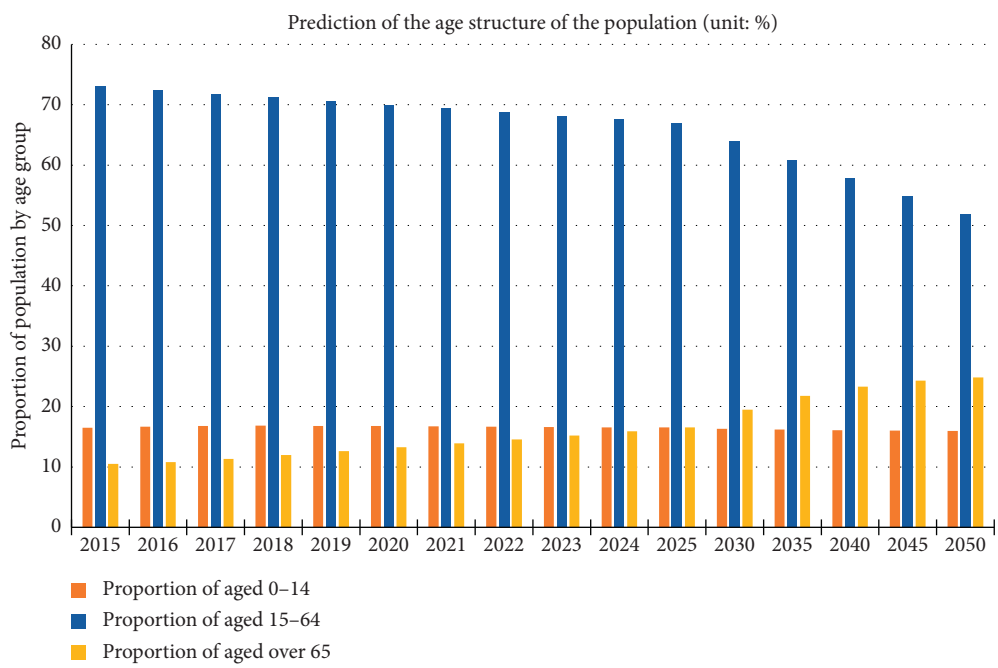

Figure 4: Column chart of predicted trends in the age structure of the population.

Table 4: Prediction of the age structure of the population.

	Year	Proportion of aged 0–14 (unit: %)	Proportion of aged 15–64 (unit: %)	Proportion of aged over 65 (unit: %)	Dependency ratio (unit: %)
The fitting samples area	2015	16.50	73.00	10.50	0.37
	2016	16.69	72.47	10.80	0.38
	2017	16.80	71.84	11.35	0.39
	2018	16.83	71.21	11.96	0.40
	2019	16.81	70.58	12.60	0.42

Table 4: Continued.

	Year	Proportion of aged 0–14 (unit: %)	Proportion of aged 15–64 (unit: %)	Proportion of aged over 65 (unit: %)	Dependency ratio (unit: %)
Short-term forecast area	2020	16.77	69.96	13.25	0.43
	2021	16.72	69.35	13.91	0.44
	2022	16.67	68.74	14.57	0.45
	2023	16.62	68.14	15.23	0.47
	2024	16.57	67.54	15.89	0.48
	2025	16.53	66.95	16.55	0.49
Medium- to long-term forecast area	2030	16.34	63.91	19.49	0.56
	2035	16.21	60.87	21.76	0.62
	2040	16.11	57.86	23.31	0.68
	2045	16.03	54.87	24.28	0.73
	2050	15.96	51.94	24.83	0.79

4. Conclusions

Based on the statistical data of China's population indices from 2015 to 2019, this paper establishes 5-dimensional grey fractional-order prediction models and makes short-term and medium- to long-term prediction of China's population and its structure. The models considered not only the total population and natural growth rate, but also the age structure of population, so they are more reliable and practical, which can describe and predict the population evolution process in a long period. The application of grey system method to population prediction has its unique advantages, which can mine the information contained in the population number series; meanwhile, the fractional-order accumulation can weaken the randomness of the original data series and reduce the influence of external disturbance factors, so it is a simple and effective method for population prediction. Scientific prediction and accurate grasp of the future trend of population change are conducive to the formulation of different population policies at different stages, so as to alleviate the adverse effects of an increasingly aging population on society, and provide scientific theoretical reference for controlling the population size and making policy.

First of all, we need to vigorously develop education and comprehensively improve the quality of the population. In order to change the present situation of unreasonable occupation composition, difficult popularization of science and technology, lack of scientific and technological personnel, and low management level, we must develop education cause actively. Therefore, we must strengthen the basic education, strengthen the pre-job training and technical training, and strive to improve the quality of labor resources. Secondly, it is necessary to solve the employment problem of working-age population through multiple channels. In the future, the increase of the working-age population in China will provide a large number of labor resources, and at the same time, it will bring the problem about employment of labor force. Accordingly, various measures should be taken to provide employment opportunities for labor force. For example, with the aging of the labor force, the proportion of the elderly labor force will continue to rise. According to the physiological characteristics and physical conditions of the labor force, the problem of employment for the elderly labor force should be solved. In addition, the aging of the population needs to be addressed. Population aging is the inevitable result of fertility decline. With the gradual increase of the proportion of the aged population, the problem of population aging is becoming more and more obvious. Consequently, it is necessary to implement the national strategy of actively coping with the aging of the population, promote the modernization of the social governance system and governance capacity for the aged, and grasp the development trend of the aging of the population comprehensively.

Data Availability

All data generated or used during the study are available within the article.

Conflicts of Interest

The authors declare that they have no conflicts of interest.

Acknowledgments

This work was supported by the Jiangsu Social Science Foundation Project of China (Grant no. 20GLD013), China Postdoctoral Science Foundation (Grant no. 2020M671491), Postdoctoral Research Foundation of Jiangsu Province of China (Grant no. 2020Z141), Funding of Nantong Science and Technology Program (Grant no. MS12019041), National Statistical Science Research Project of China (Grant no. 2020LY020), and Humanistic and Social Science Youth Foundation of Ministry of Education of China (Grant no. 18YJC630043).

References

[1] W. Sprague, "Automatic parametrization of age/sex leslie matrices for human populations," *Quantitative Biology*, vol. 1, pp. 1–26, 2012.

[2] L. Monte, "Predicting the effect of ionising radiation on biological populations: testing of a non-linear leslie model applied to a small mammal population," *Journal of Environmental Radioactivity*, vol. 122, pp. 63–69, 2013.

[3] H. Xie, T. J. Chaussalet, and P. H. Millard, "A continuous time Markov model for the length of stay of elderly people in institutional long-term care," *Journal of the Royal Statistical Society: Series A (Statistics in Society)*, vol. 168, no. 1, pp. 51–61, 2005.

[4] L. Bortolussi, R. Lanciani, and L. Nenzi, "Model checking Markov population models by stochastic approximations," *Information and Computation*, vol. 262, pp. 189–220, 2018.

[5] F. C. Billari, R. Graziani, and E. Melilli, "Stochastic population forecasting based on combinations of expert evaluations within the bayesian paradigm," *Demography*, vol. 51, no. 5, pp. 1933–1954, 2014.

[6] B. K. Chen, H. Jalal, H. Hashimoto et al., "Forecasting trends in disability in a super-aging society: adapting the future elderly model to Japan," *The Journal of the Economics of Ageing*, vol. 8, pp. 42–51, 2016.

[7] W.-Y. Wu and S.-P. Chen, "A prediction method using the grey model GMC (1, *n*) combined with the grey relational analysis: a case study on Internet access population forecast," *Applied Mathematics and Computation*, vol. 169, no. 1, pp. 198–217, 2005.

[8] J. L. Deng, "Control problems of grey systems," *Systems & Control Letters*, vol. 1, no. 5, pp. 288–294, 1982.

[9] S. F. Liu, Y. J. Yang, and J. Forrest, *Grey Data Analysis: Methods, Models and Applications*, Springer, New York, NY, USA, 2017.

[10] S. Ding, K. W. Hipel, and Y.-g. Dang, "Forecasting China's electricity consumption using a new grey prediction model," *Energy*, vol. 149, pp. 314–328, 2018.

[11] B. Zeng, H. Duan, and Y. Zhou, "A new multivariable grey prediction model with structure compatibility," *Applied Mathematical Modelling*, vol. 75, pp. 385–397, 2019.

[12] J. Ye, Y. Dang, and B. Li, "Grey-Markov prediction model based on background value optimization and central-point triangular whitenization weight function," *Communications in Nonlinear Science and Numerical Simulation*, vol. 54, pp. 320–330, 2019.

[13] B. Zeng, H. Li, and X. Ma, "A novel multi-variable grey forecasting model and its application in forecasting the grain production in China," *Computers & Industrial Engineering*, vol. 150, Article ID 106915, 2020.

[14] L. Liu, Y. Chen, and L. Wu, "The damping accumulated grey model and its application," *Communications in Nonlinear Science and Numerical Simulation*, vol. 95, Article ID 105665, 2021.

[15] B. Zeng, X. Ma, and M. Zhou, "A new-structure grey verhulst model for China's tight gas production forecasting," *Applied Soft Computing*, vol. 96, Article ID 106600, 2020.

[16] L. Tang and Y. Lu, "Study of the grey Verhulst model based on the weighted least square method," *Physica A: Statistical Mechanics and Its Applications*, vol. 545, Article ID 123615, 2020.

[17] L. Wu, S. Liu, L. Yao, S. Yan, and D. Liu, "Grey system model with the fractional order accumulation," *Communications in Nonlinear Science and Numerical Simulation*, vol. 18, no. 7, pp. 1775–1785, 2013.

[18] L. Wu, S. Liu, Z. Fang, and H. Xu, "Properties of the GM (1, 1) with fractional order accumulation," *Applied Mathematics and Computation*, vol. 252, pp. 287–293, 2015.

[19] S. L. Fang, L. F. Wu, Z. G. Fang et al., "Using fractional GM (1, 1) model to predict the maintenance cost of weapon system," *Journal of Grey System*, vol. 25, no. 3, pp. 9–15, 2013.

[20] W. Wu, X. Ma, B. Zeng, Y. Wang, and W. Cai, "Forecasting short-term renewable energy consumption of China using a novel fractional nonlinear grey Bernoulli model," *Renewable Energy*, vol. 140, pp. 70–87, 2019.

[21] C. Yan, L. F. Wu, L. Y. Liu et al., "Fractional Hausdorff grey model and its properties," *Chaos, Solitons & Fractals*, vol. 138, Article ID 109915, 2020.

[22] U. Şahin, "Future of renewable energy consumption in France, Germany, Italy, Spain, Turkey and UK by 2030 using optimized fractional nonlinear grey Bernoulli model," *Sustainable Production and Consumption*, vol. 25, pp. 1–14, 2020.

[23] C. Liu, W.-Z. Wu, W. Xie, and J. Zhang, "Application of a novel fractional grey prediction model with time power term to predict the electricity consumption of India and China," *Chaos, Solitons & Fractals*, vol. 141, Article ID 110429, 2020.

[24] W. Meng, B. Zeng, and S. L. Li, "A novel fractional-order grey prediction model and its modeling error analysis," *Information*, vol. 10, no. 5, p. 167, 2019.

[25] J. Kennedy and C. Eberhart, "Particle swarm optimization," in *Proceedings of IEEE International Conference on Neural Networks*, pp. 1942–1948, Perth, WA, Australia, November 1995.

[26] National Bureau of Statistics China, *China Statistical Yearbook 2020*, China Statistics Press, Beijing, China, 2019.

Hindawi
Journal of Mathematics
Volume 2021, Article ID 7596694, 12 pages
https://doi.org/10.1155/2021/7596694

Research Article

Grey Forecast Model with Aging Fractional Accumulation and Its Properties

Leping Tu, Yan Chen, and Lifeng Wu

School of Management Engineering and Business, Hebei University of Engineering, Handan 056038, China

Correspondence should be addressed to Lifeng Wu; wulifeng@hebeu.edu.cn

Received 9 April 2021; Revised 2 July 2021; Accepted 7 July 2021; Published 20 July 2021

Academic Editor: Ali Jaballah

A novel aging fractional accumulation operator is proposed. The aging accumulation operator can dynamically update the accumulation weight of data and flexibly change the forecast trend by adjusting the aging parameter. In addition, a new aging accumulated grey model is obtained by using the aging accumulation operator to improve the traditional grey model. In the analysis of four examples, the existing grey accumulation operator and prediction method are compared. The results show that the proposed aging accumulation operator and aging accumulation grey model have excellent performance.

1. Introduction

The grey model is a very effective forecasting method to deal with the problem with poor information and little data [1]. Other existing prediction methods such as neural network algorithm [2, 3], exponential smoothing [4], support vector regression [5], and autoregression [6] often depend on the amount of data. The grey prediction model only needs at least 4 data to make a prediction. This advantage makes the grey prediction model achieve good results even when the amount of data is small or data collection is difficult [7]. However, the traditional grey model still has some shortcomings. The improvements in recent years mainly focus on the following four aspects:

(1) Optimization of model background value: traditional background values $z^{(1)}(k) = 0.5(x^{(1)}(k) + x^{(1)}(k+1))$ are suitable for smooth sequences, which can be optimized to adapt to other situations. The model background value is reconstructed by the Simpson formula, and the unbiased GM(SD) (1, 1) model is obtained [8]. By increasing the number of parameters in the background value, the smoothness of the background value is improved and the influence of the extremum in the original sequence is weakened [9]. The NNGM (1, 1) model is constructed by a neural network algorithm, so there is no need to determine the background value [10].

(2) The extension of the modeling equation: the DGM model is proposed by using the discrete modeling method, which avoids the jumping error of GM (1, 1) from discrete equation to continuous equation [11]. An unbiased nonlinear grey Bernoulli model is constructed to achieve better performance by adjusting nonlinear parameters [12]. The GMCO (1, N) model with optimized parameters is proposed, which can accurately describe any linear dynamic grey system [13].

(3) Improvement of grey buffer operator: the original sequence is usually irregular, but its potential law can be revealed by appropriate grey buffer operators. The fractional buffer operator obtained by extending the integer buffer operator can adjust the buffer effect more accurately [14]. Three new fractional weakening buffer operators are proposed, which can effectively weaken the interference of disturbance factors on time series [15]. An optimized grey buffer operator is proposed by introducing accumulation and translation transformation [16].

(4) Error correction: the prediction accuracy can be further improved by error analysis of prediction results combined with correction technology. The Fourier error correction method is used to improve the existing grey forecasting model [17]. The triangle residual error correction method is used to eliminate the inherent error of the original grey model, and a new grey prediction model with error correction is proposed [18].

In addition to the optimization mentioned above, there are many effective improvement methods. These improvements have effectively improved the prediction accuracy of the grey model. Therefore, the grey model is widely used in energy [19], economic [20], environmental governance [21], and other related research studies. It is worth emphasizing that the advantage of the grey forecasting model compared with other forecasting methods lies in dealing with small sample problems. In fact, the grey accumulation generation plays an important role. Therefore, this paper proposes a novel aging accumulation operator to improve the traditional GM (1, 1) model. As a data preprocessing method, the aging accumulation operator can dynamically update the accumulation weight of data according to the time development. In addition, it can flexibly change the forecast trend by adjusting the aging parameter. Compared with the existing cumulative generation operator, it is an important innovation.

The other parts of this article are arranged as follows. Section 2 introduces the definition and properties of the aging accumulation operator. The aging accumulation grey model and its properties are proposed in Section 3. Section 4 introduces the optimization algorithm of the aging parameter and evaluates the performance evaluation of the proposed model by four cases. The conclusions are given in Section 5.

2. Definition and Properties of Aging Accumulation Operator

By analyzing the advantages and disadvantages of existing accumulation operators in the grey model, a new aging accumulation operator is defined. Besides, the operation details and related properties of the aging accumulation operator are introduced in detail.

2.1. Existing Accumulation Generation Operators. In the modeling process of the grey prediction model, cumulative generation is an important operation. By accumulating operation, scattered data can show certain regularity. The traditional grey prediction model uses 1-AGO to accumulate the original data. For example, the accumulation generated sequence of the original sequence $\{x^{(0)}(1), x^{(0)}(2), \ldots, x^{(0)}(m)\}$ by 1-AGO is

$$x^{(1)}(i) = \sum_{k=1}^{i} x^{(0)}(k), \quad i = 1, 2, \ldots, m. \tag{1}$$

It can be seen from equation (1) that 1-AGO treats all data indiscriminately. According to the new information priority principle, new data are more important than old data. When accumulating the original sequence, we should give full consideration to the new and old data. In other words, new information should be given more weight, and old information should be given less weight. Based on this consideration, many new cumulative generation operators have been proposed. Among them, the fractional accumulation operator is an important innovation [22]. Assuming that the original sequence is $\{x^{(0)}(1), x^{(0)}(2), \ldots, x^{(0)}(m)\}$, the fractional accumulation generated sequence is

$$x^{(r)}(i) = \sum_{k=1}^{i} \binom{i-k+r-1}{i-k} x^{(0)}(k), \quad (i = 1, 2, \ldots, m), \tag{2}$$

where $\binom{r-1}{0} = 1$, $\binom{k-1}{k} = 0$, $\binom{k-i+r-1}{k-i} = ((r+k-i-1)(r+k-i-2)\cdots(r+1)r)/(k-i)!$.

Fractional accumulation operator can effectively allocate the weight of new and old data, thus describing the development trend of series more accurately. In addition, there are some other effective grey accumulation operators [23–25]. However, most operators can only increase the weight of new data. We hope that the cumulative generation operator can dynamically update the weights of all data according to time changes. Therefore, the aging accumulation operator is proposed.

2.2. The Aging Accumulation Operator. When accumulating data, the time value of data must be fully considered. Generally speaking, the timeliness of data is decreasing. Therefore, we propose a novel aging accumulation operator. It is defined as follows.

Definition 1. Assuming that $X^{(0)} = \{x^{(0)}(1), x^{(0)}(2), \ldots, x^{(0)}(m)\}$ is the original non-negative sequence, the aging cumulative sequence $X^{(\gamma)} = \{x^{(\gamma)}(1), x^{(\gamma)}(2), \ldots, x^{(\gamma)}(m)\}$ of $X^{(0)}$ can be obtained by using the aging decreasing function $g(i)$ as the aging weighting. This transformation is called the aging accumulation operator, and its calculation formula is

$$x^{(\gamma)}(i) = \sum_{k=1}^{i} x^{(0)}(k) g(i-k), \quad i = 1, 2, \ldots, m. \tag{3}$$

The matrix form of equation (3) is

$$X^{(\gamma)} = \left[x^{(0)}(1), x^{(0)}(2), \ldots, x^{(0)}(m)\right] \begin{bmatrix} g(0) & g(1) & \cdots & g(m-1) \\ 0 & g(0) & \cdots & g(m-2) \\ \vdots & \vdots & \vdots & \vdots \\ 0 & 0 & \cdots & g(1) \\ 0 & 0 & \cdots & g(0) \end{bmatrix}, \tag{4}$$

where $g(i) = (\gamma/(i+\gamma))$ $(\gamma > 0)$ and γ is called the aging parameter. It is used to adjust the aging change of data. Obviously, no matter what the value γ is, the aging of the latest data is 1. The smaller the value γ, the more time-sensitive the new information. On the contrary, the greater the value of γ, the more consistent the timeliness of new and old information. When γ tends to infinity, aging accumulation degenerates into traditional first-order accumulation.

Property 1. Adding new data to accumulation will dynamically update the accumulation weight of existing data.

Proof. According to the definition of the aging decreasing function $g(i) = \gamma/(i+\gamma)$, we have

(1) $g(0) = \gamma/(0+\gamma) = 1$.

(2) $g(i) = \gamma/(i+\gamma)$ is the decreasing function of i.

That is to say, the aging value of the latest data is always 1, and the aging values of other data decrease with time. As shown in Figure 1, when calculating $x^{(\gamma)}(10)$, the aging value corresponding to $x^{(0)}(10)$ is $g(0) = 1$, the aging value corresponding to $x^{(0)}(9)$ is $g(1) = \gamma/(1+\gamma)$, and so on. Then, $x^{(\gamma)}(10) = \sum_{k=1}^{10} x^{(0)}(k) g(10-k)$ can be obtained. To put it simply, the addition of new data will replace the aging value of the latest data, thus pushing down the aging value of all data. This method can dynamically update the weight of all data, and the latest data always keep a higher weight. The weight generated by this accumulation method is more following the law of the development of objective things. Besides, the data metabolism can be realized by flexibly adjusting the value of the aging parameter γ.

Property 2. Assuming $X^{(0)} = \{x^{(0)}(1), x^{(0)}(2), \ldots, x^{(0)}(m)\}$ is the original non-negative sequence and its aging accumulation sequence is $X^{(\gamma)} = \{x^{(\gamma)}(1), x^{(\gamma)}(2), \ldots, x^{(\gamma)}(m)\}$, then $x^{(\gamma)}(i)$ $(i = 1, 2, \ldots, m)$ is the increasing function of the aging parameter γ.

Proof. According to Definition 1, $\forall i = 1, 2, \ldots, m$, there is

$$\begin{aligned} x^{(\gamma)}(i) &= \left[x^{(0)}(1), x^{(0)}(2), \ldots, x^{(0)}(i)\right] \left[\, g(i-1) \;\; g(i-2) \;\; \cdots \;\; g(0) \,\right]^T \\ &= \left[x^{(0)}(1), x^{(0)}(2), \ldots, x^{(0)}(i)\right] \left[\, \frac{\gamma}{i+\gamma-1} \;\; \frac{\gamma}{i+\gamma-2} \;\; \cdots \;\; 1 \,\right]^T \\ &= \left[x^{(0)}(1), x^{(0)}(2), \ldots, x^{(0)}(i)\right] \left[\, 1 - \frac{i-1}{i+\gamma-1} \;\; 1 - \frac{i-1}{i+\gamma-2} \;\; \cdots \;\; 1 \,\right]^T. \end{aligned} \tag{5}$$

Because $x^{(0)}(i)$ is non-negative and $1 - (k/(\gamma+k))$ $(k = i-1, i-2, \ldots, 1)$ is the increasing function of γ, $x^{(\gamma)}(i)$ $(i = 1, 2, \ldots, m)$ is the increasing function of γ.

Proof completed.

Lemma 1. *Let $Y = \{y_1, y_2, \ldots, y_n\}$ be a non-negative equidistant time series; then, $\Delta(k) = |y_{k+1} - y_k|$ represents the information difference between the data [26].*

Property 3. Assuming that the original non-negative sequence $X^{(0)} = \{x^{(0)}(1), x^{(0)}(2), \ldots, x^{(0)}(m)\}$ increases monotonously and its aging accumulation sequence is $X^{(\gamma)} = \{x^{(\gamma)}(1), x^{(\gamma)}(2), \ldots, x^{(\gamma)}(m)\}$, then we have

(1) The aging accumulation sequence $x^{(\gamma)}(i)$ $(i = 1, 2, \ldots, m)$ is the increasing function of i.

(2) The information difference $\Delta(i) = |x^{(\gamma)}(i+1) - x^{(\gamma)}(i)|$ between $x^{(\gamma)}(i+1)$ and $x^{(\gamma)}(i)$ is the increasing function of γ.

Proof. (1) $X^{(0)} = \{x^{(0)}(1), x^{(0)}(2), \ldots, x^{(0)}(m)\}$ is a monotonically increasing non-negative sequence; then, we have

$$x^{(0)}(i) - x^{(0)}(i-1) > 0, \quad (i = 2, 3, \ldots, m). \tag{6}$$

Also, for $1 \le i < m$, we have $g(x) = (\gamma/(i+\gamma)) > 0$. Then, we can obtain

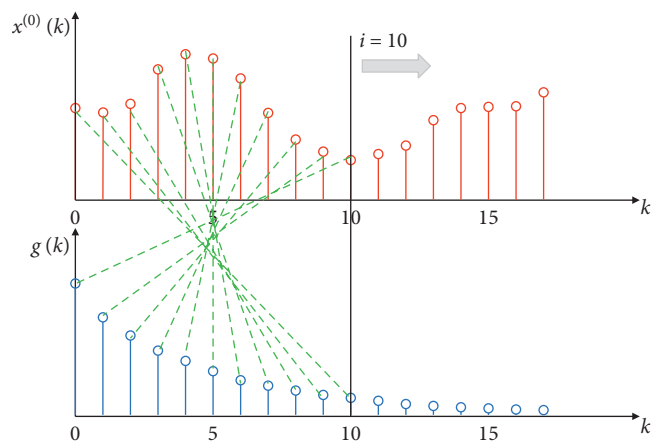

Figure 1: Dynamic update process of data aging.

(2) From (1), we know that $\forall i = 2, 3, \ldots, m$, we have

$$\begin{aligned} & x^{(\gamma)}(i+1) - x^{(\gamma)}(i) \\ & = \sum_{k=1}^{k=i+1} x^{(0)}(k) g(i+1-k) - \sum_{k=1}^{k=i} x^{(0)}(k) g(i-k) \\ & = x^{(0)}(1) g(i) + \sum_{k=2}^{k=i+1} \left[\left(x^{(0)}(k) - x^{(0)}(k-1)\right) g(i+1-k)\right] > 0. \end{aligned} \tag{7}$$

$$\begin{aligned} \Delta(i) &= \left|x^{(\gamma)}(i+1) - x^{(\gamma)}(i)\right| = x^{(\gamma)}(i+1) - x^{(\gamma)}(i) \\ &= \left[x^{(0)}(1), x^{(0)}(2), \ldots, x^{(0)}(i+1)\right] [g(i) - g(i-1), g(i-1) - g(i-2), \ldots, g(0)]^T \\ &= \left[x^{(0)}(1), x^{(0)}(2), \ldots, x^{(0)}(i+1)\right] \left[\frac{-\gamma}{(i+\gamma)(i+\gamma-1)}, \frac{-\gamma}{(i+\gamma-1)(i+\gamma-2)}, \ldots, 1\right]^T. \end{aligned} \tag{8}$$

Obviously, $(-\gamma/(k+\gamma)(k+\gamma-1))$ $(k = 1, 2, \ldots, i)$ is the increasing function of γ and $x^{(0)}(k)$ $(k = 1, 2, \ldots, m) > 0$. So, we can conclude that the information difference $\Delta(i)$ is the increasing function of γ.

Proof completed.

According to the principle of difference information, information comes from the difference [27]. Fully mining the information difference of sequence can maximize the value of data. However, in practical application, data fluctuation may lead to deviation of information difference. Based on the modeling mechanism of the grey model, the fluctuation of the older data will cause greater deviation. As an improvement, the introduction of the aging parameter γ can weaken extreme interference while retaining important difference information.

3. The Aging Accumulation Grey Model

Based on the aging accumulation operator, a new aging accumulation grey model AGM (1, 1) is proposed in this section. In order to highlight the advantages of the AGM (1, 1) model and understand its applicable scope, the validity of initial value, monotonicity, prediction trend, and reduction error of this model are analyzed and discussed.

3.1. The Definition of the Aging Accumulation Grey Model. The traditional GM (1, 1) model uses the first-order cumulative generation operation to reduce the random disturbance, which can improve the model effect to a certain extent. However, traditional 1-AGO ignores the difference of timeliness between old and new data. Therefore, in this section, the GM (1, 1) model is optimized by using the aging accumulation operator, and the aging accumulation grey model is obtained. It is defined as follows.

Definition 2. Assuming that $\{x^{(0)}(1), x^{(0)}(2), \ldots, x^{(0)}(m)\}$ is the original sequence, then the aging accumulation sequence of the original sequence can be obtained as $\{x^{(\gamma)}(1), x^{(\gamma)}(2), \ldots, x^{(\gamma)}(m)\}$ by Definition 1. Then, AGM (1, 1) can be written as

$$\frac{\mathrm{d}x^{(\gamma)}}{\mathrm{d}t} + ax^{(\gamma)} = b, \tag{9}$$

where a is the development coefficient and b is the grey action quantity. The solution of whitening differential equation (9) is $x^{(\gamma)}(i) = (x^{(0)}(1) - (b/a))e^{-a(i-1)} + (b/a)$. Its parameters generally use the least-squares solution of the AGM (1, 1) model. The least-squares estimation of the AGM (1, 1) model satisfies

$$\begin{pmatrix} \widehat{a} \\ \widehat{b} \end{pmatrix} = \left(B^T B\right)^{-1} B^T Y, \tag{10}$$

where

$$B = \begin{bmatrix} -0.5\left(x^{(\gamma)}(1) + x^{(\gamma)}(2)\right) & 1 \\ -0.5\left(x^{(\gamma)}(2) + x^{(\gamma)}(3)\right) & 1 \\ \vdots & \vdots \\ -0.5\left(x^{(\gamma)}(m-1) + x^{(\gamma)}(m)\right) & 1 \end{bmatrix},$$
$$Y = \begin{bmatrix} x^{(\gamma)}(2) - x^{(\gamma)}(1) \\ x^{(\gamma)}(3) - x^{(\gamma)}(2) \\ \vdots \\ x^{(\gamma)}(m) - x^{(\gamma)}(m-1) \end{bmatrix}. \tag{11}$$

Inputting $\widehat{a}$ and $\widehat{b}$ into the solution of the whitening differential equation, the time response equation can be obtained as

$$\widehat{x}^{(\gamma)}(i) = \left(x^{(0)}(1) - \frac{\widehat{b}}{\widehat{a}}\right)e^{-\widehat{a}(i-1)} + \frac{\widehat{b}}{\widehat{a}}, \quad i = 1, 2, \ldots, m, \ldots, m + mf, \tag{12}$$

where mf represents the number to be predicted. Then, the fitted and predicted values $\widehat{X}^{(0)} = \left\{\widehat{x}^{(0)}(1), \widehat{x}^{(0)}(2), \ldots, \widehat{x}^{(0)}(m+mf)\right\}$ can be obtained as

$$\widehat{X}^{(0)} = \left[\widehat{x}^{(\gamma)}(1), \widehat{x}^{(\gamma)}(2), \ldots, \widehat{x}^{(\gamma)}(m+mf)\right] \begin{bmatrix} g(0) & g(1) & \cdots & g(m+mf-1) \\ 0 & g(0) & \cdots & g(m+mf-2) \\ \vdots & \vdots & \vdots & \vdots \\ 0 & 0 & \cdots & g(1) \\ 0 & 0 & \cdots & g(0) \end{bmatrix}^{-1}. \tag{13}$$

3.2. The Effectiveness of the Initial Value by AGM (1, 1). The principle of minimum information is one of the six axioms of the grey theory, which holds that the existing information must be fully utilized [27]. Therefore, it is necessary to study the utilization degree of data by the grey prediction model. It has been proved that the initial value of the traditional grey prediction model is invalid [28]. This paper will prove that the initial value of the AGM(1, 1) model is valid by Property 4.

Property 4. Assuming that the fitting value $\widehat{X}^{(0)} = \left\{\widehat{x}^{(0)}(1), \widehat{x}^{(0)}(2), \ldots, \widehat{x}^{(0)}(m)\right\}$of $X^{(0)} = \{x^{(0)}(1), x^{(0)}(2), \ldots, x^{(0)}(m)\}$ is obtained by the AGM (1, 1) model, then $\widehat{X}^{(0)} = \left\{\widehat{x}^{(0)}(1), \widehat{x}^{(0)}(2), \ldots, \widehat{x}^{(0)}(m)\right\}$ will change with the change of $x^{(0)}(1)$.

Proof. A case from [29] was used for empirical analysis. The world's renewable energy is taken as the raw data:

$$X^{(0)} = \{124.1,\ 144,\ 170.6,\ 203.6,\ 238.8,\ 282.5,\ 319.5,\ 368.5,\ 416.8,\ 490.2,\ 561.3\}. \tag{14}$$

Set $\gamma = 10$, and we have

$$g(x) = \{1.00,\ 0.91,\ 0.83,\ 0.77,\ 0.71,\ 0.67,\ 0.63,\ 0.59,\ 0.56,\ 0.53,\ 0.50\}. \tag{15}$$

With equation (4), the aging accumulation sequence of $X^{(0)}$ can be calculated as

$$X^{(10)} = \{124.10,\ 256.82,\ 404.93,\ 574.15,\ 765.47,\ 986.08,\ 1227.35,\ 1500.23,\ 1801.94,\ 2155.87,\ 2555.91\}. \tag{16}$$

Then, we have

$$\begin{pmatrix} \hat{a} \\ \hat{b} \end{pmatrix} = \left(B^T B\right)^{-1} B^T Y = \begin{pmatrix} -0.12 \\ 108.58 \end{pmatrix}. \tag{17}$$

The time response function $\hat{x}^{(10)}(i) = (124.10 - (108.58/-0.12))e^{0.12(i-1)} + (108.58/-0.12)$ can be obtained by substituting $\hat{a}$ and $\hat{b}$ into equation (12). Then, the time response sequence can be calculated as

$$\hat{X}^{(10)} = \{124.10,\ 255.73,\ 404.47,\ 572.55,\ 762.48,\ 977.10,\ 1219.62,\ 1493.67,\ 1803.35,\ 2153.29,\ 2548.72\}. \tag{18}$$

Finally, the fitted values are obtained by inverse accumulation as

$$\hat{X}^{(0)} = \{124.10,\ 142.91,\ 171.14,\ 202.42,\ 237.28,\ 276.26,\ 319.97,\ 369.07,\ 424.29,\ 486.48,\ 556.56\}. \tag{19}$$

However, if the original sequence is

$$X^{(0)} = \{80.1,\ 144,\ 170.6,\ 203.6,\ 238.8,\ 282.5,\ 319.5,\ 368.5,\ 416.8,\ 490.2,\ 561.3\}, \tag{20}$$

the fitted values are obtained by the same method as

$$\hat{X}^{(0)} = \{80.10,\ 141.67,\ 170.48,\ 202.22,\ 237.42,\ 276.63,\ 320.44,\ 369.51,\ 424.53,\ 486.33,\ 555.78\}. \tag{21}$$

Proof completed.

3.3. The Monotonicity and Forecast Trend of AGM (1, 1). From equation (13), we conclude that the fitted and predicted values $\left\{\hat{x}^{(0)}(1), \hat{x}^{(0)}(2), \ldots, \hat{x}^{(0)}(m+mf)\right\}$ are related to model parameters. Therefore, the monotonicity of the predictive value is uncertain and data-driven.

We consider an example from [22]. The data from 2001 to 2007 are used for fitting, and the data from 2008 to 2009 are used for testing. The original data and model results are shown in Table 1. As for the original data, the data increased from 2001 to 2006 but decreased from 2006 to 2007, that is to say, the latest data showed a downward trend. However, the results of the traditional GM (1, 1) model increased monotonously from 2001 to 2009, which did not conform to the objective law. On the contrary, the AGM (1, 1) model perceived the trend change from 2006 to 2007, and its model results showed a downward trend from 2006 to 2009. It shows that the AGM (1, 1) model has better performance and pays more attention to new information.

In addition, by adjusting the aging parameter γ, the prediction trend of the AGM (1, 1) model can be adjusted flexibly. Figure 2 shows the results of the AGM (1, 1) model when aging parameters are 1, 3, 5, and 10, respectively. With the increase of the aging parameter, the prediction trend tends to be flat. On the contrary, the smaller the aging parameter, the steeper the prediction trend. The advantage of this flexible adjustment mechanism is that it can be analyzed by combining subjective experience with objective data, which is very suitable for forecasting uncertain systems.

3.4. The Relationship between the Error and Aging Parameter γ. Accumulation operation can make scattered data show a certain trend, but it inevitably leads to reductive error. In this section, we will further study the relationship between reductive errors and the aging parameter γ of the AGM (1, 1)

Table 1: Model results with different aging parameters.

Year	Actual value	GM (1, 1)	$AGM^{(1)}$ (1, 1)	$AGM^{(3)}$ (1, 1)	$AGM^{(5)}$ (1, 1)	$AGM^{(10)}$ (1, 1)
2001	247.84	247.84	247.84	247.84	247.84	247.84
2002	273.02	278.58	267.66	270.72	273.1685	275.9409
2003	289.01	282.20	286.13	284.76	283.7412	282.7841
2004	285.21	285.87	294.04	291.63	289.8058	287.7632
2005	288.82	289.59	295.59	294.02	292.7876	291.275
2006	297.08	293.36	293.39	293.49	293.5915	293.6141
2007	293.66	297.17	289.05	291.05	292.8283	295.005
2008	290.40	301.04	283.57	287.34	290.9281	295.6225
2009	279.14	304.95	277.55	282.82	288.2036	295.6053

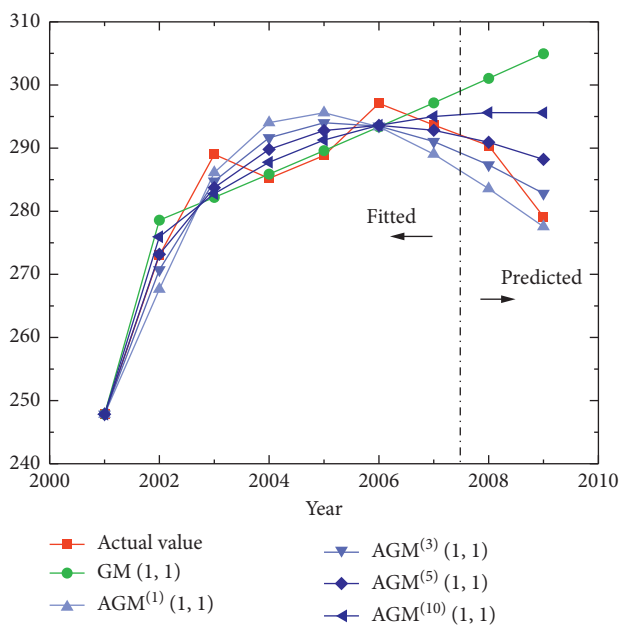

Figure 2: The results of different grey models.

model, so as to effectively control the errors caused by accumulative reduction operations.

Theorem 1. *Assume that* $X^{(\gamma)} = \{x^{(\gamma)}(1), x^{(\gamma)}(2), \ldots, x^{(\gamma)}(m)\}$ *is the accumulated sequence of the original sequence* $X^{(0)} = \{x^{(0)}(1), x^{(0)}(2), \ldots, x^{(0)}(m)\}$ *by AGM (1, 1) model with aging parameter* γ. $\widehat{X}^{(0)} = \{\widehat{x}^{(0)}(1), \widehat{x}^{(0)}(2), \ldots, \widehat{x}^{(0)}(m)\}$ *is the cumulative reduction sequence of time response sequence* $\{\widehat{x}^{(\gamma)}(1), \widehat{x}^{(\gamma)}(2), \ldots, \widehat{x}^{(\gamma)}(m)\}$.

If $|\widehat{x}^{(\gamma)}(i) - \widehat{x}^{(\gamma)}(i)| < \varepsilon$ $(1 < i \le m)$, then $|\widehat{x}^{(0)}(i) - x^{(0)}(i)| < \varepsilon * \sum_{j=1}^{i} |R(j,i)|$ $(1 < i \le m)$, where

$$R = \begin{bmatrix} g(0) & g(1) & \cdots & g(i-1) \\ 0 & g(0) & \cdots & g(i-2) \\ \vdots & \vdots & \vdots & \vdots \\ 0 & 0 & \cdots & g(1) \\ 0 & 0 & \cdots & g(0) \end{bmatrix}^{-1}. \tag{22}$$

Proof. According to the definition of AGM (1, 1), we have

$$\begin{aligned} &\left[\widehat{x}^{(0)}(1) - x^{(0)}(1), \widehat{x}^{(0)}(2) - x^{(0)}(2), \ldots, \widehat{x}^{(0)}(m) - x^{(0)}(m)\right] \\ &= \left[\widehat{x}^{(\gamma)}(1) - \widehat{x}^{(\gamma)}(1), \widehat{x}^{(\gamma)}(2) - \widehat{x}^{(\gamma)}(2), \ldots, \widehat{x}^{(\gamma)}(m) - \widehat{x}^{(\gamma)}(m)\right] \begin{bmatrix} g(0) & g(1) & \cdots & g(m-1) \\ 0 & g(0) & \cdots & g(m-2) \\ \vdots & \vdots & \vdots & \vdots \\ 0 & 0 & \cdots & g(1) \\ 0 & 0 & \cdots & g(0) \end{bmatrix}^{-1}. \end{aligned} \tag{23}$$

Let $R = \begin{bmatrix} g(0) & g(1) & \cdots & g(i-1) \\ 0 & g(0) & \cdots & g(i-2) \\ \vdots & \vdots & \vdots & \vdots \\ 0 & 0 & \cdots & g(1) \\ 0 & 0 & \cdots & g(0) \end{bmatrix}^{-1}$.

For $\forall i = 1, 2, \ldots, m$, we have

$$\begin{aligned}&\left|\hat{x}^{(0)}(i)-x^{(0)}(i)\right|\\&=\left|\left[\hat{x}^{(\gamma)}(1)-\hat{x}^{(\gamma)}(1),\hat{x}^{(\gamma)}(2)-\hat{x}^{(\gamma)}(2),\ldots,\hat{x}^{(\gamma)}(i)-\hat{x}^{(\gamma)}(i)\right]*R(\sim,i)\right|\\&<\varepsilon*\sum_{j=1}^{i}|R(j,i)|,\end{aligned}\tag{24}$$

where $R(\sim,i)$ represents the column i of the matrix R and $R(j,i)$ represents the element in row j and column i of the matrix R.

Proof completed.

When determining the value of the aging parameter γ, we should minimize $\|R\|_1$ as much as possible to avoid large reductive errors.

4. Performance Evaluation of the Proposed Model

The definition and related properties of the AGM (1, 1) model have been introduced above. In fact, the performance of AGM (1, 1) depends on the value of the aging parameter γ. In this section, an optimization algorithm is introduced to determine the optimal aging parameter, and four examples are used to prove the effectiveness of the proposed AGM (1, 1) model.

4.1. Optimization Algorithm of the Optimal Aging Parameter γ. Taking the average absolute percentage error (MAPE = $(1/m)\sum_{k=1}^{m}|(\hat{x}_1^{(0)}(k)-x_1^{(0)}(k))/x_1^{(0)}(k)|\times 100\%$) as the optimization objective and the main formula of the AGM (1, 1) model as the constraint condition, the following nonlinear programming is constructed.

$$\min Z(\gamma)=\frac{1}{m}\sum_{k=1}^{m}\left|\frac{\hat{x}_1^{(0)}(k)-x_1^{(0)}(k)}{x_1^{(0)}(k)}\right|\times 100\%,$$

$$\text{s.t.}\begin{cases}B=\begin{bmatrix}-0.5\left(x^{(\gamma)}(1)+x^{(\gamma)}(2)\right) & 1\\ -0.5\left(x^{(\gamma)}(2)+x^{(\gamma)}(3)\right) & 1\\ \vdots & \vdots\\ -0.5\left(x^{(\gamma)}(m-1)+x^{(\gamma)}(m)\right) & 1\end{bmatrix},\\ Y=\begin{bmatrix}x^{(\gamma)}(2)-x^{(\gamma)}(1)\\ x^{(\gamma)}(3)-x^{(\gamma)}(2)\\ \vdots\\ x^{(\gamma)}(m)-x^{(\gamma)}(m-1)\end{bmatrix},\\ [\hat{a},\hat{b}]^T=\left(B^TB\right)^{-1}B^TY,\\ \hat{x}^{(\gamma)}(i)=\left(x^{(0)}(1)-\frac{\hat{b}}{\hat{a}}\right)e^{-\hat{a}(i-1)}+\frac{\hat{b}}{\hat{a}},\quad i=1,2,\ldots,m.\end{cases}\tag{25}$$

Particle swarm optimization (PSO) is a mature intelligent optimization algorithm, which is derived from simulating the group behavior of bird foraging. Particle swarm optimization algorithm has the characteristics of simple operation and rapid convergence, so it has been widely used [30–32]. Figure 3 shows the flowchart for determining the optimal aging parameter γ. The specific steps of the algorithm are shown in Algorithm 1.

4.2. Application and Analysis. In addition to the MAPE, we applied the mean absolute error (MAE) and the root mean square error (RMSE) to measure the predictive performance of the AGM (1, 1) model. They are defined as follows:

$$\begin{aligned}\text{MAE}&=\frac{1}{m}\sum_{k=1}^{m}\left|\hat{x}_1^{(0)}(k)-x_1^{(0)}(k)\right|,\\ \text{RMSE}&=\sqrt{\frac{1}{m}\sum_{k=1}^{m}\left(\hat{x}_1^{(0)}(k)-x_1^{(0)}(k)\right)^2}.\end{aligned}\tag{26}$$

Case 1. Forecasting logistics demand in Jiangsu province.

This example comes from [7]. This is a case with small sample size. Similar to [7], the data from 2000 to 2005 are used for fitting, and the data of 2006 are used for the test. The smaller the sample size, the higher the prediction accuracy of the traditional GM (1, 1). Therefore, this paper compares AGM (1, 1) with GM (1, 1) models with different sample sizes, and Table 2 shows the comparison results. In the stage of fitting and testing, AGM (1, 1) with six sample sizes gets better results than GM (1, 1) with four sample sizes. The results show that with the increase of the number of samples, the special metabolic function of AGM(1, 1) can reduce the interference of old data and improve the prediction performance of the model.

Case 2. The example for the waste volume sequence of TV in China.

This example is from [33]. The data are the waste volume of TV (10000 units) in China. It is a steady growth sequence. The in-sample data and out-of-sample data are the same as [33]. To prove the performance of AGM(1,1) model, eight commonly used forecasting methods are used for comparison. The errors of the nine models are shown in Table 3. In the fitting and testing stage, MAPE, MAE, and RMSE of AGM (1, 1) are the lowest, which shows that the proposed AGM (1, 1) model has excellent performance in dealing with medium and long-term stationary sequences.

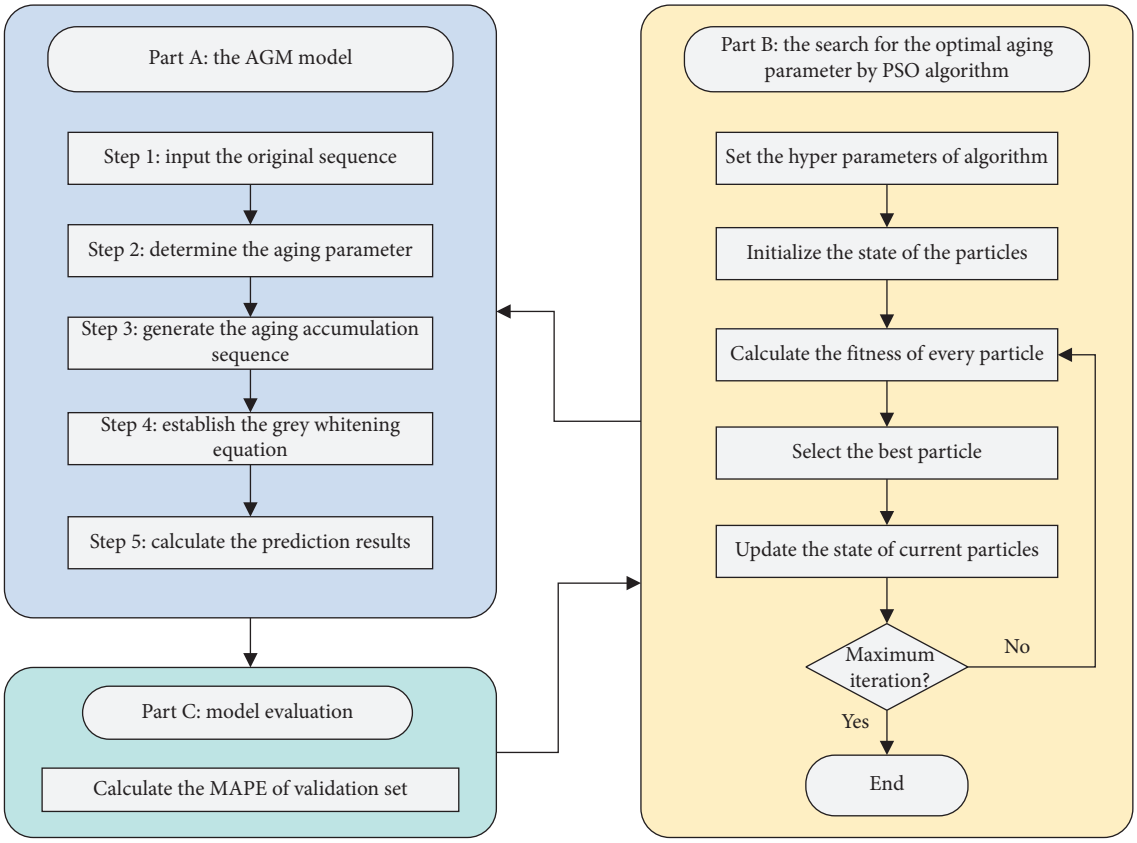

Figure 3: Flowchart for determining the optimal aging parameter.

Input: the sample set $X^{(0)} = \{x^{(0)}(1), x^{(0)}(2), \ldots, x^{(0)}(m)\}$
Output: the optimal value of γ
(1) Initialize parameters in the PSO algorithm:
Particle number N, dimension D, maximum generation T, learning factor c_1, c_2, inertia weight η.
(2) Initialize the position w_i and velocity v_i
(3) for $j = 1$: T do
(4) for $i = 1$: N do
(5) Calculate $X^{(\gamma)} = \{x^{(\gamma)}(1), x^{(\gamma)}(2), \ldots, x^{(\gamma)}(m)\}$ by Definition 1;
(6) Calculate $\{\widehat{b}_1, \widehat{b}_2, \ldots, \widehat{b}_n, \widehat{u}\}$by equation (10);
(7) Compute $\widehat{X}_1^{(0)}$ using equation (13);
(8) Compute the fitness function $Z(\gamma)$;
(9) Update the position and velocity of particles
$v_i = \eta v_i + c_1 r_1 (Q_p - w_i) + c_2 r_2 (Q_g - w_i)$;
$w_i = w_i + v_i$.
where γ are random vectors and belong to [0, 10]; Q_p and Q_g represent the individual optimal position and the global optimal position, respectively.
(10) **end for**
(11) **end for**
(12) **return optimal value of** γ

Algorithm 1: Optimization algorithm of the optimal aging parameter γ (solution to optimize the optimal aging parameter γ).

Case 3. Predicting foreign tourists to China.

This example is from [34]. The data are the annual historical data of tourists from Russia and Singapore from 2003 to 2017 in China. They are long and fluctuating sequences. Similar to [34], the data from 2003 to 2015 were used for fitting, and the data from 2016 and 2017 were used for the test. Table 4 summarizes the test results of 12 different prediction methods. In Russia, the MAPE of AGM (1, 1) is only lower than that of F-OGMp (1, 1), and MAE and RMSE are the lowest. For Singapore, the overall performance of

Table 2: The fitting and predicted values of grey models on different samples.

Serial number	Actual value	GM_6 (1, 1)	GM_5 (1, 1)	GM_4 (1, 1)	AGM (1, 1)
2000	132.4	132.4			132.40
2001	144.6	142	144.6		142.75
2002	156.3	157.3	155.3	156.3	155.57
2003	173.7	174.2	173	172.1	171.45
2004	190.2	193	192.8	192.5	191.10
2005	216.7	213.8	214.8	215.3	215.41
MAPE		1.12	0.81	0.93	**0.69**
MAE		1.63	1.24	1.33	**1.17**
RMSE		2.01	1.54	1.57	**1.38**
2006	249.4	236.8	239.4	240.8	245.50
MAPE		5.04	4.03	3.46	**1.57**
MAE		12.6	10	8.6	**3.90**

The smallest values of these model errors are in bold.

Table 3: The fitting and predicted values of nine models.

Model	Fitting value			Testing value	
	MAPE	MAE	RMSE	MAPE	MAE
AGM (1, 1)	**0.4**	**35.92**	**47.95**	**0.11**	**13.03**
EFGM	0.58	50.81	69.04	1.13	134.43
LSSVR	1.06	91.36	131.08	7.96	949.89
ANN	1.61	130.34	147.58	0.63	75.49
ARIMA	0.63	48.08	54.82	6.88	821.07
DGM (1, 1)	1.65	135.68	168.63	3.64	434.92
Verhulst	22.35	1597.68	2161.39	12.38	1477.09
GM (1, 1)	1.64	135.21	168.55	3.57	426.49
FGM (1, 1)	0.85	72.26	87.48	1.46	174.66

The smallest values of these model errors are in bold.

Table 4: The predicted values of twelve models.

Model	Russia			Singapore		
	MAPE	MAE	RMSE	MAPE	MAE	RMSE
TGM (1, 1)	9.23	**20.83**	**23.64**	1.39	1.28	1.78
Original GM (1, 1)	12.04	49.77	52.17	15.48	14.44	14.45
Optimized GM (1, 1)	11.95	49.8	51.18	15.48	14.44	14.45
Original NGBM (1, 1)	57.21	250.43	256.94	14.85	13.9	14.98
Optimized NGBM (1, 1)	10.07	44.86	48.14	1.63	1.51	1.88
ARIMA	25.29	104.66	109.39	**0.3**	**0.28**	**0.38**
BPN	9.46	43.62	53.28	2.35	8.72	8.83
Optimized GMp (1, 1)	10.09	45.43	50.64	1.58	1.48	1.48
Original F-GM (1, 1)	17.32	76.29	79.39	5.65	5.31	7.15
Optimized F-GM (1, 1)	17.34	76.32	79.3	5.67	5.34	7.47
Optimized F-GMp (1, 1)	13.19	52.21	65.27	2.89	2.72	3.85
F-OGMp (1, 1)	**6.12**	27.44	30.05	1.35	1.26	1.39

AGM (1, 1) is only lower than that of ARIMA and equivalent to F-OGMp (1, 1). This shows that the AGM (1, 1) model can well predict the development trend of medium and long-term wave series.

Case 4. Comparison of aging accumulation operator and other existing operators.

Accumulation operation is an important operation of the grey prediction model. By accumulating the data, the interference of random disturbance can be effectively reduced, and the scattered data show a certain rule. To prove the effectiveness of the proposed aging accumulation operator, seven existing grey accumulation operators such as the traditional first-order accumulation generation operation, the damping accumulation generation operation [25], the adjacent accumulation generation operation [35], the first-order new information priority accumulation generation operation [23], the conformable fractional accumulation generation operation [36], the fractional order accumulation generation operation [22], and fractional Hausdorff accumulation generation operation [37] are compared and analyzed. The data of forecasting competition are often used to verify the performance of forecasting methods [38, 39]. Take the first nine data of the $N7$ series in the $M3$ prediction contest as an example. The first seven data are used for fitting, and the last two data are used for testing.

Table 5: Grey models with different grey accumulation operators.

		GM (1, 1)	AGM (1, 1)	DAGM (1, 1)	AGM_1 (1, 1)	NGM (1, 1)	CFGM (1, 1)	FGM (1, 1)	FHGM (1, 1)
1	2399.26	2399.26	2399.26	2399.26	2399.26	2399.26	2399.26	2399.26	2399.26
2	2910.52	2989.36	2910.52	2989.36	2846.92	2910.52	2895.97	2906.43	2895.97
3	3126.62	3178.09	3192.14	3178.09	3197.53	3184.44	3202.81	3201.44	3202.81
4	3475.14	3378.73	3433.73	3378.73	3472.12	3427.27	3440.37	3436.21	3440.37
5	3750.96	3592.04	3645.29	3592.04	3687.18	3642.53	3644.95	3640.92	3644.95
6	3752.72	3818.81	3833.15	3818.81	3855.62	3833.37	3830.51	3828.03	3830.51
7	4004.02	4059.91	4001.66	4059.91	3987.53	4002.54	4004.02	4004.02	4004.02
MAPE		2.07	**1.19**	2.07	1.34	**1.19**	1.26	1.23	1.26
MAE		72.52	**42.20**	72.52	45.81	42.32	44.19	43.31	44.19
RMSE		85.28	**58.12**	85.28	58.56	58.43	59.18	59.66	59.18
8	3737.38	4316.22	4153.93	4316.22	4090.85	4152.51	4169.51	4172.66	4169.51
9	4263.98	4588.72	4292.30	4588.72	4171.77	4285.46	4329.50	4336.39	4329.51
MAPE		11.55	5.9	11.55	**5.81**	**5.81**	6.55	6.67	6.55
MAE		451.79	222.43	451.79	222.84	**218.3**	248.83	253.84	248.83
RMSE		469.31	295.23	469.31	**258.31**	293.93	309.05	312.02	309.05

Note. AGM_1 (1, 1) is the adjacent accumulation grey model. The smallest values of these model errors are in bold.

Table 5 summarizes the grey model results of different cumulative generation operators. The MAPE, MAE, and RMSE of the AGM (1, 1) model are 1.19%, 42.20, and 58.12, respectively. They are all the lowest in the fitting stage. In the testing stage, AGM (1, 1) is also superior to most models. Actually, MAPE, MAE, and RMSE are only worse than those of NGM (1, 1) and AGM_1 (1, 1) in the prediction stage, which shows that the proposed aging accumulation operator is effective.

5. Conclusions

In this paper, a novel aging accumulation operator is proposed. Different from the existing grey accumulation operator, this operator determines the accumulation weight of data at different times from back to front. The addition of new data will push the old data to roll back so that the timeliness of data can be updated dynamically with the change of the system. The aging accumulation operator is introduced into the grey model, and a new aging accumulation grey model AGM (1, 1) is obtained. Compared with the traditional grey model, AGM (1, 1) can reduce the interference of old data and improve the prediction accuracy of the model by adjusting the aging parameter γ. In addition, the prediction trend of the AGM (1, 1) model is adjustable. The effectiveness of AGM (1, 1) is proved by four case studies, and the following conclusions are obtained:

(1) The introduction of the aging parameter γ overcomes the problem that the prediction accuracy of the traditional GM (1, 1) model decreases with the increase of sample size. The AGM (1, 1) model can effectively adjust the aging weight of new and old information and get more accurate fitting and prediction results.

(2) The AGM (1, 1) model not only effectively improves the short-term forecasting ability of the grey model but also outperforms most existing forecasting methods when dealing with medium and long-term smooth and fluctuating series.

(3) As an improvement of the traditional GM (1, 1) model, the proposed aging accumulation operator is superior to most existing grey accumulation operators.

In a word, the proposed aging accumulation operator and aging accumulation grey model are very effective. Because of the excellent performance of the aging accumulation operator, it can also be used to improve other grey models and forecasting methods. Besides, when defining the aging accumulation operator, the inverse proportional function is selected as the aging decreasing function, and the better aging decreasing function can be mined.

Data Availability

The data used to support the findings of this study are available from the corresponding author upon request.

Conflicts of Interest

The authors declare that they have no conflicts of interest.

Acknowledgments

This study was supported by the Excellent Young Scientist Foundation of Hebei Education Department (SLRC2019001).

References

[1] N. Xie and R. Wang, "A historic review of grey forecasting models," *Journal of Grey System*, vol. 29, no. 4, pp. 1–29, 2017.

[2] H. Hewamalage, C. Bergmeir, and K. Bandara, "Recurrent neural networks for time series forecasting: current status and future directions," *International Journal of Forecasting*, vol. 37, no. 1, pp. 388–427, 2021.

[3] S. Ryu, J. Noh, and H. Kim, "Deep neural network based demand side short term load forecasting," *Energies*, vol. 10, no. 1, p. 3, 2016.

[4] E. M. de Oliveira and F. L. Cyrino Oliveira, "Forecasting mid-long term electric energy consumption through bagging

ARIMA and exponential smoothing methods," *Energy*, vol. 144, pp. 776–788, 2018.

[5] R. Moazenzadeh, B. Mohammadi, S. Shamshirband, and K.-w. Chau, "Coupling a firefly algorithm with support vector regression to predict evaporation in northern Iran," *Engineering Applications of Computational Fluid Mechanics*, vol. 12, no. 1, pp. 584–597, 2018.

[6] Z. Zeng and M. Li, "Bayesian median autoregression for robust time series forecasting," *International Journal of Forecasting*, vol. 37, no. 2, pp. 1000–1010, 2020.

[7] L. Wu, S. Liu, L. Yao, and S. Yan, "The effect of sample size on the grey system model," *Applied Mathematical Modelling*, vol. 37, no. 9, pp. 6577–6583, 2013.

[8] X. Ma, W. Wu, and Y. Zhang, "Improved GM(1,1) model based on Simpson formula and its applications," *Journal of Grey System*, vol. 31, no. 4, pp. 33–46, 2019.

[9] S. Li, B. Zeng, X. Mai et al., "A novel grey model with A three-parameter background value and its application in forecasting average annual water consumption per capita in urban areas along the Yangtze river basin," *Journal of Grey System*, vol. 32, no. 1, pp. 118–132, 2020.

[10] Y.-C. Hu, P. Jiang, and P.-C. Lee, "Forecasting tourism demand by incorporating neural networks into Grey-Markov models," *Journal of the Operational Research Society*, vol. 70, no. 1, pp. 12–20, 2019.

[11] N.-m. Xie and S.-f. Liu, "Discrete grey forecasting model and its optimization," *Applied Mathematical Modelling*, vol. 33, no. 2, pp. 1173–1186, 2009.

[12] C. Zheng, W.-Z. Wu, W. Xie, Q. Li, and T. Zhang, "Forecasting the hydroelectricity consumption of China by using a novel unbiased nonlinear grey Bernoulli model," *Journal of Cleaner Production*, vol. 278, Article ID 123903, 2021.

[13] X. Ma and Z. Liu, "The GMC(1, n) model with optimized parameters and its application," *Journal of Grey System*, vol. 29, no. 4, pp. 122–138, 2017.

[14] L. Wu, S. Liu, and Y. Yang, "Using the fractional order method to generalize strengthening buffer operator and weakening buffer operator," *IEEE/CAA Journal of Automatica Sinica*, vol. 5, no. 6, pp. 1074–1078, 2018.

[15] C. Li, Y. Yang, and S. Liu, "Comparative analysis of properties of weakening buffer operators in time series prediction models," *Communications in Nonlinear Science and Numerical Simulation*, vol. 68, pp. 257–285, 2019.

[16] L.-Y. He, L.-L. Pei, and Y.-H. Yang, "An optimised grey buffer operator for forecasting the production and sales of new energy vehicles in China," *Science of the Total Environment*, vol. 704, Article ID 135321, 2020.

[17] A. Bezuglov and G. Comert, "Short-term freeway traffic parameter prediction: application of grey system theory models," *Expert Systems with Applications*, vol. 62, pp. 284–292, 2016.

[18] D. Zhou, A. Al-Durra, K. Zhang, A. Ravey, and F. Gao, "A robust prognostic indicator for renewable energy technologies: a novel error correction grey prediction model," *IEEE Transactions on Industrial Electronics*, vol. 66, no. 12, pp. 9312–9325, 2019.

[19] S. Ding, R. Li, and Z. Tao, "A novel adaptive discrete grey model with time-varying parameters for long-term photovoltaic power generation forecasting," *Energy Conversion and Management*, vol. 227, Article ID 113644, 2021.

[20] E. Javanmardi and S. Liu, "Exploring grey systems theory-based methods and applications in analyzing socio-economic systems," *Sustainability*, vol. 11, no. 15, p. 4192, 2019.

[21] W. Zhou, X. Wu, S. Ding, and Y. Cheng, "Predictive analysis of the air quality indicators in the Yangtze River Delta in China: an application of a novel seasonal grey model," *Science of The Total Environment*, vol. 748, Article ID 141428, 2020.

[22] L. Wu, S. Liu, L. Yao, S. Yan, and D. Liu, "Grey system model with the fractional order accumulation," *Communications in Nonlinear Science and Numerical Simulation*, vol. 18, no. 7, pp. 1775–1785, 2013.

[23] L. Wu and Z. Zhang, "Grey multivariable convolution model with new information priority accumulation," *Applied Mathematical Modelling*, vol. 62, pp. 595–604, 2018.

[24] W. Wu, X. Ma, Y. Zhang, W. Li, and Y. Wang, "A novel conformable fractional non-homogeneous grey model for forecasting carbon dioxide emissions of BRICS countries," *Science of The Total Environment*, vol. 707, Article ID 135447, 2020.

[25] L. Liu, Y. Chen, and L. Wu, "The damping accumulated grey model and its application," *Communications in Nonlinear Science and Numerical Simulation*, vol. 95, Article ID 105665, 2021.

[26] S. Liu and Y. Lin, *Grey Systems: Theory and Applications*, Springer, London, UK, 2010.

[27] J. Deng, "Introduction to grey system theory," *Journal of Grey System*, vol. 1, no. 1, pp. 1–24, 1989.

[28] L. Wu, S. Liu, Z. Fang, and H. Xu, "Properties of the GM(1, 1) with fractional order accumulation," *Applied Mathematics and Computation*, vol. 252, pp. 287–293, 2015.

[29] L. Liu and L. Wu, "Forecasting the renewable energy consumption of the European countries by an adjacent non-homogeneous grey model," *Applied Mathematical Modelling*, vol. 89, pp. 1932–1948, 2021.

[30] N. Chouikhi, B. Ammar, N. Rokbani, and A. M. Alimi, "PSO-based analysis of Echo State Network parameters for time series forecasting," *Applied Soft Computing*, vol. 55, pp. 211–225, 2017.

[31] Z.-X. Wang and Q. Li, "Modelling the nonlinear relationship between CO2 emissions and economic growth using a PSO algorithm-based grey Verhulst model," *Journal of Cleaner Production*, vol. 207, pp. 214–224, 2019.

[32] N. Zeng, H. Zhang, W. Liu, J. Liang, and F. E. Alsaadi, "A switching delayed PSO optimized extreme learning machine for short-term load forecasting," *Neurocomputing*, vol. 240, pp. 175–182, 2017.

[33] S. Mao, Y. Kang, Y. Zhang, X. Xiao, and H. Zhu, "Fractional grey model based on non-singular exponential kernel and its application in the prediction of electronic waste precious metal content," *ISA Transactions*, vol. 107, pp. 12–26, 2020.

[34] Y.-C. Hu, "Forecasting tourism demand using fractional grey prediction models with Fourier series," *Annals of Operations Research*, vol. 300, no. 2, pp. 467–491, 2020.

[35] H. Zhao and W. Lifeng, "Forecasting the non-renewable energy consumption by an adjacent accumulation grey model," *Journal of Cleaner Production*, vol. 275, Article ID 124113, 2020.

[36] X. Ma, W. Wu, B. Zeng, Y. Wang, and X. Wu, "The conformable fractional grey system model," *ISA Transactions*, vol. 96, pp. 255–271, 2020.

[37] Y. Chen, W. Lifeng, L. Lianyi, and Z. Kai, "Fractional Hausdorff grey model and its properties," *Chaos, Solitons & Fractals*, vol. 138, Article ID 109915, 2020.

[38] A. Ingel, N. Shahroudi, M. Kängsepp, A. Tättar, V. Komisarenko, and M. Kull, "Correlated daily time series and forecasting in the M4 competition," *International Journal of Forecasting*, vol. 36, no. 1, pp. 121–128, 2020.

[39] F. Petropoulos, X. Wang, and S. M. Disney, "The inventory performance of forecasting methods: evidence from the M3 competition data," *International Journal of Forecasting*, vol. 35, no. 1, pp. 251–265, 2019.

Hindawi
Journal of Mathematics
Volume 2021, Article ID 2973361, 7 pages
https://doi.org/10.1155/2021/2973361

Research Article

Insider Trading with Memory under Random Deadline

Kai Xiao [1] **and Yonghui Zhou** [2]

[1] *School of Mathematics, Guizhou Normal University, Guiyang 550001, China*
[2] *School of Big Data and Computer Science, Guizhou Normal University, Guiyang 550001, China*

Correspondence should be addressed to Yonghui Zhou; yonghuizhou@163.com

Received 14 May 2021; Accepted 30 June 2021; Published 16 July 2021

Academic Editor: Utkucan Şahin

In this paper, we study a model of continuous-time insider trading in which noise traders have some memories and the trading stops at a random deadline. By a filtering theory on fractional Brownian motion and the stochastic maximum principle, we obtain a necessary condition of the insider's optimal strategy, an equation satisfied. It shows that when the volatility of noise traders is constant and the noise traders' memories become weaker and weaker, the optimal trading intensity and the corresponding residual information tend to those, respectively, when noise traders have no any memory. And, numerical simulation illustrates that if both the trading intensity of the insider and the volatility of noise trades are independent of trading time, the insider's expected profit is always lower than that when the asset value is disclosed at a finite fixed time; this is because the trading time ahead is a random deadline which yields the loss of the insider's information.

1. Introduction

In 1985, Kyle [1] proposed an equilibrium model of continuous insider trading, in which there are three types of traders in a market with a risky asset, whose values is normally distributed. Subsequently, Back [2] formulated and studied a revised-version of Kyle's model [1] in continuous time and, by dynamic programming principle, obtained the existence and uniqueness of equilibrium pricing rule within a certain class of insider trading. This model has been known as a classical Kyle–Back model. Later, by the same method, Caldentey and Stacchetti [3] investigated the equilibrium for a class of insider trading with a dynamic asset driven by a Brownian motion and with trading time stopped at a random deadline. Moreover, Collins-Dufresne and Fos [4] studied the impact of a stochastic volatility of noise trades on the equilibrium for some kind of insider trading with a static risky asset. Alternatively, by a filtering theory on Brownian motion and maximum principle, Aase et al. [5] solved a model of insider trading problem with volatility of noise trades' time varying. Then, Zhou [6] also obtained a close form of equilibrium when market makers have some partial observations on a risky asset. Furthermore, Ma et al. [7] studied a more general model of insider trading with an asset value driven by a conditional mean-field Ornstein–Uhlenbeck-type dynamics and obtained a closed form of optimal intensity of trading strategy as well as dynamic pricing rule. In fact, there are many research studies about insider trading, see [8–12] and so on.

Note that, in those insider trading models mentioned above, it is always assumed that noise trades are driven by Brownian motion; that is, noise traders have no memory on the history of their trades. In fact, in real financial markets, noise traders often have some memories on the history; in other words, mathematically, noise trades follow a dynamics driven by fractional Brownian motion with Hurst parameter $H > (1/2)$, which will have some impacts on the insider's benefit. Biagini etal. [13] studied insider trading in this setting, obtained an equation for the optimal trading intensity, proved that when $H \longrightarrow (1/2)$, the solution converges to the solution in the classical case driven by Brownian motion ($H = (1/2)$), and pointed out that both the optimal insider trading intensity and the expect profit of an insider decreases with increasing $H \in [1/2, 1)$; the larger the Hurst parameter H is, the stronger the memory ability of noise traders is. Then, based on the model in [4], Yang et al.

[14] proposed an insider trading model with long memory, in which the volume of noise trades is driven by a fractional Brownian motion with the Hurst parameter $H > (1/2)$, with its volatility following a general stochastic process, and found that the optimal trading strategy of the insider turns out to possess the property of long memory, and the price impact is also affected by the fractional noise.

From the abovementioned studies, in this paper, based on the two models in [3, 13], we will continue to study a model of continuous-time insider trading in which noise traders have some memories and the trading stops at a random deadline. By a filtering theory on fractional Brownian motion and the maximum principle, we will look for some necessary conditions of the insider's optimal strategy and investigate the impact of noise traders' memory and random deadline on equilibrium, especially on the insider's profit.

The rest of this paper is organized into six sections. Section 2 presents some necessary preliminaries. In Section 3, our model with equilibrium concept is proposed. In Section 4, our main theorem about a necessary condition of optimal trading intensity is stated. In Section 5, we discuss the impact of noise traders' memory and random deadline on equilibrium. Conclusions are drawn in Section 6.

2. Preliminaries

Assume that all randomness comes from a common filtered probability space $(\Omega, \mathcal{F}, \{\mathcal{F}_t\}_{t\geq 0}, P)$ satisfying the usual conditions [15]. Let us introduce the concept of fractional Brownian motion B^H with Hurst parameter $H \in (0,1)$ [13, 16].

Definition 1. A fractional Brownian motion (fBm) B^H with Hurst parameter (or scaling factor) $H \in (0,1)$ is a process satisfying these following properties:

(1) All paths are almost surely continuous.

(2) B_t^H is centered Gaussian with covariance function

$$E\left[B_t^H B_s^H\right] = \frac{1}{2}\left(t^{2H} + s^{2H} - |t-s|^{2H}\right). \tag{1}$$

(3) B_t^H has stationary increments.

For $H = 1/2$, B_t^H is a standard Brownian motion (B_m) denoted by B; the increments of the process are independent. Contrary to $H = 1/2$, the increments are not independent. More exactly, if $t - s = nh$, then the covariance between $B_{t+h}^H - B_t^H$ and $B_{s+h}^H - B_s^H$ is expressed as

$$\rho_H(n) = \frac{1}{2}h^{2H}\left[(n+1)^{2H} + (n-1)^{2H} - 2n^{2H}\right]. \tag{2}$$

In particular, for $H > (1/2)$, the two increments of form $B_{t+h}^H - B_t^H$ and $B_{t+2h}^H - B_{t+h}^H$ are positively correlated. Furthermore,

$$\lim_{n\to\infty} \frac{\rho_H(n)}{H(2H-1)n^{2H-2}} = 1, \tag{3}$$

which means that the dependence between the increments $B_{t+h}^H - B_t^H$ and $B_{s+h}^H - B_s^H$ decays slowly as n tends to infinity, or the two increments of B^H have the long-range dependence property [16] and

$$\sum_{n=1}^{\infty} \rho_H(n) = \infty. \tag{4}$$

And, paths of the process are more regular than those of B presenting an aggregation behavior, which is used to describe systems with memory and persistence.

While, for $H < (1/2)$, the two increments of form $B_{t+h}^H - B_t^H$ and $B_{t+2h}^H - B_{t+h}^H$ are negatively correlated with

$$\sum_{n=1}^{\infty} \left|\rho_H(n)\right| < \infty, \tag{5}$$

the paths of B^H are less regular than those of B, such that systems have phenomena of turbulence and antipersistence.

In this paper, we restrict ourselves to the case $H \geq (1/2)$ and understand the integral of deterministic functions with respect to fBm in the sense of that described in [17], and others are usual Lebesgue or Lebesgue–Stieltjes integral; if we denote

$$B_t^* = \int_0^t k_H(t,s)\mathrm{d}B_s^H, \tag{6}$$

where $k_H = 2H\Gamma((3/2)-H)\Gamma((1/2)+H)$, then B_t^* is a Gaussian martingale with $\langle B^*\rangle_t = \lambda_H^{-1} t^{2-2H}$ and $\lambda_H = (2H\Gamma(3-2H)\Gamma(H+(1/2))/\Gamma((3/2)-H))$. For convenience, denote L_H^2, the space of equivalence of measurable functions f, on $[0,\infty)$ such that

$$\langle\langle\langle f, g\rangle\rangle\rangle_H = H(2H-1)\int_0^\infty \int_0^\infty f(s)g(t)|s-t|^{2H-2}\mathrm{d}s\mathrm{d}t < \infty. \tag{7}$$

3. The Model with Equilibrium

There is a risky asset traded in continuous time with value v normally distributed $N(0,\sigma_v^2)$, which is made public at a random time τ. The random time τ has a geometric distribution with probability of failure $e^{-\mu t}$ for some $\mu > 0$ and is independent of the history of transactions and prices [3]. And, there are three types of agents in the market:

(i) *An insider*, who has private information of the liquidation value v at the trade beginning and submits her/his order x_t at time t.

(ii) *Noise traders*, who have no information of the liquidation value v and submit a total order z_t in the form:

$$z_t = \int_0^t \sigma_{zs}\mathrm{d}B_s^H, \tag{8}$$

where σ_z is a deterministic continuously differentiable function satisfying $\sigma_{zt} > 0$ and belongs to L_H^2.

(iii) *Market makers*, who receive the total traded volume (cannot distinguish between the insiders and noise traders),

$$y_t = x_t + z_t, \tag{9}$$

and set the market price p_t for the asset value v in a semistrong way as in [1]:

$$p_t = E\left[v|\mathcal{F}_t^M\right], \tag{10}$$

where $\mathcal{F}_t^M = \sigma\{y_s, 0 \le s \le t\}$.

As in [1, 2, 5], assume that the dynamics of the insider's strategy x_t is as

$$\mathrm{d}x_t = \beta_t (v - p_t)\mathrm{d}t, \quad x_0 = 0, \tag{11}$$

where β is a deterministic, positive, and smooth function on $[0, \infty)$, called the insider trading intensity in [1]. Then, informally, the total expected payoff of the insider is as in [3]:

$$E\int_0^\tau (v - p_s)dx_s = \int_0^{+\infty} \beta_s \exp(-\mu s)\Sigma_s \mathrm{d}s, \tag{12}$$

where $\Sigma_t = E(v - p_t)^2$, called residual information in [1].

Note that (β, p) should satisfy $E[\int_0^\infty \exp(-\mu t)\beta_t (v - p_t)^2 \mathrm{d}t] < \infty$. The collection of all these profiles (β, p) is denoted by $\mathbb{S}$.

Similar to those in [2] or [1], we give the following definition.

Definition 2. An equilibrium is a profile (β, p) in $\mathbb{S}$ such that

(i) Maximization of profit: it is given that p and β maximize

$$\int_0^\infty \beta_s \exp(-\mu s)\Sigma_s \mathrm{d}s. \tag{13}$$

(ii) Market efficiency: it is given β and p satisfy the semistrong pricing condition:

$$p_t = E\left[v|\mathcal{F}_t^M\right]. \tag{14}$$

4. The Main Theorem

Before establishing the central theorem, we give an important lemma, whose proof can be found in [4] or [13].

Lemma 1. *Let $\Sigma_0 = 1$; then the residual information*

$$\Sigma_t = \frac{1}{1 + \int_0^t \rho_s^2 \mathrm{d}l_s} \tag{15}$$

and

$$\frac{\mathrm{d}}{\mathrm{d}y}\Big|_{y=0}\Sigma(\beta + y\xi) = 2\Sigma_t^2 \int_0^t \left(\int_r^t \rho_s' K_H(s, r)\mathrm{d}s - \rho_t K_H(t, r)\right)\frac{\xi_r}{\sigma_{zr}}\mathrm{d}r, \tag{16}$$

where ξ is an arbitrary deterministic and smooth function on $[0, \infty)$, and the other functions or processes above are defined as follows:

$$\rho_t = \frac{\mathrm{d}}{\mathrm{d}l_t}\int_0^t k_H(t, s)\frac{\beta_s}{\sigma_{zs}}\mathrm{d}s, \tag{17}$$

$$\begin{aligned} \Gamma(t) &= \int_0^{+\infty} x^{t-1}e^{-x}\mathrm{d}x, \\ \mathrm{d}l_t &= \frac{(2 - 2H)t^{1-2H}}{2H\Gamma((3/2) - H)\Gamma((1/2) + H)}\mathrm{d}t, \end{aligned} \tag{18}$$

and

$$k_H(t, s) = \frac{s^{(1/2)-H}(t - s)^{(1/2)-H}}{2H\Gamma((3/2) - H)\Gamma((1/2) + H)}, \quad 0 < s < t. \tag{19}$$

Now, we will establish our central theorem below.

Theorem 1. *Suppose that the insider takes the optimal control β with its optimal expected profit:*

$$J^H(\beta) = \int_0^\infty \exp(-\mu t)\beta\Sigma(\beta)\mathrm{d}t. \tag{20}$$

Then, the residual information Σ_t satisfies the following equation:

$$\begin{aligned} \Sigma_t = -2\sigma_{zt}^{-1}\int_t^\infty \beta_r\Big(&\exp(\mu t - \mu r)\Sigma_r^2 \\ &\left(\left(\int_t^r \rho_s' K_H(s, t)\mathrm{d}s - \rho_r K_H(r, t)\right)\right)\Big)\mathrm{d}r. \end{aligned} \tag{21}$$

Proof. Assume that β is an optimal strategy of the insider. Then, if we define a real function g by

$$g(y) = J^H(\beta + y\xi), \quad y \in R, \tag{22}$$

where $y \in R$ and ξ is an arbitrary function on $[0, \infty)$, then g is maximal at $y = 0$, or

$$0 = \frac{\mathrm{d}}{\mathrm{d}y}\Big|_{y=0}J^H(\beta + y\xi) = \frac{\mathrm{d}}{\mathrm{d}y}\Big|_{y=0}\int_0^\infty \exp(-\mu t)(\beta + y\xi)\Sigma_t(\beta + y\xi)\mathrm{d}t. \tag{23}$$

From Lemma 1, we obtain

$$\begin{aligned} 0 = &\int_0^\infty \exp(-\mu t)\xi\Sigma_t \mathrm{d}t + 2\int_0^\infty \beta_t \exp(-\mu t)\Sigma_t^2 \\ &\left\{\int_0^t \left(\int_r^t \rho_s' K_H((s, r)\mathrm{d}s - \rho_t K_H(t, r)\right)\frac{\xi_r}{\sigma_{zr}}\mathrm{d}r\right\}\mathrm{d}t. \end{aligned} \tag{24}$$

Let

$$I_1 = \int_0^\infty \exp(-\mu t)\xi\Sigma_t \mathrm{d}t, \tag{25}$$

$$I_2 = 2\int_0^\infty \beta_t \exp(-\mu t)\Sigma_t^2 \left\{\int_0^t \left(\int_r^t \rho_s' K_H(s,r)\mathrm{d}s - \rho_t K_H(t,r)\right)\frac{\xi_r}{\sigma_{zr}}\mathrm{d}r\right\}\mathrm{d}t. \tag{26}$$

Changing the order of integration in (26), we have

$$I_2 = 2\int_0^\infty \frac{\xi_t}{\sigma_{zt}}\left(\int_t^\infty \left(\beta_r \exp(-\mu r)\Sigma_r^2 \left(\left(\int_t^r \rho_s' K_H(s,t)\mathrm{d}s - \rho_r K_H(r,t)\right)\right)\right)\mathrm{d}r\right)\mathrm{d}t. \tag{27}$$

Then, taking both I_2 and (25) into (23), we obtain

$$\begin{aligned} 0 &= \int_0^\infty \exp(-\mu t)\xi_t\Sigma_t \mathrm{d}t + 2\int_0^\infty \frac{\xi_t}{\sigma_{zt}}\left(\int_t^\infty \left(\beta_r \exp(-\mu r)\Sigma_r^2 \left(\left(\int_t^r \rho_s' K_H(s,t)\mathrm{d}s - \rho_r K_H(r,t)\right)\right)\right)\mathrm{d}r\right)\mathrm{d}t \\ &= \int_0^\infty \exp(-\mu t)\xi_t\left[\Sigma_t + \frac{2}{\sigma_{zt}}\left(\int_t^\infty \left(\beta_r \exp(\mu t - \mu r)\Sigma_r^2 \left(\left(\int_t^r \rho_s' K_H(s,t)\mathrm{d}s - \rho_r K_H(r,t)\right)\right)\right)\mathrm{d}r\right)\right]\mathrm{d}t. \end{aligned} \tag{28}$$

Since ξ is arbitrary, we have

$$\Sigma_t = -2\sigma_{zt}^{-1}\int_t^\infty \beta_r\left(\exp(\mu t - \mu r)\Sigma_r^2 \left(\left(\int_t^r \rho_s' K_H(s,t)\mathrm{d}s - \rho_r K_H(r,t)\right)\right)\right)\mathrm{d}r. \tag{29}$$

5. The Impact of Memory and Random Deadline on Equilibrium

The motive for is to find out the impact of memory and random deadline on equilibrium with Hurst parameter H varying.

Note that both the assumed optimal trading intensity β_t in Section 2 and the corresponding residual information Σ_t depend on Hurst parameter H, which can be written, respectively, as

$$\begin{aligned} \beta_t &= \beta_t(H), \\ \Sigma_t &= \Sigma_t(H). \end{aligned} \tag{30}$$

Equations (15) and (29) can be turned, respectively, as

$$\Sigma_t(H) = \frac{1}{1 + \int_0^t \rho_s^2(H)\mathrm{d}l_s}, \tag{31}$$

$$\Sigma_t(H) = -2\sigma_{zt}^{-1}\int_t^\infty \beta_r(H)\left(\exp(\mu t - \mu r)\Sigma_r^2(H) \left(\left(\int_t^r \rho_s' K_H(s,t)\mathrm{d}s - \rho_r K_H(r,t)\right)\right)\right)\mathrm{d}r. \tag{32}$$

Unfortunately, we are not able to solve our general equation to obtain $\beta(H)$ and $\Sigma(H)$ explicitly. However, we have the following limit theorem.

Theorem 2. *Assume that*

$$\begin{aligned} \lim_{H\longrightarrow(1/2)} \beta_t(H) &= \beta_t, \\ \lim_{H\longrightarrow(1/2)} \Sigma_t(H) &= \Sigma_t, \\ \sigma_{zt} &\equiv 1. \end{aligned} \tag{33}$$

Then,

$$\begin{aligned} \Sigma_t &= \exp(-2\mu t), \\ \beta_t &= \sqrt{2\mu}\exp(\mu t). \end{aligned} \tag{34}$$

Proof. Since $\lim_{H\to(1/2)} K_H(t,s) = 1$, it is easy to see that, by equations (31) and (32),

$$\Sigma_t = \left(1 + \int_0^t \rho_s^2 \mathrm{d}l(s)\right)^{-1}, \tag{35}$$

$$\Sigma_t = 2\beta_t\int_t^\infty \beta_r\Sigma_r^2 \exp(\mu t - \mu r)\mathrm{d}r. \tag{36}$$

Then, by equation (35), it is easy to check that

$$\begin{aligned} \frac{\mathrm{d}\Sigma_t}{\mathrm{d}t} &= -\beta_t^2\Sigma_t^2, \\ \Sigma_0 &= 1. \end{aligned} \tag{37}$$

And, by the structure of equation (36), we can assume that Σ_t is the form of $\exp(-k\mu t)$, where $k > 0$. Now, taking it into (37), we have

$$\beta_t = \sqrt{k\mu}\exp\left(\frac{k\mu t}{2}\right). \tag{38}$$

Then, taking it back into (36), we get $k = 2$. Therefore, the conclusion holds.

Remark 1. In [3], Caldentey and Stacchetti proposed a model of insider trading with a random deadline and found that the residual information Σ_t in the equilibrium is an

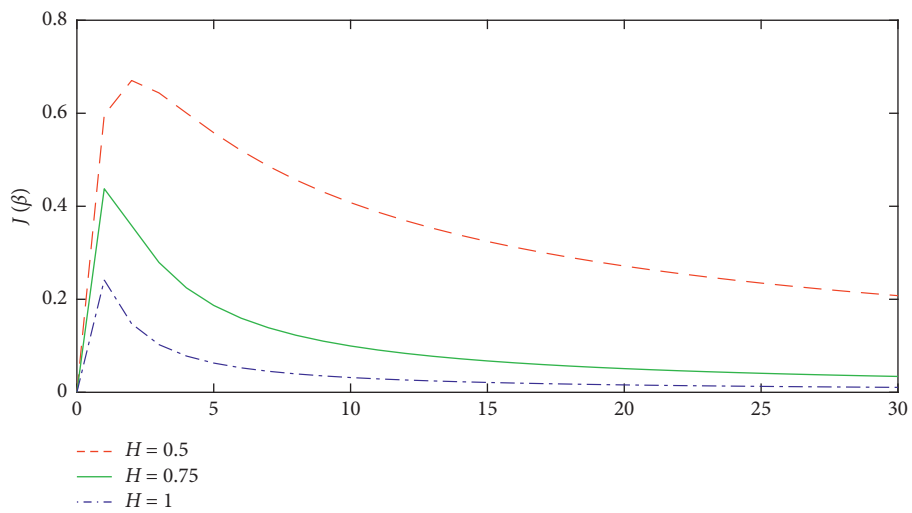

(a)

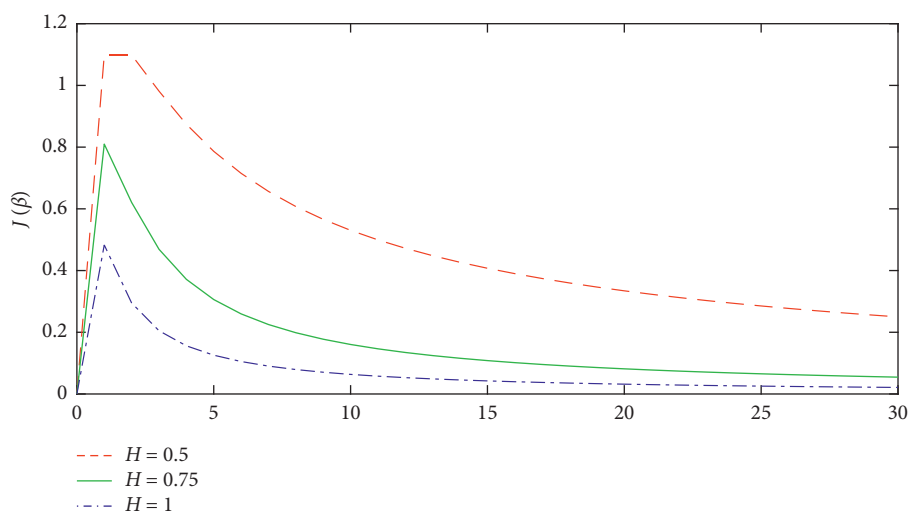

(b)

Figure 1: Hurst parameter $H = 0.5$ (top curve), Hurst parameter $H = 0.75$ (second from top), and Hurst parameter $H = 1$ (third from top). (a) Plot of the function $J(\beta)$ for 3 different values of H x-axis is β. (b) Plot of the function $J(\beta)$ for 3 different values of H x-axis is β.

exponential structure, so our exponential form of Σ_t or β_t in Theorem 2 is natural and reasonable. In fact, as in [18], when noise traders have no memories, that is, $H = (1/2)$, the optimal trading intensity and the corresponding residual information are the same as those in Theorem 2. So, Theorem 2 means that, as memories of noise traders become weaker and weaker, the optimal trading intensity and the corresponding residual information tend to those, respectively, in insider trading without any memory in [18].

Next, we will analyse the impact of memory on insider expected profit when $H \in ((1/2), 1]$. To make some conclusions about this influence in some special case, we also restrict ourselves to both insider trading intensity and the volatility of noise trades are constant numbers as in [13]; if we denote $\beta_t(H) \equiv \beta > 0$ and $\sigma_{zt} \equiv 1$, then ρ_t in (17) can be written as follows:

$$\rho_t = \frac{\mathrm{d}}{\mathrm{d}l_t} \int_0^t k_H(t,s) \frac{\beta_s}{\sigma_{zs}} \mathrm{d}s = \frac{\Gamma((3/2) - H)^2 \beta}{\Gamma(3 - 2H)}. \tag{39}$$

Hence, together with (18), we work out

$$\Sigma_t = \left(1 + \frac{\beta^2 \Gamma((3/2) - H)^3}{2H\Gamma(3 - 2H)^2 \Gamma((1/2) + H)} t^{2-2H}\right)^{-1}. \tag{40}$$

Then, by equation (12), we have

$$J^H(\beta) = \beta \int_0^\infty \exp(-\mu s)\left(1 + \frac{\beta^2 \Gamma((3/2) - H)^3}{2H\Gamma(3 - 2H)^2 \Gamma((1/2) + H)} s^{2-2H}\right)^{-1} \mathrm{d}s. \tag{41}$$

It is easy to see that

$$J^H(0) = 0,$$
$$\lim_{\beta \longrightarrow \infty} J^H(\beta) = 0, \tag{42}$$

and $J^H(\beta)$ is a continuous function of β and can attain its maximum value. Now, we choose different parameters H to show the relation between β and $J^H(\beta)$ numerically as plots. Because the trading deadline is random time τ with parameter μ, we choose $\mu = 1$ and $T = 10000$ and plot the function $J(\beta)$ for the Hurst parameters $H = 0.5, 0.75, 1$ as in Figure 1(a); to compare with the setting in [13], we also plot the function $J(\beta)$ for the Hurst parameters $H = 0.5, 0.75, 1$, as in Figure 1(b).

According to Figure 1, the expected profit in our model is always lower than that in [13]; this is because our trading deadline is random, leading to the loss of the insider's information.

6. Conclusions

In this paper, we study a model of continuous-time insider trading in which noise traders have some memories and the trading stops at a random deadline. By the filtering theorem on fractional Brownian motion in [19] and the stochastic maximum principle as in [5], the necessary condition of the insider's optimal strategy is obtained, as the equation in Theorem 1 should be satisfied by the insider's optimal strategy.

As in Theorem 2, it shows that when noise traders' memories become weaker and weaker, the optimal trading intensity and the corresponding residual information tend to those, respectively, when noise traders have any memory in [18]. And, as in Figure 1, numerical simulation shows that if both insider trading intensity and the volatility of noise trades assume two constant numbers, the expected profit with a random deadline is always lower than that when the asset value is disclosed at a finite fixed time in [13]; this is because trading time in our model is a random deadline which yields the loss of the insider's information.

Beyond that, as shown in Figure 1(a), as $H \in [1/2, 1)$ increases, both the utility value of an insider and the optimal insider trading intensity $\beta^*(H)$ decrease.

As in [13], we also think that there are two ways to reduce the complexity of the noise with increasing H: the one is that the noise process becomes long-range dependence, and the other is that the paths of the noise process become more regular, which makes market makers more easier to excavate insider's private information. And, together with trading at a random deadline, the insider's information advantage will lose more, which makes the profit more less.

Data Availability

No data were used to support this study.

Conflicts of Interest

The authors declare that they have no conflicts of interest.

Acknowledgments

This work was supported by NSF China (11861025), Guizhou QKHPTRC[2018]5769, Guizhou EDKY[2016]027, Guizhou QKZYD[2016]4006, and Guizhou ZDXK[2016]8.

References

[1] A. S. Kyle, "Continuous auctions and insider trading," *Econometrica*, vol. 53, no. 6, pp. 1315–1335, 1985.
[2] K. Back, "Insider trading in continuous time," *Review of Financial Studies*, vol. 5, no. 3, pp. 387–409, 1992.
[3] R. Caldentey and E. Stacchetti, "Insider trading with a random deadline," *Econometrica*, vol. 78, no. 1, pp. 245–283, 2010.
[4] P. Collins-Dufresne and V. Fos, "Insider trading, stochastic liquidity and equilibrium prices," *Econometrica*, vol. 84, pp. 1451–1475, 2016.
[5] K. K. Aase, T. Bjuland, and B. Øksendal, "Strategic insider trading equilibrium: a filter theory approach," *Afrika Matematika*, vol. 23, no. 2, pp. 145–162, 2012.
[6] Y. Zhou, "Existence of linear strategy equilibrium in insider trading with partial observations," *Journal of Systems Science and Complexity*, vol. 29, pp. 1–12, 2016.
[7] J. Ma, R. Sun, and Y. Zhou, "Kyle–back equilibrium models and linear conditional mean-field SDEs," *SIAM Journal on Control and Optimization*, vol. 56, no. 2, pp. 1154–1180, 2018.
[8] C. W. Holden and A. Subrahmanyam, "Long-lived private information and imperfect competition," *The Journal of Finance*, vol. 47, no. 1, pp. 247–270, 1992.
[9] K. Back and H. Pedersen, "Long-lived information and intraday pattern," *Journal of Financial Markets*, vol. 1, no. 3-4, pp. 385–402, 1998.
[10] K. H. Cho, "Continuous auctions and insider trading: uniqueness and risk aversion," *Finance and Stochastics*, vol. 7, no. 1, pp. 47–71, 2003.
[11] K. Back and S. Baruch, "Information in securities markets: kyle meets glosten and milgrom," *Econometrica*, vol. 72, no. 2, pp. 433–465, 2004.
[12] F. Gong and Y. Zhou, "Sequential fair stackelberg equilibria of linear strategies in risk-seeking insider trading," *Journal of Systems Science and Complexity*, vol. 31, no. 5, pp. 1302–1328, 2018.
[13] F. Biagini, Y. Hu, T. Meyer-Brandis, and B. Øksendal, "Insider trading equilibrium in a market with memory," *Mathematics and Financial Economics*, vol. 6, no. 3, pp. 229–247, 2012.
[14] B. Yang, X. He, and N. Huang, "Equilibrium price and optimal insider trading strategy under stochastic liquidity with long memory," *Applied Mathematics and Optimization*, vol. 1, 2020.
[15] I. Karatzas and S. Shreve, *Brownian Motion and Stochastic Calculus*, Springer-Verlag, Berlin, Germany, 1994.
[16] F. Biagini, Y. Hu, B. Øksendal, and T. Zhang, *Stochastic Calculus for Fractional Brownian Motion and Applications*, Springer, Berlin, Germany, 2008.

[17] I. Norros, E. Valkeila, and J. Virtamo, "An elementary approach to a girsanov formula and other analytical results on fractional brownian motions," *Bernoulli*, vol. 5, no. 4, pp. 571–587, 1999.

[18] K. Xiao and Y. Zhou, "Insider trading with a random deadline under partial observations: maximal principle method," *Acta Mathematicae Applicatae Sinica (English Series)*, 2021.

[19] M. Kleptsyna, A. Le Breton, and M. Roubaud, "General approach to filtering with fractional brownian noises-application to linear systems," *Stochastics and Stochastic Reports*, vol. 71, pp. 119–140, 2000.

Hindawi
Journal of Mathematics
Volume 2021, Article ID 8742330, 11 pages
https://doi.org/10.1155/2021/8742330

Research Article

An Averaging Principle for Mckean–Vlasov-Type Caputo Fractional Stochastic Differential Equations

Weifeng Wang,[1] **Lei Yan**,[2] **Junhao Hu**,[1] **and Zhongkai Guo**[1]

[1]*School of Mathematics and Statistics, South-Central University for Nationalities, Wuhan 430074, China*
[2]*School of General Quality Education, Wuchang University of Technology, Wuhan 430223, China*

Correspondence should be addressed to Zhongkai Guo; zkguo@scuec.edu.cn

Received 13 May 2021; Accepted 30 June 2021; Published 16 July 2021

Academic Editor: Lifeng Wu

In this paper, we want to establish an averaging principle for Mckean–Vlasov-type Caputo fractional stochastic differential equations with Brownian motion. Compared with the classic averaging condition for stochastic differential equation, we propose a new averaging condition and obtain the averaging convergence results for Mckean–Vlasov-type Caputo fractional stochastic differential equations.

1. Introduction

For complex systems, we usually want to locate an effective simplified model to approximate the original complex system or extract the main dynamical behavior of the original system. Based on these ideas, a lot of effective methods have been generated in dynamical systems, such as invariant manifolds, averaging principle, and homogenization principle. These effective methods have now been extended to deal with stochastic systems, such as stochastic invariant manifolds see [1, 2] and stochastic averaging principle, see [3–9].

Currently, the problem of averaging for stochastic differential equations have received a lot of attention and various types of stochastic differential equations have been studied, see [4, 6, 7, 10–12]. However, there are no relevant results of averaging principle for distribution dependent-type stochastic differential equations which we will consider in this paper.

On the contrary, the problem of averaging for stochastic fractional order differential equations have received a lot of attention in recent years, and some results [13] have been obtained under averaging condition consistence with the classic case (see [4, 5, 14]). Noting that the fractional order derivative is a nonlocal operator, therefore, the fractional order differential equation is more effective for describing certain phenomena in the real world (see [15–17]). Current research studies on stochastic fractional order differential equations mainly focused on the existence and uniqueness of the solutions, with fewer results from the dynamical system perspective.

Based on the above discussion, we shall study the averaging principle for the following Mckean–Vlasov-type Caputo fractional stochastic differential equations:

$$\begin{cases} D_t^{\alpha} X_t = f(t, X_t, \mu_t)\mathrm{d}t + g(t, X_t, \mu_t)\mathrm{d}B_t, \quad t \geq 0, \\ \mu(t) = \text{probability distribution of } X_t, \\ X_0 = x_0 \in L^2(\Omega, H), \end{cases} \tag{1}$$

where $\alpha \in (1/2, 1]$ and B_t is a scalar Brownian motion. Nonlinear terms f and g are H-valued functions defined on $R^+ \times H \times M_{\gamma^2}(H)$, and $M_{\gamma^2}(H)$ denotes a proper subset of probability measure on H. If the terms f and g do not depend on the probability distribution $\mu(t)$ of the process X at time t, such equations have been studied by [13] and other authors. If $\alpha = 1$, the equation becomes a classical Mckean–Vlasov-type stochastic differential equations which have been considered by many authors with different approaches (see [18–20]). In this paper, we just focused on $\alpha \in (1/2, 1)$, and more details can be seen in Section 2.

The paper is structured as follows. We introduce some notation and assumptions in Section 2. The existence and unique solution for distribution dependent fractional

stochastic differential equations will be discussed in Section 3. An averaging principle for the above equation is established in Section 4.

2. Preliminaries

First, we introduce some notation. Let $C(H)$ be the space of continuous functions on H. Let $\mathscr{B}(H)$ be the Borel σ-algebra of subsets of H. $M(H)$ is the space of probability measures on $\mathscr{B}(H)$ and carries the usual topology of weak convergence. (μ, ϕ) denotes $\int_H \phi(x)\mu(\mathrm{d}x)$. Let $\gamma(x) = 1 + |x|$, $\forall x \in H$, and then, define the Banach space

$$C_\rho(H) = \left\{ \phi \in C(H) \colon \|\phi\|_{C_\rho} \equiv \sup_{x\in H} \frac{|\phi(x)|}{\gamma^2(x)} + \sup_{x\neq y} \frac{|\phi(x)-\phi(y)|}{|x-y|} < \infty \right\}. \tag{2}$$

For any $p \geq 1$, let $M^s_{\gamma^p}(H)$ denote the Banach space of signed measures m on H, and $\|\mu\|_{\gamma^p} \equiv \int_H \gamma^p |m|(\mathrm{d}x) < \infty$. $|m| = m^+ + m^-$ and $m = m^+ - m^-$ are the Jordan decomposition of m. $M_{\gamma^2}(H) = M^s_{\gamma^p}(H) \cap M(H)$ is the set of probability measures on $\mathscr{B}(H)$, and there exists second moments. Define the following metric:

$$\rho(\mu,\nu) = \sup\left\{ (\phi, \mu-\nu) \colon \|\phi\|_\rho = \sup_{x\in H} \frac{|\phi(x)|}{\gamma^2(x)} + \sup_{x\neq y} \frac{|\phi(x)-\phi(y)|}{|x-y|} \leq 1 \right\}. \tag{3}$$

Then, $(M_{\gamma^2}(H), \rho)$ is a complete metric space. Let $C([0,T], (M_{\gamma^2}(H), \rho))$ be the complete metric space of continuous functions from $[0,T]$ to $(M_{\gamma^2}(H), \rho)$ with the following metric:

$$D_T(\mu,\nu) = \sup_{t\in[0,T]} \rho(\mu(t), \nu(t)), \quad \text{for } \nu, \mu \in C\left([0,T], M_{\gamma^2}(H), \rho\right). \tag{4}$$

More details can be seen in [18].

In order to obtain the existence and uniqueness of the solution of (1), we introduce the following conditions.

(i) H1 (Lipschitz condition): for all $x, y \in H$ and $t \in [0,T]$, $\mu \in C([0,T], M_{\gamma^2}(H), \rho)$, and there exists a bounded function $k_1(t) > 0$, such that

$$\begin{aligned} &|f(t,x,\mu) - f(t,y,\nu)|^2 + |g(t,x,\mu) - g(t,y,\nu)|^2 \\ &\quad \leq k_1(t)\left(|x-y|^2 + \rho^2(\mu,\nu)\right). \end{aligned} \tag{5}$$

(ii) H2 (growth condition): for all $(x,t) \in H \times [0,T]$, there exists a bounded function $k_2(t) > 0$ such that

$$|f(t,x,\mu)|^2 + |g(t,x,\mu)|^2 \leq k_2(t)\left(1 + |x|^2\right). \tag{6}$$

In this paper, we assume there existence of a constant k such that $\max\{k_1(t), k_2(t)\} \leq k$.

First, we give an important lemma, which is a type of promotion form of Gronwall's inequality with singular kernels.

Lemma 1 (see [21, 22]). *Suppose $b \geq 0$, $\beta > 0$, and $a(t)$ is a nonnegative function locally integrable on $0 \leq t < T$ (some $T \leq +\infty$), and suppose $u(t)$ is nonnegative and locally integrable on $0 \leq t < T$ with*

$$u(t) \leq a(t) + b\int_0^t (t-s)^{\beta-1} u(s)\mathrm{d}s, \tag{7}$$

on this interval. Then,

$$u(t) \leq a(t) + \int_0^t \left[\sum_{n=1}^{\infty} \frac{(b\Gamma(\beta))^n}{\Gamma(n\beta)} (t-s)^{n\beta-1} a(s)\right]\mathrm{d}s, \quad 0 \leq t < T. \tag{8}$$

3. Existence and Uniqueness

Consider the integral form of equation (1):

$$\begin{aligned} X_t = x_0 &+ \frac{1}{\Gamma(\alpha)} \int_0^t (t-s)^{\alpha-1} f(s, X_s, \mu_t)\mathrm{d}s \\ &+ \frac{1}{\Gamma(\alpha)} \int_0^t (t-s)^{\alpha-1} g(t, X_s, \mu_t)\mathrm{d}B_t. \end{aligned} \tag{9}$$

Under the assumptions of H1 and H2, we will prove the existence and uniqueness of solution for the above equation.

Definition 1. An $\mathscr{F}_t$-adapted stochastic process X_t with law $L(X_t) = \mu(t)$ is called a solution of (1) if X_t is continuous, and for $\forall t \in [0,T]$ with $X_0 = x_0$,

$$\begin{aligned} X_t = x_0 &+ \frac{1}{\Gamma(\alpha)} \int_0^t (t-s)^{\alpha-1} f(s, X_s, \mu_t)\mathrm{d}s \\ &+ \frac{1}{\Gamma(\alpha)} \int_0^t (t-s)^{\alpha-1} g(t, X_s, \mu_t)\mathrm{d}B_t, \mathbb{P}-a.s. \end{aligned} \tag{10}$$

Theorem 1. *Assume that H1 and H2 hold; then, for $\forall x_0 \in L^2(\Omega, H)$, equation (10) has a unique solution*

$X_t \in C([0,T]; L^2(\Omega, H))$ *with the associate probability distribution* $\mu_t = L(X_t)$, $t \in [0,T]$ *belonging to* $C([0,T], (M_\gamma^2(X), \rho))$, *such that*

$$\sup_{0\le t\le T} E\left|X_t\right|^2 < \infty. \tag{11}$$

We will proof the theorem by several steps.

(i) First, we prove that $X_t \in L^\infty([0,T], L^2(\Omega; H))$ for $\forall \mu \in C([0,T], (M_{\gamma^2}(H), \rho))$. Using the following inequality,

$$|a+b+c|^2 \le 3\left(|a|^2 + |b|^2 + |c|^2\right). \tag{12}$$

We see that

$$\begin{aligned} E|X(t)|^2 &\le 3E\left|x_0\right|^2 + 3E\left|\frac{1}{\Gamma(\alpha)}\int_0^t (t-s)^{\alpha-1} f(s, X_s, \mu_s)\mathrm{d}s\right|^2 \\ &\quad + 3E\left|\frac{1}{\Gamma(\alpha)}\int_0^t (t-s)^{\alpha-1} g(t, X_s, \mu_s)\mathrm{d}B_t\right|^2 \\ &:= 3I_1 + 3I_2 + 3I_3. \end{aligned} \tag{13}$$

For I_2, applying Cauchy–Schwarz's inequality and H2, it follows

$$\begin{aligned} I_2 &\le \frac{Tk}{\Gamma(\alpha)^2}\int_0^t (t-s)^{2\alpha-2}\left(1 + E|X(s)|^2 + \left\|\mu_t\right\|_\gamma^2\right)\mathrm{d}s \\ &\le \frac{Tk}{\Gamma(\alpha)^2}\left[\frac{t^{2\alpha-1}}{2\alpha-1}\left(1 + \sup_{0\le t\le T}\left\|\mu_t\right\|_\gamma^2\right) + \int_0^t (t-s)^{2\alpha-2} E|X(s)|^2\mathrm{d}s\right] \\ &\le \frac{kT^{2\alpha}}{\Gamma(\alpha)^2(2\alpha-1)}\left(1 + \sup_{0\le t\le T}\left\|\mu_t\right\|_\gamma^2\right) + \frac{Tk}{\Gamma(\alpha)^2}\int_0^t (t-s)^{2\alpha-2} E|X(s)|^2\mathrm{d}s. \end{aligned} \tag{14}$$

For I_3, by It $\widehat{o}$'s isometry formula and H2, we have

$$\begin{aligned} I_3 &\le \frac{k}{\Gamma(\alpha)^2}\int_0^t (t-s)^{2\alpha-2}\left(1 + E|X(s)|^2 + \left\|\mu_t\right\|_\gamma^2\right)\mathrm{d}s \\ &\le \frac{kT^{2\alpha-1}}{\Gamma(\alpha)^2(2\alpha-1)}\left(1 + \sup_{0\le t\le T}\left\|\mu_t\right\|_\gamma^2\right) \\ &\quad + \frac{k}{\Gamma(\alpha)^2}\int_0^t (t-s)^{2\alpha-2} E|X(s)|^2\mathrm{d}s. \end{aligned} \tag{15}$$

Combining the above estimate results, we finally obtain

$$E|X(t)|^2 \le r_1 + r_2\int_0^t (t-s)^{(2\alpha-1)-1} E|X(s)|^2\mathrm{d}s, \tag{16}$$

where

$$\begin{aligned} r_1 &:= 3E\left|x_0\right|^2 + 3\frac{\left(kT^{2\alpha-1}\right)(T+1)}{\Gamma(\alpha)^2(2\alpha-1)}\left(1 + \sup_{0\le t\le T}\left|\mu_t\right|_\gamma^2\right), \\ r_2 &:= 3\frac{k(T+1)}{\Gamma(\alpha)^2}. \end{aligned} \tag{17}$$

With the help of Lemma 1, it follows

$$\begin{aligned} E|X(t)|^2 &\le r_1\left(1 + \int_0^t \sum_{n=1}^\infty \frac{\left(r_2\Gamma(2\alpha-1)\right)^n}{\Gamma((2\alpha-1)n)}(t-s)^{(2\alpha-1)n-1}\mathrm{d}s\right) \\ &\le r_1\left(1 + \sum_{n=1}^\infty \frac{\left(r_2\Gamma(2\alpha-1)T^{2\alpha-1}\right)^n}{\Gamma((2\alpha-1)n+1)}\right) \\ &= r_1\left(1 + E_{2\alpha-1,1}\left(r_2\Gamma(2\alpha-1)T^{2\alpha-1}\right)\right) < \infty, \end{aligned} \tag{18}$$

for $\forall t \in [0,T]$, and $E_{2\alpha-1,1}(\cdot)$ is a two-parameter function of the Mittag-Leffler type [21].

Then,

$$\sup_{0\le t\le T} E|X(t)|^2 < \infty, \tag{19}$$

and $X_t \in L^\infty([0,T], L^2(\Omega; H))$.

(ii) Now, we show that $X_t \in C([0,T], L^2(\Omega; H))$ for $\forall \mu \in C([0,T], (M_{\gamma^2}(H), \rho))$:

$$\begin{aligned} E\left\|X_t - X_{t_0}\right\|^2 &\le 2E\frac{1}{\Gamma(\alpha)^2}\left\|\int_0^t (t-s)^{\alpha-1} f(s, X_s, \mu_s)\mathrm{d}s - \int_0^{t_0} (t_0-s)^{\alpha-1} f(s, X_s, \mu_s)\mathrm{d}s\right\|^2 \\ &\quad + 2E\frac{1}{\Gamma(\alpha)^2}\left\|\int_0^t (t-s)^{\alpha-1} f(s, X_s, \mu_s)\mathrm{d}B_s - \int_0^{t_0} (t_0-s)^{\alpha-1} f(s, X_s, \mu_s)\mathrm{d}B_s\right\|^2 \\ &=: 2(J_1 + J_2). \end{aligned} \tag{20}$$

For J_1, we have

$$\begin{aligned} J_1 &\le 2E\frac{1}{\Gamma(\alpha)^2}\left\|\int_{t_0}^t (t-s)^{\alpha-1} f(s, X_s, \mu_s)\mathrm{d}s\right\|^2 \\ &\quad + 2E\frac{1}{\Gamma(\alpha)^2}\left\|\int_0^{t_0}\left((t-s)^{\alpha-1} - (t_0-s)^{\alpha-1}\right) f(s, X_s, \mu_s)\mathrm{d}s\right\|^2 =: 2J_{11} + 2J_{12}. \end{aligned} \tag{21}$$

By the Cauchy–Schwartz inequality,

$$\begin{aligned} J_{11} &\le \frac{1}{\Gamma(\alpha)^2} k \int_{t_0}^t (t-s)^{2\alpha-2}\mathrm{d}s \int_{t_0}^t E\left|f(s, X_s, \mu_s)\right|^2 \mathrm{d}s \\ &\le \frac{k}{\Gamma(\alpha)^2(2\alpha-1)}(t-t_0)^{2\alpha-1}\int_{t_0}^t \left(1 + E\left|X_s\right|^2 + \left\|\mu_s\right\|^2\right)\mathrm{d}s \\ &\le \frac{Ck}{\Gamma(\alpha)^2(2\alpha-1)}(t-t_0)^{2\alpha}. \end{aligned} \tag{22}$$

For J_{12}, we have

$$\begin{aligned} J_{12} &= E\frac{1}{\Gamma(\alpha)^2}\left|\int_0^{t_0}\left((t-s)^{\alpha-1} - (t_0-s)^{\alpha-1}\right) f(s, X_s, \mu_s)\mathrm{d}s\right|^2 \\ &\le \frac{k}{\Gamma(\alpha)^2}\int_0^{t_0}\left((t-s)^{\alpha-1} - (t_0-s)^{\alpha-1}\right)^2\mathrm{d}s \int_0^{t_0}\left(1 + E\left|X_s\right|^2 + \left\|\mu_s\right\|^2\right)\mathrm{d}s \\ &\le \frac{CTk}{\Gamma(\alpha)^2}\int_0^{t_0}\left((t_0-s)^{2(\alpha-1)} - (t-s)^{2(\alpha-1)}\right)\mathrm{d}s \\ &\le \frac{CTk}{\Gamma(\alpha)^2}\left[\frac{(t-t_0)^{2\alpha-1}}{2\alpha-1} + \frac{t_0^{2\alpha-1}}{2\alpha-1} - \frac{t^{2\alpha-1}}{2\alpha-1}\right] \le \frac{CTk}{\Gamma(\alpha)^2}\frac{(t-t_0)^{2\alpha-1}}{2\alpha-1}. \end{aligned} \tag{23}$$

For J_2, using the It $\hat{o}$ isometry formula, in the similar way as J_1, we can prove that

$$J_2 \le \frac{Ck}{\Gamma(\alpha)^2}\frac{(t-t_0)^{2\alpha-1}}{2\alpha-1}. \tag{24}$$

Results of J_1 and J_2 combined together show that

$$\begin{aligned} E\left\|X_t - X_{t_0}\right\|^2 &\le \frac{Ck(1+T)}{\Gamma(\alpha)^2}\frac{(t-t_0)^{2\alpha-1}}{2\alpha-1} \\ &\quad + \frac{Ck}{\Gamma(\alpha)^2(2\alpha-1)}(t-t_0)^{2\alpha}, \end{aligned} \tag{25}$$

which implied $X_t \in C([0,T], L^2(\Omega; H))$ for each fixed $\mu \in C([0,T], (M_{\gamma^2}, \rho))$.

(iii) By virtue of the fixed point theorem for contraction mappings, we can show that, for each fixed $\mu \in C([0,T], (M_{\gamma^2}, \rho))$, equation (10) has a unique solution in $C([0,T], L^2(\Omega; H))$. Similar arguments are also discussed in [18]. Now, we define an operator $\Phi_\mu(\cdot)$ on $C([0,T], L^2(\Omega; H))$:

$$\left(\Phi_\mu X\right)(t) = x_0 + \frac{1}{\Gamma(\alpha)} \int_0^t (t-s)^{\alpha-1} f(s, X_s, \mu_s) \mathrm{d}s + \frac{1}{\Gamma(\alpha)} \int_0^t (t-s)^{\alpha-1} g(t, X_s, \mu_s) \mathrm{d}B_t. \tag{26}$$

It is easy to verify that Φ_μ is from $C([0,T], L^2(\Omega; H))$ into itself.

For $X_t, Y_t \in C([0,T], L^2(\Omega; H))$ with $x_0 = y_0$, let $|\cdot|_\zeta$ denote the norm of $C([0,T], L^2(\Omega; H))$ and $\beta = 2\alpha - 1 > 0$; then, we obtain

$$\begin{aligned} &\left|\left(\Phi_\mu X\right)(t) - \left(\Phi_\mu Y\right)(t)\right|_\varsigma^2 \\ &\quad \le 2\left|\frac{1}{\Gamma(\alpha)} \int_0^t (t-s)^{\alpha-1} \left(f(s, X_s, \mu_s) - f(s, Y_s, \mu_s)\right) \mathrm{d}s\right|_\varsigma^2 \\ &\quad + 2\left|\frac{1}{\Gamma(\alpha)} \int_0^t (t-s)^{\alpha-1} \left(g(t, X_s, \mu_s) - g(t, Y_s, \mu_s)\right) \mathrm{d}B_t\right|_\varsigma^2. \end{aligned} \tag{27}$$

Using the Cauchy–Schwartz inequality and It $\hat{o}$ isometry formula, it is readily seen that

$$\begin{aligned} &\left|\left(\Phi_\mu X\right)(t) - \left(\Phi_\mu Y\right)(t)\right|_\varsigma^2 \\ &\quad \le \frac{2Tk + 2k}{\Gamma(\alpha)^2} \int_0^t (t-s)^{\beta-1} \left|X_s - Y_s\right|_\varsigma^2 \mathrm{d}s. \end{aligned} \tag{28}$$

Our goal is now to prove the following inequality:

$$\begin{aligned} &\left|\left(\Phi_\mu^n X\right)(t) - \left(\Phi_\mu^n X\right)(t)\right|_\varsigma^2 \\ &\quad \le \frac{1}{\beta} \left(\frac{2Tk + 2k}{\Gamma(\alpha)^2}\right)^n \frac{\Gamma(\beta)^n}{\Gamma(n\beta)} t^{n\beta} \left|X_t - Y_t\right|_\varsigma^2. \end{aligned} \tag{29}$$

The proof is based on mathematical induction over n. For $n = 1$,

$$\begin{aligned} &\left|\left(\Phi_\mu X\right)(t) - \left(\Phi_\mu Y\right)(t)\right|_\varsigma^2 \\ &\quad \le \frac{2Tk + 2k}{\Gamma(\alpha)^2} \left|X_t - Y_t\right|_\varsigma^2 \frac{t^\beta}{\beta}, \end{aligned} \tag{30}$$

which is fulfilled.

For the induction step from $n = l$ to $n = l + 1$, we assume that, for $n = l$, equation (29) is satisfied; then,

$$\begin{aligned} &\left|\left(\Phi_\mu^{l+1} X\right)(t) - \left(\Phi_\mu^{l+1} Y\right)(t)\right|_\varsigma^2 \\ &\quad \le \frac{2Tk + 2k}{\Gamma(\alpha)^2} \int_0^t (t-s)^{\beta-1} \left|\left(\Phi_\mu^l X\right)(s) - \left(\Phi_\mu^l Y\right)(s)\right|_\varsigma^2 \mathrm{d}s \\ &\quad \le \frac{2Tk + 2k}{\Gamma(\alpha)^2} \int_0^t (t-s)^{\beta-1} \frac{1}{\beta} \left(\frac{2Tk + 2k}{\Gamma(\alpha)^2}\right)^l \frac{\Gamma(\beta)^l}{\Gamma(k\beta)} s^{l\beta} \left|X_s - Y_s\right|_\varsigma^2 \mathrm{d}s \\ &\quad \le \left(\frac{2Tk + 2k}{\Gamma(\alpha)^2}\right)^{l+1} \frac{1}{\beta} \frac{\Gamma(\beta)^k}{\Gamma(l\beta)} \left|X_t - Y_t\right|_\varsigma^2 \int_0^t (t-s)^{\beta-1} s^{l\beta} \mathrm{d}s. \end{aligned} \tag{31}$$

Thus, we only need to discuss the following integral:

$$\int_0^t (t-s)^{\beta-1} s^{l\beta} \mathrm{d}s. \tag{32}$$

Let $s = tz$; then,

$$\begin{aligned} \int_0^t (t-s)^{\beta-1} s^{l\beta} \mathrm{d}s &= \int_0^1 (1-z)^{\beta-1} t^{\beta-1} t^{l\beta} z^{l\beta} t \mathrm{d}z \\ &= t^{(l+1)\beta} \int_0^1 (1-z)^{\beta-1} z^{l\beta} \mathrm{d}z \\ &= t^{(l+1)\beta} B(l\beta + 1, \beta) = t^{(l+1)\beta} \frac{\Gamma(\beta)\Gamma(l\beta + 1)}{\Gamma((l+1)\beta + 1)}, \end{aligned} \tag{33}$$

where $B(\cdot, \cdot)$ is the Beta function. Substitute the above equality into (31), and we derive that

$$\begin{aligned}
&\left|\left(\Phi_\mu^{l+1}X\right)(t)-\left(\Phi_\mu^{l+1}Y\right)(t)\right|_\varsigma^2\\
&\le\left(\frac{2Tk+2k}{\Gamma^2(\alpha)}\right)^{l+1}\frac{1}{\beta}\frac{\Gamma(\beta)^l}{\Gamma(l\beta)}\left|X_t-Y_t\right|_\varsigma^2 t^{(l+1)\beta}\frac{\Gamma(\beta)\Gamma(l\beta+1)}{\Gamma((l+1)\beta+1)}\\
&=\left(\frac{2Tk+2k}{\Gamma^2(\alpha)}\right)^{l+1}\frac{1}{\beta}\Gamma(\beta)^{l+1}\frac{\Gamma(l\beta+1)}{\Gamma((l+1)\beta+1)\Gamma(l\beta)}t^{(l+1)\beta}\left|X_t-Y_t\right|_\varsigma^2\\
&=\left(\frac{2Tk+2k}{\Gamma^2(\alpha)}\right)^{l+1}\frac{1}{\beta}\Gamma(\beta)^{l+1}\frac{l\beta\Gamma(l\beta)}{(l+1)\beta\Gamma((l+1)\beta)\Gamma(l\beta)}t^{(l+1)\beta}\left|X_t-Y_t\right|_\varsigma^2\\
&\le\left(\frac{2Tk+2k}{\Gamma^2(\alpha)}\right)^{l+1}\frac{1}{\beta}\Gamma(\beta)^{l+1}\frac{t^{(l+1)\beta}}{\Gamma((l+1)\beta)}\left|X_t-Y_t\right|_\varsigma^2.
\end{aligned}\tag{34}$$

By the above discussion, we finally obtain

$$\begin{aligned}
&\left|\left(\Phi_\mu^{n}X\right)(t)-\left(\Phi_\mu^{n}Y\right)(t)\right|_\varsigma^2\\
&\le\left(\frac{2Tk+2k}{\Gamma^2(\alpha)}\right)^{n}\frac{1}{\beta}\Gamma(\beta)^{n}\frac{T^{n\beta}}{\Gamma(n\beta)}\left|X_t-Y_t\right|_\varsigma^2.
\end{aligned}\tag{35}$$

Note that $(Tk+k/\Gamma(\alpha))^n(1/\beta)\Gamma(\beta)^n(T^{n\beta}/\ \Gamma(n\beta)) \longrightarrow 0$ as $n\longrightarrow+\infty$. Then, we have $(Tk+k/\Gamma(\alpha))^n(1/\beta)\Gamma(\beta)^n(T^{n\beta}/\Gamma(n\beta))<1$ for any sufficiently large n. And, this shows that $\Phi_\mu(\cdot)$ is a contraction map on $C([0,T],L^2(\Omega;H))$. So, it has a unique fixed point for $\mu\in C([0,T],(M_{\gamma^2}(H),\rho))$.

(iv) $L(X_\mu)=\left\{L(X_\mu(t)):t\in[0,T]\right\}$ is the probability law of X_μ. Now, we prove that $L(X_\mu)\in C([0,T],(M_{\gamma^2},\rho))$. Notice that $X_\mu\in C\ ([0,T],L^2(\Omega;H)), L(X_\mu)\in M_{\gamma^2}(H)$ for $\forall t\in[0,T]$. So, we only need to prove $t\longrightarrow L(X_\mu(t))$ is continuous.

In step (ii), we have

$$E\left|X_\mu(t)-X_\mu(s)\right|^2\longrightarrow 0,\tag{36}$$

as $t\longrightarrow s$.

By the definition of ρ, we have

$$\begin{aligned}
&\left|\left(\phi,L\left(X_\mu(t)\right)-L\left(X_\mu(s)\right)\right)\right|=E\left|\phi\left(X_\mu(t)\right)-\phi\left(X_\mu(s)\right)\right|\\
&\le\|\phi\|_\rho E\left|X_\mu(t)-X_\mu(s)\right|\le\|\phi\|_\rho\left(E\left|X_\mu(t)-X_\mu(s)\right|^2\right)^{1/2},
\end{aligned}\tag{37}$$

which implies

$$\lim_{t\longrightarrow s}\rho\left(L\left(X_\mu(t)\right),L\left(X_\mu(s)\right)\right)=0.\tag{38}$$

Hence, we verify that $L(X_\mu)\in C([0,T],(M_{\gamma^2},\rho))$.

(v) Define Ψ on $C([0,T],(M_{\gamma^2},\rho))$ as follows:

$$\Psi:\mu\longrightarrow L\left(X_\mu\right).\tag{39}$$

In the following, we will show that the operator Ψ has a unique fixed point in $C([0,T],(M_{\gamma^2},\rho))$. Take $\mu,\nu\in C([0,T],(M_{\gamma^2},\rho))$, and let $X_\mu(t)$ and $X_\nu(t)$ be the corresponding solutions of the following equations:

$$\begin{aligned}
X_\mu(t)&=x_0+\frac{1}{\Gamma(\alpha)}\int_0^t(t-s)^{\alpha-1}f(s,X_s,\mu_s)\mathrm{d}s\\
&\quad+\frac{1}{\Gamma(\alpha)}\int_0^t(t-s)^{\alpha-1}g(t,X_s,\mu_s)\mathrm{d}B_t,\\
X_\nu(t)&=x_0+\frac{1}{\Gamma(\alpha)}\int_0^t(t-s)^{\alpha-1}f(s,X_s,\nu_s)\mathrm{d}s\\
&\quad+\frac{1}{\Gamma(\alpha)}\int_0^t(t-s)^{\alpha-1}g(t,X_s,\nu_s)\mathrm{d}B_t.
\end{aligned}\tag{40}$$

Thus,

$$\begin{aligned} E\left|X_\mu(t)-X_\nu(t)\right|^2 &\le \frac{2T}{\Gamma(\alpha)^2}E\int_0^t (t-s)^{2\alpha-2}\left|f\left(s,X_\mu(s),\mu_s\right)-f\left(s,X_\nu(s),\nu_s\right)\right|^2 \mathrm{d}s \\ &\quad + \frac{2}{\Gamma(\alpha)^2}E\int_0^t (t-s)^{2\alpha-2}\left|g\left(s,X_\mu(s),\mu_s\right)-g\left(s,X_\nu(s),\nu_s\right)\right|^2 \mathrm{d}s \\ &\le \frac{2kT}{\Gamma(\alpha)^2}E\int_0^t (t-s)^{2\alpha-2}\left[\left|X_\mu(s)-X_\nu(s)\right|^2+\rho^2\left(\mu_s,\nu_s\right)\right]\mathrm{d}s \\ &\quad + \frac{2k}{\Gamma(\alpha)^2}E\int_0^t (t-s)^{2\alpha-2}\left[\left|X_\mu(s)-X_\nu(s)\right|^2+\rho^2\left(\mu_s,\nu_s\right)\right]\mathrm{d}s. \end{aligned} \tag{41}$$

After simple calculation, we have that

$$\sup_{0\le t\le T} E\left|X_\mu(t)-X_\nu(t)\right|^2 \le \frac{2k(T+1)}{\Gamma(\alpha)^2}\frac{T^{2\alpha-1}}{2\alpha-1}\left[\sup_{0\le t\le T} E\left|X_\mu(t)-X_\nu(t)\right|^2+D_T^2(\mu,\nu)\right]. \tag{42}$$

Select the appropriate $T=T_0>0$, such that

$$\frac{2k(T_0+1)}{\Gamma(\alpha)^2}\frac{T_0^{2\alpha-1}}{2\alpha-1}<\frac{1}{3}. \tag{43}$$

Then, it follows

$$sup_{\ 0\le t\le T_0} E\left|X_\mu(t)-X_\nu(t)\right|^2<\frac{1}{2}D_{T_0}^2(\mu,\nu). \tag{44}$$

By the definition of $\rho(\mu,\nu)$ and $D_T^2(\mu,\nu)$, we can obtain

$$\rho^2(\mu,\nu)\le E\left|X_\mu(t)-X_\nu(t)\right|^2. \tag{45}$$

Taking sup-norm on both sides, we obtain

$$D_T^2(\Psi(\mu),\Psi(\nu))\le \sup_{0\le t\le T_0} E\left|X_\mu(t)-X_\nu(t)\right|^2. \tag{46}$$

Combine this result with equation (44), and we finally derive

$$D_{T_0}^2(\Psi(\mu),\Psi(\nu))<\frac{1}{2}D_{T_0}^2(\mu,\nu). \tag{47}$$

Since Ψ is a contraction in $C([0,T_0],(M_{\gamma^2}(H),\rho))$, it has a unique fixed point. Thus, equation (10) has a unique solution X_t with $\mu=L(X_t)$ on $[0,T_0]$. Because X_t belongs to $C([0,T],L^2(\Omega;H))$, we can extend the solution to $[0,T]$ by considering $[0,T_0]$, $[T_0,2T_0]$, and so on. This completes the proof.

4. An Averaging Principle

In this section, we study an averaging principle for the following distribution dependent fractional stochastic differential equations in H:

$$\begin{aligned} X_\epsilon(t) &= x_0+\frac{\epsilon}{\Gamma(\alpha)}\int_0^t (t-s)^{\alpha-1}f\left(s,X_\epsilon(s),\mu_\epsilon(s)\right)\mathrm{d}s \\ &\quad + \frac{\sqrt{\epsilon}}{\Gamma(\alpha)}\int_0^t (t-s)^{\alpha-1}g\left(s,X_\epsilon(s),\mu_\epsilon(s)\right)\mathrm{d}B_t, \end{aligned} \tag{48}$$

where $x_0\in L^2(\Omega;H)$. We will show that the solution of (48) will be approximated by the following simpler or averaged process under certain conditions:

$$\begin{aligned} Z_\epsilon(t) &= x_0+\frac{\epsilon}{\Gamma(\alpha)}\int_0^t (t-s)^{\alpha-1}\overline{f}\left(Z_\epsilon(s),\nu_\epsilon(s)\right)\mathrm{d}s \\ &\quad + \frac{\sqrt{\epsilon}}{\Gamma(\alpha)}\int_0^t (t-s)^{\alpha-1}\overline{g}\left(Z_\epsilon(s),\nu_\epsilon(s)\right)\mathrm{d}B_t. \end{aligned} \tag{49}$$

Equation (49) is called the averaged equation for (48). Now, we prove that the solution of (49) converges to the solution of the original equation (48) under the following additional conditions.

H3:

$$\begin{aligned} &\frac{1}{t^{2\alpha-1}}\int_0^t (t-s)^{2(\alpha-1)}\left|f(s,x,\mu)-\overline{f}(x,\mu)\right|^2\mathrm{d}s \\ &\quad \le \varphi_1(t)\left(1+|x|^2+\|\mu\|^2\right). \end{aligned} \tag{50}$$

H4:

$$\begin{aligned} &\frac{1}{t^{2\alpha-1}}\int_0^t (t-s)^{2(\alpha-1)}\left|g(s,x,\mu)-\overline{g}(x,\mu)^2\right|\mathrm{d}s \\ &\quad \le \varphi_2(t)\left(1+|x|^2+\|\mu\|^2\right), \end{aligned} \tag{51}$$

where $\varphi_i(t)$ are positive and bounded with $\lim_{t\longrightarrow+\infty}\varphi_i(t)=0$ for $i=1,2$.

Remark 1. Note that when we take $\alpha=1$, then this condition is consistence with the classic case, see [4].

Theorem 2. *Let $H1-H4$ hold. Then, for $\forall\delta_1>0$, there exist constants $L>0$, $\epsilon_1\in(0,\epsilon_0]$ and $\beta\in(0,1)$ such that, for any $\epsilon\in(0,\epsilon_1]$, $1/2<\alpha<1$, we have*

$$\sup_{0\le t\le L\epsilon^{(-\beta/2\alpha-1)}} E\left|X_\varepsilon(t)-Z_\varepsilon(t)\right|^2\le\delta_1. \tag{52}$$

Let us consider

$$\begin{aligned}X_\epsilon(t)-Z_\epsilon(t)=&\frac{\epsilon}{\Gamma(\alpha)}\int_0^t(t-s)^{\alpha-1}\left[f\left(s,X_\epsilon(s),\mu_\epsilon(s)\right)-\overline{f}\left(Z_\epsilon(s),\nu_\epsilon(s)\right)\right]\mathrm{d}s\\&+\frac{\sqrt{\epsilon}}{\Gamma(\alpha)}\int_0^t(t-s)^{\alpha-1}\left[g\left(s,X_\epsilon(s),\mu_\epsilon(s)\right)-\overline{g}\left(Z_\epsilon(s),\nu_\epsilon(s)\right)\right]\mathrm{d}B_t.\end{aligned} \tag{53}$$

By the arithmetic inequality, it follows that

$$\begin{aligned}&E\left|X_\epsilon(t)-Z_\epsilon(t)\right|^2\le\\&2\left\{\begin{array}{l}E\left|\frac{\epsilon}{\Gamma(\alpha)}\int_0^t(t-s)^{\alpha-1}\left[f\left(s,X_\epsilon(s),\mu_\epsilon(s)\right)-\overline{f}\left(Z_\epsilon(s),\nu_\epsilon(s)\right)\right]\mathrm{d}s\right|^2\\+E\left|\frac{\sqrt{\epsilon}}{\Gamma(\alpha)}\int_0^t(t-s)^{\alpha-1}\left[g\left(s,X_\epsilon(s),\mu_\epsilon(s)\right)-\overline{g}\left(Z_\epsilon(s),\nu_\epsilon(s)\right)\right]\mathrm{d}B_t\right|^2\end{array}\right\}\\&=:2\left(Q_1+Q_2\right).\end{aligned} \tag{54}$$

For Q_1, we have

$$\begin{aligned}Q_1=&E\left|\frac{\epsilon}{\Gamma(\alpha)}\int_0^t(t-s)^{\alpha-1}\left[f\left(s,X_\epsilon(s),\mu_\epsilon(s)\right)-\overline{f}\left(Z_\epsilon(s),\nu_\epsilon(s)\right)\right]\mathrm{d}s\right|^2\\\le&\frac{2\epsilon^2}{\Gamma(\alpha)^2}\left\{\begin{array}{l}E\left|\int_0^t(t-s)^{\alpha-1}\left[f\left(s,X_\epsilon(s),\mu_\epsilon(s)\right)-f\left(s,Z_\epsilon(s),\nu_\epsilon(s)\right)\right]\mathrm{d}s\right|^2\\+E\left|\int_0^t(t-s)^{\alpha-1}\left[f\left(s,Z_\epsilon(s),\nu_\epsilon(s)\right)-\overline{f}\left(Z_\epsilon(s),\nu_\epsilon(s)\right)\right]\mathrm{d}s\right|^2\end{array}\right\}.\end{aligned} \tag{55}$$

Applying the Cauchy–Schwarz inequality, H1, H3, and the definition of the metric ρ, we obtain

$$\begin{aligned} Q_1 \leq & \frac{2tk\epsilon^2}{\Gamma(\alpha)^2}\int_0^t (t-s)^{2\alpha-2}E\left[\left|X_\epsilon(s)-Z_\epsilon(s)\right|^2+\rho^2\left(\mu_\epsilon(s),\nu_\epsilon(s)\right)\right]\mathrm{d}s \\ & +\frac{2\epsilon^2}{\Gamma(\alpha)^2}t^{2\alpha}\left\{\begin{array}{c} \frac{1}{t^{2\alpha-1}}E\int_0^t (t-s)^{2\alpha-2}\left|f\left(s,Z_\epsilon(s),\nu_\epsilon(s)\right)-\overline{f}\left(Z_\epsilon(s),\nu_\epsilon(s)\right)\right|^2\mathrm{d}s \\ \leq \frac{4tk\epsilon^2}{\Gamma(\alpha)^2}\int_0^t (t-s)^{2\alpha-2}E\left|X_\epsilon(s)-Z_\epsilon(s)\right|^2\mathrm{d}s \\ +\frac{2\epsilon^2}{\Gamma(\alpha)^2}t^{2\alpha}\varphi_1(t)\left(1+E\left|Z_\epsilon(s)\right|^2+\left\|\nu_\epsilon(s)\right\|\right)^2 \end{array}\right\}. \end{aligned} \tag{56}$$

For Q_2, using the Itô isometry formula, we obtain

$$\begin{aligned} Q_2 = & \frac{\epsilon}{\Gamma(\alpha)^2}\int_0^t (t-s)^{2\alpha-2}E\left|g\left(s,X_\epsilon(s),\mu_\epsilon(s)\right)-\overline{g}\left(Z_\epsilon(s),\nu_\epsilon(s)\right)\right|^2\mathrm{d}s \\ \leq & \frac{2\epsilon}{\Gamma(\alpha)^2}\left\{\begin{array}{c} \int_0^t (t-s)^{2\alpha-2}E\left|g\left(s,X_\epsilon(s),\mu_\epsilon(s)\right)-g\left(Z_\epsilon(s),\nu_\epsilon(s)\right)\right|^2\mathrm{d}s \\ +\int_0^t (t-s)^{2\alpha-2}E\left|g\left(Z_\epsilon(s),\nu_\epsilon(s)\right)-\overline{g}\left(Z_\epsilon(s),\nu_\epsilon(s)\right)\right|^2\mathrm{d}s \end{array}\right\}. \end{aligned} \tag{57}$$

Applying conditions H1 and H4, we derive

$$\begin{aligned} Q_2 \leq & \frac{2k\epsilon}{\Gamma(\alpha)^2}\left\{\begin{array}{c} \int_0^t (t-s)^{2(\alpha-1)}\left[E\left|X_\epsilon(s)-Z_\epsilon(s)\right|^2+\rho^2\left(\mu_\epsilon(s),\nu_\epsilon(s)\right)\right]\mathrm{d}s \\ +\int_0^t (t-s)^{2(\alpha-1)}E\left|g\left(Z_\epsilon(s),\nu_\epsilon(s)\right)-\overline{g}\left(Z_\epsilon(s),\nu_\epsilon(s)\right)\right|^2\mathrm{d}s \end{array}\right\} \\ \leq & \frac{4k\epsilon}{\Gamma(\alpha)^2}\int_0^t (t-s)^{2(\alpha-1)}E\left|X_\epsilon(s)-Z_\epsilon(s)\right|^2\mathrm{d}s \\ & +\frac{2\epsilon}{\Gamma(\alpha)^2}t^{2\alpha-1}\varphi_2(t)\left(1+E\left|Z_\epsilon(s)\right|^2+\left\|\nu_\epsilon(s)\right\|^2\right). \end{aligned} \tag{58}$$

Therefore, from the above discussion, (56)–(58), and Theorem 1, we have

$$\begin{aligned} E\left|X_\epsilon(t)-Z_\epsilon(t)\right|^2 \le{}& \frac{4tk\epsilon^2}{\Gamma(\alpha)^2}\int_0^t (t-s)^{2(\alpha-1)}E\left|X_\epsilon(s)-Z_\epsilon(s)\right|^2 \mathrm{d}s \\ &+\frac{2\epsilon^2}{\Gamma(\alpha)^2}t^{2\alpha}\varphi_1\left((t)\left(1+E\left|Z_\epsilon(s)\right|^2+\left\|\nu_\epsilon(s)\right\|^2\right)\right) \\ &+\frac{4k\epsilon}{\Gamma(\alpha)^2}\int_0^t (t-s)^{2(\alpha-1)}E\left|X_\epsilon(s)-Z_\epsilon(s)\right|^2\mathrm{d}s+\frac{2\epsilon}{\Gamma(\alpha)^2}t^{2\alpha-1}\varphi_2\Gamma(\alpha)^2\left(1+E\left|Z_\epsilon(s)\right|^2+\left\|\nu_\epsilon(s)\right\|^2\right) \\ ={}& 2\epsilon T^{2\alpha-1}\left(\frac{c_1\epsilon}{\Gamma(\alpha)^2}T+\frac{c_2}{\Gamma(\alpha)^2}\right)+4\epsilon\left(\frac{k\epsilon}{\Gamma(\alpha)^2}T+\frac{k}{\Gamma(\alpha)^2}\right)\int_0^t (t-s)^{(2\alpha-1)-1}E\left|X_\epsilon(s)-Z_\epsilon(s)\right|^2\mathrm{d}s. \end{aligned} \tag{59}$$

Denote $r_1 = 2((c_1\epsilon/\Gamma(\alpha)^2)T + (c_2/\Gamma(\alpha)^2))$ and $r_2 = 4((k\epsilon/\Gamma(\alpha)^2)T + (k/\Gamma(\alpha)^2))$; using Lemma 1, we have

$$\begin{aligned} E\left|X_\epsilon(t)-Z_\epsilon(t)\right|^2 &\le \epsilon T^{2\alpha-1}r_1\left(1+\int_0^t\sum_{n=1}^{\infty}\frac{(r_2\epsilon\Gamma(2\alpha-1))^n}{\Gamma((2\alpha-1)n)}(t-s)^{(2\alpha-1)n-1}\mathrm{d}s\right) \\ &\le \epsilon T^{2\alpha-1}r_1\left(1+\sum_{n=1}^{\infty}\frac{\left(r_2\epsilon\Gamma(2\alpha-1)T^{2\alpha-1}\right)^n}{\Gamma((2\alpha-1)n+1)}\right) \\ &\le \epsilon T^{2\alpha-1}r_1\left(1+E_{2\alpha-1,1}\left(r_2\epsilon\Gamma(2\alpha-1)T^{2\alpha-1}\right)\right). \end{aligned} \tag{60}$$

Select some $\beta \in (0,1)$, $L>0$, such that, for $\forall t \in (0, L\epsilon^{(-\beta/2\alpha-1)}]$, we obtain

$$\sup_{0\le t\le L\epsilon^{(-\beta/2\alpha-1)}} E\left|X_\epsilon(t)-Z_\epsilon(t)\right|^2 \le C\epsilon^{1-\beta}, \tag{61}$$

where $C = r_1(1+E_{2\alpha-1,1}(r_2L\epsilon^{(-\beta/2\alpha-1)}\Gamma(2\alpha-1)))$.

Consequently, for $\forall\delta_1>0$, one can select some $\epsilon_1 \in (0,\epsilon_0]$ such that, for each $\epsilon \in (0,\epsilon_1]$, $\forall t \in (0, L\epsilon^{(-\beta/2\alpha-1)}]$, we have

$$\sup_{0\le t\le L\epsilon^{(-\beta/2\alpha-1)}} E\left|X_\epsilon(t)-Z_\epsilon(t)\right|^2 \le \delta_1. \tag{62}$$

This completes the proof.

Remark 2. Using the definition of ρ, we obtain

$$\rho\left(\mu_\epsilon(t),\nu_\epsilon(t)\right) \le E\left|X_\epsilon(t)-Z_\epsilon(t)\right| \le E\left|X_\epsilon(t)-Z_\epsilon(t)\right|^2. \tag{63}$$

From the above estimate, we actually obtain

$$\begin{aligned} D_T\left(\mu_\epsilon,\nu_\epsilon\right) &= \sup_{0\le t\le T}\rho\left(\mu_\epsilon(t),\nu_\epsilon(t)\right) \\ &\le s\sup_{0\le t\le T}E\left|X_\epsilon(t)-Z_\epsilon(t)\right|^2 \longrightarrow 0, \quad \epsilon\longrightarrow 0, \end{aligned} \tag{64}$$

which means that, as $\epsilon \longrightarrow 0$, $\mu_\epsilon(t)$ corresponding to $X_\epsilon(t)$ converges to $\nu_\epsilon(t)$ of $Z_\epsilon(t)$ in $C([0,T;(M_\gamma^2,\rho)])$.

Data Availability

No data were used to support this study.

Conflicts of Interest

The authors declare that they have no conflicts of interest.

Acknowledgments

This work was partiality supported by the NNSFs of China (nos. 11901584, 61876192, 11926322, and 11801575), "the Fundamental Research Funds for the Central Universities,"

the South-Central University for Nationalities (nos. CZY20013, CZY20014, CTZ20020, and KTZ20051).

References

[1] J. Duan, K. Lu, and B. r. Schmalfuss, "Smooth stable and unstable manifolds for stochastic evolutionary equations," *Journal of Dynamics and Differential Equations*, vol. 16, no. 4, pp. 949–972, 2004.

[2] J. Duan, K. Lu, and B. Schmalfuss, "Invariant manifolds for stochastic partial differential equations," *Annals of Probability*, vol. 31, no. 4, pp. 2109–2135, 2003.

[3] H. Fu and J. Liu, "Strong convergence in stochastic averaging principle for two time-scales stochastic partial differential equations," *Journal of Mathematical Analysis and Applications*, vol. 384, no. 1, pp. 70–86, 2011.

[4] Y. Xu, J. Duan, and W. Xu, "An averaging principle for stochastic dynamical systems with Lévy noise," *Physica D: Nonlinear Phenomena*, vol. 240, no. 17, pp. 1395–1401, 2011.

[5] J. Xu and J. Liu, "An Averaging principle for multivalued stochastic differential equations," *Stochastic Analysis and Applications*, vol. 32, no. 6, pp. 962–974, 2014.

[6] W. Mao, L. Hu, S. You, and X. Mao, "The averaging method for multivalued SDEs with jumps and non-Lipschitz coefficients," *Discrete & Continuous Dynamical Systems-B*, vol. 24, no. 9, p. 4937, 2019.

[7] W. Mao, S. You, X. Wu, and X. Mao, "On the averaging principle for stochastic delay differential equations with jumps," *Advances in Difference Equations*, vol. 2015, no. 1, pp. 1–19, 2015.

[8] J. Bao, G. Yin, and C. Yuan, "Two-time-scale stochastic partial differential equations driven by -stable noises: averaging principles," *Bernoulli*, vol. 23, pp. 645–669, 2017.

[9] J. Hu and C. Yuan, "Strong convergence of neutral stochastic functional differential equations with two time-scales," *Discrete and Continuous Dynamical Systems-B*, vol. 24, no. 11, p. 5831, 2019.

[10] B. Pei, Y. Xu, and J.-L. Wu, "Stochastic averaging for stochastic differential equations driven by fractional Brownian motion and standard Brownian motion," *Applied Mathematics Letters*, vol. 100, Article ID 106006, 2020.

[11] D. Luo, Q. Zhu, and Z. Luo, "An averaging principle for stochastic fractional differential equations with time-delays," *Applied Mathematics Letters*, vol. 105, Article ID 106290, 2020.

[12] X. He, S. Han, and J. Tao, "Averaging principle for SDEs of neutral type driven by G-Brownian motion," *Stochastics and Dynamics*, vol. 19, no. 01, Article ID 1950004, 2019.

[13] W. Xu, W. Xu, and S. Zhang, "The averaging principle for stochastic differential equations with Caputo fractional derivative," *Applied Mathematics Letters*, vol. 93, pp. 79–84, 2019.

[14] R. Z. Khasminskii, "On the principle of averaging the it $\hat{o}$ stochastic differential equations," *Kibernetika*, vol. 4, pp. 260–279, 1968.

[15] L. Wu, S. Liu, L. Yao, S. Yan, and D. Liu, "Grey system model with the fractional order accumulation," *Communications in Nonlinear Science and Numerical Simulation*, vol. 18, no. 7, pp. 1775–1785, 2013.

[16] C. Yan, L. Wu, L. Liu et al., "Fractional Hausdorff grey model and its properties," *Chaos Solitons and Fractals*, vol. 138, Article ID 109915, 2020.

[17] J. Wen, C. Wu, R. Zhang, X. Xiao, N. Nv, and Y. Shi, "Rear-end collision warning of connected automated vehicles based on a novel stochastic local multivehicle optimal velocity model," *Accident Analysis & Prevention*, vol. 148, Article ID 105800, 2020.

[18] T. E. Govindan and N. U. Ahmed, "On yosida approximations of McKean-Vlasov type stochastic evolution equations," *Stochastic Analysis and Applications*, vol. 33, no. 3, pp. 383–398, 2015.

[19] X. Huang and F.-Y. Wang, "Distribution dependent SDEs with singular coefficients," *Stochastic Processes and Their Applications*, vol. 129, no. 11, pp. 4747–4770, 2019.

[20] F.-Y. Wang, "Distribution dependent SDEs for Landau type equations," *Stochastic Processes and Their Applications*, vol. 128, no. 2, pp. 595–621, 2018.

[21] Y. Wang, J. Xu, and P. E. Kloeden, "Asymptotic behavior of stochastic lattice systems with a Caputo fractional time derivative," *Nonlinear Analysis: Theory, Methods & Applications*, vol. 135, pp. 205–222, 2016.

[22] H. Ye, J. Gao, and Y. Ding, "A generalized Gronwall inequality and its application to a fractional differential equation," *Journal of Mathematical Analysis and Applications*, vol. 328, no. 2, pp. 1075–1081, 2007.

Hindawi
Journal of Mathematics
Volume 2021, Article ID 4951714, 15 pages
https://doi.org/10.1155/2021/4951714

Research Article

Air Pollution and the Public Perception Level and Self-Protection Demand in Three Cities of China: Fractional Grey Modelling Analysis

Leping Tu and Yonggang Zhao

School of Management Engineering and Business, Hebei University of Engineering, Handan 056038, China

Correspondence should be addressed to Yonggang Zhao; 12075255@qq.com

Received 21 April 2021; Accepted 6 July 2021; Published 13 July 2021

Academic Editor: Firdous A. Shah

To improve air pollution and human health, a novel grey prediction model with fractional-order accumulation and new information priority accumulation is proposed to analyze and predict the public perception level, self-protection demands, and environmental protection behavior of air pollution. The study in three cities of China shows that the public' perception level will rise rapidly, and the speed will continue to accelerate with the further deterioration of air quality. Among them, Beijing's public perception is the most sensitive and strong. The protection needs of the Tianjin public are the most sensitive. The Shijiazhuang public shows a strong desire for environmental protection. This study will help in understanding the relationship between the public and air quality.

1. Introduction

Air is a necessary condition for human survival and is closely related to human health [1]. In recent years, air pollution has become serious, because of the increase in industrial production and energy consumption [2, 3]. Due to the hazards of air pollution to human health, air quality has attracted widespread attention [4]. In fact, the public's attention to air quality is closely related to air quality. First, the public's perception contributes to the promulgation of environmental laws and regulations [5]. Second, public attention to air quality can improve air quality [6]. Finally, the public's response to air treatment measures may determine the efficiency of air treatment measures [7]. Therefore, it is extremely important to understand the public's perception and response to air pollution to improve air quality.

Traditionally, the methods of analyzing the relationship between air quality and public perception and behavior are usually questionnaires and interviews [8]. The collection methods of data not only consume a lot of time, but also may not achieve the expected results [9]. With the advent of the era of big data, the public's network search behavior is widely used in forecast research [10–12]. In fact, the public's Internet search behavior can also be used to analyze air quality. The changing trends of the public's network search data reflect the development trend of air quality [4, 13]. Besides, different regions have different search habits of air quality [11].

However, there are few studies in forecasting public perception and behavior about air quality. In fact, it is of great significance for preventing major air pollution hazards. As air pollution control is a long process, this paper conducts forecast research on an annual basis. Because there is less annual data, the grey model can be used to solve this problem. Grey prediction models are widely used, because of their effectiveness in short time series prediction [14–16]. Among them, the grey multivariate model has greatly improved the prediction accuracy due to the introduction of influencing factors. For example, the multivariate grey model with optimized fractional order can be well used for the prediction of electricity consumption [17]. A novel discrete grey multivariable model is used to forecast the

output value of China's high-tech industries [18]. In the research of CO_2 emissions and economic growth, the unequal grey Verhulst model is derived [19]. However, there are some deficiencies of the existing literature. First, the grey model is rarely used to analyze public perception and behavior about air pollution. Second, there is no quantitative analysis of the relationship between public perception and behavior and air pollution. Finally, there is no effective way to predict public perception and behavior about air pollution. In this paper, a novel fractional grey multivariate model is proposed to analyze and forecast public perception and behavior about air pollution.

Compared with the existing research, there are some innovations of this paper. Firstly, a novel grey model is proposed to improve the accuracy of prediction. Secondly, based on the analysis of the relationship between the public and air quality, the future public perception level, self-protection demand, and environmental protection behavior are predicted. Finally, the study results can provide forward-looking suggestions for protecting air quality and human health.

The rest of this article is organized as follows. The research area and data sources are described in Section 2. The research methods are introduced in Section 3. We analyze the relationship between air quality and perception level, personal protection demands, and environmental protection behavior of the public and make some relevant predictions in Section 4. The conclusion and implication are drawn in Section 5.

2. Research Area and Data Sources

2.1. Research Area. The Beijing-Tianjin-Hebei region is one of the regions with the most severe air pollution in China. It is shown in Figure 1. First of all, the economic structure of Hebei Province is dominated by secondary industry, and coal combustion produces a lot of air pollutants. Secondly, Hebei Province is located in the Central Plains, where pollutants tend to accumulate in large quantities [20]. The ozone pollution in the Beijing-Tianjin-Hebei region has become more and more serious, which poses a challenge to the pollution mitigation strategy and needs to be further adjusted to solve this problem [21]. Beijing, Tianjin, and Shijiazhuang are the cities with the most serious air pollution in the Beijing-Tianjin-Hebei region, and the air quality of the three cities is closely correlated [22]. Therefore, Beijing, Tianjin, and Shijiazhuang are studied to improve air quality in this paper.

2.2. Data Sources

2.2.1. Air Quality Index. The air quality index (AQI) is a dimensionless index that describes the overall status of the city's ambient air quality. The index comprehensively considers the pollution levels of six pollutants (SO_2, NO_2, PM_{10}, $PM_{2.5}$, CO, and O_3) in the AQI Technical Regulations (HJ633-2012). The greater the value of the AQI, the greater the degree of comprehensive pollution. Therefore, the AQI can be used to reflect the air quality [23]. To assess the air pollution, AQI from 2014 to 2019 in Beijing, Tianjin, and Shijiazhuang is collected from the China Air Quality Online Monitoring and Analysis Platform (https://www.aqistudy.cn/).

2.2.2. Baidu Index. Baidu index is a data-sharing platform based on Baidu's massive netizens' behavior data and is the weighted sum of the frequency of every keyword in Baidu web search. Data sources include the number of netizens' behaviors such as reading, commenting, forwarding, praising, and disliking. In fact, the Baidu index can be used to explore the relationship between air quality and public behavior [11]. To select representative keywords, keywords need to be filtered, because grey correlation analysis is often used to analyze the degree of correlation between two variables. The higher the degree of grey correlation, the higher the degree of correlation between the two variables [24]. In this paper, based on the grey correlation analysis, the annual Baidu index for keywords with a high grey correlation with the AQI (Figure 2) is obtained from the Baidu index official website (https://index.baidu.com/).

(1) Perception Level. The level of public perception of air pollution reflects people's risk assessment and attitudes towards air pollution [25]. In fact, the level of perception depends not only on the degree of public exposure to air pollution, but also on the perception of air pollution and the sensitivity to air pollution threats [26]. The public perception based on air pollution can not only directly reflect air quality but also indirectly reflect personal protection demands and environmental protection behavior [27]. Based on the grey correlation analysis, the Baidu index $PM_{2.5}$, smog, and air quality are selected to assess the level of public perception of air pollution in Beijing, Tianjin, and Shijiazhuang.

(2) Personal Protection Demands. According to the protection motivation theory [28], the level of public perception of air pollution determines the personal protection demands of the public. The public's personal protection demands depend on the public's perception level of air pollution. Besides, the need for self-protection is affected by the public's responsiveness, the effectiveness of protective measures, and the cost of practice [29]. Based on the grey correlation analysis, the Baidu index of masks, air purifiers, and $PM_{2.5}$ detectors is used to evaluate the public's personal protection demands.

(3) Environmental Protection Behavior. Public environmental protection behavior is considered as the public's self-protection based on long-term consideration [30]. Therefore, the level of public perception of air pollution also affects the public's environmental protection behavior. Not only that, the public's environmental protection behavior can determine whether the environmental protection policies are effectively implemented [31]. The environmental protection behavior of the public includes energy saving and emission reduction, green travel, and environmental protection. Therefore, the Baidu index of energy saving and

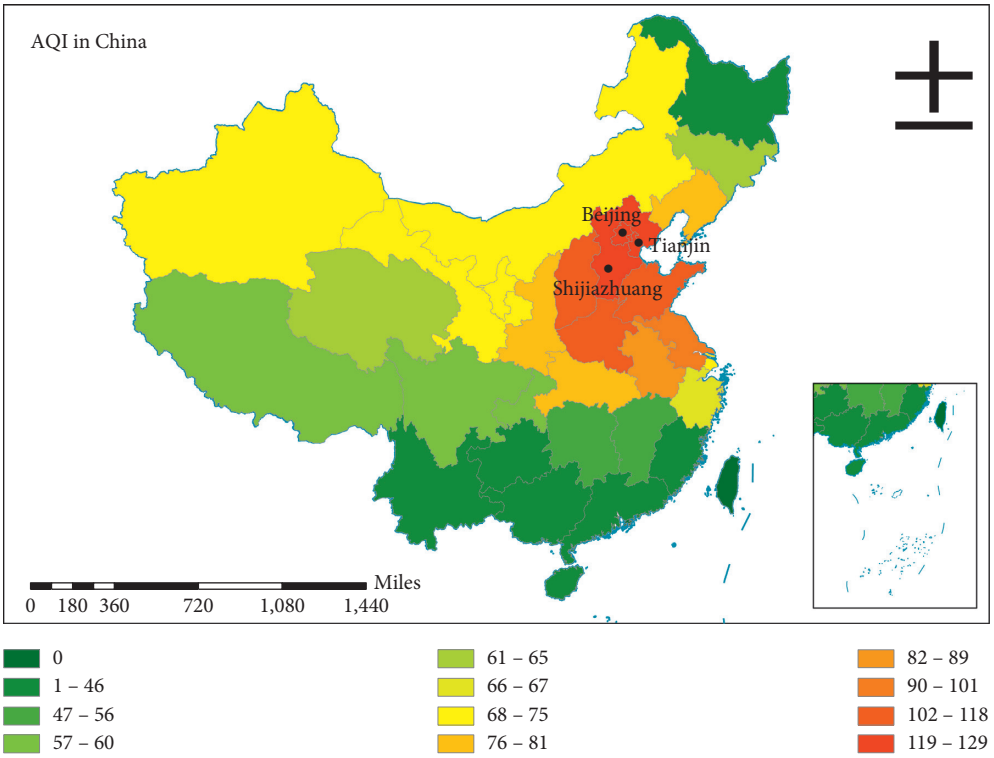

Figure 1: Location and AQI spatial patterns of Beijing, Tianjin, and Shijiazhuang in China.

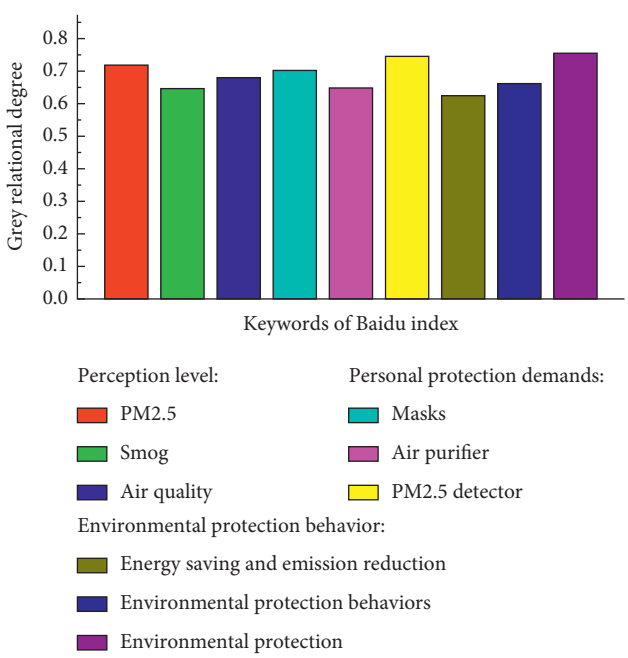

Figure 2: Grey correlation degree between AQI and Baidu index.

emission reduction, green travel, and environmental protection are used to reflect public environmental protection behavior.

3. Research Methods

The GMC (1, N) model can improve the accuracy of the grey model [32]. Considering the fractional order accumulation method [33] and new information priority accumulation [34], the GMC (1, N) model is optimized by using a combination of fractional-order accumulation and new information priority accumulation (FNGMC (1, N)). The FNGMC (1, N) model is given as follows:

The original nonnegative sequence is conventionally represented as

$$X_l^{(0,0)} = \left\{x_l^{(0,0)}(1), x_l^{(0,0)}(2), \ldots, x_l^{(0,0)}(n)\right\}, \quad l = 1, 2, \ldots, m. \tag{1}$$

Step 1. By using $x_l^{(r,0)}(k) = \sum_{i=1}^{k} C_{k-i+r-1}^{k-i} x_l^{(0,0)}(i)$, the r-order accumulation sequence is

$$X_l^{(r,0)} = \left\{x_l^{(r,0)}(1), x_l^{(r,0)}(2), \ldots, x_l^{(r,0)}(n)\right\}. \tag{2}$$

where $C_{r-1}^{0} = 1$, $C_k^{k+1} = 0$, and $C_{k-i+r-1}^{k-i} = ((k-i+r-1)(k-i+r-2), \ldots, (r+1)\, r/(k-i)!)$.

By using $x_l^{(r,\lambda)}(m) = \sum_{j=1}^{m} \lambda^{m-j} x_l^{(r,0)}(j)$, the r-order accumulation sequence of new information priority is

$$X_l^{(r,\lambda)} = \left\{x_l^{(r,\lambda)}(1), x_l^{(r,\lambda)}(2), \ldots, x_l^{(r,\lambda)}(n)\right\}. \tag{3}$$

Step 2. The whitened equation of FNGMC (1, N) model is written as

$$\frac{dx_1^{(r,\lambda)}(t)}{dt} + b_1 x_1^{(r,\lambda)}(t) = b_2 x_2^{(r,\lambda)}(t) + b_3 x_3^{(r,\lambda)}(t) + \cdots + b_N x_N^{(r,\lambda)}(t) + u. \tag{4}$$

where $b_1, b_2, \ldots, b_N$ are driving parameters, and u is the control parameter. Among them, the greater the driving parameters, the greater the influence of the corresponding factors. The grey derivative is conventionally represented as $(dx_1^{(r,\lambda)}(t)/dt) = x_1^{(r,\lambda)}(t+1) - x_1^{(r,\lambda)}(t)$. The least-squares solution of the model parameters is

$$\left[\hat{b}_1, \hat{b}_2, \ldots, \hat{b}_N, \hat{u}\right]^T = \left(B^T B\right)^{-1} B^T Y, \tag{5}$$

where

$$Y = \begin{bmatrix} x_1^{(r,\lambda)}(2) - x_1^{(r,\lambda)}(1) \\ x_1^{(r,\lambda)}(3) - x_1^{(r,\lambda)}(2) \\ \vdots \\ x_1^{(r,\lambda)}(n) - x_1^{(r,\lambda)}(n-1) \end{bmatrix},$$

$$B = \begin{bmatrix} -\frac{\left(x_1^{(r,\lambda)}(1) + x_1^{(r,\lambda)}(2)\right)}{2} & \frac{\left(x_2^{(r,\lambda)}(1) + x_2^{(r,\lambda)}(2)\right)}{2} & \cdots & \frac{\left(x_N^{(r,\lambda)}(1) + x_N^{(r,\lambda)}(2)\right)}{2} & 1 \\ -\frac{\left(x_1^{(r,\lambda)}(2) + x_1^{(r,\lambda)}(3)\right)}{2} & \frac{\left(x_2^{(r,\lambda)}(2) + x_2^{(r,\lambda)}(3)\right)}{2} & \cdots & \frac{\left(x_N^{(r,\lambda)}(2) + x_N^{(r,\lambda)}(3)\right)}{2} & 1 \\ \vdots & \vdots & \ddots & \vdots & \vdots \\ -\frac{\left(x_1^{(r,\lambda)}(n-1) + x_1^{(r,\lambda)}(n)\right)}{2} & \frac{\left(x_2^{(r,\lambda)}(n-1) + x_2^{(r,\lambda)}(n)\right)}{2} & \cdots & \frac{\left(x_N^{(r,\lambda)}(n-1) + x_N^{(r,\lambda)}(n)\right)}{2} & 1 \end{bmatrix}, \tag{6}$$

where $f(t) = b_2 x_2^{(r,\lambda)}(t) + b_3 x_3^{(r,\lambda)}(t) + \cdots + b_N x_N^{(r,\lambda)}(t) + u$.

Step 3. Then, the approximate time-response function of FNGMC (1, N) model is

$$\hat{x}_1^{(r,\lambda)}(t) = x_1^{(0,0)}(1) e^{-b_1(t-1)} + \sum_{\tau=2}^{t} \left\{ e^{-b_1(t-\tau+0.5)} \frac{f(\tau) + f(\tau-1)}{2} \right\}, \tag{7}$$

Step 4. Then, the sequence by the inverse accumulated generating operator of new information priority is

$$\hat{x}_1^{(r,0)}(1) = x_1^{(0,0)}(1), \hat{x}_1^{(r,0)}(k) = \hat{x}_1^{(r,\lambda)}(k) - \lambda \hat{x}_1^{(r,\lambda)}(k-1), \quad k = 2, 3, \ldots, n. \tag{8}$$

Finally, the predicted value is given by the inverse accumulated generating operator of r-order.

$$\hat{X}_1^{(0,0)} = \left\{ \hat{x}_1^{(0,0)}(1), \hat{x}_1^{(0,0)}(2), \ldots, \hat{x}_1^{(0,0)}(n) \right\}, \tag{9}$$

where $\hat{x}_1^{(0,0)}(k) = \hat{x}_1^{(r,0)(1-r,0)}(k) - \hat{x}_1^{(r,0)(1-r,0)}(k-1)$.

The proposed FNGMC (1, N) model can be transformed into some existing grey models. When $\lambda = 1$, the FNGMC (1, N) model yields the FGMC (1, N) model. When $r = 1$, the FNGMC (1, N) model yields the GMCN (1, N) model. When $\lambda = 1$ and $r = 1$, the FNGMC (1, N) model yields the GMC (1, N) model. As an improved model, the proposed model

not only can be flexibly transformed into a general model, but also has high prediction accuracy.

The mean absolute percentage error (MAPE) is used to verify the accuracy of the FNGMC (1, N) model. The smaller the MAPE, the higher the prediction accuracy of the model. It is calculated as

$$\mathrm{MAPE} = \frac{1}{n}\frac{\sum_{t=1}^{n}\left|x_1^{(0,0)}(t) - \hat{x}_1^{(0,0)}(t)\right|}{x_1^{(0,0)}(t)} \times 100\%. \tag{10}$$

The following example can demonstrate the validity of the FNGMC (1, N) model. The data comes from literature [35]. The tensile strength of the material is regarded as predicted sequence (X_1), while the Brinell hardness is regarded as influence sequence (X_2). The first five sets of data are used to determine the model, while the last five sets of data are used to test the model. The GMC_T (1, 2), GMC_G (1, 2), and RDGM (1, 2) models are used for comparison. The RMSPEPR and RMSPEPO of the four models are shown in Table 1.

It can be seen from Table 1 that the RMSPEPR and RMSPEPO of the FNGMC (1, N) model are as small as 0.14% and 1.72%, respectively. It shows that the FNGMC (1, N) model is better than other competition models.

4. Empirical Study

4.1. Analysis and Prediction for Perception Levels of Air Pollution in Beijing, Tianjin, and Shijiazhuang. As shown in Figure 3, the AQI of Beijing, Tianjin, and Shijiazhuang decreases from 2014 to 2018. It indicates that the air quality of the three cities has been improved. Besides, the Baidu index of $PM_{2.5}$, smog, and air quality shows a downward trend. Specifically, Beijing's AQI declined year by year, and the search index declined steadily. The AQI of Tianjin and Shijiazhuang increased from 2015 to 2017, and the search index also started to rise. This shows that the change of AQI has a significant impact on the public's perception for air quality. Moreover, this influence is positive; that is to say, the decline of AQI and the public perception level also decline. However, from 2018 to 2019, with the increase of AQI in the three cities, the Baidu index still kept declining. Presumably, there may be two reasons for this phenomenon. First, the influence of air quality on public perception level changes. Second, in recent years, the improvement of air quality has reduced the public's perception sensitivity, which has delayed this influence. Therefore, it is necessary to predict the perception level in the future. By the FNGMC (1, 2) model, the fitting results of the Baidu index in three cities are obtained (Table 2).

From Table 2, the MAPE in the three cities is low. This shows that the FNGMC (1, 2) model has high accuracy. According to the model results, the AQI has a positive impact on perception level. It is consistent with the previous analysis. Therefore, the FNGMC (1, 2) model can be used to predict the perception level from 2020 to 2024. Based on the changes from 2018 to 2019, the estimated AQI from 2020 to 2024 is obtained at growth rates of 0.95, 0.97, 1.03, 1.05, and 1.1. Then, the estimated AQI of Beijing, Tianjin, and Shijiazhuang from 2020 to 2024 is shown in Table 3.

By substituting the AQI of three cities from 2020 to 2024 into the corresponding FNGMC (1, N) models, the prediction results of $PM_{2.5}$, smog, and air quality from 2020 to 2024 can be obtained. As shown in Figure 4, the search index of $PM_{2.5}$ increased with the growth rate of AQI increase from 2020 to 2024. This shows that the reduction of air quality improves the public's perception of air pollution. In fact, $PM_{2.5}$ is the main cause of smog formation. Compared with smog and air quality, the search for $PM_{2.5}$ reflects a deeper perception. Besides, the public's deep perception of Beijing is stronger in terms of the range of change.

Similar to the prediction results of $PM_{2.5}$, a larger AQI leads to a higher smog perception level (Figure 5). However, compared with the search index of $PM_{2.5}$, the search index of smog is lower, which shows that the public's perception of smog weather not only stays on the surface, but also penetrates its causes. Besides, from the comparison results of cities, Beijing's search index is larger, indicating that Beijing's public perception of smog is still higher than that of Tianjin and Shijiazhuang. Judging from the change range, the Beijing public has higher perception sensitivity.

Similar to $PM_{2.5}$ and smog, larger AQI leads to a higher air quality search index (Figure 6). Baidu index of air quality reflects the basic public perception of air quality. Compared with $PM_{2.5}$ and smog, this perception is more comprehensive, and it includes other air pollution situations besides smog. By comparison, it is found that the public in Beijing still maintains a high level of perception of other air pollution. Besides, from the change range, this comprehensive perception is the most sensitive. Considering that the average AQI in Beijing in 2019 is as low as 86, it is speculated that the public perception level may promote air control.

To sum up, the reduction of air quality promotes the improvement of perception level at all levels, including in-depth causes ($PM_{2.5}$), major air pollution (smog), and comprehensive perception (air quality). From the prediction curves of the three indexes, the change curve of the search index caused by AQI change is a concave curve, which shows that higher AQI causes more sensitive perception. On the contrary, lower AQI leads to less sensitive perception. Retrospectively, this can explain the abnormal phenomenon from 2018 to 2019, which may be the perception delay caused by the decrease of public sensitivity to air pollution.

4.2. Analysis and Prediction for Personal Protection Demands of Air Pollution in Beijing, Tianjin, and Shijiazhuang. The Baidu index of masks, air purifiers, and $PM_{2.5}$ detectors reflects the public's personal protection needs. Taking Beijing as an example, from 2014 to 2019, with the decrease of air quality index, masks and air purifiers in Beijing showed a downward trend (Figure 7). Baidu index of Beijing masks decreased from 245 times/day to 155 times/day, Baidu index of air purifiers decreased from 680 times/day to 257 times/day, and the Baidu index of $PM_{2.5}$ detectors changed little (from 82 times/day to 76 times). The changes in Tianjin and Shijiazhuang are similar to those in Beijing. It can be seen

Table 1: The RMSPEPR and RMSPEPO of four models.

	GMC_T (1, 2)	GMC_G (1, 2)	RDGM (1, 2)	FNGMC (1, 2)
RMSPEPR (%)	0.41	0.25	0.1	0.09
RMSPEPO (%)	2.92	2.84	2.86	1.72

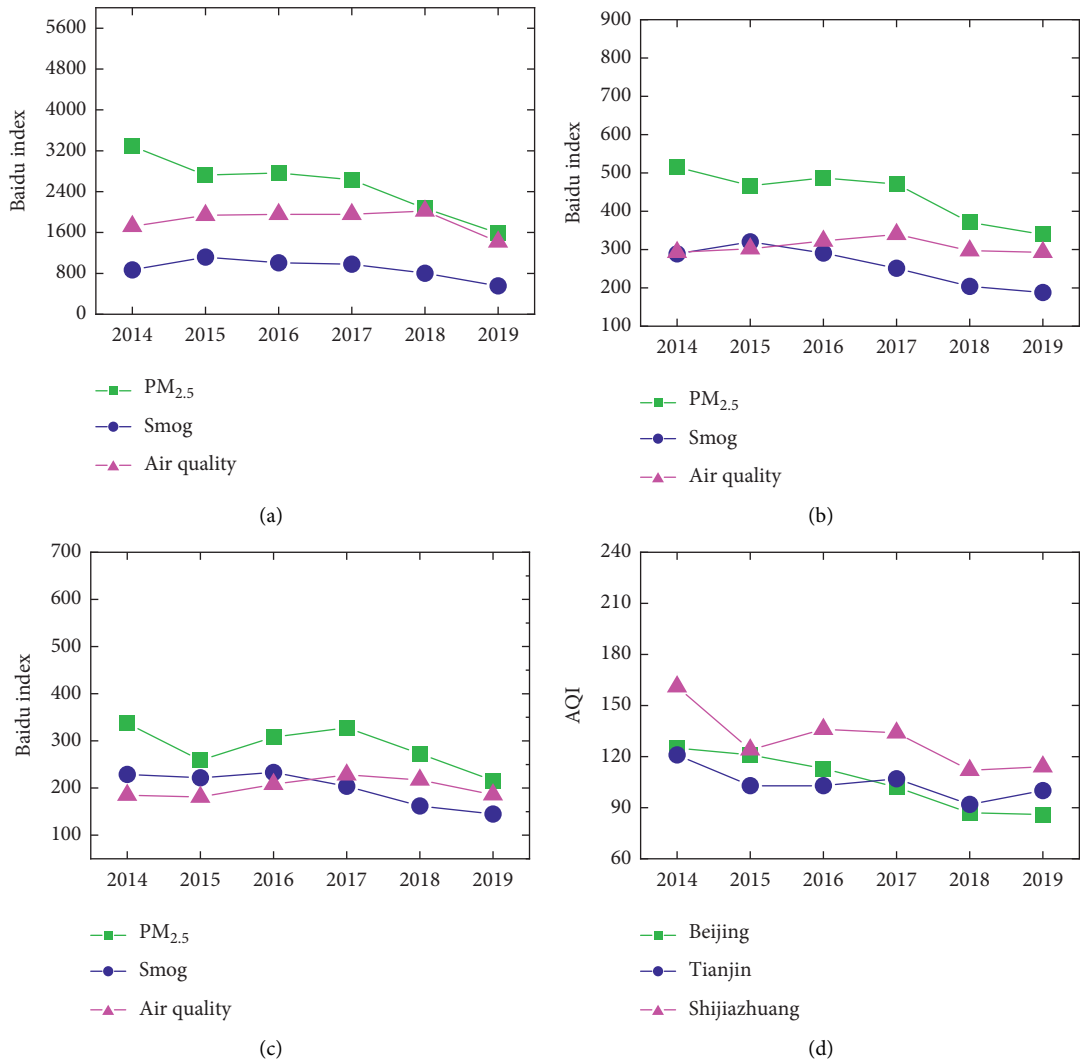

Figure 3: The relationship between Baidu index of the perception levels and AQI. (a) Beijing. (b) Tianjin. (c) Shijiazhuang. (d) AQI of three cities.

Table 2: The results of the Baidu index by the FNGMC (1, 2) model in three cities.

	Baidu index	2014	2015	2016	2017	2018	2019	MAPE (%)
Beijing	$PM_{2.5}$	3286	2749	2838	2603	2130	1626	1.61
	Smog	868	1046	1053	945	746	565	3.93
	Air quality	1721	1738	1948	2071	1865	1423	4.18
Tianjin	$PM_{2.5}$	515	467	490	451	392	335	1.91
	Smog	289	320	291	239	206	185	1.22
	Air quality	293	302	322	327	310	288	1.64
Shijiazhuang	$PM_{2.5}$	337	259	308	323	281	222	1.20
	Smog	229	222	210	204	174	138	3.69
	Air quality	185	189	210	228	217	187	1.03

Table 3: The estimated AQI from 2020 to 2024 in three cities.

	Growth rate	2020	2021	2022	2023	2024
Beijing	0.95	82	78	74	70	67
	0.97	83	81	78	76	74
	1.03	89	91	94	97	100
	1.05	90	95	100	105	110
	1.1	95	104	114	126	139
Tianjin	0.95	95	90	86	81	77
	0.97	97	94	91	89	86
	1.03	103	106	109	113	116
	1.05	105	110	116	122	128
	1.1	110	121	133	146	161
Shijiazhuang	0.95	108	103	98	93	88
	0.97	111	107	104	101	98
	1.03	117	121	125	128	132
	1.05	120	126	132	139	145
	1.1	125	138	152	167	184

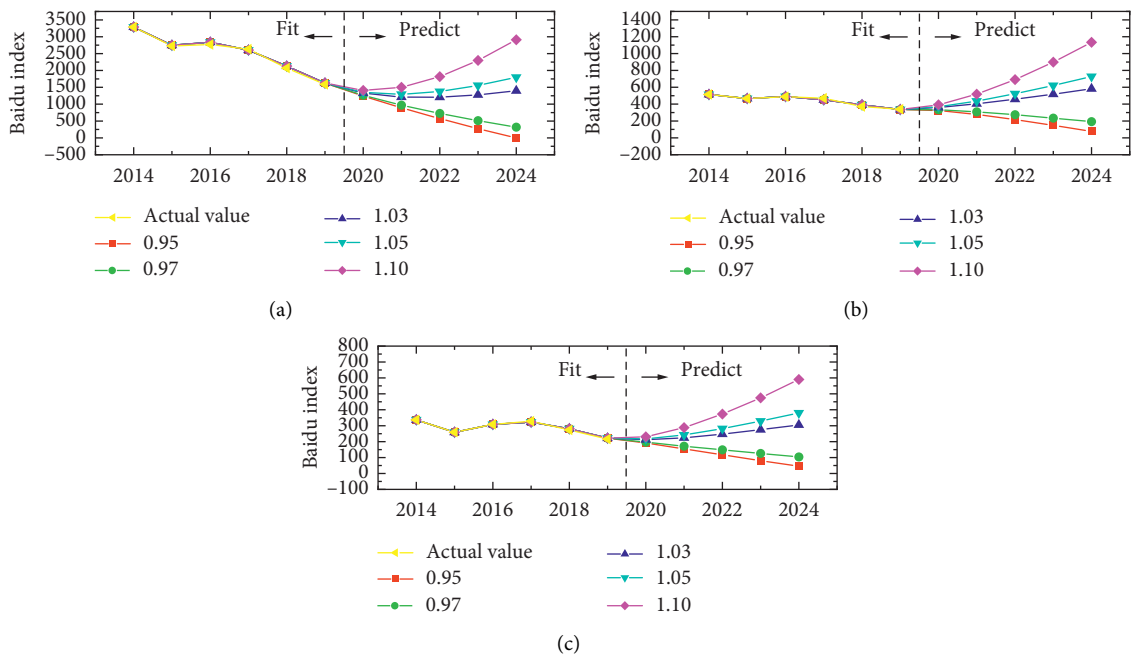

Figure 4: The predicted Baidu index of $PM_{2.5}$ in Beijing (a), Tianjin (b), and Shijiazhuang (c).

that, with the improvement of air quality, the public's demand for masks and air purifiers has decreased, while the demand for $PM_{2.5}$ detectors has not changed much. The public's demand for personal protection has generally declined. However, the air quality began to deteriorate from 2018 to 2019, and the public's demand for personal protection is still declining, which may pose a potential threat.

Therefore, the FNGMC (1, 2) model is used to forecast the personal protection needs of the public in Beijing, Tianjin, and Shijiazhuang. The results are shown in Figure 8. With the growth rate of AQI increasing, the Baidu index of masks in Tianjin also increased from 2020 to 2024. However, Beijing and Shijiazhuang continue to decline in 2020 and do not start to rise until 2021. In terms of the range of change, the public demand for the mask in Tianjin is the strongest.

Compared with the mask, the use of air purifier is a more effective way to reduce the harm of air pollution. Similar to the predicted results of masks, the larger AQI leads to higher demand for air purifiers (Figure 9). However, the search index of air purifiers is higher than that of masks. This shows that, with the aggravation of air pollution, the public tends to take more effective protective measures. In three cities, Tianjin's search index is larger. This indicates that Tianjin's public demand for air pollution protection is higher than that of Beijing and Shijiazhuang. For the change range, Tianjin public has higher demand sensitivity.

Unlike masks and air purifiers, $PM_{2.5}$ detector has no substantial protective effect, but it can serve as a reminder and warning. According to the search index, larger AQI still causes higher demand for $PM_{2.5}$ detector (Figure 10).

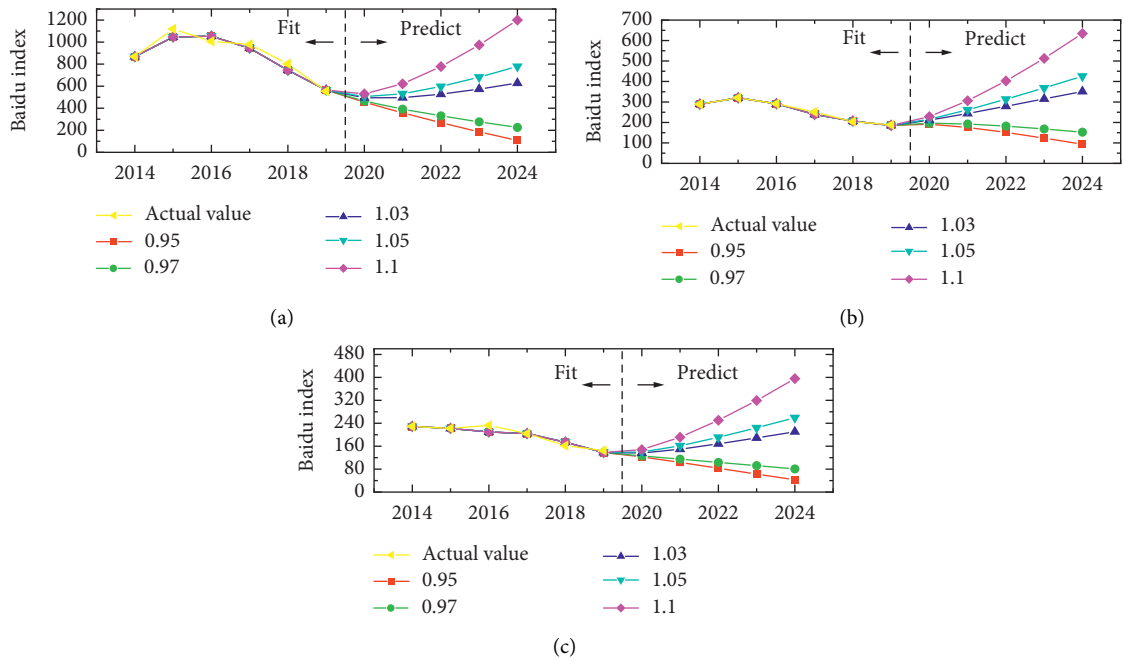

Figure 5: The predicted Baidu index of smog in Beijing (a), Tianjin (b), and Shijiazhuang (c).

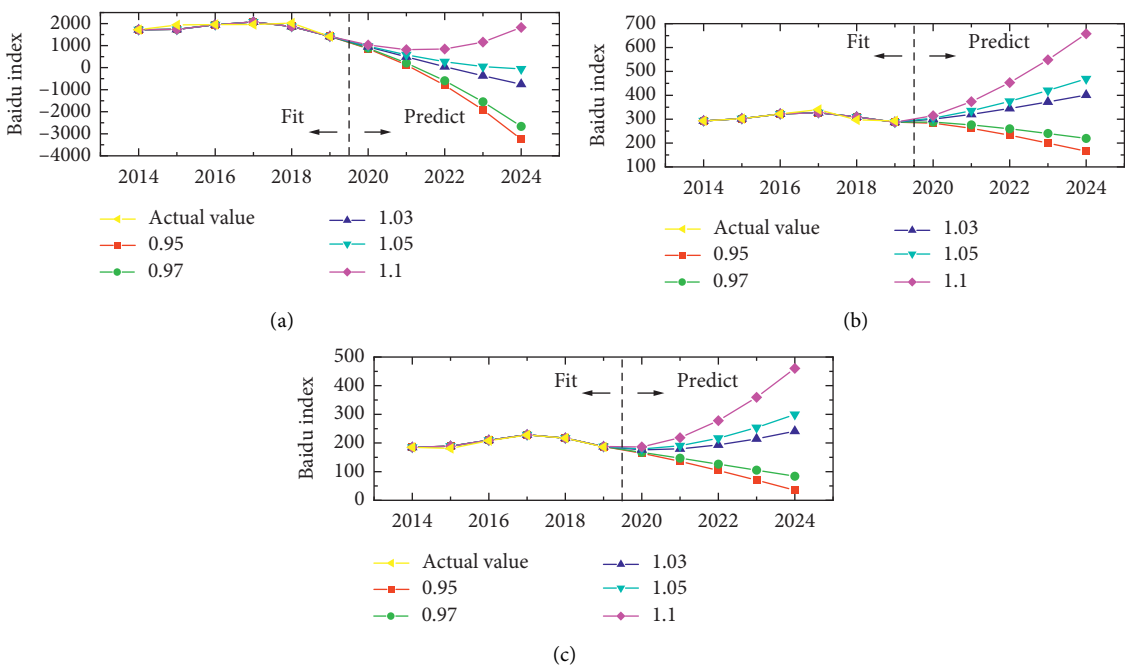

Figure 6: The predicted Baidu index of air quality in Beijing (a), Tianjin (b), and Shijiazhuang (c).

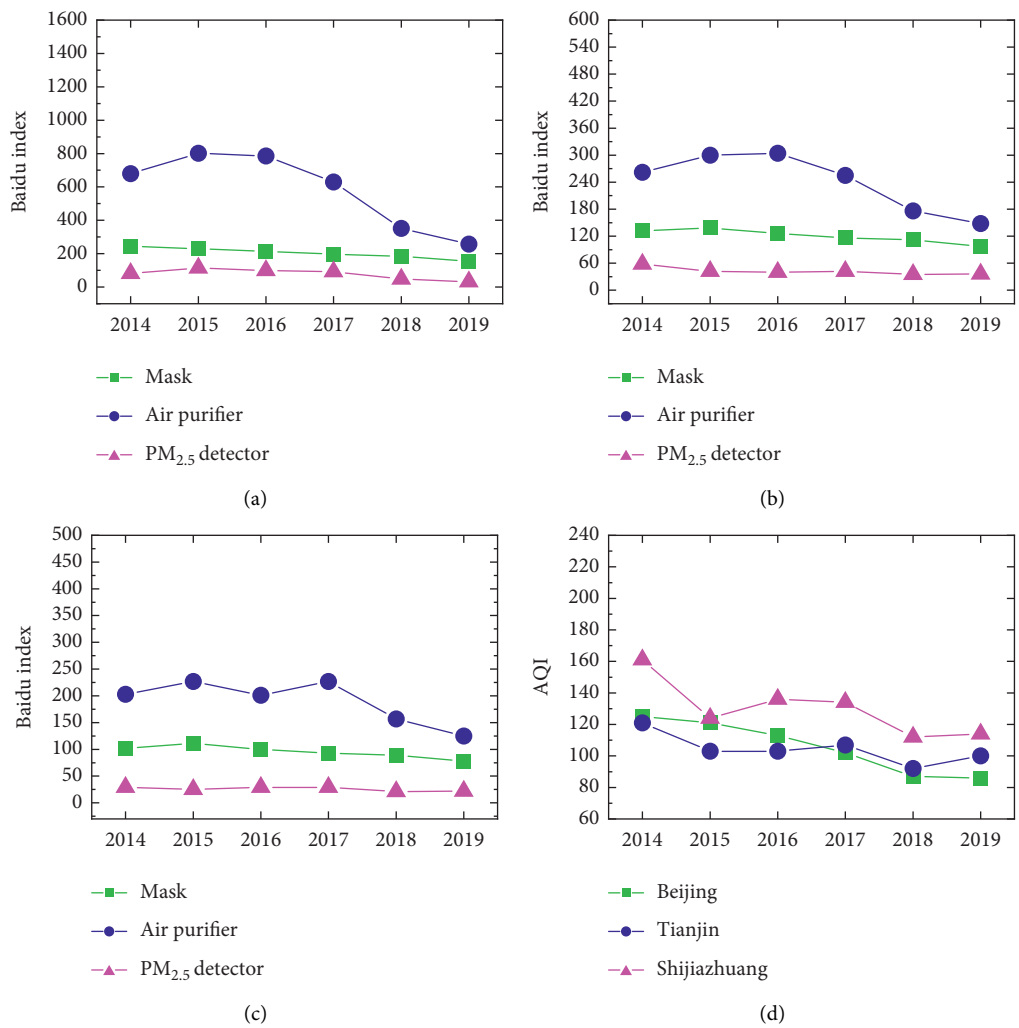

Figure 7: The relationship between Baidu index of the personal protection demands and AQI. (a) Beijing. (b) Tianjin. (c) Shijiazhuang. (d) AQI of three cities.

However, compared with masks and air purifiers, the demand for $PM_{2.5}$ detectors is the lowest, which indicates that the public is more inclined to take substantial protective measures. Besides, it is found that the public demand for $PM_{2.5}$ detector in Beijing is higher than that in Tianjin and Shijiazhuang. From the change range, Beijing public is most sensitive to the demand of $PM_{2.5}$ detector.

4.3. Analysis and Prediction for Environmental Protection Behavior of Air Pollution in Beijing, Tianjin, and Shijiazhuang. The public's search index on energy conservation and emission reduction, green travel, and environmental protection reflects the public's environmental protection behavior. Taking Beijing as an example, from 2014 to 2019, with the decline of air quality index, the Baidu index of energy conservation and emission reduction shows a downward trend (from 164 to 127), while the Baidu index of green travel and environmental protection shows an upward trend (green tourism from 121 to 138, environmental protection from 152 to 199) (Figure 11). The changes in Tianjin and Shijiazhuang are similar to those in Beijing. As a matter of fact, environmental protection often appears in the form of slogans, which cannot indicate concrete measures. Green travel and energy saving and emission reduction reflect the actual actions of the public, among which energy saving and emission reduction are more effective in air control. This shows that when the air quality is improved, the public tends to be inefficient and easy to implement. However, the air quality began to deteriorate from 2018 to 2019, and the changing trend of public environmental protection behavior remained unchanged, which may lead to further deterioration of air quality.

Therefore, the FNGMC (1, 2) model is used to predict the public's environmental protection behavior in Beijing, Tianjin, and Shijiazhuang. The results are shown in

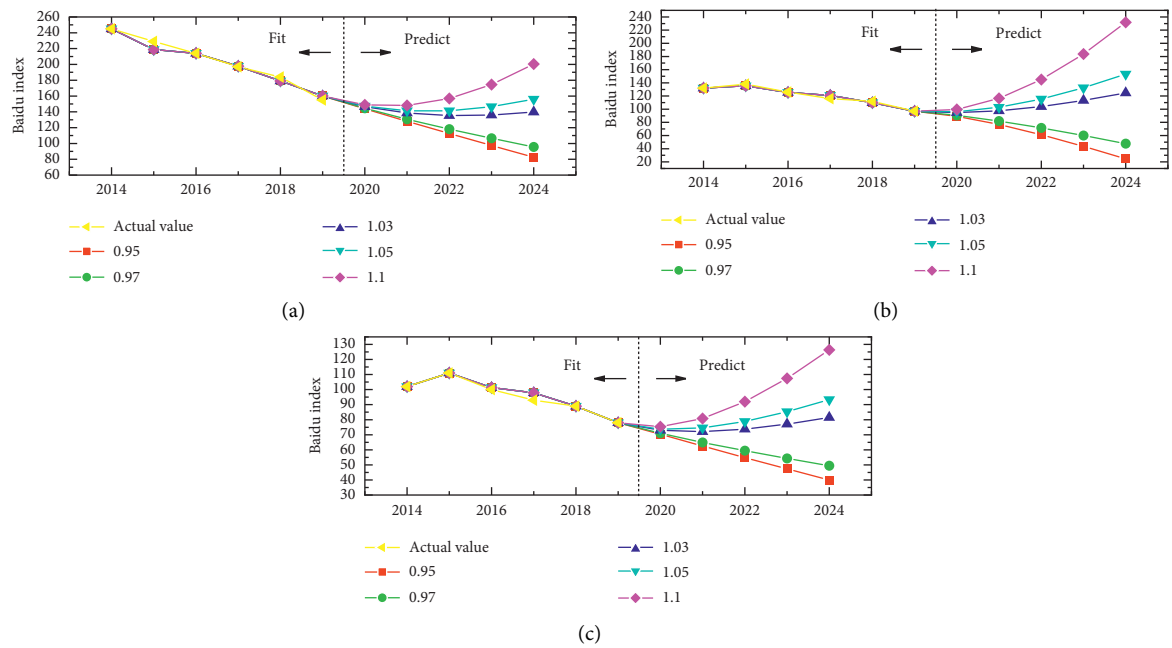

Figure 8: The predicted Baidu index of mask in Beijing (a), Tianjin (b), and Shijiazhuang (c).

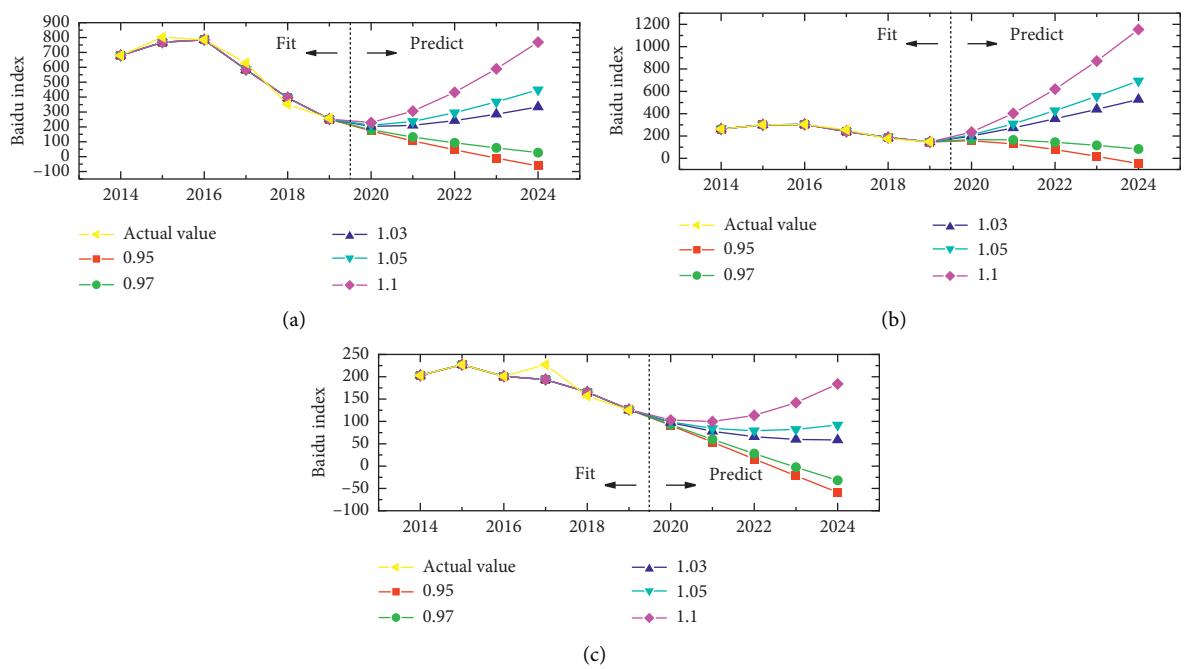

Figure 9: The predicted Baidu index of air purifier in Beijing (a), Tianjin (b), and Shijiazhuang (c).

Figure 12. With the increasing growth rate of AQI, the Baidu index of energy conservation and emission reduction in Tianjin begins to pick up in 2020. On the contrary, Beijing and Shijiazhuang continued to decline in 2020 and began to pick up in 2021. Among them, Shijiazhuang's Baidu index on energy conservation and emission reduction is picking up faster than Beijing. This may be due to the more severe air pollution in Shijiazhuang.

Compared with energy saving and emission reduction, the efficiency for air protection of green travel is low. From

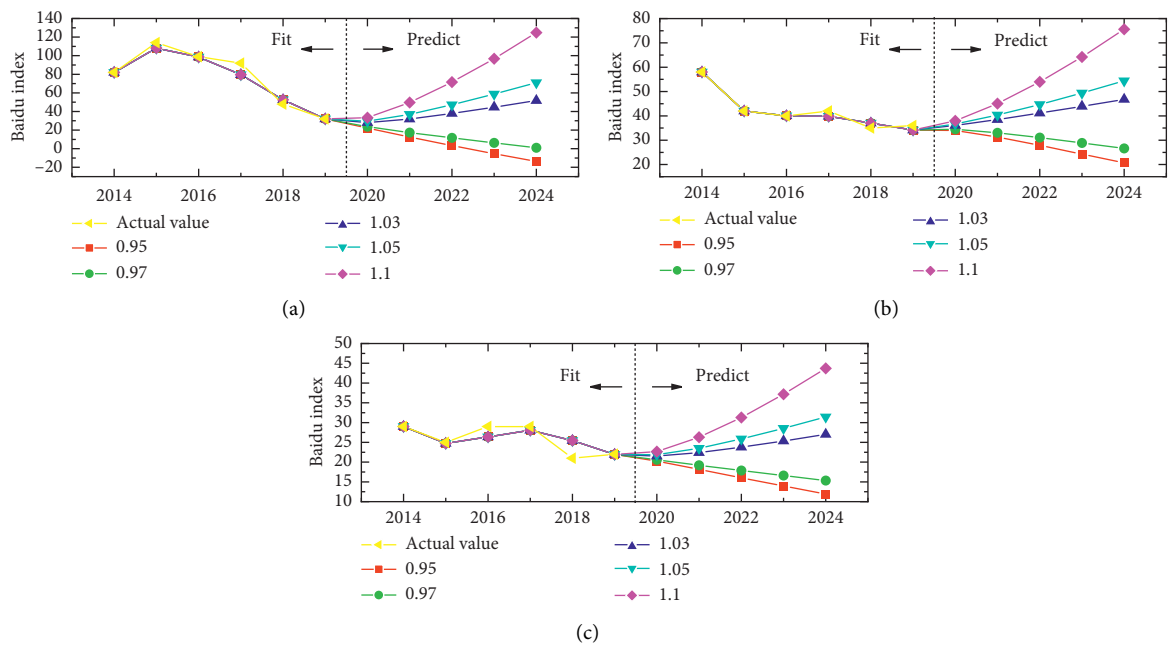

Figure 10: The predicted Baidu index of PM2.5 detector in Beijing (a), Tianjin (b), and Shijiazhuang (c).

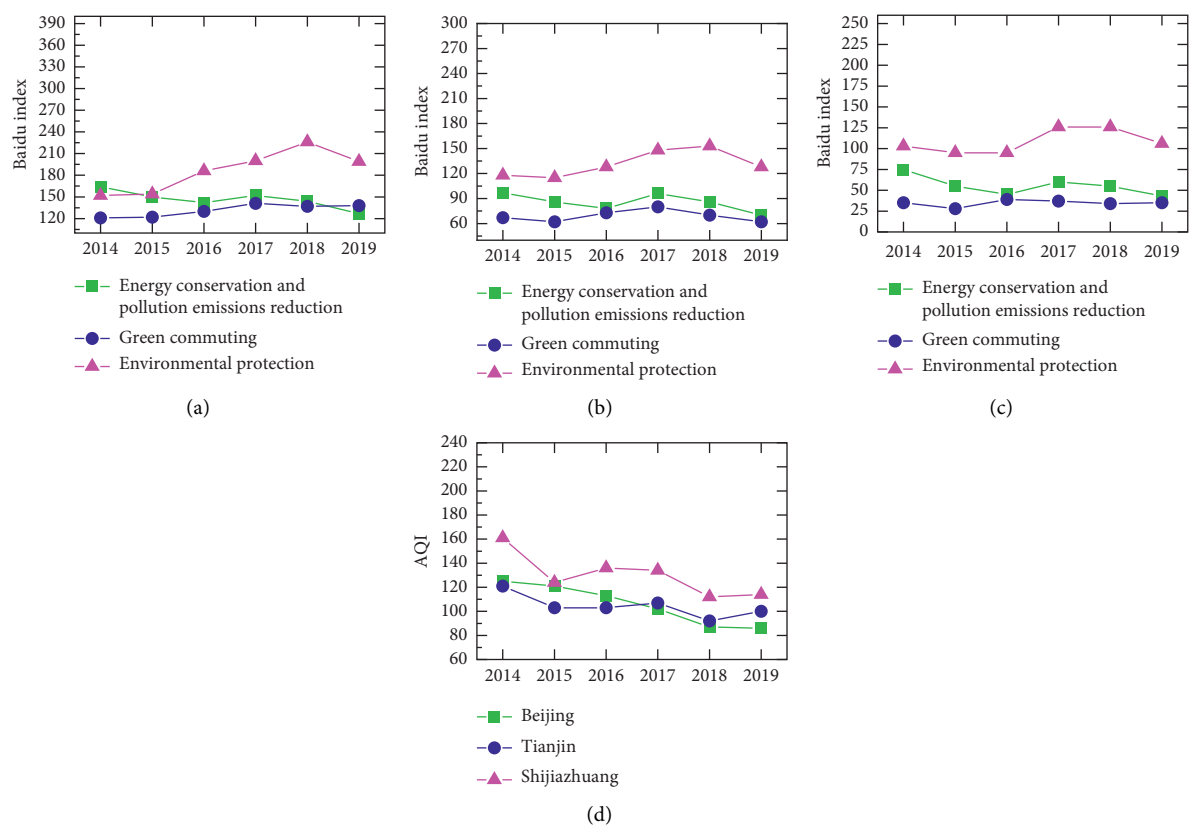

Figure 11: The relationship between Baidu index of environmental protection behavior and AQI. (a) Beijing. (b) Tianjin. (c) Shijiazhuang. (d) AQI of three cities.

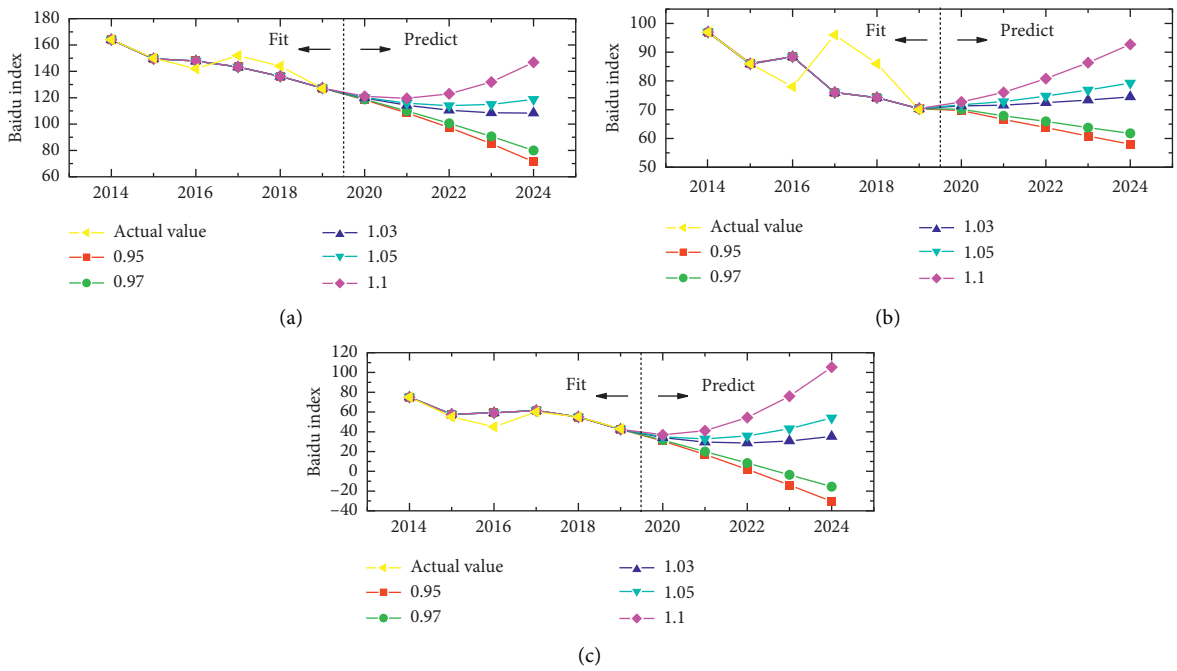

Figure 12: The predicted Baidu index of energy conservation and pollution emissions reduction in Beijing (a), Tianjin (b), and Shijiazhuang (c).

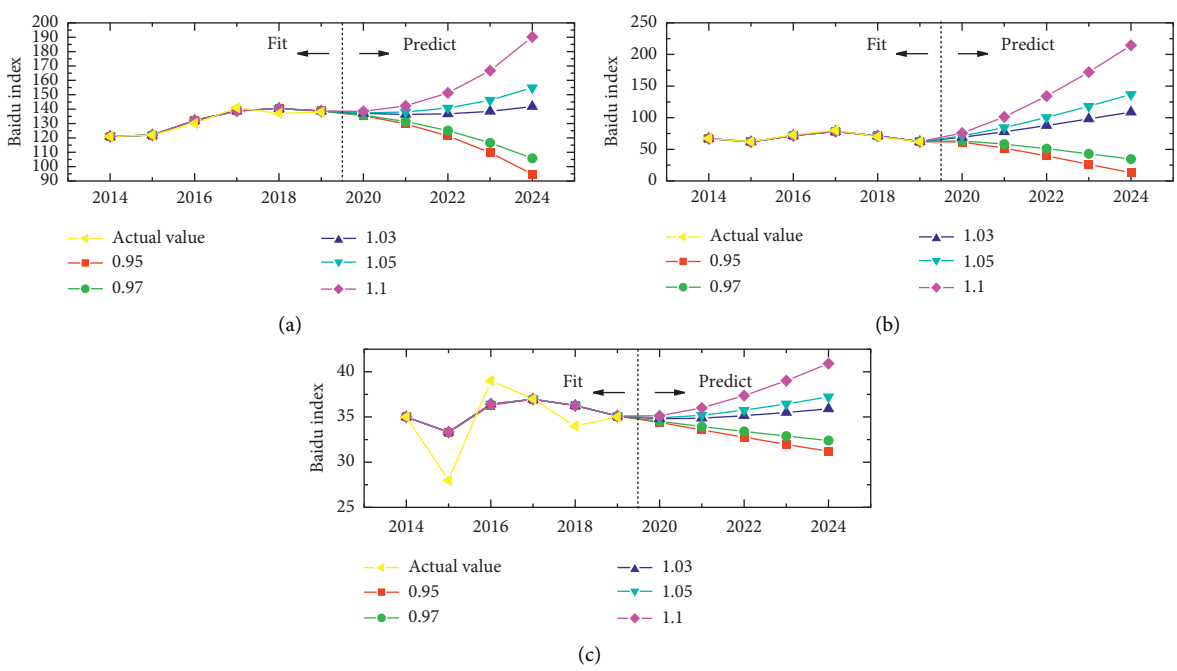

Figure 13: The predicted Baidu index of Green commuting in Beijing (a), Tianjin (b), and Shijiazhuang (c).

Figure 13, the larger AQI leads to the higher Baidu index of green travel. This shows that the aggravation of air pollution stimulates more green travel behavior. Besides, Beijing's search index is bigger than Tianjin and Shijiazhuang. It shows that Beijing's public awareness of environmental protection is stronger. Judging from the change range, Beijing's forecast curve is concave to a greater extent. It shows that, with the continuous deterioration of air quality, the public practice of green travel in Beijing is more intense.

Different from energy saving and emission reduction and green travel, environmental protection belongs to conceptual air quality control. The search may be just for understanding, without an in-depth understanding of specific protective behavior, so protective measures may

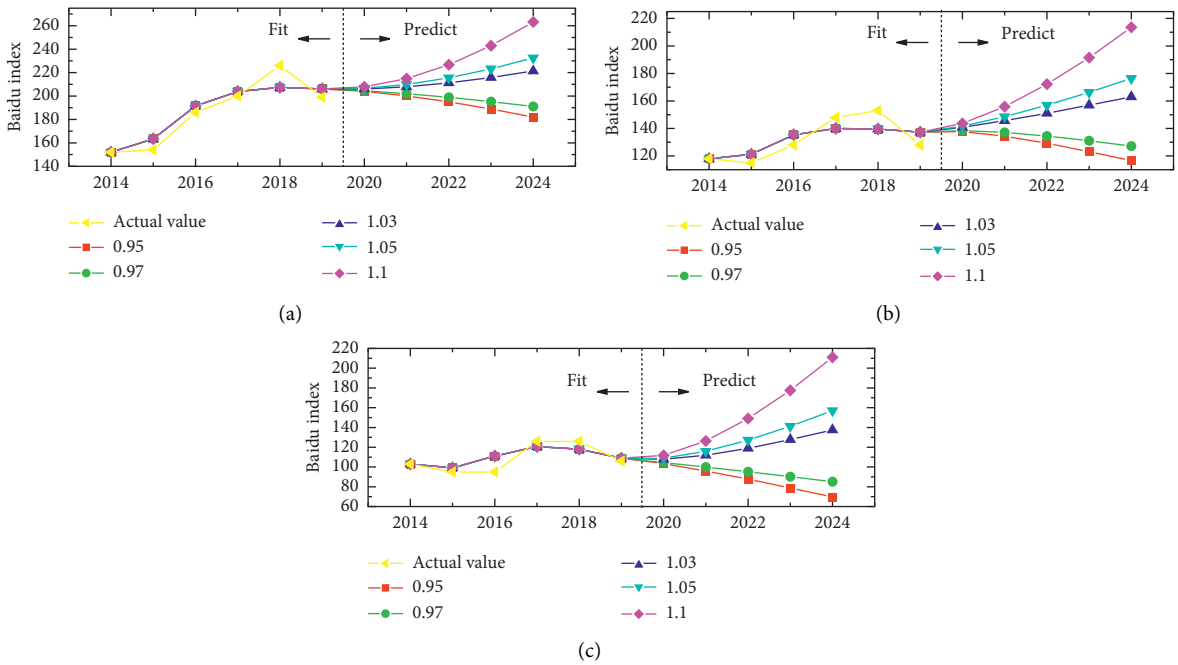

Figure 14: The predicted Baidu index of environmental protection in Beijing (a), Tianjin (b), and Shijiazhuang (c).

not be taken. According to the prediction results, a larger AQI still leads to a higher Baidu index of environmental protection (Figure 14). However, compared with energy conservation and emission reduction and green travel, the Baidu index of environmental protection is the highest, which shows that most of the public do not know enough about air protection measures and can further tap the public's environmental protection power in the future. Besides, it is found that the public's Baidu index of environmental protection in Beijing is higher than that in Tianjin and Shijiazhuang. This shows that Beijing has the greatest potential environmental protection force from the public, and the future environmental protection can be started from the public perspective.

5. Conclusion and Implication

In this paper, the public's perception level and self-protection demand of air pollution in Beijing, Tianjin, and Shijiazhuang are analyzed to improve air pollution. First of all, the Baidu index is used to measure the public's perception level and self-protection demand of air pollution. Then, an improved FNGMC (1, N) model is proposed. The numerical results show that the model has good prediction performance. According to the analysis and forecast results of the public's perception level and self-protection demand of air pollution, the main conclusions are as follows. Firstly, the public's perception of air pollution in three cities has been declining from 2014 to 2019. However, this perception level will rise in the future due to the deterioration of air quality. Among them, Beijing has the highest public perception level. Secondly, the public's self-protection demand for air pollution in three cities has been declining from 2014 to 2019. However, the self-protection demand will rise in the future due to the deterioration of air quality. Among them, Tianjin has the highest self-protection demand.

For the suggestions, first of all, environmental protection departments should raise public awareness of air pollution and make air control a positive demand, rather than a mandatory response. Secondly, it is necessary to assess the needs of people exposed to air pollution and formulate targeted air pollution protection programs. Finally, refer to the degree of air pollution and the public's willingness to formulate appropriate prevention and control measures.

For the limitations and future research directions, the Baidu index is often difficult to cover the people with the most serious air pollution, such as the elderly, children, and outdoor workers. In addition, there are few keywords in Baidu Index studied in this paper, which are not enough to express the real situation. Generally speaking, it is feasible to use the improved FNGMC (1, N) model and Baidu index to predict the public's perception level and self-protection demand of air pollution. Future research will be promoted nationwide, and the keyword types of the Baidu index will be further improved. Besides, the exposed groups of air pollution will be further divided to obtain more accurate research results.

Data Availability

The data used to support the findings of this study are included within the article.

Conflicts of Interest

The authors declare that they have no conflicts of interest.

Acknowledgments

This work was supported by the Social Science Federation Project of Handan (2021058 and 2021077).

References

[1] A. A. Almetwally, M. Bin-Jumah, and A. A. Allam, "Ambient air pollution and its influence on human health and welfare: an overview," *Environmental Science and Pollution Research*, vol. 27, no. 20, pp. 24815–24830, 2020.

[2] Y. Wang, T. Lu, and Y. Qiao, "The effect of air pollution on corporate social responsibility performance in high energy-consumption industry: evidence from Chinese listed companies," *Journal of Cleaner Production*, vol. 280, Article ID 124345, 2021.

[3] Y. Zheng, J. Peng, J. Xiao et al., "Industrial structure transformation and provincial heterogeneity characteristics evolution of air pollution: evidence of a threshold effect from China," *Atmospheric Pollution Research*, vol. 11, no. 3, pp. 598–609, 2020.

[4] S. Zhong, Z. Yu, and W. Zhu, "Study of the effects of air pollutants on human health based on Baidu indices of disease symptoms and air quality monitoring data in beijing, China," *International Journal of Environmental Research and Public Health*, vol. 16, no. 6, 1014 pages, 2019.

[5] J. Chen, J. Huang, X. Huang et al., "How does new environmental law affect public environmental protection activities in China? Evidence from structural equation model analysis on legal cognition," *Science of The Total Environment*, vol. 714, Article ID 136558, 2020.

[6] K. Yang, Y. Shi, Y. Luo et al., "Assessing spatiotemporal air environment degradation and improvement represented by $PM_{2.5}$ in China using two-phase hybrid model," *Sustainable Cities and Society*, vol. 59, Article ID 102180, 2020.

[7] W. Qu, G. Qu, X. Zhang et al., "The impact of public participation in environmental behavior on haze pollution and public health in China," *Economic Modelling*, vol. 98, pp. 319–335, 2021.

[8] T. Reames and M. Bravo, "People, place and pollution: investigating relationships between air quality perceptions, health concerns, exposure, and individual- and area-level characteristics," *Environment International*, vol. 122, pp. 244–255, 2019.

[9] A. Benedetti, B. Levis, G. Ruecker et al., "An empirical comparison of three methods for multiple cutoff diagnostic test meta-analysis of the Patient Health Questionnaire-9 (PHQ-9) depression screening tool using published data vs. individual level data," *Research Synthesis Methods*, vol. 11, 2020.

[10] D. Kostopoulos, S. Meyer, and C. Uhr, "Google search volume and individual investor trading," *Journal of Financial Markets*, vol. 49, Article ID 100544, 2020.

[11] W. Li, G. Yang, and X. Li, "Correlation between $PM_{2.5}$ pollution and its public concern in China: evidence from Baidu index," *Journal of Cleaner Production*, vol. 293, Article ID 126091, 2021.

[12] L. Wang, X. Zhou, M. Lu et al., "Impacts of haze weather on tourist arrivals and destination preference: analysis based on Baidu Index of 73 scenic spots in Beijing, China," *Journal of Cleaner Production*, vol. 273, Article ID 122887, 2020.

[13] D. Dong, X. Xu, W. Xu et al., "The relationship between the actual level of air pollution and residents' concern about air pollution: evidence from shanghai, China," *International Journal of Environmental Research and Public Health*, vol. 16, no. 23, 4784 pages, 2019.

[14] Y. Cao, K. Yin, X. Li et al., "Forecasting CO_2 emissions from Chinese marine fleets using multivariable trend interaction grey model," *Applied Soft Computing*, vol. 104, Article ID 107220, 2021.

[15] H. Duan and X. Pang, "A multivariate grey prediction model based on energy logistic equation and its application in energy prediction in China," *Energy*, vol. 229, Article ID 120716, 2021.

[16] M. Kiran, P. Shanmugam, A. Mishra et al., "A multivariate discrete grey model for estimating the waste from mobile phones, televisions, and personal computers in India," *Journal of Cleaner Production*, vol. 293, Article ID 126185, 2021.

[17] L. Wu, X. Gao, Y. Xiao et al., "Using a novel multi-variable grey model to forecast the electricity consumption of Shandong Province in China," *Energy*, vol. 157, pp. 327–335, 2018.

[18] S. Ding, "A novel discrete grey multivariable model and its application in forecasting the output value of China's high-tech industries," *Computers & Industrial Engineering*, vol. 127, pp. 749–760, 2019.

[19] Z. Wang and Q. Li, "Modelling the nonlinear relationship between CO_2 emissions and economic growth using a PSO algorithm-based grey Verhulst model," *Journal of Cleaner Production*, vol. 207, pp. 214–224, 2019.

[20] L. Jiang, S. He, and H. Zhou, "Spatio-temporal characteristics and convergence trends of $PM_{2.5}$ pollution: a case study of cities of air pollution transmission channel in Beijing-Tianjin-Hebei region, China," *Journal of Cleaner Production*, vol. 256, Article ID 120631, 2020.

[21] X. Qiu, Q. Ying, S. Wang et al., "Significant impact of heterogeneous reactions of reactive chlorine species on summertime atmospheric ozone and free-radical formation in north China," *Science of the Total Environment*, vol. 693, Article ID 133580, 2019.

[22] N. Bei, X. Li, and X. Tie, "Impact of synoptic patterns and meteorological elements on the wintertime haze in the Beijing-Tianjin-Hebei region, China from 2013 to 2017," *Science of the Total Environment*, vol. 704, Article ID 135210, 2020.

[23] B. Fu, X. Gao, and L. Wu, "Grey relational analysis for the AQI of Beijing, Tianjin, and Shijiazhuang and related countermeasures," *Grey Systems-Theory and Application*, vol. 8, no. 2, pp. 156–166, 2018.

[24] F. Yuan and C. Lee, "Intelligent sales volume forecasting using Google search engine data," *Soft Computing*, vol. 24, no. 3, pp. 2033–2047, 2020.

[25] S. Pu, Z. Shao, M. Fang et al., "Spatial distribution of the public's risk perception for air pollution: a nationwide study in China," *Science of The Total Environment*, vol. 655, pp. 454–462, 2019.

[26] D. Wu, "Empirical study of knowledge withholding in cyberspace: integrating protection motivation theory and theory of reasoned behavior," *Computers in Human Behavior*, vol. 105, Article ID 106229, 2020.

[27] G. Bradley, Z. Babutsidze, A. Chai et al., "The role of climate change risk perception, response efficacy, and psychological adaptation in pro-environmental behavior: a two nation study," *Journal of Environmental Psychology*, vol. 68, Article ID 101410, 2020.

[28] M. Clarke, Z. Ma, S. Snyder et al., "Understanding invasive plant management on family forestlands: an application of protection motivation theory," *Journal of Environmental Management*, vol. 286, Article ID 112161, 2021.

[29] S. Verkoeyen and S. Nepal, "Understanding scuba divers' response to coral bleaching: an application of protection motivation theory," *Journal of Environmental Management*, vol. 231, pp. 869–877, 2019.

[30] J. Soares, I. Miguel, C. Venâncio et al., "Public views on plastic pollution: knowledge, perceived impacts, and pro-environmental behaviours," *Journal of Hazardous Materials*, vol. 412, Article ID 125227, 2021.

[31] Y. Tan and X. Mao, "Assessment of the policy effectiveness of central inspections of environmental protection on improving air quality in China," *Journal of Cleaner Production*, vol. 288, Article ID 125100, 2021.

[32] T. Tien, "A research on the grey prediction model GM (1, n)," *Applied Mathematics and Computation*, vol. 218, no. 9, pp. 4903–4916, 2012.

[33] L. Wu, S. Liu, L. Yao et al., "Grey system model with the fractional order accumulation," *Communications in Nonlinear Science and Numerical Simulation*, vol. 18, no. 7, pp. 1775–1785, 2013.

[34] L. Wu and Z. Zhang, "Grey multivariable convolution model with new information priority accumulation," *Applied Mathematical Modelling*, vol. 62, pp. 595–604, 2018.

[35] X. Ma and Z. Liu, "Research on the novel recursive discrete multivariate grey prediction model and its applications," *Applied Mathematical Modelling*, vol. 40, no. 7-8, pp. 4876–4890, 2016.

Hindawi
Journal of Mathematics
Volume 2021, Article ID 8237600, 10 pages
https://doi.org/10.1155/2021/8237600

Research Article

A Fractional Grey Multivariable Model for Modeling Fresh Graduates' Career Choice

Xiaoen Yang, Taiming Cui, and Minghuan Shou

School of Economics, Zhejiang University of Finance & Economics, Hangzhou 310018, China

Correspondence should be addressed to Minghuan Shou; 13675778273@163.com

Received 13 June 2021; Accepted 29 June 2021; Published 7 July 2021

Academic Editor: Shuhua Mao

Aiming at exploring the effect of four factors on fresh graduate's three popular career choices of continuing studying, working in state-owned enterprises, and working in private enterprises, this paper collects the specific information of 3237 students and builds the GM (0, N) model. The four variables include student's grade point average (GPA), socioeconomic status (SES), gender, and whether the student comes from an urban household. Furthermore, this paper also considers the effect of the fractional order and proposes a fractional grey model (FGM (0, N) model) to enhance the performance of the traditional model. Eventually, the study finds that there are still some students with financial problems, which makes some negative effects on their choices of continuing studying and working in state-owned enterprises. Additionally, all the other three factors show the positive influence on the three choices. Besides, GPA shows the most positive effect on the choices of continuing studying as well as working in a state-owned enterprise; gender and SES have the greatest impact on the choice of working in a private enterprise.

1. Introduction

With the development of the society, the career choice of the fresh graduates has become more abundant; students can choose to continue studying, start their own businesses, or go directly to work in state-owned enterprises. At the same time, people's attention to employment tends to increase; there is now a large amount of literature that studies what factors affect people's career choices. Sehagl and Nasim [1] proposed that technology management skills and communication skills played an important role in choosing jobs. Gokuladas [2] focused on studying the factors influencing the first-career choice of undergraduate engineers and found that students from urban areas were more likely to be driven by intrinsic factors, while those from rural/semiurban were more likely to be influenced either by extrinsic or interpersonal reasons. Koch et al. [3] proposed that interest was also an important factor, and the high school counselor was the least influential person with respect to students' choice of careers in construction management. Mead et al. [4], Myburgh [5], and Greenman [6] made the conclusion that there were significant differences among racial/ethnic groups in factors that appeared to influence their career paths. Educational level of parents had also been proved to be an influential factor [7]. While in some papers, firsthand information sources (e.g., the work experience and personal experiences) were more influential than secondhand sources (e.g., class materials and faculty) [8]. Moreover, some people thought "students' self-efficacy and occupational aspiration" were the most important factor, followed by "tradition and cultural value," "career guidance," "support from parents," and "external consultation" [9].

In summary, there are many studies on exploring the influence of factors on fresh graduate's career choices. And, governments can take advantage of all the papers to provide the most suitable assistance to different students. However, there is no doubt that how to confirm student's need and provide suitable help is still complicated. Aiming at providing some reference for this problem, this paper selects four variables directly related to students and plans to explore the effect of these four factors on fresh graduate's career choices. These factors include student's grade point average (GPA), gender, family socioeconomic status (SES), and whether the student comes from an urban household or

not. Similarly, after summarizing the development direction of the graduates, this paper mainly selects three choices, including continuing study (Choice-1), working in private enterprises (Choice-2), and working in state-owned enterprises (Choice-3).

To finish the task, this paper builds the GM (0, N) model. And, there are two reasons for choosing this model: the first one is that grey system theory has been widely used in various fields such as natural science, social science, and engineering science [10]. And, there are many papers that can prove the good performance of the grey models. Additionally, the second reason is that, based on the results of the GM (0, N) model, this paper can obtain the effect of factors. Besides, due to the requirement of a high accuracy, the fractional orders have been added into this model, which have been proved to increase the performance of the models.

The purposes of this paper are as follows:

Firstly, some statistical description analysis can be performed to obtain the most popular career choice of fresh graduates and the specific information of students' family socioeconomic status.

Secondly, this paper plans to propose a fractional grey model (FGM (0, N) model) by considering the function of the fractional order, while building the GM (0, N) model.

Thirdly, the FGM (0, N) model is built to explore the effect of four factors on fresh graduate's career choices. Additionally, based on the results of models with similar performance, robustness of results can be tested. Accordingly, some suggestions on how to set up courses for students with different performances can be made.

There are four main contributions in this paper:

On one hand, there are two theoretical contributions: firstly, after getting the bad results of the GM (0, N) model, this paper chooses to consider the effect of the fractional order and proposes a new model, the GM (0, N) model with the fractional order (FGM (0, N) model). After comparing the accuracy, we find that the FGM (0, N) model can help scholars make better predictions. Besides it, since there are few studies on exploring the effect of SES on graduates' career choices, what we do in this paper can perfectly fill in the research gap.

On the other hand, this paper also has a significant implication contribution in two parts: the strongest one is to provide a guideline for the universities to set up the courses based on the results obtained in this paper. Students with suitable skills can be better suitable for the development of the society. Besides, this can also help save the sources of enterprises to teach students. The other contribution is that the results of data description can tell that there are still many students with financial problems, which significantly affect their career choice. Thus, scholars and governments should pay more attention to consider how to provide some necessary help.

The remaining of this paper is organized as follows: in Section 2, related works are introduced. Section 3 introduces some models used in the paper as well as the statistical description of the dataset. Section 4 shows the analysis results. Section 5 presents the conclusion and some suggestions.

2. Literature Review

To clearly show the summary of the recent studies, this paper divides the whole section into three parts. The first part contains the main studies on the effect of some factors on student's performance, while the work related to the models has been shown in parts 2 and 3.

2.1. The Relationship between Students' Performance and Their Socioeconomic Status as Well as Other Factors. Until now, the relationship between the fresh graduates' socioeconomic status backgrounds and their choices is yet to be understood completely. We focus on performance on graduates' choices in an urban school district to identify what role SES plays.

The excessive gap between the rich and the poor is still one of the important existing problems in the world. According to data released by the World Bank, 5% of the people in the United States hold more than 60% of the country's wealth. In 2018, China's Gini coefficient for measuring the gap between the rich and the poor reached 0.474, far exceeding the international warning line of 0.4, which shows that there is a large gap between the rich and poor. However, economic conditions will significantly affect people's decision-making, for example, the benevolence-dependability value of those of lower perceived socioeconomic status significantly affected their intertemporal choices [11]. The effect of poverty on students' achievement has also been widely studied. Recent studies showed that students from low socioeconomic status backgrounds had lower academic performance and a chronic risk of lower academic growth during early adolescence [12, 13]. We recognize that other factors aside from student poverty may contribute to explain variations in achievement. For example, Li et al. [14], based on a two-year longitudinal dataset of 942 middle-school students from a high-poverty district, found that emotional control had the strongest relation with GPA instead of the social perceptions and academic performance.

2.2. Recent Studies on the GM (0, N) Model. Grey systems, proposed by Deng [15, 16], have been widely utilized to cope with uncertain problems with poor and incomplete information [17]. And, there are many popular grey models, such as Grey Verhulst model [18], Grey Markov model [19], and so forth [20–22]. Among them, the GM (1, 1) model is the main forecasting model in grey systems. By accumulating generation operation in the GM (1, 1) model, the random disturbance of a short sequence is weakened [23, 24]. This model has been extensively used in various fields, especially in the field of energy consumption [25–28].

The abovementioned grey models all are used in time series prediction and not suitable for making predictions on cross-sectional data. Thus, this paper chooses to use the GM (0, N) model which can help deal with this problem and obtain the effect of input variables on the output factor. The GM (0, N) model is a special form of the GM (1, N) model with no derivatives. The two models (GM (0, N) model and GM (1, N) model) are a typical multivariable forecast model in grey system theory [29]. Kung and Wen [30] successfully used the GM (0, N) model to analyze several variables of firm attributes. Tian et al. [31] proposed a novel GM (0, N) model to solve the problem of cost forecasting of commercial aircraft. Due to the successful applications of using the GM (0, N) model to explore the influence of variables in previous papers, this study also plans to take good advantage of this method to obtain the effect of several factors on fresh graduate's career choices.

2.3. Application of the Fractional Order. Fractional calculus has been used in various fields of science, engineering, applied mathematics, and economics [32]. Similarly, numeric studies on fractional grey models have been performed in recent years. Previous GM (1, 1) models have been based on first-order accumulation techniques which revealed only partial memories and lacked the potential to represent overall memories fairly [33]. The fractional model has an accumulated generating order that can effectively manifest the nonlinear characteristics of real systems [34]. Due to the positive effect of the fractional order, scholars pay more attention to explore the possibility of combining the traditional models with the fractional order [35–37]. And, most of the results show that the performance of the fractional models can be better.

Based on the above summary, it is not difficult to get the following conclusions: firstly, fresh graduates' career choices can be affected by many variables. However, SES, as one of the main influential factors for students' performance, has not been widely used in forecasting students' career choices. Therefore, it is reasonable for us to consider the effect of SES, which is also one of the contributions in this paper. Secondly, there are many papers to prove the good performance of the GM (0, N) model in predictions and the positive effect of the fractional order to enhance the performance of the model. Thus, this paper proposes a fractional GM (0, N) model (FGM (0, N)) reasonably.

3. Methods

3.1. The Brief Introduction of Classic GM (0, N) Model. Let

$$X_1^{(0)} = \left(x_1^{(0)}(1), x_1^{(0)}(2), \ldots, x_1^{(0)}(n)\right), \tag{1}$$

be the data sequence of system behavior characteristic and

$$\begin{aligned} X_2^{(0)} &= \left(x_2^{(0)}(1), x_2^{(0)}(2), \ldots, x_2^{(0)}(n)\right), \\ X_3^{(0)} &= \left(x_3^{(0)}(1), x_3^{(0)}(2), \ldots, x_3^{(0)}(n)\right), \\ &\vdots \\ X_N^{(0)} &= \left(x_N^{(0)}(1), x_N^{(0)}(2), \ldots, x_N^{(0)}(n)\right), \end{aligned} \tag{2}$$

be the sequence of related factors:

$$X_i^{(1)} = \left(x_i^{(1)}(1), x_i^{(1)}(2), \ldots, x_i^{(1)}(n)\right), \tag{3}$$

which is the 1-AGO sequence of $X_i^{(0)}$, where $x_i^{(1)}(k) = \sum_{l=1}^{k} x_i^{(1)}(l)$, $i = 1, 2, \ldots, N$, and

$$\begin{aligned} x_1^{(1)}(k) = b_2 x_2^{(1)}(k) + b_3 x_3^{(1)}(k) + \cdots \\ + b_N x_N^{(1)}(k) + a, \quad k = 2, 3, \ldots, n, \end{aligned} \tag{4}$$

which is the basic form of the GM (0, N) model.

The GM (0, N) model has similarities with multiple regression, but there is a fundamental difference. The GM (0, N) model generates series 1-AGO series by the accumulation of the original data.

Let $X_i^{(0)}$ and $X_j^{(1)}$, $j = 2, 3, \ldots, N$, be described as in Definition 1, and the input matrix and the output vector of the model are, respectively,

$$\begin{aligned} B &= \begin{bmatrix} x_2^{(1)}(1) & x_3^{(1)}(1) & \cdots & x_N^{(1)}(1) & 1 \\ x_2^{(1)}(2) & x_3^{(1)}(2) & \cdots & x_N^{(1)}(2) & 1 \\ \vdots & \vdots & \vdots & \vdots & \vdots \\ x_2^{(1)}(n) & x_3^{(1)}(n) & \cdots & x_N^{(1)}(n) & 1 \end{bmatrix}, \\ Y &= \begin{bmatrix} x_1^{(1)}(1) \\ x_1^{(1)}(2) \\ \vdots \\ x_1^{(1)}(n) \end{bmatrix}. \end{aligned} \tag{5}$$

Let the parameters be listed as $\hat{a} = [b_2, b_3, \ldots, b_N, a]^T$, and the equation form of the GM (0, N) model is $Y = B\hat{a}$; then, the least square estimation of the model is $\hat{a} = (B^T B)^{-1} B^T Y$.

3.2. Introduction to the FGM (0, N) Model. The fractional order accumulation generation method and prediction model have been proved to be an effective method to improve the accuracy of the grey models [33]. Therefore, a novel model, the FGM (0, N) model, is proposed in this paper to reduce the prediction error.

Let

$$X_1^{(0)} = \left(x_1^{(0)}(1), x_1^{(0)}(2), \ldots, x_1^{(0)}(n)\right), \tag{6}$$

be the data sequence of system behavior characteristic and

$$\begin{aligned} X_2^{(0)} &= \left(x_2^{(0)}(1), x_2^{(0)}(2), \ldots, x_2^{(0)}(n)\right), \\ X_3^{(0)} &= \left(x_3^{(0)}(1), x_3^{(0)}(2), \ldots, x_3^{(0)}(n)\right), \\ &\vdots \\ X_N^{(0)} &= \left(x_N^{(0)}(1), x_N^{(0)}(2), \ldots, x_N^{(0)}(n)\right), \end{aligned} \tag{7}$$

be the sequence of related factors.

Let $x_i^{(r)}(k) = \sum_{l=1}^{k} \binom{k-l+r-1}{k-l} x_i^{(0)}(l)$, $i = 1, 2, \ldots, N$ and $k = 1, 2, \ldots, n$, be the $r\,(0 < r < 1)$ order-accumulated generating operator (r-AGO). Set $\binom{r-1}{0} = 1$, $\binom{k-1}{k} = 0$, $k = 1, 2, \ldots, n$, and $\binom{k-l+r-1}{k-l} = ((r + k - l - 1)\ (r + k - l - 2) \cdots (r + 1)r)/(k - l)!$:

$$X_i^{(r)} = \left(x_i^{(r)}(1), x_i^{(r)}(2), \ldots, x_i^{(r)}(n)\right), \tag{8}$$

which is the r order accumulated generation sequence.

Let

$$X_1^{(0)} = \left(x_1^{(0)}(1), x_1^{(0)}(2), \ldots, x_1^{(0)}(n)\right), \tag{9}$$

be the data sequence of system behavior characteristic. Let $\alpha^{(1)} x_1^{(1-r)}(k) = x_1^{(1-r)}(k) - x_1^{(1-r)}(k-1)$ be the $r\,(0 < r < 1)$ order-inverse accumulated generating operator (r − IAGO):

$$\alpha^{(1)} X_1^{(0)} = \alpha^{(1)} X_1^{(1-r)} = \left(\alpha^{(1)} x_1^{(1-r)}(1), \alpha^{(1)} x_1^{(1-r)}(2), \ldots \alpha^{(1)} x_1^{(1-r)}(n)\right), \tag{10}$$

which is the r order inverse accumulated generation sequence.

Let $X_i^{(0)}$ and $X_j^{(1)}$, $j = 2, 3, \ldots, N$, be described as in Definition 1:

$$x_1^{(r)}(k) = b_2 x_2^{(r)}(k) + b_3 x_3^{(r)}(k) + \cdots + b_N x_N^{(r)}(k) + a, \quad k = 2, 3, \ldots, n, \tag{11}$$

which is the basic form of the FGM (0, N) model.

The least square method is used to estimate the parameters, $\hat{a} = [b_2, b_3, \ldots, b_N, a]^T = (B^T B)^{-1} B^T Y$:

$$B = \begin{bmatrix} x_2^{(r)}(1) & x_3^{(r)}(1) & \cdots & x_N^{(r)}(1) & 1 \\ x_2^{(r)}(2) & x_3^{(r)}(2) & \cdots & x_N^{(r)}(2) & 1 \\ \vdots & \vdots & \vdots & \vdots & \vdots \\ x_2^{(r)}(n) & x_3^{(r)}(n) & \cdots & x_N^{(r)}(n) & 1 \end{bmatrix}, \quad Y = \begin{bmatrix} x_1^{(r)}(1) \\ x_1^{(r)}(2) \\ \vdots \\ x_1^{(r)}(n) \end{bmatrix}. \tag{12}$$

3.3. Modeling Steps of the FGM (0, N) Model

Step 1: determine the system behavior characteristic data sequence $X_1^{(0)}$ and related factor sequence $X_j^{(0)}$, $j = 2, 3, \ldots, N$

Step 2: calculate and generate system behavior characteristic data sequence, and related factor sequences, and $r\,(0 < r < 1)$ order accumulated generation sequences $X_i^{(r)}$, $i = 1, 2, \ldots, N$

Step 3: the FGM (0, N) model was established by the sequence generated by $r\,(0 < r < 1)$ order accumulation

Step 4: the least square method is used to estimate the parameter $\hat{a} = [b_2, b_3, \ldots, b_N, a]^T$

Step 5: according to formula (11), the prediction of sequence data is realized

Step 6: the final data $\hat{X}_1^{(0)}$ is obtained by using r − IAGO inverse accumulated generating operator to restore the predicted data

Besides, the accuracy of this article is measured by the ratio of the number of correct predictions to the total number.

4. Explore the Effect of Factors on Fresh Graduate's Career Choice: An Application of the FGM (0, N) Model

In this section, two models (GM (0, N) model and FGM (0, N) model) have been performed to forecast graduates' career choices and identify the influential factors. The career choices mainly contain three parts, including continuing studying, working in state-owned enterprises, and working in private enterprises. Besides, this paper only selects four different input variables, including GPA, gender, SES, and whether the student comes from an urban household or not.

And, in order to compare the results of models, this paper sets the ratio of the training set and test set as 8 : 2.

4.1. The Statistical Description of the Dataset. This article takes 3237 fresh graduates as the research object. It can be seen from Figure 1 that more than 60% of students still regard direct employment as their first choices after graduation and tend to choose to sign employment agreements to protect their rights and interests. As people's living standards improve, the number of students studying abroad has also increased, which accounts for 14% of the total number and even exceeds the number of people who choose to study for a postgraduate degree in China. This may be caused by the fact that the overseas postgraduate education system is shorter than that in China and studying abroad can avoid being forced to work directly because of failing to pass the postgraduate entrance examination in China. In addition, only 2% of the students do not find a job and wait for work at home, which shows that China has solved the problem of high unemployment at this stage well.

This article also counts the number of students who have declared economic problems. As shown in Figure 2, 89% of the students have no family financial problems, while 11% of the students have poor family financial status, of which 7% of students' family economic status is defined as general poverty, while 4% of students' family economic status is extremely poor. In other words, more than 10% of the families still have financial problems, and nearly 5% of the families have serious financial problems. This also reflects the large gap between the rich and the poor that has emerged in the country at this stage. And, the explanation and statistical description of whole variables have been shown in Tables 1 and 2.

4.2. Influential Factors for Fresh Graduate's Career Choice of Continuing Studying. In this part, we totally collect the specific information of 3237 students (male: 33% and female: 67%), and the average GPA is 3.73. In addition, this paper sets the output number of 26.6% of the whole dataset (choice of continuing studying) as 1 and the others as 0.

It is not difficult to obtain from Figure 3 that the results of the GM (0, N) model are 53.9% and 56.57%, respectively, for the training set and testing set. Besides, as the fractional order changes, the performance of the model changes a lot. Among them, although the training-set accuracy of the models with the fractional order ranging from 0.2 to 0.9 is all over 50%, there are much fluctuation in the testing-set accuracy. And, the testing-set accuracy is smaller than the result of the traditional model.

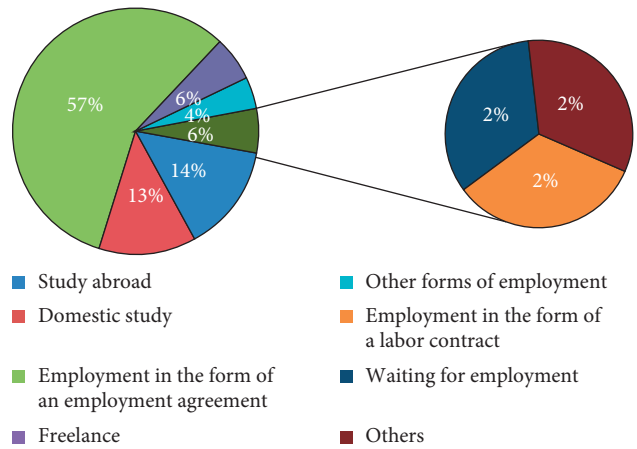

Figure 1: Career choice of graduates.

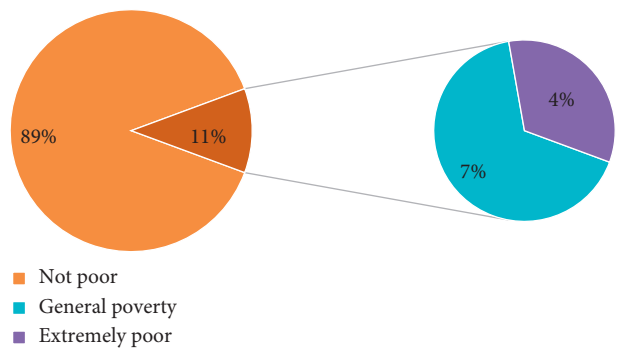

Figure 2: Students' family socioeconomic status.

However, if we set the fractional order to 0.1, the training-set and testing-set accuracy is 73.86% and 74.81%, respectively, which mean that the performance of this model is much better than the traditional one. And, we can choose this one to identify the influential factors.

From the results shown in Table 3, this paper easily gets the effect of different factors on fresh graduate's career choices according to the coefficient. And, if we set r equaling to 0.1, we can use the least square method to estimate the parameter $\hat{a} = [b_2, b_3, \ldots, b_N, a]^T = [0.095, -0.092, 0.171, 0.019, -0.858]^T$. And, the equation is

$$\begin{aligned} \text{choice}^{(0.1)}(k) &= 0.095\,\text{Town}^{(0.1)}(k) - 0.092\,\text{SES}^{(0.1)}(k) + 0.171\,\text{GPA}^{(0.1)}(k) \\ &\quad + 0.019\,\text{Gender}^{(0.1)}(k) - 0.858. \end{aligned} \tag{13}$$

If we change the value of r, the specific parameters and equation will also change.

We can get the following conclusions: firstly, GPA shows the most positive effect, followed by town. This means

Table 1: Explanation of variables.

Variable	Explanation
Town	Whether the student comes from an urban household or not (yes = 1; no = 0)
SES	Student's socioeconomic status (general = 0; poor = 1; extremely poor = 2)
GPA	Student's grade point average
Gender	Male = 1; female = 0

Table 2: Statistical description of the original data.

	Obs.	Mean	Std. dev.	Min	Max
Whether continuing studying	3237	0.2666	0.4423	0	1
GPA	3237	3.7270	0.5000	1.54	4.76
Gender	3237	0.3299	0.4703	0	1
SES	3237	0.1504	0.4508	0	2
Town	3237	0.5555	0.4970	0	1
Whether working in a state-owned enterprise	2374	0.1664	0.3725	0	1
Whether working in a private enterprise	2374	0.6184	0.4859	0	1
GPA	2374	3.6387	0.4990	1.54	4.76
Gender	2374	0.3475	0.4763	0	1
SES	2374	0.1651	0.4696	0	2
Town	2374	0.5202	0.4997	0	1

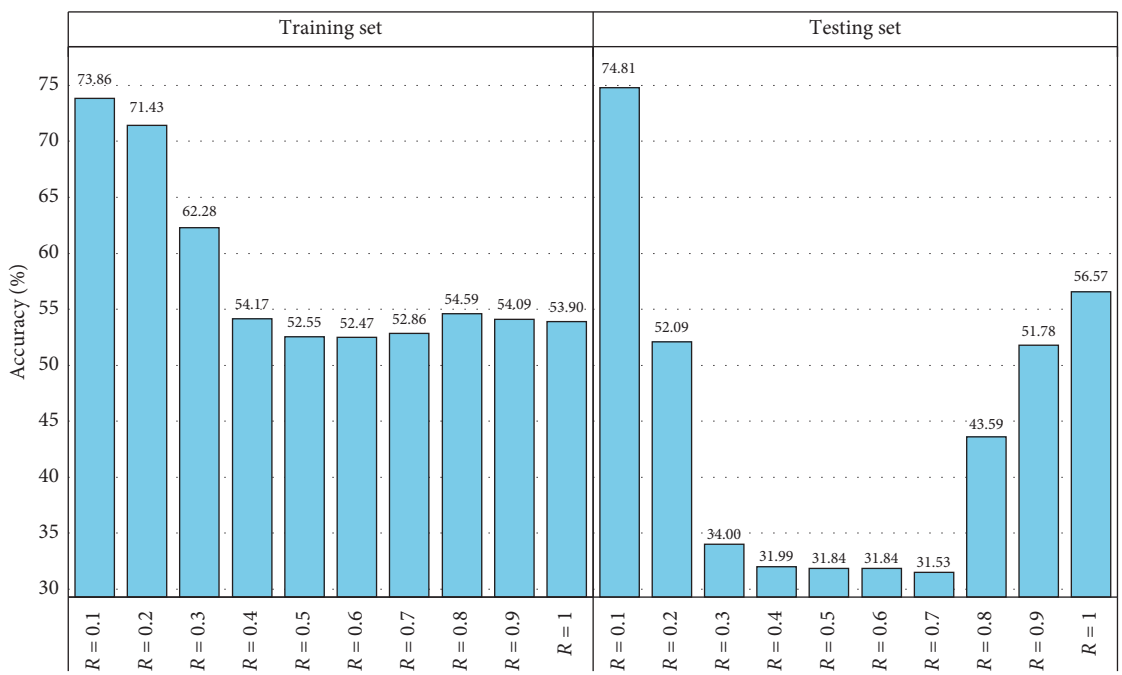

Figure 3: Results of the GM (0, N) and FGM (0, N) models: choice of continuing studying.

Table 3: Results of coefficient of variables: choice of continuing studying.

Coefficient	$r = 0.1$	$r = 0.2$	$r = 0.3$	$r = 0.4$	$r = 0.5$	$r = 0.6$	$r = 0.7$	$r = 0.8$	$r = 0.9$	$r = 1$
Constant	−0.858	−0.618	−0.792	−1.292	−2.216	−3.717	−5.998	−9.358	−14.301	−21.701
Town	0.095	0.096	0.127	0.185	0.266	0.361	0.465	0.570	0.666	0.748
SES	−0.092	−0.176	−0.291	−0.423	−0.534	−0.593	−0.600	−0.571	−0.525	−0.475
GPA	0.171	0.105	0.088	0.076	0.061	0.043	0.024	0.006	−0.011	−0.024
Gender	0.019	−0.022	−0.018	0.005	0.035	0.058	0.066	0.058	0.039	0.014

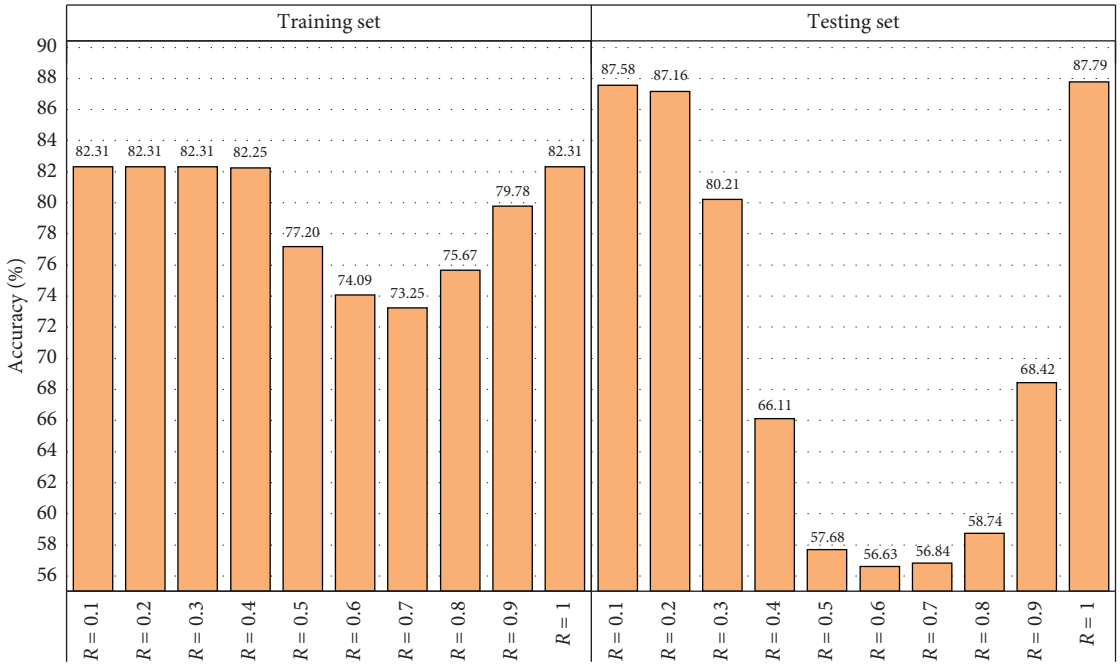

Figure 4: Results of the GM (0, N) and FGM (0, N) models: choice of working in state-owned enterprises.

Table 4: Results of coefficient of variables: choice of working in state-owned enterprises.

Coefficient	$r = 0.1$	$r = 0.2$	$r = 0.3$	$r = 0.4$	$r = 0.5$	$r = 0.6$	$r = 0.7$	$r = 0.8$	$r = 0.9$	$r = 1$
Constant	−0.200	−0.315	−0.508	−0.901	−1.642	−2.919	−4.916	−7.780	−11.627	−16.632
Town	0.072	0.064	0.055	0.049	0.043	0.036	0.027	0.019	0.011	0.005
SES	−0.038	−0.061	−0.096	−0.143	−0.187	−0.209	−0.197	−0.151	−0.081	−0.003
GPA	0.035	0.043	0.049	0.050	0.046	0.047	0.064	0.097	0.137	0.173
Gender	0.002	0.025	0.066	0.126	0.192	0.248	0.279	0.279	0.253	0.212

graduates with higher GPA and from an urban household are more likely to continue studying. Secondly, SES shows the negative influence. And, the reason may be that graduates with worse SES may choose to work aiming at weakening the family's stress.

4.3. Influential Factors for Fresh Graduate's Career Choice of Working in State-Owned Enterprises. This section selects the whole dataset except the graduates with choice of continuing studying. Eventually, we get specific information of 2374 graduates (male: 35% and female: 65%), and average GPA is 3.64. Similarly, this paper sets the output number of 16.6% of the whole dataset (choice of working in state-owned enterprises) as 1 and the others as 0.

Based on the information shown in Figure 4, we find that, in the training set, there are five models with the accuracy of 82%. However, after considering the results of the testing set, we find that the performance of two fractional models ($r = 0.1$ and 0.2) and the traditional model is much better than the others. Due to the similar performance of these three models, we choose to take advantage of all these three models to explore the effect of factors on the graduate's choice of working in state-owned enterprises.

As we can see in Table 4, results obtained from the GM (0, N) model are similar with those of the other two fractional models, which indicates the robustness. And, there are also two conclusions: on one hand, gender and GPA make the contribution to the choice of working in state-owned enterprises, which means males with higher GPA are more likely to make this choice. On the other hand, the effect of SES can diversely affect this action.

4.4. Influential Factors for Fresh Graduate's Career Choice of Working in Private Enterprises. The dataset used in this section is similar to that in Section 4.2. The only difference is that the output variable in this section is whether the students choose to work in private enterprises. After calculation, nearly 62% of the whole students take this action and we set the output number as 1.

Based on the information shown in Figure 5, we find the training-set accuracy of all the FGM (0, N) models is higher than the accuracy of the traditional model. Among them, the model with the fractional order ($r = 0.1$) has the best performance, while the testing-set accuracy of all the FGM (0, N) models is 59.68%, which may be caused by the fact that we set the situations of predictions more than 0.5 as 1 and

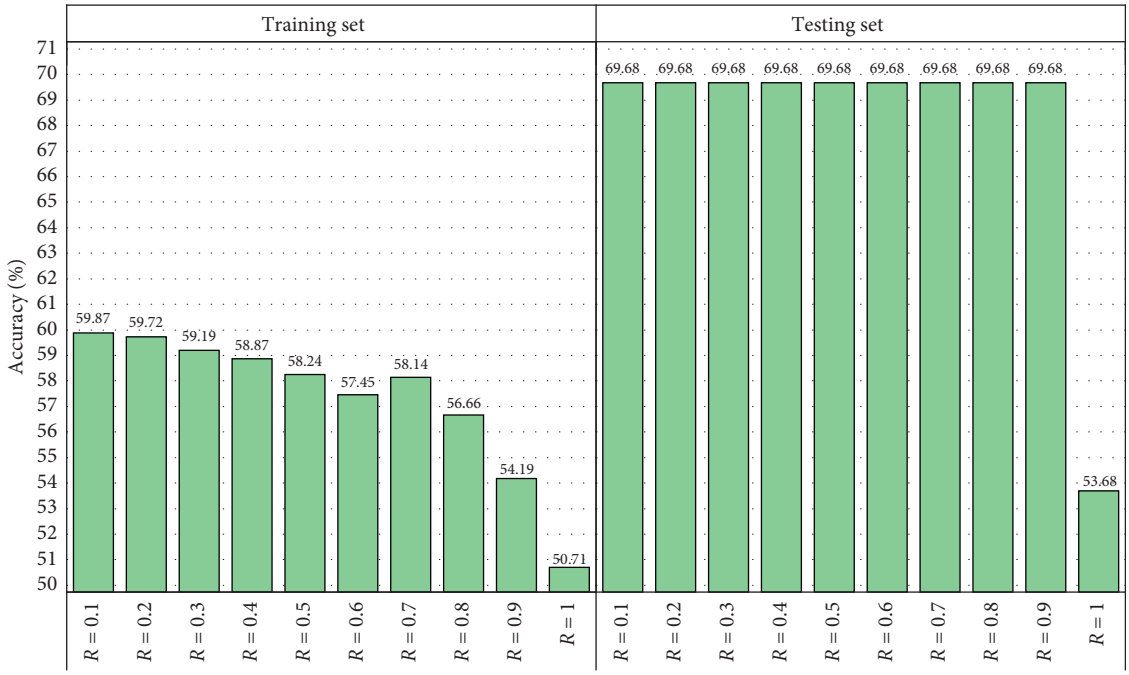

Figure 5: Results of the GM (0, N) and FGM (0, N) models: choice of working in private enterprises.

Table 5: Results of coefficient of variables: choice of working in private enterprises.

Coefficient	$r = 0.1$	$r = 0.2$	$r = 0.3$	$r = 0.4$	$r = 0.5$	$r = 0.6$	$r = 0.7$	$r = 0.8$	$r = 0.9$	$r = 1$
Constant	0.696	0.254	0.171	0.301	0.742	1.707	3.471	6.277	10.248	15.366
Town	0.052	0.109	0.103	0.088	0.075	0.065	0.059	0.056	0.054	0.054
SES	0.108	0.175	0.256	0.347	0.431	0.494	0.523	0.511	0.463	0.394
GPA	0.009	0.072	0.135	0.208	0.291	0.377	0.450	0.498	0.522	0.530
Gender	0.121	0.205	0.248	0.256	0.224	0.170	0.119	0.093	0.100	0.134

the predictions less than 0.5 as 0 and most of the predictions are around 0.5. Comprehensively comparing the performance of models, this paper sets the training-set accuracy equaling to 58.5% as the standard and chooses results of the fractional models with the fractional orders ranging from 0.1 to 0.4 to make the following analysis.

The results, as shown in Table 5, indicate that all the four factors show the positive effect on this behavior. Among these four factors, SES and gender are the most influential ones, followed by GPA. After comparing the results from the fractional models with the fraction order ranging from 0.1 to 0.4, we propose that the robustness of the results has been tested.

5. Conclusion and Suggestions

In order to confirm student's needs and provide suitable help, this paper builds the GM (0, N) models to forecast graduate's career choices. The career choices contain three parts, including continuing studying, working in state-owned enterprises, and working in private enterprises. And, GPA, SES, gender, and whether the student comes from an urban household or not are four input variables. More importantly, in order to increase the accuracy of models, we firstly combine the traditional GM (0, N) model with the fractional order and propose the FGM (0, N) model.

However, we are surprised to find that the accuracy of some models is almost 60% and the accuracy of the fractional models in previous studies is more than 90%. After reading some related studies, this paper thinks that the most possible reason is the effect of COVID-19. This epidemic has an impact on the career choice of some fresh graduates. And, the effect may also be affected by other factors. Thus, the accuracy of some models is still small.

From the above analysis, we can mainly get the following conclusions:

Firstly, after making the statistical description of the data, we find that most of the graduates are more likely to work instead of continuing studying. And, working in private enterprises is their first choice. Besides, there are still many students with financial problems, which may strongly affect their behavior.

Secondly, based on the empirical studies, we propose that, in most of times, the performance of the FGM (0, N) models is better than the traditional one. However, there is no doubt that, in some cases, the accuracy of the GM (0, N) model is also very good, even higher than that of the fractional ones.

Thirdly, GPA, gender, and town show the positive effect on all the three choices. Among these three factors, GPA is the most influential factor for the choices of continuing studying and working in state-owned enterprises.

Fourthly, the effect of SES changes in forecasting graduate's different choices: while forecasting the choice of continuing studying and working in state-owned enterprises, SES shows the negative effect. However, SES makes the diverse contribution in forecasting the choice of working in private enterprises.

Thus, based on the above conclusions, we propose the following suggestions: for the male students with higher GPA and from an urban household, schools should set up more theoretical courses and some modules about how to be better suitable for the work in state-owned enterprises. For the students with bad family socioeconomic status, schools setting up more practical courses can be better.

Data Availability

The data used to support the findings of this study are available from the corresponding author upon request.

Conflicts of Interest

The authors declare that they have no conflicts of interest.

References

[1] N. Sehagl and S. Nasim, "Total interpretive structural modelling of predictors for graduate employability for the information technology sector," *Higher Education, Skills and Work-Based Learning*, vol. 8, no. 2, pp. 495–510, 2018.

[2] V. K. Gokuladas, "Factors that influence first-career choice of undergraduate engineers in software services companies," *Career Development International*, vol. 15, no. 2, pp. 144–165, 2010.

[3] D. C. Koch, J. Greenan, and K. Newton, "Factors that influence students' choice of careers in construction management," *International Journal of Construction Education and Research*, vol. 5, no. 4, pp. 293–307, 2009.

[4] L. S. Mead, J. B. Clarke, F. Forcino, and J. J. L. Graves, "Factors influencing minority student decisions to consider a career in evolutionary biology," *Evolution: Education and Outreach*, vol. 8, no. 1, pp. 1–11, 2015.

[5] J. E. Myburgh, "An empirical analysis of career choice factors that influence first-year accounting students at the university of Pretoria: a cross-racial study," *Meditari Accountancy Research*, vol. 13, no. 2, pp. 35–48, 2005.

[6] E. Greenman, "Asian American-white differences in the effect of motherhood on career outcomes," *Work and Occupations*, vol. 38, no. 1, pp. 37–67, 2011.

[7] C. Berghammer, "The return of the male breadwinner model? educational effects on parents' work arrangements in Austria, 1980–2009," *Work, Employment and Society*, vol. 28, no. 4, pp. 611–632, 2014.

[8] B. P. Kim, K. W. McCleary, and T. Kaufman, "The new generation in the industry: hospitality/tourism students' career preferences, sources of influence and career choice factors," *Journal of Hospitality & Tourism Education*, vol. 22, no. 3, pp. 5–11, 2010.

[9] S. Qiu, L. Dooley, and T. Palkar, "What factors influence the career choice of hotel management major students in Guangzhou?" *Independent Journal of Management & Production*, vol. 8, no. 3, pp. 1092–1115, 2017.

[10] Y. T. Lee, "Structure activity relationship analysis of phenolic acid phenethylesters on oral and human breast cancers: the grey GM (0, *N*) approach," *Computers in Biology and Medicine*, vol. 41, no. 7, pp. 406–511, 2011.

[11] H. Li and G. Chen, "Benevolence-dependability value and intertemporal choice: moderating effect of perceived socioeconomic status," *Social Behavior and Personality: An International Journal*, vol. 46, no. 9, pp. 1573–1583, 2018.

[12] J. J. Cutuli, C. D. Desjardins, J. E. Herbers et al., "Academic achievement trajectories of homeless and highly mobile students: resilience in the context of chronic and acute risk," *Child Development*, vol. 84, no. 3, pp. 841–857, 2013.

[13] J. E. Herbers, J. J. Cutuli, L. M. Supkoff et al., "Early reading skills and academic achievement trajectories of students facing poverty, homelessness, and high residential mobility," *Educational Researcher*, vol. 41, no. 9, pp. 366–374, 2012.

[14] Y. Li, J. Allen, and A. Casillas, "Relating psychological and social factors to academic performance: a longitudinal investigation of high-poverty middle school students," *Journal of Adolescence*, vol. 56, pp. 179–189, 2017.

[15] J. L. Deng, "Control problem of grey systems," *System & Control Letters*, vol. 1, no. 5, pp. 288–294, 1982.

[16] J. L. Deng, "Introduction to grey system theory," *Journal of Grey Systems*, vol. 1, no. 1, pp. 1–24, 1989.

[17] W. Wu, X. Ma, Y. Wang, Y. Zhang, and B. Zeng, "Research on a novel fractional GM (α, n) model and its applications," *Grey Systems: Theory and Application*, vol. 9, no. 3, pp. 356–373, 2019.

[18] Y.-F. Zhao, M.-H. Shou, and Z.-X. Wang, "Prediction of the number of patients infected with COVID-19 based on rolling grey Verhulst models," *International Journal of Environmental Research and Public Health*, vol. 17, no. 12, p. 4582, 2020.

[19] M. H. Shou, Z. X. Wang, D. D. Li, and Y. T. Zhou, "Forecasting the price trends of digital currency: a hybrid model integrating the stochastic index and grey Markov chain models," *Grey Systems: Theory and Application*, vol. 11, no. 1, pp. 22–45, 2021.

[20] S. Ding, R. Li, S. Wu, and W. Zhou, "Application of a novel structure-adaptative grey model with adjustable time power item for nuclear energy consumption forecasting," *Applied Energy*, vol. 298, p. 117114, 2021.

[21] S. Ding, R. Li, and S. Wu, "A novel composite forecasting framework by adaptive data preprocessing and optimized nonlinear grey Bernoulli model for new energy vehicles sales," *Communications in Nonlinear Science and Numerical Simulation*, vol. 99, p. 105847, 2021.

[22] S. Ding and R. Li, "Forecasting the sales and stock of electric vehicles using a novel self-adaptive optimized grey model," *Engineering Applications of Artificial Intelligence*, vol. 100, p. 104148, 2021.

[23] N.-M. Xie, C.-Q. Yuan, and Y.-J. Yang, "Forecasting China's energy demand and self-sufficiency rate by grey forecasting model and Markov model," *International Journal of Electrical Power & Energy Systems*, vol. 66, pp. 1–8, 2015.

[24] Z.-X. Wang, D.-D. Li, and H.-H. Zheng, "Model comparison of GM (1, 1) and DGM (1, 1) based on Monte-Carlo

simulation," *Physica A: Statistical Mechanics and Its Applications*, vol. 542, p. 123341, 2020.

[25] J. Ye, Y. Dang, S. Ding, and Y. Yang, "A novel energy consumption forecasting model combining an optimized DGM (1, 1) model with interval grey numbers," *Journal of Cleaner Production*, vol. 229, pp. 256–267, 2019.

[26] C. Yuan, Y. Zhu, D. Chen, S. Liu, and Z. Fang, "Using the GM (1, 1) model cluster to forecast global oil consumption," *Grey Systems: Theory and Application*, vol. 7, no. 2, pp. 286–296, 2017.

[27] Z.-X. Wang, Q. Li, and L.-L. Pei, "A seasonal GM (1, 1) model for forecasting the electricity consumption of the primary economic sectors," *Energy*, vol. 154, pp. 522–534, 2018.

[28] S. Ding, "A novel discrete grey multivariable model and its application in forecasting the output value of China's high-tech industries," *Computers & Industrial Engineering*, vol. 127, pp. 749–760, 2019.

[29] N. Xie, "Estimating civil aircraft's research and manufacture cost by using grey system model and neural network algorithm," *Grey Systems: Theory and Application*, vol. 5, no. 1, pp. 89–104, 2015.

[30] C.-Y. Kung and K.-L. Wen, "Applying grey relational analysis and grey decision-making to evaluate the relationship between company attributes and its financial performance-a case study of venture capital enterprises in Taiwan," *Decision Support Systems*, vol. 43, no. 3, pp. 842–852, 2007.

[31] M. Tian, Y. Cao, N. Xie, and S. Liu, "IN-GM (0, *N*) cost forecasting model of commercial aircraft based on interval grey numbers," *Kybernetes*, vol. 41, no. 7/8, pp. 886–896, 2012.

[32] H. Dehestani, Y. Ordokhani, and M. Razzaghi, "Fractional-order Legendre-Laguerre functions and their applications in fractional partial differential equations," *Applied Mathematics and Computation*, vol. 336, pp. 433–453, 2018.

[33] L. Wu, "Using fractional GM (1, 1) model to predict the life of complex equipment," *Grey Systems: Theory and Application*, vol. 6, no. 1, pp. 32–40, 2016.

[34] L. Wu, S. Liu, Z. Fang, and H. Xu, "Properties of the GM (1, 1) with fractional order accumulation," *Applied Mathematics and Computation*, vol. 252, pp. 287–293, 2015.

[35] Y. X. Kang, S. H. Mao, and Y. H. Zhang, "Variable order fractional grey model and its application," *Applied Mathematical Modelling*, vol. 97, pp. 619–635, 2021.

[36] W. Wu, X. Ma, B. Zeng, Y. Wang, and W. Cai, "Forecasting short-term renewable energy consumption of China using a novel fractional nonlinear grey Bernoulli model," *Renewable Energy*, vol. 140, pp. 70–87, 2019.

[37] X. H. Gao and L. Wu, "Using fractional order weakening buffer operator to forecast the main indices of online shopping in China," *Grey Systems: Theory and Application*, vol. 9, no. 1, pp. 128–140, 2019.

Hindawi
Journal of Mathematics
Volume 2021, Article ID 9962565, 11 pages
https://doi.org/10.1155/2021/9962565

Research Article

An Improved Nonhomogeneous Grey Model with Fractional-Order Accumulation and Its Application

Shuanghua Liu,[1] Qin Qi,[2] and Zhiming Hu[3]

[1]*School of Mathematics and Statistics, Baise University, Baise 533000, China*
[2]*School of Economics and Management, Tongji University, Shanghai 200092, China*
[3]*Zhejiang College, Shanghai University of Finance & Economics, Jinhua 321013, China*

Correspondence should be addressed to Qin Qi; qiqin_jxsh@163.com

Received 31 March 2021; Revised 14 May 2021; Accepted 4 June 2021; Published 21 June 2021

Academic Editor: Lifeng Wu

The nonhomogeneous grey model has been seen as an effective method for forecasting time series with approximate nonhomogeneous index law, which has been widely used in diverse disciplines on account of its high prediction precision. However, there remains room for improvements. For this, this study presents an improved nonhomogeneous grey model by incorporating the dynamic integral mean value theorem and fractional accumulation simultaneously. In order to promote the efficacy of the optimised model, we apply the whale optimization algorithm (WOA) to ascertain its optimal parameter. In particular, two examples are conducted to validate the superiority of the proposed model in contrast with other benchmarks, and the experimental results show that the mean absolute percentage error of the proposed approach is 808692% and 6.0706%, respectively, indicating the proposed approach performs better than other competing models.

1. Introduction

The prediction plays an important role in management and decision-making science. In the past decades, there are a variety of forecasting technique, such as autoregressive integrated moving average (ARIMA), artificial neural networks, and support vector machine. These models have their modeling mechanism and application scope. However, these models have a common flaw that they usually require more samples to build the model so as to obtain relatively high prediction precision. However, the behaviors of most systems in practice are often uncertain and unknown, and the effect of large-sized sample-based prediction models may be relatively poor. On this basis, grey system models focusing on small-sized observations have been received more attention in the recent decades [1].

As previous literature revealed, for the ability to analyse and process data sequences, grey-based models have been broadly applied among diverse disciplines because of their excellent implementation on small-scale sample modeling, such as natural gas consumption [2–4], electric power supply and demand [5–8], renewable energy [9, 10], industry [11, 12], and medicine [13, 14]. Although grey-based models have their own advantages, there still exist some shortcomings. For instance, the traditional grey model (denoted as GM(1, 1)) only fits time-series sequence with pure exponential characteristics well but fails to fit time series with other features. To this end, Cui et al. [15] brought forward a nonhomogeneous grey model for forecasting data series with approximate nonhomogeneous index feature. In fact, the nonhomogeneous grey model is nascent, and this model has certain defects. To be specific, these defects mainly exist in the background value, cumulative order, time response function, and application scope. Later, to improve the nonhomogeneous grey model, many scholars have paid their attention to this issue. For example, Ma and Liu [16] optimised the background value in accord with general expression for its time response function, also notable is that this optimised model was successful to apply in practice. Tong et al. [17] designed a newly designed nonhomogeneous grey model to simultaneously fit time approximately homogeneous and nonhomogeneous index features.

Considering the vital impact of the background value on the prediction performance of the nonhomogeneous grey model, Zeng and Liu [18] presented an improved nonhomogeneous grey model based on fractional-order accumulation, which can achieve high accurate prediction by virtue of fractional-order accumulation. Subsequently, a series of variants of the nonhomogeneous grey model with fractional-order accumulation have emerged. For example, Wu et al. [19] established a discrete nonhomogeneous grey model based on fractional-order accumulation. Later, Wu et al. [20] presented a conformable fractional nonhomogeneous grey model to predict carbon emissions for BRIC countries. The abovementioned optimization measures have dramatically improved the prediction performance of the existing grey-based model and enriched the grey modeling theory.

Admitted, there exist a variety of nonhomogeneous grey models; however, these approaches are not universal. That is, many optimization approaches are only suitable for special cases. The optimization methods for increasing the prediction precision of the grey models include fractional accumulation and integral median theorem aiming to optimize the background value. Recalling, Wu et al. [21] first placed the fractional accumulation on the grey system models, which is a significant innovation to improve the prediction precision of grey models, on the foundation of grey-based models with fractional-order accumulation [22–25].

To further increase the prediction performance of the abovementioned models, there are a variety of studies that are committed to explore the combination of fractional-order accumulation and grey modeling technique. For instance, Zhu et al. [26] brought forward a newly designed fractional grey model, of which the fractional accumulated generating operation sequence is dependent on an adaptive grey score weight; additionally, this model is applied to predict Jiangsu's electricity consumption. Chen et al. [27] put forward a fractional Hausdorff grey model, and Ma et al. [28] presented a novel grey model by using conformable fractional-order accumulation. These studies greatly enriched the grey system theory and enabled the combination of fractional calculus with the grey modeling technique. On the other hand, the adaptation of the integral median value theorem for improving the background value can enhance the prediction precision of the grey-based models [29, 30].

On the foundation of the previous knowledge, this study constructs a novel discrete nonhomogeneous grey model by incorporating the idea of fractional accumulation and the dynamic integral median theorem; the composite grey model (denoted as FDNGM(1,1) for short) is developed thereby, which can fit diverse series sequence through altering the fractional accumulation order and background-value coefficients. The principal innovations and contributions are outlined as follows. (1) We combine the dynamic background value with the grey modeling technique. (2) An effective intelligent technique, namely, the whale optimization algorithm, is utilized to ascertain the proper parameters for the proposed approach. (3) The several examples are used to certify the feasibility of this model.

The rest of this study is listed as follows. Section 2 briefly depicts the computational steps of the basic nonhomogeneous grey model. The proposed approach is studied in Section 3. Section 4 introduces the solution method for the proposed model. Section 5 reports the experimental results, and Section 6 concludes.

2. Basic NGM(1,1,*k*,*c*) Model

Assuming a raw sequence can be denoted as $S^0 = \{s^0(k)|k = 1, 2, \ldots, n\}, n \geq 4$, whose 1st-order accumulative generation operator data series is calculated as

$$S^1 = \left\{s^1(i)|i = 1, 2, \ldots, n\right\}, \tag{1}$$

where $s^1(i) = \sum_{j=1}^{i} s^0(j)$, $i = 1, 2, \ldots, n$.

Then, the differential equation for the basic NGM(1,1,*k*,*c*) model is written as

$$\frac{\mathrm{d}s^1(t)}{\mathrm{d}t} + as^1(t) = bt + c. \tag{2}$$

For the sake of estimating the system parameters for the abovementioned model, we get the discrete formula for equation (2) as

$$s^0(i) + az^1(i) = b\frac{i^2 - (i-1)^2}{2} + c. \tag{3}$$

In equation (3), z^1 refers to the background value, for which $z^1(i) = 0.5(s^1(i) + s^1(i-1))$.

With the help of the least-squares method, the system parameters for the conventional NGM(1,1,*k*,*c*) model should be computed as

$$(\tilde{a}, \tilde{b}, \tilde{c})^T = \left(\gamma^T\gamma\right)^{-1}\gamma^T\Omega, \tag{4}$$

where

$$\gamma = \begin{pmatrix} -z^1(2) & \frac{3}{2} & 1 \\ -z^1(3) & \frac{5}{2} & 1 \\ \vdots & \vdots & \vdots \\ -z^1(n) & \frac{\left(n^2 - (n-1)^2\right)}{2} & 1 \end{pmatrix}, \tag{5}$$

$$\Omega = \begin{pmatrix} s^0(2) \\ s^0(3) \\ \vdots \\ s^0(n) \end{pmatrix}.$$

After that, we get the time response function for equation (2) calculated as

$$s^1(i) = \left\{ s^0(1) + \frac{b - ac - ab}{a^2} \right\} \exp(-a(k-1)) + \frac{bk}{a} + \frac{(ac-b)}{a^2}. \tag{6}$$

Eventually, the restored values of the raw data are given by

$$\tilde{x}^{(0)}(k) = \begin{cases} \tilde{x}^{(1)}(k) - \tilde{x}^{(1)}(k-1), & k = 2, 3, \ldots, \\ \tilde{x}^{(1)}(1), & k = 1. \end{cases} \tag{7}$$

We observe from the modeling procedure above that the prediction precision is dependent on the system parameters influenced by the background value and cumulative sum operator. In NGM(1,1,k,c), we apply the integer-order accumulation and trapezoid formula to generate the accumulated sequence and background value, and it is evident that the fixed accumulation order and approximate discrete error will impair the prediction performance to a large degree. For this, we apply the fractional accumulation and dynamic integral median theorem on the modeling procedure for improving the prediction capacity of the existing nonhomogeneous model.

3. Presentation of FDNGM(1,1,k,c)

Suppose that

$$S^0 = \left\{ s^0(i) | i = 1, 2, \ldots, n \right\}, \tag{8}$$

is the given data sequence that is nonnegative, then its r-order fractional accumulating generation operation data series can be calculated as

$$S^r = \left\{ s^r(i) | i = 1, 2, \ldots, n \right\}, \tag{9}$$

where $s^r(i) == \sum_{j=1}^{i} \binom{i-j+r-1}{i-j} s^0(j)$, $i = 1, 2, v, n$.

Based on S^r, the differential equation for the proposed model is obtained as

$$\frac{\mathrm{d}s^r(t)}{\mathrm{d}t} + as^r(t) = bt + c. \tag{10}$$

In this study, we place the dynamic integral median theorem on the background value for the proposed model so as to eliminate the discretization error generated by the transition process.

Theorem 1. *If $s^r(j)$ is continuous over given interval $[i-1, i]$, then we get*

$$\int_{i-1}^{i} s^r(j)\mathrm{d}j = s^r(I) = (1-\varphi)s^r(i-1) + \varphi s^r(i), \tag{11}$$

where $\varphi \in [0, 1]$ and $I \in [i-1, i]$.

Proof. Since $s^r(j)$ keeps continduous over $[i-1, i]$, there exist the maximum value D and minimum value d for $s^r(j)$ over $[i-1, i]$, which makes $d \le s^r(j) \le D$ hold true; then, we have

$$\varphi d \le \varphi s^r(i) \le \varphi D, \tag{12}$$

which is also

$$(1-\varphi)d \le (1-\varphi)s^r(i-1) \le (1-\varphi)D. \tag{13}$$

Combining equations (12) and (13), we have

$$d \le (1-\varphi)s^r(i-1) + \varphi s^r(i) \le D. \tag{14}$$

In accord with the intermediate value theorem, $\phi \in [k-1, k]$ that makes $s^r(\phi) = (1-\varphi)s^r(i-1) + \varphi s^r(i)$ hold. It can be further concluded that for any value $s^r(\tilde{\phi})$ of the continuous function $s^r(i)$ on $[i-1, i]$, there exists $\varphi_1 \in [0, 1]$ that makes $s^r(\tilde{\phi}) = (1-\varphi_1)s^r(i-1) + \varphi_1 s^r(i)$ hold true. Thereafter, in accord with the integral mean value theorem, we get

$$\int_{i-1}^{i} s^r(j)\mathrm{d}j = s^r(I), \quad I \in [i-1, i]. \tag{15}$$

Furthermore, we have

$$\int_{i-1}^{i} s^r(j)\mathrm{d}j = s^r(I) = (1-\varphi)s^r(i-1) + \varphi s^r(i). \tag{16}$$

It is proved.

Therefore, the newly designed background value for the proposed model can be given as

$$\tilde{z}^r(i) = (1-\varphi_1)s^r(i-1) + \varphi_1 s^r(i), \quad i = 2, 3, \ldots, n. \tag{17}$$

Then, we get the least-squares estimation for system parameters expressed as

$$(\tilde{a}, \tilde{b}, \tilde{c})^T = \left(\vartheta^T \vartheta\right)^{-1} \vartheta^T \omega, \tag{18}$$

where

$$\vartheta = \begin{pmatrix} -\tilde{z}^r(2) & \frac{3}{2} & 1 \\ -\tilde{z}^r(3) & \frac{5}{2} & 1 \\ \vdots & \vdots & \vdots \\ -\tilde{z}^r(n) & \frac{\left(n^2 - (n-1)^2\right)}{2} & 1 \end{pmatrix}, \tag{19}$$

$$\omega = \begin{pmatrix} s^{r-1}(2) \\ s^{r-1}(3) \\ \vdots \\ s^{r-1}(n) \end{pmatrix}.$$

Similar to the calculation steps mentioned in Section 2, the time response function for the proposed model can be acquired. Moreover, the predicted values of the original data series is given as

$$\tilde{s}^0(i) = \left\{\alpha^1\tilde{s}^r(1), \alpha^1\tilde{s}^r(2), \ldots, \alpha^1\tilde{s}^r(n)\right\}. \tag{20}$$

4. Determination of Parameter

Notice that the proposed model is constructed under the assumption that the emerging coefficients φ_1, r are known. Thus, they have a significant impact on the prediction precision directly. Aiming to effectively enhance the prediction precision of the proposed model, a relative simple optimization problem can be established, whose calculation formula can be defined as

$$\begin{cases} \min f(r,\varphi_1) = \dfrac{1}{n-1}\displaystyle\sum_{i=2}^{n}\dfrac{\left|\tilde{s}^r(i) - s^r(i)\right|}{s^r(i)} \times 100\% \\ \varphi_1 \in [0,1], \quad r \geq 0 \\ (\tilde{a},\tilde{b},\tilde{c}) = \left(\vartheta^T\vartheta\right)^{-1}\vartheta^T\omega, \\ \vartheta = \begin{pmatrix} -\tilde{z}^r(2) & \dfrac{3}{2} & 1 \\ -\tilde{z}^r(3) & \dfrac{5}{2} & 1 \\ \vdots & \vdots & \vdots \\ -\tilde{z}^r(n) & \dfrac{\left(n^2-(n-1)^2\right)}{2} & 1 \end{pmatrix}, \\ \omega = \begin{pmatrix} s^{r-1}(2) \\ s^{r-1}(3) \\ \vdots \\ s^{r-1}(n) \end{pmatrix}, \\ s^1(i) = \left\{s^0(1) + \dfrac{b-ac-ab}{a^2}\right\}\exp(-a(k-1)) + \dfrac{bk}{a} + \dfrac{(ac-b)}{a^2}. \end{cases} \tag{21}$$

As previous literature revealed, the abovementioned equation is difficult to solve by the ordinary approach on account of its nonlinear features. Therefore, this study introduces a metaheuristic technique, namely, the whale optimization algorithm (denoted as WOA), to search the best values of the background-value coefficients and fractional accumulation order.

In 2016, Mirijalili and Lewis [31] designed the whale optimization algorithm which describes the social behavior of the whale group. Over the past 5 years, this algorithm has been applied in various fields [32, 33]. More importantly, this approach is regarded as an effective technique to solve nonlinear optimization problems [34]. This is the main motivation for us to choose the WOA to solve the abovementioned equation. To be specific, the modeling steps of the WOA are listed.

Whales move in spiral to surround the school of fish, which is considered the best solution for predation. After that, they change their position by reference to the candidate solution. We get the expression of this behavior shown as

$$\overrightarrow{P}(i+1)=\begin{cases}\overrightarrow{P}^{*}(i)-(2f(i)\overrightarrow{r}-f(i))\overrightarrow{D}, & \xi<0.5\,(a),\\ \left|\overrightarrow{P}^{*}(i)-\overrightarrow{P}(i)\right|e^{\beta i}\cos(2\pi l)+\overrightarrow{P}^{*}(i), & \xi\geq 0.5\,(b).\end{cases} \tag{22}$$

In equation (22), $\overrightarrow{P}(i)$, $\overrightarrow{P}^{*}(i)$ denote the whales' current position and their current best position, respectively. $\overrightarrow{r}$ refers to a arbitrary number generated within [0, 1], l is a random number produced from [−1, 1], β is the key for controlling the shape of whales' moving spiral, T is denoted as the maximum number of iterations, and the movement strategy will be chosen by the probability ξ. Whales change their position according to the equation expressed as

$$\overrightarrow{P}(i+1)=\overrightarrow{P}_{r}(i)-\overrightarrow{C}\left|2\overrightarrow{P}_{r}(i)\overrightarrow{r}-\overrightarrow{P}(i)\right|. \tag{23}$$

In equation (23), $\overrightarrow{p}_{r}(i)$ denotes the position of random whale in the group. Additionally, we define the fitness function for calculating the fitness of each whale expressed as

$$\text{fitness}=\frac{1}{n-1}\sum_{i=2}^{n}\left|\frac{\overline{s}^{0}(i)-s^{0}(i)}{s^{0}(i)}\right|\times 100\%. \tag{24}$$

The flowchart of the proposed model based on the WOA technique is shown in Figure 1.

5. Application

This section conducts two real cases to demonstrate the superiority of the proposed approach in contrast with other benchmark models. The models used for comparison include the polynomial regression model (PR) proposed by literature [35], the FHGM(1,1) model proposed by literature [26], and the ONGM(1,1,k,c) model proposed by literature [36].

Case 1. (Prognosticating Chongqing's electric power consumption) With the depletion of nonrenewable energy sources such as coal, crude oil, and nuclear energy, electrical energy is becoming more and more important in our lives and production. Overestimation and underestimation of short-term electricity consumption will waste the energy or cause unnecessary loss. Therefore, accurate and effective forecasting of electricity consumption can help power system operators and market participants to propose bidding strategies and ensure consumer's electricity supply based on corresponding forecast information, thereby reducing the cost of electricity consumption and reducing energy consumption.

The original data were gathered from the Statistical Yearbook of China. Regarding the calculation procedure, first, the searching process by the WOA is given in Figure 2; accordingly, all the system parameters are listed in Table 1. By reference with this study and references therein, the predicted values and error-value metrics generated by the competing models are given in Tables 2 and 3, respectively. What is more, the error distribution is shown in Figure 3.

In accord with the predicted values mentioned in Table 2, we find that the predicted values by the NGM(1,1,k,c), FHGM(1,1), and ONGM(1,1,k,c) models all deviate far away from the actual series, and those of the proposed approach are much closer to the actual data. In addition, we observe from Table 3 that the MAPE values of the FDNGM(1,1,k,c) model are obviously lower than those of others. Moreover, the same discovery can be supported in Figure 3, indicating the proposed approach is more suitable for predicting the electric power consumption in Chongqing than other competitors.

Case 2. (Forecasting China's natural gas consumption) Chinese economy experienced a high growth in the new stage; additionally, natural gas, as a clean energy, has been regarded as an alternative source. Under the background of oil and gas system reform, the supply and demand for natural gas have dramatically changed as time goes on. Developing a accurate and sustainable forecasting model for the development trend of natural gas is of great practical significance.

Analogous with Case 1, the original series is gathered from Statistical Yearbook of China, as given in Table 4. First, the searching process by the WOA technique-based proposed approach is shown in Figure 4. By referring to the current study and references therein, we tabulate the predicted values of China's natural gas consumption and corresponding error-value indices by using different models in Tables 4 and 5, respectively.

By screening the predicted values of natural gas consumption in Table 5 that the predicted values of NGM(1,1,k,c), FHGM(1,1), and ONGM(1,1) models deviate away from the observations, and the those of the proposed approach are much closer to the actual data. What is more, the error of the proposed model is smaller than other benchmarks, as shown in Figure 5. Specifically, the APEs and MAPEs of the proposed approach in this case, referring that the proposed model, should be regarded as a promising approach in this case.

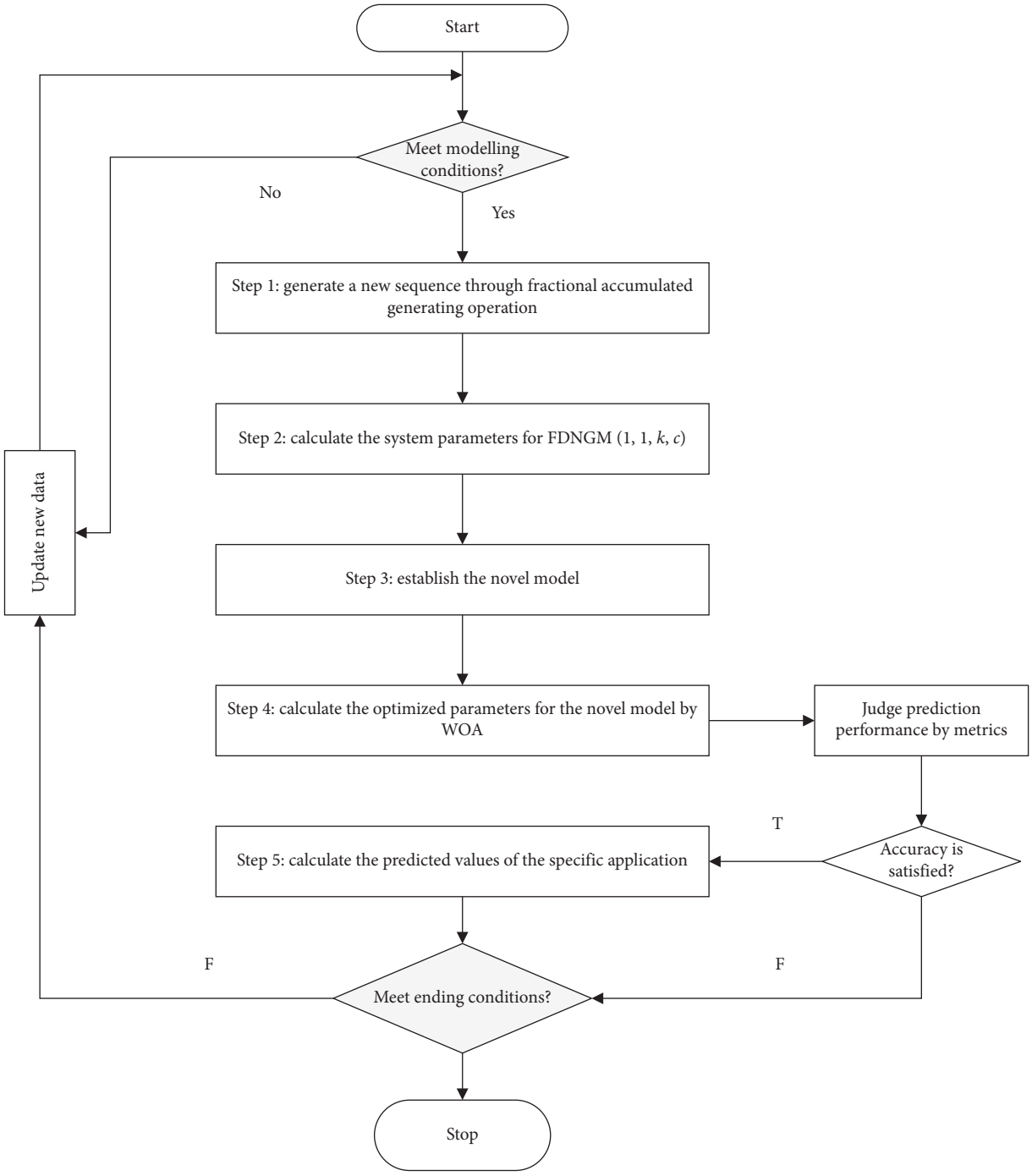

Figure 1: Schematic diagram of the calculation process of the FDNGM(1,1,k,c) model.

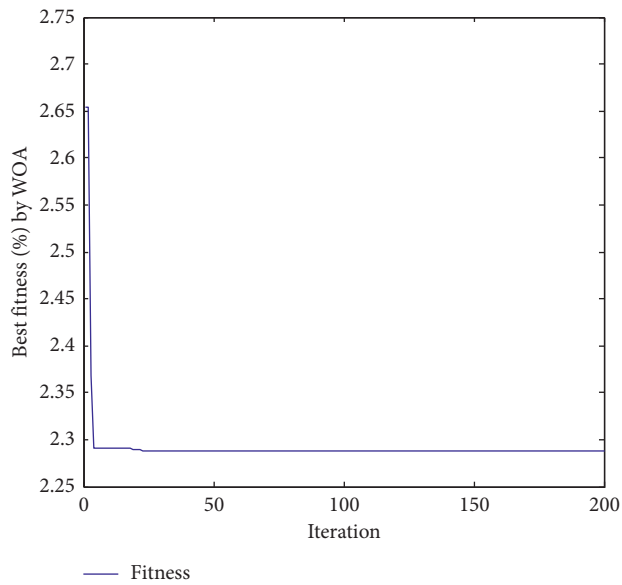

Figure 2: Searching process of the WOA-based FDNGM(1,1,k,c) model in Case 1.

Table 1: Parameters of the competitors in the two real-world cases.

Parameter	Case 1				Case 2			
φ_1	0.85363				0.98361			
φ_2	0.69486				0.99217			
φ_3	0.62772				0.70541			
φ_4	0.49884				0.99948			
φ_5	0.66898				0.75600			
φ_6	0.10179				0.03251			
φ_7	0.02099				0.98822			
φ_8	0.63933				0.96816			
φ_9	0.37460				0.99913			
r	0.28715				0.02580			
–	NGM	FHGM	FDNGM	ONGM	NGM	FHGM	FDNGM	ONGM
A	−0.06433	−0.05620	0.00113	−0.05620	−0.12639	−0.10767	0.10902	−0.10767
B	22.33115	26.88054	4.67769	26.88054	21.76010	35.34812	25.82133	35.34812
C	244.6430	237.2880	90.1820	237.2880	193.2125	160.5392	16.92224	160.5392

Table 2: The predicted values of original domain by employing the competing models in Case 1.

Year	Data	NGM	FHGM(1,1)	FDNGM	PR(3)	ONGM
2003	294.19	294.19	294.83	294.19	294.09	294.19
2004	309.06	306.71	302.47	305.74	314.59	302.43
2005	347.68	350.15	347.61	348.78	347.42	347.57
2006	405.20	396.48	395.35	398.12	390.42	395.31
2007	449.22	445.90	445.86	450.10	441.44	445.81
2008	484.41	498.59	499.28	503.75	498.32	499.23
2009	533.80	554.79	555.79	558.71	558.93	555.74
2010	626.44	614.72	615.57	614.86	621.10	615.52
2011	717.03	678.63	678.81	672.13	682.68	678.75
2012	723.50	746.79	745.70	730.52	741.53	745.64
2013	813.30	819.48	816.46	790.01	795.49	816.40
2014	867.24	897.00	891.30	850.59	842.41	891.24
2015	875.37	979.67	970.48	912.28	880.13	970.41
2016	924.89	1067.83	1054.23	975.06	906.51	1054.16
2017	996.55	1161.85	1142.82	1038.95	919.40	1142.75
2018	1118.79	1262.12	1236.54	1103.93	916.64	1236.46

Table 3: The error-value indices of the competing models in Case 1.

Year	Data	NGM (%)	FHGM (%)	FDNGM (%)	PR(3)	ONGM (%)
2003	294.19	0.0000	0.2159	0.0000	0.0332	0.0000
2004	309.06	0.7614	2.1318	1.0743	1.7908	2.1437
2005	347.68	0.7111	0.0210	0.3173	0.0745	0.0322
2006	405.20	2.1508	2.4305	1.7479	3.6479	2.4406
2007	449.22	0.7399	0.7488	0.1961	1.7325	0.7584
2008	484.41	2.9274	3.0699	3.9915	2.8725	3.0604
2009	533.80	3.9316	4.1202	4.6662	4.7076	4.1110
2010	626.44	1.8714	1.7347	1.8493	0.8526	1.7429
2011	717.03	5.3555	5.3306	6.2615	4.7901	5.3382
2012	723.50	3.2189	3.0683	2.3416	2.4921	3.0603
MAPE		2.4076	2.2872	2.1920	2.2994	2.5209
2013	813.30	0.7596	0.3881	2.8641	2.1901	0.3806
2014	867.24	3.4312	2.7748	1.9197	2.8637	2.7674
2015	875.37	11.9145	10.8650	4.2162	0.5438	10.8573
2016	924.89	15.4547	13.9845	5.4247	1.9871	13.9767
2017	996.55	16.5873	14.6781	4.2545	7.7419	14.6704
2018	1118.79	12.8112	10.5247	1.3278	18.0688	10.5175
MAPE		10.1598	8.8692	3.3345	5.5659	8.8616

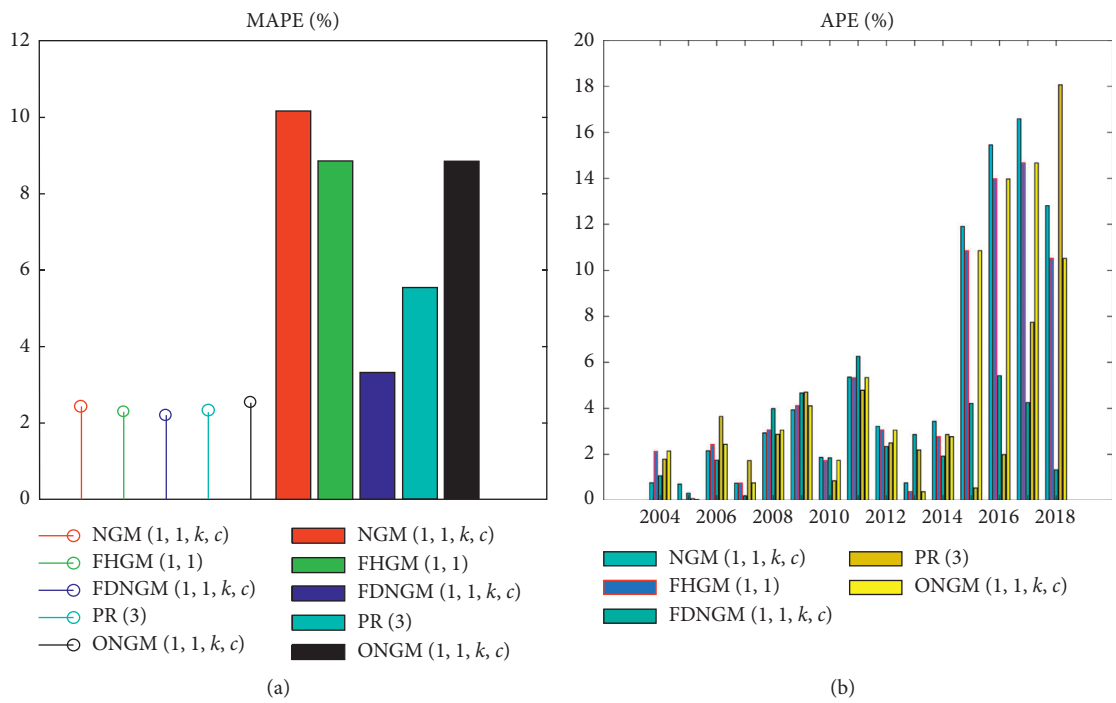

Figure 3: APEs and MAPEs of the competitive models in Case 1.

Table 4: The error-value indices of the competing models in Case 2.

Year	Data	NGM (%)	FHGM (%)	FDNGM (%)	PR(3)	ONGM (%)
2001	274.30	0.0000	3.7915	0.0000	0.1272	0.0000
2002	291.84	4.9274	11.7633	0.0012	0.2375	12.1678
2003	339.08	0.3097	4.4149	1.4094	1.4931	4.8043
2004	396.72	2.5333	0.3907	0.0003	0.0835	0.0215
2005	467.63	3.6653	2.8313	1.8665	1.9901	2.4816
2006	561.41	2.1125	2.0377	1.7288	2.0552	1.7143
2007	705.23	4.4709	4.2454	3.6870	3.3347	4.5319
2008	812.94	3.1097	2.8981	1.6931	1.5280	3.1753
2009	895.20	2.4330	2.3727	3.8457	3.5135	2.0920
2010	1069.41	0.5330	1.0726	0.0003	1.1227	1.3341
MAPE		2.6772	3.5818	1.5814	1.5486	3.5914
2011	1305.30	5.7519	6.8781	6.7281	8.8285	7.1163
2012	1463.00	2.9973	4.9200	6.1571	9.6438	5.1568
2013	1705.37	4.2114	6.9715	9.9952	14.9601	7.1983
2014	1868.94	0.4216	3.4672	8.8931	15.8696	3.6971
2015	1931.75	11.4466	5.9433	2.9000	12.7471	5.6952
2016	2078.06	18.6741	11.4756	1.1905	14.0055	11.2188
2017	2393.70	17.8744	9.3366	6.6300	21.7045	9.0883
MAPE		8.7682	6.9989	6.0706	13.9656	7.0244

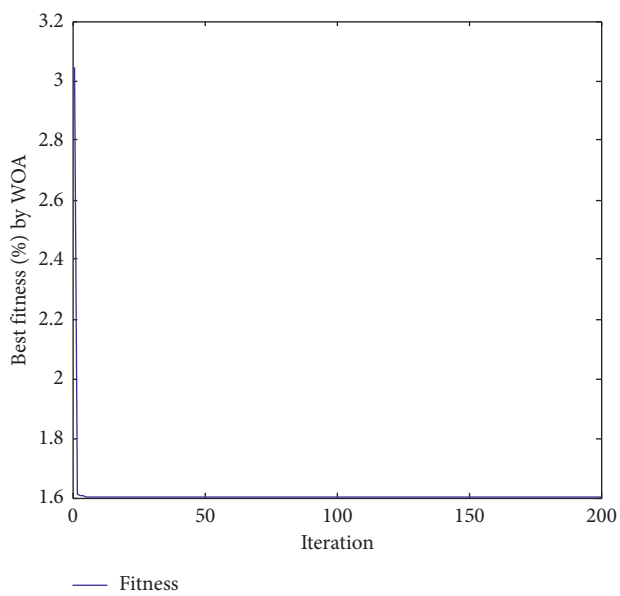

Figure 4: Searching process of the WOA-based FDNGM(1,1,k,c) model in Case 2.

Table 5: The predicted values of original domain by employing the competing models in Case 2.

Year	Data	NGM	FHGM	FDNGM	PR(3)	ONGM
2001	274.30	274.30	284.70	274.30	274.65	274.30
2002	291.84	277.46	257.51	291.84	292.53	256.33
2003	339.08	338.03	324.11	334.30	334.02	322.79
2004	396.72	406.77	398.27	396.72	396.39	396.81
2005	467.63	484.77	480.87	476.36	476.94	479.23
2006	561.41	573.27	572.85	571.12	572.95	571.03
2007	705.23	673.70	675.29	679.23	681.71	673.27
2008	812.94	787.66	789.38	799.18	800.52	787.13
2009	895.20	916.98	916.44	929.63	926.65	913.93
2010	1069.41	1063.71	1057.94	1069.41	1057.40	1055.14
2011	1305.30	1230.22	1215.52	1217.48	1190.06	1212.41

Table 5: Continued.

Year	Data	NGM	FHGM	FDNGM	PR(3)	ONGM
2012	1463.00	1419.15	1391.02	1372.92	1321.91	1387.56
2013	1705.37	1633.55	1586.48	1534.92	1450.24	1582.61
2014	1868.94	1876.82	1804.14	1702.73	1572.35	1799.84
2015	1931.75	2152.87	2046.56	1875.73	1685.51	2041.77
2016	2078.06	2466.12	2316.53	2053.32	1787.02	2311.19
2017	2393.70	2821.56	2617.19	2235.00	1874.16	2611.25

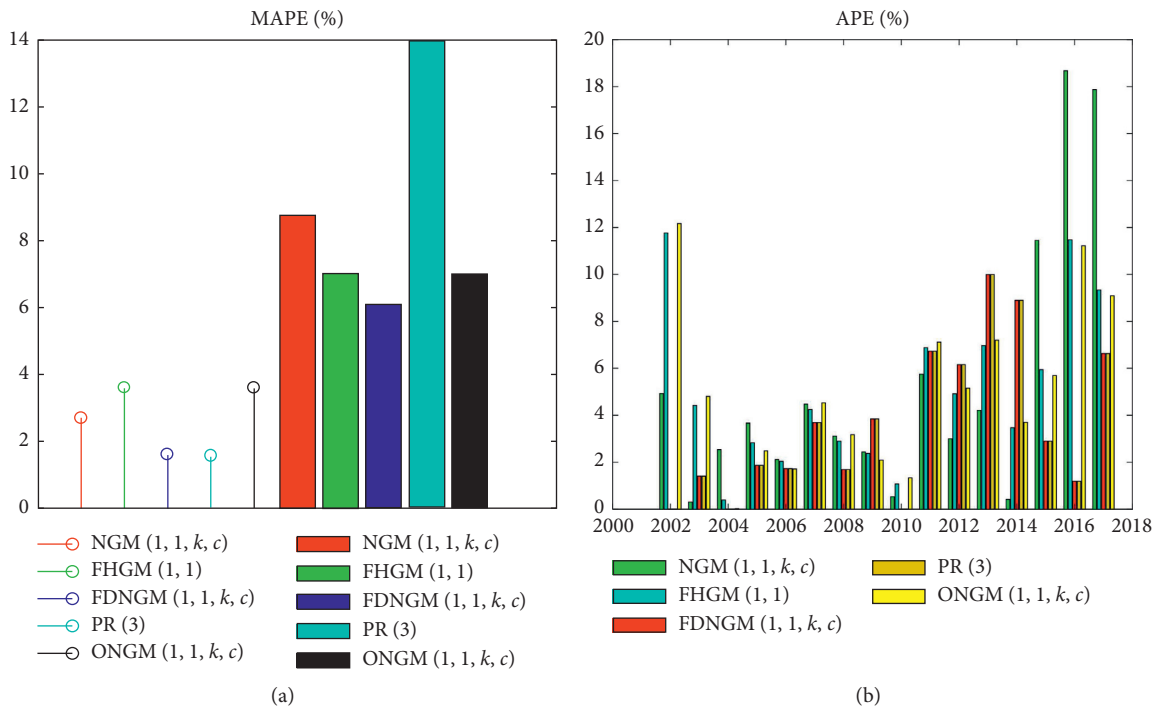

Figure 5: APEs and MAPEs of the competitive models in Case 2.

6. Conclusion

Aiming to improve the prediction precision of the existing NGM(1,1,k,c) model, this study establishes an optimised NGM(1,1,k,c) model by combining the ideal of fractional accumulation and dynamic integral median theorem. As a result, a novel model named FDNGM(1,1,k,c) is proposed thereby. The proposed model is proved to grasp a more flexible and general structure to fit different series by changing the variable of fractional accumulation parameter and dynamic background-value coefficients, thus obtaining a much stronger adaptability in practice. To demonstrate the performance of this approach, we carried out two practical examples to certify the feasibility of the FDNGM(1,1) approach. Additionally, this study presents the dynamic parameters to perfect the background value for the grey modeling technique, applicable for all grey forecasting models.

In addition, we have discussed the superiorities of the proposed FDNGM(1,1,k,c) model; however, it still has some shortcomings, for example, many parameters are contained in the proposed model (elaborated on in Section 3), which brings trouble into the calculation process. How to simplify the model structure will be addressed in our next work.

Data Availability

The data used to support the findings of this study are included within the article.

Conflicts of Interest

The authors declare that they have no conflicts of interest.

Acknowledgments

This work was supported by the National Natural Science Foundation of China (11661001).

References

[1] J. L. Deng, "Control problems of grey systems," *System Control Letter*, vol. 1, no. 5, pp. 288–294, 1982.
[2] C. Liu, W.-Z. Wu, W. Xie, T. Zhang, and J. Zhang, "Forecasting natural gas consumption of China by using a novel

fractional grey model with time power term," *Energy Reports*, vol. 7, pp. 788–797, 2021.

[3] B. Zeng, M. Zhou, X. Liu, and Z. Zhang, "Application of a new grey prediction model and grey average weakening buffer operator to forecast China's shale gas output," *Energy Reports*, vol. 6, pp. 1608–1618, 2020.

[4] W. Zhou, X. Wu, S. Ding, and J. Pan, "Application of a novel discrete grey model for forecasting natural gas consumption: a case study of Jiangsu Province in China," *Energy*, vol. 200, Article ID 117443, 2020.

[5] C. Zheng, W.-Z. Wu, W. Xie, Q. Li, and T. Zhang, "Forecasting the hydroelectricity consumption of China by using a novel unbiased nonlinear grey Bernoulli model," *Journal of Cleaner Production*, vol. 278, Article ID 123903, 2021.

[6] U. Şahin, "Projections of Turkey's electricity generation and installed capacity from total renewable and hydro energy using fractional nonlinear grey Bernoulli model and its reduced forms," *Sustainable Production and Consumption*, vol. 23, pp. 52–62, 2020.

[7] C. Liu, W.-Z. Wu, W. Xie, and J. Zhang, "Application of a novel fractional grey prediction model with time power term to predict the electricity consumption of India and China," *Chaos, Solitons & Fractals*, vol. 141, Article ID 110429, 2020.

[8] C. Liu, T. Lao, W. Z. Wu, and W. Xie, "Application of optimized fractional grey model-based variable background value to predict electricity consumption," *Fractals*, vol. 29, no. 2, 2020.

[9] H. Zhao and W. Lifeng, "Forecasting the non-renewable energy consumption by an adjacent accumulation grey model," *Journal of Cleaner Production*, vol. 275, Article ID 124113, 2020.

[10] S.-L. Lu, "Integrating heuristic time series with modified grey forecasting for renewable energy in Taiwan," *Renewable Energy*, vol. 133, pp. 1436–1444, 2019.

[11] S. Ding, "A novel discrete grey multivariable model and its application in forecasting the output value of China's high-tech industries," *Computers & Industrial Engineering*, vol. 127, pp. 749–760, 2019.

[12] L. Zeng, "Analysing the high-tech industry with a multivariable grey forecasting model based on fractional order accumulation," *Kybernetes*, vol. 48, no. 6, pp. 1158–1174, 2019.

[13] U. Şahin and T. Şahin, "Forecasting the cumulative number of confirmed cases of COVID-19 in Italy, UK and USA using fractional nonlinear grey Bernoulli model," *Chaos, Solitons, and Fractals*, vol. 138, Article ID 109948, 2020.

[14] Z. Lixia, T. Hong, and H. Miao, "Grey system analysis in the field of medicine and health," *Grey Systems: Theory and Application*, vol. 9, no. 2, pp. 251–258, 2019.

[15] J. Cui, Y. G. Dang, and S. F. Liu, "Novel grey forecasting model and its modeling mechanism," *Control and Decision*, vol. 24, no. 11, pp. 1702–1706, 2009.

[16] X. Ma and Z. Liu, "Predicting the cumulative oil field production using the novel grey ENGM model," *Journal of Computational and Theoretical Nanoscience*, vol. 13, no. 1, pp. 89–95, 2016.

[17] M. Tong, X. Zhou, and B. Zeng, "Optimization of background value in grey NGM(1,1,k) model," *Control and Decision*, vol. 32, no. 3, pp. 507–514, 2017.

[18] B. Zeng and S. Liu, "A self-adaptive intelligence gray prediction model with the optimal fractional order accumulating operator and its application," *Mathematical Methods in the Applied Sciences*, vol. 40, no. 18, pp. 7843–7857, 2017.

[19] L.-F. Wu, S.-F. Liu, W. Cui, D.-L. Liu, and T.-X. Yao, "Non-homogenous discrete grey model with fractional-order accumulation," *Neural Computing and Applications*, vol. 25, no. 5, pp. 1215–1221, 2014.

[20] W. Wu, X. Ma, Y. Zhang, W. Li, and Y. Wang, "A novel conformable fractional non-homogeneous grey model for forecasting carbon dioxide emissions of BRICS countries," *Science of the Total Environment*, vol. 707, Article ID 135447, 2020.

[21] L. Wu, S. Liu, L. Yao, S. Yan, and D. Liu, "Grey system model with the fractional order accumulation," *Communications in Nonlinear Science and Numerical Simulation*, vol. 18, no. 7, pp. 1775–1785, 2013.

[22] C. Liu, W. Xie, T. Lao et al., "Application of a novel grey forecasting model with time power term to predict China's GDP," *Grey Systems Theory and Application Ahead-of-Print*, vol. 93, 2020.

[23] S. Mao, M. Gao, X. Xiao, and M. Zhu, "A novel fractional grey system model and its application," *Applied Mathematical Modelling*, vol. 40, no. 7-8, pp. 5063–5076, 2016.

[24] X. Ma, X. Mei, W. Wu, X. Wu, and B. Zeng, "A novel fractional time delayed grey model with Grey Wolf Optimizer and its applications in forecasting the natural gas and coal consumption in Chongqing China," *Energy*, vol. 178, pp. 487–507, 2019.

[25] C. Liu, W. Xie, W.-Z. Wu, and H. Zhu, "Predicting Chinese total retail sales of consumer goods by employing an extended discrete grey polynomial model," *Engineering Applications of Artificial Intelligence*, vol. 102, no. 3, Article ID 104261, 2021.

[26] X. Zhu, Y. Dang, and S. Ding, "Using a self-adaptive grey fractional weighted model to forecast Jiangsu's electricity consumption in China," *Energy*, vol. 190, Article ID 116417, 2020.

[27] Y. Chen, W. Lifeng, L. Lianyi, and Z. Kai, "Fractional Hausdorff grey model and its properties," *Chaos, Solitons & Fractals*, vol. 138, Article ID 109915, 2020.

[28] X. Ma, W. Wu, B. Zeng, Y. Wang, and X. Wu, "The conformable fractional grey system model," *ISA Transactions*, vol. 96, pp. 255–271, 2020.

[29] S. Li, B. Zeng, X. Ma, and D. Zhang, "A novel grey model with A three-parameter background value and its application in forecasting average annual water consumption per capita in urban areas along the yangtze river basin," *Journal of Grey System*, vol. 32, no. 1, 2020.

[30] W. Zhang, R. Xiao, B. Shi, H.-h. Zhu, and Y.-j. Sun, "Forecasting slope deformation field using correlated grey model updated with time correction factor and background value optimization," *Engineering Geology*, vol. 260, Article ID 105215, 2019.

[31] S. Mirjalili and A. Lewis, "The whale optimization algorithm," *Advances in Engineering Software*, vol. 95, pp. 51–67, 2016.

[32] G. Xiong, J. Zhang, D. Shi, and Y. He, "Parameter extraction of solar photovoltaic models using an improved whale optimization algorithm," *Energy Conversion and Management*, vol. 174, pp. 388–405, 2018.

[33] M. A. E. Aziz, A. A. Ewees, and A. E. Hassanien, "Whale optimization algorithm and moth-flame optimization for multilevel thresholding image segmentation," *Expert Systems with Applications*, vol. 83, pp. 242–256, 2017.

[34] Z. Alameer, M. A. Elaziz, A. A. Ewees, H. Ye, and Z. Jianhua, "Forecasting gold price fluctuations using improved multilayer perceptron neural network and whale optimization algorithm," *Resources Policy*, vol. 61, pp. 250–260, 2019.

[35] B. Chen, *Polynomial Regression*, Springer Texts in Statistics, Berlin, Germany, 1986.

[36] Z. Liu, Y. G. Dang, and L. Wei, "Optimization of background value and time response function in NGM(1,1,k) control and decision," 2016.

Hindawi
Journal of Mathematics
Volume 2021, Article ID 9988073, 20 pages
https://doi.org/10.1155/2021/9988073

Research Article

New Stability Criterion for Fractional-Order Quaternion-Valued Neural Networks Involving Discrete and Leakage Delays

Bingjun Li[1] and Bingnan Tang[2]

[1]*School of Mathematics & Statistics Guizhou University of Finance and Economics, Guiyang 550025, China*
[2]*Business School, Jiangsu University of Technology, Changzhou 213001, China*

Correspondence should be addressed to Bingnan Tang; regales1988@sina.com

Received 29 March 2021; Revised 28 April 2021; Accepted 7 May 2021; Published 3 June 2021

Academic Editor: Lifeng Wu

In the current work, we are devoted to the issue of uniform stability of fractional-order quaternion-valued neural networks involving discrete and leakage delays. Making use of the contracting mapping theory, we prove that the equilibrium point of the involved fractional-order quaternion-valued neural networks exists and is unique. Taking advantage of mathematical analysis strategy, a sufficient criterion involving delay to verify the global uniform stability for the considered fractional-order quaternion-valued neural networks is set up. Computer simulation figures are displayed to sustain the rationality of the established conclusions. This study generalizes and supplements the research of Xiu et al. (2020).

1. Introduction

It is public knowledge that that neural networks own broad application prospects in numerous aspects and many demesnes such as pattern recognition, artificial intelligence, graph manipulation, psychophysics, control engineering, bioscience, and so on [1–3]. Generally speaking, time delay usually arises in artificial neural networks and biological systems due to the time lag of signal transmission. The study shows that the time delay often brings about some unexpected dynamical phenomena such as loss of stability, periodic vibration, chaos, and so on [4]. Thus, it is an important task for us to reveal the influence of time delay on various dynamical phenomena in delayed neural networks. During the past several decades, plenty of scholars made great effort to investigate a great variety of dynamical behaviors of delayed neural networks and fruitful results have been reported. For instance, Kong et al. [5] discussed the periodic and homoclinic solutions of discontinuous delayed neural networks. In 2019, Aouiti et al. [6] obtained the sufficient condition to ensure the existence and exponential stability of piecewise pseudo almost periodic solution to neutral-type inertial neural networks involving delays and impulses. In 2019, Huang et al. [7] set up a sufficient criterion to guarantee the existence of anti-periodic solutions and exponential stability for shunting inhibitory cellular neural networks involving proportional time delays by applying Lyapunov functional, inequality shills, and some mathematical analyses. In 2020, Abdelaziz and Chérif [8] carried out the study on the piecewise asymptotic almost periodic solutions of fuzzy Cohen–Grossberg neural networks involving impulsive effect. Xu and Li [9] did a valuable and novel work on anti-periodic solution to delayed cellular neural networks involving D operator. For more detailed publications, one can refer to [10–12].

All the above works are only concerned with real-valued neural networks. Here we would like to point out that there are other types of multidimensional valued neural networks. As the extension of real-valued neural networks (RVNNs), complex-valued neural networks (CVNNs) occupy an important position in handling signal and intrinsic information of neural networks. Especially, they are often applied in different physical waves such as sound wave, elastic wave, electronic wave, optical wave, and so on. In 1843, Hamilton [13] proposed quaternion-valued neural networks (QVNNs), which are extension version of RVNNs and

CVNNs. The skew of quaternion is given by $\mathcal{Q}: = \{y = y^R + iy^I + jy^J + ky^K\}$, where $y^R, y^I, y^J, y^K \in R$ and i, j, k obey the following operation:

$$\begin{aligned} ij &= -ji = k, \\ jk &= -kj = i, \\ ki &= -ik = j, \\ i^2 &= j^2 = k^2 = ijk = -1. \end{aligned} \tag{1}$$

The investigation on QVNNs has attracted great attention from a lot of scholars since they have been found to have tremendous application in numerous areas such as color night vision, image impression, spatial rotation, three dimension geometrical affine transformation, and so on [14–16]. At present, some fruits on the dynamics of QVNNs have been reported. For example, Lin et al. [17] dealt with the global exponential synchronization problem of inertial memristor-based QVNNs with delays. Jiang and Wang [18] studied the almost periodic solutions of delayed QVNNs. You et al. [19] made a detailed analysis on the exponential stability of discrete-time quaternion-valued neural networks with leakage delay and discrete delays. For more concrete literatures, we refer the readers to [20–24].

It is worth mentioning that all the above works on quaternion-valued neural networks mainly focus on the integer-order case and does not involve the fractional-order ones. The study on fractional-order neural networks has been keeping a very slow level due to the lack of actual background and fractional calculus theories. With the development of the research on fractional calculus, it is recognized that fractional-order differential system has greater advantages than classical integer-order one since it can give a description of the hereditary trait and memory nature for many materials and dynamic processes [14, 15]. Recently, lots of fractional-order neural networks have already aroused high attention from academic circles and a great deal of excellent fruits on fractional-order neural networks have been reported constantly. For instance, Udhayakumar et al. [25] focused on the multiple ψ-type stability issue for fractional-order quaternion-valued neural networks. Liu et al. [26] set up a set of sufficient conditions to guarantee the asymptotic synchronization of fractional-order neural networks involving delays. Du and Lu [27] investigated the finite-time synchronization problem for fractional-order delayed memristor-based neural networks. For more detailed studies, we refer the readers to [28–37]. However, there are few publications on fractional-order quaternion-valued neural networks. Stimulated by the discussion above, in this work, we will explore the research on the stability for fractional-order quaternion-valued neural networks involving delays. In a word, this work will mainly focus on the following issues: (a) prove the existence and uniqueness of equilibrium point of fractional-order quaternion-valued neural networks; (b) set up the sufficient criterion to ensure global uniform stability of fractional-order quaternion-valued neural networks.

In 2017, Zhang et al. [4] studied the following complex-valued neural networks:

$$\frac{d^\rho u_i(t)}{dt^\rho} = -\gamma_i u_i(t - \rangle) + \sum_{h=1}^{m} \alpha_{ih} g_h(u_h(t)) + \sum_{h=1}^{m} \beta_{ih} g_h(u_h(t - \vartheta)) + L_i, \tag{2}$$

where $i = 1, 2, \ldots, m$, $\rho \in (0, 1)$, $u_i(t) \in \mathscr{C}$ ($\mathscr{C}$ denotes the set of complex numbers) stands for the state of the ith neuron at time t, $\alpha_{ih}, \beta_{ih} \in \mathscr{C}$ stand for the connection weight without and with time delays, respectively, $L_i \in \mathscr{C}$ denotes the external input, $\vartheta, \varrho \geq 0$ stand for the transmission delay and the leakage delay, respectively, and $g_h \in \mathscr{C}$ denotes the activation function. For details, one can see [4]. Making use of contraction mapping principle, a sufficient condition to ensure the existence and uniqueness of the equilibrium point for system (2) is set up. Applying mathematical analysis skills, a set of delay-dependent criteria to check the global uniform stability of system (2) is established.

In this present work, we modify system (2) as the following fractional-order quaternion-valued neural networks:

$$\frac{d^\rho u_i(t)}{dt^\rho} = -\gamma_i u_i(t - \rangle) + \sum_{h=1}^{m} \alpha_{ih} g_h(u_h(t)) + \sum_{h=1}^{m} \beta_{ih} g_h(u_h(t - \vartheta)) + L_i, \tag{3}$$

where $i = 1, 2, \ldots, m$, $\rho \in (0, 1)$, $u_i(t) \in \mathcal{Q}$ stands for the state of the ith neuron at time t, $\alpha_{ih}, \beta_{ih} \in \mathcal{Q}$ stand for the connection weight without and with time delays, respectively, $L_i \in \mathcal{Q}$ denotes the external input, $\vartheta, \varrho \geq 0$ stand for the transmission delay and the leakage delay, respectively, and $g_h \in \mathcal{Q}$ denotes the activation function.

This paper is organized as follows. In Section 2, the basic definitions, lemmas, and essential theories on fractional calculus and quaternion algebra are given. In Section 3, the existence and uniqueness of solution of model (3) are stated. In Section 4, a new delay-dependent criterion to check the global uniform stability of model (3) is derived. In Section 5, software simulation plots are presented to support the derived chief conclusions of this study. Section 6 ends this paper.

2. Preliminaries and Assumptions

Now we give some related notations. $\mathscr{Z}_+$ stands for the set of positive integer numbers, and i, j, k are imaginary units. $\mathcal{Q}^n, \mathscr{R}^{m\times n}, \mathcal{Q}^{m\times n}$ stand for the set of n-dimensional quaternion-valued vectors, $m \times n$ real-valued matrices, and quaternion-valued matrices. The norm of quaternion-valued matrices $M = (m_{ij})_{n\times n} \in \mathcal{Q}^{n\times n}$ is given by $\|M\| = \sqrt{\sum_{i=1}^{n}\sum_{j=1}^{n} |m_{ij}|^2}$. Denote $C([-T, 0], R^m)$ the Banach space of continuous m-real vector functions defined on $[-T, 0]$ with the norm $\|\phi(t)\| = \max_{i=1,2,\ldots,m}\sup_{t\in[-T,0]}\{e^t|\phi_i(t)|\}$, where $\phi \in C([-T, 0], R^m)$. For $u(t) = (u_1(t), u_2(t), \ldots, u_m(t))^T \in C([0, +\infty), R^m)$, the norm of $u(t)$ is defined by $\|u(t)\| = \max_{i=1,2,\ldots,m}\sup_{t\in[0,+\infty)}\{e^t|u_i(t)|\}$.

Definition 1 (see [38]). The Caputo fractional-order derivative with order ρ for the function $u(\alpha)$ is given by

$$\mathscr{D}^{\rho}u(\beta)=\frac{1}{\Gamma(l-\rho)}\int_{\beta_0}^{\beta}\frac{u^{(l)}(\nu)}{(\beta-\nu)^{\rho-l+1}}\mathrm{d}\nu, \tag{4}$$

where $u(\beta)\in([\beta_0,\infty),R)$, $\Gamma(s)=\int_0^{\infty}\beta^{s-1}e^{-\beta}d\beta$, $\beta\geq\beta_0$, and $l\in\mathscr{Z}^{+}$, $l-1\leq\rho<l$; $\mathscr{D}^{\rho}u(\beta)$ implies that $d^{\rho}u(\beta)/d\beta$ is a Caputo fractional-order derivative operator.

For each $y=y^R+iy^I+jy^J+ky^K\in\mathbb{Q}$ and each activation $g\colon\mathbb{Q}\longrightarrow\mathbb{Q}$, g_h has the form:

$$g(y)=g^R\left(y^R,y^I,y^J,y^K\right)+g^I\left(y^R,y^I,y^J,y^K\right)+g^J\left(y^R,y^I,y^J,y^K\right)+g^K\left(y^R,y^I,y^J,y^K\right). \tag{5}$$

Thus, $g_h(u)$ in system (3) has the following form:

$$g_h(u_h)=g_h^R\left(y_h^R,y_h^I,y_h^J,y_h^K\right)+g_h^I\left(y_h^R,y_h^I,y_h^J,y_h^K\right)+g_h^J\left(y_h^R,y_h^I,y_h^J,y_h^K\right)+g_h^K\left(y_h^R,y_h^I,y_h^J,y_h^K\right), \tag{6}$$

where $h=1,2,\ldots,m$.

System (3) can be rewritten as the following equivalent form:

$$\frac{d^{\rho}u(t)}{\mathrm{d}t^{\rho}}=-\mathscr{A}u(t-\rangle)+\mathscr{B}g(u(t))+\mathscr{C}g(u(t-\vartheta))+\mathscr{L}, \tag{7}$$

where $u(t)=(u_1(t),u_2(t),\ldots,u_m(t))^T\in\mathbb{Q}^m$, $\mathscr{A}=(\gamma_1,\gamma_2,\ldots,\gamma_m)^T\in R^{m\times m}$, $\mathscr{B}=(\alpha_{ih})_{m\times m}\in\mathbb{Q}^{m\times m}$, $\mathscr{C}=(\beta_{ih})_{m\times m}\in\mathbb{Q}^{m\times m}$, $\mathscr{L}=(L_i)_{m\times m}\in\mathbb{Q}^{m\times m}$, $g(u(t))=(g_1(u_1(t)),g_2(u_2(t)),\ldots,g_m(u_m(t)))\in\mathbb{Q}^{m\times m}$, $\rho\in(0,1)$, and $\vartheta,\varrho\geq0$.

The initial values of (3) can be written as follows:

$$u_h(s)=\phi_h^R(s)+i\phi_h^I(s)+j\phi_h^J(s)+k\phi_h^K(s),\quad s\in[-\tau,0],\ h=1,2,\ldots,m, \tag{8}$$

where
$\tau=\max\{\rangle,\vartheta\}$, $\phi_h^R(s),\phi_h^I(s),\phi_h^J(s),\phi_h^K(s)\in C([-\tau,0],R)$.

Definition 2 (see [39]). We say that the equilibrium point u^* of model (3) is stable provided that for every $\epsilon>0$, $\exists\ \zeta=\eta(t_0,\varepsilon)>0$ which satisfies $t\geq t_0\geq0$, $\|\phi(t)-u^*\|\leq\zeta$ which implies $\|u(t,t_0,\phi)-u^*\|\leq\varepsilon$ for every solution $u(t,t_0,\phi)$ of model (1). The equilibrium point u^* of model (3) is uniformly stable provided that η has nothing to do with t_0.

Lemma 1 (see [40]). *Let $u(t)\in C^n[0,\infty)$ and $n-1<\rho<n\in\mathscr{Z}_+$; then, the following equalities hold.*

(i) $\mathscr{D}^{-r_1}\mathscr{D}^{-r_2}u(t)=\mathscr{D}^{-(r_1+r_2)}u(t)$, $r_1,r_2\geq0$.

(ii) $\mathscr{D}^{r}\mathscr{D}^{-r}u(t)=u(t)$, $r\geq0$.

(iii) $\mathscr{D}^{-r}\mathscr{D}^{r}u(t)=u(t)-\sum_{l=0}^{n-1}(t^l/l!)u^{(l)}(0)$, $r\geq0$.

In order to obtain the key results of this study, we give the hypotheses as follows.

$(\mathscr{H}_1)$ $g_h(0,0,0,0)=0$ *and* $\exists$ *positive constants* $\mathscr{G}_h^{RR},\mathscr{G}_h^{RI},\mathscr{G}_h^{RJ},\mathscr{G}_h^{RK},\mathscr{G}_h^{IR},\mathscr{G}_h^{II},\mathscr{G}_h^{IJ},\mathscr{G}_h^{IK},\mathscr{G}_h^{JR},\mathscr{G}_h^{JI},\mathscr{G}_h^{JJ},\mathscr{G}_h^{JK},\mathscr{G}_h^{KR},\mathscr{G}_h^{KI},\mathscr{G}_h^{KJ},\mathscr{G}_h^{KK}$ *such that*

$$\begin{cases}\left|g_h^R\left(y_h^R,y_h^I,y_h^J,y_h^K\right)-g_h^R\left(x_h^R,x_h^I,x_h^J,x_h^K\right)\right|\leq\mathscr{G}_h^{RR}\left|y_h^R-x_h^R\right|+\mathscr{G}_h^{RI}\left|y_h^I-x\right|_h^I+\mathscr{G}_h^{RJ}\left|y_h^J-x_h^J\right|+\mathscr{G}_h^{RK}\left|y_h^K-x_h^K\right|,\\ \left|g_h^I\left(y_h^R,y_h^I,y_h^J,y_h^K\right)-g_h^I\left(x_h^R,x_h^I,x_h^J,x_h^K\right)\right|\leq\mathscr{G}_h^{IR}\left|y_h^R-x_h^R\right|+\mathscr{G}_h^{II}\left|y_h^I-x_h^I\right|+\mathscr{G}_h^{IJ}\left|y_h^J-x_h^J\right|+\mathscr{G}_h^{IK}\left|y_h^K-x_h^K\right|,\\ \left|g_h^J\left(y_h^R,y_h^I,y_h^J,y_h^K\right)-g_h^J\left(x_h^R,x_h^I,x_h^J,x_h^K\right)\right|\leq\mathscr{G}_h^{JR}\left|y_h^R-x_h^R\right|+\mathscr{G}_h^{JI}\left|y_h^I-x_h^I\right|+\mathscr{G}_h^{JJ}\left|y_h^J-x_h^J\right|+\mathscr{G}_h^{JK}\left|y_h^K-x_h^K\right|,\\ \left|g_h^K\left(y_h^R,y_h^I,y_h^J,y_h^K\right)-g_h^K\left(x_h^R,x_h^I,x_h^J,x_h^K\right)\right|\leq\mathscr{G}_h^{KR}\left|y_h^R-x_h^R\right|+\mathscr{G}_h^{KI}\left|y_h^I-x_h^I\right|+\mathscr{G}_h^{KJ}\left|y_h^J-x_h^J\right|+\mathscr{G}_h^{KK}\left|y_h^K-x_h^K\right|,\end{cases} \tag{9}$$

for every $x_h^R, x_h^I, x_h^J, x_h^K \in R$ *and* $h = 1, 2, \ldots, m$.

3. Existence and Uniqueness

In this part, we investigate the existence and uniqueness of the equilibrium point for model (3) (i.e., (7)). Let $u^* \in \mathbb{Q}^m$ be the equilibrium point for model (7); then, we have

$$-\mathscr{A}u^* + \mathscr{B}g(u^*) + \mathscr{C}g(u^*) + \mathscr{L} = 0. \tag{10}$$

Then,

$$u^* = \mathscr{A}^{-1}(\mathscr{B} + \mathscr{C})g(u^*) + \mathscr{A}^{-1}\mathscr{L}. \tag{11}$$

From (11), we know that if we can prove the following map: Γ: $\mathbb{Q}^m \longrightarrow \mathbb{Q}^m$,

$$\Gamma(u) = \mathscr{A}^{-1}(\mathscr{B} + \mathscr{C})g(u^*) + \mathscr{A}^{-1}\mathscr{L} \tag{12}$$

has a unique fixed point, then we can conclude that the equilibrium point of model (7) exists and is unique.

$(\mathscr{H}_2)\theta\|\mathscr{U}\| < 1$, where $\theta = \max_{h=1,2,\ldots,m}\{\sqrt{\theta_{h1}}, \sqrt{\theta_{h2}}, \sqrt{\theta_{h3}}, \sqrt{\theta_{h4}}\}$, $\mathscr{U} = \mathscr{A}^{-1}(\mathscr{B} + \mathscr{C})$ and

$$\begin{cases}
\theta_{h1} = \left(\mathscr{G}_h^{RR}\right)^2 + \mathscr{G}_h^{RR}\mathscr{G}_h^{RI}\mathscr{G}_h^{RR}\mathscr{G}_h^{RJ} + \mathscr{G}_h^{RR}\mathscr{G}_h^{RK} + \left(\mathscr{G}_h^{IR}\right)^2 + \mathscr{G}_h^{IR}\mathscr{G}_h^{II} + \mathscr{G}_h^{IR}\mathscr{G}_h^{IJ} \\
+ \mathscr{G}_h^{IR}\mathscr{G}_h^{IK} + \left(\mathscr{G}_h^{JR}\right)^2 + \mathscr{G}_h^{JR}\mathscr{G}_h^{JI} + \mathscr{G}_h^{JR}\mathscr{G}_h^{JJ} + \mathscr{G}_h^{JR}\mathscr{G}_h^{JK} + \left(\mathscr{G}_h^{KR}\right)^2 \\
+ \mathscr{G}_h^{KR}\mathscr{G}_h^{KI} + \mathscr{G}_h^{KR}\mathscr{G}_h^{KJ} + \mathscr{G}_h^{KR}\mathscr{G}_h^{KK}, \\
\theta_{h1} = \left(\mathscr{G}_h^{RI}\right)^2 + \mathscr{G}_h^{RR}\mathscr{G}_h^{RI} + \mathscr{G}_h^{RI}\mathscr{G}_h^{RJ} + \left(\mathscr{G}_h^{II}\right)^2 + \mathscr{G}_h^{IR}\mathscr{G}_h^{II} + \mathscr{G}_h^{II}\mathscr{G}_h^{IJ} + \left(\mathscr{G}_h^{JI}\right)^2 \\
+ \mathscr{G}_h^{JR}\mathscr{G}_h^{JI} + \mathscr{G}_h^{JI}\mathscr{G}_h^{JJ} + \left(\mathscr{G}_h^{KI}\right)^2 + \mathscr{G}_h^{KR}\mathscr{G}_h^{KI} + \mathscr{G}_h^{KI}\mathscr{G}_h^{KJ}, \\
\theta_{h1} = \left(\mathscr{G}_h^{RJ}\right)^2\mathscr{G}_h^{RR}\mathscr{G}_h^{RJ} + \mathscr{G}_h^{RI}\mathscr{G}_h^{RJ} + \mathscr{G}_h^{RJ}\mathscr{G}_h^{RK} + \mathscr{G}_h^{RJ}\mathscr{G}_h^{RK} + \left(\mathscr{G}_h^{IJ}\right)^2 + \mathscr{G}_h^{IR}\mathscr{G}_h^{IJ} \\
+ \mathscr{G}_h^{II}\mathscr{G}_h^{IJ} + \mathscr{G}_h^{IJ}\mathscr{G}_h^{IK} + \mathscr{G}_h^{IJ}\mathscr{G}_h^{IK} + \left(\mathscr{G}_h^{JJ}\right)^2 + \mathscr{G}_h^{JR}\mathscr{G}_h^{JJ} + \mathscr{G}_h^{JI}\mathscr{G}_h^{JJ} + \mathscr{G}_h^{JJ}\mathscr{G}_h^{JK} \\
+ \mathscr{G}_h^{JJ}\mathscr{G}_h^{JK} + \left(\mathscr{G}_h^{KJ}\right)^2 + \mathscr{G}_h^{KR}\mathscr{G}_h^{KJ} + \mathscr{G}_h^{KI}\mathscr{G}_h^{KJ} + \mathscr{G}_h^{KJ}\mathscr{G}_h^{KK} + \mathscr{G}_h^{KJ}\mathscr{G}_h^{KK}, \\
\theta_{h1} = \left(\mathscr{G}_h^{RK}\right)^2 + \mathscr{G}_h^{RR}\mathscr{G}_h^{RK} + \mathscr{G}_h^{RJ}\mathscr{G}_h^{RK} + \mathscr{G}_h^{RJ}\mathscr{G}_h^{RK} + \left(\mathscr{G}_h^{IK}\right)^2 + \mathscr{G}_h^{IR}\mathscr{G}_h^{IK} + \mathscr{G}_h^{IJ}\mathscr{G}_h^{IK} \\
+ \mathscr{G}_h^{IJ}\mathscr{G}_h^{IK} + \left(\mathscr{G}_h^{JK}\right)^2 + \mathscr{G}_h^{JR}\mathscr{G}_h^{JK} + \mathscr{G}_h^{JJ}\mathscr{G}_h^{JK} + \mathscr{G}_h^{JJ}\mathscr{G}_h^{JK} + \left(\mathscr{G}_h^{KK}\right)^2 + \mathscr{G}_h^{KR}\mathscr{G}_h^{KK} \\
+ \mathscr{G}_h^{KJ}\mathscr{G}_h^{KK} + \mathscr{G}_h^{KJ}\mathscr{G}_h^{KK}.
\end{cases} \tag{13}$$

Theorem 1. *If* $(\mathscr{H}_1)$ *and* $(\mathscr{H}_2)$ *hold, then model (3) owns a unique equilibrium point.*

Proof. Let $u_1 = u_1^R + iu_1^I + ju_1^J + ku_1^K$ and $u_2 = u_2^R + iu_2^I + ju_2^J + ku_2^K$. Then,

$$\begin{aligned}
&\left|g_h(u_1) - g_h(u_2)\right|^2 \\
&= \left|g_h^R(u_1) + ig_h^I(u_1) + jg_h^J(u_1) + kg_h^K(u_1) - \left(g_h^R(u_2) + ig_h^I(u_2) + jg_h^J(u_2) + kg_h^K(u_2)\right)\right|^2 \\
&= \left|g_h^R(u_1) - g_h^R(u_2)\right|^2 + \left|g_h^I(u_1) - g_h^I(u_2)\right|^2 + \left|g_h^J(u_1) - g_h^J(u_2)\right|^2 + \left|g_h^K(u_1) - g_h^K(u_2)\right|^2 \\
&\le \left[\mathscr{G}_h^{RR}\left|u_{1h}^R - u_{2h}^R\right| + \mathscr{G}_h^{RI}\left|u_{1h}^I - u_{2h}^I\right| + \mathscr{G}_h^{RJ}\left|u_{1h}^J - u_{2h}^J\right| + \mathscr{G}_h^{RK}\left|u_{1h}^K - u_{2h}^K\right|\right]^2 \\
&\quad + \left[\mathscr{G}_h^{IR}\left|u_{1h}^R - u_{2h}^R\right| + \mathscr{G}_h^{II}\left|u_{1h}^I - u_{2h}^I\right| + \mathscr{G}_h^{IJ}\left|u_{1h}^J - u_{2h}^J\right| + \mathscr{G}_h^{IK}\left|u_{1h}^K - u_{2h}^K\right|\right]^2 \\
&\quad + \left[\mathscr{G}_h^{JR}\left|u_{1h}^R - u_{2h}^R\right| + \mathscr{G}_h^{JI}\left|u_{1h}^I - u_{2h}^I\right| + \mathscr{G}_h^{JJ}\left|u_{1h}^J - u_{2h}^J\right| + \mathscr{G}_h^{JK}\left|u_{1h}^K - u_{2h}^K\right|\right]^2 \\
&\quad + \left[\mathscr{G}_h^{KR}\left|u_{1h}^R - u_{2h}^R\right| + \mathscr{G}_h^{KI}\left|u_{1h}^I - u_{2h}^I\right| + \mathscr{G}_h^{KJ}\left|u_{1h}^J - u_{2h}^J\right| + \mathscr{G}_h^{KK}\left|u_{1h}^K - u_{2h}^K\right|\right]^2
\end{aligned}$$

$$
\begin{aligned}
&= \left(\mathcal{G}_h^{RR}\right)^2\left|u_{1h}^R - u_{2h}^R\right|^2 + \left(\mathcal{G}_h^{RI}\right)^2\left|u_{1h}^I - u_{2h}^I\right|^2 + \left(\mathcal{G}_h^{RJ}\right)^2\left|u_{1h}^J - u_{2h}^J\right|^2 + \left(\mathcal{G}_h^{RK}\right)^2\left|u_{1h}^K - u_{2h}^K\right|^2 \\
&\quad + 2\mathcal{G}_h^{RR}\mathcal{G}_h^{RI}\left|u_{1h}^R - x_h^R\right|\left|u_{1h}^I - u_{2h}^I\right| + 2\mathcal{G}_h^{RR}\mathcal{G}_h^{RJ}\left|u_{1h}^R - u_{2h}^R\right|\left|u_{1h}^J - u_{2h}^J\right| \\
&\quad + 2\mathcal{G}_h^{RR}\mathcal{G}_h^{RK}\left|u_{1h}^R - x_h^R\right|\left|u_{1h}^K - u_{2h}^K\right| + 2\mathcal{G}_h^{RI}\mathcal{G}_h^{RJ}\left|u_{1h}^I - u_{2h}^I\right|\left|u_{1h}^J - u_{2h}^J\right| \\
&\quad + 2\mathcal{G}_h^{RJ}\mathcal{G}_h^{RK}\left|u_{1h}^J - x_h^J\right|\left|u_{1h}^K - u_{2h}^K\right| + 2\mathcal{G}_h^{RJ}\mathcal{G}_h^{RK}\left|u_{1h}^J - u_{2h}^J\right|\left|u_{1h}^K - u_{2h}^K\right| \\
&\quad + \left(\mathcal{G}_h^{IR}\right)^2\left|u_{1h}^R - u_{2h}^R\right|^2 + \left(\mathcal{G}_h^{II}\right)^2\left|u_{1h}^I - u_{2h}^I\right|^2 + \left(\mathcal{G}_h^{IJ}\right)^2\left|u_{1h}^J - u_{2h}^J\right|^2 + \left(\mathcal{G}_h^{IK}\right)^2\left|u_{1h}^K - u_{2h}^K\right|^2 \\
&\quad + 2\mathcal{G}_h^{IR}\mathcal{G}_h^{II}\left|u_{1h}^R - x_h^R\right|\left|u_{1h}^I - u_{2h}^I\right| + 2\mathcal{G}_h^{IR}\mathcal{G}_h^{IJ}\left|u_{1h}^R - u_{2h}^R\right|\left|u_{1h}^J - u_{2h}^J\right| \\
&\quad + 2\mathcal{G}_h^{IR}\mathcal{G}_h^{IK}\left|u_{1h}^R - x_h^R\right|\left|u_{1h}^K - u_{2h}^K\right| + 2\mathcal{G}_h^{II}\mathcal{G}_h^{IJ}\left|u_{1h}^I - u_{2h}^I\right|\left|u_{1h}^J - u_{2h}^J\right| \\
&\quad + 2\mathcal{G}_h^{IJ}\mathcal{G}_h^{IK}\left|u_{1h}^J - x_h^J\right|\left|u_{1h}^K - u_{2h}^K\right| + 2\mathcal{G}_h^{IJ}\mathcal{G}_h^{IK}\left|u_{1h}^J - u_{2h}^J\right|\left|u_{1h}^K - u_{2h}^K\right| \\
&\quad + \left(\mathcal{G}_h^{JR}\right)^2\left|u_{1h}^R - u_{2h}^R\right|^2 + \left(\mathcal{G}_h^{JI}\right)^2\left|u_{1h}^I - u_{2h}^I\right|^2 + \left(\mathcal{G}_h^{JJ}\right)^2\left|u_{1h}^J - u_{2h}^J\right|^2 + \left(\mathcal{G}_h^{JK}\right)^2\left|u_{1h}^K - u_{2h}^K\right|^2 \\
&\quad + 2\mathcal{G}_h^{JR}\mathcal{G}_h^{JI}\left|u_{1h}^R - x_h^R\right|\left|u_{1h}^I - u_{2h}^I\right| + 2\mathcal{G}_h^{JR}\mathcal{G}_h^{JJ}\left|u_{1h}^R - u_{2h}^R\right|\left|u_{1h}^J - u_{2h}^J\right| \\
&\quad + 2\mathcal{G}_h^{JR}\mathcal{G}_h^{JK}\left|u_{1h}^R - x_h^R\right|\left|u_{1h}^K - u_{2h}^K\right| + 2\mathcal{G}_h^{JI}\mathcal{G}_h^{JJ}\left|u_{1h}^I - u_{2h}^I\right|\left|u_{1h}^J - u_{2h}^J\right| \\
&\quad + 2\mathcal{G}_h^{JJ}\mathcal{G}_h^{JK}\left|u_{1h}^J - x_h^J\right|\left|u_{1h}^K - u_{2h}^K\right| + 2\mathcal{G}_h^{JJ}\mathcal{G}_h^{JK}\left|u_{1h}^J - u_{2h}^J\right|\left|u_{1h}^K - u_{2h}^K\right| \\
&\quad + \left(\mathcal{G}_h^{KR}\right)^2\left|u_{1h}^R - u_{2h}^R\right|^2 + \left(\mathcal{G}_h^{KI}\right)^2\left|u_{1h}^I - u_{2h}^I\right|^2 + \left(\mathcal{G}_h^{KJ}\right)^2\left|u_{1h}^J - u_{2h}^J\right|^2 + \left(\mathcal{G}_h^{KK}\right)^2\left|u_{1h}^K - u_{2h}^K\right|^2 \\
&\quad + 2\mathcal{G}_h^{KR}\mathcal{G}_h^{KI}\left|u_{1h}^R - x_h^R\right|\left|u_{1h}^I - u_{2h}^I\right| + 2\mathcal{G}_h^{KR}\mathcal{G}_h^{KJ}\left|u_{1h}^R - u_{2h}^R\right|\left|u_{1h}^J - u_{2h}^J\right| \\
&\quad + 2\mathcal{G}_h^{KR}\mathcal{G}_h^{KK}\left|u_{1h}^R - x_h^R\right|\left|u_{1h}^K - u_{2h}^K\right| + 2\mathcal{G}_h^{KI}\mathcal{G}_h^{KJ}\left|u_{1h}^I - u_{2h}^I\right|\left|u_{1h}^J - u_{2h}^J\right| \\
&\quad + 2\mathcal{G}_h^{KJ}\mathcal{G}_h^{KK}\left|u_{1h}^J - x_h^J\right|\left|u_{1h}^K - u_{2h}^K\right| + 2\mathcal{G}_h^{KJ}\mathcal{G}_h^{KK}\left|u_{1h}^J - u_{2h}^J\right|\left|u_{1h}^K - u_{2h}^K\right| \\
&\le \left(\mathcal{G}_h^{RR}\right)^2\left|u_{1h}^R - u_{2h}^R\right|^2 + \left(\mathcal{G}_h^{RI}\right)^2\left|u_{1h}^I - u_{2h}^I\right|^2 + \left(\mathcal{G}_h^{RJ}\right)^2\left|u_{1h}^J - u_{2h}^J\right|^2 + \left(\mathcal{G}_h^{RK}\right)^2\left|u_{1h}^K - u_{2h}^K\right|^2 \\
&\quad + \mathcal{G}_h^{RR}\mathcal{G}_h^{RI}\left(\left|u_{1h}^R - x_h^R\right|^2 + \left|u_{1h}^I - u_{2h}^I\right|^2\right) + \mathcal{G}_h^{RR}\mathcal{G}_h^{RJ}\left(\left|u_{1h}^R - u_{2h}^R\right|^2 + \left|u_{1h}^J - u_{2h}^J\right|^2\right) \\
&\quad + \mathcal{G}_h^{RR}\mathcal{G}_h^{RK}\left(\left|u_{1h}^R - x_h^R\right|^2 + \left|u_{1h}^K - u_{2h}^K\right|^2\right) + \mathcal{G}_h^{RI}\mathcal{G}_h^{RJ}\left(\left|u_{1h}^I - u_{2h}^I\right|^2 + \left|u_{1h}^J - u_{2h}^J\right|^2\right) \\
&\quad + \mathcal{G}_h^{RJ}\mathcal{G}_h^{RK}\left(\left|u_{1h}^J - x_h^J\right|^2 + \left|u_{1h}^K - u_{2h}^K\right|^2\right) + \mathcal{G}_h^{RJ}\mathcal{G}_h^{RK}\left(\left|u_{1h}^J - u_{2h}^J\right|^2 + \left|u_{1h}^K - u_{2h}^K\right|^2\right) \\
&\quad + \left(\mathcal{G}_h^{IR}\right)^2\left|u_{1h}^R - u_{2h}^R\right|^2 + \left(\mathcal{G}_h^{II}\right)^2\left|u_{1h}^I - u_{2h}^I\right|^2 + \left(\mathcal{G}_h^{IJ}\right)^2\left|u_{1h}^J - u_{2h}^J\right|^2 + \left(\mathcal{G}_h^{IK}\right)^2\left|u_{1h}^K - u_{2h}^K\right|^2 \\
&\quad + \mathcal{G}_h^{IR}\mathcal{G}_h^{II}\left(\left|u_{1h}^R - x_h^R\right|^2 + \left|u_{1h}^I - u_{2h}^I\right|^2\right) + \mathcal{G}_h^{IR}\mathcal{G}_h^{IJ}\left(\left|u_{1h}^R - u_{2h}^R\right|^2 + \left|u_{1h}^J - u_{2h}^J\right|\right)^2 \\
&\quad + \mathcal{G}_h^{IR}\mathcal{G}_h^{IK}\left(\left|u_{1h}^R - x_h^R\right|^2 + \left|u_{1h}^K - u_{2h}^K\right|^2\right) + \mathcal{G}_h^{II}\mathcal{G}_h^{IJ}\left(\left|u_{1h}^I - u_{2h}^I\right|^2 + \left|u_{1h}^J - u_{2h}^J\right|^2\right) \\
&\quad + \mathcal{G}_h^{IJ}\mathcal{G}_h^{IK}\left(\left|u_{1h}^J - x_h^J\right|^2 + \left|u_{1h}^K - u_{2h}^K\right|^2\right) + \mathcal{G}_h^{IJ}\mathcal{G}_h^{IK}\left(\left|u_{1h}^J - u_{2h}^J\right|^2 + \left|u_{1h}^K - u_{2h}^K\right|^2\right) \\
&\quad + \left(\mathcal{G}_h^{JR}\right)^2\left|u_{1h}^R - u_{2h}^R\right|^2 + \left(\mathcal{G}_h^{JI}\right)^2\left|u_{1h}^I - u_{2h}^I\right|^2 + \left(\mathcal{G}_h^{JJ}\right)^2\left|u_{1h}^J - u_{2h}^J\right|^2 + \left(\mathcal{G}_h^{JK}\right)^2\left|u_{1h}^K - u_{2h}^K\right|^2 \\
&\quad + \mathcal{G}_h^{JR}\mathcal{G}_h^{JI}\left(\left|u_{1h}^R - x_h^R\right|^2 + \left|u_{1h}^I - u_{2h}^I\right|^2\right) + \mathcal{G}_h^{JR}\mathcal{G}_h^{JJ}\left(\left|u_{1h}^R - u_{2h}^R\right|^2 + \left|u_{1h}^J - u_{2h}^J\right|^2\right) \\
&\quad + \mathcal{G}_h^{JR}\mathcal{G}_h^{JK}\left(\left|u_{1h}^R - x_h^R\right|^2 + \left|u_{1h}^K - u_{2h}^K\right|^2\right) + \mathcal{G}_h^{JI}\mathcal{G}_h^{JJ}\left(\left|u_{1h}^I - u_{2h}^I\right|^2 + \left|u_{1h}^J - u_{2h}^J\right|^2\right) \\
&\quad + \mathcal{G}_h^{JJ}\mathcal{G}_h^{JK}\left(\left|u_{1h}^J - x_h^J\right|^2 + \left|u_{1h}^K - u_{2h}^K\right|^2\right) + \mathcal{G}_h^{JJ}\mathcal{G}_h^{JK}\left(\left|u_{1h}^J - u_{2h}^J\right|^2 + \left|u_{1h}^K - u_{2h}^K\right|^2\right) \\
&\quad + \left(\mathcal{G}_h^{KR}\right)^2\left|u_{1h}^R - u_{2h}^R\right|^2 + \left(\mathcal{G}_h^{KI}\right)^2\left|u_{1h}^I - u_{2h}^I\right|^2 + \left(\mathcal{G}_h^{KJ}\right)^2\left|u_{1h}^J - u_{2h}^J\right|^2 + \left(\mathcal{G}_h^{KK}\right)^2\left|u_{1h}^K - u_{2h}^K\right|^2 \\
&\quad + \mathcal{G}_h^{KR}\mathcal{G}_h^{KI}\left(\left|u_{1h}^R - x_h^R\right|^2 + \left|u_{1h}^I - u_{2h}^I\right|^2\right) + \mathcal{G}_h^{KR}\mathcal{G}_h^{KJ}\left(\left|u_{1h}^R - u_{2h}^R\right|^2 + \left|u_{1h}^J - u_{2h}^J\right|^2\right) \\
&\quad + \mathcal{G}_h^{JR}\mathcal{G}_h^{JI}\left(\left|u_{1h}^R - x_h^R\right|^2 + \left|u_{1h}^I - u_{2h}^I\right|^2\right) + \mathcal{G}_h^{JR}\mathcal{G}_h^{JJ}\left(\left|u_{1h}^R - u_{2h}^R\right|^2 + \left|u_{1h}^J - u_{2h}^J\right|^2\right) \\
&\quad + \mathcal{G}_h^{KJ}\mathcal{G}_h^{KK}\left(\left|u_{1h}^J - x_h^J\right|^2 + \left|u_{1h}^K - u_{2h}^K\right|^2\right) + \mathcal{G}_h^{KJ}\mathcal{G}_h^{KK}\left(\left|u_{1h}^J - u_{2h}^J\right|^2 + \left|u_{1h}^K - u_{2h}^K\right|^2\right) \\
&= \theta_{h1}\left|u_{1h}^R - u_{2h}^R\right|^2 + \theta_{h2}\left|u_{1h}^I - u_{2h}^I\right|^2 + \theta_{h3}\left|u_{1h}^J - u_{2h}^J\right|^2 + \theta_{h4}\left|u_{1h}^K - u_{2h}^K\right|^2.
\end{aligned}
\tag{14}
$$

Then, for any $u_1, u_2 \in \mathcal{Q}^m$, one has

$$\left\|\Gamma(u_1) - \Gamma(u_2)\right\| = \left\|\mathcal{U}(g(u_1) - g(u_2))\right\| \le \theta\|\mathcal{U}\|\left\|u_1 - u_2\right\|. \tag{15}$$

In view of $(\mathcal{H}_2)$, one can easily know that $\Gamma(u)$ is contractive map. Thus, $\Gamma(u)$ owns a unique fixed point, which implies that model (3) owns a unique equilibrium point. The proof finishes. □

4. Uniform Stability

In the current part, we explore the global uniform stability issue of the equilibrium point for model (3). Let

$$\begin{cases} \mathcal{A}_1^{p_1} = 1 - \left[e^{-\rangle}\gamma + \sum_{h=1}^{m}\left(\left|\alpha_{p_1h}^R\right|\mathcal{G}_h^{RR} + \left|\alpha_{p_1h}^I\right|\mathcal{G}_h^{IR} + \left|\alpha_{p_1h}^J\right|\mathcal{G}_h^{JR} + \left|\alpha_{p_1h}^K\right|\mathcal{G}_h^{KR}\right) + e^{-\vartheta}\sum_{h=1}^{m}\left(\left|\beta_{p_1h}^R\right|\mathcal{G}_h^{RR} + \left|\beta_{p_1h}^I\right|\mathcal{G}_h^{IR} + \left|\beta_{p_1h}^J\right|\mathcal{G}_h^{JR} + \left|\beta_{p_1h}^K\right|\mathcal{G}_h^{KR}\right)\right] \\ \mathcal{A}_2^{p_1} = \sum_{h=1}^{m}\left(\left|\alpha_{p_1h}^R\right|\mathcal{G}_h^{RI} + \left|\alpha_{p_1h}^I\right|\mathcal{G}_h^{II} + \left|\alpha_{p_1h}^J\right|\mathcal{G}_h^{JI} + \left|\alpha_{p_1h}^K\right|\mathcal{G}_h^{KI}\right) + e^{-\vartheta}\sum_{h=1}^{m}\left(\left|\beta_{p_1h}^R\right|\mathcal{G}_h^{RI} + \left|\beta_{p_1h}^I\right|\mathcal{G}_h^{II} + \left|\beta_{p_1h}^J\right|\mathcal{G}_h^{JI} + \left|\beta_{p_1h}^K\right|\mathcal{G}_h^{KI}\right), \end{cases} \tag{16}$$

$$\begin{cases} \mathcal{A}_3^{p_1} = \sum_{h=1}^{m}\left(\left|\alpha_{p_1h}^R\right|\mathcal{G}_h^{RJ} + \left|\alpha_{p_1h}^I\right|\mathcal{G}_h^{IJ} + \left|\alpha_{p_1h}^J\right|\mathcal{G}_h^{JJ} + \left|\alpha_{p_1h}^K\right|\mathcal{G}_h^{KJ}\right) + e^{-\vartheta}\sum_{h=1}^{m}\left(\left|\beta_{p_1h}^R\right|\mathcal{G}_h^{RJ} + \left|\beta_{p_1h}^I\right|\mathcal{G}_h^{IJ} + \left|\beta_{p_1h}^J\right|\mathcal{G}_h^{JJ} + \left|\beta_{p_1h}^K\right|\mathcal{G}_h^{KJ}\right), \\ \mathcal{A}_4^{p_1} = \sum_{h=1}^{m}\left(\left|\alpha_{p_1h}^R\right|\mathcal{G}_h^{RK} + \left|\alpha_{p_1h}^I\right|\mathcal{G}_h^{IK} + \left|\alpha_{p_1h}^J\right|\mathcal{G}_h^{JK} + \left|\alpha_{p_1h}^K\right|\mathcal{G}_h^{KK}\right) + e^{-\vartheta}\sum_{h=1}^{m}\left(\left|\beta_{p_1h}^R\right|\mathcal{G}_h^{RK} + \left|\beta_{p_1h}^I\right|\mathcal{G}_h^{IK} + \left|\beta_{p_1h}^J\right|\mathcal{G}_h^{JK} + \left|\beta_{p_1h}^K\right|\mathcal{G}_h^{KK}\right), \\ \mathcal{A}_5^{p_1} = 1 + e^{-\rangle}\gamma + e^{-\vartheta}\sum_{h=1}^{m}\left(\left|\beta_{p_1h}^R\right|\mathcal{G}_h^{RR} + \left|\beta_{p_1h}^I\right|\mathcal{G}_h^{IR} + \left|\beta_{p_1h}^J\right|\mathcal{G}_h^{JR} + \left|\beta_{p_1h}^K\right|\mathcal{G}_h^{KR}\right), \\ \mathcal{A}_6^{p_1} = e^{-\vartheta}\sum_{h=1}^{m}\left(\left|\beta_{p_1h}^R\right|\mathcal{G}_h^{RI} + \left|\beta_{p_1h}^I\right|\mathcal{G}_h^{II} + \left|\beta_{p_1h}^J\right|\mathcal{G}_h^{JI} + \left|\beta_{p_1h}^K\right|\mathcal{G}_h^{KI}\right), \\ \mathcal{A}_7^{p_1} = e^{-\vartheta}\sum_{h=1}^{m}\left(\left|\beta_{p_1h}^R\right|\mathcal{G}_h^{RJ} + \left|\beta_{p_1h}^I\right|\mathcal{G}_h^{IJ} + \left|\beta_{p_1h}^J\right|\mathcal{G}_h^{JJ} + \left|\beta_{p_1h}^K\right|\mathcal{G}_h^{KJ}\right), \\ \mathcal{A}_8^{p_1} = e^{-\vartheta}\sum_{h=1}^{m}\left(\left|\beta_{p_1h}^R\right|\mathcal{G}_h^{RK} + \left|\beta_{p_1h}^I\right|\mathcal{G}_h^{IK} + \left|\beta_{p_1h}^J\right|\mathcal{G}_h^{JK} + \left|\beta_{p_1h}^K\right|\mathcal{G}_h^{KK}\right), \\ \mathcal{B}_1^{p_2} = 1 - \left[e^{-\rangle}\gamma + \sum_{h=1}^{m}\left(\left|\alpha_{p_2h}^I\right|\mathcal{G}_h^{II} + \left|\alpha_{p_2h}^R\right|\mathcal{G}_h^{RI} + \left|\alpha_{p_2h}^J\right|\mathcal{G}_h^{JI} + |\alpha|_{p_2h}^K\mathcal{G}_h^{KI}\right) + e^{-\vartheta}\sum_{h=1}^{m}\left(\left|\beta_{p_2h}^I\right|\mathcal{G}_h^{II} + \left|\beta_{p_2h}^R\right|\mathcal{G}_h^{RI} + \left|\beta_{p_2h}^J\right|\mathcal{G}_h^{JI} + \left|\beta_{p_2h}^K\right|\mathcal{G}_h^{KI}\right)\right], \end{cases}$$

$$\begin{cases} \mathcal{B}_2^{p_2} = \sum_{h=1}^{m}\left(\left|\alpha_{p_2h}^I\right|\mathcal{G}_h^{IR} + \left|\alpha_{p_2h}^R\right|\mathcal{G}_h^{RR} + \left|\alpha_{p_2h}^J\right|\mathcal{G}_h^{JR} + \left|\alpha_{p_2h}^K\right|\mathcal{G}_h^{KR}\right) + e^{-\vartheta}\sum_{h=1}^{m}\left(\left|\beta_{p_2h}^I\right|\mathcal{G}_h^{IR} + \left|\beta_{p_2h}^R\right|\mathcal{G}_h^{RR} + \left|\beta_{p_2h}^J\right|\mathcal{G}_h^{JR} + \left|\beta_{p_2h}^K\right|\mathcal{G}_h^{KR}\right), \\ \mathcal{B}_3^{p_2} = \sum_{h=1}^{m}\left(\left|\alpha_{p_2h}^I\right|\mathcal{G}_h^{IJ} + \left|\alpha_{p_2h}^R\right|\mathcal{G}_h^{RJ} + \left|\alpha_{p_2h}^J\right|\mathcal{G}_h^{JJ} + \left|\alpha_{p_2h}^K\right|\mathcal{G}_h^{KJ}\right) + e^{-\vartheta}\sum_{h=1}^{m}\left(\left|\beta_{p_2h}^I\right|\mathcal{G}_h^{IJ} + \left|\beta_{p_2h}^I\right|\mathcal{G}_h^{RJ} + \left|\beta_{p_2h}^J\right|\mathcal{G}_h^{JJ} + \left|\beta_{p_2h}^K\right|\mathcal{G}_h^{KJ}\right), \\ \mathcal{B}_4^{p_2} = \sum_{h=1}^{m}\left(\left|\alpha_{p_2h}^I\right|\mathcal{G}_h^{IK} + \left|\alpha_{p_2h}^I\right|\mathcal{G}_h^{RK} + \left|\alpha_{p_2h}^J\right|\mathcal{G}_h^{JK} + \left|\alpha_{p_2h}^K\right|\mathcal{G}_h^{KK}\right) + e^{-\vartheta}\sum_{h=1}^{m}\left(\left|\beta_{p_2h}^I\right|\mathcal{G}_h^{IK} + \left|\beta_{p_2h}^I\right|\mathcal{G}_h^{RK} + \left|\beta_{p_2h}^J\right|\mathcal{G}_h^{JK} + \left|\beta_{p_2h}^K\right|\mathcal{G}_h^{KK}\right), \\ \mathcal{B}_5^{p_2} = 1 + e^{-\rangle}\gamma + e^{-\vartheta}\sum_{h=1}^{m}\left(\left|\beta_{p_2h}^I\right|\mathcal{G}_h^{II} + \left|\beta_{p_2h}^I\right|\mathcal{G}_h^{RI} + \left|\beta_{p_2h}^J\right|\mathcal{G}_h^{JI} + \left|\beta_{p_2h}^K\right|\mathcal{G}_h^{KI}\right), \\ \mathcal{B}_6^{p_2} = e^{-\vartheta}\sum_{h=1}^{m}\left(\left|\beta_{p_2h}^I\right|\mathcal{G}_h^{IR} + \left|\beta_{p_2h}^I\right|\mathcal{G}_h^{RR} + \left|\beta_{p_2h}^J\right|\mathcal{G}_h^{JR} + \left|\beta_{p_2h}^K\right|\mathcal{G}_h^{KR}\right), \\ \mathcal{B}_7^{p_2} = e^{-\vartheta}\sum_{h=1}^{m}\left(\left|\beta_{p_2h}^I\right|\mathcal{G}_h^{IJ} + \left|\beta_{p_2h}^I\right|\mathcal{G}_h^{RJ} + \left|\beta_{p_2h}^J\right|\mathcal{G}_h^{JJ} + \left|\beta_{p_2h}^K\right|\mathcal{G}_h^{KJ}\right), \\ \mathcal{B}_8^{p_2} = e^{-\vartheta}\sum_{h=1}^{m}\left(\left|\beta_{p_2h}^I\right|\mathcal{G}_h^{IK} + \left|\beta_{p_2h}^R\right|\mathcal{G}_h^{RK} + \left|\beta_{p_2h}^J\right|\mathcal{G}_h^{JK} + \left|\beta_{p_2h}^K\right|\mathcal{G}_h^{KK}\right), \\ \mathcal{C}_1^{p_3} = 1 - \left[e^{-\rangle}\gamma + \sum_{h=1}^{m}\left(\left|\alpha_{p_3h}^J\right|\mathcal{G}_h^{JJ} + \left|\alpha_{p_3h}^I\right|\mathcal{G}_h^{IJ} + \left|\alpha_{p_3h}^R\right|\mathcal{G}_h^{RJ} + \left|\alpha_{p_3h}^K\right|\mathcal{G}_h^{KJ}\right) + e^{-\vartheta}\sum_{h=1}^{m}\left(\left|\beta_{p_3h}^J\right|\mathcal{G}_h^{JJ} + \left|\beta_{p_3h}^I\right|\mathcal{G}_h^{IJ} + \left|\beta_{p_3h}^R\right|\mathcal{G}_h^{RJ} + \left|\beta_{p_3h}^K\right|\mathcal{G}_h^{KJ}\right)\right], \end{cases} \tag{17}$$

$$
\begin{cases}
\mathscr{C}_2^{p_3} = \sum_{h=1}^{m}\left(\left|\alpha_{p_3h}^{J}\right|\mathscr{G}_h^{JI} + \left|\alpha_{p_3h}^{I}\right|\mathscr{G}_h^{II} + \left|\alpha_{p_3h}^{R}\right|\mathscr{G}_h^{RI} + \left|\alpha_{p_3h}^{K}\right|\mathscr{G}_h^{KI}\right) + e^{-\vartheta}\sum_{h=1}^{m}\left(\left|\beta_{p_3h}^{J}\right|\mathscr{G}_h^{JI} + \left|\beta_{p_3h}^{I}\right|\mathscr{G}_h^{II} + \left|\beta_{p_3h}^{R}\right|\mathscr{G}_h^{RI} + \left|\beta_{p_3h}^{K}\right|\mathscr{G}_h^{KI}\right),\\
\mathscr{C}_3^{p_3} = \sum_{h=1}^{m}\left(\left|\alpha_{p_3h}^{J}\right|\mathscr{G}_h^{JR} + \left|\alpha_{p_3h}^{I}\right|\mathscr{G}_h^{IR} + \left|\alpha_{p_3h}^{R}\right|\mathscr{G}_h^{RR} + \left|\alpha_{p_3h}^{K}\right|\mathscr{G}_h^{KR}\right) + e^{-\vartheta}\sum_{h=1}^{m}\left(\left|\beta_{p_3h}^{J}\right|\mathscr{G}_h^{JR} + \left|\beta_{p_3h}^{I}\right|\mathscr{G}_h^{IR} + \left|\beta_{p_3h}^{R}\right|\mathscr{G}_h^{RR} + \left|\beta_{p_3h}^{K}\right|\mathscr{G}_h^{KR}\right),\\
\mathscr{C}_4^{p_3} = \sum_{h=1}^{m}\left(\left|\alpha_{p_3h}^{J}\right|\mathscr{G}_h^{JK} + \left|\alpha_{p_3h}^{I}\right|\mathscr{G}_h^{IK} + \left|\alpha_{p_3h}^{R}\right|\mathscr{G}_h^{RK} + \left|\alpha_{p_3h}^{K}\right|\mathscr{G}_h^{KK}\right) + e^{-\vartheta}\sum_{h=1}^{m}\left(\left|\beta_{p_1h}^{J}\right|\mathscr{G}_h^{JK} + \left|\beta_{p_3h}^{I}\right|\mathscr{G}_h^{IK} + \left|\beta_{p_3h}^{J}\right|\mathscr{G}_h^{RK} + \left|\beta_{p_3h}^{K}\right|\mathscr{G}_h^{KK}\right),\\
\mathscr{C}_5^{p_3} = 1 + e^{-\rangle}\gamma + e^{-\vartheta}\sum_{h=1}^{m}\left(\left|\beta_{p_3h}^{J}\right|\mathscr{G}_h^{JJ} + \left|\beta_{p_3h}^{I}\right|\mathscr{G}_h^{IJ} + \left|\beta_{p_3h}^{R}\right|\mathscr{G}_h^{RJ} + \left|\beta_{p_3h}^{K}\right|\mathscr{G}_h^{KJ}\right),\\
\mathscr{C}_6^{p_3} = e^{-\vartheta}\sum_{h=1}^{m}\left(\left|\beta_{p_3h}^{J}\right|\mathscr{G}_h^{JI} + \left|\beta_{p_3h}^{I}\right|\mathscr{G}_h^{II} + \left|\beta_{p_3h}^{R}\right|\mathscr{G}_h^{RI} + \left|\beta_{p_3h}^{K}\right|\mathscr{G}_h^{KI}\right),\\
\mathscr{C}_7^{p_3} = e^{-\vartheta}\sum_{h=1}^{m}\left(\left|\beta_{p_3h}^{J}\right|\mathscr{G}_h^{JR} + \left|\beta_{p_3h}^{I}\right|\mathscr{G}_h^{IR} + \left|\beta_{p_3h}^{J}\right|\mathscr{G}_h^{RR} + \left|\beta_{p_3h}^{K}\right|\mathscr{G}_h^{KR}\right),\\
\mathscr{C}_8^{p_3} = e^{-\vartheta}\sum_{h=1}^{m}\left(\left|\beta_{p_3h}^{J}\right|\mathscr{G}_h^{JK} + \left|\beta_{p_3h}^{I}\right|\mathscr{G}_h^{IK} + \left|\beta_{p_3h}^{R}\right|\mathscr{G}_h^{RK} + \left|\beta_{p_3h}^{K}\right|\mathscr{G}_h^{KK}\right),\\
\mathscr{D}_1^{p_4} = 1 - \left[e^{-\rangle}\gamma + \sum_{h=1}^{m}\left(\left|\alpha_{p_4h}^{K}\right|\mathscr{G}_h^{KK} + \left|\alpha_{p_4h}^{I}\right|\mathscr{G}_h^{IK} + \left|\alpha_{p_4h}^{J}\right|\mathscr{G}_h^{JK} + \left|\alpha_{p_4h}^{R}\right|\mathscr{G}_h^{RK}\right) + e^{-\vartheta}\sum_{h=1}^{m}\left(\left|\beta_{p_4h}^{K}\right|\mathscr{G}_h^{KK} + \left|\beta_{p_4h}^{I}\right|\mathscr{G}_h^{IK} + \left|\beta_{p_4h}^{J}\right|\mathscr{G}_h^{JK} + \left|\beta_{p_4h}^{R}\right|\mathscr{G}_h^{RK}\right)\right],
\end{cases}
$$

$$
\begin{cases}
\mathscr{D}_4^{p_4} = \sum_{h=1}^{m}\left(\left|\alpha_{p_4h}^{K}\right|\mathscr{G}_h^{KI} + \left|\alpha_{p_4h}^{I}\right|\mathscr{G}_h^{II} + \left|\alpha_{p_4h}^{J}\right|\mathscr{G}_h^{JI} + \left|\alpha_{p_4h}^{R}\right|\mathscr{G}_h^{RI}\right) + e^{-\vartheta}\sum_{h=1}^{m}\left(\left|\beta_{p_4h}^{K}\right|\mathscr{G}_h^{KI} + \left|\beta_{p_4h}^{I}\right|\mathscr{G}_h^{II} + \left|\beta_{p_4h}^{J}\right|\mathscr{G}_h^{JI} + \left|\beta_{p_4h}^{R}\right|\mathscr{G}_h^{RI}\right),\\
\mathscr{D}_4^{p_4} = \sum_{h=1}^{m}\left(\left|\alpha_{p_4h}^{K}\right|\mathscr{G}_h^{KJ} + \left|\alpha_{p_4h}^{I}\right|\mathscr{G}_h^{IJ} + \left|\alpha_{p_4h}^{J}\right|\mathscr{G}_h^{JJ} + \left|\alpha_{p_4h}^{R}\right|\mathscr{G}_h^{RJ}\right) + e^{-\vartheta}\sum_{h=1}^{m}\left(\left|\beta_{p_4h}^{K}\right|\mathscr{G}_h^{KJ} + \left|\beta_{p_4h}^{I}\right|\mathscr{G}_h^{IJ} + \left|\beta_{p_4h}^{J}\right|\mathscr{G}_h^{JJ} + \left|\beta_{p_4h}^{R}\right|\mathscr{G}_h^{RJ}\right),\\
\mathscr{D}_4^{p_4} = \sum_{h=1}^{m}\left(\left|\alpha_{p_4h}^{K}\right|\mathscr{G}_h^{KR} + \left|\alpha_{p_4h}^{I}\right|\mathscr{G}_h^{IR} + \left|\alpha_{p_4h}^{J}\right|\mathscr{G}_h^{JR} + \left|\alpha_{p_4h}^{R}\right|\mathscr{G}_h^{RR}\right) + e^{-\vartheta}\sum_{h=1}^{m}\left(\left|\beta_{p_4h}^{K}\right|\mathscr{G}_h^{KR} + \left|\beta_{p_4h}^{I}\right|\mathscr{G}_h^{IR} + \left|\beta_{p_4h}^{J}\right|\mathscr{G}_h^{JR} + \left|\beta_{p_4h}^{R}\right|\mathscr{G}_h^{RR}\right),\\
\mathscr{D}_5^{p_4} = 1 + e^{-\rangle}\gamma + e^{-\vartheta}\sum_{h=1}^{m}\left(\left|\beta_{p_1h}^{K}\right|\mathscr{G}_h^{KK} + \left|\beta_{p_4h}^{I}\right|\mathscr{G}_h^{IK} + \left|\beta_{p_4h}^{J}\right|\mathscr{G}_h^{JK} + \left|\beta_{p_4h}^{R}\right|\mathscr{G}_h^{RK}\right),\\
\mathscr{D}_6^{p_4} = e^{-\vartheta}\sum_{h=1}^{m}\left(\left|\beta_{p_4h}^{K}\right|\mathscr{G}_h^{KI} + \left|\beta_{p_4h}^{I}\right|\mathscr{G}_h^{II} + \left|\beta_{p_4h}^{J}\right|\mathscr{G}_h^{JI} + \left|\beta_{p_4h}^{R}\right|\mathscr{G}_h^{RI}\right),\\
\mathscr{D}_7^{p_4} = e^{-\vartheta}\sum_{h=1}^{m}\left(\left|\beta_{p_4h}^{K}\right|\mathscr{G}_h^{KJ} + \left|\beta_{p_4h}^{I}\right|\mathscr{G}_h^{IJ} + \left|\beta_{p_4h}^{J}\right|\mathscr{G}_h^{JJ} + \left|\beta_{p_4h}^{R}\right|\mathscr{G}_h^{RJ}\right),\\
\mathscr{D}_8^{p_4} = e^{-\vartheta}\sum_{h=1}^{m}\left(\left|\beta_{p_4h}^{K}\right|\mathscr{G}_h^{KR} + \left|\beta_{p_4h}^{I}\right|\mathscr{G}_h^{IR} + \left|\beta_{p_4h}^{J}\right|\mathscr{G}_h^{JR} + \left|\beta_{p_4h}^{R}\right|\mathscr{G}_h^{RR}\right),
\end{cases}
\tag{18}
$$

where $\gamma = \max_{i=1,2,\ldots,m}\{\gamma_i\}$ and $p_1, p_2, p_3, p_4 \in \{1, 2, \ldots, m\}$. Assume that $(\mathscr{H}_3)$ $\mathscr{W} = \min\{\mathscr{W}_1, \mathscr{W}_2, \mathscr{W}_3, \mathscr{W}_4\} > 0$, where

$$
\begin{cases}
\mathscr{W}_1 = \mathscr{A}_1^{p_1} - \mathscr{B}_2^{p_2} - \mathscr{C}_2^{p_3} - \mathscr{D}_2^{p_4},\\
\mathscr{W}_2 = \mathscr{B}_1^{p_1} - \mathscr{A}_2^{p_1} - \mathscr{C}_3^{p_3} - \mathscr{D}_3^{p_4},\\
\mathscr{W}_3 = \mathscr{C}_1^{p_3} - \mathscr{A}_1^{p_1} - \mathscr{B}_3^{p_2} - \mathscr{D}_4^{p_4},\\
\mathscr{W}_4 = \mathscr{D}_1^{p_4} - \mathscr{A}_4^{p_1} - \mathscr{B}_4^{p_2} - \mathscr{C}_3^{p_3}.
\end{cases}
\tag{19}
$$

Theorem 2. *If $(\mathscr{H}_1)$-$(\mathscr{H}_3)$ hold, then equilibrium point of system (3) is uniformly stable.*

Proof. In view of Theorem 1, we know that system (3) has a unique equilibrium point $u^* = (u_1^*, u_2^*, \ldots, u_m^*)^T$. Let $\overline{u}(t) = u(t) - u^*$; then, system (3) becomes

$$
\frac{d^{\rho}\overline{u}(t)}{dt^{\rho}} = -\mathscr{A}\overline{u}(t - \rangle) + \mathscr{B}f(\overline{u}) + \mathscr{C}f(\overline{u}(t - \vartheta)),
\tag{20}
$$

where $f(\overline{u}(t)) = g(u(t)) - g(u^*)$. The initial value

$$
\overline{u}_h(s) = \overline{\phi}_h^R(s) + i\overline{\phi}_h^I(s) + j\overline{\phi}_h^J(s) + k\overline{\phi}_h^K(s), \quad s \in [-\tau, 0],\ h = 1, 2, \ldots, m,
\tag{21}
$$

where $\tau = \max\{\rangle, \vartheta\}$, $\phi_h^R(s), \overline{\phi}_h^I(s), \overline{\phi}_h^J(s), \overline{\phi}_h^K(s) \in C([-\tau, 0], R)$, and $\overline{\phi}_h^R(s) = \phi_h^R(s) - u_h^*, \overline{\phi}_h^I(s) = \phi_h^I(s) - u_h^*, \overline{\phi}_h^J(s) = \phi_h^J(s) - u_h^*, \overline{\phi}_h^K(s) = \phi_h^K(s) - u_h^*$ and $\overline{u}(t) = (\overline{u}_1(t), \overline{u}_2(t), \ldots, \overline{u}_m(t))^T$. Let $\overline{u}(t) = \overline{u}^R(t) + i\overline{u}^I(t) + j\overline{u}^J(t) + k\overline{u}^K(t)$, where $\overline{u}^R(t) = (\overline{u}_1^R(t), \overline{u}_2^R(t), \ldots, \overline{u}_m^R(t)^T)$, $\overline{u}^I(t) = (\overline{u}_1^I(t), \overline{u}_2^I(t), \ldots, \overline{u}_m^I(t)^T)$, $\overline{u}^J(t) = (\overline{u}_1^J(t), \overline{u}_2^J(t), \ldots, \overline{u}_m^J(t)^T)$, $\overline{u}^K(t) = \overline{u}_1^K(t), \overline{u}_2^K(t), \ldots, \overline{u}_m^K(t)^T$. It follows from (20) that

$$
\begin{aligned}
&\frac{d^\rho \overline{u}_i^R(t)}{dt^\rho} + i\frac{d^\rho \overline{u}_i^I(t)}{dt^\rho} + j\frac{d^\rho \overline{u}_i^J(t)}{dt^\rho} + k\frac{d^\rho \overline{u}_i^K(t)}{dt^\rho} \\
&\quad = -\gamma_i \overline{u}_i^R(t - \rangle) + \sum_{h=1}^{m}\left[\alpha_{ih}^R g_h^R - \alpha_{ih}^I g_h^I - \alpha_{ih}^J g_h^J - \alpha_{ih}^K g_h^K\right] \\
&\quad + \sum_{h=1}^{m}\left[\beta_{ih}^R \tilde{g}_h^R - \beta_{ih}^I \tilde{g}_h^I - \beta_{ih}^J \tilde{g}_h^J - \beta_{ih}^K \tilde{g}_h^K\right] \\
&\quad + i\left\{-\gamma_i \overline{u}_i^I(t - \rangle) + \sum_{h=1}^{m}\left[\alpha_{ih}^I g_h^R + \alpha_{ih}^R(t) g_h^I - \alpha_{ih}^K(t) g_h^J + \alpha_{ih}^J g_h^K\right] + \sum_{h=1}^{m}\left[\beta_{ih}^I \tilde{g}_h^R + \beta_{ih}^R \tilde{g}_h^I - \beta_{ih}^K \tilde{g}_h^J + \beta_{ih}^J \tilde{g}_h^K\right]\right\} \\
&\quad + j\left\{-\gamma_i \overline{u}_i^J(t - \rangle) + \sum_{h=1}^{m}\left[\alpha_{ih}^J g_h^R + \alpha_{ih}^K g_h^I + \alpha_{ih}^R g_h^J - \alpha_{ih}^I\left(g_h^K\right)\right] + \sum_{h=1}^{m}\left[\beta_{ih}^J \tilde{g}_h^R + \beta_{ih}^K \tilde{g}_h^I + \beta_{ih}^R \tilde{g}_h^J - \beta_{ih}^I \tilde{g}_h^K\right]\right\} \\
&\quad + k\left\{-\gamma_i \overline{u}_i^K(t - \rangle) + \sum_{h=1}^{m}\left[\alpha_{ih}^K g_h^R - \alpha_{ih}^J g_h^I + \alpha_{ih}^I g_h^J + \alpha_{ih}^R g_h^K\right] + \sum_{h=1}^{m}\left[\beta_{ih}^K \tilde{g}_h^R - \beta_{ih}^J \tilde{g}_h^I + \beta_{ih}^I \tilde{g}_h^J + \beta_{ih}^R \tilde{g}_h^K\right]\right\},
\end{aligned}
\tag{22}
$$

where

$$
\begin{cases}
g_h^R = g_h^R\left(\overline{u}_h^R(t), \overline{u}_h^i(t), \overline{u}_h^J(t), \overline{u}_h^K(t)\right), \\
g_h^I = g_h^I\left(\overline{u}_h^R(t), \overline{u}_h^i(t), \overline{u}_h^J(t), \overline{u}_h^K(t)\right), \\
g_h^J = g_h^J\left(\overline{u}_h^R(t), \overline{u}_h^i(t), \overline{u}_h^J(t), \overline{u}_h^K(t)\right), \\
g_h^K = g_h^K\left(\overline{u}_h^R(t), \overline{u}_h^i(t), \overline{u}_h^J(t), \overline{u}_h^K(t)\right), \\
\tilde{g}_h^R = \tilde{g}_h^R\left(\overline{u}_h^R(t - \vartheta), \overline{u}_h^i(t - \vartheta), \overline{u}_h^J(t - \vartheta), \overline{u}_h^K(t - \vartheta)\right), \\
\tilde{g}_h^I = \tilde{g}_h^I\left(\overline{u}_h^R(t - \vartheta), \overline{u}_h^i(t - \vartheta), \overline{u}_h^J(t - \vartheta), \overline{u}_h^K(t - \vartheta)\right), \\
\tilde{g}_h^J = \tilde{g}_h^J\left(\overline{u}_h^R(t - \vartheta), \overline{u}_h^i(t - \vartheta), \overline{u}_h^J(t - \vartheta), \overline{u}_h^K(t - \vartheta)\right), \\
\tilde{g}_h^K = \tilde{g}_h^K\left(\overline{u}_h^R(t - \vartheta), \overline{u}_h^i(t - \vartheta), \overline{u}_h^J(t - \vartheta), \overline{u}_h^K(t - \vartheta)\right).
\end{cases}
\tag{23}
$$

It follows from (22) that

$$\begin{cases} \dfrac{d^{\rho}\overline{u}_i^R(t)}{\mathrm{d}t^{\rho}} = -\gamma_i\overline{u}_i^R(t-\rangle) + \sum_{h=1}^{m}\left[\alpha_{ih}^R g_h^R - \alpha_{ih}^I g_h^I - \alpha_{ih}^J g_h^J - \alpha_{ih}^K g_h^K\right] + \sum_{h=1}^{m}\left[\beta_{ih}^R \tilde{g}_h^R - \beta_{ih}^I \tilde{g}_h^I - \beta_{ih}^J \tilde{g}_h^J - \beta_{ih}^K \tilde{g}_h^K\right], \\ \dfrac{d^{\rho}\overline{u}_i^I(t)}{\mathrm{d}t^{\rho}} = -\gamma_i\overline{u}_i^I(t-\rangle) + \sum_{h=1}^{m}\left[\alpha_{ih}^I g_h^R + \alpha_{ih}^R g_h^I - \alpha_{ih}^K g_h^J + \alpha_{ih}^J g_h^K\right] + \sum_{h=1}^{m}\left[\beta_{ih}^I \tilde{g}_h^R + \beta_{ih}^R \tilde{g}_h^I - \beta_{ih}^K \tilde{g}_h^J + \beta_{ih}^J \tilde{g}_h^K\right] \\ \dfrac{d^{\rho}\overline{u}_i^J(t)}{\mathrm{d}t^{\rho}} = -\gamma_i\overline{u}_i^J(t-\rangle) + \sum_{h=1}^{m}\left[\alpha_{ih}^J g_h^R + \alpha_{ih}^K g_h^I + \alpha_{ih}^R g_h^J - \alpha_{ih}^I g_h^K\right] + \sum_{h=1}^{m}\left[\beta_{ih}^J \tilde{g}_h^R + \beta_{ih}^K \tilde{g}_h^I + \beta_{ih}^R \tilde{g}_h^J - \beta_{ih}^I \tilde{g}_h^K\right], \\ \dfrac{d^{\rho}\overline{u}_i^K(t)}{\mathrm{d}t^{\rho}} = -\gamma_i\overline{u}_i^K(t-\rangle) + \sum_{h=1}^{m}\left[\alpha_{ih}^K g_h^R - \alpha_{ih}^J g_h^I + \alpha_{ih}^I g_h^J + \alpha_{ih}^R g_h^K\right] + \sum_{h=1}^{m}\left[\beta_{ih}^K \tilde{g}_h^R - \beta_{ih}^J \tilde{g}_h^I + \beta_{ih}^I \tilde{g}_h^J + \beta_{ih}^R \tilde{g}_h^K\right], \end{cases} \tag{24}$$

where $i = 1, 2, \ldots, m$. In view of Lemma 1, one gets

$$\begin{cases} \overline{u}_i^R(t) - \overline{u}_i^R(0) = \dfrac{d^{-\rho}\overline{u}_i^R(t)}{\mathrm{d}t^{-\rho}}\left\{-\gamma_i\overline{u}_i^R(t-\rangle) + \sum_{h=1}^{m}\left[\alpha_{ih}^R g_h^R - \alpha_{ih}^I g_h^I - \alpha_{ih}^J g_h^J - \alpha_{ih}^K g_h^K\right] + \sum_{h=1}^{m}\left[\beta_{ih}^R \tilde{g}_h^R - \beta_{ih}^I \tilde{g}_h^I - \beta_{ih}^J(t)\tilde{g}_h^J - \beta_{ih}^K \tilde{g}_h^K\right]\right\}, \\ \overline{u}_i^I(t) - \overline{u}_i^I(0) = \dfrac{d^{-\rho}\overline{u}_i^I(t)}{\mathrm{d}t^{-\rho}}\left\{-\gamma_i\overline{u}_i^I(t-\rangle) + \sum_{h=1}^{m}\left[\alpha_{ih}^I g_h^R + \alpha_{ih}^R g_h^I - \alpha_{ih}^K g_h^J + \alpha_{ih}^J g_h^K\right] + \sum_{h=1}^{m}\left[\beta_{ih}^I \tilde{g}_h^R + \beta_{ih}^R \tilde{g}_h^I - \beta_{ih}^K \tilde{g}_h^J + \beta_{ih}^J \tilde{g}_h^K\right]\right\}, \\ \overline{u}_i^J(t) - \overline{u}_i^J(0) = \dfrac{d^{-\rho}\overline{u}_i^J(t)}{\mathrm{d}t^{-\rho}}\left\{-\gamma_i\overline{u}_i^J(t-\rangle) + \sum_{h=1}^{m}\left[\alpha_{ih}^J g_h^R + \alpha_{ih}^K g_h^I + \alpha_{ih}^R g_h^J - \alpha_{ih}^I g_h^K\right] + \sum_{h=1}^{m}\left[\beta_{ih}^J \tilde{g}_h^R + \beta_{ih}^K \tilde{g}_h^I + \beta_{ih}^R \tilde{g}_h^J - \beta_{ih}^I \tilde{g}_h^K\right]\right\}. \end{cases} \tag{25}$$

From the first equation of (25), one has

$$\overline{u}_i^R(t) = \overline{u}_i^R(0) + \frac{1}{\Gamma(\rho)}\int_0^t (t-s)^{\rho-1}\left\{-\gamma_i\overline{u}_i^R(t-\varrho) + \sum_{h=1}^{m}\left[\alpha_{ih}^R g_h^R - \alpha_{ih}^I g_h^I - \alpha_{ih}^J g_h^J - \alpha_{ih}^K g_h^K\right] + \sum_{h=1}^{m}\left[\beta_{ih}^R \tilde{g}_h^R - \beta_{ih}^I \tilde{g}_h^I - \beta_{ih}^J \tilde{g}_h^J - \beta_{ih}^K \tilde{g}_h^K\right]\right\}\mathrm{d}s, \tag{26}$$

which leads to

$$\begin{aligned} \left|\overline{u}_i^R(t)\right| &\le \left|\overline{u}_i^R(0)\right| + \frac{1}{\Gamma(\rho)}\int_0^t (t-s)^{\rho-1} \\ &\left\{\gamma_i\left|\overline{u}_i^R(t-\rangle)\right| + \sum_{h=1}^{m}\left[\left|\alpha_{ih}^R\right|\left|g_h^R\right| + \left|\alpha_{ih}^I\right|\left|g_h^I\right| + \left|\alpha_{ih}^J\right|\left|g_h^J\right| + \left|\alpha_{ih}^K\right|\left|g_h^K\right|\right] + \sum_{h=1}^{m}\left[\left|\beta_{ih}^R\right|\left|\tilde{g}_h^R\right| + \left|\beta_{ih}^I\right|\left|\tilde{g}_h^I\right| + \left|\beta_{ih}^J\right|\left|\tilde{g}_h^J\right| + \left|\beta_{ih}^K\right|\left|\tilde{g}_h^K\right|\right]\right\} \\ &\le \left|\overline{u}_i^R(0)\right| + \gamma_i\frac{1}{\Gamma(\rho)}\int_0^t (t-s)^{\rho-1}\left|\overline{u}_i^R(t-\rangle)\right|\mathrm{d}s + \sum_{h=1}^{m}\left|\alpha_{ih}^R\right|\frac{1}{\Gamma(\rho)}\int_0^t (t-s)^{\rho-1}\left|g_h^R\right|\mathrm{d}s \\ &\quad + \sum_{h=1}^{m}\left|\alpha_{ih}^I\right|\frac{1}{\Gamma(\rho)}\int_0^t (t-s)^{\rho-1}\left|g_h^I\right|\mathrm{d}s + \sum_{h=1}^{m}\left|\alpha_{ih}^J\right|\frac{1}{\Gamma(\rho)}\int_0^t (t-s)^{\rho-1}\left|g_h^J\right|\mathrm{d}s \end{aligned}$$

$$
\begin{aligned}
&+\sum_{h=1}^{m}\left|\alpha_{ih}^{K}\right|\frac{1}{\Gamma(\rho)}\int_{0}^{t}(t-s)^{\rho-1}\left|g_{h}^{K}\right|\mathrm{d}s+\sum_{h=1}^{m}\left|\beta_{ih}^{R}\right|\frac{1}{\Gamma(\rho)}\int_{0}^{t}(t-s)^{\rho-1}\left|\widetilde{g}_{h}^{R}\right|\mathrm{d}s\\
&+\sum_{h=1}^{m}\left|\beta_{ih}^{I}\right|\frac{1}{\Gamma(\rho)}\int_{0}^{t}(t-s)^{\rho-1}\left|\widetilde{g}_{h}^{I}\right|\mathrm{d}s+\sum_{h=1}^{m}\left|\beta_{ih}^{J}\right|\frac{1}{\Gamma(\rho)}\int_{0}^{t}(t-s)^{\rho-1}\left|\widetilde{g}_{h}^{J}\right|\mathrm{d}s\\
&+\sum_{h=1}^{m}\left|\beta_{ih}^{K}\right|\frac{1}{\Gamma(\rho)}\int_{0}^{t}(t-s)^{\rho-1}\left|\widetilde{g}_{h}^{K}\right|\mathrm{d}s\\
\leq&\left|\overline{u}_{i}^{R}(0)\right|+\gamma_{i}\frac{1}{\Gamma(\rho)}\int_{0}^{t}(t-s)^{\rho-1}\left|\overline{u}_{i}^{R}(t-\rangle)\right|\mathrm{d}s\\
&+\sum_{h=1}^{m}\left|\alpha_{ih}^{R}\right|\frac{1}{\Gamma(\rho)}\int_{0}^{t}(t-s)^{\rho-1}\left[\mathcal{G}_{h}^{RR}\left|\overline{u}_{h}^{R}(s)\right|+\mathcal{G}_{h}^{RI}\left|\overline{u}_{h}^{I}(s)\right|+\mathcal{G}_{h}^{RJ}\left|\overline{u}_{h}^{J}(s)\right|+\mathcal{G}_{h}^{RK}\left|\overline{u}_{h}^{K}(s)\right|\right]\mathrm{d}s\\
&+\sum_{h=1}^{m}\left|\alpha_{ih}^{I}\right|\frac{1}{\Gamma(\rho)}\int_{0}^{t}(t-s)^{\rho-1}\left[\mathcal{G}_{h}^{IR}\left|\overline{u}_{h}^{R}(s)\right|+\mathcal{G}_{h}^{II}\left|\overline{u}_{h}^{I}(s)\right|+\mathcal{G}_{h}^{IJ}\left|\overline{u}_{h}^{J}(s)\right|+\mathcal{G}_{h}^{IK}\left|\overline{u}_{h}^{K}(s)\right|\right]\mathrm{d}s\\
&+\sum_{h=1}^{m}\left|\alpha_{ih}^{J}\right|\frac{1}{\Gamma(\rho)}\int_{0}^{t}(t-s)^{\rho-1}\left[\mathcal{G}_{h}^{JR}\left|\overline{u}_{h}^{R}(s)\right|+\mathcal{G}_{h}^{JI}\left|\overline{u}_{h}^{I}(s)\right|+\mathcal{G}_{h}^{JJ}\left|\overline{u}_{h}^{J}(s)\right|+\mathcal{G}_{h}^{JK}\left|\overline{u}_{h}^{K}(s)\right|\right]\mathrm{d}s\\
&+\sum_{h=1}^{m}\left|\alpha_{ih}^{K}\right|\frac{1}{\Gamma(\rho)}\int_{0}^{t}(t-s)^{\rho-1}\left[\mathcal{G}_{h}^{KR}\left|\overline{u}_{h}^{R}(s)\right|+\mathcal{G}_{h}^{KI}\left|\overline{u}_{h}^{I}(s)\right|+\mathcal{G}_{h}^{KJ}\left|\overline{u}_{h}^{J}(s)\right|+\mathcal{G}_{h}^{KK}\left|\overline{u}_{h}^{K}(s)\right|\right]\mathrm{d}s\\
&+\sum_{h=1}^{m}\left|\beta_{ih}^{R}\right|\frac{1}{\Gamma(\rho)}\int_{0}^{t}(t-s)^{\rho-1}\left[\mathcal{G}_{h}^{RR}\left|\overline{u}_{h}^{R}(s-\vartheta)\right|+\mathcal{G}_{h}^{RI}\left|\overline{u}_{h}^{I}(s-\vartheta)\right|+\mathcal{G}_{h}^{RJ}\left|\overline{u}_{h}^{J}(s-\vartheta)\right|+\mathcal{G}_{h}^{RK}\left|\overline{u}_{h}^{K}(s-\vartheta)\right|\right]\mathrm{d}s\\
&+\sum_{h=1}^{m}\left|\beta_{ih}^{I}\right|\frac{1}{\Gamma(\rho)}\int_{0}^{t}(t-s)^{\rho-1}\left[\mathcal{G}_{h}^{IR}\left|\overline{u}_{h}^{R}(s-\vartheta)\right|+\mathcal{G}_{h}^{II}\left|\overline{u}_{h}^{I}(s-\vartheta)\right|+\mathcal{G}_{h}^{IJ}\left|\overline{u}_{h}^{J}(s-\vartheta)\right|+\mathcal{G}_{h}^{IK}\left|\overline{u}_{h}^{K}(s-\vartheta)\right|\right]\mathrm{d}s\\
&+\sum_{h=1}^{m}\left|\beta_{ih}^{J}\right|\frac{1}{\Gamma(\rho)}\int_{0}^{t}(t-s)^{\rho-1}\left[\mathcal{G}_{h}^{JR}\left|\overline{u}_{h}^{R}(s-\vartheta)\right|+\mathcal{G}_{h}^{JI}\left|\overline{u}_{h}^{I}(s-\vartheta)\right|+\mathcal{G}_{h}^{JJ}\left|\overline{u}_{h}^{J}(s-\vartheta)\right|+\mathcal{G}_{h}^{JK}\left|\overline{u}_{h}^{K}(s-\vartheta)\right|\right]\mathrm{d}s\\
&+\sum_{h=1}^{m}\left|\beta_{ih}^{K}\right|\frac{1}{\Gamma(\rho)}\int_{0}^{t}(t-s)^{\rho-1}\left[\mathcal{G}_{h}^{KR}\left|\overline{u}_{h}^{R}(s-\vartheta)\right|+\mathcal{G}_{h}^{KI}\left|\overline{u}_{h}^{I}(s-\vartheta)\right|+\mathcal{G}_{h}^{KJ}\left|\overline{u}_{h}^{J}(s-\vartheta)\right|+\mathcal{G}_{h}^{KK}\left|\overline{u}_{h}^{K}(s-\vartheta)\right|\right]\mathrm{d}s\\
=&\left|\overline{u}_{i}^{R}(0)\right|+\gamma_{i}\frac{1}{\Gamma(\rho)}\int_{0}^{t}(t-s)^{\rho-1}\left|\overline{u}_{i}^{R}(t-\rangle)\right|\mathrm{d}s\\
&+\sum_{h=1}^{m}\left(\left|\alpha_{ih}^{R}\right|\mathcal{G}_{h}^{RR}+\left|\alpha_{ih}^{I}\right|\mathcal{G}_{h}^{IR}+\left|\alpha_{ih}^{J}\right|\mathcal{G}_{h}^{JR}+\left|\alpha_{ih}^{K}\right|\mathcal{G}_{h}^{KR}\right)\frac{1}{\Gamma(\rho)}\int_{0}^{t}(t-s)^{\rho-1}\left|\overline{u}_{h}^{R}(s)\right|\mathrm{d}s\\
&+\sum_{h=1}^{m}\left(\left|\alpha_{ih}^{R}\right|\mathcal{G}_{h}^{RI}+\left|\alpha_{ih}^{I}\right|\mathcal{G}_{h}^{II}+\left|\alpha_{ih}^{J}\right|\mathcal{G}_{h}^{JI}+\left|\alpha_{ih}^{K}\right|\mathcal{G}_{h}^{KI}\right)\frac{1}{\Gamma(\rho)}\int_{0}^{t}(t-s)^{\rho-1}\left|\overline{u}_{h}^{I}(s)\right|\mathrm{d}s\\
&+\sum_{h=1}^{m}\left(\left|\alpha_{ih}^{R}\right|\mathcal{G}_{h}^{RJ}+\left|\alpha_{ih}^{I}\right|\mathcal{G}_{h}^{IJ}+\left|\alpha_{ih}^{J}\right|\mathcal{G}_{h}^{JJ}+\left|\alpha_{ih}^{K}\right|\mathcal{G}_{h}^{KJ}\right)\frac{1}{\Gamma(\rho)}\int_{0}^{t}(t-s)^{\rho-1}\left|\overline{u}_{h}^{J}(s)\right|\mathrm{d}s\\
&+\sum_{h=1}^{m}\left(\left|\alpha_{ih}^{R}\right|\mathcal{G}_{h}^{RK}+\left|\alpha_{ih}^{I}\right|\mathcal{G}_{h}^{IK}+\left|\alpha_{ih}^{J}\right|\mathcal{G}_{h}^{JK}+\left|\alpha_{ih}^{K}\right|\mathcal{G}_{h}^{KK}\right)\frac{1}{\Gamma(\rho)}\int_{0}^{t}(t-s)^{\rho-1}\left|\overline{u}_{h}^{K}(s)\right|\mathrm{d}s\\
&+\sum_{h=1}^{m}\left(\left|\beta_{ih}^{R}\right|\mathcal{G}_{h}^{RR}+\left|\beta_{ih}^{I}\right|\mathcal{G}_{h}^{IR}+\left|\beta_{ih}^{J}\right|\mathcal{G}_{h}^{JR}+\left|\beta_{ih}^{K}\right|\mathcal{G}_{h}^{KR}\right)\frac{1}{\Gamma(\rho)}\int_{0}^{t}(t-s)^{\rho-1}\left|\overline{u}_{h}^{R}(s-\vartheta)\right|\mathrm{d}s\\
&+\sum_{h=1}^{m}\left(\left|\beta_{ih}^{R}\right|\mathcal{G}_{h}^{RI}+\left|\beta_{ih}^{I}\right|\mathcal{G}_{h}^{II}+\left|\beta_{ih}^{J}\right|\mathcal{G}_{h}^{JI}+\left|\beta_{ih}^{K}\right|\mathcal{G}_{h}^{KI}\right)\frac{1}{\Gamma(\rho)}\int_{0}^{t}(t-s)^{\rho-1}\left|\overline{u}_{h}^{I}(s-\vartheta)\right|\mathrm{d}s\\
&+\sum_{h=1}^{m}\left(\left|\beta_{ih}^{R}\right|\mathcal{G}_{h}^{RJ}+\left|\beta_{ih}^{I}\right|\mathcal{G}_{h}^{IJ}+\left|\beta_{ih}^{J}\right|\mathcal{G}_{h}^{JJ}+\left|\beta_{ih}^{K}\right|\mathcal{G}_{h}^{KJ}\right)\frac{1}{\Gamma(\rho)}\int_{0}^{t}(t-s)^{\rho-1}\left|\overline{u}_{h}^{J}(s-\vartheta)\right|\mathrm{d}s\\
&+\sum_{h=1}^{m}\left(\left|\beta_{ih}^{R}\right|\mathcal{G}_{h}^{RK}+\left|\beta_{ih}^{I}\right|\mathcal{G}_{h}^{IK}+\left|\beta_{ih}^{J}\right|\mathcal{G}_{h}^{JK}+\left|\beta_{ih}^{K}\right|\mathcal{G}_{h}^{KK}\right)\frac{1}{\Gamma(\rho)}\int_{0}^{t}(t-s)^{\rho-1}\left|\overline{u}_{h}^{K}(s-\vartheta)\right|\mathrm{d}s.
\end{aligned}
\tag{27}
$$

Multiplying by e^{-t} by (23) leads to

$$
\begin{aligned}
e^{-t}\left|\overline{u}_i^R(t)\right| &= e^{-t}\left|\overline{u}_i^R(0)\right| + \gamma_i \frac{1}{\Gamma(\rho)} \int_0^t (t-s)^{\rho-1} e^{-t}\left|\overline{u}_i^R(t-\varrho)\right| \mathrm{d}s \\
&+ \sum_{h=1}^{m}\left(\left|\alpha_{ih}^R\right|\mathcal{G}_h^{RR} + \left|\alpha_{ih}^I\right|\mathcal{G}_h^{IR} + \left|\alpha_{ih}^J\right|\mathcal{G}_h^{JR} + \left|\alpha_{ih}^K\right|\mathcal{G}_h^{KR}\right)\frac{1}{\Gamma(\rho)} \int_0^t (t-s)^{\rho-1} e^{-t}\left|\overline{u}_h^R(s)\right| \mathrm{d}s \\
&+ \sum_{h=1}^{m}\left(\left|\alpha_{ih}^R\right|\mathcal{G}_h^{RI} + \left|\alpha_{ih}^I\right|\mathcal{G}_h^{II} + \left|\alpha_{ih}^J\right|\mathcal{G}_h^{JI} + \left|\alpha_{ih}^K\right|\mathcal{G}_h^{KI}\right)\frac{1}{\Gamma(\rho)} \int_0^t (t-s)^{\rho-1} e^{-t}\left|\overline{u}_h^I(s)\right| \mathrm{d}s \\
&+ \sum_{h=1}^{m}\left(\left|\alpha_{ih}^R\right|\mathcal{G}_h^{RJ} + \left|\alpha_{ih}^I\right|\mathcal{G}_h^{IJ} + \left|\alpha_{ih}^J\right|\mathcal{G}_h^{JJ} + \left|\alpha_{ih}^K\right|\mathcal{G}_h^{KJ}\right)\frac{1}{\Gamma(\rho)} \int_0^t (t-s)^{\rho-1} e^{-t}\left|\overline{u}_h^J(s)\right| \mathrm{d}s \\
&+ \sum_{h=1}^{m}\left(\left|\alpha_{ih}^R\right|\mathcal{G}_h^{RK} + \left|\alpha_{ih}^I\right|\mathcal{G}_h^{IK} + \left|\alpha_{ih}^J\right|\mathcal{G}_h^{JK} + \left|\alpha_{ih}^K\right|\mathcal{G}_h^{KK}\right)\frac{1}{\Gamma(\rho)} \int_0^t (t-s)^{\rho-1} e^{-t}\left|\overline{u}_h^K(s)\right| \mathrm{d}s \\
&+ \sum_{h=1}^{m}\left(\left|\beta_{ih}^R\right|\mathcal{G}_h^{RR} + \left|\beta_{ih}^I\right|\mathcal{G}_h^{IR} + \left|\beta_{ih}^J\right|\mathcal{G}_h^{JR} + \left|\beta_{ih}^K\right|\mathcal{G}_h^{KR}\right)\frac{1}{\Gamma(\rho)} \int_0^t (t-s)^{\rho-1} e^{-t}\left|\overline{u}_h^R(s-\vartheta)\right| \mathrm{d}s \\
&+ \sum_{h=1}^{m}\left(\left|\beta_{ih}^R\right|\mathcal{G}_h^{RI} + \left|\beta_{ih}^I\right|\mathcal{G}_h^{II} + \left|\beta_{ih}^J\right|\mathcal{G}_h^{JI} + \left|\beta_{ih}^K\right|\mathcal{G}_h^{KI}\right)\frac{1}{\Gamma(\rho)} \int_0^t (t-s)^{\rho-1} e^{-t}\left|\overline{u}_h^I(s-\vartheta)\right| \mathrm{d}s \\
&+ \sum_{h=1}^{m}\left(\left|\beta_{ih}^R\right|\mathcal{G}_h^{RJ} + \left|\beta_{ih}^I\right|\mathcal{G}_h^{IJ} + \left|\beta_{ih}^J\right|\mathcal{G}_h^{JJ} + \left|\beta_{ih}^K\right|\mathcal{G}_h^{KJ}\right)\frac{1}{\Gamma(\rho)} \int_0^t (t-s)^{\rho-1} e^{-t}\left|\overline{u}_h^J(s-\vartheta)\right| \mathrm{d}s \\
&+ \sum_{h=1}^{m}\left(\left|\beta_{ih}^R\right|\mathcal{G}_h^{RK} + \left|\beta_{ih}^I\right|\mathcal{G}_h^{IK} + \left|\beta_{ih}^J\right|\mathcal{G}_h^{JK} + \left|\beta_{ih}^K\right|\mathcal{G}_h^{KK}\right)\frac{1}{\Gamma(\rho)} \int_0^t (t-s)^{\rho-1} e^{-t}\left|\overline{u}_h^K(s-\vartheta)\right| \mathrm{d}s \\
&= e^{-t}\left|\overline{u}_i^R(0)\right| + \gamma_i \frac{1}{\Gamma(\rho)} \int_0^t (t-s)^{\rho-1} e^{-t+s} e^{-\varrho} e^{-s+\varrho}\left|\overline{u}_i^R(t-\varrho)\right| \mathrm{d}s \\
&+ \sum_{h=1}^{m}\left(\left|\alpha_{ih}^R\right|\mathcal{G}_h^{RR} + \left|\alpha_{ih}^I\right|\mathcal{G}_h^{IR} + \left|\alpha_{ih}^J\right|\mathcal{G}_h^{JR} + \left|\alpha_{ih}^K\right|\mathcal{G}_h^{KR}\right)\frac{1}{\Gamma(\rho)} \int_0^t (t-s)^{\rho-1} e^{-t+s} e^{-s}\left|\overline{u}_h^R(s)\right| \mathrm{d}s \\
&+ \sum_{h=1}^{m}\left(\left|\alpha_{ih}^R\right|\mathcal{G}_h^{RI} + \left|\alpha_{ih}^I\right|\mathcal{G}_h^{II} + \left|\alpha_{ih}^J\right|\mathcal{G}_h^{JI} + \left|\alpha_{ih}^K\right|\mathcal{G}_h^{KI}\right)\frac{1}{\Gamma(\rho)} \int_0^t (t-s)^{\rho-1} e^{-t+s} e^{-s}\left|\overline{u}_h^I(s)\right| \mathrm{d}s \\
&+ \sum_{h=1}^{m}\left(\left|\alpha_{ih}^R\right|\mathcal{G}_h^{RJ} + \left|\alpha_{ih}^I\right|\mathcal{G}_h^{IJ} + \left|\alpha_{ih}^J\right|\mathcal{G}_h^{JJ} + \left|\alpha_{ih}^K\right|\mathcal{G}_h^{KJ}\right)\frac{1}{\Gamma(\rho)} \int_0^t (t-s)^{\rho-1} e^{-t+s} e^{-s}\left|\overline{u}_h^J(s)\right| \mathrm{d}s \\
&+ \sum_{h=1}^{m}\left(\left|\alpha_{ih}^R\right|\mathcal{G}_h^{RK} + \left|\alpha_{ih}^I\right|\mathcal{G}_h^{IK} + \left|\alpha_{ih}^J\right|\mathcal{G}_h^{JK} + \left|\alpha_{ih}^K\right|\mathcal{G}_h^{KK}\right)\frac{1}{\Gamma(\rho)} \int_0^t (t-s)^{\rho-1} e^{-t+s} e^{-s}\left|\overline{u}_h^K(s)\right| \mathrm{d}s \\
&+ \sum_{h=1}^{m}\left(\left|\beta_{ih}^R\right|\mathcal{G}_h^{RR} + \left|\beta_{ih}^I\right|\mathcal{G}_h^{IR} + \left|\beta_{ih}^J\right|\mathcal{G}_h^{JR} + \left|\beta_{ih}^K\right|\mathcal{G}_h^{KR}\right)\frac{1}{\Gamma(\rho)} \\
&\times \int_0^t (t-s)^{\rho-1} e^{-t+s} e^{-\vartheta} e^{-s+\vartheta}\left|\overline{u}_h^R(s-\vartheta)\right| \mathrm{d}s
\end{aligned}
$$

$$
\begin{aligned}
&+\sum_{h=1}^{m}\left(\left|\beta_{ih}^{R}\right|\mathcal{G}_{h}^{RI}+\left|\beta_{ih}^{I}\right|\mathcal{G}_{h}^{II}+\left|\beta_{ih}^{J}\right|\mathcal{G}_{h}^{JI}+\left|\beta_{ih}^{K}\right|\mathcal{G}_{h}^{KI}\right)\frac{1}{\Gamma(\rho)}\\
&\times\int_{0}^{t}(t-s)^{\rho-1}e^{-t}e^{-t+s}e^{-\vartheta}e^{-s+\vartheta}\left|\overline{u}_{h}^{I}(s-\vartheta)\right|\mathrm{d}s\\
&+\sum_{h=1}^{m}\left(\left|\beta_{ih}^{R}\right|\mathcal{G}_{h}^{RJ}+\left|\beta_{ih}^{I}\right|\mathcal{G}_{h}^{IJ}+\left|\beta_{ih}^{J}\right|\mathcal{G}_{h}^{JJ}+\left|\beta_{ih}^{K}\right|\mathcal{G}_{h}^{KJ}\right)\frac{1}{\Gamma(\rho)}\times\int_{0}^{t}(t-s)^{\rho-1}e^{-t}e^{-t+s}e^{-\vartheta}e^{-s+\vartheta}\left|\overline{u}_{h}^{J}(s-\vartheta)\right|\mathrm{d}s\\
&+\sum_{h=1}^{m}\left(\left|\beta_{ih}^{R}\right|\mathcal{G}_{h}^{RK}+\left|\beta_{ih}^{I}\right|\mathcal{G}_{h}^{IK}+\left|\beta_{ih}^{J}\right|\mathcal{G}_{h}^{JK}+\left|\beta_{ih}^{K}\right|\mathcal{G}_{h}^{KK}\right)\frac{1}{\Gamma(\rho)}\\
&\times\int_{0}^{t}(t-s)^{\rho-1}e^{-t}e^{-t+s}e^{-\vartheta}e^{-s+\vartheta}\left|\overline{u}_{h}^{K}(s-\vartheta)\right|\mathrm{d}s=e^{-t}\left|\overline{u}_{i}^{R}(0)\right|\\
&+e^{-\varrho}\gamma_{i}\frac{1}{\Gamma(\rho)}\left(\int_{0}^{\varrho}+\int_{\varrho}^{t}\right)(t-s)^{\rho-1}e^{-t+s}e^{-\varrho}e^{-s+\varrho}\left|\overline{u}_{i}^{R}(t-\varrho)\right|\mathrm{d}s\\
&+\sum_{h=1}^{m}\left(\left|\alpha_{ih}^{R}\right|\mathcal{G}_{h}^{RR}+\left|\alpha_{ih}^{I}\right|\mathcal{G}_{h}^{IR}+\left|\alpha_{ih}^{J}\right|\mathcal{G}_{h}^{JR}+\left|\alpha_{ih}^{K}\right|\mathcal{G}_{h}^{KR}\right)\frac{1}{\Gamma(\rho)}\int_{0}^{t}(t-s)^{\rho-1}e^{-t+s}e^{-s}\left|\overline{u}_{h}^{R}(s)\right|\mathrm{d}s\\
&+\sum_{h=1}^{m}\left(\left|\alpha_{ih}^{R}\right|\mathcal{G}_{h}^{RI}+\left|\alpha_{ih}^{I}\right|\mathcal{G}_{h}^{II}+\left|\alpha_{ih}^{J}\right|\mathcal{G}_{h}^{JI}+\left|\alpha_{ih}^{K}\right|\mathcal{G}_{h}^{KI}\right)\frac{1}{\Gamma(\rho)}\int_{0}^{t}(t-s)^{\rho-1}e^{-t+s}e^{-s}\left|\overline{u}_{h}^{I}(s)\right|\mathrm{d}s\\
&+\sum_{h=1}^{m}\left(\left|\alpha_{ih}^{R}\right|\mathcal{G}_{h}^{RJ}+\left|\alpha_{ih}^{I}\right|\mathcal{G}_{h}^{IJ}+\left|\alpha_{ih}^{J}\right|\mathcal{G}_{h}^{JJ}+\left|\alpha_{ih}^{K}\right|\mathcal{G}_{h}^{KJ}\right)\frac{1}{\Gamma(\rho)}\int_{0}^{t}(t-s)^{\rho-1}e^{-t+s}e^{-s}\left|\overline{u}_{h}^{J}(s)\right|\mathrm{d}s\\
&+\sum_{h=1}^{m}\left(\left|\alpha_{ih}^{R}\right|\mathcal{G}_{h}^{RK}+\left|\alpha_{ih}^{I}\right|\mathcal{G}_{h}^{IK}+\left|\alpha_{ih}^{J}\right|\mathcal{G}_{h}^{JK}+\left|\alpha_{ih}^{K}\right|\mathcal{G}_{h}^{KK}\right)\frac{1}{\Gamma(\rho)}\int_{0}^{t}(t-s)^{\rho-1}e^{-t+s}e^{-s}\left|\overline{u}_{h}^{K}(s)\right|\mathrm{d}s\\
&+\sum_{h=1}^{m}\left(\left|\beta_{ih}^{R}\right|\mathcal{G}_{h}^{RR}+\left|\beta_{ih}^{I}\right|\mathcal{G}_{h}^{IR}+\left|\beta_{ih}^{J}\right|\mathcal{G}_{h}^{JR}+\left|\beta_{ih}^{K}\right|\mathcal{G}_{h}^{KR}\right)\frac{1}{\Gamma(\rho)}\\
&\times\left(\int_{0}^{\vartheta}+\int_{\vartheta}^{t}\right)(t-s)^{\rho-1}e^{-t+s}e^{-\vartheta}e^{-s+\vartheta}\left|\overline{u}_{h}^{R}(s-\vartheta)\right|\mathrm{d}s\\
&+\sum_{h=1}^{m}\left(\left|\beta_{ih}^{R}\right|\mathcal{G}_{h}^{RI}+\left|\beta_{ih}^{I}\right|\mathcal{G}_{h}^{II}+\left|\beta_{ih}^{J}\right|\mathcal{G}_{h}^{JI}+\left|\beta_{ih}^{K}\right|\mathcal{G}_{h}^{KI}\right)\frac{1}{\Gamma(\rho)}\\
&\times\left(\int_{0}^{\vartheta}+\int_{\vartheta}^{t}\right)(t-s)^{\rho-1}e^{-t+s}e^{-\vartheta}e^{-s+\vartheta}\left|\overline{u}_{h}^{I}(s-\vartheta)\right|\mathrm{d}s\\
&+\sum_{h=1}^{m}\left(\left|\beta_{ih}^{R}\right|\mathcal{G}_{h}^{RJ}+\left|\beta_{ih}^{I}\right|\mathcal{G}_{h}^{IJ}+\left|\beta_{ih}^{J}\right|\mathcal{G}_{h}^{JJ}+\left|\beta_{ih}^{K}\right|\mathcal{G}_{h}^{KJ}\right)\frac{1}{\Gamma(\rho)}\\
&\times\left(\int_{0}^{\vartheta}+\int_{\vartheta}^{t}\right)(t-s)^{\rho-1}e^{-t+s}e^{-\vartheta}e^{-s+\vartheta}\left|\overline{u}_{h}^{J}(s-\vartheta)\right|\mathrm{d}s\\
&+\sum_{h=1}^{m}\left(\left|\beta_{ih}^{R}\right|\mathcal{G}_{h}^{RK}+\left|\beta_{ih}^{I}\right|\mathcal{G}_{h}^{IK}+\left|\beta_{ih}^{J}\right|\mathcal{G}_{h}^{JK}+\left|\beta_{ih}^{K}\right|\mathcal{G}_{h}^{KK}\right)\frac{1}{\Gamma(\rho)}\\
&\times\left(\int_{0}^{\vartheta}+\int_{\vartheta}^{t}\right)(t-s)e^{-t+s}e^{-\vartheta}e^{-s+\vartheta}\left|\overline{u}_{h}^{K}(s-\vartheta)\right|\mathrm{d}s\leq e^{-t}\left|\overline{u}_{i}^{R}(0)\right|\\
&+e^{-\varrho}\gamma_{i}\left[\sup_{s\in[-\varrho,0]}\left\{e^{-s}\left|\overline{\phi}_{i}^{R}(s)\right|\right\}+\sup_{s\in[0,t-\varrho]}\left\{e^{-s}\left|\overline{u}_{i}^{R}(s)\right|\right\}\right]\frac{1}{\Gamma(\rho)}\int_{0}^{t}\nu^{\rho-1}e^{-\nu}\mathrm{d}\nu\\
&+\sum_{h=1}^{m}\left(\left|\alpha_{ih}^{R}\right|\mathcal{G}_{h}^{RR}+\left|\alpha_{ih}^{I}\right|\mathcal{G}_{h}^{IR}+\left|\alpha_{ih}^{J}\right|\mathcal{G}_{h}^{JR}+\left|\alpha_{ih}^{K}\right|\mathcal{G}_{h}^{KR}\right)\sup_{s\in[0,t]}\left\{e^{-t}\left|\overline{u}_{i}^{R}(s)\right|\right\}\frac{1}{\Gamma(\rho)}\int_{0}^{t}\nu^{\rho-1}e^{-\nu}\mathrm{d}\nu\\
&+\sum_{h=1}^{m}\left(\left|\alpha_{ih}^{R}\right|\mathcal{G}_{h}^{RI}+\left|\alpha_{ih}^{I}\right|\mathcal{G}_{h}^{II}+\left|\alpha_{ih}^{J}\right|\mathcal{G}_{h}^{JI}+\left|\alpha_{ih}^{K}\right|\mathcal{G}_{h}^{KI}\right)\sup_{s\in[0,t]}\left\{e^{-t}\left|\overline{u}_{i}^{I}(s)\right|\right\}\frac{1}{\Gamma(\rho)}\int_{0}^{t}\nu^{\rho-1}e^{-\nu}\mathrm{d}\nu
\end{aligned}
$$

$$
\begin{aligned}
&+\sum_{h=1}^{m}\left(\left|\alpha_{ih}^{R}\right|\mathcal{G}_{h}^{RJ}+\left|\alpha_{ih}^{I}\right|\mathcal{G}_{h}^{IJ}+\left|\alpha_{ih}^{J}\right|\mathcal{G}_{h}^{JJ}+\left|\alpha_{ih}^{K}\right|\mathcal{G}_{h}^{KJ}\right)\sup_{s\in[0,t]}\left\{e^{-t}\left|\overline{u}_{i}^{J}(s)\right|\right\}\frac{1}{\Gamma(\rho)}\int_{0}^{t}v^{\rho-1}e^{-v}\mathrm{d}v\\
&+\sum_{h=1}^{m}\left(\left|\alpha_{ih}^{R}\right|\mathcal{G}_{h}^{RK}+\left|\alpha_{ih}^{I}\right|\mathcal{G}_{h}^{IK}+\left|\alpha_{ih}^{J}\right|\mathcal{G}_{h}^{JK}+\left|\alpha_{ih}^{K}\right|\mathcal{G}_{h}^{KK}\right)\sup_{s\in[0,t]}\left\{e^{-t}\left|\overline{u}_{i}^{K}(s)\right|\right\}\frac{1}{\Gamma(\rho)}\int_{0}^{t}v^{\rho-1}e^{-v}\mathrm{d}v\\
&+e^{-\vartheta}\sum_{h=1}^{m}\left(\left|\beta_{ih}^{R}\right|\mathcal{G}_{h}^{RR}+\left|\beta_{ih}^{I}\right|\mathcal{G}_{h}^{IR}+\left|\beta_{ih}^{J}\right|\mathcal{G}_{h}^{JR}+\left|\beta_{ih}^{K}\right|\mathcal{G}_{h}^{KR}\right)\\
&\times\left[\sup_{s\in[-\vartheta,0]}\left\{e^{-s}\left|\overline{\phi}_{h}^{R}(s)\right|\right\}+\sup_{s\in[0,t-\vartheta]}\left\{e^{-s}\left|\overline{u}_{h}^{R}(s)\right|\right\}\right]\frac{1}{\Gamma(\rho)}\int_{0}^{t}v^{\rho-1}e^{-v}\mathrm{d}v\\
&+e^{-\vartheta}\sum_{h=1}^{m}\left(\left|\beta_{ih}^{R}\right|\mathcal{G}_{h}^{RI}+\left|\beta_{ih}^{I}\right|\mathcal{G}_{h}^{II}+\left|\beta_{ih}^{J}\right|\mathcal{G}_{h}^{JI}+\left|\beta_{ih}^{K}\right|\mathcal{G}_{h}^{KI}\right)\\
&\times\left[\sup_{s\in[-\vartheta,0]}\left\{e^{-s}\left|\overline{\phi}_{h}^{R}(s)\right|\right\}+\sup_{s\in[0,t-\vartheta]}\left\{e^{-s}\left|\overline{u}_{h}^{I}(s)\right|\right\}\right]\frac{1}{\Gamma(\rho)}\int_{0}^{t}v^{\rho-1}e^{-v}dv\\
&+e^{-\vartheta}\sum_{h=1}^{m}\left(\left|\beta_{ih}^{R}\right|\mathcal{G}_{h}^{RJ}+\left|\beta_{ih}^{I}\right|\mathcal{G}_{h}^{IJ}+\left|\beta_{ih}^{J}\right|\mathcal{G}_{h}^{JJ}+\left|\beta_{ih}^{K}\right|\mathcal{G}_{h}^{KJ}\right)\\
&\times\left[\sup_{s\in[-\vartheta,0]}\left\{e^{-s}\left|\overline{\phi}_{h}^{R}(s)\right|\right\}+\sup_{s\in[0,t-\vartheta]}\left\{e^{-s}\left|\overline{u}_{h}^{J}(s)\right|\right\}\right]+\frac{1}{\Gamma(\rho)}\int_{0}^{t}v^{\rho-1}e^{-v}dv\\
&+e^{-\vartheta}\sum_{h=1}^{m}\left(\left|\beta_{ih}^{R}\right|\mathcal{G}_{h}^{RK}+\left|\beta_{ih}^{I}\right|\mathcal{G}_{h}^{IK}+\left|\beta_{ih}^{J}\right|\mathcal{G}_{h}^{JK}+\left|\beta_{ih}^{K}\right|\mathcal{G}_{h}^{KK}\right)\\
&\times\left[\sup_{s\in[-\vartheta,0]}\left\{e^{-s}\left|\overline{\phi}_{h}^{R}(s)\right|\right\}+\sup_{s\in[0,t-\vartheta]}\left\{e^{-s}\left|\overline{u}_{h}^{K}(s)\right|\right\}\right]\frac{1}{\Gamma(\rho)}\int_{0}^{t}v^{\rho-1}e^{-v}dv\\
\le{}&\|\overline{\phi}(t)\|+e^{-\rangle}\gamma\|\overline{\phi}(t)\|+e^{-\rangle}\gamma\left\|\overline{u}_{i}^{R}(s)\right\|\\
&+\sum_{h=1}^{m}\left(\left|\alpha_{ih}^{R}\right|\mathcal{G}_{h}^{RR}+\left|\alpha_{ih}^{I}\right|\mathcal{G}_{h}^{IR}+\left|\alpha_{ih}^{J}\right|\mathcal{G}_{h}^{JR}+\left|\alpha_{ih}^{K}\right|\mathcal{G}_{h}^{KR}\right)\left\|\overline{u}_{i}^{R}(s)\right\|\\
&+\sum_{h=1}^{m}\left(\left|\alpha_{ih}^{R}\right|\mathcal{G}_{h}^{RI}+\left|\alpha_{ih}^{I}\right|\mathcal{G}_{h}^{II}+\left|\alpha_{ih}^{J}\right|\mathcal{G}_{h}^{JI}+\left|\alpha_{ih}^{K}\right|\mathcal{G}_{h}^{KI}\right)\left\|\overline{u}_{i}^{I}(s)\right\|\\
&+\sum_{h=1}^{m}\left(\left|\alpha_{ih}^{R}\right|\mathcal{G}_{h}^{RJ}+\left|\alpha_{ih}^{I}\right|\mathcal{G}_{h}^{IJ}+\left|\alpha_{ih}^{J}\right|\mathcal{G}_{h}^{JJ}+\left|\alpha_{ih}^{K}\right|\mathcal{G}_{h}^{KJ}\right)\left\|\overline{u}_{i}^{J}(s)\right\|\\
&+\sum_{h=1}^{m}\left(\left|\alpha_{ih}^{R}\right|\mathcal{G}_{h}^{RK}+\left|\alpha_{ih}^{I}\right|\mathcal{G}_{h}^{IK}+\left|\alpha_{ih}^{J}\right|\mathcal{G}_{h}^{JK}+\left|\alpha_{ih}^{K}\right|\mathcal{G}_{h}^{KK}\right)\left\|\overline{u}_{i}^{K}(s)\right\|\\
&+e^{-\vartheta}\sum_{h=1}^{m}\left(\left|\beta_{ih}^{R}\right|\mathcal{G}_{h}^{RR}+\left|\beta_{ih}^{I}\right|\mathcal{G}_{h}^{IR}+\left|\beta_{ih}^{J}\right|\mathcal{G}_{h}^{JR}+\left|\beta_{ih}^{K}\right|\mathcal{G}_{h}^{KR}\right)\left(\left\|\overline{\phi}_{h}^{R}(t)\right\|+\left\|\overline{u}_{h}^{R}(s)\right\|\right)\\
&+e^{-\vartheta}\sum_{h=1}^{m}\left(\left|\beta_{ih}^{R}\right|\mathcal{G}_{h}^{RI}+\left|\beta_{ih}^{I}\right|\mathcal{G}_{h}^{II}+\left|\beta_{ih}^{J}\right|\mathcal{G}_{h}^{JI}+\left|\beta_{ih}^{K}\right|\mathcal{G}_{h}^{KI}\right)\left(\left\|\overline{\phi}_{h}^{I}(t)\right\|+\left\|\overline{u}_{h}^{I}(s)\right\|\right)\\
&+e^{-\vartheta}\sum_{h=1}^{m}\left(\left|\beta_{ih}^{R}\right|\mathcal{G}_{h}^{RJ}+\left|\beta_{ih}^{I}\right|\mathcal{G}_{h}^{IJ}+\left|\beta_{ih}^{J}\right|\mathcal{G}_{h}^{JJ}+\left|\beta_{ih}^{K}\right|\mathcal{G}_{h}^{KJ}\right)\left(\left\|\overline{\phi}_{h}^{J}(t)\right\|+\left\|\overline{u}_{h}^{J}(s)\right\|\right)\\
&+e^{-\vartheta}\sum_{h=1}^{m}\left(\left|\beta_{ih}^{R}\right|\mathcal{G}_{h}^{RK}+\left|\beta_{ih}^{I}\right|\mathcal{G}_{h}^{IK}+\left|\beta_{ih}^{J}\right|\mathcal{G}_{h}^{JK}+\left|\beta_{ih}^{K}\right|\mathcal{G}_{h}^{KK}\right)\left(\left\|\overline{\phi}_{h}^{K}(t)\right\|+\left\|\overline{u}_{h}^{K}(s)\right\|\right)\\
={}&\left\|\overline{\phi}^{R}(t)\right\|+e^{-\rangle}\gamma\left\|\overline{\phi}^{R}(t)\right\|+e^{-\rangle}\gamma\left\|\overline{u}_{i}^{R}(s)\right\|\\
&+\sum_{h=1}^{m}\left(\left|\alpha_{ih}^{R}\right|\mathcal{G}_{h}^{RR}+\left|\alpha_{ih}^{I}\right|\mathcal{G}_{h}^{IR}+\left|\alpha_{ih}^{J}\right|\mathcal{G}_{h}^{JR}+\left|\alpha_{ih}^{K}\right|\mathcal{G}_{h}^{KR}\right)\left\|\overline{u}_{i}^{R}(s)\right\|
\end{aligned}
$$

$$
\begin{aligned}
&+\sum_{h=1}^{m}\left(\left|\alpha_{ih}^{R}\right|\mathcal{G}_{h}^{RI}+\left|\alpha_{ih}^{I}\right|\mathcal{G}_{h}^{II}+\left|\alpha_{ih}^{J}\right|\mathcal{G}_{h}^{JI}+\left|\alpha_{ih}^{K}\right|\mathcal{G}_{h}^{KI}\right)\left\|\overline{u}_{i}^{I}(s)\right\| \\
&+\sum_{h=1}^{m}\left(\left|\alpha_{ih}^{R}\right|\mathcal{G}_{h}^{RJ}+\left|\alpha_{ih}^{I}\right|\mathcal{G}_{h}^{IJ}+\left|\alpha_{ih}^{J}\right|\mathcal{G}_{h}^{JJ}+\left|\alpha_{ih}^{K}\right|\mathcal{G}_{h}^{KJ}\right)\left\|\overline{u}_{i}^{J}(s)\right\| \\
&+\sum_{h=1}^{m}\left(\left|\alpha_{ih}^{R}\right|\mathcal{G}_{h}^{RK}+\left|\alpha_{ih}^{I}\right|\mathcal{G}_{h}^{IK}+\left|\alpha_{ih}^{J}\right|\mathcal{G}_{h}^{JK}+\left|\alpha_{ih}^{K}\right|\mathcal{G}_{h}^{KK}\right)\left\|\overline{u}_{i}^{K}(s)\right\| \\
&+e^{-\vartheta}\sum_{h=1}^{m}\left(\left|\beta_{ih}^{R}\right|\mathcal{G}_{h}^{RR}+\left|\beta_{ih}^{I}\right|\mathcal{G}_{h}^{IR}+\left|\beta_{ih}^{J}\right|\mathcal{G}_{h}^{JR}+\left|\beta_{ih}^{K}\right|\mathcal{G}_{h}^{KR}\right)\left(\left\|\overline{\phi}_{h}^{R}(t)\right\|+\left\|\overline{u}_{h}^{R}(s)\right\|\right) \\
&+e^{-\vartheta}\sum_{h=1}^{m}\left(\left|\beta_{ih}^{R}\right|\mathcal{G}_{h}^{RI}+\left|\beta_{ih}^{I}\right|\mathcal{G}_{h}^{II}+\left|\beta_{ih}^{J}\right|\mathcal{G}_{h}^{JI}+\left|\beta_{ih}^{K}\right|\mathcal{G}_{h}^{KI}\right)\left(\left\|\overline{\phi}_{h}^{I}(t)\right\|+\left\|\overline{u}_{h}^{I}(s)\right\|\right) \\
&+e^{-\vartheta}\sum_{h=1}^{m}\left(\left|\beta_{ih}^{R}\right|\mathcal{G}_{h}^{RJ}+\left|\beta_{ih}^{I}\right|\mathcal{G}_{h}^{IJ}+\left|\beta_{ih}^{J}\right|\mathcal{G}_{h}^{JJ}+\left|\beta_{ih}^{K}\right|\mathcal{G}_{h}^{KJ}\right)\left(\left\|\overline{\phi}_{h}^{J}(t)\right\|+\left\|\overline{u}_{h}^{J}(s)\right\|\right) \\
&+e^{-\vartheta}\sum_{h=1}^{m}\left(\left|\beta_{ih}^{R}\right|\mathcal{G}_{h}^{RK}+\left|\beta_{ih}^{I}\right|\mathcal{G}_{h}^{IK}+\left|\beta_{ih}^{J}\right|\mathcal{G}_{h}^{JK}+\left|\beta_{ih}^{K}\right|\mathcal{G}_{h}^{KK}\right)\left(\left\|\overline{\phi}_{h}^{K}(t)\right\|+\left\|\overline{u}_{h}^{K}(s)\right\|\right).
\end{aligned}
\tag{28}
$$

It is easy to see that $\exists\, p_1 \in \{1, 2, \ldots, m\}$ such that

$$
\max_i\left\{\sup_t\left\{e^{-t}\left|\overline{u}_i^R(t)\right|\right\}\right\} = \sup_t\left\{e^{-t}\left|\overline{u}_{p_1}^R(t)\right|\right\}. \tag{29}
$$

Then, it follows from (28) that

$$
\begin{aligned}
&\left\|\overline{u}^R(t)\right\| = \max_i\left\{\sup_t\left\{e^{-t}\left|\overline{u}_i^R(t)\right|\right\}\right\} = \sup_t\left\{e^{-t}\left|\overline{u}_{p_1}^R(t)\right|\right\} \\
&\quad\le\left[e^{-\rangle}\gamma+\sum_{h=1}^{m}\left(\left|\alpha_{p_1h}^{R}\right|\mathcal{G}_{h}^{RR}+\left|\alpha_{p_1h}^{I}\right|\mathcal{G}_{h}^{IR}+\left|\alpha_{p_1h}^{J}\right|\mathcal{G}_{h}^{JR}+\left|\alpha_{p_1h}^{K}\right|\mathcal{G}_{h}^{KR}\right)+e^{-\vartheta}\sum_{h=1}^{m}\left(\left|\beta_{p_1h}^{R}\right|\mathcal{G}_{h}^{RR}+\left|\beta_{p_1h}^{I}\right|\mathcal{G}_{h}^{IR}+\left|\beta_{p_1h}^{J}\right|\mathcal{G}_{h}^{JR}+\left|\beta_{p_1h}^{K}\right|\mathcal{G}_{h}^{KR}\right)\right] \\
&\quad\left\|\overline{u}^R(s)\right\| \\
&+\left[\sum_{h=1}^{m}\left(\left|\alpha_{p_1h}^{R}\right|\mathcal{G}_{h}^{RI}+\left|\alpha_{p_1h}^{I}\right|\mathcal{G}_{h}^{II}+\left|\alpha_{p_1h}^{J}\right|\mathcal{G}_{h}^{JI}+\left|\alpha_{p_1h}^{K}\right|\mathcal{G}_{h}^{KI}\right)+e^{-\vartheta}\sum_{h=1}^{m}\left(\left|\beta_{p_1h}^{R}\right|\mathcal{G}_{h}^{RI}+\left|\beta_{p_1h}^{I}\right|\mathcal{G}_{h}^{II}+\left|\beta_{p_1h}^{J}\right|\mathcal{G}_{h}^{JI}+\left|\beta_{p_1h}^{K}\right|\mathcal{G}_{h}^{KI}\right)\right] \\
&\quad\left\|\overline{u}^I(s)\right\| \\
&+\left[\sum_{h=1}^{m}\left(\left|\alpha_{p_1h}^{R}\right|\mathcal{G}_{h}^{RJ}+\left|\alpha_{p_1h}^{I}\right|\mathcal{G}_{h}^{IJ}+\left|\alpha_{p_1h}^{J}\right|\mathcal{G}_{h}^{JJ}+\left|\alpha_{p_1h}^{K}\right|\mathcal{G}_{h}^{KJ}\right)+e^{-\vartheta}\sum_{h=1}^{m}\left(\left|\beta_{p_1h}^{R}\right|\mathcal{G}_{h}^{RJ}+\left|\beta_{p_1h}^{I}\right|\mathcal{G}_{h}^{IJ}+\left|\beta_{p_1h}^{J}\right|\mathcal{G}_{h}^{JJ}+\left|\beta_{p_1h}^{K}\right|\mathcal{G}_{h}^{KJ}\right)\right] \\
&\quad\left\|\overline{u}^J(s)\right\| \\
&+\left[\sum_{h=1}^{m}\left(\left|\alpha_{p_1h}^{R}\right|\mathcal{G}_{h}^{RK}+\left|\alpha_{p_1h}^{I}\right|\mathcal{G}_{h}^{IK}+\left|\alpha_{p_1h}^{J}\right|\mathcal{G}_{h}^{JK}+\left|\alpha_{p_1h}^{K}\right|\mathcal{G}_{h}^{KK}\right)+e^{-\vartheta}\sum_{h=1}^{m}\left(\left|\beta_{p_1h}^{R}\right|\mathcal{G}_{h}^{RK}+\left|\beta_{p_1h}^{I}\right|\mathcal{G}_{h}^{IK}+\left|\beta_{p_1h}^{J}\right|\mathcal{G}_{h}^{JK}+\left|\beta_{p_1h}^{K}\right|\mathcal{G}_{h}^{KK}\right)\right] \\
&\quad\left\|\overline{u}^K(s)\right\| \\
&+\left[1+e^{-\rangle}\gamma+e^{-\vartheta}\sum_{h=1}^{m}\left(\left|\beta_{p_1h}^{R}\right|\mathcal{G}_{h}^{RR}+\left|\beta_{p_1h}^{I}\right|\mathcal{G}_{h}^{IR}+\left|\beta_{p_1h}^{J}\right|\mathcal{G}_{h}^{JR}+\left|\beta_{p_1h}^{K}\right|\mathcal{G}_{h}^{KR}\right)\right]\left\|\overline{\phi}^R(t)\right\| \\
&+\left[e^{-\vartheta}\sum_{h=1}^{m}\left(\left|\beta_{p_1h}^{R}\right|\mathcal{G}_{h}^{RI}+\left|\beta_{p_1h}^{I}\right|\mathcal{G}_{h}^{II}+\left|\beta_{p_1h}^{J}\right|\mathcal{G}_{h}^{JI}+\left|\beta_{p_1h}^{K}\right|\mathcal{G}_{h}^{KI}\right)\right]\left\|\overline{\phi}^I(t)\right\| \\
&+\left[e^{-\vartheta}\sum_{h=1}^{m}\left(\left|\beta_{p_1h}^{R}\right|\mathcal{G}_{h}^{RJ}+\left|\beta_{p_1h}^{I}\right|\mathcal{G}_{h}^{IJ}+\left|\beta_{p_1h}^{J}\right|\mathcal{G}_{h}^{JJ}+\left|\beta_{p_1h}^{K}\right|\mathcal{G}_{h}^{KJ}\right)\right]\left\|\overline{\phi}^J(t)\right\| \\
&+\left[e^{-\vartheta}\sum_{h=1}^{m}\left(\left|\beta_{p_1h}^{R}\right|\mathcal{G}_{h}^{RK}+\left|\beta_{p_1h}^{I}\right|\mathcal{G}_{h}^{IK}+\left|\beta_{p_1h}^{J}\right|\mathcal{G}_{h}^{JK}+\left|\beta_{p_1h}^{K}\right|\mathcal{G}_{h}^{KK}\right)\right]\left\|\overline{\phi}^K(t)\right\|.
\end{aligned}
\tag{30}
$$

Then, we have

$$\left\|\overline{u}^{R}(t)\right\| \leq \frac{1}{\mathscr{A}_{1}^{p_1}}\left[\mathscr{A}_{2}^{p_1}\left\|\overline{u}^{I}(t)\right\| + \mathscr{A}_{3}^{p_1}\left\|\overline{u}^{J}(t)\right\| + \mathscr{A}_{4}^{p_1}\left\|\overline{u}^{K}(t)\right\| + \mathscr{A}_{5}^{p_1}\left\|\overline{\phi}^{R}(t)\right\| + \mathscr{A}_{6}^{p_1}\left\|\overline{\phi}^{I}(t)\right\| + \mathscr{A}_{7}^{p_1}\left\|\overline{\phi}^{J}(t)\right\| + \mathscr{A}_{8}^{p_1}\left\|\overline{\phi}^{K}(t)\right\|\right]. \tag{31}$$

In a similar way, we can obtain

$$\left\|\overline{u}^{I}(t)\right\| \leq \frac{1}{\mathscr{B}_{1}^{p_2}}\left[\mathscr{B}_{2}^{p_2}\left\|\overline{u}^{R}(t)\right\| + \mathscr{B}_{3}^{p_2}\left\|\overline{u}^{J}(t)\right\| + \mathscr{B}_{4}^{p_2}\left\|\overline{u}^{K}(t)\right\| + \mathscr{B}_{5}^{p_2}\left\|\overline{\phi}^{R}(t)\right\| + \mathscr{B}_{6}^{p_2}\left\|\overline{\phi}^{I}(t)\right\| + \mathscr{B}_{7}^{p_2}\left\|\overline{\phi}^{J}(t)\right\| + \mathscr{B}_{8}^{p_2}\left\|\overline{\phi}^{K}(t)\right\|\right], \tag{32}$$

$$\left\|\overline{u}^{J}(t)\right\| \leq \frac{1}{\mathscr{C}_{1}^{p_3}}\left[\mathscr{C}_{2}^{p_3}\left\|\overline{u}^{R}(t)\right\| + \mathscr{C}_{3}^{p_3}\left\|\overline{u}^{I}(t)\right\| + \mathscr{C}_{4}^{p_3}\left\|\overline{u}^{K}(t)\right\| + \mathscr{C}_{5}^{p_3}\left\|\overline{\phi}^{R}(t)\right\| + \mathscr{C}_{6}^{p_3}\left\|\overline{\phi}^{I}(t)\right\| + \mathscr{C}_{7}^{p_3}\left\|\overline{\phi}^{J}(t)\right\| + \mathscr{C}_{8}^{p_3}\left\|\overline{\phi}^{K}(t)\right\|\right], \tag{33}$$

$$\left\|\overline{u}^{K}(t)\right\| \leq \frac{1}{\mathscr{D}_{1}^{p_4}}\left[\mathscr{C}_{2}^{p_4}\left\|\overline{u}^{R}(t)\right\| + \mathscr{D}_{3}^{p_4}\left\|\overline{u}^{I}(t)\right\| + \mathscr{D}_{4}^{p_4}\left\|\overline{u}^{J}(t)\right\| + \mathscr{D}_{5}^{p_4}\left\|\overline{\phi}^{R}(t)\right\| + \mathscr{D}_{6}^{p_4}\left\|\overline{\phi}^{I}(t)\right\| + \mathscr{D}_{7}^{p_4}\left\|\overline{\phi}^{J}(t)\right\| + \mathscr{D}_{8}^{p_4}\left\|\overline{\phi}^{K}(t)\right\|\right]. \tag{34}$$

By (31)–(34), we obtain

$$\begin{aligned}
&\left(\mathscr{A}_{1}^{p_1} - \mathscr{B}_{2}^{p_2} - \mathscr{C}_{2}^{p_3} - \mathscr{D}_{2}^{p_4}\right)\left\|\overline{u}^{R}(t)\right\| + \left(\mathscr{B}_{1}^{p_1} - \mathscr{A}_{2}^{p_1} - \mathscr{C}_{3}^{p_3} - \mathscr{D}_{3}^{p_4}\right)\left\|\overline{u}^{I}(t)\right\| \\
&+\left(\mathscr{C}_{1}^{p_3} - \mathscr{A}_{1}^{p_1} - \mathscr{B}_{3}^{p_2} - \mathscr{D}_{4}^{p_4}\right)\left\|\overline{u}^{J}(t)\right\| + \left(\mathscr{D}_{1}^{p_4} - \mathscr{A}_{4}^{p_1} - \mathscr{B}_{4}^{p_2} - \mathscr{C}_{3}^{p_3}\right)\left\|\overline{u}^{K}(t)\right\| \\
&\leq \left(\mathscr{A}_{5}^{p_1} + \mathscr{B}_{5}^{p_2} + \mathscr{C}_{5}^{p_3} + \mathscr{D}_{5}^{p_4}\right)\left\|\overline{\phi}^{R}(t)\right\| + \left(\mathscr{A}_{6}^{p_1} + \mathscr{B}_{6}^{p_2} + \mathscr{C}_{6}^{p_3} + \mathscr{D}_{6}^{p_4}\right)\left\|\overline{\phi}^{I}(t)\right\| \\
&+\left(\mathscr{A}_{7}^{p_1} + \mathscr{B}_{7}^{p_2} + \mathscr{C}_{7}^{p_3} + \mathscr{D}_{7}^{p_4}\right)\left\|\overline{\phi}^{J}(t)\right\| + \left(\mathscr{A}_{8}^{p_1} + \mathscr{B}_{8}^{p_2} + \mathscr{C}_{8}^{p_3} + \mathscr{D}_{8}^{p_4}\right)\left\|\overline{\phi}^{K}(t)\right\|.
\end{aligned} \tag{35}$$

It follows from (35) that

$$\left\|\overline{u}^{R}(t)\right\| + \left\|\overline{u}^{I}(t)\right\| + \left\|\overline{u}^{J}(t)\right\| + \left\|\overline{u}^{K}(t)\right\| \leq \Pi_1\left\|\overline{\phi}^{R}(t)\right\| + \Pi_2\left\|\overline{\phi}^{I}(t)\right\| + \Pi_3\left\|\overline{\phi}^{J}(t)\right\| + \Pi_4\left\|\overline{\phi}^{K}(t)\right\|, \tag{36}$$

where

$$\begin{cases}
\Pi_1 = \dfrac{\mathscr{A}_{5}^{p_1} + \mathscr{B}_{5}^{p_2} + \mathscr{C}_{5}^{p_3} + \mathscr{D}_{5}^{p_4}}{\mathscr{W}} > 0, \\[2ex]
\Pi_2 = \dfrac{\mathscr{A}_{6}^{p_1} + \mathscr{B}_{6}^{p_2} + \mathscr{C}_{6}^{p_3} + \mathscr{D}_{6}^{p_4}}{\mathscr{W}} > 0, \\[2ex]
\Pi_3 = \dfrac{\mathscr{A}_{7}^{p_1} + \mathscr{B}_{7}^{p_2} + \mathscr{C}_{7}^{p_3} + \mathscr{D}_{7}^{p_4}}{\mathscr{W}} > 0, \\[2ex]
\Pi_4 = \dfrac{\mathscr{A}_{8}^{p_1} + \mathscr{B}_{8}^{p_2} + \mathscr{C}_{8}^{p_3} + \mathscr{D}_{8}^{p_4}}{\mathscr{W}} > 0.
\end{cases} \tag{37}$$

Thus, we can come to the conclusion that the unique equilibrium point u^* of system (3) is uniformly stable. This ends the proof. □

Remark 1. In 2017, Zhang et al. [4] analyzed the stability issue of fractional-order complex-valued neural networks involving leakage and discrete delays. In this study, we have investigated the stability of fractional-order quaternion-valued neural networks involving discrete and leakage delays. The investigation on the stability of fractional-order quaternion-valued neural networks becomes more complex than that of Zhang et al. [4] since the fractional-order quaternion-valued neural networks has been decomposed into more multidimensional neural networks. This study replenishes the research of Zhang et al. [4].

5. Simulation Results

Consider the fractional-order quaternion-valued neural networks:

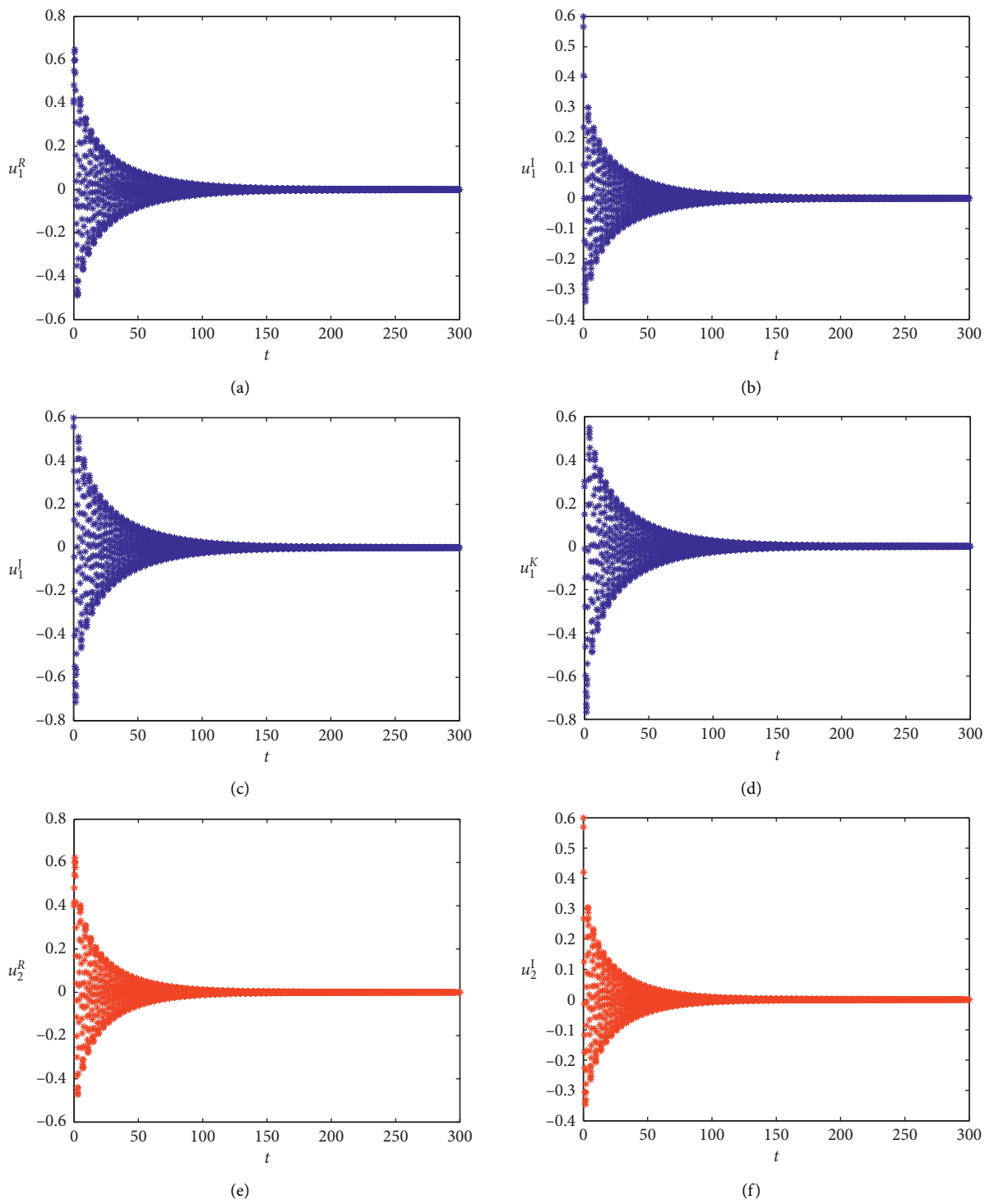

Figure 1: Continued.

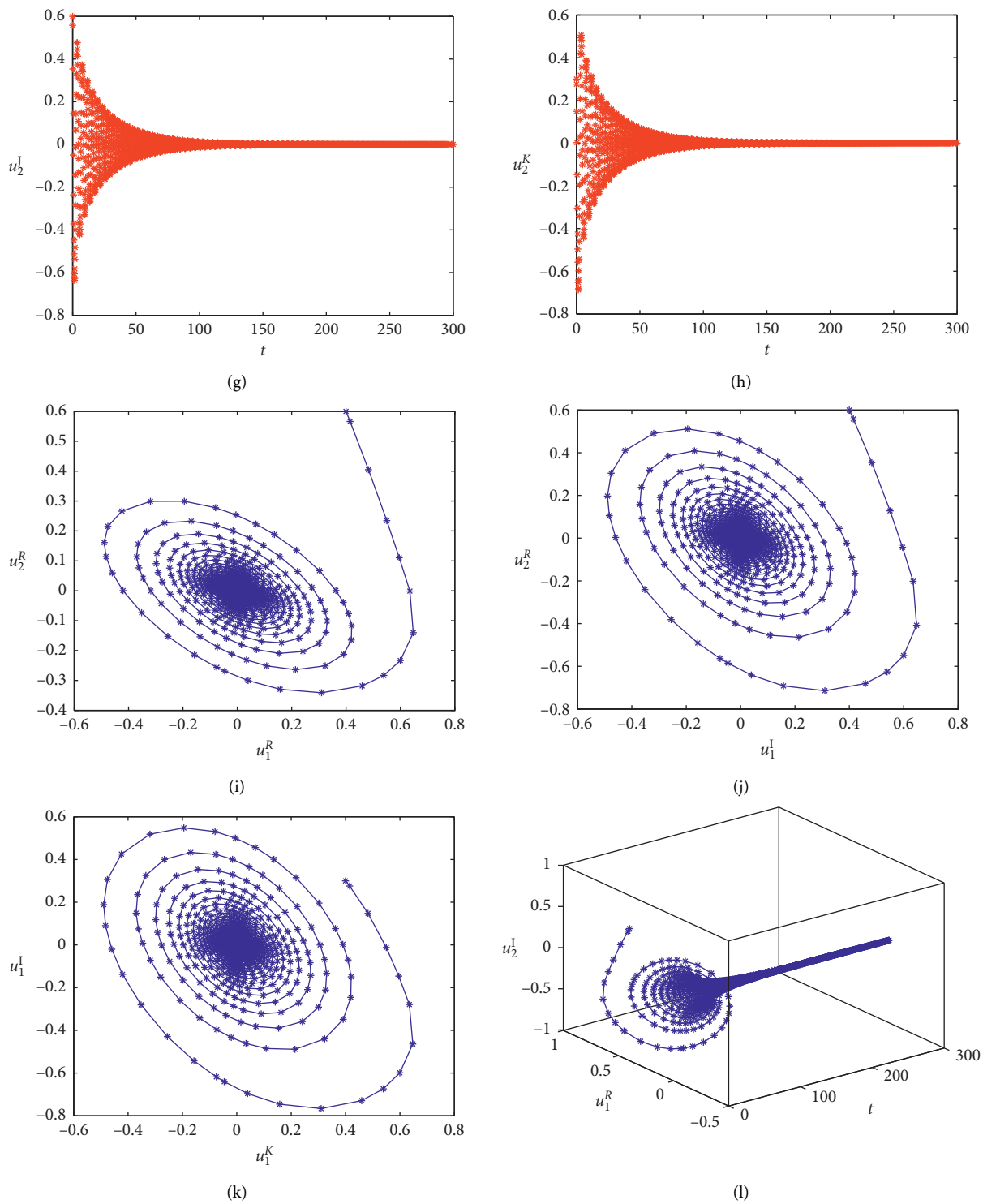

Figure 1: Continued.

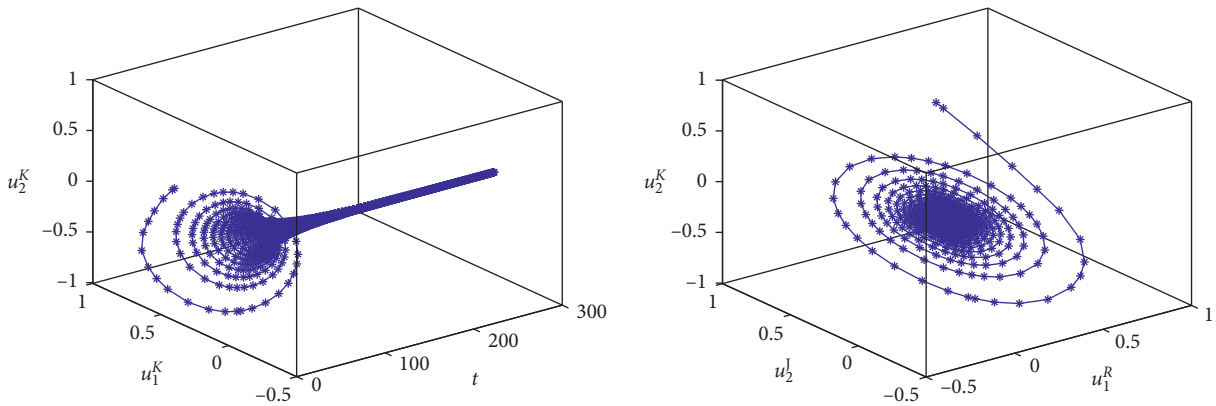

(m) (n)

Figure 1: The simulation trajectories of system (38).

$$\begin{cases} \dfrac{d^{0.72}u_1(t)}{dt^{0.72}} = -\gamma_1 u_1(t-0.52) + \sum_{h=1}^{2} \alpha_{1h} g_h(u_h(t)) + \sum_{h=1}^{2} \beta_{1h} g_h(u_h(t-0.44)) + L_1, \\ \dfrac{d^{0.72}u_2(t)}{dt^{0.72}} = -\gamma_2 u_2(t-0.52) + \sum_{h=1}^{2} \alpha_{2h} g_h(u_h(t)) + \sum_{h=1}^{2} \beta_{2h} g_h(u_h(t-0.44)) + L_2, \end{cases} \tag{38}$$

where $u_1(t) = u_1^R(t) + i\, u_1^I(t) + j u_1^J(t) + k u_1^K(t), u_2(t) = u_2^R(t) + i u_2^I(t) + j\, u_2^J(t) + k u_2^K(t)$, and

$$\begin{cases} \alpha_{11} = 0.22 + 0.25i + 0.34j + 0.53k, \\ \alpha_{12} = 0.33 + 0.43i - 0.67j + 0.45k, \\ \alpha_{21} = 0.19 + 0.65i - 0.67j - 0.88k, \\ \alpha_{22} = 0.43 + 0.35i - 0.23j - 0.38k, \\ \beta_{11} = 0.56 - 0.55i - 0.76j + 0.39k, \\ \beta_{12} = 0.22 + 0.79i + 0.81j - 0.66k, \\ \beta_{21} = 0.89 + 0.34i + 0.73j - 0.48k, \\ \beta_{22} = 0.35 + 0.84i + 0.67j - 0.85k, \\ L_1 = 0.77 + 0.33i + 0.28j - 0.36k, \\ L_2 = 0.67 + 0.34i + 0.57j - 0.62k, \\ g_h(u_h) = 0.3\cos u_h^R + 0.4i \sin\left(u_h^I + u_h^J + u_h^K\right) + 0.5j \sin u_h^J + 0.2k \sin\left(u_h^R + u_h^J + u_h^K\right). \end{cases} \tag{39}$$

It is easy to obtain that model (38) owns the zero equilibrium point. Let $\mathcal{G}_h^{RR} = \mathcal{G}_h^{RI} = \mathcal{G}_h^{RJ} = \mathcal{G}_h^{RK} = \mathcal{G}_h^{IR} = \mathcal{G}_h^{II} = \mathcal{G}_h^{IJ} = \mathcal{G}_h^{IK} = \mathcal{G}_h^{JR}, \mathcal{G}_h^{JI} = \mathcal{G}_h^{JJ} = \mathcal{G}_h^{JK} = \mathcal{G}_h^{KR} = \mathcal{G}_h^{KI} = \mathcal{G}_h^{KJ} = \mathcal{G}_h^{KK} = 1$. Utilizing the Matlab software, we obtain that $\theta = 0.7845$ and $\|\mathcal{U}\| = 0.6812$, $\mathcal{W} = 0.6008$. Thus, we can check that all the hypotheses of Theorem 2 are fulfilled. Thus, one can conclude that the zero equilibrium point of model (38) is uniformly stable. Figure 1 shows that the state of four parts will be close to zero gradually.

6. Conclusions

Based on earlier research studies, a class of fractional-order quaternion-valued neural networks involving discrete and

leakage delays has been set up. A set of sufficient conditions guaranteeing the existence and uniqueness of the equilibrium point for the investigated fractional-order quaternion-valued neural networks has been derived. In addition, the global uniform stability of the involved fractional-order quaternion-valued neural networks has been systematically discussed. This work generalizes the work of Zhang et al. [4]. The research idea can also be utilized to investigate many other types of fractional-order quaternion-valued neural networks. In addition, we know that Clifford analysis is more general than quaternion one [36, 37]. We will study the global uniform stability of Clifford-valued neural networks in the near future.

Data Availability

No data were used to support this study.

Conflicts of Interest

The authors declare that they have no conflicts of interest.

Acknowledgments

This work was supported by Natural Science Foundation of Guizhou Province (no. ZK2021019) and Guizhou University of Finance and Economics (nos. 2018YJ19 and 2018JGZZD04).

References

[1] C. Xiu, R. Zhou, and Y. Liu, "New chaotic memristive cellular neural network and its application in secure communication system," *Chaos, Solitons & Fractals*, vol. 141, Article ID 110316, 2020.

[2] M. Akhmet, R. Seilova, M. Tleubergenova, and A. Zhamanshin, "Shunting inhibitory cellular neural networks with strongly unpredictable oscillations," *Communications in Nonlinear Science and Numerical Simulation*, vol. 89, Article ID 105287, 2020.

[3] V. Limbachiya and R. Shamass, "Application of artificial neural networks for web-post shear resistance of cellular steel beams," *Thin-Walled Structures*, vol. 161, Article ID 107414, 2021.

[4] L. Zhang, Q. Song, and Z. Zhao, "Stability analysis of fractional-order complex-valued neural networks with both leakage and discrete delays," *Applied Mathematics and Computation*, vol. 298, pp. 296–309, 2017.

[5] F. C. Kong, Q. X. Zhu, C. Aouitic, and F. Dridi, "Periodic and homoclinic solutions of discontinuous CohenCGrossberg neural networks with time-varying delays," *European Journal of Control*, vol. 59, 2020.

[6] C. Aouiti, E. A. Assali, I. B. Gharbia, and Y. E. Foutayeni, "Existence and exponential stability of piecewise pseudo almost periodic solution of neutral-type inertial neural networks with mixed delay and impulsive perturbations," *Neurocomputing*, vol. 357, pp. 292–309, 2019.

[7] C. Huang, S. Wen, and L. Huang, "Dynamics of anti-periodic solutions on shunting inhibitory cellular neural networks with multi-proportional delays," *Neurocomputing*, vol. 357, pp. 47–52, 2019.

[8] M. Abdelaziz and F. Chérif, "Piecewise asymptotic almost periodic solutions for impulsive fuzzy Cohen-Grossberg neural networks," *Chaos, Solitons & Fractals*, vol. 132, Article ID 109575, 2020.

[9] C. Xu and P. Li, "On anti-periodic solutions for neutral shunting inhibitory cellular neural networks with time-varying delays and D operator," *Neurocomputing*, vol. 275, pp. 377–382, 2018.

[10] Z. Huang, X. Wang, and Y. Xia, "Exponential attractor of -almost periodic sequence solution of discrete-time bidirectional neural networks," *Simulation Modelling Practice and Theory*, vol. 18, no. 3, pp. 317–337, 2010.

[11] P. Jiang, Z. Zeng, and J. Chen, "Almost periodic solutions for a memristor-based neural networks with leakage, time-varying and distributed delays," *Neural Networks*, vol. 68, pp. 34–45, 2015.

[12] C. Xu, "Local and global Hopf bifurcation analysis on simplified bidirectional associative memory neural networks with multiple delays," *Mathematics and Computers in Simulation*, vol. 149, pp. 69–90, 2018.

[13] A. Sudbery, "Quaternionic analysis," *Mathematical Proceedings of the Cambridge Philosophical Society*, vol. 85, no. 2, pp. 199–225, 1979.

[14] H. Kusamichi, T. Isokawa, N. Matsui, Y. Ogawa, and K. Maeda, "A new scheme for color night vision by quaternion neural network," in *Proceedings of the 2004 International Conference on Autonomous Robots and Agents*, pp. 101–106, Palmerston North, New Zealand, December 2004.

[15] T. Isokawa, T. Kusakabe, N. Matsui, and F. Peper, "Quaternion neural network and its application," in *Proceedings of the 2003 7th International Conference on Knowledge-Based Intelligent Information*, pp. 318–324, Oxford, UK, September 2003.

[16] P. Arena, L. Fortuna, G. Muscato, and M. Xibilia, "Neural networks in multidimensional domains," in *Fundamentals And New Trends In Modelling And Control*Springer, London, UK, 1998.

[17] D. Lin, X. Chen, G. Yu, Z. Li, and Y. Xia, "Global exponential synchronization via nonlinear feedback control for delayed inertial memristor-based quaternion-valued neural networks with impulses," *Applied Mathematics and Computation*, vol. 401, Article ID 126093, 2021.

[18] Q. D. Jiang and Q. R. Wang, "Almost periodic solutions for quaternion-valued neural networks with mixed delays on time scales," *Neurocomputing*, vol. 439, pp. 363–373, 2021.

[19] X. You, S. Dian, R. Guo, and S. Li, "Exponential stability analysis for discrete-time quaternion-valued neural networks with leakage delay and discrete time-varying delays," *Neurocomputing*, vol. 430, pp. 71–81, 2021.

[20] H. Wang, G. Wei, S. Wen, and T. Huang, "Impulsive disturbance on stability analysis of delayed quaternion-valued neural networks," *Applied Mathematics and Computation*, vol. 390, Article ID 125680, 2021.

[21] D. Li, Z. Q. Zhang, Z. Zhang, and X. Zhang, Periodic solutions of discrete-time Quaternion-valued BAM neural networks," *Chaos, Solitons & Fractals*, vol. 138, Article ID 110144, 2020.

[22] Q. Song, L. Long, Z. Zhao, Y. Liu, and F. E. Alsaadi, "Stability criteria of quaternion-valued neutral-type delayed neural networks," *Neurocomputing*, vol. 412, pp. 287–294, 2020.

[23] C. Xu, M. Liao, P. Li, Z. Liu, and S. Yuan, "New results on pseudo almost periodic solutions of quaternion-valued fuzzy cellular neural networks with delays," *Fuzzy Sets and Systems*, vol. 411, pp. 25–47, 2021.

[24] Z. Tu, D. Wang, X. Yang, and J. Cao, "Lagrange stability of memristive quaternion-valued neural networks with neutral items," *Neurocomputing*, vol. 399, pp. 380–389, 2020.

[25] K. Udhayakumar, R. Rakkiyappan, X. Li, and J. Cao, "Mutiple ψ-type stability of fractional-order quaternion-valued neural networks," *Applied Mathematics and Computation*, vol. 401, Article ID 126092, 2021.

[26] P. Liu, M. Kong, M. Xu, J. Sun, and N. Liu, "Pinning synchronization of coupled fractional-order time-varying delayed neural networks with arbitrary fixed topology," *Neurocomputing*, vol. 400, pp. 46–52, 2020.

[27] F. Du and J.-G. Lu, "New criterion for finite-time synchronization of fractional order memristor-based neural networks with time delay," *Applied Mathematics and Computation*, vol. 389, Article ID 125616, 2021.

[28] S. Yang, H. Jiang, C. Hu, and J. Yu, "Synchronization for fractional-order reaction-diffusion competitive neural networks with leakage and discrete delays," *Neurocomputing*, vol. 436, pp. 47–57, 2021.

[29] M. Syed Ali, G. Narayanan, S. Saroha, B. Priya, and G. K. Thakur, "Finite-time stability analysis of fractional-order memristive fuzzy cellular neural networks with time delay and leakage term," *Mathematics and Computers in Simulation*, vol. 185, pp. 468–485, 2021.

[30] Y. Xu, J. Yu, W. Li, and J. Feng, "Global asymptotic stability of fractional-order competitive neural networks with multiple time-varying-delay links," *Applied Mathematics and Computation*, vol. 389, Article ID 125498, 2021.

[31] S. A. Karthick, R. Sakthivel, Y. K. Ma, S. Mohanapriya, and A. Leelamani, "Disturbance rejection of fractional-order T-S fuzzy neural networks based on quantized dynamic output feedback controller," *Applied Mathematics and Computation*, vol. 361, pp. 846–857, 2019.

[32] Y. Chatibi, E. H. El Kinani, and A. Ouhadan, "Variational calculus involving nonlocal fractional derivative with Mittag-Leffler kernel," *Chaos, Solitons & Fractals*, vol. 118, pp. 117–121, 2019.

[33] Y. Chatibi, E. H. El Kinani, and A. Ouhadan, "On the discrete symmetry analysis of some classical and fractional differential equations," *Mathematical Methods in the Applied Sciences*, vol. 44, no. 4, pp. 2868–2878, 2019.

[34] Y. Chatibi, E. H. El Kinani, E. Hassan El Kinani, and A. Ouhadan, "Lie symmetry analysis of conformable differential equations," *AIMS Mathematics*, vol. 4, no. 4, pp. 1133–1144, 2019.

[35] Y. Chatibi, E. H. El Kinani, and A. Ouhadan, "Lie symmetry analysis and conservation laws for the time fractional Black-Scholes equation," *International Journal of Geometric Methods in Modern Physics*, vol. 17, no. 1, Article ID 2050010, 2020.

[36] C. Xu, M. Liao, P. Li, Y. Guo, and Z. Liu, "Bifurcation properties for fractional order delayed BAM neural networks," *Cognitive Computation*, vol. 13, no. 2, pp. 322–356, 2021.

[37] C. Xu and C. Aouiti, "Comparative analysis on Hopf bifurcation of integer-order and fractional-order two-neuron neural networks with delay," *International Journal of Circuit Theory and Applications*, vol. 48, no. 9, pp. 1459–1475, 2020.

[38] I. Podlubny, *Fractional Differential Equations*, Academic Press, Cambridge, MA, USA, 1999.

[39] R. Rakkiyappan, J. Cao, and G. Velmurugan, "Existence and uniform stability analysis of fractional-order complex-valued neural networks with time delays," *IEEE Transactions on Neural Networks and Learning Systems*, vol. 26, no. 1, pp. 84–97, 2015.

[40] C. Li and W. Deng, "Remarks on fractional derivatives," *Applied Mathematics and Computation*, vol. 187, no. 2, pp. 777–784, 2007.

Hindawi
Journal of Mathematics
Volume 2021, Article ID 9936968, 13 pages
https://doi.org/10.1155/2021/9936968

Research Article

Prediction of High-Tech Talents Flow Impact on Labor Income Share: Based on DEA and Fractional Hausdorff Grey Model

Wei Cui, Anwei Wan, and Yongbo Yang

Faculty of Finance and Economics, Jiangsu University, Zhenjiang, Jiangsu 212013, China

Correspondence should be addressed to Anwei Wan; 1044258119@qq.com

Received 13 March 2021; Revised 5 April 2021; Accepted 12 April 2021; Published 26 April 2021

Academic Editor: Lifeng Wu

The purpose of this paper is to analyze the impact of high-tech talents flow on labor income share and explore the influencing mechanism. It can be proved that high-tech talents flow affects labor income share by production function, with technological progress as a mediator variable. The labor income share is the dependent variable, and the gravity of high-tech talents as the independent variable is the index to measure the high-tech talents flow, constructing the panel data model with the Malmquist index of technological progress as a mediator variable. Furthermore, the Malmquist index of technological progress is decomposed into catching-up of technological progress index and leapfrogging of technological progress index, which, respectively, replaces the Malmquist index of technological progress as a mediator variable in the panel data model. Regression analysis shows that technological progress is a mediator variable for high-tech talents flow to reduce labor income share, and the impact mainly comes from leapfrogging of technological progress. However, although the mediating effect of catching-up technological progress index is not significant at the significance level of 10%, it is a mediator variable for high-tech labor mobility to increase income share at the significance level of 20%. Finally, this paper predicts the change in labor income share from 2018 to 2027 by the fractional Hausdorff grey model, and the results show that it is an increasing trend. However, the Gini coefficient whose change trend is opposite to the labor income share remains high in the past two years, indicating that there are other factors affecting the income gap, such as the urbanization rate and the transportation convenience. The innovation of this paper is mainly to reveal that the leapfrogging of technological progress is the major cause of the high-tech talents flow rising income inequality gap, while the catching-up of technological progress is the source of the former narrowing the latter. The fractional Hausdorff grey model predicts that the key determinants of income inequality gap are more than labor income share.

1. Introduction

China's carbon emissions are among the top in the world, so it has great pressure and potential to reduce carbon emissions. One of the best ways to reduce carbon emissions is technological progress [1]. Technological progress requires the introduction of high-tech talents, which may lead to two outcomes. Firstly, the introduction of high-tech talents improves the level of automation and increases machine input and energy consumption, but increases carbon emissions. So carbon reduction equipment is needed in order to reduce carbon emissions from machines. Thus, there is a need for more labor to operate, maintain, and repair these carbon emissions to reduce devices, where labor and capital are in complementary relationship. Therefore, total labor income of the whole society increases in order to manage carbon emission from capital expansion; that is, labor income share may increase [2, 3]. Secondly, the increase in the employment of labor force due to carbon emission reduction also means an increase in production costs, a corresponding increase in commodity prices, and a decrease in demand, which leads to a decrease in demand for labor force, so the possibility of a decrease in labor income share is enhanced [2, 4].

Accordingly, the impact of the introduction of high-tech talents on the labor income share is uncertain on account of carbon emission reduction technological progress. However, changes in the labor income share significantly affecting the equality of income distribution are obvious. If the labor income share is low, social wealth tends to be allocated to

capital owners. Also, it may widen the gap between rich and poor to increase social instability [5]. If the labor income share is too high, it will lead to inflation [6]. The wage income of labor will be devalued, which not only reduces their quality of life but also hinders economic development. Therefore, labor income share should be kept within a reasonable range. Since technological progress is an important mediator variable for the introduction of high-tech talents to change labor income share, the law of technological progress deeply analyzed may be the key to mining the impact of high-tech talents flow on labor income share.

If technological progress is taken as a mediator variable, the reason for the uncertainty of the impact of the high-tech talents flow on the labor income share may be related to the mode of technological progress. Technological progress is divided into two modes [7], namely, catching-up and leapfrogging [8]. Technological progress was slow in the early stage of the emergence of new technologies. With the continuous promotion and popularization of technology, the progress speed was accelerating until natural limits or physical limits. At this time, the technology reached the mature stage, and the technological progress also encountered bottlenecks. It requires longer time and more resources to breaking through this bottleneck to achieve the leapfrogging of technological progress. The catching-up of technological progress is mainly technology promotion, which is manifested in the popularization of new machinery and equipment or the promotion of new production process. The leapfrogging of technological progress is mainly the replacement of old and new technologies, which is manifested as the emergence of new production tools. Therefore, the path of technological progress presents an S-curve trend [9]. Although the high-tech talents flow has an impact on the technological progress of the two models, the mechanism of technological change is different, and the role of the catching-up of technological progress is to improve production efficiency. By comparison, the role of the leapfrogging of technological progress is to produce new technologies. Consequently, the impact of high-tech talents flow on labor income share may be different due to different types of technological progress. On deep analysis, this impact may be the key to formulating income distribution policies and revealing the specific path of technological progress affecting labor income share.

The innovation of this paper is that the mediator variable of high-tech talents flow affecting labor income share is mainly the leapfrogging of technological progress rather than the catching-up of technological progress. Furthermore, the leapfrogging of technological progress is a mediator variable for high-tech talents flow to reduce labor income share at a significance level of 10%. Also, the catching-up of technological progress is a mediator variable for high-tech talents flow to increase labor income share at a significance level of 20%. Moreover, the impact of high-tech talents flow on labor income share is constrained by carbon emission reduction regulations. Fractional Hausdorff grey model predicts that the key determinants of income inequality gap are more than labor income share.

The rest of the article is arranged as follows. Section 2 is literature review. Section 3 is mechanism analysis. Section 4 is model construction. Section 5 is empirical analysis. Section 6 is conclusion.

2. Literature Review

2.1. Labor Mobility Affects Labor Income Share. The more skilled the labor, the greater the labor income share in developed countries; the more skilled the labor, the smaller the labor income share in developing countries [10]. This is related to differences in industrial efficiency and elasticity of substitution among products among countries. Differences in industrial efficiency lead to differences in product prices, triggering the labor flow. If substitution elasticity between products is greater than 1, labor flows from low-technology to high-technology sectors. If the elasticity of substitution between products is less than 1, the result of labor flows is opposite [11]. High-tech industries in developed countries are more efficient and match highly skilled labor, so the more the labor, the greater the labor income share. However, developing countries are completely opposite [12]. Therefore, the technical level is related to labor mobility and its labor income share. Panel data from 11 industrialized countries show that both technological advances in the industrial sector prior to the Second World War and subsequent technological advances in the agricultural sector are drivers of labor mobility [13]. Similar conclusions were obtained by the industrial evolution model and counterfactual analysis with data from 45 countries from 1970 to 2005. This may be because technological progress has changed productivity across sectors and has led to transsectoral labor mobility [14]; for example, the industrial structure of the United States changed from industry to service with the flow of labor and the corresponding change in the labor income share in various industries from 1960 to 2005 [15]. Thus, technological progress is an important mediator between labor mobility and labor income share.

2.2. Impact of Technological Progress on Labor Income Share. The impact of technological progress on the share of labor income is uncertain. Zeira [16] constructed an automated economic growth model. This model showed that the higher the proportion of automation input, the higher the proportion of capital output. Based on this study, Aghion et al. [17] analyzed the impact of technological progress on income share in terms of automation and Baumol's disease. On the one hand, automation inputs increase returns on capital and capital income share, while they decrease labor income share, that is, substitution effects [18, 19]. On the other hand, the labor income share increased because of Baumol's disease, that is, countervailing effect [20, 21].

Technological progress can lead to higher unemployment while improving labor productivity, that is, substitution effect [22, 23]. So 47% of jobs in the US, 59% in Germany, and 1.7% in Canada are replaced by machines with technological advances [24, 25]. The reason for the large difference in substitution rates among the three countries

may be because the statistical calibers are inconsistent. After unification, the values of the three countries become 9%, 12%, and 9%, respectively [26].

In fact, however, employment in countries of the twentieth century has maintained a trend of growth [27], which suggests that technological progress can also increase jobs [28] and therefore has a countervailing effect. Although scientific and technological progress has led to a greater substitution effect than complementary effects for industrial machines to labor in the United States, adding one machine will reduce employment by 0.18–0.34 percent [18], but this result is related to the nature of the industry. The textile, steel, and automotive industries are substitution effects in the US, while the nonmanufacturing industry is the complementary effect, and the increase in mechanization has increased employment between capital and labor [29]. Similar phenomena exist in Germany. The promotion of machines reduces manufacturing employment but increases employment in services [30]. The increase in employment means that the labor income share may increase.

Income distribution inequality is generally increased whether scientific and technological progress increases or decreases the labor income share. Even though low-skilled and high-skilled labor may be replaced by machines in technological progress, the former increases income inequality and the latter reduces income inequality [31]. However, capital returns are higher because machines are replicable [32]. Furthermore, machine costs fall led to labor income share fall as technology matures [33]. Therefore, income inequality shows an increasing trend.

A considerable number of environmental technology innovation results have been produced in response to global environmental protection pressure. At present, environmental regulation is an important constraint for technological innovation, and its impact on labor income share has also become the focus of academic circles.

2.3. Impact of Environmental Regulation on Labor Income Share. Environmental regulation has a significant effect on labor income share [34]. Environmental protection policy and labor employment may be negative correlation. Developed countries began to attach importance to environmental protection and introduced stricter environmental protection systems, which led to an increase in unemployment in the 1970s [35]. A survey shows that one-third of interviewee feedback that their work is threatened by environmental regulation in 1990 [2], but there are also scholars who argue that these interviewees are overstated because they ignore environmental regulation also creates jobs [36]. Therefore, the direct impact of environmental regulation on employment is still unclear [37].

On the one hand, environmental regulation increases marginal costs, which results in lower output and reducing labor demand. Greenstone (2002) analyzed the impact of the Clean Air Act Amendments on the labor demand of the industrial sector and found that the labor force in counties that failed to meet the air emission requirements of the Act Amendments decreased by 590000 people from 1972 to 1987 in order to meet the air emission standards in the United States. Similar cases occurred in Spain. In 1990, this country amended the Clean Air Act. Walker [38] estimated a 15 percent decline in labor force in the industrial sector in counties not meeting the standard to counties meeting the standard. Therefore, the introduction of new environmental protection bills or amendments to environmental protection regulations may lead to reduced labor demand and increased unemployment [3, 37, 39].

On the other hand, environmental regulation may also increase the employment rate. More workers are needed to install, operate, and repair new machines because of new technologies. Numerous studies have shown that this phenomenon is widespread. For example, the United States SCAQMD Act and CAFÉ standards created 300,000 jobs [4, 40]. Although these policies aim to reduce carbon emissions and improve energy efficiency, they also create more jobs [41].

Thus, the correlation between environmental regulation and labor income share is also uncertain. Britain's carbon tax policy has not significantly changed manufacturing employment rate [42], but British Columbia's carbon tax police has significantly increased employment [43]. However, this result was denied by Chi [44], and he found that the policy led to an increase of 1.3% in unemployment.

Existing studies have shown that high-tech labor mobility accelerates technological innovation spillover, which may change the labor income share. However, there are three points that need further analysis. Firstly, although the flow of high-tech labor force can change the labor income share, it is not clear whether it is caused by catching-up of technological progress or leapfrogging of technological progress, which leads to the failure to correctly guide the flow of talents to improve labor income share. Secondly, there is opposite correlation among technological progress, environmental regulation, and labor income share in different literature studies, but there is no literature systematically discussing the reasons, which makes it impossible to find incentive measures for scientific and technological progress to effectively improve labor income share under different environmental regulations. Thirdly, the literature of the impact of labor mobility on labor income share ignores the mediator variable of technological progress, leading to the lack of an effective method of technological innovation path improving labor income share.

In view of this, this paper introduces the Malmquist index of carbon emission reduction technological progress and uses the IDA (Index Decomposition Analysis) to decompose it into catching-up of technological progress index and the leapfrogging of technological progress index. This paper analyzes the influence of the high-tech labor flow on the labor income share with these two kinds of technological progress indexes as mediator variables and then gives the possible path to increase the labor income share. Also, fractional Hausdorff grey model is used to predict the change in labor income share to forecast the fairness of income distribution.

2.4. Mechanism Analysis of High-Tech Talents Flow Affecting Labor Income Share. An aggregate production function, *F(L, M, A)*, includes two inputs, which are L and M. A is a technology index in *F(L, M, A)*. And L is unskilled workman, while M could be capital, skilled labor, or land according to Acemoglu [45]. But skilled labor should not belong to M but to L according to the definition of labor. So L and M are high-tech talent and capital, respectively, in the *F(L, M, A)*.

Without loss of generality, imagine that $\partial F/\partial A > 0$; the more the introduction of talents are, the greater the level A is, the better the technology is. Introducing the talents could improve technology from two aspects, which is, respectively, the leapfrogging and the catching-up.

Technical change is the leapfrogging if the production function takes the more special form$F(\mathrm{AL}, M)$. Also, technical change is the catching-up if the production function takes the more special form $F(L, \mathrm{AM})$. $F(\mathrm{AL}, M)$ means labor efficiency improvement breaks through old technologies to realize the leapfrogging of technological progress because of more and more knowledgeable, capable, and intelligent workers in the employment market. However, $F(L, \mathrm{AM})$ means the capital efficiency improvement may be caused by new machines usage or new technical skill extension which is the catching-up of technological progress.

Technical change is L-biased, which means increment of labor income share, if

$$\frac{\partial(\partial F/\partial L)/(\partial F/\partial M)}{\partial A} > 0, \tag{1}$$

that is, technical change increases the marginal product of high-tech talent more than M.

The constant elasticity of substitution (CES) production function is calculated in equation (2), and the relative marginal product of L and M is calculated in equation (3). For more details on the properties of production function and marginal function, refer to [45]:

$$y = \left[\gamma\left(A_L L\right)^{(\sigma-1/\sigma)} + (1-\gamma)\left(A_M M\right)^{(\sigma-1/\sigma)}\right]^{(\sigma/\sigma-1)}, \tag{2}$$

$$\frac{\mathrm{MP}_M}{\mathrm{MP}_L} = \frac{1-\gamma}{\gamma}\left(\frac{A_M}{A_L}\right)^{(\sigma-1/\sigma)}\left(\frac{M}{L}\right)^{-1/\sigma}, \tag{3}$$

with A_M (capital efficiency) and A_L (labor efficiency) calculated in equations (4) and (5) based on Box–Cox transformations according to Bencik, *M*. [46]:

$$A_M = M_0 e^{g_M(t)}, \tag{4}$$

$$A_L = L_0 e^{g_L(t)}, \tag{5}$$

in which $g_M(t)$ and $g_L(t)$ are the contribution of capital efficiency and labor efficiency, respectively.

Then, equations (4) and (5) replace A_M and A_M in equation (3), respectively. And the result is shown in the following equation:

$$Q = \frac{\mathrm{MP}_M}{\mathrm{MP}_L} = \frac{1-\gamma}{\gamma}\left(\frac{A_M}{A_L}\right)^{(\sigma-1/\sigma)}\left(\frac{M}{L}\right)^{-1/\sigma}. \tag{6}$$

Technical change is the leapfrogging of technological progress or the catching-up of technological progress, which is decided by technical bias. Also, the technical bias could be calculated by time derivative of equation (6). The result is shown as follows:

$$\frac{\mathrm{d}Q}{\mathrm{d}t} = \frac{1-r}{r}\left(\frac{M_0}{L_0}\right)^{(\sigma-1/\sigma)}\left(\frac{M}{L}\right)^{-1/\sigma}\left(\frac{\sigma-1}{\sigma}\right)\left[\frac{e^{g_M(t)}}{e^{g_L(t)}}\right]^{-1/\sigma}\frac{e^{g_M(t)}\cdot e^{g_L(t)}\left[g'_M(t)-g'_L(t)\right]}{\left[e^{g_L(t)}\right]^2}. \tag{7}$$

If $\sigma < 1$, high-tech talents and capital are complementary effects with increasing returns to scale Also, new technology replaces old technology, which is the leapfrogging of technological progress, so the marginal contribution of labor efficiency is more than capital efficiency [47] because new technological breakthrough relies on high-tech talents, that is, as shown in equation (8). However, $\sigma < 1$ means that more capital needs to be put on production. Hence, $\mathrm{d}Q/\mathrm{d}t > 0$ in equation (7). This means the technical bias is capital bias. In other words, the leapfrogging of technological progress would increase capital income share and decrease high-tech talent income share. Moreover, the unskilled labor efficiency is lower than the high-tech talent efficiency, so the unskilled labor income share also decreases when the high-tech talent income share decreases. Consequently, the leapfrogging of technological progress, which means increasing returns to scale, could decrease labor income share:

$$g'_M(t) < g'_L(t). \tag{8}$$

If $\sigma > 1$, it means the substitution effect between high-tech talent and capital with constant returns to scale. Also, the new technology is promoting after the leapfrogging of technological progress, such as the application of new machines and new process. Therefore, the marginal contribution of capital efficiency is more than labor efficiency [8], so the technical change is capital-biased, that is, equation (9). Also, $\mathrm{d}Q/\mathrm{d}t > 0$ in equation (7), but the technical bias would change equation (9) into equation (10) because of the law of diminishing marginal returns and $\mathrm{d}Q/\mathrm{d}t < 0$. If $\mathrm{d}Q/\mathrm{d}t > 0$, the catching-up of technological progress would decrease high-tech talent income share. If $\mathrm{d}Q/\mathrm{d}t < 0$, the catching-up of technological progress would increase high-tech talent income share, so the catching-up of technological progress may increase or decrease the labor income share because high-tech talent is part of labor:

$$g'_M(t) > g'_L(t), \tag{9}$$

$$g'_M(t) < g'_L(t). \tag{10}$$

Thus, because of high-tech talents flow, the leapfrogging of technological progress decreases the labor income share, while the catching-up of technological progress ambiguously impacts on labor income share.

3. Malmquist Index with DEA, Panel Model, and Fractional Hausdorff Grey Model

3.1. Malmquist Index and Decomposition Analysis Based on DEA. Technological progress as a mediator variable can be measured by Malmquist index [48]. Färe et al. [49] developed it as a nonparametric method described by Shephard distance function. The advantage of this method is that it is easy to determine the optimal solution to improve technological progress, and the disadvantage is that it is unable to solve the measurement model of technological progress with CO_2 constraints. Thus, it is necessary to combine the static environmental performance measurement method by Tyteca [50] to define the distance function of CO_2 as in equation (11). K, L, and E are input capital, labor, and energy. Y and C are output GDP and CO_2. The δ value indicates the maximum promotion of technological progress under the pressure of carbon emission reduction. On this basis, Malmquist index MQI can be constructed. Malmquist index can be based on both t-period technology and $(t+1)$ period, so the geometric average of the Malmquist index in these two periods is used to measure the technological progress under the constraint of carbon emission reduction from t-period to $(t+1)$ period in order to avoid different measurement results due to different periods, as shown in formula (12):

$$D(K, L, E, Y, C) = \sup\{\delta\colon\ (K, L, E, Y, C/\delta) \in P(K, L, E)\}, \tag{11}$$

$$MQI(t, t+1) = \frac{D^t\left(K^t, L^t, E^t, Y^t, C^t\right) \cdot D^{t+1}\left(K^t, L^t, E^t, Y^t, C^t\right)}{D^t\left(K^{t+1}, L^{t+1}, E^{t+1}, Y^{t+1}, C^{t+1}\right) D^{t+1}\left(K^{t+1}, L^{t+1}, E^{t+1}, Y^{t+1}, C^{t+1}\right)}, \tag{12}$$

where $(K^t, L^t, E^t, Y^t, C^t)$ and $(K^{t+1}, L^{t+1}, E^{t+1}, Y^{t+1}, C^{t+1})$ are t-period and $(t+1)$ period of input-output, respectively; D^t and D^{t+1}, respectively, represent the distance function of technological progress in period t and $(t+1)$. Solving the method of distance function is environmental DEA model [51]. Hence, the Malmquist index of technological progress of carbon emission reduction is based on four periods of technology, so four distance functions are solved, as shown in formula (13), where p and q represent periods and $p, q \in (t, t+1)$:

$$\begin{aligned} &\min \delta = \left[D^p\left(K^q, L^q, E^q, Y^q, C^q\right)\right]^{-1} \\ &s.t.\ \sum_{i=1}^{I} \lambda_i K_i^p \le K_i^q, \sum_{i=1}^{I} \lambda_i L_i^p \le L_i^q, \sum_{i=1}^{I} \lambda_i E_i^p \le E_i^q, \sum_{i=1}^{I} \lambda_i Y_i^p \ge Y_i^q, \sum_{i=1}^{I} \lambda_i C_i^p = \delta C_i^q, \quad \lambda_i \ge 0, i = 1, 2, \ldots, I. \end{aligned} \tag{13}$$

Malmquist index of carbon emission reduction technological progress can be further decomposed into catching-up index (CCI) and leapfrogging index (LFI), that is, MQI = CCI · LFI, as shown in (14) and (15), respectively. Also, MQI > 1 represents carbon emission reduction technological advances. CCI > 1 and LFI > 1 mean that the catching-up of technological progress and the leapfrogging of technological progress are the reasons for carbon emission reduction technological progress, respectively. Also, the meaning of MQI < 1,CCI < 1, and LFI < 1 is opposite:

$$\mathrm{CCI}(t, t+1) = \frac{D^t\left(K^{t+1}, L^{t+1}, E^{t+1}, Y^{t+1}, C^{t+1}\right) \cdot D^t\left(K^t, L^t, E^t, Y^t, C^t\right)}{D^{t+1}\left(K^t, L^t, E^t, Y^t, C^t\right) D^{t+1}\left(K^{t+1}, L^{t+1}, E^{t+1}, Y^{t+1}, C^{t+1}\right)}, \tag{14}$$

$$\mathrm{LFI}(t, t+1) = \frac{D^{t+1}\left(K^{t+1}, L^{t+1}, E^{t+1}, Y^{t+1}, C^{t+1}\right)}{D^t\left(K^t, L^t, E^t, Y^t, C^t\right)}. \tag{15}$$

3.2. Panel Model. According to the mechanism analysis, a panel data model is used to analyze the impact of high-tech talents on labor income share. According to a study by Grunewald et al. [52], the dependent variable is labor income share (LSrate); the core independent variable is the labor gravitation (Labor_grav). The mediator variable is carbon emission reduction technology (CERT). Furthermore, the control variables include the level of urbanization (Urb), education level (Edu) [53], basic pension insurance (Pen) [54], unemployment insurance (Unempl) [55], health insurance (Heal) [56], highway density (Hwd), and railway density (Rwd) [57]. All control variables are referred to the research by Wei [58] and represented by γ_{ij}. The specific models are as follows:

$$\mathrm{LSrate}_{it} = \lambda_0 + \lambda_1 \mathrm{Labor\_grav}_{it} + \sum \lambda_{it} \cdot \gamma_{it} + u_{it}, \tag{16}$$

$$\mathrm{CERT}_{it} = \tau_0 + \tau_1 \mathrm{Labor\_grav}_{it} + \sum \tau_{it} \cdot \gamma_{it} + \varepsilon_{it}, \tag{17}$$

$$\mathrm{LSrate}_{it} = \beta_0 + \beta_1 \mathrm{Labor\_grav}_{it} + \beta_2 \mathrm{CERT}_{it} + \sum \beta_{it} \cdot \gamma_{it} + \xi_{it}. \tag{18}$$

It divides into three steps to judge the mediating effect. The first step is to check whether the labor gravitation has a significant impact on the labor income share, as shown in equation (14). If it is significant, then the second step is to test whether the labor gravitation significantly affects the carbon emission reduction technology, as shown in equation (15). If it is significant, then the third step is to examine the significance of the impact of labor gravitation and carbon emission reduction technology on the labor income share. If the impact of labor gravitation is significant, the carbon emission reduction technology is the mediator variable of the labor gravitation impacting the labor income share.

3.3. Fractional Hausdorff Grey Model. The data for this article are from 2007 to 2017 because of some unpublished data, so it is necessary for the prediction model to predict the change in labor income share in the future. Because of the small amount of data in this paper, grey theory may be suitable for building the prediction model. At present, the prediction accuracy of fractional Hausdorff grey model (FHGM) is higher than that of other models, which is suitable for the prediction analysis in this paper. For the specific form of FHGM, this study refers to the research of Meng et al. and Shi and Wu [59, 60].

$$\hat{x}^{(0)}(k+1) = \frac{\left(1 - e^{\hat{a}}\right)\left(x^{(0)}(1) - \hat{b}/\hat{a}\right)e^{-\hat{a}k}}{(k+1)^r - k^r}, \quad (k = 1, 2, \ldots, n). \tag{19}$$

4. Index, Data, and Results

4.1. Index Selection, Data Sources, and Descriptive Statistics. This paper studies the impact of high-tech talents flow on labor income share based on the carbon emission reduction technology as the mediator variable in China. The variable Labor_grav is the labor gravitation measured by gravitation in the high tech workforce, and its calculation method refers to the research of Witt & Witt (1995) [61]. The mediator variable CERT is carbon emission reduction efficiency based on environmental DEA methodology measuring carbon emission reduction technology. The control variables include Urb measured by the proportion of urban population in each province; Edu is measured by the average education years using the concrete calculation method of (6 + Edu)/28 because most Chinese citizens begin attending elementary school at the age of 6 and graduate with a doctoral degree at the age of 28; Pen, Unempl, and Heal are pension, unemployment insurance, and health insurance, respectively, measured by the ratio of each type of insurance participant to the total population in each province; Hwd and Rwd are, respectively, measured by the ratio of highway and railway mileage to the total population in each province [58].

The data selection, data sources, and data calculation methods are as follows. The data pertaining to population, capital, labor, and GDP are also from the China Statistical Yearbook. The perpetual inventory method is used to calculate capital, taking 2000 as the basic period. Similarly, we calculate the actual GDP taking 2000 as the basic period. The data regarding energy consumption come from the China Energy Statistical Yearbook. CO_2 data are from the "Energy" section in the "2006 IPCC Guidelines for National Greenhouse Gas Inventories" designated by the Intergovernmental Panel on Climate Change, which can be specifically calculated using the final consumption of industrial energy data from the China Energy Statistical Yearbook. The Urb, Edu, Pen, Unempl, and Heal data are all from the China Urban Statistical Yearbook. The data regarding highway and railway mileage are from the China Transportation Statistical Yearbook. In the absence of data from individual indices in some provinces, we use a balanced data set with annual measurements from 2007 to 2017, covering 25 provinces. The summary statistics of these data are shown in Table 1.

4.2. Results

4.2.1. Results of Malmquist Index. The carbon emission reduction efficiency measuring as Malmquist index of 25 provinces is calculated in China using formulas (12) and (13), as shown in Table 2. It can decompose into the catching-up and the leapfrogging of technological progress using formulas (14), (15), and (13), as shown in Tables 3 and 4, respectively.

4.2.2. Results of Panel Data Model. Malmquist index of carbon emission reduction technology is used as a mediator variable to verify the impact of high-tech talents flow on labor income share. High-tech talents flow reduces labor income share at a significance level of 5% according to formula (16) and model 1 in Table 5. Then, according to formula (17), high-tech talents flow promotes technological progress in carbon emission reduction at a significance level of 5% according to model 2 in Table 5. Also, at a significance

Table 1: Summary statistics for our balanced panel set.

Variable	Unit	Mean	SD	Min	Max
Main variables					
G	Percentage scale	0.378	0.050	0.251	0.490
δ	Percentage scale	0.636	0.264	0.124	1.000
Mediator variables					
Labor_grav	Percentage scale	0.004	0.006	4.361E-05	0.033
Controls					
Urb	Percentage scale	0.528	0.136	0.275	0.896
Edu	Percentage scale	0.544	0.049	0.449	0.732
Pen	Percentage scale	0.402	0.214	0.051	0.811
Unempl	Percentage scale	0.119	0.084	0.035	0.513
Heal	Percentage scale	0.358	0.226	0.059	1.093
Hwd	Kilometer/hundred person	0.366	0.228	0.057	1.384
Rwd	Kilometer/thousand person	0.102	0.092	0.017	0.497

Data source: calculation. Total number of observations is 275.

Table 2: Calculation results of Malmquist index of carbon emission reduction technology of 25 provinces.

	2007	2008	2009	2010	2011	2012	2013	2014	2015	2016	2017
Beijing	1.0000	1.0000	1.0000	1.0000	1.0000	1.0000	1.0000	1.0000	1.0000	1.0000	1.0000
Hebei	0.2840	0.2645	0.2476	0.2314	0.2010	0.1666	0.1743	0.1431	0.1412	0.1233	0.1146
Liaoning	0.1852	0.1694	0.1581	0.1359	0.1453	0.1206	0.1237	0.1073	0.1035	0.0948	0.0842
Shanghai	0.2074	0.1822	0.1685	0.1564	0.1553	0.1119	0.1167	0.1240	0.1172	0.1043	0.0981
Jiangsu	0.3533	0.3200	0.3313	0.2954	0.2761	0.2512	0.2635	0.2318	0.2254	0.2053	0.1449
Zhejiang	0.8659	0.4150	0.3903	0.3333	0.3249	0.2601	0.2623	0.2577	0.2301	0.1976	0.1762
Fujian	1.0000	0.7574	1.0000	1.0000	1.0000	1.0000	1.0000	0.4726	0.4919	0.4741	0.4711
Guangdong	0.6185	0.6034	0.5831	0.5742	0.5243	0.4164	0.4246	0.3648	0.3586	0.3417	0.3183
Hainan	0.7009	0.6355	0.6114	0.5829	0.6022	0.5157	0.4977	0.4676	0.4589	0.4322	0.4253
Shanxi	0.4249	0.3764	0.3442	0.3230	0.3394	0.2657	0.2784	0.2389	0.2369	0.2273	0.2151
Heilongjiang	0.7007	0.6160	0.5712	0.5357	0.5538	0.4150	0.4530	0.4425	0.4298	0.4397	0.4746
Anhui	0.5827	0.5054	0.5032	0.4438	0.4821	0.3972	0.4418	0.3278	0.3214	0.2980	0.2865
Jiangxi	0.4209	0.3613	0.3510	0.3221	0.3042	0.2540	0.2775	0.2722	0.2665	0.2662	0.2573
Henan	0.4129	0.3917	0.3970	0.3782	0.3332	0.2488	0.2803	0.3333	0.3367	0.3385	0.3298
Hubei	1.0000	1.0000	1.0000	1.0000	1.0000	1.0000	1.0000	1.0000	1.0000	1.0000	1.0000
Inner Mongolia	0.5355	0.4898	0.4714	0.4176	0.3963	0.3210	0.3302	0.3128	0.3098	0.3211	0.2952
Guangxi	0.7791	0.6714	0.5717	0.5318	0.5836	0.4174	0.4343	0.4035	0.3961	0.3687	0.3998
Sichuan	0.5419	0.5057	0.4022	0.3986	0.4415	0.3321	0.3507	0.4164	0.3837	0.3922	0.3949
Chongqing	0.5957	0.4973	0.4516	0.4041	0.3968	0.3557	0.3518	0.3379	0.3440	0.3513	0.3593
Guizhou	0.1620	0.1551	0.1716	0.1547	0.1609	0.1289	0.1306	0.1382	0.1504	0.1592	0.1488
Shaanxi	0.4854	0.3937	0.3700	0.3541	0.3300	0.2656	0.2603	0.2655	0.2577	0.2424	0.2356
Gansu	0.3034	0.2744	0.2468	0.2496	0.2071	0.1720	0.1700	0.1609	0.1601	0.1492	0.1483
Qinghai	0.3096	0.2985	0.2595	0.2370	0.2707	0.2108	0.1954	0.1850	0.1813	0.1613	0.1367
Ningxia	0.1453	0.1314	0.1322	0.1221	0.1182	0.0722	0.0796	0.0763	0.0735	0.0660	0.0663
Xinjiang	0.3158	0.2832	0.2528	0.2025	0.2151	0.1577	0.1385	0.1159	0.1032	0.0908	0.0775

Data source: calculation.

level of 10 percent, high-tech talents flow reduces the labor income share through technological advances in carbon emission reduction according to formula (18) and model 3, as shown in Table 5.

It is noteworthy that carbon emission reduction technology has a full mediating effect. Then, it can be proved that the real mediating variable is leapfrogging rather than catching-up of technological progress, as shown in Tables 6 and 7. In model 4, high-tech talents flow promotes leapfrogging of technological progress at a significance level of 10% in Table 6. Also, leapfrogging of carbon emission reduction technological progress as a mediator variable reduces labor income share with high-tech talents flow in model 5 in Table 6. If catching-up of technological progress is taken as the mediator variable, high-tech talents are introduced to enhance catching-up

Table 3: Calculation results of the catching-up index of carbon emission reduction technology of 25 provinces.

	2007	2008	2009	2010	2011	2012	2013	2014	2015	2016	2017
Beijing	0.9446	0.9457	0.9524	0.9658	0.8997	0.9548	0.9556	0.9556	0.9214	0.9569	0.9446
Hebei	1.0263	1.0266	1.0365	1.2359	1.4518	0.8332	1.3260	0.9366	1.1145	1.0602	1.0263
Liaoning	1.0724	1.0425	1.2363	0.8162	1.4020	0.8307	1.1872	0.9811	1.0120	1.1599	1.0724
Shanghai	1.1533	1.0561	1.0575	0.9455	1.8105	0.8391	0.7910	1.0219	1.0714	1.0344	1.1533
Jiangsu	1.0954	0.8462	1.1477	1.0494	1.2848	0.8284	1.1547	0.9651	1.0231	1.8397	1.0954
Zhejiang	3.9718	1.0373	1.2618	0.9638	1.6673	0.8959	0.9256	1.1459	1.1502	1.1526	3.9718
Fujian	1.3510	0.6361	0.8955	0.9148	1.0991	0.8334	2.8946	0.8428	0.9319	0.9271	1.3510
Guangdong	0.9489	0.9769	0.9536	1.1109	1.7218	0.8514	1.2096	0.9449	0.9354	1.0549	0.9489
Hainan	1.0866	0.9768	1.0040	0.8610	1.5238	0.8919	1.0119	0.9482	0.9572	0.9454	1.0866
Shanxi	1.1439	1.0853	1.0432	0.8373	1.7721	0.8303	1.2128	0.9287	0.9227	1.0225	1.1439
Heilongjiang	1.1570	1.0495	1.0294	0.8728	1.8425	0.7653	0.9361	0.9677	0.8112	0.7858	1.1570
Anhui	1.1848	0.9097	1.1665	0.7849	1.5672	0.7369	1.6225	0.9496	0.9881	0.9901	1.1848
Jiangxi	1.2237	0.9598	1.0798	1.0459	1.3491	0.7635	0.9284	0.9527	0.8512	0.9799	1.2237
Henan	0.9951	0.8830	1.0078	1.1832	1.9368	0.7182	0.6317	0.8950	0.8401	0.9646	0.9951
Hubei	0.9782	0.9519	0.9612	0.9858	1.1457	0.9099	0.9538	0.9148	0.9099	0.9929	0.9782
Inner Mongolia	1.0685	0.9725	1.1531	1.0356	1.4335	0.8619	0.9953	0.9309	0.7904	1.0830	1.0685
Guangxi	1.2016	1.2232	1.0483	0.7745	1.8389	0.8419	1.0350	0.9473	0.9803	0.7784	1.2016
Sichuan	1.0237	1.4018	0.9239	0.7602	1.8070	0.8177	0.6335	1.0754	0.8125	0.9031	1.0237
Chongqing	1.2734	1.0912	1.1330	0.9675	1.3034	0.9318	0.9681	0.8812	0.8137	0.8754	1.2734
Guizhou	0.9740	0.7245	1.1168	0.8621	1.4658	0.8872	0.7985	0.7707	0.7578	1.0482	0.9740
Shaanxi	1.3562	1.0042	0.9906	1.0737	1.4602	0.9488	0.8585	0.9689	0.9596	0.9696	1.3562
Gansu	1.0873	1.0969	0.8864	1.3545	1.3644	0.9326	0.9972	0.9231	0.9777	0.9258	1.0873
Qinghai	0.9594	1.1734	1.0877	0.7152	1.5505	1.0609	0.9969	0.9489	1.0723	1.2762	0.9594
Ningxia	1.0923	0.8763	1.0631	0.9953	2.5201	0.7490	0.9739	0.9827	1.0514	0.9085	1.0923
Xinjiang	1.1100	1.1129	1.4142	0.8259	1.7506	1.1823	1.2763	1.1507	1.0958	1.2594	1.1100

Data source: calculation.

Table 4: Calculation results of the leapfrogging index of carbon emission reduction technology of 25 provinces.

	2007	2008	2009	2010	2011	2012	2013	2014	2015	2016	2017
Beijing	0.9446	0.9457	0.9524	0.9658	0.8997	0.9548	0.9556	0.9556	0.9214	0.9569	0.9446
Hebei	1.0263	1.0266	1.0365	1.2359	1.4518	0.8332	1.3260	0.9366	1.1145	1.0602	1.0263
Liaoning	1.0724	1.0425	1.2363	0.8162	1.4020	0.8307	1.1872	0.9811	1.0120	1.1599	1.0724
Shanghai	1.1533	1.0561	1.0575	0.9455	1.8105	0.8391	0.7910	1.0219	1.0714	1.0344	1.1533
Jiangsu	1.0954	0.8462	1.1477	1.0494	1.2848	0.8284	1.1547	0.9651	1.0231	1.8397	1.0954
Zhejiang	3.9718	1.0373	1.2618	0.9638	1.6673	0.8959	0.9256	1.1459	1.1502	1.1526	3.9718
Fujian	1.3510	0.6361	0.8955	0.9148	1.0991	0.8334	2.8946	0.8428	0.9319	0.9271	1.3510
Guangdong	0.9489	0.9769	0.9536	1.1109	1.7218	0.8514	1.2096	0.9449	0.9354	1.0549	0.9489
Hainan	1.0866	0.9768	1.0040	0.8610	1.5238	0.8919	1.0119	0.9482	0.9572	0.9454	1.0866
Shanxi	1.1439	1.0853	1.0432	0.8373	1.7721	0.8303	1.2128	0.9287	0.9227	1.0225	1.1439
Heilongjiang	1.1570	1.0495	1.0294	0.8728	1.8425	0.7653	0.9361	0.9677	0.8112	0.7858	1.1570
Anhui	1.1848	0.9097	1.1665	0.7849	1.5672	0.7369	1.6225	0.9496	0.9881	0.9901	1.1848
Jiangxi	1.2237	0.9598	1.0798	1.0459	1.3491	0.7635	0.9284	0.9527	0.8512	0.9799	1.2237
Henan	0.9951	0.8830	1.0078	1.1832	1.9368	0.7182	0.6317	0.8950	0.8401	0.9646	0.9951
Hubei	0.9782	0.9519	0.9612	0.9858	1.1457	0.9099	0.9538	0.9148	0.9099	0.9929	0.9782
Inner Mongolia	1.0685	0.9725	1.1531	1.0356	1.4335	0.8619	0.9953	0.9309	0.7904	1.0830	1.0685
Guangxi	1.2016	1.2232	1.0483	0.7745	1.8389	0.8419	1.0350	0.9473	0.9803	0.7784	1.2016
Sichuan	1.0237	1.4018	0.9239	0.7602	1.8070	0.8177	0.6335	1.0754	0.8125	0.9031	1.0237
Chongqing	1.2734	1.0912	1.1330	0.9675	1.3034	0.9318	0.9681	0.8812	0.8137	0.8754	1.2734
Guizhou	0.9740	0.7245	1.1168	0.8621	1.4658	0.8872	0.7985	0.7707	0.7578	1.0482	0.9740
Shaanxi	1.3562	1.0042	0.9906	1.0737	1.4602	0.9488	0.8585	0.9689	0.9596	0.9696	1.3562
Gansu	1.0873	1.0969	0.8864	1.3545	1.3644	0.9326	0.9972	0.9231	0.9777	0.9258	1.0873
Qinghai	0.9594	1.1734	1.0877	0.7152	1.5505	1.0609	0.9969	0.9489	1.0723	1.2762	0.9594
Ningxia	1.0923	0.8763	1.0631	0.9953	2.5201	0.7490	0.9739	0.9827	1.0514	0.9085	1.0923
Xinjiang	1.1100	1.1129	1.4142	0.8259	1.7506	1.1823	1.2763	1.1507	1.0958	1.2594	1.1100

Data source: calculation.

Table 5: The estimation results of 25 provinces and Malmquist index is the mediator variable.

Variable	Model 1	Model 2	Model 3
Labor_grav	−1.82E-06**	33.7047**	−8.97E−07
δ	—	—	$-6.45E-09^{*}$
Urb	−7.20E−08	-1.7256^{***}	$7.13E-08^{**}$
Edu	$-1.43E-07^{*}$	-0.8861^{***}	$-1.48E-08$
Pen	$-1.68E-08$	0.3854^{***}	$-1.05E-08$
Unempl	$3.41E-07^{***}$	−0.2192	$-2.81E-08$
Heal	$-4.54E-08^{***}$	−0.0621	$5.11E-09$
Hwd	$1.41E-07^{***}$	−0.3283	$-1.35E-07^{***}$
Rwd	$5.91E-08$	0.3233	$2.86E-08$
β_0	$1.01E-07^{**}$	2.2256^{***}	$8.60E-08^{***}$

*Significance under level of 10%; **significance under level of 5%; ***significance under level of 1%. Data source: calculation.

Table 6: The estimation results of 25 provinces and the leapfrogging index is the mediator variable.

Variable	Model 1	Model 4	Model 5
Labor_grav	$-1.82E-06^{**}$	45.6037^{*}	$-9.99E-07^{*}$
δ	—	—	$-2.25E-09^{*}$
Urb	$-7.20E-08$	-3.2636^{**}	$7.41E-08^{**}$
Edu	$-1.43E-07^{*}$	-1.7484^{***}	$-1.35E-08$
Pen	$-1.68E-08$	0.7745^{***}	$-1.10E-08^{*}$
Unempl	$3.41E-07^{***}$	−0.5750	$-2.81E-08$
Heal	$-4.54E-08^{***}$	−0.1777	$5.06E-09$
Hwd	$1.41E-07^{***}$	−0.9849	$-1.36E-07^{***}$
Rwd	$5.91E-08$	1.1321	$2.94E-08$
β_0	$1.01E-07^{**}$	3.6416^{***}	$8.09E-08^{***}$

*Significance under level of 10%; **significance under level of 5%; ***significance under level of 1%. Data source: calculation.

Table 7: The estimation results of 25 provinces and the catching-up index is the mediator variable.

Variable	Model 1	Model 6	Model 7
Labor_grav	$-1.82E-06^{**}$	15.63299^{*}	$-4.75E-07$
δ	—	—	$7.47E-09$
Urb	$-7.20E-08$	−0.0463	$-5.91E-08^{**}$
Edu	$-1.43E-07^{*}$	−0.4683	$5.88E-08$
Pen	$-1.68E-08$	0.1568	$2.66E-08$
Unempl	$3.41E-07^{***}$	−0.1812	$-5.97E-08^{**}$
Heal	$-4.54E-08^{***}$	−0.0101	$4.61E-09$
Hwd	$1.41E-07^{***}$	0.0710	$-1.12E-07^{***}$
Rwd	$5.91E-08$	−0.1601	$1.84E-08$
β_0	$1.01E-07^{**}$	0.4337^{**}	$8.60E-08^{***}$

*Significance under level of 10%; **significance under level of 5%; ***significance under level of 1%. Data source: calculation.

of technological progress at the significance level of 10% in model 6, but catching-up of technological progress as a mediator variable has no significant effect on the change in labor income share in model 7. Therefore, leapfrogging of carbon emission reduction technological progress is a factor by which high-tech talents reduce labor income share.

4.2.3. Labor Income Share Forecast Based on Fractional Hausdorff Grey Model. Fractional Hausdorff grey model is used to predict the labor income share from 2018 to 2027, as shown in Table 8. Table 8 shows an increasing trend of labor income share in 25 provinces, indicating a clear and sustainable tendency in leapfrogging of technological progress over the next 10 years.

Table 8: Forecast of labor income share in 25 provinces by fractional Hausdorff grey model (unit: 10^{-8}).

	2018	2019	2020	2021	2022	2023	2024	2025	2026	2027
Beijing	4.913	5.011	5.161	5.368	5.261	5.524	5.579	5.133	5.594	5.650
Hebei	4.922	5.020	5.171	5.270	5.378	5.534	5.589	5.142	5.605	5.661
Liaoning	1.773	1.809	1.863	1.938	1.994	1.899	2.014	1.853	2.019	2.040
Shanghai	4.237	4.322	4.452	4.630	4.537	4.764	4.811	4.873	4.427	4.825
Jiangsu	3.343	3.410	3.512	3.653	3.580	3.759	3.796	3.492	3.807	3.845
Zhejiang	2.593	2.724	2.644	2.833	2.915	2.776	2.944	2.709	2.952	2.982
Fujian	3.844	3.921	4.038	4.200	4.116	4.322	4.377	4.016	4.365	4.421
Guangdong	3.476	3.546	3.652	3.798	3.722	3.908	3.947	3.632	3.958	3.998
Hainan	4.454	4.543	4.679	4.867	4.769	5.008	5.058	4.653	5.072	5.123
Shanxi	0.960	0.979	1.008	1.048	1.027	1.079	1.090	1.002	1.093	1.104
Heilongjiang	1.609	1.641	1.690	1.758	1.723	1.809	1.827	1.681	1.832	1.850
Anhui	2.500	2.550	2.626	2.731	2.676	2.810	2.838	2.611	2.846	2.875
Jiangxi	2.216	2.261	2.329	2.422	2.373	2.492	2.517	2.316	2.524	2.549
Henan	3.118	3.180	3.276	3.541	3.339	3.506	3.407	3.257	3.550	3.586
Hubei	0.952	0.971	1.000	1.040	1.019	1.070	1.081	0.995	1.084	1.095
Inner Mongolia	1.257	1.282	1.321	1.314	1.346	1.414	1.428	1.374	1.432	1.446
Guangxi	1.890	1.927	1.985	2.065	2.023	2.124	2.146	1.974	2.152	2.173
Sichuan	1.901	1.939	1.998	2.077	2.036	2.138	2.159	1.986	2.165	2.187
Chongqing	0.928	0.946	0.975	1.014	0.993	1.043	1.054	0.969	1.057	1.067
Guizhou	3.236	3.300	3.399	3.535	3.465	3.638	3.674	3.380	3.685	3.721
Shaanxi	15.551	15.862	16.338	16.991	16.652	17.484	17.659	16.246	17.708	17.886
Gansu	3.808	3.884	4.000	4.160	4.077	4.281	4.324	3.978	4.336	4.379
Qinghai	1.995	2.035	2.096	2.180	2.136	2.243	2.266	2.084	2.272	2.295
Ningxia	5.761	5.876	6.053	6.295	6.169	6.477	6.542	6.019	6.560	6.626
Xinjiang	4.147	4.229	4.356	4.531	4.440	4.662	4.709	4.332	4.722	4.769

Data source: calculation.

5. Conclusions and Discussion

Based on the marginal substitution theory, if it is a leapfrogging of technological progress, then there is an increasing return to scale, and there is a complementary relationship between capital and labor; that is, capital income share increases, while labor income share decreases. If the catching-up of technological advances is made possible, production efficiency improves, capital income share increases, while labor income share decreases in the initial stage due to the popularization and application of new equipment. However, the marginal output decreases, and the carbon emissions are close to or exceed the delimitation with the continuous input of machinery and equipment. The relationship between capital and labor becomes substitution, and labor replaces capital, so the share of labor income increases. However, the marginal output decreases with the continuous input of machinery and equipment, and carbon emissions are close to or exceed the emission standard. The relationship between capital and labor becomes substitution relationship, and labor replaces capital, so the labor income shares increase.

The results can be proved by relevant data of 25 provinces in China. The introduction of high-tech talents significantly reduces labor income share by using Malmquist index as a mediator variable. If the Malmquist index is decomposed into the leapfrogging of technological progress index and the catching-up technological progress index, the former as a mediator variable is the reason for the introduction of high-tech talents to reduce the labor income share, and the latter is not significant. However, catching-up of technological progress is a mediator variable between the introduction of high-tech talents and the labor income share at a significance level of 20%. While the confidence level is only 80 percent, it is worth noting that catching-up of technological advances helps to increase the labor income share.

Thus, the leapfrogging of technological progress helps to increase the capital income share, while the catching-up of technological progress helps to increase the labor income share. In 2019, China's Gini coefficient reached 0.465, still above the international alert line. If the income inequality gap can be narrowed, on the one hand, we should start from redistribution, improve the collection system of personal income tax, and increase the proportion of personal income tax in total tax. The primary means is to improve the education of workers because the catching-up of technological progress is manifested as technological diffusion. Also, the effectiveness of technology diffusion depends on whether the workers who learn technology have the ability to learn and whether they have the ability to use new production machines and participate in new production processes. If workers are well educated, their learning capacity increases accordingly.

It is found that the labor income share predicting by fractional Hausdorff grey model is increasing in 25 provinces and regions in China after 2018. This shows that the labor income share slows down the increase in income inequality gap after 2018, but the Gini coefficient of China is still above 0.46 after 2018 according to "China Statistical

Yearbook." Therefore, there are other factors leading to the high-income inequality gap in China besides labor income share, for instance, urbanization level and traffic convenience.

The promotion of urbanization is also an important factor in assisting the catching-up of technological progress and increasing the labor income share. The higher the level of urbanization, the higher the concentration of labor, which is conducive to the spread of new technologies between labors. If workers gather together, then the frequency of knowledge exchange between them increases, and new technologies can be transmitted at the fastest speed. Then, workers in this region will increase their income due to the improvement of skills.

In addition, convenient transportation is also conducive to the spread of catching-up of technological progress. The speed at which new technologies are disseminated within regions depends on the agglomeration degree of labors, while the speed at which they are transmitted to other regions depends on the accessibility of traffic, such as the number of roads and railways between regions, so if a region is at a transport hub, it could become a distributing centre for advanced technology. Thus, taking advantage of this advantage, the region prioritizes access to advanced technologies from other regions and is likely to stimulate local economic growth, thereby boosting local income levels.

Data Availability

The data used to support the findings of this study are available from the corresponding author upon request.

Conflicts of Interest

The authors declare that they have no conflicts of interest.

Acknowledgments

This research was supported by the National Social Science Fund (Grant no. 16BGL210), Universities' Philosophy and Social Science Project of Jiangsu Province (Grant no. 2020SJA2057), and National Bureau of Statistics (Grant no. 2019LY84).

References

[1] A. Mushtaq, Z. Chen, N. Ud Din, B. Ahmad, and X. Zhang, "Income inequality, innovation and carbon emission: perspectives on sustainable growth," *Economic Research-Ekonomska Istraživanja*, vol. 33, no. 1, pp. 769–787, 2020.

[2] R. D. Morgenstern, W. A. Pizer, and J.-S. Shih, "Jobs versus the environment: an industry-level perspective," *Journal of Environmental Economics and Management*, vol. 43, no. 3, pp. 412–436, 2002.

[3] G. Sheriff, A. E. Ferris, and R. J. Shadbegian, "How did air quality standards affect employment at us power plants? the importance of timing, geography, and stringency," *Journal of the Association of Environmental and Resource Economists*, vol. 6, no. 1, pp. 111–149, 2019.

[4] E. Berman and L. T. M. Bui, "Environmental regulation and labor demand: evidence from the south coast air basin," *Journal of Public Economics*, vol. 79, no. 2, pp. 265–295, 2001.

[5] E. Özgür and G. Türkmen, "The effects of technological development on the labor share of national income," *Economic Modelling*, vol. 87, no. 5, pp. 158–171, 2020.

[6] N. Batini, B. Jackson, and S. Nickell, "An open-economy new keynesian phillips curve for the UK," *Journal of Monetary Economics*, vol. 52, no. 6, pp. 1061–1071, 2005.

[7] L. Soete, "International diffusion of technology, industrial development and technological leapfrogging," *World Development*, vol. 13, no. 3, pp. 409–422, 1985.

[8] K. Lee and C. Lim, "Technological regimes, catching-up and leapfrogging: findings from the Korean industries," *Research Policy*, vol. 30, no. 3, pp. 459–483, 2001.

[9] R. H. Becker and L. M. Speltz, "Putting the s-curve concept to work," *Research Management*, vol. 26, no. 5, pp. 31–33, 1983.

[10] Y. Chen and I. Diwan, "When the bureaucrats move out of business : a cost-benefit assessment of labor retrenchment in China," *Policy Research Working Paper Series*, 2000.

[11] L. R. Ngai and C. A. Pissarides, "Structural change in a multisector model of growth," *American Economic Review*, vol. 97, no. 1, pp. 429–443, 2007.

[12] R. Koopman, W. Powers, Z. Wang, and S. J. Wei, "Give credit where credit is due: tracing value added in global production chains," *NBER Working Papers*, 2010.

[13] F. Alvarez-Cuadrado and M. Poschke, "Structural change out of agriculture: labor push versus labor pull," *American Economic Journal: Macroeconomics*, vol. 3, no. 3, pp. 127–15810, 2011.

[14] M. Duarte and D. Restuccia, "The role of the structural transformation in aggregate productivity," *Quarterly Journal of Economics*, vol. 125, no. 1, pp. 129–173, 2010.

[15] F. Alvarez-Cuadrado, N. V. Long, and M. Poschke, "Capital-labor substitution, structural change and the labor income share," *Journal of Economic Dynamics and Control*, vol. 87, pp. 206–231, 2018.

[16] J. Zeira, "Workers, machines, and economic growth," *The Quarterly Journal of Economics*, vol. 113, no. 4, pp. 1091–1117, 1998.

[17] P. Aghion, B. F. Jones, and C. I. Jones, "Artificial intelligence and economic growth," *NBER Working Papers*, 2017.

[18] D. Acemoglu and P. Restrepo, *Robots and Jobs: Evidence from Us Labor Markets*, Boston University - Department of Economics - The Institute for Economic Development Working Papers Series, Boston, MA, USA, 2017.

[19] T. Gregory, A. Salomons, and U. Zierahn, "Racing With or Against the Machine? Evidence from Europe," *ZEW - Centre for European Economic Research Discussion Paper No. 16-053*, 2019, https://ssrn.com/abstract=2815469.

[20] D. Acemoglu and P. Restrepo, *Artificial Intelligence, Automation and Work*, Social Science Electronic Publishing, New York, NY, USA, 2018.

[21] N. Salomons, M. V. D. Linden, S. S. Sebo, and B. Scassellati, "Humans conform to robots: disambiguating trust, truth, and conformity," in *Proceedings of the 2018 ACM/IEEE international conference*, ACM, Barcelona, Spain, 2018.

[22] G. Graetz and G. Michaels, *Robots at Work: The Impact on Productivity and Jobs*, CentrePiece - The Magazine for Economic Performance, 2015.

[23] L. Kromann, N. Malchow-Mller, J. R. Skaksen, and A. Srensen, "Automation and productivity—a cross-country, cross-industry comparison," *Industrial and Corporate Change*, vol. 29, no. 1, pp. 265–287, 2020.

[24] C. B. Frey and M. A. Osborne, "The future of employment: how susceptible are jobs to computerisation?" *Technological Forecasting and Social Change*, vol. 114, pp. 254–280, 2017.

[25] M. Oschinski and R. Wyonch, "Future Shock? The Impact of Automation on Canada's Labour Market," *C.D. Howe Institute*, Toronto, Canada, 2017.

[26] M. Arntz, T. Gregory, and U. Zierahn, "The risk of automation for jobs in OECD countries: a comparative analysis OECD Social Employment & Migration Working Papers," 2016.

[27] J. Bessen, *Ai and Jobs: The Role of Demand*, Social Science Electronic Publishing, New York, NY, USA, 2018.

[28] D. Acemoglu and P. Restrepo, "The race between man and machine: implications of technology for growth, factor shares, and employment," *American Economic Review*, vol. 108, no. 6, pp. 1488–1542, 2018.

[29] J. Bessen, "Automation and jobs: when technology boosts employment," *Economic Policy*, vol. 34, no. 100, pp. 589–626, 2019.

[30] W. Dauth, S. Findeisen, J. Sudekum, and N. Woessner, "German robots - the impact of industrial robots on workers Cepr Discussion Papers," 2017.

[31] A. Daron and R. Pascual, "Low-skill and high-skill automation," *Journal of Human Capital*, vol. 12, no. 2, pp. 204–232, 2018.

[32] E. Brynjolfsson, A. Mcafee, and M. Spence, "New world order : labor, capital, and ideas in the power law economy," *Forgn Affairs*, vol. 93, no. 4, pp. 10–44, 2014.

[33] R. Freeman, "Who owns the robots rules the world," *IZA World of Labor*, vol. 5, pp. 1–10, 2015.

[34] International Labour Organization (ILO), "Green policies and jobs: a double dividend?," in *The Global Jobs Crisis and beyond, World of Work Report 2009*, J. P. Bustamante, M. Charpe, and R. Torres, Eds., pp. 97–107, International Labour Organization (ILO),, Geneva, Switzerland, 2009.

[35] J. M. Mcneill and J. B. Williams, "The employment effects of sustainable development policies," *Ecological Economics*, vol. 64, no. 1, pp. 216–223, 2007.

[36] E. B. Goodstein, *Jobs and the Environment: The Myth of a National Trade-Off*, Economic Policy Institute, Washington, DC, USA, 1994.

[37] M. Liu, R. Shadbegian, and B. Zhang, "Does environmental regulation affect labor demand in China? evidence from the textile printing and dyeing industry," *Journal of Environmental Economics and Management*, vol. 86, no. 11, pp. 277–294, 2017.

[38] W. R. Walker, "Environmental regulation and labor reallocation: evidence from the clean air act," *American Economic Review*, vol. 101, no. 3, pp. 442–447, 2011.

[39] W. B. Gray, R. J. Shadbegian, C. Wang, and M. Meral, "Do epa regulations affect labor demand? evidence from the pulp and paper industry," *Journal of Environmental Economics and Management*, vol. 68, no. 1, pp. 188–202, 2014.

[40] R. H. Bezdek, R. M. Wendling, and P. Diperna, "Environmental protection, the economy, and jobs: national and regional analyses," *Journal of Environmental Management*, vol. 86, no. 1, pp. 63–79, 2008.

[41] J. P. Barrett and J. A. Hoerner, *Clean Energy and Jobs: A Comprehensive Approach to Climate Change and Energy Policy*, Economic Policy Institute, Washington, DC, USA, 2002.

[42] R. Martin, L. B. De Preux, and U. J. Wagner, "The impact of a carbon tax on manufacturing: evidence from microdata," *Journal of Public Economics*, vol. 117, pp. 1–14, 2014.

[43] A. Yamazaki, "Jobs and climate policy: evidence from british columbia's revenue-neutral carbon tax," *Journal of Environmental Economics and Management*, vol. 83, pp. 197–216, 2017.

[44] M. Y. Chi, "On the labor market consequences of environmental taxes," *Journal of Environmental Economics & Management*, vol. 89, pp. 136–152, 2018.

[45] D. Acemoglu, "Directed technical change," *NBER Working Papers*, vol. 69, no. 4, pp. 781–809, 2001.

[46] M. Bencik, "Capturing changes in factor effectivity with estimates of a ces production function with flexible trends," *Ekonomick Casopis*, vol. 68, p. 563, 2020.

[47] C. M. Christensen, "Exploring the limits of the technology s-curve," *Production and Operations Management*, vol. 1, no. 4, pp. 334–366, 1994.

[48] D. W. Caves, L. R. Christensen, and W. E. Diewert, "Multilateral comparisons of output, input, and productivity using superlative index numbers," *Economic Journal*, vol. 92, no. 365, pp. 73–86, 2002.

[49] R. Färe, S. Grosskopf, M. Norris, and Z. Z. Zhang, "Productivity growth, technical progress, and efficiency change in industrialized countries," *American Economic Review*, vol. 84, no. 1, pp. 66–83, 1994.

[50] D. Tyteca, "On the measurement of the environmental performance of firms- A literature review and a productive efficiency perspective," *Journal of Environmental Management*, vol. 46, no. 3, pp. 281–308, 1996.

[51] Z. Geng, J. Dong, Y. Han, and Q. Zhu, "Energy and environment efficiency analysis based on an improved environment DEA cross-model: case study of complex chemical processes," *Applied Energy*, vol. 205, pp. 465–476, 2017.

[52] N. Grunewald, S. Klasen, I. Martínez-Zarzoso, and C. Muris, "The trade-off between income inequality and carbon dioxide emissions," *Ecological Economics*, vol. 142, pp. 249–256, 2017.

[53] A. Panori and Y. Psycharis, "Exploring the links between education and income inequality at the municipal level in Greece," *Applied Spatial Analysis and Policy*, vol. 12, no. 1, pp. 101–126, 2019.

[54] J. Been, K. Caminada, K. Goudswaard, and O. van Vliet, "Public/private pension mix, income inequality and poverty among the elderly in Europe: an empirical analysis using new and revised OECD data," *Social Policy & Administration*, vol. 51, no. 7, pp. 1079–1100, 2017.

[55] G. J. Countryman, "The effect of unemployment insurance benefits on income inequality in the canadian provinces," *Canadian Public Policy/Analyse de Politiques*, vol. 25, no. 4, pp. 539–556, 1999.

[56] M. Johar, P. Soewondo, R. Pujisubekti, H. K. Satrio, and A. Adji, "Inequality in access to health care, health insurance and the role of supply factors," *Social Science & Medicine*, vol. 213, pp. 134–145, 2018.

[57] A. Banerjee, E. Duflo, and N. Qian, *On the Road: Access to Transportation Infrastructure and Economic Growth in China (No. W17897)*, National Bureau of Economic Research, Cambridge, UK, 2012.

[58] W. Cui, A. Wan, F. Xin, and Q. Li, "How does carbon emission reduction efficiency affect regional income inequality? The mediator effect of interregional labor flow," *Mathematical Problems in Engineering*, vol. 2021, Article ID 5578027, 14 pages, 2021.

[59] X. Meng, F. Fan, and L. Wu, "Prediction of major pollutants discharge from wastewater in 31 cities of China," *Sustainable Production and Consumption*, vol. 26, pp. 54–64, 2021.

[60] K. Shi and L. Wu, "Forecasting air quality considering the socio-economic development in Xingtai," *Sustainable Cities and Society*, vol. 61, Article ID 102337, 2020.

[61] S. F. Witt and C. A. Witt, "Forecasting tourism demand: a review of empirical research," *International Journal of Forecasting*, vol. 11, no. 3, pp. 447–475, 1995.

Hindawi
Journal of Mathematics
Volume 2021, Article ID 5599633, 8 pages
https://doi.org/10.1155/2021/5599633

Research Article

Coordinated Development of Urban Land Use and Ecological Economics in China

Zhiyuan Zhu [1] and Gang Du [2]

[1] *School of Mathematics and Information Science, Weifang University, Weifang 261061, China*
[2] *School of Economics and Management, Nanjing University of Aeronautics and Astronautics, Nanjing 210016, Jiangsu, China*

Correspondence should be addressed to Zhiyuan Zhu; zhuzhiyuanncu@163.com

Received 3 March 2021; Revised 15 April 2021; Accepted 17 April 2021; Published 26 April 2021

Academic Editor: Lifeng Wu

To analyze the coordination between land use and the ecological economy in China, ecoefficiency and land use intensity were measured using the nonradial, nonoriented slacks-based measure (SBM) and the vertical and horizontal scatter degree method. The TOPSIS method was then used to comprehensively evaluate regional differences in coordination. Our research indicates that the level of coordinated development between intensive urban land use and the ecological economy in China showed an overall upward trend from 2006 to 2017. The level of coordination was high in Beijing, Shanghai, and Tianjin and was low in Gansu, Ningxia, and Xinjiang. Changes in ecoefficiency were not consistent with the degree of coordination, and intensive urban land use was positively correlated with the level of coordination, which showed a mutually reinforcing relationship. Improving ecoefficiency is necessary for intensive urban land use, and for ecological improvement, coordinated development between ecoefficiency and urban land use intensity is essential. The establishment of environmentally friendly land use patterns could promote urban land use.

1. Introduction

Present urban land use in China, which has experienced an acceleration of industrialization and urbanization, directly affects urban economics, social development, and the construction of human settlements. When considering urban land use, ecological functions are typically ignored in favor of economic and social functions. The depletion of natural resources and overextension of environmental carrying capacity caused by urban land expansion have seriously hindered the development of urbanization in China. Construction on urban land in China increased from 6720 km^2 in 1986 to 49,983 km^2 in 2014, with an average annual growth rate of 7.43%. The first national pollution bulletin showed that China's industrial emissions of sulfur dioxide and soot were 21,197,500 and 11,666,400 tons, respectively, accounting for 91.4% and 84.2% of total pollution emissions. The direct economic loss caused by the destruction of natural resources and the environment is substantial. The importance of land use regulations should not be ignored in the pursuit of ecological development.

Coordination between intensive urban land use and ecological economics can also be conceived of as coordination among internal components of urban economic, social, and ecological development during the process of urbanization. Research on the relationship between intensive urban land use and ecological economics has concentrated mainly on urban land use and ecology in a single region; aspects that have been considered include the effects of intensive land use [1, 2], the ecoefficiency of land use [3–5], the impact of ecology on intensive land use [6, 7], and the relationships among these aspects [8, 9]. With continuing urbanization, research efforts are increasingly being devoted to the study of regional development, in three main respects: (1) the relationship between economic development and the ecological environment, (2) the relationship between land expansion and population growth, and (3) the coordination of the internal unit of urbanization. For

example, using spatial lag, spatial error, and spatial Durbin models, Tang et al. analyzed the relationship between urban land and regional economic development at the county level in the Beijing–Tianjin–Hebei region, based on analysis of cross-sectional data from 2015 [10]. Lv et al. empirically analyzed the interaction between land urbanization and population urbanization in Nanchang from 2002 to 2017 using the coupling coordination model (CCM) [11]. Cui developed a "comprehensive coordinated development index" for an urbanization–resources–environment (URE) system (URECDI) to represent the relationships among urbanization, resources, and environmental subsystems [12]. Liu et al. stated that the interaction among urban economic, social, and ecological systems in China, at the prefecture level and above, could be modeled using a CCM. Their results showed that coordinated urban development in China is spatially heterogeneous [13].

These studies provide a basis for further exploration of regional coordinated development. From a quantitative and dynamic perspective, there are few studies that focus on the coordinated relationship between land use and ecological development and propose effective regulatory approaches.

During the process of urbanization, can ecological improvement and intensive use of urban land coexist? Also, how strongly do they interact? To answer these questions, we empirically studied ecological efficiency in the context of intensive urban land use and provide suggestions for its optimization.

2. Evaluation Index System and Data Sources

2.1. Evaluation Index System Construction. Intensive urban land use is a dynamic and complex process related to the level of economic development and scientific and technological progress. The basic aim is to increase the input of elements per unit area and optimize the structural layout, to improve the utilization rate of urban land for greater economic, social, and environmental benefits. Based on the research of Zhang et al. [14–17], the following indicators of intensive urban land use were selected for this study: per capita fixed asset investment; number of employees in secondary and tertiary industries; per capita gross domestic product (GDP); per capita fiscal revenue; per capita construction land; per capita total retail sales of social consumer goods; per capita road area; per capita green space area; the green coverage rate of the built-up area; and population density.

According to the definition of ecoefficiency of the World Business Council for Sustainable Development (WBCSD) [18], which is based on the environmental and economic situation of Germany and the regional ecological efficiency evaluation index system constructed by Zhang [19] and Seppälä [20], resource consumption is the main index of ecological efficiency. The most important resources consumed are energy, water, land, and minerals. Seppälä [20] suggested that GDP, industrial added value, and total product value could be used as indicators of economic value in ecoefficiency analysis. To determine the overall developmental level of a region, the desirable output index (represented by GDP) was used, based on the constant price in 2000. Three indicators for environmental pollution and ecological destruction were used: (1) wastewater emissions, (2) industrial SO_2 emissions, and (3) smoke (powder) dust emissions.

2.2. Data. All the data were collected from the China Statistical Yearbook (2007–2018) and China urban statistical yearbook (2007–2018). Considering availability of the data, Tibet, Hong Kong, Macao, and Taiwan are not included in our data collection. We set the research period from 2006 to 2017.

3. Research Methods

3.1. Vertical and Horizontal Scatter Degree Method. Urban land use intensity is a dynamic phenomenon that changes continuously with time. The measurement of urban land use intensity should not only reflect the state of land use intensity at a certain cross-sectional moment in each evaluation area but should also describe the changing trends of urban land across time. The vertical and horizontal scatter degree method is an evaluation method based on a multidimensional time series table that is used to determine weights [21]. It not only reflects the "horizontal" level of intensity in all study areas at different times but also reflects the "vertical" intensity of each area. The intensity status at different times can be determined by comprehensively considering the maximization of differences between "horizontal" and "vertical" land intensification, which will reflect the differences between the evaluated objects.

Table 1, referred to as a multidimensional time series data table, shows the data from the evaluation indices in different regions at different times. Here, $t_i\,(i = 1, 2, \ldots, N)$ represents time, $S_i\,(i = 1, 2, \ldots, n)$ represents geographic regions, and $x_i\,(i = 1, 2, \ldots, m)$ represents the evaluation indices.

The dynamic comprehensive evaluation function supported by Table 1 is

$$y_i(t_k) = \sum_{j=1}^{m} w_j x_{ij}(t_k), \quad k = 1, 2, \ldots, N,\ i = 1, 2, \ldots, n, \tag{1}$$

where $y_i(t_k)$ is the comprehensive evaluation value of city S_i at time t_k and w_j is the weight coefficient.

The overall difference for each object in the multidimensional time series data table is expressed as the sum of the total deviation of squares of $y_i(t_k)$:

$$\sigma^2 = \sum_{k=1}^{N}\sum_{i=1}^{n}\left(y_i(t_k) - y\right)^2. \tag{2}$$

After standardizing the original data, we get $\overline{y} = 0$; hence,

$$\sigma^2 = \sum_{k=1}^{N}\sum_{i=1}^{n}\left(y_i(t_k)\right)^2 = \sum_{k=1}^{N} w^T H_k w = w^T \sum_{k=1}^{N} H_k w = w^T H w, \tag{3}$$

where $w = (w_1, w_2, \ldots, w_m)^T$, $H = \sum_{k=1}^{N} H_k$, and $H_k = A_k^T A_k$,

$$A_k = \begin{pmatrix} x_{11}(t_k) & x_{12}(t_k) & \cdots & x_{1m}(t_k) \\ x_{21}(t_k) & x_{22}(t_k) & \cdots & x_{2m}(t_k) \\ \cdots & \cdots & \cdots & \cdots \\ x_{n1}(t_k) & x_{n2}(t_k) & \cdots & x_{nm}(t_k) \end{pmatrix}, \quad k = 1, 2, \ldots, N. \tag{4}$$

If $w^T w = 1$ is limited, when w is the (standard) eigenvector corresponding to the maximum eigenvalue of H, σ^2 is the maximum, and $\max_{\|w\|} w^T H w = \lambda_{\max}(H)$. When the element of H_k is greater than 0, there must be an element of H greater than 0 and a positive weight coefficient vector. Therefore, the normalized eigenvector corresponding to $\lambda_{\max}(H)$ is the weight vector w.

3.2. SBM Model. Regional development can lead to economic growth, but can also have a negative impact on the environment. For example, water and soil pollution can be classified as "undesirable outputs." There are five main methods for modeling undesirable outputs. The first is to treat pollutants as inputs [22, 23]. The second is hyperbolic measurement [24]. The third method involves converting undesirable outputs into new variables [25]. However, these methods do not reflect actual production processes [26]. Chung et al. proposed a directional distance function approach, which has been adopted by many researchers [27]. The fifth method is the nonradial slacks-based measure (SBM). Traditional radial efficiency measures may introduce error as they neglect slack variables [28]. Hence, a series of models considering the nonradial, nonoriented SBM have been proposed [29–31].

The SBM is described as follows [30]: Suppose there are n homogeneous decision-making units (DMUs) and each DMU has three factors—inputs $x \in R^m$, desirable outputs $y^g \in R^{s_1}$, and undesirable outputs $y^b \in R^{s_2}$. The three matrices are defined as

$$\begin{aligned} X &= (x_1, x_2, \ldots, x_n) \in R^{m\times n}, \quad x_i \in R^m, \\ Y^g &= (y_1^g, y_2^g, \ldots, y_n^g) \in R^{s_1\times n}, \quad y_i^g \in R^{s_1}, \\ Y^b &= (y_1^b, y_2^b, \ldots, y_n^b) \in R^{s_2\times n}, \quad y_i^b \in R^{s_2}. \end{aligned} \tag{5}$$

Here, $x_i > 0$, $y_i^g > 0$, $y_i^b > 0$. Under the situation of constant return to scale (CRS), the production possibility set (PPS) is as follows:

$$P(x) = \left\{(x, y^g, y^b) | x \geq X\lambda, y^g \leq Y^g\lambda, \lambda \geq 0\right\}. \tag{6}$$

Here, λ is a nonnegative multiplier vector. Based on the PPS, the SBM model considering undesirable outputs can be expressed as

$$\rho^* = \frac{1 - (1/m)\sum_{i=1}^{m}(s_i^-/x_{io})}{1 + (1/s_1 + s_2)\left(\sum_{r=1}^{s_1} s_r^g/y_{ro}^g + \sum_{r=1}^{s_2} s_r^b/y_{ro}^b\right)},$$

$$s.t. \begin{cases} x_o = X\lambda + s^-, \\ y_o^g = Y^g\lambda - s^g, \\ y_o^b = Y^b\lambda + s^b, \\ s^- \geq 0, s^g \geq 0, s^b \geq 0, \lambda \geq 0. \end{cases} \tag{7}$$

3.3. TOPSIS Method. The maximum "positive intensive land use index" and "regional ecological efficiency index" values are obtained for each province. The minimum negative index value is taken as the positive ideal solution (that is, the optimally coordinated state). The minimum value is selected from the positive index, and the maximum value from the negative index is taken as the negative ideal solution (least well-coordinated state). The proximity of each province to the positive ideal solution obtained by the TOPSIS algorithm defines the level of coordination between intensive urban land utilization and the ecological economy in that province (see [32] for details of the TOPSIS algorithm).

4. Results

4.1. Intensive Land Use. China is divided into four main economic regions: east, central, west, and northeast. The eastern region includes Beijing, Fujian, Guangdong, Hebei, Jiangsu, Shandong, Shanghai, Tianjin, and Zhejiang. The central region includes Anhui, Henan, Hubei, Hunan, Jiangxi, and Shanxi. The western region includes Gansu, Guangxi, Guizhou, Inner Mongolia, Ningxia, Qinghai, Shaanxi, Sichuan, Xinjiang, and Yunnan. The northeastern region includes Heilongjiang, Jilin, and Liaoning.

Using the vertical and horizontal scatter degree method, the land use intensity of 30 provinces in China was measured for the period 2006–2017 (Table 2). Intensive urban land utilization, in China as a whole and in all four economic regions, showed an overall upward trend, although intensive land use decreased significantly after 2009, which was related to the national macrocontrol policy. A series of stimulus policies introduced by the Chinese government in response to the financial crisis further accelerated the pace of urban expansion, thereby reducing the intensity of urban land use. Intensive urban land use increased most rapidly from 2006 to 2009, by 32.6%. Spatially, the level of intensive land use in China fluctuated between 2006 and 2017. Intensive urban land use decreased in all four main economic regions, although it was still seen in parts of the eastern region, especially Shanghai and Beijing. Intensive land use was also seen in Zhejiang, Shandong, Fujian, Jiangsu, and Hebei, with an annual average of more than 0.5. Urban land use was less intensive in Jilin, Heilongjiang, Gansu, Ningxia, and

Table 1: Multidimensional time series data table.

Region	t_1 $x_1 x_2, \ldots, x_m$	t_2 $x_1, x_2, \ldots, x_m$	$\cdots$ $\cdots$	t_N $x_1, x_2, \ldots, x_m$
S_1	$x_{11}(t_1), x_{12}(t_1), \ldots, x_{1m}(t_1)$	$x_{11}(t_2) x_{12}(t_2), \ldots, x_{1m}(t_2)$	$\cdots$	$x_{11}(t_N) x_{12}(t_N), \ldots, x_{1m}(t_N)$
S_2	$x_{21}(t_1) x_{22}(t_1). \ldots, x_{2m}(t_1)$	$x_{21}(t_2) x_{22}(t_2), \ldots, x_{2m}(t_2)$	$\cdots$	$x_{21}(t_N) x_{22}(t_N), \ldots, x_{2m}(t_N)$
$\cdots$	$\cdots$	$\cdots$	$\cdots$	$\cdots$
S_n	$x_{n1}(t_1) x_{n2}(t_1), \ldots, x_{nm}(t_1)$	$x_{n1}(t_2) x_{n2}(t_2), \ldots, x_{nm}(t_2)$	$\cdots$	$x_{n1}(t_N) x_{n2}(t_N), \ldots, x_{nm}(t_N)$

Table 2: Values of urban land intensive use in China (2006–2017).

Province	2006	2007	2008	2009	2010	2011	2012	2013	2014	2015	2016	2017
Beijing	0.52	0.52	0.61	0.63	0.64	0.64	0.70	0.64	0.61	0.63	0.63	0.65
Tianjin	0.48	0.48	0.56	0.55	0.52	0.62	0.63	0.63	0.61	0.60	0.64	0.64
Hebei	0.43	0.43	0.54	0.39	0.38	0.43	0.45	0.45	0.45	0.44	0.45	0.46
Shanxi	0.34	0.39	0.39	0.41	0.40	0.44	0.46	0.45	0.48	0.47	0.46	0.47
Inner Mongolia	0.27	0.35	0.37	0.39	0.38	0.39	0.42	0.42	0.46	0.49	0.46	0.49
Liaoning	0.31	0.34	0.36	0.36	0.33	0.34	0.36	0.36	0.37	0.33	0.34	0.35
Jilin	0.22	0.25	0.27	0.26	0.25	0.27	0.28	0.29	0.28	0.31	0.31	0.33
Heilongjiang	0.14	0.21	0.20	0.24	0.25	0.29	0.31	0.31	0.32	0.30	0.32	0.34
Shanghai	0.57	0.68	0.54	0.57	0.58	0.62	0.64	0.63	0.64	0.62	0.65	0.66
Jiangsu	0.61	0.60	0.64	0.61	0.56	0.55	0.55	0.53	0.52	0.51	0.52	0.54
Zhejiang	0.59	0.54	0.54	0.51	0.56	0.49	0.52	0.52	0.50	0.50	0.50	0.52
Anhui	0.31	0.38	0.47	0.44	0.44	0.45	0.50	0.48	0.47	0.51	0.52	0.54
Fujian	0.64	0.56	0.61	0.60	0.56	0.54	0.60	0.60	0.61	0.58	0.60	0.61
Jiangxi	0.46	0.45	0.52	0.50	0.47	0.43	0.51	0.51	0.44	0.47	0.48	0.47
Shandong	0.49	0.60	0.57	0.55	0.56	0.53	0.55	0.54	0.52	0.51	0.53	0.53
Henan	0.42	0.50	0.42	0.51	0.52	0.51	0.54	0.53	0.54	0.55	0.57	0.57
Hubei	0.33	0.42	0.46	0.40	0.39	0.40	0.42	0.43	0.43	0.42	0.43	0.44
Hunan	0.44	0.45	0.51	0.49	0.48	0.49	0.54	0.54	0.55	0.57	0.59	0.60
Guangdong	0.51	0.52	0.53	0.51	0.53	0.51	0.52	0.53	0.52	0.51	0.54	0.56
Guangxi	0.36	0.41	0.43	0.40	0.43	0.44	0.48	0.45	0.41	0.44	0.43	0.45
Hainan	0.39	0.43	0.38	0.38	0.40	0.43	0.48	0.45	0.38	0.44	0.45	0.46
Chongqing	0.29	0.31	0.41	0.44	0.44	0.46	0.45	0.48	0.44	0.42	0.45	0.48
Sichuan	0.39	0.47	0.38	0.41	0.38	0.39	0.41	0.51	0.46	0.46	0.46	0.47
Guizhou	0.38	0.32	0.45	0.43	0.38	0.43	0.42	0.41	0.40	0.43	0.44	0.45
Yunnan	0.41	0.44	0.49	0.48	0.48	0.48	0.52	0.52	0.49	0.40	0.46	0.49
Shaanxi	0.43	0.41	0.32	0.30	0.37	0.41	0.40	0.43	0.43	0.42	0.44	0.46
Gansu	0.31	0.28	0.25	0.25	0.26	0.26	0.28	0.31	0.31	0.33	0.34	0.36
Qinghai	0.31	0.35	0.39	0.38	0.39	0.42	0.50	0.43	0.39	0.42	0.41	0.44
Ningxia	0.10	0.28	0.26	0.25	0.28	0.29	0.26	0.25	0.30	0.28	0.31	0.32
Xinjiang	0.26	0.30	0.32	0.27	0.27	0.27	0.28	0.28	0.30	0.29	0.31	0.33
China	0.39	0.42	0.44	0.43	0.43	0.44	0.47	0.46	0.45	0.45	0.47	0.48
East	0.52	0.54	0.55	0.53	0.53	0.54	0.56	0.55	0.54	0.53	0.55	0.56
Central	0.38	0.43	0.46	0.46	0.45	0.45	0.49	0.49	0.48	0.50	0.51	0.52
West	0.31	0.34	0.35	0.35	0.36	0.38	0.39	0.40	0.38	0.38	0.40	0.42
Northeast	0.22	0.26	0.28	0.29	0.28	0.30	0.31	0.32	0.33	0.31	0.32	0.34

Data are calculated according to equation (1).

Xinjiang, but showed a rapidly increasing trend in the latter two regions (average annual growth rate >3.2%).

In summary, intensive urban land use in China increased significantly between 2006 and 2017. Urban land use intensity was the highest in the eastern region, but showed a rapidly increasing trend in the central and western regions. Urban land use intensity was relatively low in the northeastern region.

4.2. Measurement of Regional Ecoefficiency. The regional ecoefficiency of 30 provinces in China was calculated for the period 2006–2017 using DEA Solver Pro5.0 software (Saitech Inc., Fremont, CA, USA) (Table 3). During this period, regional ecoefficiency showed a fluctuating trend (i.e., improvement followed by deterioration and then by further improvement). The number of effective units in the data envelopment analysis (DEA) showed a decreasing, followed by an increasing, trend from seven in 2012 to eight in 2017.

Beijing, Tianjin, Shanghai, Jiangsu, Zhejiang, Fujian, and Guangdong have always been the major production areas in China. Low ecoefficiency areas are mainly in the western region. The ecoefficiency of areas with inconsistent input and undesired output is low, as seen in Liaoning with respect

Table 3: Ecoefficiency values for 30 regions in China (2006–2017).

Province	2006	2007	2008	2009	2010	2011	2012	2013	2014	2015	2016	2017
Beijing	1.00	1.00	1.00	1.00	1.00	1.00	1.00	1.00	1.00	1.00	1.00	1.00
Tianjin	1.00	1.00	1.00	1.00	1.00	1.00	1.00	1.00	1.00	1.00	1.00	1.00
Hebei	0.57	0.55	0.56	0.54	0.49	0.41	0.43	0.47	0.46	0.45	0.45	0.43
Shanxi	0.38	0.34	0.35	0.35	0.30	0.29	0.27	0.26	0.26	0.27	0.27	0.24
Inner Mongolia	0.31	0.29	0.31	0.31	0.31	0.27	0.27	0.28	0.27	0.28	0.28	0.26
Liaoning	0.52	0.48	0.48	0.47	0.48	0.48	0.47	0.45	0.45	0.44	0.42	0.41
Jilin	0.38	0.36	0.36	0.39	0.40	0.40	0.39	0.40	0.40	0.40	0.40	0.40
Heilongjiang	1.00	0.46	0.46	0.45	0.47	0.44	0.45	0.41	0.41	0.41	0.41	0.42
Shanghai	1.00	1.00	1.00	1.00	1.00	1.00	1.00	1.00	1.00	1.00	1.00	1.00
Jiangsu	1.00	1.00	1.00	1.00	1.00	1.00	1.00	1.00	1.00	1.00	1.00	1.00
Zhejiang	1.00	1.00	1.00	1.00	1.00	1.00	1.00	1.00	1.00	1.00	1.00	1.00
Anhui	0.50	0.49	0.48	0.45	0.44	0.44	0.48	0.46	0.46	0.47	0.46	0.45
Fujian	1.00	1.00	1.00	1.00	1.00	1.00	1.00	1.00	1.00	1.00	1.00	1.00
Jiangxi	0.49	0.47	0.45	0.45	0.44	0.43	0.43	0.43	0.44	0.45	0.46	0.45
Shandong	1.00	0.58	0.58	0.57	0.57	0.56	0.60	0.57	0.60	0.62	0.63	0.65
Henan	0.57	0.51	0.50	0.49	0.47	0.47	0.46	0.45	0.46	0.46	0.45	0.43
Hubei	0.56	0.54	0.54	0.51	0.50	0.47	0.46	0.45	0.45	0.45	0.43	0.42
Hunan	0.46	0.46	0.48	0.50	0.44	0.46	0.45	0.47	0.47	0.47	0.43	0.45
Guangdong	1.00	1.00	1.00	1.00	1.00	1.00	1.00	1.00	1.00	1.00	1.00	1.00
Guangxi	0.36	0.39	0.40	0.37	0.41	0.42	0.42	0.39	0.40	0.40	0.38	0.40
Hainan	1.00	1.00	1.00	1.00	1.00	1.00	0.51	0.57	1.00	1.00	1.00	1.00
Chongqing	0.49	0.44	0.43	0.42	0.41	0.41	0.41	0.42	0.42	0.43	0.44	0.45
Sichuan	0.50	0.50	0.49	0.47	0.45	0.45	0.49	0.47	0.48	0.48	0.48	0.48
Guizhou	0.28	0.26	0.27	0.27	0.26	0.27	0.25	0.24	0.25	0.25	0.25	0.26
Yunnan	1.00	0.44	0.38	0.37	0.36	0.35	0.33	0.34	0.34	0.35	0.36	0.35
Shaanxi	0.45	0.41	0.42	0.41	0.43	0.43	0.42	0.40	0.40	0.41	0.42	0.41
Gansu	0.28	0.28	0.27	0.27	0.26	0.25	0.24	0.24	0.25	0.24	0.23	0.24
Qinghai	0.30	0.29	0.29	0.30	0.29	0.29	0.27	0.27	0.27	0.28	0.27	0.28
Ningxia	0.13	0.13	0.15	0.12	0.12	0.13	0.12	0.12	0.12	0.12	0.12	0.11
Xinjiang	0.30	0.26	0.26	0.24	0.22	0.22	0.20	0.18	0.18	0.18	0.19	0.19

Data are calculated according to equation (7).

to urban water. Industrial SO_2 emissions and smoke (powder) dust emissions were higher than the national average in Liaoning, while the GDP of Ningxia and Xinjiang over the 12-year period was markedly different from the national average. These factors were responsible for the relatively low ecoefficiencies in these areas.

The analysis showed that GDP is not necessarily reflected in regional ecoefficiency. In 2015, Sichuan, Hubei, and Hunan had larger GDP values, but lower ecoefficiency, than Fujian; economically underdeveloped areas can still achieve ecological efficiency by rationally adjusting their industrial structure and optimizing output. For example, in 2006, the GDP of Yunnan was less than a fifth of that of Shandong, but its ecoefficiency was 60% higher. Thus, regional ecoefficiency is not dependent only on the economic output.

4.3. Coordinated Development. The TOPSIS algorithm was used to measure the level of intensity of urban land use and regional ecological development in various provinces of China from 2006 to 2017 (Table 4). Spatial and temporal aspects of coordinated development were analyzed. Based on K-means clustering and regional economic and social development data, the study area was divided into four categories: low coordination (0–0.3), moderate coordination (0.3–0.5), moderate-to-high coordination (0.5–0.7), and high coordination (0.7–1.0). Figure 1 shows the classifications for 30 provinces from 2006 to 2017.

The average coordination value between intensive land use and the ecological economy in China for the period 2006–2017 was 0.524, indicating considerable room for improvement. Most provinces had moderate or moderate-to-high coordination. The number of provinces with low and moderate coordination values showed an upward trend over the period 2006–2017, while the moderate-to-high coordination areas showed a fluctuating, but ultimately decreasing, trend.

Despite some volatility, there was significant overall improvement in the level of coordination, particularly after 2007 and 2012. Implementation of the Eleventh Five-Year Plan and Twelfth Five-Year Plan promoted rational allocation of production and coordinated overall development of the Chinese economy and society. From 2007 to 2011, economic development was rapid, environmental pollution control efforts were strengthened, and the degree of coordination was high. From 2012 to 2017, the rate of urban construction in China began to slow down; more attention was paid to ecological construction, and coordination showed an upward trend.

Areas with high coordination were mainly distributed within the economically developed coastal areas in the east. Areas with high-to-moderate and moderate

Table 4: Coordinated development values for 30 regions in China (2006–2017).

Province	2006	2007	2008	2009	2010	2011	2012	2013	2014	2015	2016	2017
Beijing	0.89	0.80	0.74	0.71	0.88	0.93	0.88	0.88	0.89	0.92	0.91	0.94
Tianjin	0.76	0.66	0.74	0.72	0.71	0.76	0.83	0.84	0.85	0.86	0.89	0.86
Hebei	0.58	0.54	0.57	0.60	0.60	0.62	0.57	0.57	0.58	0.58	0.61	0.59
Shanxi	0.42	0.36	0.35	0.37	0.33	0.36	0.33	0.33	0.34	0.34	0.36	0.37
Inner Mongolia	0.28	0.29	0.31	0.36	0.31	0.31	0.32	0.32	0.33	0.34	0.32	0.32
Liaoning	0.66	0.60	0.67	0.71	0.70	0.71	0.55	0.60	0.61	0.63	0.65	0.65
Jilin	0.34	0.29	0.29	0.30	0.28	0.31	0.26	0.27	0.28	0.29	0.32	0.31
Heilongjiang	0.50	0.49	0.52	0.54	0.57	0.59	0.61	0.62	0.63	0.64	0.63	0.65
Shanghai	1.00	1.00	1.00	1.00	0.99	0.90	0.90	1.00	1.00	1.00	1.00	1.00
Jiangsu	0.78	0.70	0.83	0.83	0.89	0.89	0.86	0.86	0.88	0.90	0.94	0.95
Zhejiang	0.74	0.74	0.79	0.79	0.78	0.80	0.82	0.83	0.83	0.85	0.87	0.86
Anhui	0.34	0.42	0.47	0.45	0.48	0.50	0.48	0.48	0.49	0.50	0.52	0.52
Fujian	0.84	0.75	0.84	0.88	0.91	0.89	0.90	0.92	0.93	0.94	0.92	0.96
Jiangxi	0.52	0.46	0.43	0.49	0.53	0.55	0.51	0.54	0.54	0.56	0.57	0.56
Shandong	0.80	0.74	0.82	0.83	0.83	0.86	0.85	0.86	0.87	0.88	0.84	0.83
Henan	0.58	0.55	0.54	0.54	0.49	0.48	0.47	0.48	0.49	0.52	0.54	0.58
Hubei	0.49	0.49	0.57	0.51	0.59	0.57	0.53	0.55	0.56	0.57	0.58	0.62
Hunan	0.48	0.48	0.46	0.45	0.52	0.54	0.52	0.54	0.54	0.56	0.57	0.59
Guangdong	0.68	0.64	0.68	0.70	0.72	0.74	0.76	0.77	0.78	0.82	0.85	0.85
Guangxi	0.31	0.38	0.33	0.32	0.36	0.38	0.40	0.42	0.44	0.45	0.47	0.45
Hainan	0.60	0.60	0.68	0.71	0.73	0.79	0.51	0.60	0.63	0.73	0.75	0.76
Chongqing	0.42	0.37	0.44	0.48	0.47	0.52	0.46	0.47	0.49	0.52	0.53	0.54
Sichuan	0.47	0.55	0.53	0.53	0.56	0.55	0.53	0.55	0.56	0.57	0.59	0.60
Guizhou	0.42	0.25	0.32	0.28	0.21	0.27	0.24	0.25	0.27	0.33	0.36	0.39
Yunnan	0.70	0.39	0.37	0.35	0.36	0.35	0.37	0.38	0.38	0.40	0.42	0.43
Shaanxi	0.52	0.52	0.53	0.56	0.55	0.53	0.52	0.54	0.54	0.56	0.55	0.54
Gansu	0.23	0.17	0.13	0.14	0.15	0.14	0.13	0.14	0.15	0.16	0.17	0.17
Qinghai	0.26	0.31	0.25	0.25	0.25	0.31	0.35	0.36	0.37	0.38	0.39	0.39
Ningxia	0.00	0.00	0.05	0.06	0.13	0.14	0.06	0.08	0.09	0.10	0.15	0.16
Xinjiang	0.23	0.15	0.15	0.14	0.13	0.12	0.14	0.14	0.15	0.19	0.22	0.24
Average	0.53	0.49	0.51	0.52	0.53	0.55	0.52	0.54	0.55	0.57	0.58	0.59

Data are calculated according to Section 3.3.

Figure 1: Coordinated development value of 30 provinces in China.

coordination were mainly distributed in the central and northeastern regions. Low coordination regions were mainly in the west.

The coordination between intensive urban land use and the development of the ecological economy shows a significant regional variation in China. Coordination differs according to the level of economic development and regional development policies. With further regional economic integration, different regions must implement land regulations and environmental management policies to promote sustainable development of economic society.

5. Conclusions

We constructed a model based on the TOPSIS method to measure coordination between intensive urban land use and the ecological economy in China, for the period 2006–2017. We then analyzed spatial and temporal aspects of coordination across Chinese provinces. Our conclusions are as follows:

(1) Despite large regional differences in the intensity of urban land use, there was an overall upward trend. The intensity of urban land use was consistent with the degree of economic development. The intensity was the highest in the eastern region, possibly due to the rational allocation of production and efficient use of resources in this region. The western and northeastern regions had the least intense land use. Due to its rich resources and industrial history, the eastern region lags behind in resource utilization efficiency and industrial adjustment. The central region has benefitted from the transfer of industrial

activity from the eastern region, reflected in intensive land use.

(2) Ecoefficiency showed a downward trend over the study period at the regional level. In the eastern coastal areas, ecological efficiency did not accord with GDP. Rational allocation of production could improve regional ecological efficiency.

(3) The average coordination value (between intensive land use and the ecological economy) for the period 2006–2017 in China was ~0.524, indicating considerable room for improvement. The low and moderate coordination provinces accounted for about 46% of all provinces in all years of the study period, indicating that improving coordination between land use and economic development will be a difficult, but important, task. The degree of coordination is consistent with the intensity of urban land use; improvement in the latter could provide ecological benefits.

Based on these findings, the following conclusions can be drawn:

(1) Under resource and environmental constraints, an improper relationship between the development of land resources and ecological protection measures may weaken regional cooperation and hinder the implementation of policies promoting urban development. More attention should be paid to rational allocation of production at the regional level, mutually beneficial development policies, and land regulations that promote ecoefficiency. Regional environmental protection policies could not only benefit economic and social development but also resolve the tension between the former and ecological construction.

(2) Land resources should be rationally allocated at the policy level; the scale of urban development should be effectively controlled by improving natural resource taxation. Furthermore, environmental pollutants should be monitored more closely, and the economical, societal, and ecological needs should all be considered. Finally, enthusiasm for ecological protection should be fostered among all relevant stakeholders by establishing a mechanism for cross-regional ecological compensation.

Data Availability

The data, models, or code used to support the findings of this study are available from the corresponding author upon request.

Conflicts of Interest

The authors declare that they have no conflicts of interest.

References

[1] J. Zhan, J. Liu, Y. Lin, F. Wu, and E. Ma, "Land use change dynamics model compatible with climate models," *Land Use Impacts on Climate*, pp. 19–46, 2014.

[2] C. Wei, Z. Zhi-yuan, and F. Jun-chao, "Urban construction land deployment based on ecological efficiency Malmquist index," *Metallurgical and Mining Industry*, vol. 7, no. 8, pp. 114–118, 2015.

[3] Z. Zhi-yuan, M. Jianjun, and C. Wei, "Measuring regional eco-efficiency: a non-oriented slacks-based measure analysis," *International Journal of Earth Sciences and Engineering*, vol. 7, no. 6, pp. 2520–2527, 2014.

[4] Z. Zhi-yuan, M. Jianjun, and C. Wei, "Regional eco-efficiency variation: a data envelopment analysis approach," *International Journal of Earth Sciences and Engineering*, vol. 8, no. 2, pp. 977–984, 2015.

[5] M. Xiangmei, F. Feifei, and W. Lifeng, "Prediction of major pollutants discharge from wastewater in 31 cities of China," *Sustainable Production and Consumption*, vol. 26, pp. 54–64, 2021.

[6] S. Cheng-Shun, T. Li, and Z. Wen-Xia, "Evaluation of intensive utilization of urban land based on set pair analysis," *Scientific and Technological Management of Land and Resources*, vol. 36, no. 3, pp. 27–39, 2019.

[7] K. Shi and L. Wu, "Forecasting air quality considering the socio-economic development in Xingtai," *Sustainable Cities and Society*, vol. 61, Article ID 102337, 2020.

[8] K. Wang, Y. Tang, Y. Chen et al., "The coupling and coordinated development from urban land using benefits and urbanization level: case study from Fujian province (China)," *International Journal of Environmental Research and Public Health*, vol. 17, no. 16, p. 5647, 2020.

[9] X. Cen, C. Wu, X. Xing, M. Fang, Z. Garang, and Y. Wu, "Coupling intensive land use and landscape ecological security for urban sustainability: an integrated socioeconomic data and spatial metrics analysis in Hangzhou city," *Sustainability*, vol. 7, no. 2, pp. 1459–1482, 2015.

[10] Z. Tang, Z. Zhang, L. Zuo, X. Wang, S. Hu, and Z. Zhu, "Spatial econometric analysis of the relationship between urban land and regional economic development in the Beijing-Tianjin-Hebei coordinated development region," *Sustainability*, vol. 12, no. 20, p. 8451, 2020.

[11] T. Lv, L. Wang, X. Zhang et al., "Coupling coordinated development and exploring its influencing factors in Nanchang, China: from the perspectives of land urbanization and population urbanization," *Land*, vol. 8, no. 12, p. 178, 2019.

[12] X. Cui, C. Fang, H. Liu, and X. Liu, "Assessing sustainability of urbanization by a coordinated development index for an urbanization-resources-environment complex system: a case study of Jing-Jin-Ji region, China," *Ecological Indicators*, vol. 96, pp. 383–391, 2019.

[13] H. Liu and L. Ma, "Spatial pattern and effects of urban coordinated development in China's urbanization," *Sustainability*, vol. 12, no. 6, p. 2389, 2020.

[14] Q. Sun, X. Zhang, H. Zhang, and H. Niu, "Coordinated development of a coupled social economy and resource environment system: a case study in Henan Province, China," *Environment, Development and Sustainability*, vol. 20, no. 3, pp. 1385–1404, 2018.

[15] H. Liu, Y. Liu, H. Wang, J. Yang, and X. Zhou, "Research on the coordinated development of greenization and urbanization based on system dynamics and data envelopment analysis-a case study of Tianjin," *Journal of Cleaner Production*, vol. 214, pp. 195–208, 2019.

[16] H. Zhang, C. Lu, K. Yang et al., "Evaluation on intensive use of urban land based on PSR model taking Henan Province as an example," *Journal of Physics: Conference Series*, vol. 1419, no. 1, Article ID 012016, 2019.

[17] P. Zhang, D. Yang, M. Qin, and W. Jing, "Spatial heterogeneity analysis and driving forces exploring of built-up land development intensity in Chinese prefecture-level cities and implications for future Urban Land intensive use," *Land Use Policy*, vol. 99, Article ID 104958, 2020.

[18] B. Stigson, *Eco-Efficiency: Creating More Value with Less Impact*, WBCSD, Geneva, Switzerland, 2000.

[19] B. Zhang, J. Bi, Z. Fan, Z. Yuan, and J. Ge, "Eco-efficiency analysis of industrial system in China: a data envelopment analysis approach," *Ecological Economics*, vol. 68, no. 1-2, pp. 306–316, 2008.

[20] J. Seppälä, M. Melanen, I. Mäenpää et al., "How can the eco-efficiency of a region be measured and monitored?" *Journal of Industrial Ecology*, vol. 9, pp. 117–130, 2005.

[21] Y. Guo, *Comprehensive Evaluation Theory, Method and Application*, Science Press, Beijing, China, 2007.

[22] J.-D. Lee, J.-B. Park, and T.-Y. Kim, "Estimation of the shadow prices of pollutants with production/environment inefficiency taken into account: a nonparametric directional distance function approach," *Journal of Environmental Management*, vol. 64, no. 4, pp. 365–375, 2002.

[23] L. M. Seiford and J. Zhu, "Modeling undesirable factors in efficiency evaluation," *European Journal of Operational Research*, vol. 142, no. 1, pp. 16–20, 2002.

[24] J. L. Zofío and A. M. Prieto, "Environmental efficiency and regulatory standards: the case of CO_2 emissions from OECD industries," *Resource and Energy Economics*, vol. 23, no. 1, pp. 63–83, 2001.

[25] G. R. Jahanshahloo, A. Hadi Vencheh, A. A. Foroughi, and R. Kazemi Matin, "Inputs/outputs estimation in DEA when some factors are undesirable," *Applied Mathematics and Computation*, vol. 156, no. 1, pp. 19–32, 2004.

[26] A. J. Picazo-Tadeo and D. Prior, "Environmental externalities and efficiency measurement," *Journal of Environmental Management*, vol. 90, no. 11, pp. 3332–3339, 2009.

[27] B. Arabi, S. Munisamy, A. Emrouznejad, and F. Shadman, "Power industry restructuring and eco-efficiency changes: a new slacks-based model in Malmquist-Luenberger index measurement," *Energy Policy*, vol. 68, pp. 132–145, 2014.

[28] H. Fukuyama and W. L. Weber, "A directional slacks-based measure of technical inefficiency," *Socio-Economic Planning Sciences*, vol. 43, no. 4, pp. 274–287, 2009.

[29] K. Tone, "A slacks-based measure of efficiency in data envelopment analysis," *European Journal of Operational Research*, vol. 130, no. 3, pp. 498–509, 2001.

[30] K. Tone, "Dealing with undesirable outputs in DEA: a slacks-based measure (SBM) approach," in *Proceedings of the North American Productivity Workshop 2004*, pp. 44-45, Presentation at NAPW III, Toronto, Canada, 2004.

[31] P. Zhou and B. W. Ang, "Linear programming models for measuring economy-wide energy efficiency performance," *Energy Policy*, vol. 36, no. 8, pp. 2911–2916, 2008.

[32] B. B. Zaidan and A. A. Zaidan, "Comparative study on the evaluation and benchmarking information hiding approaches based multi-measurement analysis using TOPSIS method with different normalisation, separation and context techniques," *Measurement*, vol. 117, pp. 277–294, 2018.